frontiers | Research Topics

Immunodynamics of cardiorespiratory disease

Edited by
Szandor Simmons, Kathleen Pappritz and Jana Grune

Published in
Frontiers in Immunology

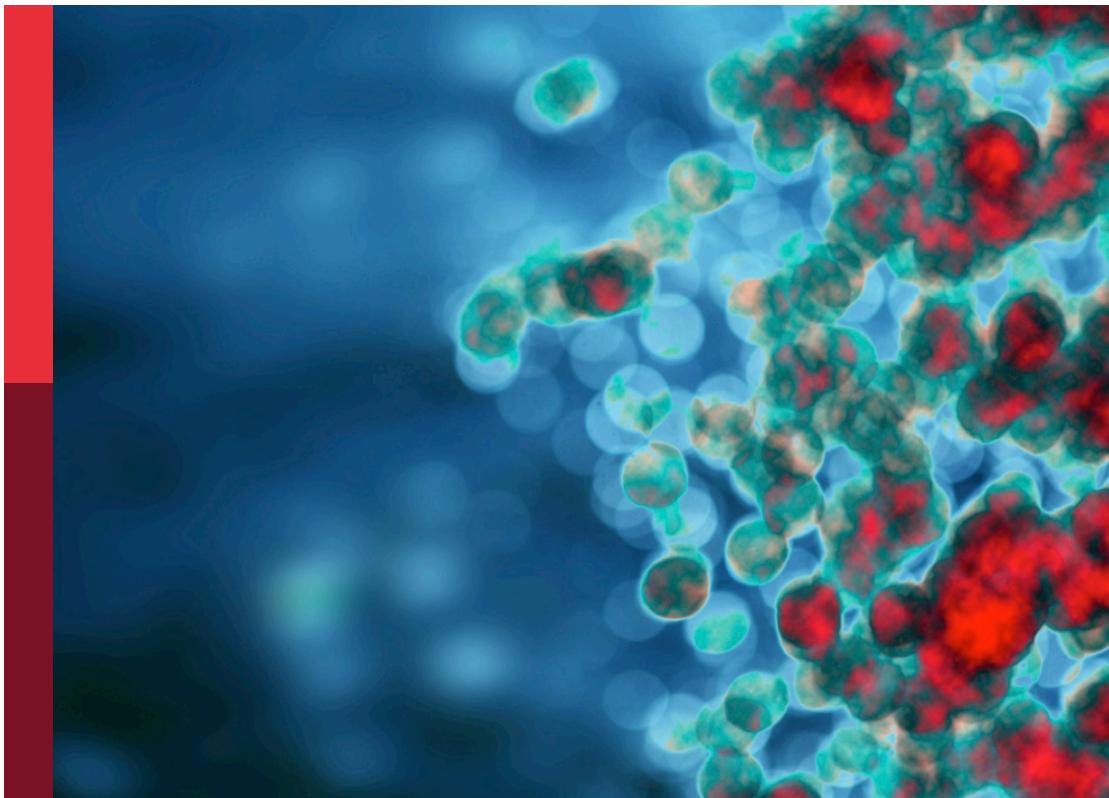

ISSN 1664-8714
ISBN 978-2-8325-2389-6
DOI 10.3389/978-2-8325-2389-6

About Frontiers

Frontiers is more than just an open access publisher of scholarly articles: it is a pioneering approach to the world of academia, radically improving the way scholarly research is managed. The grand vision of Frontiers is a world where all people have an equal opportunity to seek, share and generate knowledge. Frontiers provides immediate and permanent online open access to all its publications, but this alone is not enough to realize our grand goals.

Frontiers journal series

The Frontiers journal series is a multi-tier and interdisciplinary set of open-access, online journals, promising a paradigm shift from the current review, selection and dissemination processes in academic publishing. All Frontiers journals are driven by researchers for researchers; therefore, they constitute a service to the scholarly community. At the same time, the *Frontiers journal series* operates on a revolutionary invention, the tiered publishing system, initially addressing specific communities of scholars, and gradually climbing up to broader public understanding, thus serving the interests of the lay society, too.

Dedication to quality

Each Frontiers article is a landmark of the highest quality, thanks to genuinely collaborative interactions between authors and review editors, who include some of the world's best academicians. Research must be certified by peers before entering a stream of knowledge that may eventually reach the public - and shape society; therefore, Frontiers only applies the most rigorous and unbiased reviews. Frontiers revolutionizes research publishing by freely delivering the most outstanding research, evaluated with no bias from both the academic and social point of view. By applying the most advanced information technologies, Frontiers is catapulting scholarly publishing into a new generation.

What are Frontiers Research Topics?

Frontiers Research Topics are very popular trademarks of the *Frontiers journals series*: they are collections of at least ten articles, all centered on a particular subject. With their unique mix of varied contributions from Original Research to Review Articles, Frontiers Research Topics unify the most influential researchers, the latest key findings and historical advances in a hot research area.

Find out more on how to host your own Frontiers Research Topic or contribute to one as an author by contacting the Frontiers editorial office: frontiersin.org/about/contact

Immunodynamics of cardiorespiratory disease

Topic editors

Szandor Simmons — Charité – Universitätsmedizin Berlin, Germany
Kathleen Pappritz — Charité Medical University of Berlin, Germany
Jana Grune — Charité Medical University of Berlin, Germany

Citation

Simmons, S., Pappritz, K., Grune, J., eds. (2023). *Immunodynamics of cardiorespiratory disease*. Lausanne: Frontiers Media SA.
doi: 10.3389/978-2-8325-2389-6

Table of contents

frontiers in Immunology

ORIGINAL RESEARCH
published: 11 March 2022
doi: 10.3389/fimmu.2022.844701

Disease Severity in Moderate-to-Severe COVID-19 Is Associated With Platelet Hyperreactivity and Innate Immune Activation

Kai Jakobs[1,2], Leander Reinshagen[1,2], Marianna Puccini[1,2], Julian Friebel[1,2,3], Anne-Christin Beatrice Wilde[4], Ayman Alsheik[1], Andi Rroku[1,2], Ulf Landmesser[1,2,3], Arash Haghikia[1,2,3], Nicolle Kränkel[1,2†] and Ursula Rauch-Kröhnert[1,2*†]*

[1] Department of Cardiology, Charité University Medicine Berlin, Campus Benjamin Franklin, Berlin, Germany, [2] German Centre for Cardiovascular Research (DZHK), Partner Site Berlin, Berlin, Germany, [3] Berlin Institute of Health (BIH), Berlin, Germany, [4] Department of Hepatology and Gastroenterology, Charité University Medicine Berlin, Campus Virchow, Berlin, Germany

Background: Hemostasis and inflammation are both dysregulated in patients with moderate-to-severe coronavirus disease 2019 (COVID-19). Yet, both processes can also be disturbed in patients with other respiratory diseases, and the interactions between coagulation, inflammation, and disease severity specific to COVID-19 are still vague.

Methods: Hospitalized patients with acute respiratory symptoms and with severe acute respiratory syndrome coronavirus 2 (SARS-CoV2)-positive (COV^{pos}) and SARS-CoV2-negative (COV^{neg}) status were included. We assessed adenosine diphosphate (ADP)-, thrombin receptor activator peptide 6 (TRAP)-, and arachidonic acid (AA)-induced platelet reactivity by impedance aggregometry, as well as leukocyte subtype spectrum and platelet-leukocyte aggregates by flow cytometry and inflammatory cytokines by cytometric bead array.

Results: ADP-, TRAP-, and AA-induced platelet reactivity was significantly higher in COV^{pos} than in COV^{neg} patients. Disease severity, assessed by sequential organ failure assessment (SOFA) score, was higher in COV^{pos} than in COV^{neg} patients and again higher in deceased COV^{pos} patients than in surviving COV^{pos}. The SOFA score correlated significantly with the mean platelet volume and TRAP-induced platelet aggregability. A larger percentage of classical and intermediate monocytes, and of $CD4^{pos}$ T cells (T_H) aggregated with platelets in COV^{pos} than in COV^{neg} patients. Interleukin (IL)-1 receptor antagonist (RA) and IL-6 levels were higher in COV^{pos} than in COV^{neg} patients and again higher in deceased COV^{pos} patients than in surviving COV^{pos}. IL-1RA and IL-6 levels correlated with the SOFA score in COV^{pos} but not in COV^{neg} patients. In both respiratory disease groups, absolute levels of B-cell-platelet aggregates and NK-cell-platelet aggregates were correlated with *ex vivo* platelet aggegation upon stimulation with AA and ADP, respectively, indicating a universal, but not a COVID-19-specific mechanism.

OPEN ACCESS

Edited by:
Fabrice Cognasse, Santé Ingéniérie Biologie (INSERM), France

Reviewed by:
Sanjay B. Maggirwar, George Washington University, United States
Wared Nour-Eldine, Qatar Biomedical Research Institute, Qatar

***Correspondence:**
Ursula Rauch-Kröhnert
ursula.rauch@charite.de
Nicolle Kränkel
nicolle.kraenkel@charite.de

†These authors have contributed equally to this work and share senior authorship

Specialty section:
This article was submitted to Inflammation, a section of the journal Frontiers in Immunology

Received: *28 December 2021*
Accepted: *11 February 2022*
Published: *11 March 2022*

Citation:
Jakobs K, Reinshagen L, Puccini M, Friebel J, Wilde A-CB, Alsheik A, Rroku A, Landmesser U, Haghikia A, Kränkel N and Rauch-Kröhnert U (2022) Disease Severity in Moderate-to-Severe COVID-19 Is Associated With Platelet Hyperreactivity and Innate Immune Activation. Front. Immunol. 13:844701. doi: 10.3389/fimmu.2022.844701

Conclusion: In moderate-to-severe COVID-19, but not in other respiratory diseases, disease severity was associated with platelet hyperreactivity and a typical inflammatory signature. In addition to a severe inflammatory response, platelet hyperreactivity associated to a worse clinical outcome in patients with COVID-19, pointing to the importance of antithrombotic therapy for reducing disease severity.

Keywords: COVID-19, platelet hyperactivity, immunothrombosis, inflammation, platelet-leucocyte aggregates, disease severity, survival

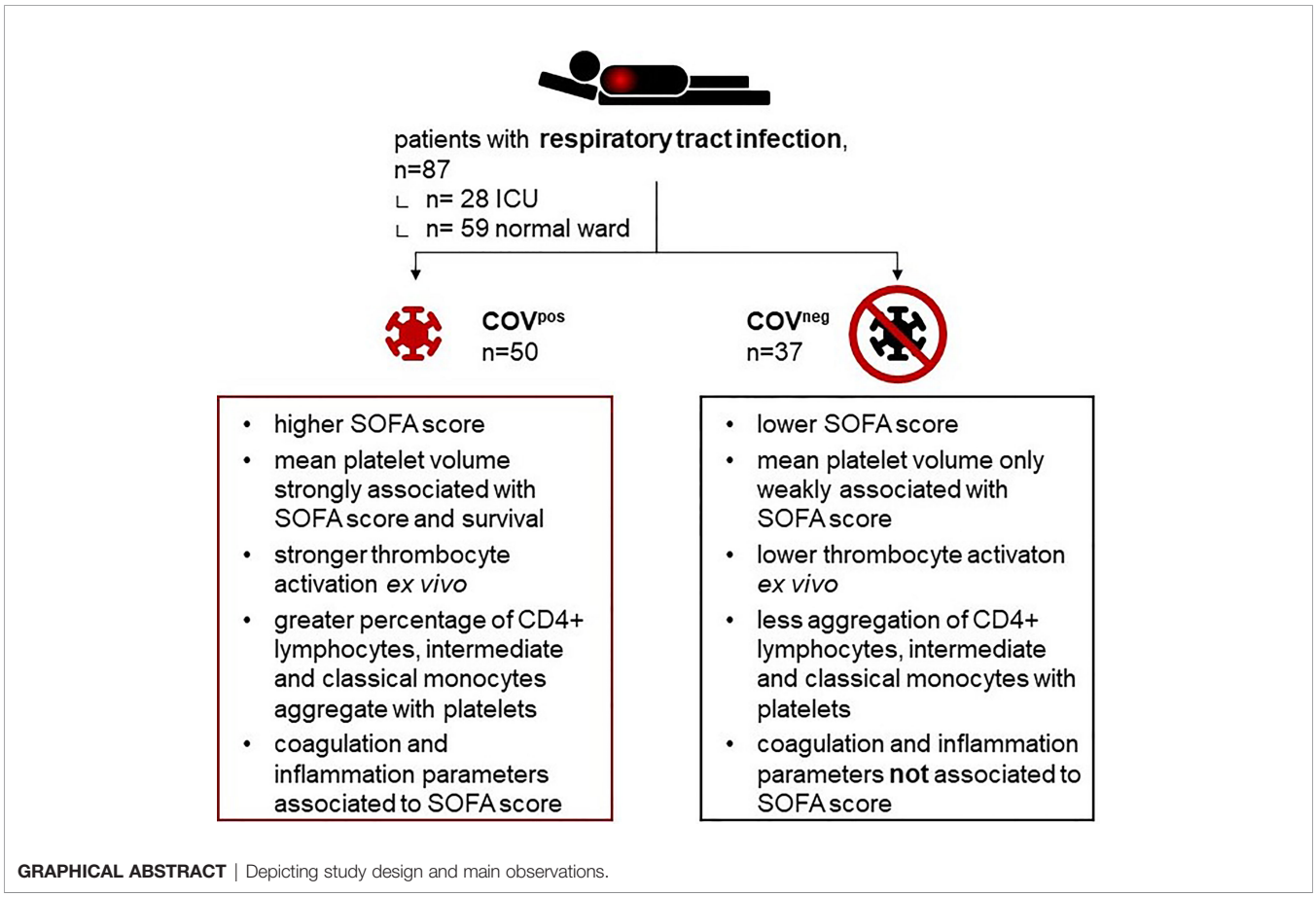

GRAPHICAL ABSTRACT | Depicting study design and main observations.

INTRODUCTION

The coronavirus disease 2019 (COVID-19) pandemic, caused by severe acute respiratory syndrome coronavirus 2 (SARS-CoV2), continues to affect humans all around the world (1). While vaccinations have greatly helped to lower the number of patients admitted to intensive care with severe COVID-19, newly emerging SARS-CoV-2 variants and refusal to receive vaccination in some countries still heavily fill ICU wards (2).

Acute dysregulations in hemostasis and inflammation are prominent features of patients with moderate-to-severe COVID-19 (3). Thrombi have been detected in the lung, heart, brain, and liver of COVID-19 patients, and the prevalence of deep vein thrombosis in hospitalized patients with an infection is significantly increased (4–6). Microthrombosis, also extensively documented by autopsy reports, reflects the increased platelet activation and subsequent fibrin clot formation in the pulmonary microvasculature in 80%–100% of lungs examined (7). The increased risk of thromboembolic events observed during moderate-to-severe COVID-19 is associated with the increased morbidity and mortality of these patients (8, 9).

Upon stimulation with thrombin, platelets from patients with COVID-19 released more interleukin (IL)-1β and soluble cluster of differentiation 40 ligand (sCD40L) than platelets of healthy controls (4). Moreover, lower amounts of thrombin were required for platelets from COVID-19 patients to achieve aggregation than for platelets from healthy controls, further suggesting that these platelets have an increased hyperactive

potential, contributing to the overall inflammation often observed during the infection with SARS-CoV2 (10). Platelet-specific granule content, including platelet factor 4 (PF4) and serotonin was significantly elevated in the plasma of patients with COVID-19 (11, 12).

Crosstalk between platelets and the immune system involves a variety of mechanisms (13, 14). Beyond paracrine mechanisms, platelets can also form aggregates with various leukocyte subtypes, such as neutrophils, monocytes, and T cells (11, 14, 15). Platelet-leukocyte aggregates have been suggested to drive vascular disease and may potentially represent a biomarker for thrombotic events (9, 16).

Increased levels of IL-6 and C-reactive protein (CRP) are associated with a worse outcome from COVID-19, suggesting that inflammation contributes as a critical mediator to the heightened mortality of those patients (17, 18).

The actual processes governing interactions between platelets, coagulation, and inflammation in COVID-19 are still not well known. In particular, knowledge about distinct immuno-thrombotic pathways in COVID-19 which may differ from other infectious respiratory diseases is limited. Importantly, subjects without acute respiratory symptoms, such as healthy persons or patients without any respiratory symptoms have been chosen as control groups in many clinical studies (15, 19–21). While these comparisons give valuable first insight, similar mechanisms might be active in COVID-19 and in other respiratory diseases (22). Thus, there is still a lack of knowledge about the typical features that characterize the patients with acute respiratory syndromes caused by COVID-19 as compared with those with non-COVID-19-associated acute respiratory infections.

MATERIAL AND METHODS

Study Design and Subjects

All patients that were included into this study were admitted to our clinic due to acute respiratory infectious disease. COV^{pos} had to be SARS-CoV2 positive confirmed by polymerase chain reaction (PCR) testing. COV^{neg} suffered from pneumonia or infect-triggered acute exacerbation of COPD and had to be SARS-CoV2 negative confirmed by PCR. Individuals had to be at least 18 years old and did not suffer from a known hematological or hemostatic disease, coagulopathy, or acute bleeding event. Patients form ICU or normal floor were eligible. Dual antiplatelet therapy was prohibited. Patients were recruited between May 2020 and May 2021. Routinely clinically assessed blood values were determined by the hospital laboratory (Labor Berlin, Berlin, Germany). Mean platelet volume is assessed by the routine diagnostics lab by impedance-based particle counting. Within the same measurement, counts and size of platelets, as well as erythrocytes and leukocytes, are assessed in diluted samples and without lysis. Leukocyte counts are assessed in a separate measurement after erythrocyte lysis. The study was approved by the local ethics committee (EA2/066/20, EA4/147/15). The study was conducted in compliance with the 1964 Declaration of Helsinki and its amendments and the Principles of Good Clinical Practice by the International Council for Harmonization 1996.

Blood Sampling

Blood was drawn from the cubital veins using ethylenediaminetetraacetic acid (EDTA) (3 ml, Vacurette®, Greiner Bio-One, Kremsmünster, Austria), citrate (3 ml, 3.2% sodium citrate, Vacurette®, Greiner Bio-One, Kremsmünster, Austria), and hirudin tubes (Sarstedt-Monovette®, Sarstedt, Nümbrecht, Germany). Whole blood was separated for the experiments requiring plasma by centrifugation (1,200×*g*, 10 min, room temperature) and stored at −80° for further analysis.

Multiple Electrode Aggregometry

In hirudinized whole blood which was previously diluted with 0.9% sodium chloride, platelet's reactivity to TRAP (32 µmol/l), ADP (6.4 µmol/l), and AA (0.5 mmol/l) was measured by multiple electrode aggregometry (MEA; Multiplate® Analyzer; Roche, Germany; regents also by Roche) not later than 3 h after sampling. According to the manufacturers' instructions, a measurement time of 6 min was set, and the area under the curve was calculated and translated to Multiplate®-specific units. The exact method was reported previously (23, 24).

Flow Cytometric Quantification of Leukocytes and Platelet-Leukocyte Aggregates

Flow cytometric characterization of leukocytes was performed as previously established (25). Within 1 h of collection, 100 µl of EDTA-anticoagulated whole blood was added to a master mix consisting of 100 µl fluorescence-activated cell scanning (FACS) staining buffer (BioLegend, San Diego, CA, USA) and 2 µl of each of the following antibodies: anti-human CD14-Pacific Blue™, CD16-Brilliant Violet 510™, CD4-Brilliant Violet 605™, CD45-Brilliant Violet 711™, CD3-Alexa Fluor 488™, CD26-PE, CD19-PE/Dazzle 594™, CD8-PE/Cyanine7, and CD41-Alexa Fluor 647™ (all BioLegend, San Diego, CA, USA). The mixture was incubated in the dark at room temperature for 30 min. Stained samples were fixed by adding 800 µl of 0.5% paraformaldehyde in phosphate-buffered saline (Sigma-Aldrich, St. Louis, MO, USA) and kept at +4°C in the dark. Samples were acquired on an Attune NxT Acoustic Focusing Cytometer (ThermoFisherScientific, Waltham, MA, USA) within 3 days. Stability of signal detection was verified and documented by daily measurements of Attune Performance tracking beads. Kaluza version 2.1 software (Beckman Coulter, Brea, CA, USA) was used for gating. Scatter parameters were interpreted as measures of morphological features, i.e., side scatter as a measure of granularity and forward scatter as a measure of cell size.

Cytokine Measurements

The cytokines IL-1RA, IL-2, IL-6, IL-7, IL-10, monocyte chemotactic protein 1 (MCP-1), chemokine (C-C motif) ligand (CCL) 3, chemokine (C-X-C Motif) ligand (CXCL) 8, CXCL10, interferon (IFN)-α2, IFN-γ, granulocyte colony-stimulating factor (GCSF), and tumor necrosis factor alpha

(TNF-α) were determined in platelet-depleted plasma samples using the "COVID-19 Cytokine Storm Panel 1" 13-plex bead array (BioLegend, San Diego, CA, USA) according to the manufacturer's instructions. Data were acquired on the flow cytometer mentioned above and analyzed using Kaluza version 2.1 software.

ELISA

Thrombin-antithrombin complex (TAT) ELISA (AssayPro, St. Charles, MO, USA) was performed according to manufacturer's instructions and measured using the plate reader Tecan Infinite 200Pro (Tecan Group, Maennedorf, Switzerland).

Statistics

All reported probability values are two sided, and a value of $p < 0.05$ was considered statistically significant. Median values and quartiles are reported, and nonparametric tests were used if not stated otherwise. If not stated differently, Mann–Whitney *U* test or Chi-squared test were used to evaluate differences between two groups. Correlations were calculated with Spearman's test. For network building $p < 0.01$ and $r > 0.3$ or $r < -0.3$ were used as cutoffs for showing connections. Statistics were calculated using SPSS Statistics, version 27 for Windows and macOS (IBM, Armonk, NY, USA) and R version 4.1.0 (2021-05-18). Graphs and networks were plotted using R within R Studio version 1.3.1093 (RStudio PBC, Boston, MA, USA).

RESULTS

Patients' Characteristics

More patients in the COV^{neg} group had chronic obstructive lung disease (**Table 1**). More patients had received prophylactic and less received intermediate-dose anticoagulation in the COV^{neg} than COV^{pos} cohort (**Table 2**). There was no difference in the frequency of patients receiving therapeutic dose anticoagulation (**Table 2**). Administration of oral glucocorticoids and inhalative bronchodilators was more common in COV^{pos} (**Table 2**). In COV^{pos}, 10 out of 50 individuals died compared with none in COV^{neg} patients. The sequential organ failure assessment (SOFA) score was calculated for all patients with sufficient data (COV^{pos} $n = 33$, COV^{neg} $n = 21$). Laboratory parameters did not differ significantly between COV^{neg} and COV^{pos} patients (**Table 3**). Four COV^{pos} patients and two COV^{neg} patients had thrombocytopenia as defined by <150 thrombocytes/nL. No patient participating on our study had received vaccination against SARS-CoV2 prior to study participation.

Higher Platelet Reactivity in Patients With COVID-19 Is Associated With Disease Severity and Death

Platelets from COV^{pos} patients exhibited higher TRAP-induced aggregability than platelets from COV^{neg} patients (**Figure 1A**). As TRAP is a strong coagulation stimulus, this observation points to the hyperaggregability of platelets under stimulation with a thrombin-substitute in COVID-19. ADP-induced platelet aggregability was also increased COV^{pos} as compared with COV^{neg} patients (**Figure 1B**), although ADP is a much weaker platelet agonist than TRAP. Additionally, also AA-induced platelet aggregation was higher in COV^{pos} than COV^{neg} patients (**Figure 1C**). No significant differences between COV^{pos} and COV^{neg} patients were observed for platelet counts or MPV (**Supplemental Figure 1**).

Since TAT is a surrogate parameter for thrombin generation and thrombin is the strongest known platelet activator (26), TAT was quantified in both patient groups. Higher TAT levels were measured in COV^{pos} than COV^{neg} patients, reflecting the linkage between higher platelet reactivity and activated coagulation system (**Figure 2**).

In our study, SOFA score values differed significantly between COV^{pos} and COV^{neg} (**Figure 3A**) and between COV^{surv} and $COV^{non\text{-}surv}$ patients (**Figure 3B**). MPV was higher in $COV^{non\text{-}surv}$ compared with COV^{surv} patients (**Figure 3C**). MPV- (**Figure 3D**) and TRAP-6-induced platelet aggregation (**Figure 3E**) correlated positively with the SOFA score values only in COV^{pos} but not in COV^{neg} patients. These findings point

TABLE 1 | Patient characteristics—demographics and preexisting conditions.

	COV^{neg} ($n = 37$)	COV^{pos} ($n = 50$)	Mann–Whitney *U* or Chi-squared test
Demographics			
Age (years)	73 (58; 81)	69 (54.8; 76.5)	0.078
Men (% per group)	57%	70%	0.259
BMI (kg/m^2)	25.1 (23.2; 29.3)	28.7 (24.7; 76.5)	0.1030
Patients on ICU (% per group)	22%	40%	0.104
Respiratory rate (breaths per minute)	18 (16.25; 19)	18.7 (18; 21.3)	0.078
Heart rate (beats per minute)	77 (70; 88.5)	81.5 (72.8; 94.8)	0.259
Systolic blood pressure (mmHg)	131 (116; 149.5)	123.5 (110; 140)	0.103
Diastolic blood pressure (mmHg)	75 (66; 85.5)	70 (60; 80)	0.141
Preexisting conditions			
Coronary artery disease (% per group)	32.4%	14%	0.065
Arterial hypertension (% per group)	67.6%	62%	0.655
Diabetes (% per group)	48.6%	58%	0.632
Dyslipidemia (% per group)	29.7%	28%	1
COPD (% per group)	35.1%	6%	0.001

Data about demographics and preexisting conditions of COV^{pos} and COV^{neg} absolute numbers or median values with quartiles are shown.

TABLE 2 | Patient characteristics—concomitant medication.

	COV^{neg} (n = 37)	COV^{pos} (n = 50)	Mann–Whitney U or Chi-squared test
Acetylsalicylic acid (% per group)	32.4%	36%	0.821
Clopidogrel (% per group)	0%	4%	0.505
Prophylactic anticoagulation (% per group)	56.8%	24%	0.003
Intermediate dose anticoagulation (% per group)	8.1%	32%	0.009
Therapeutic dose anticoagulation (% per group)	35.1%	44%	0.51
Statins (% per group)	24.3%	24%	1
ACE blocker (% per group)	35.1%	24%	0.339
Angiotensin II receptor blocker (% per group)	16.2%	22%	0.591
Beta blocker (% per group)	46%	28%	0.113
Aldosterone antagonist (% per group)	13.5%	6%	0.277
Diuretics (% per group)	50%	38%	0.383
Oral glucocorticoids (% per group)	19%	56%	0.001
Remdesivir (% per group)	0%	2%	1
Tocilizumab (% per group)	0%	2%	1
Inhalative bronchodilators (% per group)	59.5%	84%	0.014

Data about concomitant medication of COV^{pos} and COV^{neg} in absolute numbers are shown.

TABLE 3 | Patient characteristics—laboratory values.

	COV^{neg} (n = 37)	COV^{pos} (n = 50)	Mann–Whitney U or Chi-squared test
Creatinine (mg/dl)	0.94 (0.79; 1.3)	0.90 (0.66; 1.16)	0.354
Urea (mg/dl)	34 (24.5; 52.5)	48 (27.3; 64.5)	0.164
NT-proBNP (ng/l)	468 (251; 2318)	498 (125; 1834)	0.499
CRP (mg/dl)	62.1 (37.7; 103.5)	69.8 (18.9; 126.9)	0.880
Hemoglobin (g/dl)	11.7 (10.1; 13.4)	10.9 (9.3; 21.4)	0.140
Leukocytes (n/nl)	9.3 (6.7; 11.8)	8.5 (6.8; 12.6)	0.837
Lymphocytes (n/nl)	1.22 (0.87; 1.96)	1.06 (0.74; 1.50)	0.214
Lymphocytes (% of leukocytes)	12 (9.7; 23.2)	13.2 (8; 18.1)	0.508
Thrombocytes (n/pl)	279 (209; 321)	300.5 (247; 397)	0.057
Mean platelet volume (fl)	10.3 (9.7; 10.9)	10.4 (9.8; 11.6)	0.269
INR	1.07 (1.00; 1.25)	1.12 (1.05; 1.21)	0.307
aPPT (s)	36.4 (31.4; 43.3)	38.8 (32.8; 47.5)	0.435

Data about laboratory values of COV^{pos} and COV^{neg} in median values with quartiles are shown.

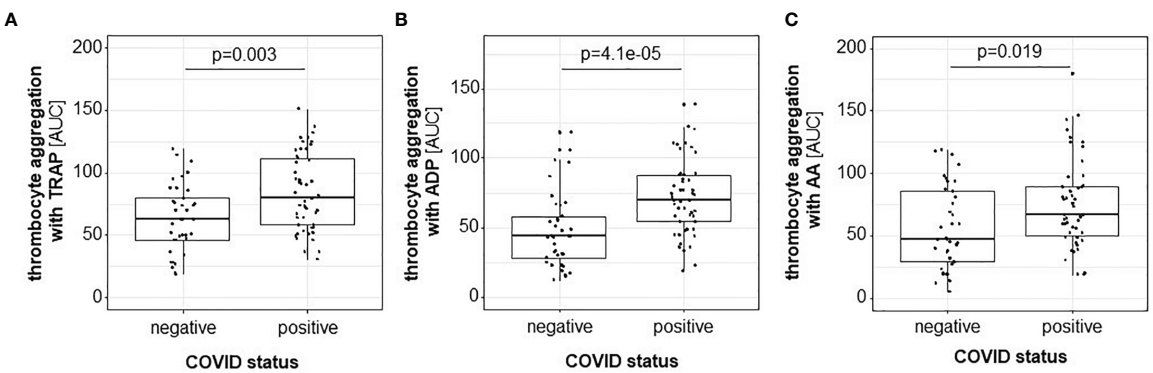

FIGURE 1 | Platelet aggregation induced by TRAP **(A)**, ADP **(B)**, and AA **(C)**, as assessed by MEA, is higher in COV^{pos} (n = 50) than in COV^{neg} (n = 37) patients.

to an important role of platelet function for the clinical prognosis of patients suffering from COVID-19. Instead, levels of individual leukocyte subtype aggregates with platelets did not correlate with SOFA score in COV^{pos} or in COV^{neg} patients.

Inflammation Characteristics Related to COVID-19 and Clinical Outcome

We observed more than 2-fold higher plasma levels of IL-6, IL-7, IL-10, IL-1RA, MCP1, and CXCL10 in COV^{pos} as compared with

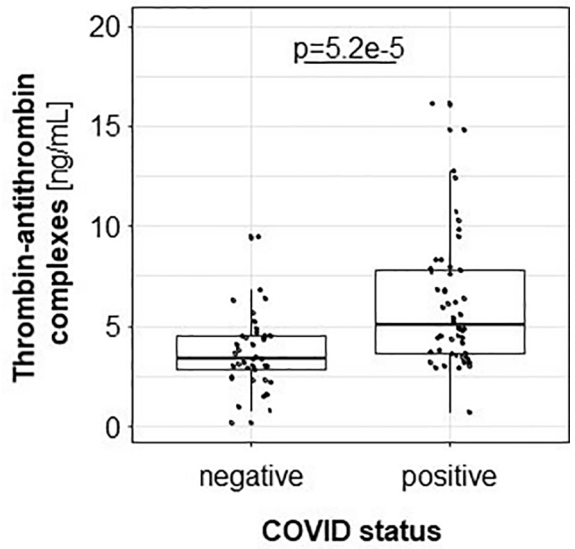

FIGURE 2 | Thrombin-antithrombin complex is higher in COV^{pos} (n = 50) than in COV^{neg} (n = 37).

COV^{neg} patients, pointing to the severe cytokine burst (**Figure 4A**). The cytokines IL-2, CXCL8, IFN-α2, IFN-γ, GCSF, and TNF-α were less than 2-fold higher in COV^{pos} in comparison with COV^{neg} patients (**Figure 4A**). Moreover, a higher percentage of $CD4^{pos}$ T_H lymphocytes, $CD14^{hi}CD16^{neg}$ classical monocytes, and $CD14^{hi}CD16^{pos}$ intermediate monocytes formed aggregates with platelets in COV^{pos} as compared with COV^{neg} patients (**Figure 4A** and **Supplemental Figure 2**). The granularity of $CD14^{lo}CD16^{pos}$ nonclassical monocytes was higher and the granularity of $CD19^{pos}$ B lymphocytes was lower in COV^{pos} in comparison with COV^{neg} (**Figure 4A** and **Supplemental Figure 2**), potentially indicating a differential activation state of these cell types.

Within the COV^{pos} group, we also compared our panel of inflammatory parameters between COV^{surv} and $COV^{non\text{-}surv}$ patients (**Figure 4B**). Values of IL-6, IL-1RA, CXCL8, MCP1, and CXCL10 were over 2-fold higher in $COV^{non\text{-}surv}$ than in COV^{surv}. Moreover, lower relative lymphocyte abundance and higher absolute leukocyte count, IL-2, and CCL3 levels were observed in the $COV^{non\text{-}surv}$ versus COV^{surv} patients. In $COV^{non\text{-}surv}$ patients, the granularity of $CD8^{pos}$ cytotoxic T cells as well as the percentage of T_H cells forming aggregates with platelets were lower than in COV^{surv} patients.

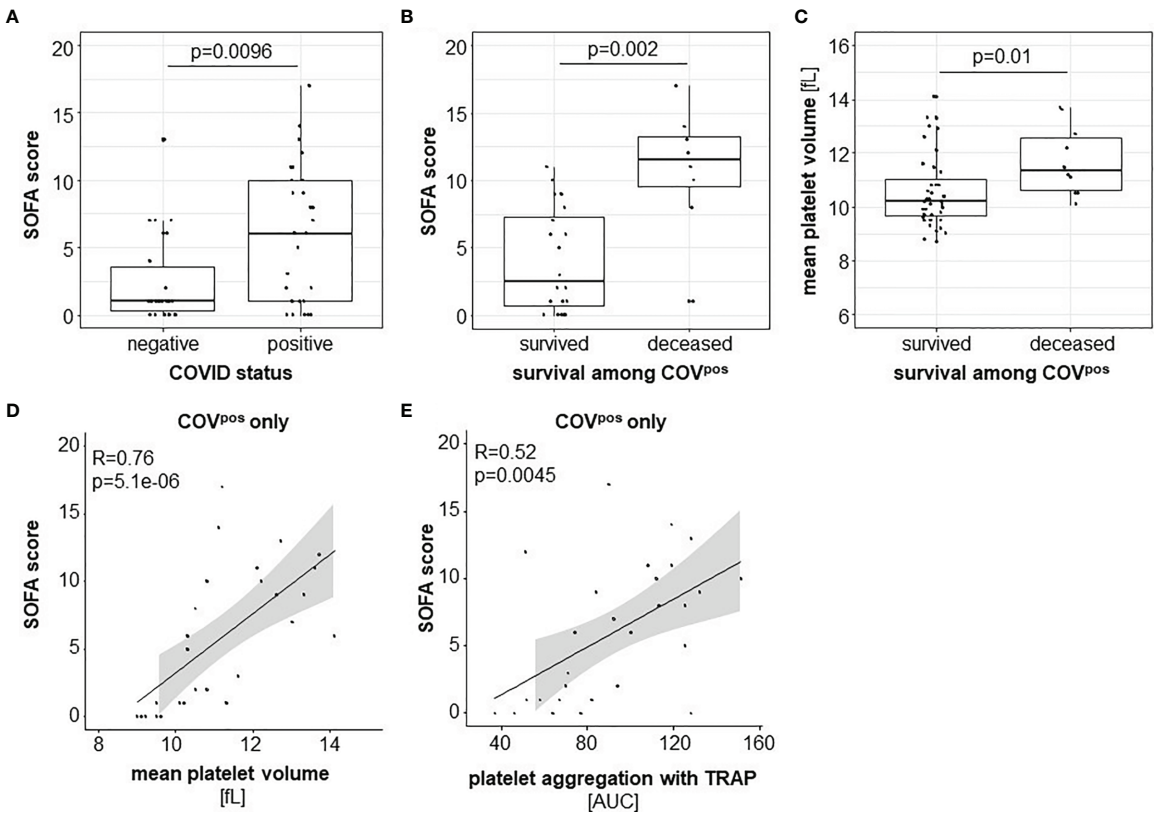

FIGURE 3 | Disease severity indicated by the SOFA score was higher in COV^{pos} (n = 50) than in COV^{neg} (n = 37) patients **(A)** and higher among $COV^{non\text{-}surv}$ (n = 10) than COV^{surv} (n = 40) COV^{pos} patients **(B)**. MPV was higher in $COV^{non\text{-}surv}$ than in COV^{surv} COV^{pos} patients **(C)**. Within COV^{pos}, SOFA score correlated with MPV **(D)** and TRAP-initiated platelet activation **(E)**.

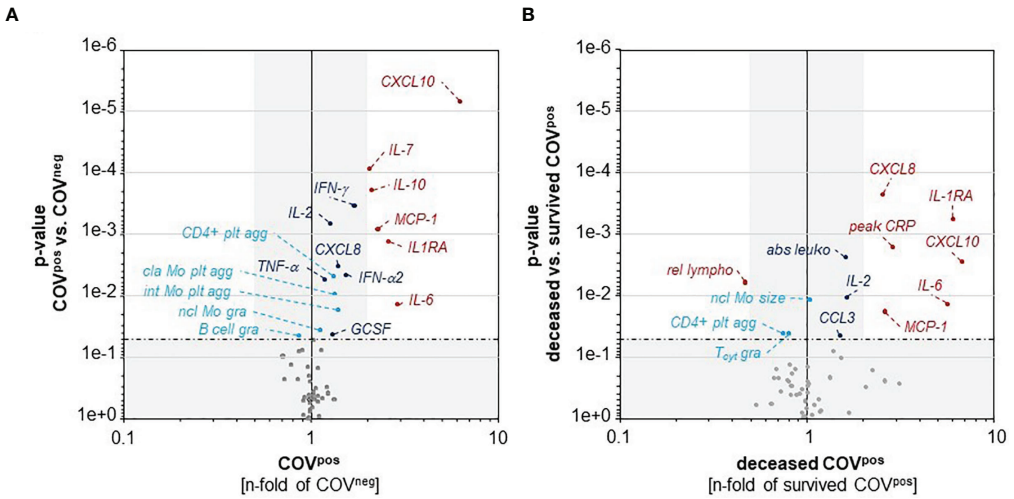

FIGURE 4 | CXCL10, IL-6, MCP-1, and IL-1RA are higher in COV^{pos} than in COV^{neg} patients **(A)** and also higher in deceased than in surviving COV^{pos} patients **(B)**. A higher percentage of classical and intermediate monocytes and $CD4^{pos}$ T_H lymphocytes form aggregates with platelets in COV^{pos} than in COV^{neg} patients **(A)**. Deceased COV^{pos} patients showed lower relative abundance of lymphocytes and higher total leukocyte counts than surviving COV^{pos} patients **(B)**. *p*-value of 0.05 is indicated by the horizontal dashed-dotted line. *p*-values higher than 0.05 and less-than-twofold changes between groups are underlaid in grey. plt agg, platelet aggregates; gra, granularity; cla Mo, classical monocytes; int Mo, intermediate monocytes; ncl Mo, nonlassical monocytes.

SOFA Score Correlated With Typical Markers of Platelet Reactivity and Inflammation in COVID-19 Only

Correlations between the SOFA score, parameters of platelet function, and inflammation are visualized by networks for patients with COVID-19 (**Figure 5A**), with other respiratory disease (**Figure 5B**), and for parameters correlated in both cohorts to elucidate common effects (**Supplemental Figure 3**).

In COV^{pos} patients, the SOFA score correlated with CRP at the time of blood sampling, peak CRP level during hospital stay, leukocyte count, and MPV- and TRAP-induced platelet aggregation. Peak CRP level during hospital stay was strongly correlated with platelet aggregation after stimulation with TRAP-6 and AA (**Figure 5A**). Moreover, IL-6 was correlated with MPV, platelet aggregation after stimulation with TRAP-6 and AA in COV^{pos} but not in COV^{neg} patients (**Figures 5A, B**). In contrast to COV^{pos}, only peak CRP but no platelet function marker correlated with the SOFA score in COV^{neg} patients (**Figure 5B**). Correlation between SOFA and peak CRP was much stronger in COV^{pos} than in the COV^{neg} group (**Supplemental Figure 3**). These findings support a link between characteristic markers of inflammation and platelet reactivity and SOFA score for patients with COVID-19 but not for those with other acute respiratory diseases. This panel of characteristic markers is associated with the clinical outcome in COVID-19.

In both patient groups with respiratory symptoms, platelet aggregation upon stimulation with ADP or with AA correlates with the absolute number of platelet aggregates formed with B lymphocytes and with NK cells, respectively (**Supplemental Figure 3**).

DISCUSSION

The central findings of our study are as follows:

- The platelet reactivity is higher in COV^{pos} than in COV^{neg} patients with an acute respiratory disease and is associated with higher mortality in COV^{pos} patients.
- A higher percentage of T_H lymphocytes and classical and intermediate monocytes form aggregates with platelets in COV^{pos} than in COV^{neg} patients.
- The SOFA score as a measure for the clinical outcome strongly correlates with markers of platelet hyperreactivity, CRP, and leukocyte count in COV^{pos} but not in COV^{neg} patients.

These findings suggest a relation between increased markers of platelet reactivity, inflammation, and the clinical outcome for patients with COVID-19 but not for those with other acute respiratory diseases.

Higher Platelet Reactivity Relates to Survival in Patients With COVID-19

We demonstrated higher platelet reactivity measured by MEA in COVID-19 compared with patients with other acute respiratory disease. Less ADP- and TRAP-induced aggregation (20) and no significant differences for TRAP- and AA-induced aggregation compared with healthy volunteers or reference ranges (19) have previously been reported in patients hospitalized or receiving ICU-level care. Another study demonstrated a predictive value of ADP- and TRAP-induced platelet activation for the duration of the hospital stay (20). However, in these studies, COVID-19 patients were compared only with healthy controls but not with

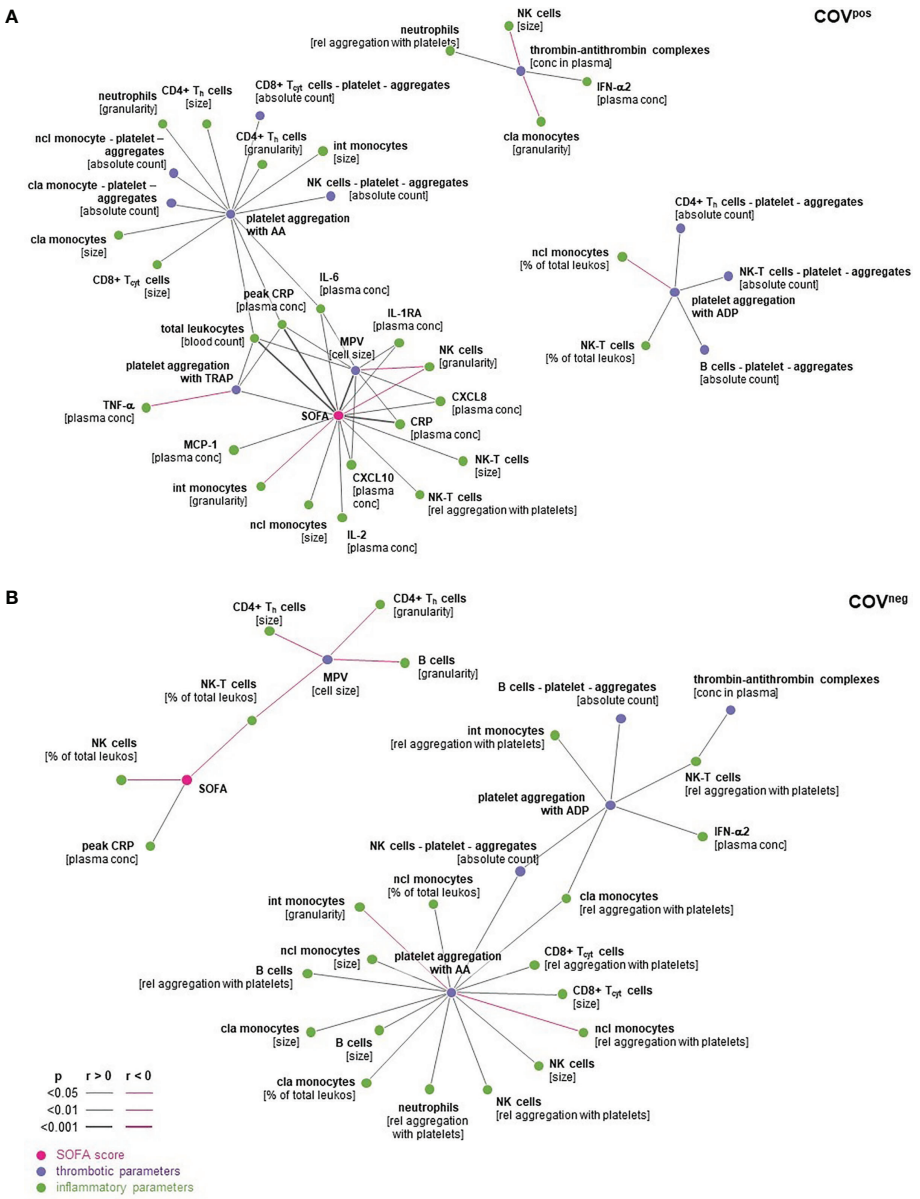

FIGURE 5 | Spearman's correlations in COV^{pos} **(A)** and COV^{neg} **(B)** were expressed as dark grey lines if positively correlated and pink lines if correlated inversely. Correlations with $p < 0.05$ are depicted. cla Mo, classical monocytes; int Mo, intermediate monocytes; ncl Mo, nonclassical monocytes; T_h, CD4^{pos} helper T cells; T_{cyt}, CD8^{pos} cytoxic T cells; NK-T, natural killer T cells; NK cells, natural killer cells; peak CRP, highest CPR level during hospital stay.

diseased individuals. In our study, platelets of patients with COVID-19 reacted stronger to TRAP, ADP, and AA compared with those patients suffering from other pulmonary infections. In linkage between coagulation system and platelet hyperreactivity, we found TAT to be higher in COV^{pos} than in COV^{neg} patients. Elevated thrombin level may explain the increased platelet reactivity as well as the higher numbers of platelet-leukocyte complexes despite antiplatelet therapy in patients with COVID-19.

Comparing COV^{surv} and COV$^{non\text{-}surv}$ groups, we observed a higher MPV in COV$^{non\text{-}surv}$, pointing to a hyperreactivity of platelets *in vivo* (27). A retrospective analysis including patients hospitalized for COVID-19 also suggested that MPV relates to the clinical outcome (28). The SOFA score values predict disease severity and mortality in patients with COVID-19 (29, 30). Our data additionally link TRAP-induced platelet aggregation and MPV as markers of platelet reactivity with SOFA score. This once again stresses the important relation between hyperreactive platelets and disease severity.

In patients with COVID-19, thrombocytopenia has been shown to be associated with a worse clinical outcome (31). In our patients, we found four COV^{pos} and two COV^{neg} individuals

presenting thrombocytopenia at the time point of platelet function measurement, reflecting the disease severity of our patient cohort.

Cytokine Signature in COV^{pos} Compared with COV^{neg}

Cytokines typically associated with COVID-19-induced "cytokine storm" were mostly higher in COV^{pos} compared with COV^{neg}, verifying earlier reports and also in comparison with patients with non-COVID-19 respiratory diseases (32–34). Regarding disease severity, we observed higher levels of IL-6, IL-1RA, MCP1, CXCL8, and CXCL10 comparing COVID survivors and nonsurvivors. MCP1 and CXCL10 as chemotactic agents for monocytes and CXCL8 and CXCL10 as monocyte-derived cytokines point to the central role of monocytes in this setting (35). IL-6 as cytokine amplifier is known to play a prognostic role in COVID-19 (35). IL-1RA antagonizes IL-1 and can also be derived from monocytes (36). Plasma values of IL-1RA correlate with a worse clinical prognosis in COVID-19 (36). Within our COVID cohort, nonsurvivors were characterized by higher cytokine levels, especially IL-1RA, IL-6, MCP-1, CXCL8, and CXCL10 than patients who survived COVID-19.

Differential Leukocyte-Platelet Aggregate Formation in COV^{pos} Compared With COV^{neg}

In COVID-19, monocytes have been shown to release procoagulant proteins in a platelet-dependent manner (22). In line with other studies, we here demonstrate differences in monocyte-platelet conjugates in comparison with patients with acute respiratory diseases other than COVID-19. We found a higher proportion of classical and intermediate monocyte-platelet aggregates in COV^{pos} compared with COV^{neg}. These findings are in line with data of other studies, which also demonstrated more platelet aggregates with monocytes in patients with COVID-19 compared with healthy individuals (15, 37) or not further specified patients as controls (22). This points to the importance of the innate immune system interacting with platelets in COVID-19.

In this study, more T_H lymphocytes formed aggregates with platelets in COV^{pos} than in COV^{neg} patients. These conjugates seem to have proinflammatory effects in autoimmune neuroinflammation (38). Further research is needed to elucidate the interplay between T_H cells and platelets, explaining its relevance for COVID-19.

Granularity of B cells was lower in COV^{pos} than COV^{neg}, potentially indicating release of synthesized proteins—presumably immunoglobulins—from B cells surpasses synthesis within the cell. Similarly, granularity of $CD8^{pos}$ T_{cyt} lymphocytes was lower in $COV^{non\text{-}surv}$ than COV^{surv}, also potentially reflecting a predominant degranulation in these patients, who died from COVID-19 (39). The lower relative lymphocyte abundance and higher leukocyte count in those patients who died confirm previous findings (40).

The SOFA Score Correlates With Platelet Hyperreactivity and Inflammatory Markers in COV^{pos} But Not in COV^{neg} Patients—Clinical Implications

A positive correlation was observed between the SOFA score as marker for disease severity and CRP, leukocytes, and markers of platelet hyperreactivity in patients with COVID-19 only but not in those with acute respiratory disease of other reason. The peak CRP level correlated with AA- and TRAP-induced platelet aggregation and IL-6 with MPV, reflecting an interplay between platelet hyperreactivity and inflammation. Importantly, none of these relations could be demonstrated in COV^{neg} patients.

Since platelet hyperreactivity contributes to worse clinical outcome in COVID-19, it is tempting to speculate that antiplatelet-directed therapies would improve the clinical prognosis. In a pandemic retrospective analysis, aspirin administration in patients with COVID-19 reduced the risk for mechanical ventilation, ICU admission, and in-hospital mortality (41). Within the RECOVERY trial, the aspirin group did show a significant reduction in hospital stay duration, thromboembolic events, and percentage of patients who had been discharged alive compared with best medical care in COVID-19 (42). These clinical data are in line with our experimental findings and highlight the clinical impact of platelet hyperreactivity on the clinical outcome, pointing to the importance of antithrombotic therapy in COVID-19.

CONCLUSION

In moderate-to-severe COVID-19, but not in other respiratory diseases, we found features of platelet hyperreactivity to be relevant for the disease severity of the patients. Our data suggest that platelet hyperreactivity together with a heightened inflammation contributes to a worse clinical outcome in patients with COVID-19, thereby pointing to the importance of antithrombotic therapy for reducing disease severity. Further clinical investigations are warranted to make use of the above-described targets.

DATA AVAILABILITY STATEMENT

The raw data supporting the conclusions of this article will be made available by the authors, without undue reservation.

ETHICS STATEMENT

The studies involving human participants were reviewed and approved by Ethikkommission der Charité - Universitätsmedizin Berlin. The patients/participants provided their written informed consent to participate in this study.

AUTHOR CONTRIBUTIONS

Conception and design: KJ, UR-K, AH, and NK. Development of methodology: KJ, UR-K, and NK. Sample collection: A-CW, LR, AR, and AH. Acquisition of data: KJ, LR, MP, AR, and AA. Analysis and interpretation of data: KJ, UR-K, and NK. Writing: KJ. Review of the manuscript: UR-K, NK, MP, JF, A-CW, AR, AH, and UL. All authors contributed to the article and approved the submitted version.

FUNDING

AH is participant in the BIH-Charité Advanced Clinician Scientist Pilotprogram, and JF is participant in the BIH-Charité Clinician Scientist both funded by the Charité - Universitätsmedizin Berlin and the Berlin Institute of Health. The study was supported by a research grant within the BIH & MDC Focus Area Translational Vascular Biomedicine.

ACKNOWLEDGMENTS

Additionally, we would like to thank Kerstin Kamprath and Sabine Knüppel for excellent technical support.

SUPPLEMENTARY MATERIAL

The Supplementary Material for this article can be found online at: https://www.frontiersin.org/articles/10.3389/fimmu.2022.844701/full#supplementary-material

REFERENCES

1. World Health Organization. *Weekly Epidemiological Update on COVID-19 - 21 December 2021* (2021). Available at: https://www.who.int/publications/m/item/weekly-epidemiological-update-on-covid-19—21-december-2021.
2. European Centre for Disease Prevention and Control. *Data on Hospital and ICU Admission Rates and Current Occupancy for COVID-19* (2021). Available at: https://www.ecdc.europa.eu/en/publications-data/download-data-hospital-and-icu-admission-rates-and-current-occupancy-covid-19.
3. Bonaventura A, Vecchie A, Dagna L, Martinod K, Dixon DL, Van Tassell BW, et al. Endothelial Dysfunction and Immunothrombosis as Key Pathogenic Mechanisms in COVID-19. *Nat Rev Immunol* (2021) 21(5):319–29. doi: 10.1038/s41577-021-00536-9
4. Zhang L, Feng X, Zhang D, Jiang C, Mei H, Wang J, et al. Deep Vein Thrombosis in Hospitalized Patients With COVID-19 in Wuhan, China: Prevalence, Risk Factors, and Outcome. *Circulation* (2020) 142(2):114–28. doi: 10.1161/CIRCULATIONAHA.120.046702
5. McConnell MJ, Kondo R, Kawaguchi N, Iwakiri Y. Covid-19 and Liver Injury: Role of Inflammatory Endotheliopathy, Platelet Dysfunction, and Thrombosis. *Hepatol Commun* (2021) 6(2):255–69. doi: 10.1002/hep4.1843
6. Qureshi AI, Baskett WI, Huang W, Shyu D, Myers D, Raju M, et al. Acute Ischemic Stroke and COVID-19: An Analysis of 27 676 Patients. *Stroke* (2021) 52(3):905–12. doi: 10.1161/STROKEAHA.120.031786
7. McFadyen JD, Stevens H, Peter K. The Emerging Threat of (Micro) Thrombosis in COVID-19 and Its Therapeutic Implications. *Circ Res* (2020) 127(4):571–87. doi: 10.1161/CIRCRESAHA.120.317447
8. Guo T, Fan Y, Chen M, Wu X, Zhang L, He T, et al. Cardiovascular Implications of Fatal Outcomes of Patients With Coronavirus Disease 2019 (COVID-19). *JAMA Cardiol* (2020) 5(7):811–8. doi: 10.1001/jamacardio.2020.1017
9. Canzano P, Brambilla M, Porro B, Cosentino N, Tortorici E, Vicini S, et al. Platelet and Endothelial Activation as Potential Mechanisms Behind the Thrombotic Complications of COVID-19 Patients. *JACC Basic Transl Sci* (2021) 6(3):202–18. doi: 10.1016/j.jacbts.2020.12.009
10. Zaid Y, Puhm F, Allaeys I, Naya A, Oudghiri M, Khalki L, et al. Platelets Can Associate With SARS-Cov-2 RNA and Are Hyperactivated in COVID-19. *Circ Res* (2020) 127(11):1404–18. doi: 10.1161/CIRCRESAHA.120.317703
11. Koupenova M, Clancy L, Corkrey HA, Freedman JE. Circulating Platelets as Mediators of Immunity, Inflammation, and Thrombosis. *Circ Res* (2018) 122(2):337–51. doi: 10.1161/CIRCRESAHA.117.310795
12. Cloutier N, Pare A, Farndale RW, Schumacher HR, Nigrovic PA, Lacroix S, et al. Platelets can Enhance Vascular Permeability. *Blood* (2012) 120(6):1334–43. doi: 10.1182/blood-2012-02-413047
13. Hottz ED, Quirino-Teixeira AC, Merij LB, Pinheiro MBM, Rozini SV, Bozza FA, et al. Platelet-Leukocyte Interactions in the Pathogenesis of Viral Infections. *Platelets* (2021) 33(2):1–8. doi: 10.1080/09537104.2021.1952179
14. Tschoepe D, Rauch U, Schwippert B. Platelet-Leukocyte-Cross-Talk in Diabetes Mellitus. *Horm Metab Res* (1997) 29(12):631–5. doi: 10.1055/s-2007-979115
15. Manne BK, Denorme F, Middleton EA, Portier I, Rowley JW, Stubben C, et al. Platelet Gene Expression and Function in Patients With COVID-19. *Blood* (2020) 136(11):1317–29. doi: 10.1182/blood.2020007214
16. Sefer D, Miljic P, Kraguljac-Kurtovic N, Bizic-Radulovic S, Bogdanovic A, Knezevic V, et al. Correlation Between Leukocyte-Platelet Aggregates and Thrombosis in Myeloproliferative Neoplasms. *Int J Lab Hematol* (2021). doi: 10.1111/ijlh.13754
17. Santa Cruz A, Mendes-Frias A, Oliveira AI, Dias L, Matos AR, Carvalho A, et al. Interleukin-6 Is a Biomarker for the Development of Fatal Severe Acute Respiratory Syndrome Coronavirus 2 Pneumonia. *Front Immunol* (2021) 12:613422. doi: 10.3389/fimmu.2021.613422
18. Luan YY, Yin CH, Yao YM. Update Advances on C-Reactive Protein in COVID-19 and Other Viral Infections. *Front Immunol* (2021) 12:720363. doi: 10.3389/fimmu.2021.720363
19. Heinz C, Miesbach W, Herrmann E, Sonntagbauer M, Raimann FJ, Zacharowski K, et al. Greater Fibrinolysis Resistance But No Greater Platelet Aggregation in Critically Ill COVID-19 Patients. *Anesthesiology* (2021) 134(3):457–67. doi: 10.1097/ALN.0000000000003685
20. Bertolin AJ, Dalcoquio TF, Salsoso R, de MFRH, Kalil-Filho R, Hajjar LA, et al. Platelet Reactivity and Coagulation Markers in Patients With COVID-19. *Adv Ther* (2021) 38(7):3911–23. doi: 10.1007/s12325-021-01803-w
21. Herrmann J, Notz Q, Schlesinger T, Stumpner J, Kredel M, Sitter M, et al. Point of Care Diagnostic of Hypercoagulability and Platelet Function in COVID-19 Induced Acute Respiratory Distress Syndrome: A Retrospective Observational Study. *Thromb J* (2021) 19(1):39. doi: 10.1186/s12959-021-00293-8
22. Hottz ED, Azevedo-Quintanilha IG, Palhinha L, Teixeira L, Barreto EA, Pao CRR, et al. Platelet Activation and Platelet-Monocyte Aggregate Formation Trigger Tissue Factor Expression in Patients With Severe COVID-19. *Blood* (2020) 136(11):1330–41. doi: 10.1182/blood.2020007252
23. Schuette C, Steffens D, Witkowski M, Stellbaum C, Bobbert P, Schultheiss HP, et al. The Effect of Clopidogrel on Platelet Activity in Patients With and Without Type-2 Diabetes Mellitus: A Comparative Study. *Cardiovasc Diabetol* (2015) 14:15. doi: 10.1186/s12933-015-0182-7
24. Stellbaum C, Ayral Y, Morguet A, Schultheiss HP, Rauch U. Doubling the Clopidogrel Dose in Patients With Reduced Responsiveness to the Standard Dose Is Associated With a Limited Effectiveness as Evaluated by Impedance Aggregometry. *Cardiovasc Revasc Med* (2012) 13(3):159–66. doi: 10.1016/j.carrev.2012.02.009
25. Leistner DM, Krankel N, Meteva D, Abdelwahed YS, Seppelt C, Stahli BE, et al. Differential Immunological Signature at the Culprit Site Distinguishes Acute Coronary Syndrome With Intact From Acute Coronary Syndrome With Ruptured Fibrous Cap: Results From the Prospective Translational OPTICO-ACS Study. *Eur Heart J* (2020) 41(37):3549–60. doi: 10.1093/eurheartj/ehaa703

26. Diquelou A, Lemozy S, Dupouy D, Boneu B, Sakariassen K, Cadroy Y. Effect of Blood Flow on Thrombin Generation Is Dependent on the Nature of the Thrombogenic Surface. *Blood* (1994) 84(7):2206–13. doi: 10.1182/blood.V84.7.2206.2206
27. Gasparyan AY, Ayvazyan L, Mikhailidis DP, Kitas GD. Mean Platelet Volume: A Link Between Thrombosis and Inflammation? *Curr Pharm Des* (2011) 17 (1):47–58. doi: 10.2174/138161211795049804
28. Barrett TJ, Bilaloglu S, Cornwell M, Burgess HM, Virginio VW, Drenkova K, et al. Platelets Contribute to Disease Severity in COVID-19. *J Thromb Haemost* (2021) 19(12):3139–53. doi: 10.1111/jth.15534
29. Yang Z, Hu Q, Huang F, Xiong S, Sun Y. The Prognostic Value of the SOFA Score in Patients With COVID-19: A Retrospective, Observational Study. *Med (Baltimore)* (2021) 100(32):e26900. doi: 10.1097/MD.0000000000026900
30. Zhou F, Yu T, Du R, Fan G, Liu Y, Liu Z, et al. Clinical Course and Risk Factors for Mortality of Adult Inpatients With COVID-19 in Wuhan, China: A Retrospective Cohort Study. *Lancet* (2020) 395(10229):1054–62. doi: 10.1016/S0140-6736(20)30566-3
31. Zong X, Gu Y, Yu H, Li Z, Wang Y. Thrombocytopenia Is Associated With COVID-19 Severity and Outcome: An Updated Meta-Analysis of 5637 Patients With Multiple Outcomes. *Lab Med* (2021) 52(1):10–5. doi: 10.1093/labmed/lmaa067
32. Laing AG, Lorenc A, Del Molino Del Barrio I, Das A, Fish M, Monin L, et al. A Dynamic COVID-19 Immune Signature Includes Associations With Poor Prognosis. *Nat Med* (2020) 26(10):1623–35. doi: 10.1038/s41591-020-1038-6
33. de la Rica R, Borges M, Gonzalez-Freire M. COVID-19: In the Eye of the Cytokine Storm. *Front Immunol* (2020) 11:558898. doi: 10.3389/fimmu.2020.558898
34. Huang C, Wang Y, Li X, Ren L, Zhao J, Hu Y, et al. Clinical Features of Patients Infected With 2019 Novel Coronavirus in Wuhan, China. *Lancet* (2020) 395(10223):497–506. doi: 10.1016/S0140-6736(20)30183-5
35. Hojyo S, Uchida M, Tanaka K, Hasebe R, Tanaka Y, Murakami M, et al. How COVID-19 Induces Cytokine Storm With High Mortality. *Inflammation Regener* (2020) 40:37. doi: 10.1186/s41232-020-00146-3
36. Zhao Y, Qin L, Zhang P, Li K, Liang L, Sun J, et al. Longitudinal COVID-19 Profiling Associates IL-1RA and IL-10 With Disease Severity and RANTES With Mild Disease. *JCI Insight* (2020) 5(13):e139834. doi: 10.1172/jci.insight.139834
37. Le Joncour A, Biard L, Vautier M, Bugaut H, Mekinian A, Maalouf G, et al. Neutrophil-Platelet and Monocyte-Platelet Aggregates in COVID-19 Patients. *Thromb Haemost* (2020) 120(12):1733–5. doi: 10.1055/s-0040-1718732
38. Starossom SC, Veremeyko T, Yung AW, Dukhinova M, Au C, Lau AY, et al. Platelets Play Differential Role During the Initiation and Progression of Autoimmune Neuroinflammation. *Circ Res* (2015) 117(9):779–92. doi: 10.1161/CIRCRESAHA.115.306847
39. Rha MS, Shin EC. Activation or Exhaustion of CD8(+) T Cells in Patients With COVID-19. *Cell Mol Immunol* (2021) 18(10):2325–33. doi: 10.1038/s41423-021-00750-4
40. Huang G, Kovalic AJ, Graber CJ. Prognostic Value of Leukocytosis and Lymphopenia for Coronavirus Disease Severity. *Emerg Infect Dis* (2020) 26 (8):1839–41. doi: 10.3201/eid2608.201160
41. Chow JH, Khanna AK, Kethireddy S, Yamane D, Levine A, Jackson AM, et al. Aspirin Use Is Associated With Decreased Mechanical Ventilation, Intensive Care Unit Admission, and In-Hospital Mortality in Hospitalized Patients With Coronavirus Disease 2019. *Anesth Analg* (2021) 132(4):930–41. doi: 10.1213/ANE.0000000000005292
42. Group RC. Aspirin in Patients Admitted to Hospital With COVID-19 (RECOVERY): A Randomised, Controlled, Open-Label, Platform Trial. *Lancet* (2021) 399(10320):143–51. doi: 10.1016/S0140-6736(21)01825-0

Conflict of Interest: The authors declare that the research was conducted in the absence of any commercial or financial relationships that could be construed as a potential conflict of interest.

Publisher's Note: All claims expressed in this article are solely those of the authors and do not necessarily represent those of their affiliated organizations, or those of the publisher, the editors and the reviewers. Any product that may be evaluated in this article, or claim that may be made by its manufacturer, is not guaranteed or endorsed by the publisher.

frontiers | Frontiers in Immunology

ORIGINAL RESEARCH
published: 27 April 2022
doi: 10.3389/fimmu.2022.853769

Microvesicle-Mediated Communication Within the Alveolar Space: Mechanisms of Uptake by Epithelial Cells and Alveolar Macrophages

*Sanooj Soni[1], Kieran P. O'Dea[1], Eiko Abe[1], Maryam Khamdan[1], Sneh V. Shah[1], Padmini Sarathchandra[2], Michael R. Wilson[1] and Masao Takata[1]**

[1] Division of Anaesthetics, Pain Medicine and Intensive Care, Faculty of Medicine, Imperial College London, Chelsea and Westminster Hospital, London, United Kingdom, [2] National Heart & Lung Institute, Imperial College London, Heart Science Centre, Harefield Hospital, Harefield, United Kingdom

OPEN ACCESS

Edited by:
Szandor Simmons, Charité Universitätsmedizin Berlin, Germany

Reviewed by:
Laura Michalick, Charité Universitätsmedizin Berlin, Germany
Matthias Clauss, Indiana University Bloomington, United States

***Correspondence:**
Masao Takata
m.takata@imperial.ac.uk

Specialty section:
This article was submitted to Inflammation, a section of the journal Frontiers in Immunology

Received: *13 January 2022*
Accepted: *24 March 2022*
Published: *27 April 2022*

Citation:
Soni S, O'Dea KP, Abe E, Khamdan M, Shah SV, Sarathchandra P, Wilson MR and Takata M (2022) Microvesicle-Mediated Communication Within the Alveolar Space: Mechanisms of Uptake by Epithelial Cells and Alveolar Macrophages. Front. Immunol. 13:853769. doi: 10.3389/fimmu.2022.853769

Intra-alveolar microvesicles (MVs) are important mediators of inter-cellular communication within the alveolar space, and are key components in the pathophysiology of lung inflammation such as acute respiratory distress syndrome (ARDS). Despite the abundance of data detailing the pro-inflammatory effects of MVs, it remains unclear how MVs interact or signal with target cells in the alveolus. Using both *in vivo* and *in vitro* alveolar models, we analyzed the dynamics of MV uptake by resident alveolar cells: alveolar macrophages and epithelial cells. Under resting conditions, the overwhelming majority of MVs were taken up by alveolar macrophages. However, following lipopolysaccharide (LPS)-mediated inflammation, epithelial cells internalized significantly more MVs ($p<0.01$) whilst alveolar macrophage internalization was significantly reduced ($p<0.01$). We found that alveolar macrophages adopted a pro-inflammatory phenotype after internalizing MVs under resting conditions, but reduction of MV uptake following LPS pre-treatment was associated with loss of inflammatory phenotype. Instead, MVs induced significant epithelial cell inflammation following LPS pre-treatment, when MV internalization was most significant. Using pharmacological inhibitors, we interrogated the mechanisms of MV internalization to identify which endocytic pathways and cell surface receptors are involved. We demonstrated that epithelial cells are exclusively dependent on the clathrin and caveolin dependent endocytotic pathway, whereas alveolar macrophage uptake may involve a significant phagocytic component. Furthermore, alveolar macrophages predominantly engulf MVs *via* scavenger receptors whilst, epithelial cells internalize MVs *via* a phosphatidylserine/integrin receptor mediated pathway (specifically alpha V beta III), which can be inhibited with phosphatidylserine-binding protein (i.e. annexin V). In summary, we have undertaken a comprehensive evaluation of MV internalization within the alveolar space. Our results demonstrate that different environmental conditions can modulate MV internalization, with inflammatory stimuli strongly enhancing epithelial cell uptake of MVs and inducing epithelial cell

activation. Our data reveal the unique mechanisms by which alveolar macrophages and epithelial cells internalize MVs thereby elucidating how MVs exert their pathophysiological effect during lung inflammation and injury. As MVs are potential novel therapeutic targets in conditions such as ARDS, these data provide crucial insights into the dynamics of MV-target cell interactions and highlight potential avenues for researchers to modulate and inhibit their pro-inflammatory actions within the alveolar space.

Keywords: extracellular vesicles, microvesicle internalization, alveolar space, intercellular communication, microvesicle processing

INTRODUCTION

Microvesicles (MVs) are cell membrane-circumscribed extracellular particles, carrying a variety of molecular cargo, such as proteins, receptors and nucleic acids (1–3) over a distance to remote cells (1–3). They provide an alternative yet essential pathway for inter-cellular communication (2, 4) and have been implicated in the pathophysiology of various inflammatory diseases (5–8). This has led to a considerable amount of interest regarding the role of MVs in inflammatory lung diseases such as acute respiratory distress syndrome (ARDS). Indeed, we have previously demonstrated that intra-alveolar MVs, particularly alveolar macrophage-derived MVs, are potent initiators of acute lung injury (ALI), mediated by molecular cargo packaged within them (9, 10) and it is now evident that MVs are key components in the pathophysiology of lung inflammation as well as potential novel therapeutic targets (9, 11–13).

Despite the abundance of data detailing the pro-inflammatory effects of MVs, it remains unclear how MVs interact or signal with target cells in the alveolus *in vivo*. Several mechanisms have been postulated based largely on extra-pulmonary models of inflammation (**Figure 1**): 1) *via* direct MV-cellular interaction forming a ligand-receptor complex (14); 2) through a paracrine fashion where MVs release their cargo near target cells, which subsequently act upon membrane receptors (15); 3) by endocytosis or internalization of MVs (and their cargo) by target cells (16, 17); and 4) through fusion of MVs with target cell membranes, thereby transferring their intra-vesicular cargo (18). Whist some of these data may be applicable to the alveolar space, it is important to note that within the unique environment of the alveolus, MVs may have prolonged or enhanced effects as the alveolus acts a semi-closed environment, protected from the rapid dilution or washout of MVs by blood flow. Therefore, the dynamics of MV communication in the alveolus are likely to differ from more commonly studied compartments such as the circulation.

To date, studies on MV interactions with alveolar cells have focused on the process of endocytosis. Alveolar macrophages, as resident professional phagocytes, internalize MVs resulting in lung inflammation (11), while a recent study has shown that insulin-like growth factor-1 (IGF-1) augments particle engulfment function of non-professional phagocytic cells such as epithelial cells, resulting in enhancement of MV uptake by

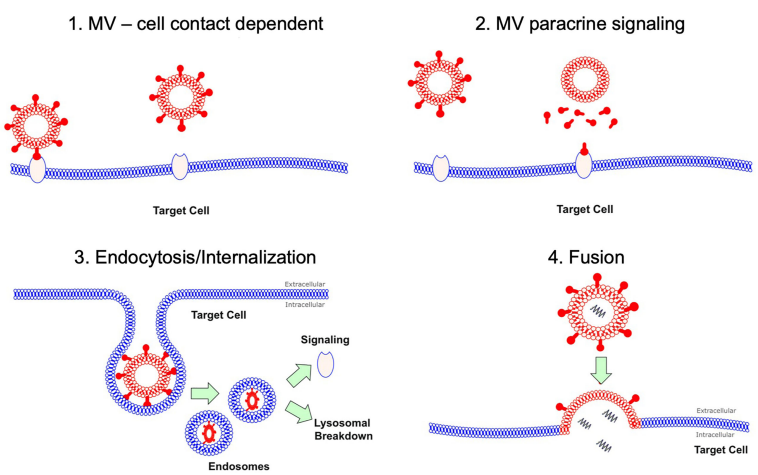

FIGURE 1 | MV interaction with target cells. There are several hypotheses how MVs may interact with their target cells. Firstly this could be as simple MV and cell contact *via* a receptor *via* ligand-receptor interaction. Secondly this could occur through a paracrine fashion with MVs releasing soluble factors at a target cell site. MVs could undergo endocytosis, where they are internalized and then subsequently either undergo lysosomal degradation or activate endosomal signaling. Finally MV could fuse with their target cells resulting in fusion of 2 initially distinct membranes and subsequent release of contents into target cell cytoplasm.

airway epithelial cells *in vitro* (19). However these studies have focused on individual alveolar cells, predominantly in the *in vitro* setting and have not considered the alveolus as a whole, where alveolar macrophages and epithelial cells lie in close proximity to each other. This could lead to competition for uptake, which would not be apparent using isolated cells *in vitro*. Furthermore, it remains unknown whether differential uptake mechanisms/pathways occur between these different alveolar cells or if specific cellular populations preferentially take up MVs. Since MVs are a promising therapeutic avenue in lung inflammatory diseases such as ARDS, it is crucial to address these points but also to understand how MVs interact with these different cells in the alveolar environment.

In this study, we performed a comprehensive analysis of MV communication with target intra-alveolar cells in both *in vivo* and *in vitro* models, identifying key receptors and pathways involved in MV internalization in resting as well as inflammatory conditions. We showed that MV uptake and internalization in the alveolar space is performed primarily by alveolar macrophages rather than epithelial cells. However, following exposure to lipopolysaccharide (LPS), epithelial cell uptake is significantly increased, enhancing epithelial cell inflammation, whilst alveolar macrophage internalization of MVs is reduced. Furthermore, we demonstrated clear differences in MV uptake mechanism between these two cell types, i.e. MV uptake by alveolar macrophages is predominantly a scavenger receptor mediated process, whilst epithelial cells rely upon integrin receptors. These data provide crucial mechanistic information and delineate potential means to interrupt MV-mediated signaling in the alveolus for therapeutic purposes.

MATERIALS AND METHODS

Animal Experiments

All protocols were approved by the Ethical Review Board of Imperial College London, carried out under the authority of the UK Home Office in accordance with the Animals (Scientific Procedures) Act 1986, UK and reported in compliance with the ARRIVE guidelines. One hundred and fifty-six male C57BL/6 mice (Charles River, Margate, UK), aged 10-14 weeks were used. Mice were housed in individual ventilated cages (maximum number of 5 per cage) and exposed to 12-hour light and dark cycles. All experiments were initiated and completed during the light cycle and no unexpected adverse effects were observed in any of the treatment groups.

In Vitro MV Production and Fluorescent Labeling

RAW 264.7 macrophages cells (Sigma-Aldrich, UK) were washed and pre-treated with 1μg/ml of 'Ultrapure' lipopolysaccharide (LPS) (*In vivo*gen Toulouse, strain: E. coli O111:B4) for 1 hour to induce inflammatory conditions as previously described (9, 10). Cells were then stimulated with 3mM of ATP disodium salt (Biotechne, UK) to induce release of 'pro-inflammatory' MVs. Supernatants were collected, centrifuged to remove cells (200g 10 minutes at 4°C) and then labeled with 5μM of 1,1'-Dioctadecyl-3,3,3',3'-Tetramethylindodicarbocyanine Perchlorate (DiD) (ThermoFisher Scientific, UK) in Diluent C, in dark at room temperature for 7 minutes. DiD-labeled MVs were then pelleted (20,000*g* for 30 min at 4°C) and washed twice to remove unbound dye. The relative fluorescence of MVs was assessed using a fluorescence plate reader (Bio-tek FLX 800; Bio-tek instruments, USA), and a standardized amount of fluorescent MVs (25,000 relative fluorescence units (RFU), which corresponds to approximately 1 x 10^6 MVs) was then added to our *in vitro* or *in vivo* models [**Supplementary Figures 1**, **2** (20)]. This dose of MVs was chosen as we have previously observed up to approximately 1 x 10^6/ml of alveolar macrophage-derived MVs in bronchoalveolar lavage fluid (BALF) samples in i.t. LPS-induced ALI in mice at 1 hour (9).

MVs were identified by flow cytometry (CyAn^{TM} ADP flow cytometer, Beckman Coulter, UK) as events under 1μm in size (forward scatter and side scatter with a trigger threshold of 0.01 were used to elucidate a 1μm gate that was delineated using sizing beads) and positive for specific surface marker CD11b (M1/70; Biolegend, CA) and DiD (**Figure 2A**). MVs were also enumerated using Accucheck counting beads (Invitrogen, Paisley, UK) as previously shown (9, 10, 20). Data were analysed using FlowJo software. All stained MV samples were also treated with 0.1% triton detergent in order to correctly differentiate MVs from non-vesicular antibody-bound events (21). The centrifugation and flow cytometry methods to isolate and characterise MVs in this study have been previously validated both by high-resolution imaging and electron microscopy (10).

In Vivo MV Production

In vivo-derived MVs were harvested from our LPS model of ALI as previously described (composed primarily of alveolar macrophage and epithelial cell-derived MVs) (9). In brief, mice were anesthetized (intraperitoneal ketamine 90mg/kg; xylazine 10mg/kg) and 20μg LPS in 50μl was instilled intratracheally (i.t.). After 1 hour, animals were euthanized and tracheostomized, BALF were obtained by flushing and gently aspirating 700μl of 0.9% saline in and out of the lungs *via* the endotracheal tube three times, and centrifuged to remove cells and larger particles (200g, 10mins at 4°C). Cell free supernatants were then stained with DiD as described above. DiD-labeled *in vivo* generated MVs were then pelleted (20,000g for 30 min at 4°C) and washed twice to remove unbound dye and other stimulatory factors.

In Vivo Model of Intra-Alveolar MV Uptake

Fluorescent-labeled RAW macrophage-derived MVs (25,000 RFU, resuspended in 50μl normal saline) or post-wash supernatant (50μl of supernatant following second wash step as control) was instilled i.t. into the lungs of randomly selected mice by an investigator blinded to the treatment groups (**Supplementary Figure 1**). In a separate set of experiments, *in vivo* derived MVs (25,000 RFU, obtained as described above) were also instilled i.t. into the lungs of randomly selected mice (**Supplementary Figure 2**). Either 1 or 4 hours after instillation, mice were euthanized, lungs were removed and mechanically disrupted in warm fixation buffer using a GentleMACS

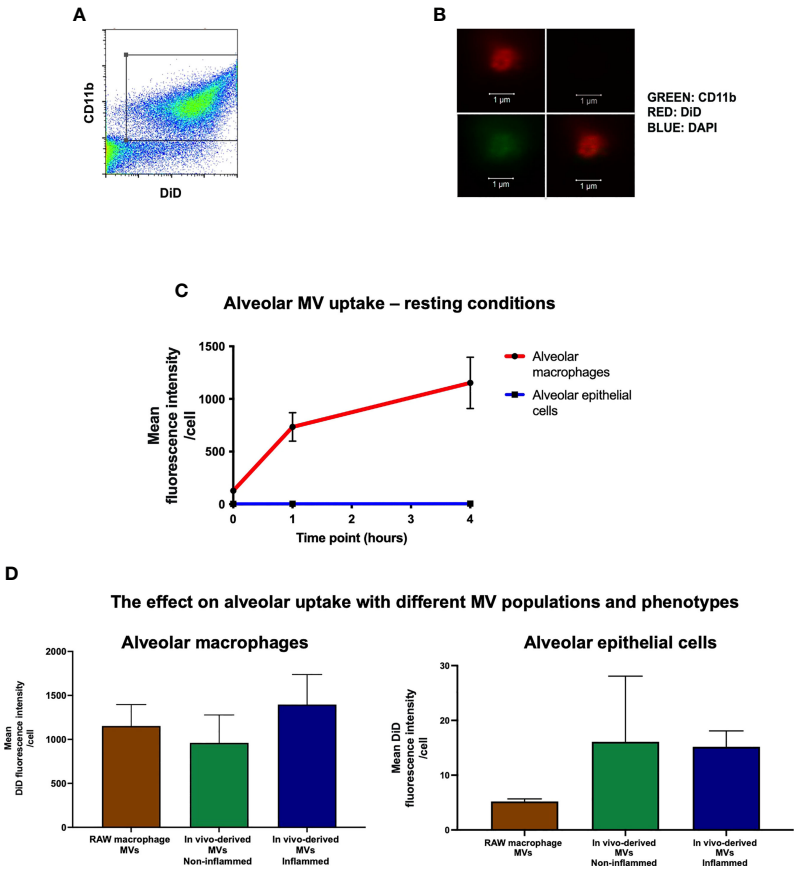

FIGURE 2 | *In vivo* uptake of MVs. **(A)** Flow cytometry plot of RAW macrophage derived MVs, demonstrating that DiD labeled events were also positive for CD11b, confirming their identity as macrophage-derived MVs. **(B)** These particles were readily visualized by confocal microscopy as DiD (red, top left panel), particles negative for nuclear materials ($DAPI^-$, top-right), but positive for CD11b (green, bottom-left, co-localization shown in the bottom-right combined image) (n = 3). **(C)** DiD labeled RAW macrophage MVs (25,000 RFU) were instilled into the trachea of untreated mice and *in vivo* MV uptake by alveolar macrophages and epithelial cells was assessed by flow cytometry at 1 and 4 hours. Time 0 represents baseline auto-fluorescence, i.e. no MVs added. Alveolar macrophages significantly internalized the majority of MVs compared to alveolar epithelial cells at both time points [1 hour: alveolar macrophage 734 ± 135 RFU vs. epithelial cells 4.78 ± 0.57 RFU; 4 hours: alveolar macrophage 1153 ± 243 RFU vs. epithelial cells 5.21 ± 0.47 RFU (n = 5)]. **(D)** Alveolar macrophages, as compared to epithelial cells, internalized the majority of MVs at 1 hour after installation *in vivo* regardless of the MV phenotypes used: 1) *in vitro*-derived RAW macrophage MVs (i.e. from stimulated RAW macrophage culture); 2) *in vivo*-derived MVs, non-inflamed (intra-alveolar MVs harvested by lung lavage from untreated mice); and 3) *in vivo*-derived MVs, inflamed (intra-alveolar MVs harvested by lung lavage from LPS-treated mice). (n = 3-6, not significant by one way ANOVA).

dissociator [Miltenyi Biotec, Surrey, UK (20)]. Samples were then passed through 40μm sieves, washed and resuspended twice in flow cytometry buffer (2% fetal calf serum, 2mM EDTA and 0.1% sodium azide constituted in PBS) to yield a fixed single cell suspension. Uptake was then evaluated by assessing mean fluorescence intensity (MFI) of DiD in alveolar cells by flow cytometry. As described previously (9), alveolar macrophages were identified as $CD45^+$ (clone 30-F11; Biolegend), $CD11c^+$ (clone N418; eBioscience, CA), $CD11b^-$, $F4/80^+$ (BM8; eBioscience). Epithelial cells were identified as $CD45^-$, $CD31^-$ (MEC 13.3; BD Bioscience, CA), and $T1alpha^+$ (8.1.1; Biolegend) events (9). In some experiments, mice were pre-treated with i.t. 20ng LPS (in 50μl normal saline) or saline (50 μl) for 1 hour in order to assess the effect of underlying lung inflammation on MV uptake.

In Vitro Model of Intra-Alveolar MV Uptake

In order to model the intra-alveolar environment *in vitro*, we created a co-culture system comprised of primary alveolar macrophages and Murine Lung Epithelial (MLE-12) cells (ATCC, UK). MLE-12 cells were seeded overnight in a 24 well-plate at a density of 10^5 cells/well and primary alveolar macrophages [harvested by lung lavage from untreated mice as described previously (9)] were added to MLE cells for one hour in the ratio of 1:5 (22). DiD-labeled RAW macrophage-derived MVs or post-wash supernatant were then incubated in this *in vitro* model of the alveolus. After 1 or 4 hours, cells were detached using EDTA containing solution (Versene, Life Technologies), stained with the fluorescently conjugated antibodies against CD45, CD11c and T1α and DiD MFI of individual cells were assessed.

Mechanisms of MV Uptake

In our *in vitro* alveolar co-culture model, we examined the surface expression of variety of scavenger/integrin receptors in each cell type *via* flow cytometry: MERTK (2B10C42; biolegend), TIM4 (RMT4-54; biolegend), Alpha V Beta III (2C9.G2; Biolegend), Alpha V Beta V (RMV-7; Biolegend), Macrophage Scavenger Receptor 1 (REA148; Miltenyi), MARCO, CD36 (HM36; Biolegend); CD68 (FA-11; Biolegend).

In separate experiments, to assess mechanism of MVs internalization, we pre-incubated the cells in the alveolar co-culture model with 2μM Cytochalasin D or 0.25mM Dynasore prior to treatment with DiD-labeled RAW MVs. DiD fluorescence was then assessed in these cells as described above.

Confocal Microscopy

Primary alveolar macrophages and MLE cells were seeded on coverslips and then incubated with DiD-labeled RAW MVs for 1 hour. In separate experiments, to visualize DiD-labeled MVs *via* confocal microscopy, MVs were placed on poly-L-ornithine coated coverslips to encourage adherence for 6 hours. Thereafter both MVs and cells were washed, fixed, permeabilized with 0.5% triton-X 100 and incubated with 3% bovine serum albumin (Sigma-Aldrich) for 30mins. Slides were then incubated with 5μg/ml T1 alpha (ab109059; Abcam, Cambridge UK) or 5μg/ml CD45 (ab23910; Abcam) overnight in the dark at 4°C, followed by washing and incubation with secondary antibodies (1:1000) for 1 hour. After washing, slides were treated with 4',6-diamidino-2-phenylindole (DAPI) intra-nuclear stain (1:10000) solution (pre-made) for 10mins. Coverslips were placed on slides with Mounting PermaFluor (ThermoFisher Scientific) and viewed using a Zeiss LSM880 NLO multiphoton confocal imaging system with Axio Observer 1 microscope. The objective lens used was a Plan Apochromat 40x/1.3 oil DIC UVVIS-IR. The imaging medium was oil and the temperature -20°C. The fluorochromes used were Alexa-Fluor 488 and Alexa-Fluor 594. CZI Images were acquired using Zen software, which were then exported as 16 bit Tiff images. No image processing software was used.

Statistical Analysis

Shapiro-Wilk normality tests were carried out (IBM SPSS). Comparisons between two data sets were performed using either paired T-tests or Wilcoxon Rank Sum test. All data was analyzed on GraphPad Prism and are expressed as Mean ± SD, or Median ± Interquartile range. A $p<0.05$ was defined as the minimum threshold for statistical significance.

RESULTS

In Vivo Uptake of MVs

We have previously shown that 'pro-inflammatory' macrophage-derived MVs are rapidly released within the alveolus *in vivo* and involved in the early pathogenesis of ALI (9). To model this effect, RAW macrophages were stimulated with LPS (inflammatory stimulus) followed by ATP (danger signal) to induce release of pro-inflammatory MVs, which were then labeled with the fluorescence lipophilic dye DiD (17) for detection by flow cytometry and confocal microscopy (**Figures 2A, B**). A known fluorescent quantity of these MVs [25,000 RFU which corresponds to 1 x 10^6 MVs; we previously found up to approximately 1 x 10^6/ml of alveolar macrophage-derived MVs in BALF in i.t. LPS-induced ALI in mice at 1 hour (9)] was instilled into the trachea of untreated mice, and MV uptake by different alveolar cells was assessed by flow cytometric analysis of lung single cell suspensions. One hour after instillation, we found that alveolar macrophages rather than epithelial cells internalized the majority of MVs (**Figure 2C**), despite several studies previously demonstrating that epithelial cells rapidly take up MVs (19, 23, 24). This difference persisted over time, such that at 4 hours alveolar macrophage still internalized the majority of MVs (1153 ± 244 RFU for alveolar macrophages vs. 5.21 ± 0.47 RFU for epithelial cells).

To assess the uptake of the mixed populations of MVs released *in vivo* within the alveolus, we used intra-alveolar MVs harvested from an *in vivo* model of ALI. These MVs contained 'mixed' populations, predominantly composed of alveolar macrophage- and epithelial cell-derived MVs (with concentrations of ~1000 MVs/μL and ~650 MVs/μL respectively in the original BALF samples), and have significant pro-inflammatory activity (9). We also used intra-alveolar MVs harvested from untreated mice as a control, which are composed of both alveolar macrophage- and epithelial cell-derived MVs (~300 and ~180 MVs/μL in the original BALF samples), and devoid of inflammatory activity. Both types of MVs were labelled and instilled i.t. into another mice (**Supplementary Figure 2**). Alveolar macrophages still internalized the overwhelming majority of these primary, *in vivo*-generated 'inflamed' or 'non-inflamed' MVs compared to epithelial cells 1 hour after installation (**Figure 2D**). Interestingly, there was a trend that epithelial cells internalized more *in vivo* derived MVs compared to RAW MVs but this did not reach statistical significance (epithelial uptake of RAW MV: 5.21 ± 0.47 RFU vs. non-inflamed *in vivo* MVs: 16.1 ± 12.0 RFU vs. inflamed *in vivo* MVs: 15.9 ± 2.9 RFU). Nevertheless, these data suggest that irrespective of MV population (either alveolar macrophage- or epithelial cell-derived MVs) and phenotype (inflamed or no-inflamed), alveolar macrophages internalize the majority of MVs within the alveolar space under normal physiological conditions, within the time frame of our observations.

In Vitro Uptake of MVs

In order to model the environment with the lungs, we created an *in vitro* alveolar system composed of primary alveolar macrophages (obtained from untreated mice) and murine lung epithelial (MLE-12) cells (22). This co-culture system allowed us to confirm our *in vivo* results and explore the dynamics and mechanisms of MV-mediated communication with alveolar cells in detail. DiD labeled RAW-derived MVs were incubated within this *in vitro* environment for 1 or 4 hours, and the uptake of MVs by individual cells was measured by flow cytometry and confocal microscopy. As occurred *in vivo*, substantial amounts of MVs

were internalized by alveolar macrophages, after both 1 and 4 hours incubation time (**Figure 3A**), while epithelial cells did internalize MVs but this process occurred to a much lesser extent compared to alveolar macrophages (**Figure 3B**). As would be expected from this *in vitro* alveolar model (which is essentially a completely closed system), the amount of MVs recovered in the cell culture supernatant substantively decreased over time, consistent with these MVs being taken up by alveolar cells (**Figure 3C**). These findings were also confirmed by confocal microscopy (**Figure 3D**), where alveolar macrophages can be seen to internalize MVs.

Interestingly, we found that when we increased MV numbers in our co-culture system, alveolar macrophages appeared to become saturated and unable to internalize any further MVs. Instead, epithelial cells started taking up MVs to almost a similar extent as alveolar macrophages at 4 hours of incubation, presumably as there is less competition from alveolar macrophages (**Supplementary Figure 3**). There may also be increased uptake efficiency of the epithelial cells at higher MV concentrations. However, it is important to note that the number of MVs required to precipitate this effect (0.5 to 1.5 x 10^7/ml) far exceeds the number of macrophage MVs measured in BALF (~1 x 10^6/ml) in our *in vivo* models of ALI (9).

Effects of Inflammation on MV Internalization

Next, we assessed whether MV internalization in the alveolar space would differ during inflammation. DiD-labeled RAW macrophage-derived MVs were instilled into the trachea of mice that were pre-treated with either 20ng LPS or saline. We found that LPS pre-treatment caused a significant switch in MV uptake: alveolar macrophage internalization was reduced (~<50%, p<0.01) whilst epithelial cell uptake was increased (~>150%, p<0.01) (**Figure 4A**). This pattern was replicated in our *in vitro* model when the co-culture was pretreated with 1μg/ml LPS (**Figure 4B**). These findings demonstrated that inflammatory conditions substantively modulate MV uptake within the alveolar space, producing a partial shift of MV uptake/internalization from alveolar macrophages to epithelial cells.

We also assessed whether MV uptake caused a change in alveolar cell phenotype or activation status. Using ICAM-1 as a surrogate marker of cell activation (25, 26), we found that alveolar macrophages adopted a pro-inflammatory phenotype after internalizing RAW macrophage-derived MVs under resting conditions (p<0.01, **Figure 5A**). Interestingly, when uptake was reduced following pre-treatment with 1μg/ml LPS, the pro-inflammatory effect of MVs was no longer evident (**Figure 5A**).

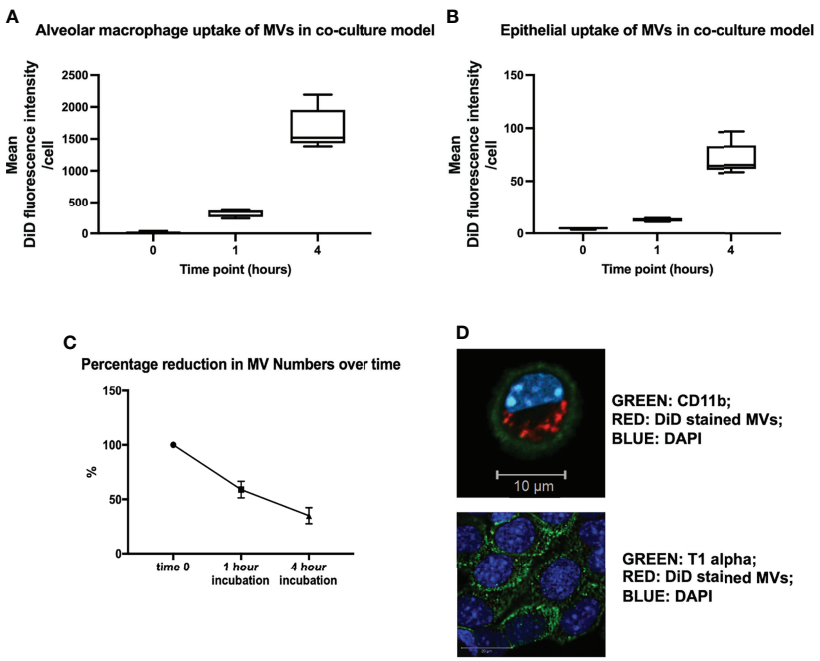

FIGURE 3 | **(A)** *In vitro* uptake of DiD labeled uptake in our in vitro alveolar system. Under resting conditions, a known quantity of raw cell derived-MVs (25,000 RFU) were introduced into our in vitro alveolar system consisting of alveolar macrophages and MLE cells at a ratio of 1:5. Substantial amount of MVs were internalized by alveolar macrophage rather than MLEs cells at either 1 or 4 hours. **(B)** Epithelial cells did take up MVs albeit to a much lesser extent compared to alveolar macrophages, with a rise in uptake after 4 hours. **(C)** The amount of MVs, recovered from our co-culture system decreased over time, in keeping with increased uptake of MVs by the cells in the co-culture system. **(D)** Confocal microscopy of MV uptake by alveolar cells after 1 hour incubation. The green dye represents cell surface integrin CD11b, which depicts the cell membrane. Our image demonstrates the presence of DiD stained MVs clearly within the membrane (likely to be localized to the cytoplasm) of the macrophage confirming our flow cytometry results. However MLE cells (bottom) take up a very small amount of MVs, as minimal amounts of red stained MVs are present within these cells (n = 3). Parametric or non-parametric data displayed as mean ± s.d. or box–whisker plots showing the median, IQR and minimum/maximum values respectively (**A–C** experiments n = 5-6).

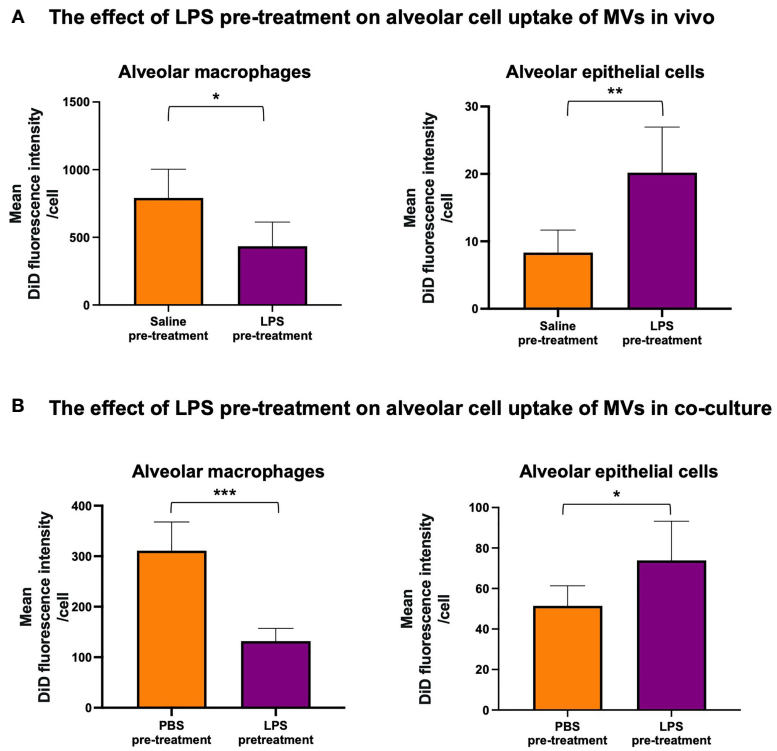

FIGURE 4 | The effect of LPS on internalization of RAW macrophage derived MVs by alveolar cells. **(A)** 20ng LPS pre-treatment (via intra-tracheal instillation) caused a decrease in MV uptake by alveolar macrophages (left), but produced a marked increase in MV uptake by epithelial cells (right). **(B)** This phenomenon was repeated *in vitro* such that pre-treatment with 1μg/ml LPS for 1 hour caused a significant decrease in MV uptake by alveolar macrophages (left) but a significant increase in epithelial cell uptake (right). Parametric data displayed as mean ± s.d. *p < 0.05, **p < 0.01, ***p < 0.001 (all experiments n=5).

Conversely, MVs only induced significant epithelial cell activation following pre-treatment with LPS, when MV internalization was most significant (**Figure 5B**).

Endocytosis of MVs

We then investigated the mechanisms of MV internalization in both alveolar macrophages and epithelial cells. Firstly, MV uptake experiments were carried out at 4°C which abolished MV uptake in both alveolar macrophages and epithelial cells, indicating that an active, energy dependent process is involved (**Figure 6A**). We next assessed the effect of inhibitors of endocytosis on MV uptake by each of these cells. Cytochalasin (generalized inhibitor of endocytosis) reduced alveolar macrophage uptake by 59.5%, and dynasore (cell-permeable inhibitor of the clathrin and caveolin dependent endocytosis pathway) inhibited macrophage uptake by 47.9% (**Figure 6A**). In contrast, epithelial cell uptake was inhibited by 62.7% by cytochalasin but completely blocked by dynasore (**Figure 6A**). The absolute effects of dynasore on epithelial cells, but not on alveolar macrophages, suggests that epithelial cells are exclusively dependent on the clathrin and caveolin dependent endocytotic pathway, whereas alveolar macrophage uptake may involve a significant phagocytic component.

Receptor-Mediated Mechanism of MV Uptake

To identify receptor-mediated mechanisms involved in MV internalization by alveolar cells, we examined the presence of cell surface receptors that have been implicated in the uptake of endogenous and foreign particles or apoptotic cells, and thus may be involved in MV uptake. In particular, we investigated the relative expression of integrin receptors which bind to phosphatidylserine (PS) such as MerTK (27, 28), alpha V beta III (29, 30) and alpha V beta V (31), and scavenger receptors such as macrophage scavenger receptor A (32), MARCO (33), CD36 (34) and CD68 (35). We also studied the expression of the integrin TIM4 since it is expressed on the surface of macrophages and has a role in MV and exosome internalization (36, 37). We found that alveolar macrophages express MerTK and Alpha V beta III integrin receptors whereas epithelial cells only express Alpha V beta III integrin receptor (**Figure 6B**). In addition, we detected a variety of scavenger receptors on alveolar macrophages including MARCO, CD36 and CD68, but expression of scavenger receptors was low or undetectable on epithelial cells (**Figure 6C**). Based on these profiles, we hypothesized that both integrin (MerTK and alpha V beta III) and scavenger receptors (MARCO, CD36, and CD68) were involved in MV uptake by alveolar macrophages, whereas

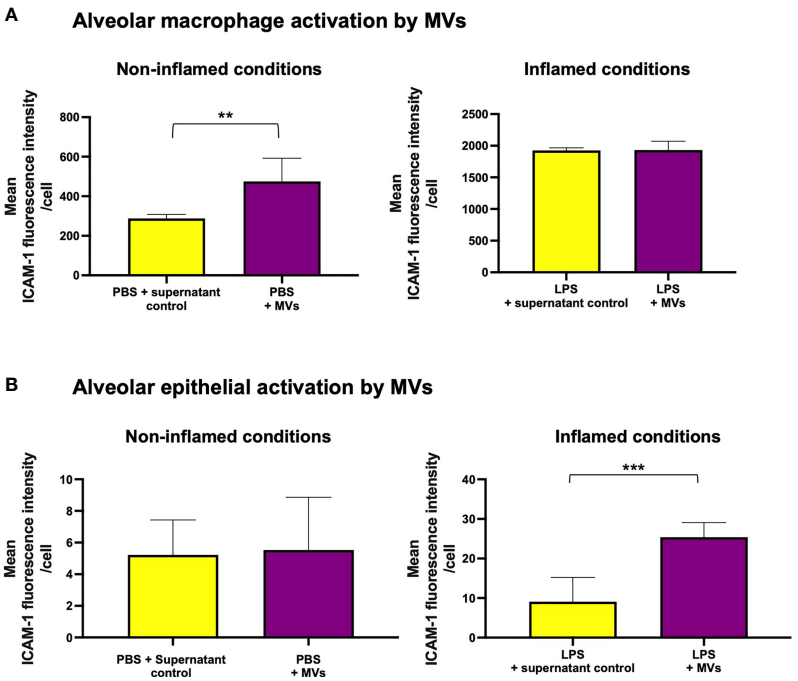

FIGURE 5 | MV mediated inflammation within our *in vitro* alveolar system. (**A**, left) Under resting conditions, addition of RAW macrophage derived MVs caused a significant increase in ICAM-1 expression on alveolar macrophages. (**A**, right) However, when exposed to 1μg/ml LPS (where MV uptake is substantively reduced), MVs no longer have a pro-inflammatory effect on alveolar macrophages. **(B)** However this trend is reversed within epithelial cells when ICAM-1 expression significantly increases only in epithelial cells that have been pre-treated with LPS (where MV uptake is maximal). Parametric data displayed as mean ± s.d. **$p < 0.01$, ***$p < 0.001$. (all experiments n = 5).

epithelial cell uptake occurred principally *via* integrin receptors (specifically alpha V beta III).

To examine this hypothesis, we pre-treated our co-culture system with either polyinosinic acid (50μg/mL) (Class A scavenger receptor inhibitor) or annexin V [binds to PS expressed on MVs preventing integrin/PS mediated MV uptake (38, 39)] and assessed their effect on MV uptake by each cells (**Figures 6D, E**). As predicted, annexin V inhibited uptake by both alveolar macrophages and epithelial cells but had a greater effect on uptake by epithelial cells. Conversely, scavenger receptor inhibitor polyinosinic acid dramatically reduced alveolar macrophage internalization of MVs, with a lesser effect on epithelial cell uptake. The results suggest that integrin receptors play an essential role in MV uptake by epithelial cells, whereas scavenger receptors play a more predominant role in that by alveolar macrophages.

DISCUSSION

Elevated production of MVs is a common feature in the pathophysiology of alveolar inflammation, particularly in conditions such as ARDS (9) or COPD (8), yet there is a paucity of data describing MV communication or cellular uptake within the alveolus. This study demonstrates several novel findings detailing MV trafficking within the unique environment of the alveolar space, under both resting and inflammatory states. We have provided convincing data that the overwhelming majority of MV uptake is performed by alveolar macrophages under resting conditions, irrespective of MV phenotype or origin and inducing a pro-inflammatory phenotype in these cells. Although epithelial cells internalized MVs only to a limited extent, this was substantively enhanced by LPS priming, leading to significant MV-induced epithelial cell activation. Furthermore, our data indicate that MVs are internalized by distinct receptor-mediated pathways: alveolar macrophages predominantly internalize MVs *via* scavenger receptors, whilst epithelial cells endocytose MVs through a PS/integrin receptor mediated pathway.

Within the alveolus, the major resident cell populations directly exposed to the air space are alveolar macrophages and epithelial cells. Previous studies investigating MV mediated communication within the alveolus have been performed mostly in an *in vitro* setting, concentrating on MV uptake by either epithelial cells (19, 23, 24) or alveolar macrophages (11, 28) alone. This is the first study to analyze MV internalization by different alveolar cells '*in vivo*', and we have shown that the degree of uptake by each of these alveolar cells is dependent on the environmental condition to which they are exposed. Under normal physiological conditions, alveolar macrophages internalize the overwhelming majority of MVs, inducing an inflammatory phenotype, while epithelial cells

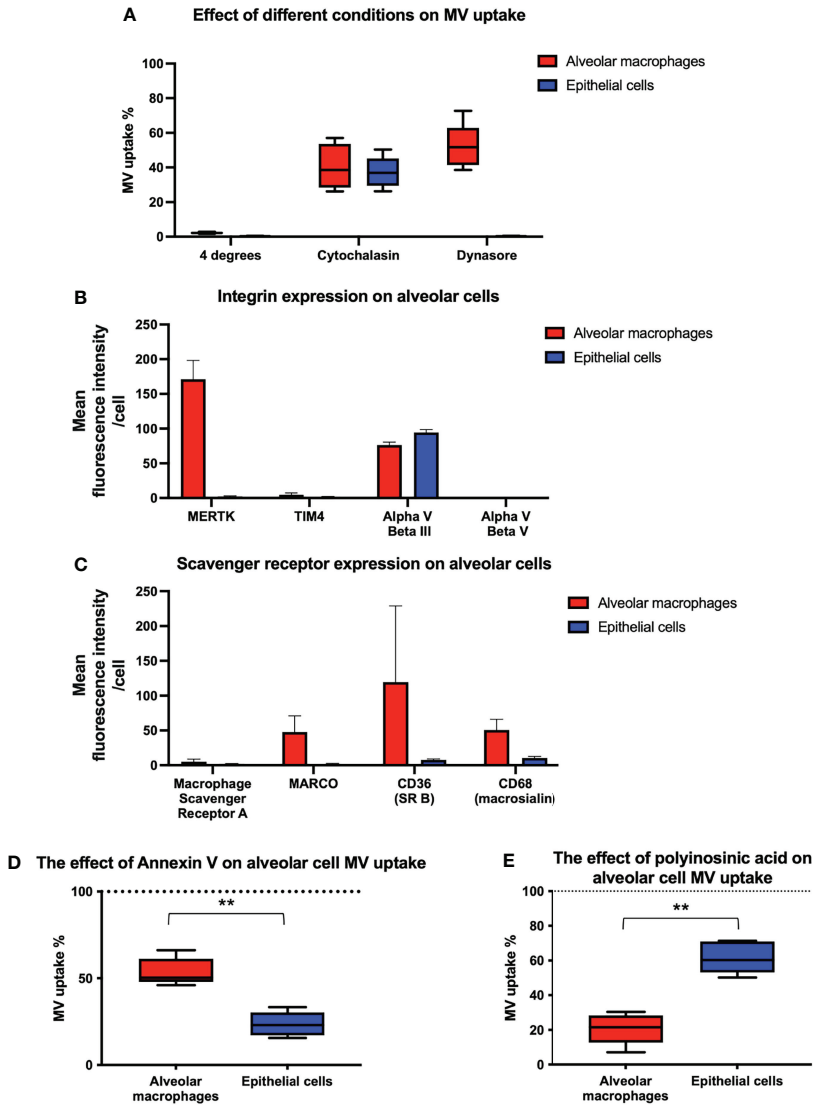

FIGURE 6 | Inhibition of endocytosis in alveolar cells. **(A)** Performing experiments at 4°C completely obliterated MV engulfment in both alveolar macrophages and epithelial cells. When our co-culture system was pre-incubated with either cytochalasin or dynasore, endocytosis was significantly inhibited in both cell types. However dynasore had a greater effect upon epithelial cells, completely abrogating internalization, which may have some mechanistic significance. Results expressed as a percentage of control MV uptake (compared to experiments where no inhibitor used). **(B)** Flow cytometry analysis of integrins on the surface of alveolar macrophages and MLE cells. Alveolar macrophages express MERTK and Alpha V Beta III integrin receptors on their surface whilst epithelial cells only express Alpha V Beta III. **(C)** Flow cytometry analysis of scavenger receptors on the surface of alveolar macrophages and MLE cells. Alveolar macrophages express a variety of scavenger receptors including MARCO, CD36 and CD68 whereas epithelial cells do not. **(D)** The effect of blocking integrin on alveolar cell uptake. MVs were pre-incubated with annexin V prior to alveolar cells treatment. Annexin V binding to PS on surface of MVs and subsequent integrin receptor blockade, had a significant effect on epithelial cell blockade compared to alveolar macrophages, although alveolar macrophage uptake was also inhibited. Results expressed as a percentage of control MV uptake (where no annexin V used). **(E)** The effect of blocking scavenger receptors on alveolar cell uptake. Our alveolar cells *in vitro* were pre-incubated with polyinosinic acid, a scavenger receptor inhibitor, prior to MV treatment. This significantly abrogated alveolar macrophage engulfment whilst have little effect upon epithelial cells. Results expressed as a percentage of control MV uptake (where polycytidylic acid used rather than polyinosinic acid). Results expressed as mean fluorescence intensity. Parametric data displayed as mean ± s.d. and non-parametric data displayed as box–whisker plots showing the median, IQR and minimum/maximum values. $^{**}p < 0.01$ All experiments n = 5.

internalize only a very modest proportion of MVs. Hence, in non-inflamed alveoli, any pro-inflammatory effects of MVs seems to be mediated largely by alveolar macrophages. However, in reality, MVs are actively produced within the alveolus when cells are exposed to injury/inflammation causing release of danger associated molecular patterns such as ATP (40, 41). Therefore, any study examining MV pro-inflammatory signaling in the alveolus should rather be conducted under

inflammatory stress to better simulate clinically-relevant disease states. We found that during inflammation, alveolar macrophage uptake of MVs is substantively reduced, with the pro-inflammatory effect of MVs upon macrophages being no longer evident. In sharp contrast, MV uptake by alveolar epithelial cells was markedly enhanced, inducing significant epithelial cell activation. We have previously observed a similar phenomenon of uptake shift of circulating MVs such that LPS injection reduced MV uptake by liver Kupfer cells but enhanced internalization of MVs by monocytes marginated within the pulmonary vasculature, leading to significant pulmonary vascular inflammation (20). Previous studies have demonstrated the reduced expression of scavenger receptors such as CD36 and Marco on the surface of inflamed/M1-polarized macrophages, potentially explaining this finding (42, 43).

The mechanisms detailing MV communication and interaction with target cells remain poorly understood and this is particularly true within the alveolus during inflammatory lung diseases. It is thought that this interaction occurs primarily through endocytosis (3, 23), which consists of a number of pathways including macropinocytosis, phagocytosis, clathrin-dependent, caveolin-dependent, or clathrin/caveolin-independent pathways. Alveolar macrophages and epithelial cells are likely to internalize MVs *via* different endocytosis pathways (44, 45), and we undertook a series of experiments to identify the mechanisms and receptors involved in MV uptake by these alveolar cells. Our confocal microscopy images demonstrated that MVs are internalized by alveolar macrophages rather than fusion with cell membranes. This internalization is an active process, and cytochalasin D, an actin polymerization inhibitor and a generalized suppressor of endocytosis (38, 46), reduced but did not completely abolish MV uptake in both cell types to a similar extent as previously reported (47). Dynasore, a dynamin inhibitor which inhibits both clathrin and caveolin-dependent endocytosis (48), had a much more profound effect on epithelial cells, effectively abolishing epithelial cell uptake. This suggests that there are mechanistic differences in MV uptake between the two cell types: epithelial cell uptake is dependent upon clathrin and caveolin-dependent endocytosis whereas alveolar macrophages may be more reliant upon other endocytic mechanisms (e.g macropinocytosis and phagocytosis), which is consistent with recent data of endocytosis mechanisms of nanoparticle uptake by alveolar cells (49). Indeed, the different speed and capacity of uptake mechanism may explain to some extent why alveolar macrophages (via phagocytosis by forming large phagosomes) take up the majority of MVs in the alveolar space compared to epithelial cells (via clathrin and caveolin-dependent endocytosis by forming much smaller plasma membrane vesicles).

Since MVs express PS on their surface and integrins have been implicated in the uptake of apoptotic material *via* binding of PS, we investigated the expression of various integrin receptors in these alveolar cells. We found that alpha V beta III was the only integrin expressed by murine epithelial cells whilst alveolar macrophages expressed both MERTK and alpha V beta III. Inhibition of integrin/PS binding with annexin V substantially blocked epithelial cell uptake while alveolar macrophage uptake was moderately inhibited. We also investigated the expression of scavenger receptors on both cell types, and as expected, identified several on alveolar macrophages, particularly MARCO (class A) and CD36 (class B), both of which have been shown to play a prominent role in removing apoptotic material (50, 51) and particles (32, 52, 53), but not on epithelial cells. Polyinosinic acid, a known inhibitor of scavenger receptors particularly class A (33, 54), markedly reduced MV internalization in macrophages whilst having little effect on epithelial cells. These results suggest that integrin/PS binding (specifically *via* alpha V beta III) plays a crucial role in MV uptake by epithelial cells, while MV uptake by alveolar macrophages are largely dependent on scavenger receptors but integrin/PS binding may also play a role.

There are some caveats to our work. We used a membrane-bound dye DiD to measure MV uptake, but this dye may affect the functional structure of MVs. However, the use of fluorescent markers is the current gold standard method of visualizing MV internalization, and these stained MVs had similar pro-inflammatory effects to un-stained MVs used in our previous studies (9). There is also a possibility that DiD may leak from stained MVs and cells, falsely conveying uptake in recipient cells. However this is unlikely since alveolar macrophages were preferentially stained with DiD, compared to epithelial cells which would be uniformly stained if DiD was truly leaking from vesicle membranes. In addition to this, uptake was inhibited by low temperature, endocytosis and receptor-mediated uptake inhibition, making significant DiD leak or artefactual uptake of precipitated DiD by cells very unlikely. Furthermore, whilst we have presented a comprehensive evaluation of MV uptake mechanisms within the alveolar space, this was based on pharmacological inhibitor studies and more specific evidence would be required to confirm the molecular pathways. For example, scavenger receptors MARCO and CD36 have been implicated in EV uptake previously (55, 56), but it was beyond the scope of the study to precisely define whether these specific scavenger receptors were responsible for initiating MV endocytosis. Further studies, potentially using MARCO or CD36 knockout mice/SiRNA knockdown cells, would be prudent to elicit if alveolar macrophages were reliant on a particular scavenger receptor during MV internalization.

On the other hand, our data have a number of strengths as a study investigating MV interaction with target cells within the lungs. Firstly, we have investigated MV uptake in the alveolus as a whole, rather than just concentrating upon individual alveolar cells. We have comprehensively characterized MV processing in the alveolar space using both *in vitro* and *in vivo* models, while previous studies have just investigated internalization using *in vitro* models (19, 24). Furthermore, we have used MVs from different sources, both *in vitro* and *in vivo* generated, to demonstrate that alveolar macrophages take up the majority of MVs irrespective of their phenotype or origin (19, 23, 24). Finally, we have employed robust methodologies to reliably assess MV uptake by different cells in these models, e.g. reproducible standardization of administered MV doses using fluorescence, sensitive quantification of MV uptake by individual cells using flow cytometry, morphological confirmation of MV

internalization by confocal microscopy, and mechanistic investigations into MV uptake using combined surface marker assessment/inhibition experiments.

In conclusion, this study demonstrates, for the first time, that alveolar macrophages internalize the majority of MVs within the alveolar space under resting conditions, but during intra-alveolar inflammation, MV uptake by epithelial cells is substantially increased, leading to MV-mediated alveolar epithelial activation. Furthermore we have established that alveolar macrophages and epithelial cells internalize MVs *via* contrasting mechanistic pathways: alveolar macrophages predominantly engulf MVs *via* scavenger receptors, whilst epithelial cells internalize MVs through a PS/integrin receptor-mediated endocytosis pathway. These data elucidate crucial mechanistic information describing how MVs can produce alveolar epithelial injury, exacerbating lung inflammation and have key implications when understanding MV signaling within the alveolar space and MV interactions with target cells. As potential novel therapeutic targets, these data highlight future areas of study by which researchers can modulate the actions of MVs within the alveolar space.

DATA AVAILABILITY STATEMENT

The original contributions presented in the study are included in the article/**Supplementary Material**. Further inquiries can be directed to the corresponding author.

ETHICS STATEMENT

The animal study was reviewed and approved by Ethical Review Board of Imperial College London.

AUTHOR CONTRIBUTIONS

SS and MT contributed to the study design, protocol and study materials. SS, KO'D, EA, MK, SVS, and PS contributed to collection of data. SS and MT performed the statistical analysis. SS, MW, and MT wrote the first draft of the manuscript. All authors contributed to interpretation of the data.

FUNDING

P54008: Medical research Council and British Journal of Anaesthesia; P86239: Academy of Medical Sciences; Chelsea and Westminster Health Charity.

SUPPLEMENTARY MATERIAL

The Supplementary Material for this article can be found online at: https://www.frontiersin.org/articles/10.3389/fimmu.2022.853769/full#supplementary-material

REFERENCES

1. Wang J-G, Williams JC, Davis BK, Jacobson K, Doerschuk CM, Ting JP-Y, et al. Monocytic Microparticles Activate Endothelial Cells in an IL-1β–Dependent Manner. *Blood* (2011) 118(8):2366–74. doi: 10.1182/blood-2011-01-330878
2. Lee TH, D'Asti E, Magnus N, Al-Nedawi K, Meehan B, Rak J. Microvesicles as Mediators of Intercellular Communication in Cancer—the Emerging Science of Cellular 'Debris'. *Semin Immunopathol* (2011) 33(5):455–67. doi: 10.1007/s00281-011-0250-3
3. Ismail N, Wang Y, Dakhlallah D, Moldovan L, Agarwal K, Batte K, et al. Macrophage Microvesicles Induce Macrophage Differentiation and miR-223 Transfer. *Blood* (2013) 121(6):984–95. doi: 10.1182/blood-2011-08-374793
4. Islam MN, Das SR, Emin MT, Wei M, Sun L, Westphalen K, et al. Mitochondrial Transfer From Bone-Marrow-Derived Stromal Cells to Pulmonary Alveoli Protects Against Acute Lung Injury. *Nat Med* (2012) 18 (5):759–65. doi: 10.1038/nm.2736
5. Hulsmans M, Holvoet P. MicroRNA-Containing Microvesicles Regulating Inflammation in Association With Atherosclerotic Disease. *Cardiovasc Res* (2013) 100(1):7–18. doi: 10.1093/cvr/cvt161
6. Knijff-Dutmer E, Koerts J, Nieuwland R, Kalsbeek-Batenburg E, Van De Laar M. Elevated Levels of Platelet Microparticles Are Associated With Disease Activity in Rheumatoid Arthritis. *Arthritis Rheumatol* (2002) 46(6):1498–503. doi: 10.1002/art.10312
7. Reid V, Webster N. Role of Microparticles in Sepsis. *Br J Anaesth* (2012) 109 (4):503–13. doi: 10.1093/bja/aes321
8. Soni S, Garner JL, O'Dea KP, Koh M, Finney L, Tirlapur N, et al. Intra-Alveolar Neutrophil-Derived Microvesicles Are Associated With Disease Severity in COPD. *Am J Physiol Lung Cell Mol Physiol* (2021) 320(1):L73–83. doi: 10.1152/ajplung.00099.2020
9. Soni S, Wilson MR, O'dea KP, Yoshida M, Katbeh U, Woods SJ, et al. Alveolar Macrophage-Derived Microvesicles Mediate Acute Lung Injury. *Thorax* (2016) 71(11):1020–9. doi: 10.1136/thoraxjnl-2015-208032
10. Soni S, O'Dea KP, Tan YY, Cho K, Abe E, Romano R, et al. ATP Redirects Cytokine Trafficking and Promotes Novel Membrane TNF Signaling *via* Microvesicles. *FASEB J* (2019) 33(5):6442–55. doi: 10.1096/fj.201802386R
11. Lee H, Zhang D, Wu J, Otterbein LE, Jin Y. Lung Epithelial Cell–Derived Microvesicles Regulate Macrophage Migration *via* MicroRNA-17/221–Induced Integrin β1 Recycling. *J Immunol* (2017) 199(4):1453–64. doi: 10.4049/jimmunol.1700165
12. Takahashi T, Kobayashi S, Fujino N, Suzuki T, Ota C, He M, et al. Increased Circulating Endothelial Microparticles in COPD Patients: A Potential Biomarker for COPD Exacerbation Susceptibility. *Thorax* (2012) 67 (12):1067–74. doi: 10.1136/thoraxjnl-2011-201395
13. Bacha NC, Blandinieres A, Rossi E, Gendron N, Nevo N, Lecourt S, et al. Endothelial Microparticles are Associated to Pathogenesis of Idiopathic Pulmonary Fibrosis. *Stem Cell Rev Rep* (2018) 14(2):223–35. doi: 10.1007/s12015-017-9778-5
14. Beyer C, Pisetsky DS. The Role of Microparticles in the Pathogenesis of Rheumatic Diseases. *Nat Rev Rheumatol* (2010) 6(1):21–9. doi: 10.1038/nrrheum.2009.229
15. Pizzirani C, Ferrari D, Chiozzi P, Adinolfi E, Sandona D, Savaglio E, et al. Stimulation of P2 Receptors Causes Release of IL-1β–Loaded Microvesicles From Human Dendritic Cells. *Blood* (2007) 109(9):3856–64. doi: 10.1182/blood-2005-06-031377
16. Dasgupta SK, Le A, Chavakis T, Rumbaut RE, Thiagarajan P. Developmental Endothelial Locus-1 (Del-1) Mediates Clearance of Platelet Microparticles by the Endothelium. *Circulation* (2012) 125(13):1664–72. doi: 10.1161/CIRCULATIONAHA.111.068833
17. Tan YY, O'Dea KP, Soni S, Shah S, Patel BV, Takata M. Enhanced Recognition and Internalisation of Microvesicles by Lung-Marginated, Ly-6chigh Monocytes During Endotoxaemia. *FASEB J* (2017) 31(1 Supplement):327.7. doi: 10.1096/fasebj.31.1_supplement.327.7
18. Parolini I, Federici C, Raggi C, Lugini L, Palleschi S, De Milito A, et al. Microenvironmental pH Is a Key Factor for Exosome Traffic in Tumor Cells. *J Biol Chem* (2009) 284(49):34211–22. doi: 10.1074/jbc.M109.04115

19. Han CZ, Juncadella IJ, Kinchen JM, Buckley MW, Klibanov AL, Dryden K, et al. Macrophages Redirect Phagocytosis by Non-Professional Phagocytes and Influence Inflammation. *Nature* (2016) 539(7630):570–4. doi: 10.1038/nature20141
20. O'Dea KP, Tan YY, Shah S, V Patel B, C Tatham K, Wilson MR, et al. Monocytes Mediate Homing of Circulating Microvesicles to the Pulmonary Vasculature During Low-Grade Systemic Inflammation. *J Extracell Vesicles* (2020) 9(1):1706708. doi: 10.1080/20013078.2019.1706708
21. Osteikoetxea X, Sódar B, Németh A, Szabó-Taylor K, Pálóczi K, Vukman KV, et al. Differential Detergent Sensitivity of Extracellular Vesicle Subpopulations. *Org Biomol Chem* (2015) 13(38):9775–82. doi: 10.1039/C5OB01451D
22. Fritz JM, Dwyer-Nield LD, Malkinson AM. Stimulation of Neoplastic Mouse Lung Cell Proliferation by Alveolar Macrophage-Derived, Insulin-Like Growth Factor-1 Can be Blocked by Inhibiting MEK and PI3K Activation. *Mol Cancer* (2011) 10(1):76. doi: 10.1186/1476-4598-10-76
23. Bourdonnay E, Zasłona Z, Penke LRK, Speth JM, Schneider DJ, Przybranowski S, et al. Transcellular Delivery of Vesicular SOCS Proteins From Macrophages to Epithelial Cells Blunts Inflammatory Signaling. *J Exp Med* (2015) 212(5):729–42. doi: 10.1084/jem.20141675
24. Schneider DJ, Speth JM, Penke LR, Wettlaufer SH, Swanson JA, Peters-Golden M. Mechanisms and Modulation of Microvesicle Uptake in a Model of Alveolar Cell Communication. *J Biol Chem* (2017) 292(51):20897–910. doi: 10.1074/jbc.M117.792416
25. Sharma AK, Fernandez LG, Awad AS, Kron IL, Laubach VE. Proinflammatory Response of Alveolar Epithelial Cells Is Enhanced by Alveolar Macrophage-Produced TNF-α During Pulmonary Ischemia-Reperfusion Injury. *Am J Physiol Lung Cell Mol Physiol* (2007) 293(1): L105–L13. doi: 10.1152/ajplung.00470.2006
26. Bachurski CJ, Pryhuber GS, Glasser SW, Kelly SE, Whitsett JA. Tumor Necrosis Factor-α Inhibits Surfactant Protein C Gene Transcription. *J Biol Chem* (1995) 270(33):19402–7. doi: 10.1074/jbc.270.33.19402
27. Kazeros A, Harvey B-G, Carolan BJ, Vanni H, Krause A, Crystal RG. Overexpression of Apoptotic Cell Removal Receptor MERTK in Alveolar Macrophages of Cigarette Smokers. *Am J Respir Cell Mol Biol* (2008) 39 (6):747–57. doi: 10.1165/rcmb.2007-0306OC
28. Mohning MP, Thomas SM, Barthel L, Mould KJ, McCubbrey AL, Frasch SC, et al. Phagocytosis of Microparticles by Alveolar Macrophages During Acute Lung Injury Requires MerTK. *Am J Physiol Lung Cell Mol Physiol* (2017) 314 (1):L69–82. doi: 10.1152/ajplung.00058.2017
29. Hoffmann PR, Ogden CA, Leverrier Y, Bratton DL, Daleke DL, Ridley AJ, et al. Phosphatidylserine (PS) Induces PS Receptor–Mediated Macropinocytosis and Promotes Clearance of Apoptotic Cells. *J Cell Biol* (2001) 155(4):649–60. doi: 10.1083/jcb.200108080
30. Odrljin TM, Haidaris CG, Lerner NB, Simpson-Haidaris PJ. Integrin α V β 3-Mediated Endocytosis of Immobilized Fibrinogen by A549 Lung Alveolar Epithelial Cells. *Am J Respir Cell Mol Biol* (2001) 24(1):12–21. doi: 10.1165/ajrcmb.24.1.3992
31. Pande P, Mosleh TA, Aust AE. Role of αvβ5 Integrin Receptor in Endocytosis of Crocidolite and Its Effect on Intracellular Glutathione Levels in Human Lung Epithelial (A549) Cells. *Toxicol Appl Pharmacol* (2006) 210(1-2):70–7. doi: 10.1016/j.taap.2005.07.017
32. França A, Aggarwal P, Barsov EV, Kozlov SV, Dobrovolskaia MA, González-Fernández Á. Macrophage Scavenger Receptor A Mediates the Uptake of Gold Colloids by Macrophages *In Vitro*. *Nanomedicine* (2011) 6(7):1175–88. doi: 10.2217/nnm.11.41
33. Palecanda A, Paulauskis J, Al-Mutairi E, Imrich A, Qin G, Suzuki H, et al. Role of the Scavenger Receptor MARCO in Alveolar Macrophage Binding of Unopsonized Environmental Particles. *J Exp Med* (1999) 189(9):1497–506. doi: 10.1084/jem.189.9.1497
34. Dodd CE, Pyle CJ, Glowinski R, Rajaram MV, Schlesinger LS. CD36-Mediated Uptake of Surfactant Lipids by Human Macrophages Promotes Intracellular Growth of Mycobacterium Tuberculosis. *J Immunol* (2016) 197(12):4727–35. doi: 10.4049/jimmunol.1600856
35. Song L, Lee C, Schindler C. Deletion of the Murine Scavenger Receptor CD68. *J Lipid Res* (2011) 52(8):1542–50. doi: 10.1194/jlr.M015412
36. Feng D, Zhao WL, Ye YY, Bai XC, Liu RQ, Chang LF, et al. Cellular Internalization of Exosomes Occurs Through Phagocytosis. *Traffic* (2010) 11(5):675–87. doi: 10.1111/j.1600-0854.2010.01041
37. Miyanishi M, Tada K, Koike M, Uchiyama Y, Kitamura T, Nagata S. Identification of Tim4 as a Phosphatidylserine Receptor. *Nature* (2007) 450 (7168):435. doi: 10.1038/nature06307
38. Mulcahy LA, Pink RC, Carter DRF. Routes and Mechanisms of Extracellular Vesicle Uptake. *J Extracell Vesicles* (2014) 3(1):24641. doi: 10.3402/jev.v3.24641
39. Al-Nedawi K, Meehan B, Kerbel RS, Allison AC, Rak J. Endothelial Expression of Autocrine VEGF Upon the Uptake of Tumor-Derived Microvesicles Containing Oncogenic EGFR. *Proc Natl Acad Sci* (2009) 106(10):3794–9. doi: 10.1073/pnas.0804543106
40. Soni S, Tirlapur N, O'Dea KP, Takata M, Wilson MR. Microvesicles as New Therapeutic Targets for the Treatment of the Acute Respiratory Distress Syndrome (ARDS). *Expert Opin Ther Targets* (2019) 23(11):931–41. doi: 10.1080/14728222.2019.1692816
41. Cicko S, Köhler TC, Ayata CK, Müller T, Ehrat N, Meyer A, et al. Extracellular ATP Is a Danger Signal Activating P2X7 Receptor in a LPS Mediated Inflammation (ARDS/ALI). *Oncotarget* (2018) 9(55):30635. doi: 10.18632/oncotarget.25761
42. Raggi F, Pelassa S, Pierobon D, Penco F, Gattorno M, Novelli F, et al. Regulation of Human Macrophage M1–M2 Polarization Balance by Hypoxia and the Triggering Receptor Expressed on Myeloid Cells-1. *Front Immunol* (2017) 8:1097. doi: 10.3389/fimmu.2017.01097
43. Ganesan S, Faris AN, Comstock AT, Sonstein J, Curtis JL, Sajjan US. Elastase/LPS-Exposed Mice Exhibit Impaired Innate Immune Responses to Bacterial Challenge: Role of Scavenger Receptor A. *Am J Pathol* (2012) 180(1):61–72. doi: 10.1016/j.ajpath.2011.09.029
44. Doherty GJ, McMahon HT. Mechanisms of Endocytosis. *Ann Rev Biochem* (2009) 78:857–902. doi: 10.1146/annurev.biochem.78.081307.110540
45. Voigt J, Christensen J, Shastri VP. Differential Uptake of Nanoparticles by Endothelial Cells Through Polyelectrolytes With Affinity for Caveolae. *Proc Natl Acad Sci* (2014) 111(8):2942–7. doi: 10.1073/pnas.1322356111
46. Montecalvo A, Larregina AT, Shufesky WJ, Stolz DB, Sullivan ML, Karlsson JM, et al. Mechanism of Transfer of Functional microRNAs Between Mouse Dendritic Cells *via* Exosomes. *Blood* (2012) 119(3):756–66. doi: 10.1182/blood-2011-02-338004
47. Fitzner D, Schnaars M, van Rossum D, Krishnamoorthy G, Dibaj P, Bakhti M, et al. Selective Transfer of Exosomes From Oligodendrocytes to Microglia by Macropinocytosis. *J Cell Sci* (2011) 124(3):447–58. doi: 10.1242/jcs.074088
48. Macia E, Ehrlich M, Massol R, Boucrot E, Brunner C, Kirchhausen T. Dynasore, a Cell-Permeable Inhibitor of Dynamin. *Dev Cell* (2006) 10 (6):839–50. doi: 10.1016/j.devcel.2006.04.002
49. Kuhn DA, Vanhecke D, Michen B, Blank F, Gehr P, Petri-Fink A, et al. Different Endocytotic Uptake Mechanisms for Nanoparticles in Epithelial Cells and Macrophages. *Beilstein J Nanotechnol* (2014) 5:1625. doi: 10.3762/bjnano.5.174
50. Platt N, Suzuki H, Kurihara Y, Kodama T, Gordon S. Role for the Class A Macrophage Scavenger Receptor in the Phagocytosis of Apoptotic Thymocytes *In Vitro*. *Proc Natl Acad Sci* (1996) 93(22):12456–60. doi: 10.1073/pnas.93.22.12456
51. Platt N, Gordon S. Is the Class A Macrophage Scavenger Receptor (SR-A) Multifunctional?—The Mouse's Tale. *J Clin Invest* (2001) 108(5):649–54. doi: 10.1172/JCI13903
52. Nishikawa K, Arai H, Inoue K. Scavenger Receptor-Mediated Uptake and Metabolism of Lipid Vesicles Containing Acidic Phospholipids by Mouse Peritoneal Macrophages. *J Biol Chem* (1990) 265(9):5226–31. doi: 10.1016/S0021-9258(19)34110-9
53. Podrez EA, Febbraio M, Sheibani N, Schmitt D, Silverstein RL, Hajjar DP, et al. Macrophage Scavenger Receptor CD36 Is the Major Receptor for LDL Modified by Monocyte-Generated Reactive Nitrogen Species. *J Clin Invest* (2000) 105(8):1095–108. doi: 10.1172/JCI8574
54. Thelen T, Hao Y, Medeiros AI, Curtis JL, Serezani CH, Kobzik L, et al. The Class A Scavenger Receptor, Macrophage Receptor With Collagenous Structure, Is the Major Phagocytic Receptor for Clostridium Sordellii Expressed by Human Decidual Macrophages. *J Immunol* (2010) 185 (7):4328–35. doi: 10.4049/jimmunol.1000989
55. Pfeiler S, Thakur M, Grünauer P, Megens RT, Joshi U, Coletti R, et al. CD36-Triggered Cell Invasion and Persistent Tissue Colonization by Tumor Microvesicles During Metastasis. *FASEB J* (2019) 33(2):1860–72. doi: 10.1096/fj.201800985R

56. Kanno S, Hirano S, Sakamoto T, Furuyama A, Takase H, Kato H, et al. Scavenger Receptor MARCO Contributes to Cellular Internalization of Exosomes by Dynamin-Dependent Endocytosis and Macropinocytosis. *Sci Rep* (2020) 10(1):1–12. doi: 10.1038/s41598-020-78464-2

Conflict of Interest: The authors declare that the research was conducted in the absence of any commercial or financial relationships that could be construed as a potential conflict of interest.

Publisher's Note: All claims expressed in this article are solely those of the authors and do not necessarily represent those of their affiliated organizations, or those of the publisher, the editors and the reviewers. Any product that may be evaluated in this article, or claim that may be made by its manufacturer, is not guaranteed or endorsed by the publisher.

frontiers | Frontiers in Immunology

ORIGINAL RESEARCH
published: 09 June 2022
doi: 10.3389/fimmu.2022.895501

Endothelin B Receptor Immunodynamics in Pulmonary Arterial Hypertension

*Christoph Tabeling[1,2,3], Carla R. González Calera[1], Jasmin Lienau[1], Jakob Höppner[4], Thomas Tschernig[5], Olivia Kershaw[6], Birgitt Gutbier[1], Jan Naujoks[2], Julia Herbert[1], Bastian Opitz[2], Achim D. Gruber[6], Berthold Hocher[7,8,9], Norbert Suttorp[2,10], Harald Heidecke[11], Gerd-R. Burmester[4], Gabriela Riemekasten[12], Elise Siegert[3,4], Wolfgang M. Kuebler[10,13,14,15,16] and Martin Witzenrath[1,2,10]**

[1] Division of Pulmonary Inflammation, Charité - Universitätsmedizin Berlin, Corporate Member of Freie Universität Berlin and Humboldt-Universität zu Berlin, Berlin, Germany, [2] Department of Infectious Diseases and Respiratory Medicine, Charité - Universitätsmedizin Berlin, Corporate Member of Freie Universität Berlin and Humboldt-Universität zu Berlin, Berlin, Germany, [3] Berlin Institute of Health at Charité - Universitätsmedizin Berlin, Berlin, Germany, [4] Department of Rheumatology and Clinical Immunology, Charité - Universitätsmedizin Berlin, Corporate Member of Freie Universität Berlin and Humboldt-Universität zu Berlin, Berlin, Germany, [5] Institute of Anatomy and Cell Biology, University of Saarland, Homburg, Germany, [6] Department of Veterinary Pathology, Freie Universität Berlin, Berlin, Germany, [7] Fifth Department of Medicine (Nephrology/Endocrinology/Rheumatology), University of Heidelberg, University Medical Centre Mannheim, Heidelberg, Germany, [8] Key Laboratory of Study and Discovery of Small Targeted Molecules of Hunan Province, School of Medicine, Hunan Normal University, Changsha, China, [9] Reproductive and Genetic Hospital of CITIC-Xiangya, Changsha, China, [10] German Center for Lung Research (DZL), Partner Site Charité, Berlin, Germany, [11] CellTrend GmbH, Luckenwalde, Germany, [12] Department of Rheumatology, University of Lübeck, Lübeck, Germany, [13] Institute of Physiology, Charité - Universitätsmedizin Berlin, Corporate Member of Freie Universität Berlin and Humboldt-Universität zu Berlin, Berlin, Germany, [14] German Center for Cardiovascular Research (DZHK), Partner Site, Berlin, Germany, [15] St. Michael's Hospital, Keenan Research Centre for Biomedical Science, Toronto, ON, Canada, [16] Departments of Physiology and Surgery, University of Toronto, Toronto, ON, Canada

OPEN ACCESS

Edited by:
Rudolf Lucas,
Augusta University, United States

Reviewed by:
Dustin Fraidenburg,
University of Illinois at Chicago, United States
Robert Naeije,
Université libre de Bruxelles, Belgium

***Correspondence:**
Martin Witzenrath
martin.witzenrath@charite.de

Specialty section:
This article was submitted to Inflammation, a section of the journal Frontiers in Immunology

Received: 13 March 2022
Accepted: 09 May 2022
Published: 09 June 2022

Citation:
Tabeling C, González Calera CR, Lienau J, Höppner J, Tschernig T, Kershaw O, Gutbier B, Naujoks J, Herbert J, Opitz B, Gruber AD, Hocher B, Suttorp N, Heidecke H, Burmester GR, Riemekasten G, Siegert E, Kuebler WM and Witzenrath M (2022) Endothelin B Receptor Immunodynamics in Pulmonary Arterial Hypertension. Front. Immunol. 13:895501. doi: 10.3389/fimmu.2022.895501

Introduction: Inflammation is a major pathological feature of pulmonary arterial hypertension (PAH), particularly in the context of inflammatory conditions such as systemic sclerosis (SSc). The endothelin system and anti-endothelin A receptor (ET_A) autoantibodies have been implicated in the pathogenesis of PAH, and endothelin receptor antagonists are routinely used treatments for PAH. However, immunological functions of the endothelin B receptor (ET_B) remain obscure.

Methods: Serum levels of anti-ET_B receptor autoantibodies were quantified in healthy donors and SSc patients with or without PAH. Age-dependent effects of overexpression of prepro-endothelin-1 or ET_B deficiency on pulmonary inflammation and the cardiovascular system were studied in mice. Rescued ET_B-deficient mice ($ET_B^{-/-}$) were used to prevent congenital Hirschsprung disease. The effects of pulmonary T-helper type 2 (Th2) inflammation on PAH-associated pathologies were analyzed in $ET_B^{-/-}$ mice. Pulmonary vascular hemodynamics were investigated in isolated perfused mouse lungs. Hearts were assessed for right ventricular hypertrophy. Pulmonary inflammation and collagen deposition were assessed *via* lung microscopy and bronchoalveolar lavage fluid analyses.

Results: Anti-ET_B autoantibody levels were elevated in patients with PAH secondary to SSc. Both overexpression of prepro-endothelin-1 and rescued ET_B deficiency led to pulmonary hypertension, pulmonary vascular hyperresponsiveness, and right ventricular hypertrophy with accompanying lymphocytic alveolitis. Marked perivascular lymphocytic infiltrates were exclusively found in $ET_B^{-/-}$ mice. Following induction of pulmonary Th2 inflammation, PAH-associated pathologies and perivascular collagen deposition were aggravated in $ET_B^{-/-}$ mice.

Conclusion: This study provides evidence for an anti-inflammatory role of ET_B. ET_B seems to have protective effects on Th2-evoked pathologies of the cardiovascular system. Anti-ET_B autoantibodies may modulate ET_B-mediated immune homeostasis.

Keywords: endothelin B receptor, autoantibody, Th2 inflammation, pulmonary vascular hyperresponsiveness, pulmonary arterial hypertension, systemic sclerosis

INTRODUCTION

Despite modern therapy, pulmonary arterial hypertension (PAH) remains a fatal condition. PAH is characterized by construction and remodelling of pulmonary arteries leading to increased pulmonary vascular resistance and right heart failure (1).

An increasing body of evidence points to inflammation as a central pathogenic factor in idiopathic PAH (iPAH) as well as PAH secondary to other conditions (2–8). Perivascular inflammation and lymphoid tissue are found in lungs of PAH patients, and concordantly in murine models of pulmonary hypertension (2, 9–12). Elevated numbers of mast cells and T-helper type 2 (Th2) lymphocytes as well as increased expression of Th2 cytokines were repeatedly found in patients with pulmonary hypertension (2, 8, 13–16). Analogously, preclinical studies indicate an important underlying role of Th2-mediated immune signaling in the induction of morphological and functional changes found in PAH (2, 16–23).

The concept that the endothelium-derived peptide endothelin-1 (ET-1) serves as a major driver of PAH pathobiology is broadly accepted (1, 24–26). Prepro-endothelin-1 is the precursor of big-ET-1, which is converted to mature, bioactive ET-1 (24, 26, 27). Patients with pulmonary hypertension show elevated pulmonary vascular expression of ET-1 as well as increased levels of circulating ET-1 (25, 28).

ET-1 is a potent vasoconstrictor in the pulmonary circulation through activation of the G protein-coupled receptors endothelin A receptor (ET_A) and endothelin B receptor (ET_B) expressed on pulmonary arterial smooth muscle cells (PASMCs) (26, 27). The vasoconstrictive response induced by ET-1 involves thromboxane A_2 (TXA_2) release and consecutive TXA_2 receptor activation (29, 30). Downstream signalling of ET-1-evoked vasoconstriction critically depends on protein kinase C isozyme alpha (PKCα) (31). Contrariwise, activation of ET_B located on endothelial cells induces vasodilation *via* release of nitric oxide (NO) and prostaglandins (26, 27), partially dampening the vasoconstrictive effects of ET-1.

Besides its vasomotor actions, ET-1 promotes immune cell trafficking (32), such as *via* release of tumor necrosis factor alpha (TNF-α), interleukin (IL)-1β, and IL-6 from monocytes and macrophages (33), or *via* ET_A-dependent release of IL-6 from vascular smooth muscle cells (34).

Endothelin receptor antagonists (ERAs) are routinely used for the treatment of PAH. However, whether ET_A-selective targeting or dual inhibition of ET_A/ET_B is superior to the other is controversially discussed.

In systemic sclerosis (SSc), PAH is a common vascular complication, and an important driver of mortality (24). The prognosis of PAH secondary to SSc (SSc-PAH) has been critically linked to the presence of anti-ET_A autoantibodies (AAb) (35). Autoimmunity is believed to play a significant role in PAH pathobiology (2, 5, 6, 35–40), and blood plasmablast levels were shown to be elevated in PAH patients (36). However, the potential involvement of anti-ET_B AAb in PAH is currently unknown and the immunomodulatory role of ET_B in the context of pulmonary hypertension remains largely elusive.

In this study, anti-ET_B AAb levels were assessed in PAH patients for the first time. To better characterize the immunomodulatory functions of ET_B, we additionally studied the effects of rescued ET_B deficiency in mice on pulmonary vascular disease, independent of and dependent on pulmonary Th2 inflammation.

Circulating ET-1 is cleared from the blood *via* ET-1/ET_B complex internalization (27, 41–43) and ET_B deficiency results in increased ET-1 plasma levels (44–46). Thus, effects on PAH-associated cardiovascular pathologies were studied in parallel in

Abbreviations: AT_1R, angiotensin II type 1 receptor; AAb, autoantibody; BAL, bronchoalveolar lavage; BMPR2, bone morphogenetic protein receptor type 2; C_{dyn}, dynamic lung compliance; ET-1, endothelin-1; ET_A, endothelin A receptor; ET_B, endothelin B receptor; ERA, endothelin receptor antagonist; H&E, hematoxylin and eosin; IgG, immunoglobulin G; IL, interleukin; IL-12p40, IL-12 subunit p40; NO, nitric oxide; OVA, ovalbumin; OVA/OVA, OVA-sensitized and OVA-challenged; PAH, pulmonary arterial hypertension; PBS, phosphate buffered saline; PBS/PBS, non-sensitized and non-challenged (PBS-treated); PASMCs, pulmonary arterial smooth muscle cells; Ppa, pulmonary arterial pressure; SSc, systemic sclerosis; Th2, T-helper type 2; TNF-α, tumor necrosis factor alpha; TXA_2, thromboxane A_2; TXB_2, thromboxane B_2; VIP, vasoactive intestinal peptide.

mice overexpressing prepro-ET-1 ($_{pre}ET^{tg}$) to allow differentiation between ET-1- and ET_B-mediated effects.

We hypothesized that ET_B plays an anti-inflammatory role, alleviating Th2-evoked pathologies of the cardiovascular system.

MATERIALS AND METHODS

Patients and Clinical Manifestations

Serum samples from 177 SSc patients referred to the Department of Rheumatology and Clinical Immunology at Charité - Universitätsmedizin Berlin were collected. Patients with SSc met the American College of Rheumatology/European League Against Rheumatism 2013 classification (47). SSc patients were classified as having either limited cutaneous SSc or diffuse cutaneous SSc or SSc sine scleroderma, according to the LeRoy criteria, depending on the distribution and history of skin sclerosis at the study visit. The first non-Raynaud symptom was considered as disease onset.

Under clinical routine conditions, patients were screened for PAH at least in 1-year intervals by assessment of World Health Organization functional class, echocardiography, lung function including single-breath diffusion capacity for carbon monoxide ($DLCO_{SB}$), and, during the last few years, also by the detection of N-terminal pro-brain natriuretic peptide (NT-proBNP) levels. In all SSc patients in which PAH was suspected, diagnosis was confirmed by right heart catheterization. Interstitial lung disease was identified on the basis of a high-resolution computed tomographic scan, as confirmed by an expert radiologist. Additional serum samples were obtained from 10 iPAH patients, confirmed by right heart catheterization. Control serum samples were obtained from 26 healthy subjects.

The epidemiologic data of patients and healthy donors are shown in **Supplementary Table 1**. The study protocol was approved by the ethics committee (Charité - Universitätsmedizin Berlin; EA1/179/17). A written informed consent was obtained from each patient. The study was conducted in accordance with the principles of the Declaration of Helsinki.

Detection of Anti-ET_B AAb

Prior to analysis, serum samples were stored at −80°C. Serum ET_B antibody levels were measured in duplicate by ELISA (CellTrend GmbH, Luckenwalde, Germany) in a blinded manner as described (35, 48). In brief, microtiter plates were coated with extracts from Chinese hamster ovary cells overexpressing human ET_B. Calcium chloride (1 mmol/L) was administered to each buffer for maintenance of conformational epitopes. Diluted serum samples were incubated (1:100, 4°C, 2 h). For detection, plates were washed and incubated for 1 h with horseradish peroxidase-labeled goat anti-human immunoglobulin G (IgG; 1:20,000; Jackson, West Grove, Pennsylvania, USA), followed by enzymatic substrate reaction. Optical densities were converted into concentrations (U/ml) by comparison to a standard curve. Concentrations below the limit of detection (LOD) were depicted as LOD/√2.

Mice

All animal procedures were approved by institutional authorities of the Charité - Universitätsmedizin Berlin and the Local State Office of Health and Social Affairs Berlin (LAGeSo; Berlin, Germany). Transgenic mice overexpressing human prepro-ET-1 ($_{pre}ET^{tg}$) on a mixed NMRI/C57BL/6 background rescued endothelin B receptor-deficient mice ($ET_B^{-/-}$) on a mixed C57BL/6/129 background and the respective corresponding wild-type mice were housed under specific pathogen-free conditions. The generation of $_{pre}ET^{tg}$ mice (49) and rescued ET_B-deficient mice (50) has been described elsewhere. Rescued ET_B-deficient mice hold a dopamine-β-hydroxylase ET_B transgene to prevent fatal congenital Hirschsprung disease (50).

Isolated Perfused Mouse Lung

Here, we used the isolated perfused mouse lung preparation to evaluate pulmonary hemodynamics *ex vivo*. While this approach does not allow determining whether a specific model fulfills the clinical criteria of pulmonary hypertension *in vivo* (which is, however, obscured anyway by the fact that invasive hemodynamic measurements in mice are commonly restricted to recordings of right ventricular systolic pressure rather than mean Ppa), constant perfusion rates and defined left atrial pressures allow for a sensitive assessment of differences in pulmonary vascular resistance independent of right and left ventricular function.

Anesthetized mice were prepared, lungs were isolated, and pulmonary artery and left atrium were cannulated as described (51–53). Lungs were perfused constantly (1 mL/min, nonrecirculating, left atrial pressure 2.2 cmH_2O) with 37°C sterile Krebs-Henseleit hydroxyethyl amylopectin buffer (Serag-Wiessner, Naila, Germany). Negative pressure ventilation was performed (*P*exp −4.5, *P*ins −9.0 cmH_2O, 90 breaths/min). Pulmonary arterial pressure (Ppa) and dynamic lung compliance (C_{dyn}) were measured and recorded *via* Pulmodyn software (17). ET-1, thromboxane analog U46619, or serotonin (all Merck KGaA, Darmstadt, Germany) was administered to the perfusion buffer for 10, 3, or 0.5 min, respectively (31). Doses were increased following intervals of 24 (ET-1), 12 (U46619), or 8 min (serotonin). Vasopressor responses were calculated (maximal difference in Ppa, Δ Ppa). To determine the role of ET_A, ET_A inhibitor BQ-123 (8 µmol/L; Merck KGaA) or solvent (aqua dest.) was added to the perfusion buffer 10 min prior to ET-1 application. Lungs with signs of edema, atelectasis, or hemostasis were excluded from further analyses.

Fulton Index

Hearts were excised. Right ventricle and left ventricle plus adjacent septum were microscopically dissected and weighed. Fulton index [quotient of right ventricle (RV) and left ventricle (LV) including septum (S)] was calculated.

Pulmonary Th2 Inflammation

After systemic sensitization *via* i.p. injections of 20 µg of ovalbumin (OVA; grade V; Merck KGaA) dissolved in 100 µL of aluminum hydroxide suspension (1.3%; SERVA

Electrophoresis GmbH, Heidelberg, Germany) and 10 µL of phosphate-buffered saline (PBS) on days 0 and 14, mice were repeatedly exposed to aerosolized ovalbumin (1%) in PBS on days 28–30 for 20 min/day (53, 54). On the respective days, sham-treated mice received i.p. injections of 100 µL of aluminum hydroxide suspension and 10 µL of PBS, followed by exposure to aerosolized PBS. Effects of pulmonary Th2 inflammation were analyzed on day 32.

Bronchoalveolar Lavage

Bronchoalveolar lavage (BAL) of the right lung was performed twice with 650 µL of ice-cold PBS containing protease inhibitor (cOmplete™ mini; Merck KGaA) (55, 56). Total cell numbers and leukocyte differentiation were determined by microscopic analysis blinded to the study groups. Cytokines from the BAL fluid supernatant of the first lavage were quantified according to the manufacturer´s instructions using a cytokine multiplex assay (Bioplex®; Bio-Rad Laboratories GmbH, Feldkirchen, Germany).

Lung Histopathology

Lungs were removed and immersion fixed for 24 h with 4% buffered formaldehyde solution pH 7.0 (Merck KGaA). After embedding in paraffin, tissue sections were cut with a microtome, mounted onto glass slides, and stained.

For histopathological analyses of naïve mice, 3-µm sections were either stained with hematoxylin and eosin (H&E) or immunostained for CD45R/B220 (B cells, monoclonal, 1:1,000, clone RA3-6B2, 553086; BD Biosciences, Heidelberg, Germany) or CD3 (T cells, polyclonal, 1:800; reference A0452; Dako, Santa Clara, CA, USA). Positive immunostaining was visualized using diaminobenzidine, and slides were counterstained with hematoxylin. For analyses of the effects of pulmonary Th2 inflammation, 5-µm tissue sections were either stained with H&E or Masson–Goldner trichrome.

Microscopic analyses were performed (Axiophot; Carl Zeiss Microscopy GmbH, Jena, Germany) in a blinded fashion by a board-certified veterinary pathologist or an anatomist and images were digitized (Color View II camera, CellSens software; Olympus Europa SE Co. KG, Hamburg, Germany).

Real-Time Quantitative RT-PCR

Gene expression was analyzed as described (31, 57). Lung tissue was homogenized in Trizol (Thermo Fisher Scientific, Dreieich, Germany), and RNA was extracted. Reverse transcription (RT) of total RNA was performed (high-capacity reverse transcription kit; Thermo Fisher Scientific). For quantitative RT-PCR (ABI 7300 instrument; Thermo Fisher Scientific), TaqMan assays (Life Technologies) were applied for the target genes ET_A, TXA_2 receptor, and ET-1. TaqMan assay IDs were Mm01243722_m1 (ET_A), Mm00436917_m1 (TXA_2 receptor), and Mm00438656_m1 (ET-1). Glyceraldehyde 3-phosphate dehydrogenase (GAPDH) served as internal reference. GAPDH primer sequences were TGTGTCCGTCGTGGATCTGA (forward, 5' to 3'), CCTGCTTCACCACCTTCTTGA (reverse, 5' to 3'), and CCGCCTGGAGAAACCTGCCAAGTATG (probe, 5'-FAM to 3'-TAMRA) (57). The relative expression (relative quantity, RQ) of each target gene was quantified using the comparative C_t method, with relative expression set to 1 in PBS-treated WT mice (31, 57).

TXB_2 and VIP Quantification

Thromboxane B_2 (TXB_2) perfusate levels and vasoactive intestinal peptide (VIP) plasma levels were quantified *via* enzyme immunoassay (EIA) according to the respective manufacturer's guide (TXB_2 EIA; Cayman Chemical, MI, USA; detection limit 7.8 pg/mL; VIP EIA; Phoenix Europe GmbH, Karlsruhe, Germany; detection limit 0.05 ng/mL).

Statistical Analysis

For comparison of autoantibody levels, data were analyzed by one-way ANOVA followed by Dunnett's multiple comparisons test. Dose–response curves were compared using two-way repeated measures ANOVA. Mann–Whitney *U* test was performed for comparison between two groups. $*p < 0.05$, $**p < 0.01$, $***p < 0.001$.

RESULTS

Elevated Anti-ET_B Autoantibody Serum Levels in Patients With PAH Secondary to Systemic Sclerosis

Autoantibodies against ET_A were shown to be elevated in SSc-PAH patients (35). Analogously, in this study, anti-ET_B autoantibody serum levels were quantified in SSc patients with or without PAH as well as in iPAH patients and healthy donors. Compared to healthy donors, SSc-PAH patients showed increased levels of anti-ET_B AAb (**Figure 1**). In SSc patients without PAH as well as in iPAH patients, anti-ET_B AAb serum levels were increased by trend when compared to healthy donors (**Figure 1**). However, the relatively small number of iPAH serum samples needs to be considered. Detailed patient characteristics are found in **Supplementary Table 1**.

Pulmonary Hypertension, Right Ventricular Hypertrophy, and Lymphocytic Alveolitis in $_{pre}ET^{tg}$ and $ET_B^{-/-}$ Mice

To confirm the dual vasomotor role of ET-1 *via* ET_A and ET_B receptors in the pulmonary vasculature, functional analyses in isolated perfused mouse lungs were performed. In isolated WT lungs, application of the ET_A inhibitor BQ-123 resulted in an almost complete reduction of the pulmonary vascular pressure response to ET-1 compared with the solvent control (**Supplementary Figure 1A**), while rescued ET_B deficiency resulted in an elevated pulmonary vascular pressure response to ET-1 or the thromboxane receptor agonist U46619 compared to WT controls (**Supplementary Figures 1B, C**).

To dissect ET-1-specific as well as ET_B-specific effects on pulmonary inflammation and PAH-associated cardiovascular pathologies independent of additional inflammatory stimuli, we first investigated age-dependent effects in two transgenic mouse models of (i) prepro-ET-1 overexpression ($_{pre}ET^{tg}$) and (ii) rescued ET_B deficiency ($ET_B^{-/-}$). In line with the literature (58), young to mature-adult (2–6 months old) $_{pre}ET^{tg}$ mice did not

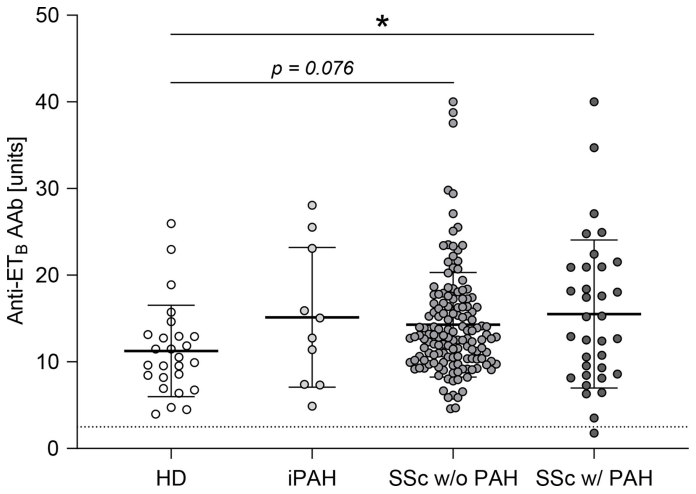

FIGURE 1 | Anti-ET_B autoantibody serum levels were elevated in patients with PAH secondary to SSc. Serum levels of anti-endothelin B receptor (ET_B) autoantibodies (AAb) were quantified in healthy donors (HD), patients with idiopathic pulmonary arterial hypertension (iPAH), and systemic sclerosis (SSc) patients (+/- interstitial lung disease) with or without PAH. Data are expressed as single values with mean ± SD; *N* = 26 (HD) or *N* = 10 (iPAH) or *N* = 143 (SSc w/o PAH) or *N* = 34 (SSc w/PAH). The dotted line indicates the lower detection limit of the ELISA. *$p < 0.05$ (one-way ANOVA and Dunnett's multiple comparisons test).

show pulmonary hypertension. However, in highly aged (16–18 months old) mice, prepro-ET-1 overexpression resulted in a significant increase in pulmonary arterial pressure compared to corresponding WT controls (**Figure 2A**). Furthermore, 2- to 6-month-old $_{pre}ET^{tg}$ mice demonstrated a moderate increase in pulmonary vascular responsiveness to thromboxane receptor agonist U46619 compared to corresponding WT mice, whereas pulmonary vascular responsiveness of 16- to 18-month old mice was comparable within both groups ($_{pre}ET^{tg}$ vs. WT) (**Figure 2B**). Cardiac analysis using the Fulton index (right ventricular weight/weight of left ventricle including septum) revealed right ventricular hypertrophy associated with chronic prepro-ET-1 overexpression in 16- to 18-month-old but not in 2- to 6-month-old mice (**Figure 2C**). Long-term overexpression of prepro-ET-1 was also associated with an increase in lymphocyte numbers in the BAL (**Figure 2D**). Independent of prepro-ET-1 overexpression, less BAL macrophages were found in 16- to 18-month-old vs. 2- to 6-month-old mice (**Figure 2D**).

In mature-adult (6 months old) $ET_B^{-/-}$ mice, basal pulmonary arterial pressure was significantly increased compared to WT mice of the same age (**Figure 3A**). Weight analysis of cardiac compartments revealed that $ET_B^{-/-}$ mice of both age groups exhibited right ventricular hypertrophy compared with their respective WT counterparts (**Figure 3B**). Furthermore, splenomegaly was present in $ET_B^{-/-}$ compared to WT mice and was progressive with age (**Figure 3C)** whereas relative liver weight was comparable in all groups (**Supplementary Figure 2A**). Cellular analysis of BAL fluid showed increased numbers of lymphocytes and macrophages in young $ET_B^{-/-}$ compared to WT mice (**Figure 3D**).

Basal dynamic lung compliance was found to be reduced in $ET_B^{-/-}$ compared to corresponding WT mice in both age groups (**Supplementary Figure 2B**), in contrast to $_{pre}ET^{tg}$ mice, which showed unaltered dynamic lung compliance (**Supplementary Figure 3**).

Perivascular Lymphoid Infiltrates in $ET_B^{-/-}$ Lungs

Compared to WT controls, $ET_B^{-/-}$ mice developed marked perivascular lymphocytic infiltrates (**Supplementary Figure 4**). In $ET_B^{-/-}$ mice, perivascular lymphocytic infiltrates were particularly observed in the peripheral lung tissue, which were absent from WT lungs (**Figure 4A**). These infiltrates mostly consisted of B cells (**Figure 4B**) and T cells (**Figure 4C**). Both the prevalence and number of these cell clusters increased with age, and infiltrates were present in almost all (14/15) >16 months old $ET_B^{-/-}$ mice (**Figure 4D**). Such perivascular cell clusters adjacent to small pulmonary arteries were absent in $_{pre}ET^{tg}$ mice (**Supplementary Figure 5**) pointing to an immunomodulatory role of ET_B in the lungs in the context of pulmonary hypertension.

Th2 Inflammation Aggravates PAH-Associated Pathologies in $ET_B^{-/-}$ Lungs

Next, we studied the effects of pulmonary Th2 inflammation as a second inflammatory hit in $ET_B^{-/-}$ mice. Pulmonary Th2 inflammation was induced *via* systemic ovalbumin sensitization and ovalbumin airway exposure (OVA/OVA).

Pulmonary arterial pressure was elevated in $ET_B^{-/-}$ compared to WT mice as described before, independent of pulmonary Th2 inflammation (**Figure 5A**). Following OVA/OVA treatment, pulmonary vascular hyperresponsiveness to ET-1 and U46619 was highly increased in $ET_B^{-/-}$ mice compared to WT mice (**Figure 5A**). Pulmonary vascular hyperresponsiveness to serotonin, however, was not increased in $ET_B^{-/-}$ as compared to WT mice (**Supplementary Figure 6A**).

Importantly, pulmonary Th2 inflammation aggravated right ventricular hypertrophy as well as splenomegaly in $ET_B^{-/-}$ mice compared to WT controls (**Figure 5B**). Liver weight in relation to body weight was comparable in all groups (**Supplementary Figure 6B**).

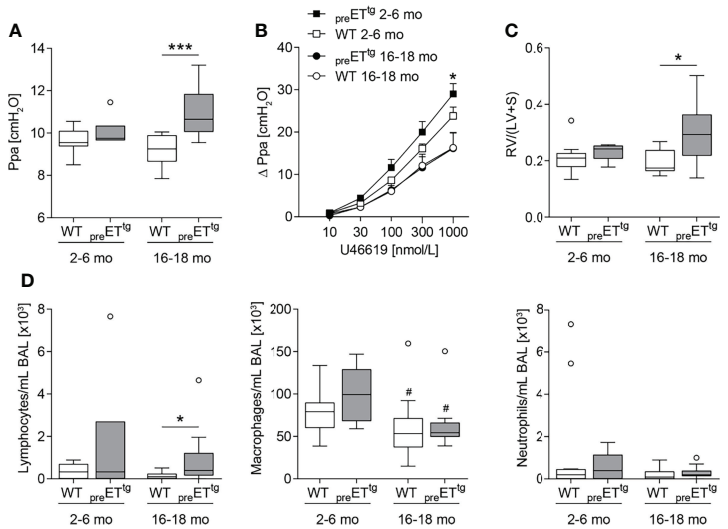

FIGURE 2 | Prepro-endothelin-1 overexpression was age-dependently associated with increased pulmonary arterial pressure, vascular hyperresponsiveness, right ventricular hypertrophy, and increased number of lymphocytes in bronchoalveolar lavage. Lungs and hearts of 2- to 6-month (mo)-old or 16- to 18-mo-old prepro-endothelin-1 overexpressing ($_{pre}ET^{tg}$) mice and corresponding wild-type (WT) mice were prepared, or bronchoalveolar lavage (BAL) was performed. **(A)** In isolated perfused and ventilated lungs, under basal conditions, 16- to 18-mo-old $_{pre}ET^{tg}$ showed a higher pulmonary arterial pressure (Ppa) compared to WT mice of the same age. **(B)** Pulmonary vascular responsiveness to intravascular application of the thromboxane receptor agonist U46619 was increased in 2- to 6-mo-old $_{pre}ET^{tg}$ mice compared to WT controls of the same age. Data (Δ Ppa) represent the difference between the highest pressure response to U46619 and the basal Ppa. **(C)** Fulton index [quotient of right ventricle (RV) and left ventricle (LV) including septum (S)] determined after weighing the cardiac compartments was higher in 16- to 18-mo-old $_{pre}ET^{tg}$ compared to WT mice of the same age. **(D)** Analysis of differentially quantified leukocytes in BAL showed increased number of lymphocytes in 16- to 18-mo-old $_{pre}ET^{tg}$ compared to WT mice of the same age, whereas macrophages decreased with age, independent of prepro-ET-1 overexpression. In **(A, C, D),** data are represented as *box plots* depicting median, quartiles, and ranges excluding outliers (*open circles*), and analyzed using Mann–Whitney *U* test. # indicates significant difference between 16- to 18-mo-old vs. 2- to 6-mo-old groups, * indicates significant difference between $_{pre}ET^{tg}$ vs. corresponding WT group (as indicated). In **(B)**, values are given as mean and SEM, and analyzed using two-way repeated measures ANOVA, followed by a single Mann–Whitney *U* test between values of $_{pre}ET^{tg}$ and WT mice of the same age at the highest dose of U46619 (*). In **(A–C)**, $N = 5–12$; in **(D)**, $N = 7–17$. $^{*/\#}p < 0.05$, $^{***}p < 0.001$.

The Th2-mediated inflammatory cell influx into the lung was increased in $ET_B^{-/-}$ mice as reflected by elevated BAL cell numbers including lymphocytes, neutrophils, and eosinophils (**Figure 5C**) and as revealed by more pronounced perivascular leukocyte infiltrates in $ET_B^{-/-}$ lungs (**Supplementary Figure 7**). While BAL Th2 cytokines IL-4, IL-5, and IL-13 in OVA/OVA-treated $ET_B^{-/-}$ mice were comparable with the respective WT mice (**Supplementary Table 2**), IL-12 subunit p40 (IL-12p40) levels were greatly increased in BAL of $ET_B^{-/-}$ mice (**Figure 5D**).

ET_B Deficiency Aggravates Th2-Mediated Collagen Deposition in the Lung

Th2 immune responses have been associated with pulmonary collagen deposition (59) and IL-12p40 is believed to possess profibrotic properties in the lung (60). Dynamic lung compliance was lowest in $ET_B^{-/-}$ mice after induction of pulmonary Th2 inflammation (**Figure 5E**). Accordingly, histological analyses of Masson–Goldner trichrome-stained lung slices revealed more pronounced collagen deposition in $ET_B^{-/-}$ lungs than in WT lungs following OVA/OVA treatment (**Figure 5F**).

ET_B Mediates Thromboxane Release Evoked by ET-1

To mechanistically dissect the pronounced increase in pulmonary vascular responsiveness to ET-1 in $ET_B^{-/-}$ mice (**Figure 5A**), we indirectly assessed pulmonary vascular TXA_2 release in isolated mouse lungs *via* quantification of stable TXB_2 in the perfusate before and after intravascular application of ET-1. Indeed, vascular thromboxane release following ET-1 application was highly elevated in $ET_B^{-/-}$ lungs (**Figure 6A**).

Increased vascular hyperresponsiveness secondary to ET_A and/or TXA_2 receptor upregulation, however, was ruled out *via* mRNA expression analyses. In $ET_B^{-/-}$ lungs, ET_A mRNA expression was downregulated while TXA_2 receptor mRNA expression was comparable (**Figure 6B**). Of note, rescued ET_B deficiency led to increased pulmonary ET-1 expression following induction of pulmonary Th2 inflammation (**Figure 6B**).

To investigate a potential pathomechanistic link between the endothelin system in pulmonary Th2 inflammation and the VIP, VIP plasma levels were quantified. Neither rescued ET_B deficiency nor OVA/OVA treatment had an effect on VIP plasma levels (**Supplementary Figure 8**).

DISCUSSION

In our study, we evaluated anti-ET_B AAb in PAH patients for the first time and found increased levels in SSc-PAH patients. Furthermore, we characterized the immunomodulatory role of

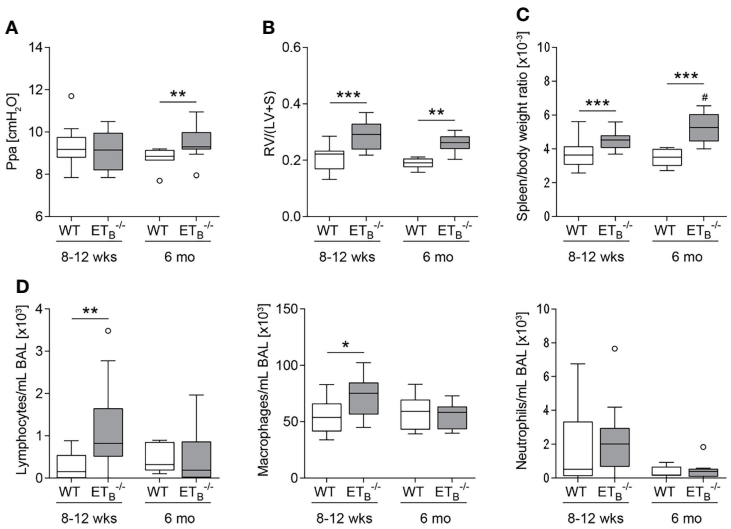

FIGURE 3 | ET_B deficiency was age-dependently associated with increased pulmonary arterial pressure, right ventricular hypertrophy, splenomegaly, and increased number of lymphocytes in bronchoalveolar lavage. Lungs, hearts, and spleens of 8- to 12-week (wk)-old and 6-mo-old rescued endothelin B receptor-deficient ($ET_B^{-/-}$) and corresponding wild-type (WT) mice were removed, or bronchoalveolar lavage (BAL) was performed. **(A)** In isolated perfused and ventilated lungs, under basal conditions, pulmonary arterial pressure (Ppa) was increased in 6-mo-old $ET_B^{-/-}$ compared to WT mice of the same age. **(B)** Fulton index [ratio of right ventricle (RV) and left ventricle (LV) including septum (S)] determined after weighing the cardiac compartments was higher in $ET_B^{-/-}$ compared to WT mice. **(C)** Determination of spleen weight related to body weight revealed splenomegaly in $ET_B^{-/-}$ mice. **(D)** Analysis of differentially quantified leukocytes in BAL revealed increased number of lymphocytes and macrophages in BAL from 8- to 12-wk-old $ET_B^{-/-}$ vs. WT mice of the same age. Data are represented as *box plots* depicting median, quartiles, and ranges excluding outliers (*open circles*). In **(A–C)**, $N = 7–28$; in **(D)**, $N = 7–17$. # indicates significant difference in the 6-mo-old vs. the corresponding 8- to 12-wk-old group, * indicates significant difference between $ET_B^{-/-}$ vs. the corresponding WT group. $^{*/\#}p < 0.05$, $^{**}p < 0.01$, $^{***}p < 0.001$ (Mann–Whitney *U* test).

ET_B in the context of PAH using a mouse model of PAH due to rescued ET_B deficiency. Our data point to an important role of ET_B in immune homeostasis, with functional ET_B deficiency unleashing PAH development under inflammatory conditions.

ET_B deficiency is associated with defective ET-1 clearance (27, 41–43), and increased levels of plasma ET-1 (44–46). In order to distinguish ET-1- and ET_B-dependent effects in $ET_B^{-/-}$ mice, we studied a second transgenic mouse model in parallel, namely, prepro-endothelin-1 overexpressing ($_{pre}ET^{tg}$) mice.

Here, we show that pulmonary hypertension, pulmonary vascular hyperresponsiveness, and right ventricular hypertrophy were present in $_{pre}ET^{tg}$ as well as in $ET_B^{-/-}$ mice, arguing for ET-1-specific effects. In $_{pre}ET^{tg}$ mice, both

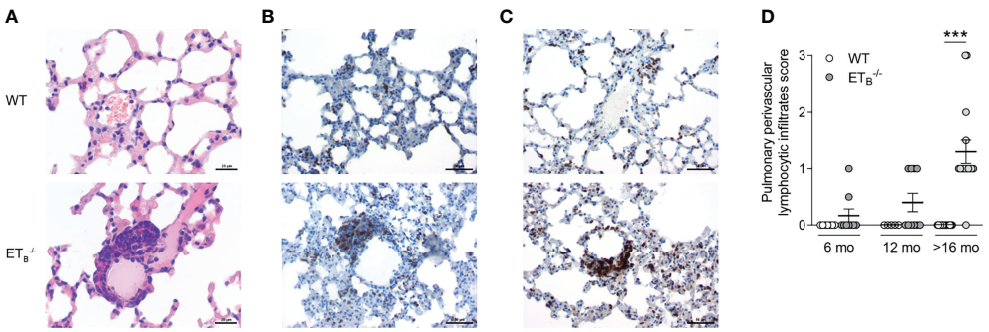

FIGURE 4 | ET_B deficiency was associated with peripheral perivascular lymphocytic infiltrates in the lung. Lungs of 6-, 12-, and >16-mo-old rescued endothelin B receptor-deficient ($ET_B^{-/-}$) and the corresponding wild-type (WT) mice were assessed histologically following hematoxylin and eosin (H&E) stain **(A)** or immunohistochemical stains for CD45R/B220 (B cells; **B**) or CD3 (T cells; **C**). The scale bars represent 20 µm **(A)** or 50 µm **(B, C)**. Representative images of ≥12-mo-old mice are shown; $N = 20–25$ per group **(A)** or $N = 3–5$ per group **(B, C)**. **(D)** H&E-stained lung sections were analyzed and scored (0, no peripheral perivascular infiltrates; 1, mild; 2 moderate; 3, pronounced) by an independent board-certified pathologist, blinded to the study groups. Data are expressed as single values with mean ± SEM; $N = 7–9$ (6-mo-old group), $N = 5–10$ (12-mo-old group), or $N = 15$ (>16-mo-old group). $^{***}p < 0.001$ (Mann–Whitney *U* test).

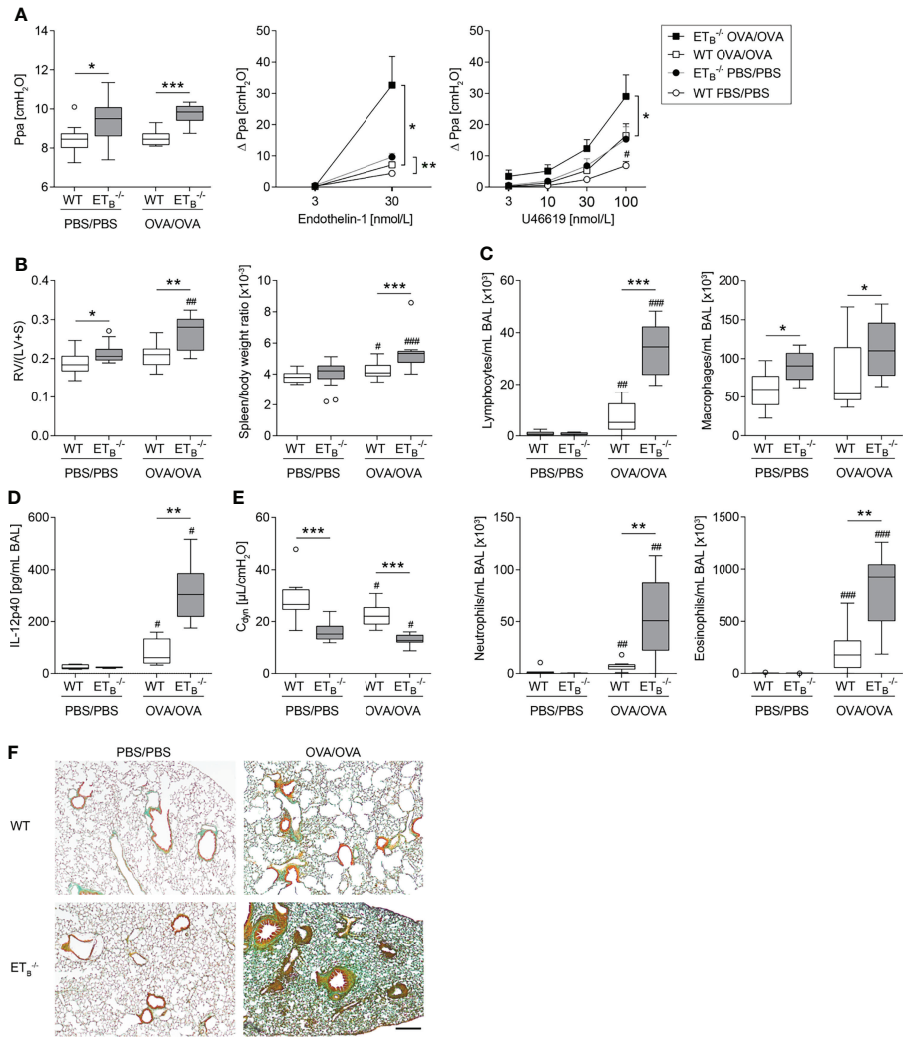

FIGURE 5 | ET_B deficiency aggravated Th2-mediated vascular pathologies and inflammation in the lung. Rescued endothelin B receptor-deficient ($ET_B^{-/-}$) and corresponding wild-type (WT) mice were systemically sensitized with ovalbumin (OVA) (or PBS as control) and repeatedly exposed to aerosolized OVA (OVA/OVA) or PBS (PBS/PBS). Forty-eight hours after the last challenge, lungs, hearts, and spleens of 12-wk-old mice were harvested, or bronchoalveolar lavage (BAL) was performed. **(A)** In isolated perfused and ventilated lungs, pulmonary arterial pressure (Ppa) was measured under basal conditions, and pulmonary vascular responsiveness to increasing concentrations of endothelin-1 or thromboxane receptor agonist U46619 was determined. Data (Δ Ppa) represent the difference between the highest pressure response to the respective stimulus and the basal Ppa. **(B)** Fulton index [quotient of right ventricle (RV) and left ventricle (LV) including septum (S)] was determined after weighing the cardiac compartments (left) and spleen weight was determined and related to body weight (right). **(C)** Leukocytes were differentially quantified in BAL. **(D)** IL-12p40 was determined in BAL (lower detection limit was 0.54 pg/mL). **(E)** In isolated perfused and ventilated mouse lungs, dynamic lung compliance (C_{dyn}) was measured. **(F)** Lung tissue sections were stained with Masson–Goldner trichrome that revealed more pronounced pulmonary collagen deposition in $ET_B^{-/-}$ than WT mice after OVA/OVA treatment. The scale bar represents 100 μm and is valid for all photomicrographs. Representative images (N = 7 per group) are shown. In **(A left, B–E),** data are represented as *box plots* depicting median, quartiles, and ranges excluding outliers (*open circles*), and analyzed using Mann–Whitney U test. # indicates significant difference between OVA/OVA vs. the corresponding PBS/PBS group, * indicates significant difference between $ET_B^{-/-}$ vs. the corresponding WT group. In **(A middle-right)**, values are given as mean and SEM, and analyzed using two-way repeated measures ANOVA (*). In **(A right)**, additional Mann–Whitney U test was performed comparing values of $ET_B^{-/-}$ and WT mice treated with PBS at the highest dose of U46619 (#). N = 5–14 **(A–C, E)** or N = 3–6 **(D)**. $^{*/\#}p < 0.05$, $^{**/\#\#}p < 0.01$, $^{***/\#\#\#}p < 0.001$.

pulmonary hypertension and right ventricular hypertrophy, however, were exclusively detected in highly aged (≥16 months old) mice, possibly as a result of decreasing NO-mediated compensatory effects with increasing age (61). In contrast, in $ET_B^{-/-}$ mice, PAH-associated alterations were generally observed at a younger age than in $_{pre}ET^{tg}$ mice, which may be the result of synergistic unfavorable effects of ET_B deficiency and consecutive defective clearance of ET-1. Yet, as opposed to the characteristic findings in PAH patients, relevant pulmonary arterial remodeling was absent in both transgenic mouse lines, suggesting that the observed pulmonary hypertensive phenotypes are primarily driven by an increased vascular tone

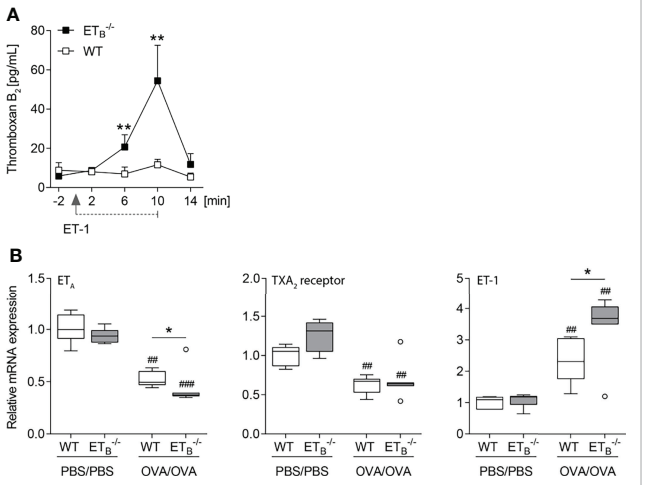

FIGURE 6 | ET-1-mediated thromboxane release is increased in $ET_B^{-/-}$ mice. **(A)** In isolated perfused lungs of 10- to 12-wk-old rescued endothelin B receptor-deficient ($ET_B^{-/-}$) and corresponding wild-type (WT) mice, perfusate samples were collected 2 min before application of 100 nmol/L ET-1 (for 10 min), and 2, 6, 10, and 14 min after the start of ET-1 application, and TXB_2 levels were determined. The detection limit was 7.8 pg/ml. Values are given as mean and SEM ($N = 7$), and analyzed using Mann–Whitney *U* tests at each time point comparing both groups. **(B)** $ET_B^{-/-}$ and corresponding WT mice were systemically sensitized with OVA (or PBS as control) and repeatedly exposed to aerosolized OVA (OVA/OVA) or PBS (PBS/PBS). Forty-eight hours after the last inhalative OVA challenge, lungs of 15- to 17-wk-old mice were isolated for mRNA expression analyses by quantitative PCR. Relative quantification of mRNA was performed using the comparative C_t method. Data are represented as *box plots* depicting median, quartiles, and ranges excluding outliers (*open circles*), and analyzed using Mann–Whitney *U* test; $N = 6$–7 per group. # indicates significant difference between OVA/OVA vs. the corresponding PBS/PBS group, * indicates significant difference between $ET_B^{-/-}$ vs. the corresponding WT group. $^{*}/^{\#\#}p < 0.01$, $^{\#\#\#}p < 0.001$.

due to an imbalance of vasoconstrictive and vasodilatory mechanisms, rather than by extensive vascular remodeling in the pulmonary circulation.

Increased numbers of lymphocytes were found in BAL of both transgenic mouse models, again pointing to ET-1 as causative trigger. This finding is in line with previously described chronic lymphocytic lung inflammation as a result of prepro-ET-1 overexpression (58).

Of note, pronounced peripheral perivascular cluster of lymphoid infiltrates were exclusively found in $ET_B^{-/-}$ lungs, arguing for a dysregulation of the immune system due to the loss of ET_B. The perivascular space is a unique lung compartment, which might have been underestimated (62). Capillaries as well as lymphatic vessels from the periphery are found in the perivascular space, predominantly around the pulmonary arteries. This compartment is rather inactive in healthy lungs, but gains major significance in many types of lung inflammation. It is hypothesized that in certain conditions, inflammatory mediators induce extravasation of fluid and leukocytes from the periarterial capillaries, leading to thick cellular cuffs around the pulmonary arteries (63, 64). This defense mechanism may contribute to secondary lesions or processes such as the development of tertiary lymphoid tissue.

The data presented here give a strong hint that ET_B is involved in the regulation of perivascular infiltration of pulmonary arteries. This finding is of specific interest as perivascular infiltrates and lymphoid tissue are commonly found in lungs of PAH patients and in preclinical models of pulmonary hypertension (2, 9–12).

As previously shown by us and others, induction of pulmonary Th2 inflammation in mice induces relevant PAH-associated features such as perivascular inflammation, hyperresponsiveness of the pulmonary vasculature to vasoconstrictive stimuli, complex pulmonary arterial remodeling, and increase in right ventricular systolic pressure (2, 16–23). Importantly, a key role of Th2 inflammation in the pathogenesis of pulmonary hypertension has been demonstrated in lung-specific IL-13-overexpressing mice, which develop spontaneous pulmonary hypertension, pulmonary arterial remodeling, and right ventricular hypertrophy (22). Interestingly, also in Fra-2 transgenic mice, a well-described model of SSc-PAH and interstitial lung disease, a strong underlying Th2 phenotype is present (56, 65).

Here, we analyzed the effects of pulmonary Th2 inflammation as a second hit in $ET_B^{-/-}$ mice. Notably, both pulmonary vascular hyperresponsiveness and right ventricular hypertrophy were aggravated secondary to Th2 inflammation in $ET_B^{-/-}$ mice. Moreover, in $ET_B^{-/-}$ lungs, pulmonary perivascular inflammation and collagen deposition were increased.

On the cytokine level, IL-12 subunit p40 (IL-12p40) levels were largely increased in BAL of $ET_B^{-/-}$ mice, whereas Th2 cytokines were similar in $ET_B^{-/-}$ and WT mice. Increased IL-12p40 levels are notable with respect to the exaggerated PAH phenotype in $ET_B^{-/-}$ mice as well as the increased pulmonary collagen deposition, since PAH patients show elevated levels of circulating IL-12p40 (12). Analogously, IL-12p40 serum levels are increased in mice deficient for chemokine receptor CCR7, which develop pulmonary hypertension, pulmonary arterial remodeling, and perivascular lymphoid infiltrates in the lung (12). Moreover, IL-12p40 has been identified as a central profibrotic mediator in murine lung fibrosis (60).

Pulmonary vascular hyperresponsiveness to the stimuli ET-1 and TXA_2 analog U46619 was shown to be aggravated in $ET_B^{-/-}$ lungs compared to the WT lungs. Interestingly, pulmonary vascular hyperresponsiveness to serotonin was unchanged in $ET_B^{-/-}$ lungs, arguing for stimulus-specific alterations of the here assessed vasomotor responses. Mechanistically, ET-1-evoked hyperresponsiveness was most likely based on increased TXA_2 release following vascular ET-1 application in $ET_B^{-/-}$ mice, as indicated here by the elevated TXB_2 perfusate levels.

Increased responsiveness as a result of ET_A and/or TXA_2 receptor upregulation, however, was ruled out in this study. In fact, ET_A was downregulated in $ET_B^{-/-}$ lungs following induction of Th2 inflammation, possibly as a counter-response to the increase in local ET-1 expression in $ET_B^{-/-}$ lungs. Taken together, both the upregulation of ET-1 expression and the increased release of IL-12p40 may have contributed to the here

observed exaggeration of the PAH phenotype in $ET_B^{-/-}$ mice following induction of pulmonary Th2 inflammation.

It can be assumed that the anti-inflammatory effects of ET_B signaling described in this study are primarily mediated *via* ET_B receptor activation on vascular and inflammatory cells. In contrast, secondary immunomodulatory effects in response to ET_B-regulated sodium and water reabsorption in the kidney are unlikely to underlie the detected anti-inflammatory properties of ET_B in the lung. Specifically, ET_B exerts natriuretic functions (66), and collecting duct-specific deficiency of ET_B accordingly causes systemic hypertension with decreased urinary aldosterone excretion and plasma renin activity (67). Reduced activation of the renin–angiotensin–aldosterone system is, however, characteristically associated with mitigated inflammation (68). The same holds true for natriuretic peptides, which are abundantly released upon volume expansion (69) and have protective immunomodulatory properties (70). These anti-inflammatory effects of renal ET_B deficiency stand in contrast to the pro-inflammatory effects in the lung detected in our study. Therefore, the anti-inflammatory role of ET_B in the lung seems unrelated to its natriuretic function.

Our finding that Th2 inflammation as a second hit augments hallmarks of PAH is in line with previous findings in mice expressing a hypomorphic bone morphogenetic protein receptor type 2 (BMPR2) transgene, which showed an increase in right ventricular systolic pressure following induction of a Th2 immune response (23). As Th2-mediated aggravation of PAH phenotypes has been repeatedly shown, it is tempting to speculate that mediators of Th2 signaling may serve as potential targets in PAH. This needs to be evaluated in further studies.

PAH may occur in SSc patients with or without accompanying interstitial lung disease and/or digital ulcers (71, 72). The endothelin system is believed to play a central role in SSc-PAH, and SSc-PAH patients benefit from ERA treatment (24, 71, 72). ERAs are further indicated to treat SSc-related digital ulcers (72). Additional SSc-associated complications seem to involve the endothelin system. Alveolitis is frequently observed in SSc patients (73, 74). Intriguingly, alveolitis was also experimentally induced in mice treated with anti-ET_A AAb and anti-angiotensin II type 1 receptor (AT_1R) AAb-positive IgG derived from SSc patients (75). Moreover, expression of type I collagen in fibroblasts following treatment with IgG from SSc patients correlated with anti-ET_A AAb levels, suggesting an underlying role of the endothelin system in SSc-associated fibrosis (75), as also discussed elsewhere (76).

The immunomodulatory actions of ET_B shown here may be of relevance for the early phase of PAH, in which inflammation, endothelial dysfunction, and hyperresponsiveness of the pulmonary vasculature are believed to play relevant mechanistic roles. In the chronic disease state, reflected by profound remodeling of the pulmonary arteries, ET_B, however, may play a less prominent role, as indicated by the fact that ET_A-selective blockers do not appear to be superior to dual ET_A/ET_B therapy in established PAH (77, 78). Prospective clinical trials comparing selective ERA (inhibition of ET_A) head-to-head against dual ERA (combined inhibition of ET_A/ET_B) therapy at early disease time points may be required to identify a potential advantage of selective ERA therapy in PAH.

In conclusion, our data show an anti-inflammatory role of ET_B. ET_B deficiency as a single hit is associated with spontaneous formation of marked lymphoid infiltrates in the perivascular space of the lung, in addition to pulmonary hypertension, pulmonary vascular hyperresponsiveness, and right ventricular hypertrophy. Th2 inflammation as a second hit aggravates PAH-associated pathologies in $ET_B^{-/-}$ mice. The pathogenic role of anti-ET_B AAb in SSc-PAH needs to be evaluated in further studies.

DATA AVAILABILITY STATEMENT

The raw data supporting the conclusions of this article will be made available by the authors, without undue reservation.

ETHICS STATEMENT

The studies involving human participants were reviewed and approved by the ethics committee (Charité - Universitätsmedizin Berlin, Germany; EA1/179/17). The patients/participants provided their written informed consent to participate in this study. The animal study was reviewed and approved by institutional authorities of the Charité – Universitätsmedizin Berlin, Germany, and the Local State Office of Health and Social Affairs Berlin (LAGeSo; Berlin, Germany).

AUTHOR CONTRIBUTIONS

CT and MW conceived and designed the research. CT, CG, TT, OK, BG, JN, and JHe performed experiments. CT, CG, JL, JHö, TT, OK, BG, JN, BO, AG, HH, ES, and MW analyzed data. All authors interpreted the results of the experiments. CT, CG, JL, JHö, TT, OK, and ES prepared figures. CT and JL drafted the manuscript. All authors edited and revised the manuscript and approved the final version of the manuscript.

FUNDING

This study received funding from the German Research Foundation (SFB-TR84, C6/C9 to MW and Z01b to AG) and Actelion Pharmaceuticals Germany GmbH. The funders were not involved in the study design, collection, analysis, interpretation of data, the writing of this article or the decision to submit it for publication.

ACKNOWLEDGMENTS

The authors would like to thank Udo Schneider, Daniel Grund, and Vincent Casteleyn for their support on patient recruitment.

The technical assistance of Katharina Krause-Relle is greatly appreciated. The present study is part of the doctoral thesis of CG. CT and ES are participants in the BIH-Charité Clinician Scientist Program funded by the Charité - Universitätsmedizin Berlin and the Berlin Institute of Health.

SUPPLEMENTARY MATERIAL

The Supplementary Material for this article can be found online at: https://www.frontiersin.org/articles/10.3389/fimmu.2022.895501/full#supplementary-material

REFERENCES

1. Gaine S. Pulmonary Hypertension. *JAMA* (2000) 284(24):3160–8. doi: 10.1001/jama.284.24.3160
2. Price LC, Wort SJ, Perros F, Dorfmüller P, Huertas A, Montani D, et al. Inflammation in Pulmonary Arterial Hypertension. *Chest* (2012) 141(1):210–21. doi: 10.1378/chest.11-0793
3. Hassoun PM, Mouthon L, Barberà JA, Eddahibi S, Flores SC, Grimminger F, et al. Inflammation, Growth Factors, and Pulmonary Vascular Remodeling. *J Am Coll Cardiol* (2009) 54(1 Suppl):S10–9. doi: 10.1016/j.jacc.2009.04.006
4. Huertas A, Tu L, Humbert M, Guignabert C. Chronic Inflammation Within the Vascular Wall in Pulmonary Arterial Hypertension: More Than a Spectator. *Cardiovasc Res* (2020) 116(5):885–93. doi: 10.1093/cvr/cvz308
5. Kherbeck N, Tamby MC, Bussone G, Dib H, Perros F, Humbert M, et al. The Role of Inflammation and Autoimmunity in the Pathophysiology of Pulmonary Arterial Hypertension. *Clin Rev Allergy Immunol* (2013) 44 (1):31–8. doi: 10.1007/s12016-011-8265-z
6. Le Pavec J, Humbert M, Mouthon L, Hassoun PM. Systemic Sclerosis-Associated Pulmonary Arterial Hypertension. *Am J Respir Crit Care Med* (2010) 181(12):1285–93. doi: 10.1164/rccm.200909-1331PP
7. Dorfmüller P, Perros F, Balabanian K, Humbert M. Inflammation in Pulmonary Arterial Hypertension. *Eur Respir J* (2003) 22(2):358–63. doi: 10.1183/09031936.03.00038903
8. Soon E, Holmes AM, Treacy CM, Doughty NJ, Southgate L, Machado RD, et al. Elevated Levels of Inflammatory Cytokines Predict Survival in Idiopathic and Familial Pulmonary Arterial Hypertension. *Circulation* (2010) 122 (9):920–7. doi: 10.1161/CIRCULATIONAHA.109.933762
9. Hu Y, Chi L, Kuebler WM, Goldenberg NM. Perivascular Inflammation in Pulmonary Arterial Hypertension. *Cells* (2020) 9(11):2338. doi: 10.3390/cells9112338
10. Colvin KL, Cripe PJ, Ivy DD, Stenmark KR, Yeager ME. Bronchus-Associated Lymphoid Tissue in Pulmonary Hypertension Produces Pathologic Autoantibodies. *Am J Respir Crit Care Med* (2013) 188(9):1126–36. doi: 10.1164/rccm.201302-0403OC
11. Perros F, Dorfmüller P, Montani D, Hammad H, Waelput W, Girerd B, et al. Pulmonary Lymphoid Neogenesis in Idiopathic Pulmonary Arterial Hypertension. *Am J Respir Crit Care Med* (2012) 185(3):311–21. doi: 10.1164/rccm.201105-0927OC
12. Larsen KO, Yndestad A, Sjaastad I, Løberg EM, Goverud IL, Halvorsen B, et al. Lack of CCR7 Induces Pulmonary Hypertension Involving Perivascular Leukocyte Infiltration and Inflammation. *Am J Physiol Lung Cell Mol Physiol* (2011) 301(1):L50–9. doi: 10.1152/ajplung.00048.2010
13. Harbaum L, Renk E, Yousef S, Glatzel A, Lüneburg N, Hennigs JK, et al. Acute Effects of Exercise on the Inflammatory State in Patients With Idiopathic Pulmonary Arterial Hypertension. *BMC Pulm Med* (2016) 16(1):145. doi: 10.1186/s12890-016-0301-6
14. Heath D, Yacoub M. Lung Mast Cells in Plexogenic Pulmonary Arteriopathy. *J Clin Pathol* (1991) 44(12):1003–6. doi: 10.1136/jcp.44.12.1003
15. Hamada H, Terai M, Kimura H, Hirano K, Oana S, Niimi H. Increased Expression of Mast Cell Chymase in the Lungs of Patients With Congenital Heart Disease Associated With Early Pulmonary Vascular Disease. *Am J Respir Crit Care Med* (1999) 160(4):1303–8. doi: 10.1164/ajrccm.160.4.9810058
16. Kumar R, Mickael C, Chabon J, Gebreab L, Rutebemberwa A, Garcia AR, et al. The Causal Role of Il-4 and Il-13 in Schistosoma Mansoni Pulmonary Hypertension. *Am J Respir Crit Care Med* (2015) 192(8):998–1008. doi: 10.1164/rccm.201410-1820OC
17. Haberberger RV, Tabeling C, Runciman S, Gutbier B, König P, Andratsch M, et al. Role of Sphingosine Kinase 1 in Allergen-Induced Pulmonary Vascular Remodeling and Hyperresponsiveness. *J Allergy Clin Immunol* (2009) 124 (5):933–41.e1-9. doi: 10.1016/j.jaci.2009.06.034
18. Witzenrath M, Ahrens B, Kube SM, Hocke AC, Rosseau S, Hamelmann E, et al. Allergic Lung Inflammation Induces Pulmonary Vascular Hyperresponsiveness. *EurRespirJ* (2006) 28(2):370–7. doi: 10.1183/09031936.06.00080105
19. Daley E, Emson C, Guignabert C, de Waal MR, Louten J, Kurup VP, et al. Pulmonary Arterial Remodeling Induced by a Th2 Immune Response. *J Exp Med* (2008) 205(2):361–72. doi: 10.1084/jem.20071008
20. Gomez-Arroyo J, Saleem SJ, Mizuno S, Syed AA, Bogaard HJ, Abbate A, et al. A Brief Overview of Mouse Models of Pulmonary Arterial Hypertension: Problems and Prospects. *Am J Physiol Lung Cell Mol Physiol* (2012) 302(10): L977–91. doi: 10.1152/ajplung.00362.2011
21. Mushaben EM, Hershey GK, Pauciulo MW, Nichols WC, Le Cras TD. Chronic Allergic Inflammation Causes Vascular Remodeling and Pulmonary Hypertension in BMPR2 Hypomorph and Wild-Type Mice. *PloS One* (2012) 7(3):e32468. doi: 10.1371/journal.pone.0032468
22. Cho WK, Lee CM, Kang MJ, Huang Y, Giordano FJ, Lee PJ, et al. Il-13 Receptor α2-Arginase 2 Pathway Mediates Il-13-Induced Pulmonary Hypertension. *Am J Physiol Lung Cell Mol Physiol* (2013) 304(2):L112–24. doi: 10.1152/ajplung.00101.2012
23. Park SH, Chen WC, Hoffman C, Marsh LM, West J, Grunig G. Modification of Hemodynamic and Immune Responses to Exposure With a Weak Antigen by the Expression of a Hypomorphic BMPR2 Gene. *PloS One* (2013) 8(1): e55180. doi: 10.1371/journal.pone.0055180
24. McLaughlin V, Humbert M, Coghlan G, Nash P, Steen V. Pulmonary Arterial Hypertension: The Most Devastating Vascular Complication of Systemic Sclerosis. *Rheumatol (Oxford)* (2009) 48(Suppl 3):iii25–31. doi: 10.1093/rheumatology/kep107
25. Giaid A, Yanagisawa M, Langleben D, Michel RP, Levy R, Shennib H, et al. Expression of Endothelin-1 in the Lungs of Patients With Pulmonary Hypertension. *N Engl J Med* (1993) 328(24):1732–9. doi: 10.1056/NEJM199306173282402
26. Dhaun N, Webb DJ. Endothelins in Cardiovascular Biology and Therapeutics. *Nat Rev Cardiol* (2019) 16(8):491–502. doi: 10.1038/s41569-019-0176-3
27. Davenport AP, Hyndman KA, Dhaun N, Southan C, Kohan DE, Pollock JS, et al. Endothelin. *Pharmacol Rev* (2016) 68(2):357–418. doi: 10.1124/pr.115.011833
28. Stewart DJ, Levy RD, Cernacek P, Langleben D. Increased Plasma Endothelin-1 in Pulmonary Hypertension: Marker or Mediator of Disease? *Ann Intern Med* (1991) 114(6):464–9. doi: 10.7326/0003-4819-114-6-464
29. de Nucci G, Thomas R, D'Orleans-Juste P, Antunes E, Walder C, Warner TD, et al. Pressor Effects of Circulating Endothelin Are Limited by Its Removal in the Pulmonary Circulation and by the Release of Prostacyclin and Endothelium-Derived Relaxing Factor. *Proc Natl Acad Sci USA* (1988) 85 (24):9797–800. doi: 10.1073/pnas.85.24.9797
30. Horgan MJ, Pinheiro JM, Malik AB. Mechanism of Endothelin-1-Induced Pulmonary Vasoconstriction. *Circ Res* (1991) 69(1):157–64. doi: 10.1161/01.res.69.1.157
31. Tabeling C, Noe E, Naujoks J, Doehn JM, Hippenstiel S, Opitz B, et al. PKCα Deficiency in Mice Is Associated With Pulmonary Vascular Hyperresponsiveness to Thromboxane A2 and Increased Thromboxane Receptor Expression. *J Vasc Res* (2015) 52(4):279–88. doi: 10.1159/000443402
32. Cabral-Marques O, Riemekasten G. Functional Autoantibodies Targeting G Protein-Coupled Receptors in Rheumatic Diseases. *Nat Rev Rheumatol* (2017) 13(11):648–56. doi: 10.1038/nrrheum.2017.134
33. Helset E, Sildnes T, Seljelid R, Konopski ZS. Endothelin-1 Stimulates Human Monocytes in Vitro to Release TNF-alpha, Il-1beta and Il-6. *Mediat Inflamm* (1993) 2(6):417–22. doi: 10.1155/S0962935193000596

34. Browatzki M, Schmidt J, Kübler W, Kranzhöfer R. Endothelin-1 Induces Interleukin-6 Release *Via* Activation of the Transcription Factor NF-kappaB in Human Vascular Smooth Muscle Cells. *Basic Res Cardiol* (2000) 95(2):98–105. doi: 10.1007/s003950050170
35. Becker MO, Kill A, Kutsche M, Guenther J, Rose A, Tabeling C, et al. Vascular Receptor Autoantibodies in Pulmonary Arterial Hypertension Associated With Systemic Sclerosis. *Am J Respir Crit Care Med* (2014) 190(7):808–17. doi: 10.1164/rccm.201403-0442OC
36. Blum LK, Cao RRL, Sweatt AJ, Bill M, Lahey LJ, Hsi AC, et al. Circulating Plasmablasts Are Elevated and Produce Pathogenic Anti-Endothelial Cell Autoantibodies in Idiopathic Pulmonary Arterial Hypertension. *Eur J Immunol* (2018) 48(5):874–84. doi: 10.1002/eji.201747460
37. Tamby MC, Humbert M, Guilpain P, Servettaz A, Dupin N, Christner JJ, et al. Antibodies to Fibroblasts in Idiopathic and Scleroderma-Associated Pulmonary Hypertension. *Eur Respir J* (2006) 28(4):799–807. doi: 10.1183/09031936.06.00152705
38. Tamby MC, Chanseaud Y, Humbert M, Fermanian J, Guilpain P, Garcia-de-la-Peña-Lefebvre P, et al. Anti-Endothelial Cell Antibodies in Idiopathic and Systemic Sclerosis Associated Pulmonary Arterial Hypertension. *Thorax* (2005) 60(9):765–72. doi: 10.1136/thx.2004.029082
39. Arends SJ, Damoiseaux JG, Duijvestijn AM, Debrus-Palmans L, Boomars KA, Brunner-La Rocca HP, et al. Functional Implications of IgG Anti-Endothelial Cell Antibodies in Pulmonary Arterial Hypertension. *Autoimmunity* (2013) 46(7):463–70. doi: 10.3109/08916934.2013.812080
40. Arends SJ, Damoiseaux J, Duijvestijn A, Debrus-Palmans L, Boomars K, Broers B, et al. Prevalence of Anti-Endothelial Cell Antibodies in Idiopathic Pulmonary Arterial Hypertension. *Eur Respir J* (2010) 35(4):923–5. doi: 10.1183/09031936.00164209
41. Kelland NF, Kuc RE, McLean DL, Azfer A, Bagnall AJ, Gray GA, et al. Endothelial Cell-Specific ETB Receptor Knockout: Autoradiographic and Histological Characterisation and Crucial Role in the Clearance of Endothelin-1. *Can J Physiol Pharmacol* (2010) 88(6):644–51. doi: 10.1139/Y10-041
42. Fukuroda T, Fujikawa T, Ozaki S, Ishikawa K, Yano M, Nishikibe M. Clearance of Circulating Endothelin-1 by ETB Receptors in Rats. *Biochem Biophys Res Commun* (1994) 199(3):1461–5. doi: 10.1006/bbrc.1994.1395
43. Dupuis J, Goresky CA, Fournier A. Pulmonary Clearance of Circulating Endothelin-1 in Dogs in Vivo: Exclusive Role of ETB Receptors. *J Appl Physiol (1985)* (1996) 81(4):1510–5. doi: 10.1152/jappl.1996.81.4.1510
44. Ivy DD, Yanagisawa M, Gariepy CE, Gebb SA, Colvin KL, McMurtry IF. Exaggerated Hypoxic Pulmonary Hypertension in Endothelin B Receptor-Deficient Rats. *Am J Physiol Lung Cell Mol Physiol* (2002) 282(4):L703–12. doi: 10.1152/ajplung.00272.2001
45. Gariepy CE, Ohuchi T, Williams SC, Richardson JA, Yanagisawa M. Salt-Sensitive Hypertension in Endothelin-B Receptor-Deficient Rats. *J Clin Invest* (2000) 105(7):925–33. doi: 10.1172/JCI8609
46. Bagnall AJ, Kelland NF, Gulliver-Sloan F, Davenport AP, Gray GA, Yanagisawa M, et al. Deletion of Endothelial Cell Endothelin B Receptors Does Not Affect Blood Pressure or Sensitivity to Salt. *Hypertension* (2006) 48(2):286–93. doi: 10.1161/01.HYP.0000229907.58470.4c
47. van den Hoogen F, Khanna D, Fransen J, Johnson SR, Baron M, Tyndall A, et al. Classification Criteria for Systemic Sclerosis: An American College of Rheumatology/European League Against Rheumatism Collaborative Initiative. *Ann Rheum Dis* (2013) 72(11):1747–55. doi: 10.1136/annrheumdis-2013-204424
48. Riemekasten G, Philippe A, Näther M, Slowinski T, Müller DN, Heidecke H, et al. Involvement of Functional Autoantibodies Against Vascular Receptors in Systemic Sclerosis. *Ann Rheum Dis* (2011) 70(3):530–6. doi: 10.1136/ard.2010.135772
49. Hocher B, Thöne-Reineke C, Rohmeiss P, Schmager F, Slowinski T, Burst V, et al. Endothelin-1 Transgenic Mice Develop Glomerulosclerosis, Interstitial Fibrosis, and Renal Cysts But Not Hypertension. *J Clin Invest* (1997) 99(6):1380–9. doi: 10.1172/JCI119297
50. Quaschning T, Rebhan B, Wunderlich C, Wanner C, Richter CM, Pfab T, et al. Endothelin B Receptor-Deficient Mice Develop Endothelial Dysfunction Independently of Salt Loading. *J Hypertens* (2005) 23(5):979–85. doi: 10.1097/01.hjh.0000166838.55688.7e
51. von Bethmann AN, Brasch F, Nüsing R, Vogt K, Volk HD, Müller KM, et al. Hyperventilation Induces Release of Cytokines From Perfused Mouse Lung. *Am J Respir Crit Care Med* (1998) 157(1):263–72. doi: 10.1164/ajrccm.157.1.9608052
52. Tabeling C, Yu H, Wang L, Ranke H, Goldenberg NM, Zabini D, et al. CFTR and Sphingolipids Mediate Hypoxic Pulmonary Vasoconstriction. *Proc Natl Acad Sci USA* (2015) 112(13):E1614–23. doi: 10.1073/pnas.1421190112
53. Tabeling C, Scheer H, Schönrock SM, Runge F, Gutbier B, Lienau J, et al. Nucleotide Oligomerization Domain 1 Ligation Suppressed Murine Allergen-Specific T-Cell Proliferation and Airway Hyperresponsiveness. *Am J Respir Cell Mol Biol* (2014) 50(5):903–11. doi: 10.1165/rcmb.2013-0333OC
54. Schulze T, Golfier S, Tabeling C, Räbel K, Gräler MH, Witzenrath M, et al. Sphingosine-1-Phospate Receptor 4 ($S1P_4$) Deficiency Profoundly Affects Dendritic Cell Function and Th17-Cell Differentiation in a Murine Model. *FASEB J* (2011) 25(11):4024–36. doi: 10.1096/fj.10-179028
55. Heine G, Tabeling C, Hartmann B, González Calera CR, Kühl AA, Lindner J, et al. 25-Hydroxvitamin D3 Promotes the Long-Term Effect of Specific Immunotherapy in a Murine Allergy Model. *J Immunol* (2014) 193(3):1017–23. doi: 10.4049/jimmunol.1301656
56. Tabeling C, Wienhold SM, Birnhuber A, Brack MC, Nouailles G, Kershaw O, et al. Pulmonary Fibrosis in Fra-2 Transgenic Mice Is Associated With Decreased Numbers of Alveolar Macrophages and Increased Susceptibility to Pneumococcal Pneumonia. *Am J Physiol Lung Cell Mol Physiol* (2021) 320(5):L916–L25. doi: 10.1152/ajplung.00505.2020
57. Naujoks J, Tabeling C, Dill BD, Hoffmann C, Brown AS, Kunze M, et al. IFNs Modify the Proteome of Legionella-Containing Vacuoles and Restrict Infection *Via* IRG1-Derived Itaconic Acid. *PloS Pathog* (2016) 12(2):e1005408. doi: 10.1371/journal.ppat.1005408
58. Hocher B, Schwarz A, Fagan KA, Thöne-Reineke C, El Hag K, Kusserow H, et al. Pulmonary Fibrosis and Chronic Lung Inflammation in ET-1 Transgenic Mice. *Am J Respir Cell Mol Biol* (2000) 23(1):19–26. doi: 10.1165/ajrcmb.23.1.4030
59. Tabeling C, Herbert J, Hocke AC, Lamb DJ, Wollin SL, Erb KJ, et al. Spleen Tyrosine Kinase Inhibition Blocks Airway Constriction and Protects From Th2-Induced Airway Inflammation and Remodeling. *Allergy* (2017) 72(7):1061–72. doi: 10.1111/all.13101
60. Huaux F, Arras M, Tomasi D, Barbarin V, Delos M, Coutelier JP, et al. A Profibrotic Function of Il-12p40 in Experimental Pulmonary Fibrosis. *J Immunol* (2002) 169(5):2653–61. doi: 10.4049/jimmunol.169.5.2653
61. Kalk P, Mach A, Thone-Reineke C, Godes M, Heiden S, Sharkovska Y, et al. Pulmonary Fibrosis in L-NAME-Treated Mice Is Dependent on an Activated Endothelin System. *Can J Physiol Pharmacol* (2008) 86(8):541–5. doi: 10.1139/Y08-047
62. Pabst R, Tschernig T. Perivascular Capillaries in the Lung: An Important But Neglected Vascular Bed in Immune Reactions? *J Allergy Clin Immunol* (2002) 110(2):209–14. doi: 10.1067/mai.2002.126836
63. Lindsey AS, Sullivan LM, Housley NA, Koloteva A, King JA, Audia JP, et al. Analysis of Pulmonary Vascular Injury and Repair During Pseudomonas Aeruginosa Infection-Induced Pneumonia and Acute Respiratory Distress Syndrome. *Pulm Circ* (2019) 9(1):2045894019826941. doi: 10.1177/2045894019826941
64. Pabst R, Tschernig T. Periarterial Leukocyte Accumulation in Allergic Airway Inflammation. *Am J Respir Crit Care Med* (2006) 174(7):840. doi: 10.1164/ajrccm.174.7.840
65. Birnhuber A, Biasin V, Schnoegl D, Marsh LM, Kwapiszewska G. Transcription Factor Fra-2 and Its Emerging Role in Matrix Deposition, Proliferation and Inflammation in Chronic Lung Diseases. *Cell Signal* (2019) 64:109408. doi: 10.1016/j.cellsig.2019.109408
66. Zhang Y, Jose PA, Zeng C. Regulation of Sodium Transport in the Proximal Tubule by Endothelin. *Contrib Nephrol* (2011) 172:63–75. doi: 10.1159/000328684
67. Ge Y, Bagnall A, Stricklett PK, Strait K, Webb DJ, Kotelevtsev Y, et al. Collecting Duct-Specific Knockout of the Endothelin B Receptor Causes Hypertension and Sodium Retention. *Am J Physiol Renal Physiol* (2006) 291(6):F1274–80. doi: 10.1152/ajprenal.00190.2006
68. Pacurari M, Kafoury R, Tchounwou PB, Ndebele K. The Renin-Angiotensin-Aldosterone System in Vascular Inflammation and Remodeling. *Int J Inflam* (2014) 2014:689360. doi: 10.1155/2014/689360

69. McFarlane SI, Winer N, Sowers JR. Role of the Natriuretic Peptide System in Cardiorenal Protection. *Arch Intern Med* (2003) 163(22):2696–704. doi: 10.1001/archinte.163.22.2696
70. Ramakrishnan V, Burnett JCJr. Natriuretic Peptides, Inflammation, and Sounding the Alarm. *Circ Heart Fail* (2020) 13(7):e007208. doi: 10.1161/CIRCHEARTFAILURE.120.007208
71. Naranjo M, Hassoun PM. Systemic Sclerosis-Associated Pulmonary Hypertension: Spectrum and Impact. *Diagnostics (Basel)* (2021) 11(5):911. doi: 10.3390/diagnostics11050911
72. Kowal-Bielecka O, Fransen J, Avouac J, Becker M, Kulak A, Allanore Y, et al. Update of EULAR Recommendations for the Treatment of Systemic Sclerosis. *Ann Rheum Dis* (2017) 76(8):1327–39. doi: 10.1136/annrheumdis-2016-209909
73. Manganelli P, Salaffi F, Pesci A. Clinical and Subclinical Alveolitis in Connective Tissue Diseases Assessed by Bronchoalveolar Lavage. *Semin Arthritis Rheum* (1997) 26(5):740–54. doi: 10.1016/s0049-0172(97)80042-x
74. Schmidt K, Martinez-Gamboa L, Meier S, Witt C, Meisel C, Hanitsch LG, et al. Bronchoalveoloar Lavage Fluid Cytokines and Chemokines as Markers and Predictors for the Outcome of Interstitial Lung Disease in Systemic Sclerosis Patients. *Arthritis Res Ther* (2009) 11(4):R111. doi: 10.1186/ar2766
75. Kill A, Tabeling C, Undeutsch R, Kühl AA, Gunther J, Radic M, et al. Autoantibodies to Angiotensin and Endothelin Receptors in Systemic Sclerosis Induce Cellular and Systemic Events Associated With Disease Pathogenesis. *Arthritis Res Ther* (2014) 16(1):R29. doi: 10.1186/ar4457
76. Grune J, Kuebler WM. Is There a Role for Endothelin-1 Receptor Antagonists in the Treatment of Lung Fibrosis Associated With Pulmonary Hypertension? *Eur Respir J* (2018) 52(2):1801287. doi: 10.1183/13993003.01287-2018
77. Vizza CD, Fedele F, Pezzuto B, Rubin LJ. Safety and Efficacy Evaluation of Ambrisentan in Pulmonary Hypertension. *Expert Opin Drug Saf* (2012) 11(6):1003–11. doi: 10.1517/14740338.2012.714770
78. Dupuis J, Hoeper MM. Endothelin Receptor Antagonists in Pulmonary Arterial Hypertension. *Eur Respir J* (2008) 31(2):407–15. doi: 10.1183/09031936.00078207

Conflict of Interest: CT received funding for research from Deutsche Gesellschaft für Pneumologie, Bayer HealthCare, Boehringer Ingelheim, and for lectures from Actelion Pharmaceuticals, Boehringer Ingelheim. HH is CEO of CellTrend GmbH, Luckenwalde, Germany. MW received funding for research from Deutsche Forschungsgemeinschaft, Bundesministerium für Bildung und Forschung, Deutsche Gesellschaft für Pneumologie, European Respiratory Society, Marie Curie Foundation, Else Kröner Fresenius Stiftung, CAPNETZ STIFTUNG, International Max Planck Research School, Actelion, Bayer Health Care, Biotest AG, Boehringer Ingelheim, NOXXON Pharma, Pantherna, Quark Pharma, Silence Therapeutics, Vaxxilon, and for lectures and advisory from Actelion, Alexion, Aptarion, Astra Zeneca, Bayer Health Care, Berlin Chemie, Biotest, Boehringer Ingelheim, Chiesi, Glaxo Smith Kline, Insmed, Novartis, Teva and Vaxxilon.

The remaining authors declare that the research was conducted in the absence of any commercial or financial relationships that could be construed as a potential conflict of interest.

frontiers | Frontiers in Immunology

ORIGINAL RESEARCH
published: 04 July 2022
doi: 10.3389/fimmu.2022.898690

Colchicine Impacts Leukocyte Trafficking in Atherosclerosis and Reduces Vascular Inflammation

Ulrike Meyer-Lindemann[1,2†], Carina Mauersberger[1,2†], Anna-Christina Schmidt[1,2†], Aldo Moggio[1†], Julia Hinterdobler[1,2], Xinghai Li[1], David Khangholi[1,2], Jan Hettwer[1,2], Christian Gräßer[1,2], Alexander Dutsch[1,2], Heribert Schunkert[1,2], Thorsten Kessler[1,2‡] and Hendrik B. Sager[1,2‡]*

[1] Department of Cardiology, German Heart Centre Munich, Technical University Munich, Munich, Germany, [2] DZHK (German Centre for Cardiovascular Research), Partner Site Munich Heart Alliance, Munich, Germany

OPEN ACCESS

Edited by:
Szandor Simmons,
Charité – Universitätsmedizin Berlin,
Germany

Reviewed by:
Norbert Gerdes,
Heinrich Heine University Düsseldorf,
Germany
Ingrid E. Dumitriu,
University of Birmingham,
United Kingdom

***Correspondence:**
Hendrik B. Sager
hendrik.sager@tum.de

[†]These authors have contributed equally to this work and share first authorship

[‡]These authors have contributed equally to this work and share last authorship

Specialty section:
This article was submitted to Inflammation, a section of the journal Frontiers in Immunology

Received: 17 March 2022
Accepted: 13 June 2022
Published: 04 July 2022

Citation:
Meyer-Lindemann U, Mauersberger C, Schmidt A-C, Moggio A, Hinterdobler J, Li X, Khangholi D, Hettwer J, Gräßer C, Dutsch A, Schunkert H, Kessler T and Sager HB (2022) Colchicine Impacts Leukocyte Trafficking in Atherosclerosis and Reduces Vascular Inflammation. Front. Immunol. 13:898690. doi: 10.3389/fimmu.2022.898690

Background: Inflammation strongly contributes to atherosclerosis initiation and progression. Consequently, recent clinical trials pharmacologically targeted vascular inflammation to decrease the incidence of atherosclerosis-related complications. Colchicine, a microtubule inhibitor with anti-inflammatory properties, reduced cardiovascular events in patients with recent acute coronary syndrome and chronic coronary disease. However, the biological basis of these observations remains elusive. We sought to explore the mechanism by which colchicine beneficially alters the course of atherosclerosis.

Methods and Results: In mice with early atherosclerosis (*Apoe*$^{-/-}$ mice on a high cholesterol diet for 8 weeks), we found that colchicine treatment (0.25 mg/kg bodyweight once daily over four weeks) reduced numbers of neutrophils, inflammatory monocytes and macrophages inside atherosclerotic aortas using flow cytometry and immunohistochemistry. Consequently, colchicine treatment resulted in a less inflammatory plaque composition and reduced plaque size. We next investigated how colchicine prevented plaque leukocyte expansion and found that colchicine treatment mitigated recruitment of blood neutrophils and inflammatory monocytes to plaques as revealed by adoptive transfer experiments. Causally, we found that colchicine reduced levels of both leukocyte adhesion molecules and receptors for leukocyte chemoattractants on blood neutrophils and monocytes. Further experiments showed that colchicine treatment reduced vascular inflammation also in post-myocardial infarction accelerated atherosclerosis through similar mechanisms as documented in early atherosclerosis. When we examined whether colchicine also decreased numbers of macrophages inside atherosclerotic plaques by impacting monocyte/macrophage transitioning or *in-situ* proliferation of macrophages, we report that colchicine treatment did not influence macrophage precursor differentiation or macrophage proliferation using cell culture experiments with bone marrow derived macrophages.

Conclusions: Our data reveal that colchicine prevents expansion of plaque inflammatory leukocytes through lowering recruitment of blood myeloid cells to plaques. These data provide novel mechanistic clues on the beneficial effects of colchicine in the treatment of atherosclerosis and may inform future anti-inflammatory interventions in patients at risk.

Keywords: atherosclerosis, innate immunity, vascular inflammation, anti-inflammatory treatment, colchicine, leukocyte recruitment, monocytes/macrophages, neutrophils

INTRODUCTION

A large body of evidence has demonstrated that inflammation contributes to all stages of atherosclerotic plaque formation (1–3). Atheroma initiation is characterized by hyperlipidemia-activated endothelial cells, which upregulate leukocyte adhesion molecules and leukocyte attracting chemokines. Consequently, leukocytes – the effector cells of the immune system – are recruited from the blood stream and accumulate in the arterial intima. Intimal leukocytes, mainly myeloid cells (neutrophils, monocytes and macrophages), fuel plaque initiation and progression through 1) release of pro-inflammatory cytokines and chemokines, 2) lipid core formation and enlargement, and 3) thinning of the fibrous cap. As a consequence, plaque destabilization with fibrous cap erosion/rupture may occur resulting in complications such as myocardial infarction (MI) or stroke. Given this background, clinical studies recently probed whether therapeutic targeting of inflammatory pathways may be beneficial in prevention and treatment of atherosclerosis (4). Indeed, the Canakinumab Anti-inflammatory Thrombosis Outcomes Study (CANTOS) provided the first proof of the contribution of inflammation to atherosclerosis in humans and demonstrated that neutralizing interleukin-1 beta (IL-1β) reduces cardiovascular events in patients with atherosclerosis and prior MI (5, 6). This concept was further reinforced by two recent trials using the anti-inflammatory drug colchicine (7, 8): In the Colchicine Cardiovascular Outcomes Trial (COLCOT), colchicine led to a significantly lower risk of ischemic cardiovascular events in patients with prior MI (7) while in the Low-Dose Colchicine (LoDoCo) 2 trial, it reduced cardiovascular events in chronic coronary disease patients (8). Colchicine, an orally administered plant alkaloid used to treat gout and pericarditis, is a potent anti-inflammatory agent mainly acting by inhibiting tubulin assembly and suppressing microtubule formation (key components of the cellular cytoskeleton), but also interfering with NLRP3 (NACHT, LRR and PYD domains-containing protein 3)-inflammasome formation and thereby reducing the release of activated pro-inflammatory IL-1β and interleukin-18 (IL-18) (9).

Although large randomized trials using colchicine to treat atherosclerosis showed promising results, we do not completely understand the biological basis of the beneficial effects. In this study, we sought to explore how colchicine prevents progression of atherosclerosis. Our results show that colchicine reduces vascular inflammation by dampening uptake of inflammatory leukocytes into plaques through altering the recruitment profile of circulating monocytes and neutrophils.

MATERIALS AND METHODS

Mouse Studies

Apoe$^{-/-}$ (B6.129P2-Apoetm1Unc/J) and *Ubc-GFP* mice (C57BL/6-Tg(UBC-GFP)30Scha/J) were purchased from the The Jackson Laboratory (Bar Harbor, ME, USA) and expanded by in-house breeding. C57BL/6 J mice were purchased from Charles River Laboratories (Sulzfeld, Germany). For experiments, *Apoe*$^{-/-}$ mice were fed a high cholesterol diet (HCD, 21.2% fat by weight and 0.2% cholesterol, TD.88137, Envigo, Indianapolis, IN, USA) for a total period of eight weeks. During the last four weeks of HCD, a sterile solution of vehicle [phosphate buffered saline (PBS)] or colchicine (dissolved in sterile PBS, 0.25 mg/kg bodyweight (BW); C3915, Sigma Aldrich, St. Louis, MO, USA) was injected intraperitoneally once daily. The colchicine dosage used was based on previously published studies (10, 11). Unfortunately, it was not possible to quantify plasma concentrations of colchicine in our mice.

For MI experiments, *Apoe*$^{-/-}$ mice were fed a HCD for four weeks and anaesthetized with a combination of midazolam (5.0 mg/kg BW), medetomidine (0.5 mg/kg BW) and fentanyl (0.05 mg/kg BW). C57BL/6 J mice were anaesthetized without prior HCD treatment. After thoracotomy in the left intercostal space, the left anterior descending coronary artery was located and permanently occluded using an 8-0 prolene suture to induce MI. For analgesia, mice received buprenorphine every 8 hours for 3 days. *Apoe*$^{-/-}$ mice were fed the HCD for an additional 5 weeks, with PBS or colchicine injections for the last 4 weeks as described above, while C57BL/6 J mice received vehicle or colchicine (0.25 mg/kg BW every 8 hours) during the first three days after MI.

For all experiments, age- and sex-matched littermates at 8 to 12 weeks of age were used. Assignment to groups was random. Animal experiments were conducted in accordance with the German legislation on protection of animals and approved by the local animal care committee (AZ: ROB-55.2-2532.Vet_02-16-92).

Tissue Processing

For *in vivo* staining of circulating blood leukocytes, an antibody directed against CD45-BV605 (clone 30-F11, 1:10 in 100 µl PBS, BioLegend, San Diego, CA, USA) was injected intravenously 5 min before euthanizing the animals under isoflurane anesthesia. Blood samples were obtained by retrobulbar collection into EDTA-coated tubes. Lysis of erythrocytes was performed in blood samples in 1X RBC Lysis Buffer (420302, BioLegend). After stopping the reaction with PBS, samples were centrifuged at 400 g for 10 min at 4°C and resuspended in FACS Buffer (PBS

containing 0.5% bovine serum albumin, A2153, Sigma Aldrich). Bone marrow was sampled from femurs by flushing the bones with PBS. Cells were then filtered using a 40 µm cell strainer.

For analysis of aortic plaques and cardiac leukocytes, hearts were perfused through the left ventricle with PBS, aortas were extracted carefully from root to common iliac artery bifurcation removing the surrounding tissue. Hearts and aortas were minced in respective digestion buffer. Then, tissues were digested in a solution composed of collagenase I (450 U/ml, C0130), collagenase XI (125 U/ml, C7657), DNase I (60 U/ml, D5319-500UG), and hyaluronidase (60 U/ml, H3506, all Sigma Aldrich) in PBS for 1 h under agitation at 37°C.

For flow cytometric analysis of aortic endothelial cells, digestion buffer consisted of 1X PBS containing DNase I (250 U/ml) and collagenase IV (2500 U/ml, LS004212, CellSystems, Troisdorf, Germany) and aortas were digested for 40 min under agitation at 37°C.

Subsequently, cell suspensions were filtered using a 40 µm cell strainer and resuspended in FACS buffer.

Flow Cytometry and Fluorescence Activated Cell Sorting

Aortic and cardiac cell suspensions were stained with antibodies labelling murine hematopoietic lineage markers (B220 (clone RA3-6B2); CD90.2 (clone 53-2.1, 1:300 dilution); CD49b (clone DX5, 1:1200 dilution); NK1.1 (clone PK136); Ter-119 (clone TER-119) and Ly6G (clone 1A8), all conjugated with phycoerythrin (PE)) and antibodies directed against CD45.2 (PerCP/Cy5.5-conjugated, clone 104, 1:300); CD11b (APC/Cy7-conjugated, clone M1/70); F4/80 (PE/Cy7-conjugated, clone BM8); and Ly6C (BV421- or FITC-conjugated, clone HK1.4). For blood and bone marrow analysis, an antibody against CD115 (BV711-conjugated, clone AFS98) was added to the staining mixture. For BrdU experiments, cells were subsequently fixed and permeabilized and additionally stained in an APC-conjugated anti-BrdU antibody according to the manufacturer's recommendations (552598, BD Biosciences). All antibodies were used in 1:600 dilutions and purchased from BioLegend unless indicated otherwise.

Aortic endothelial cell samples were stained with antibodies against CD54-APC (ICAM1) (clone YN1/1.7.4, 1:600 dilution); CD102-biotin (ICAM2) (clone 3C4, 1:600 dilution; streptavidin-BV510 (1:600 dilution) was used for secondary labelling)); CD106-PE/Cy7 (VCAM1) (clone 429, 1:100 dilution); CD62E-PE (E-Selectin) (clone 10E9.6, 1:50 dilution, BD Biosciences, San Jose, CA, USA); CD62P-FITC (P-Selectin) (clone RB40.34, 1:300 dilution, BD Biosciences); CD31-BV421 (clone 390, 1:600 dilution); CD107a-APC/Cy7 (LAMP1) (clone 1D4B, 1:300 dilution); and CD45.2-PerCP/Cy5.5 (clone 104, 1:300 dilution, all BioLegend unless indicated otherwise).

Cell suspensions were submitted to flow cytometric analysis on a BD LSRFortessa (BD Biosciences) and files were analyzed using FlowJo software (version 9 or 10). Therefore, cells were pre-gated on viable (FSC-A vs. SSC-A) and single (FSC-A vs. FSC-W and SSC-A vs. SSC-W) cells. Myeloid cells were characterized as follows: neutrophils as CD45.2^{high}CD11b^{high}lineage^{high}CD115^{low}Ly6C^{intermediate}, monocytes as CD45.2^{high}CD11b^{high}lineage^{low}F4/80^{low}Ly6C$^{high/low}$ (in aortic cell suspensions) or CD45.2^{high}CD11b^{high}lineage^{low}CD115^{high}Ly6C$^{high/low}$ (in blood and bone marrow) and macrophages as CD45.2^{high}CD11b^{high}lineage^{low}Ly6C$^{low/intermediate}$F4/80^{high}. Contaminating blood leukocytes were excluded by omitting CD45-BV605^{+} cells in the gating. Endothelial cells were identified as CD45.2^{low}CD31^{high}CD107a$^{intermediate/high}$ and adhesion molecule expression was quantified using respective histograms.

For fluorescence-activated cell sorting (FACS), blood leukocytes and aortic endothelial cells were sorted on a FACS Aria III using FACSDiva Software version 6 (BD Biosciences). Neutrophils were identified as CD45.2^{high}CD11b^{high}lineage^{high}CD115^{low}Ly6C^{intermediate}, Ly6C^{high} and Ly6C^{low} monocytes as CD45.2^{high}CD11b^{high}lineage^{low}CD115^{high}Ly6C$^{high/low}$, and endothelial cells as CD45.2^{low}CD31^{high} cells. Cells were directly sorted into RNA extraction buffer (KIT0204, Thermo Fisher Scientific) containing tubes and snap-frozen to -80°C.

Histology

Aortic roots were excised, embedded in optimal cutting temperature compound (Sakura Finetek, Tokyo, Japan) and snap frozen to -80°C. Samples were cut into 5 µm cross-sections. Per staining, 5 sections were examined at 25 µm intervals per mouse.

The absolute size of the plaques was determined by Masson trichrome staining (HT15-1KT, Sigma Aldrich). Sections were fixed in 4% PFA for 45 seconds and stained corresponding to the manufacturer's protocol. Mean total plaque area [in µm (2)] was evaluated for sections showing at least two complete cusps and analyzed using ImageJ. An average value per mouse was then calculated.

To analyze the distribution of CD11b^{+} cells, sections were fixated in ice-cold acetone for 10 min and blocked in 10% rabbit serum (Vector Laboratories, Burlingame, CA, USA). Specimens were stained with an anti-CD11b antibody (101202, BioLegend) or anti-Ly6G antibody (clone 1A8, BioLegend), respectively, followed by a HRP conjugated secondary antibody (ab6734) and AEC substrate (ab64252, both abcam, Cambridge, MA, USA). Cell nuclei were counterstained with Gill's hematoxylin solution II (1051752500, Merck Millipore). The CD11b or Ly6G content was determined by quantifying the CD11b- or Ly6G-positive area per total plaque area using ImageJ software.

Isolation of Nucleic Acids and Real-Time Quantitative Polymerase Chain Reaction (qPCR)

Aortic arches were minced in 500 µl of Qiazol lysis reagent (Qiagen, Hilden, Germany) with the aid of a mechanical disruptor (TH220) using soft tissue tips (all OMNI International, Kennesaw, GA, USA). Total ribonucleic acid (RNA) was extracted by using the RNeasy Mini Kit (Qiagen)

corresponding to the manufacturer´s instructions, involving an additional DNA removal step (RNase-free DNase set, Qiagen).

RNA of FACS-sorted leukocytes and aortic endothelial cells was isolated according to the manufacturer's instructions (PicoPure™ RNA Isolation Kit, Thermo Fisher Scientific).

RNA quality was assessed using a NanoQuant Plate on an Infinite M200 PRO plate reader (both TECAN, Männedorf, Switzerland) and first-strand cDNA was generated using the High-Capacity RNA-to-cDNA kit (Applied Biosystems, Waltham, MA).

Real-time qPCR was performed using TaqMan probes (listed in **Supplementary Table S1**) and TaqMan Fast Universal PCR Master Mix (4352042) over 40 cycles on a ViiA 7 system (all Thermo Fisher Scientific, Waltham, MA, USA). *Gapdh* was used as a housekeeping gene and data were converted to $2^{-\triangle\triangle Ct}$ values.

Cell Sorting and Adoptive Transfer

Ubc-GFP donor animals were subjected to the experiments either untreated or after one week of treatment with PBS or colchicine (0.25 mg/kg BW) injected intraperitoneally once daily. Single cell suspensions were prepared from the bone marrow as described above. Neutrophils and monocytes were isolated by staining the cells with Ly6G-PE (clone 1A8) and CD115-biotin (clone AFS98, both BioLegend) followed by linking to magnetic beads (anti-PE and streptavidin microbeads, Miltenyi Biotec, Bergisch Gladbach, Germany) and enrichment on magnetic-activated specific columns (130-042-401, Miltenyi Biotec). The degree of purification of the separated cells was determined by flow cytometry.

Equal cell amounts were injected intravenously into *Apoe*$^{-/-}$ mice 24 h before harvest. Quantification of recruited $CD11b^{high}GFP^{high}$ cells within aortas was assessed by flow cytometry.

Cell Culture

Bone marrow cells were isolated from C57BL/6 J mice by flushing the femurs with RPMI 1640 (A1049101, Thermo Fisher Scientific) containing 2% of fetal bovine serum (FBS; S0615, Sigma Aldrich). Erythrocytes were removed by incubating the cells in 1X RBC lysis buffer (BioLegend). Subsequently, cells were cultured for the indicated time in RPMI 1640 containing 10% FBS, 100 U/ml penicillin-streptomycin (15140122, Thermo Fisher Scientific) and 50 ng/ml recombinant mouse M-CSF (R&D Systems, Minneapolis, MN, USA) in 6-well plates [80,000 cells/cm (2)] in a humidified incubator with 5% CO_2 at 37°C. Fresh medium was added every day, and every third day the medium was partially replaced with fresh medium containing the resuspended non-adherent cells. In the respective experiments, colchicine (0, 1, or 10 ng/ml final concentration) was added along with the culture medium daily for one to six days as indicated in the respective figures.

For BrdU experiments, bone marrow cells were cultured into macrophages in 100 mm dishes for two or three days, respectively, and reseeded in 6-well plates [80,000 cells/cm (2)]. Colchicine (0, 1, or 10 ng/ml final concentration) was added along with fresh culture medium for the last 24 or 48 hours as indicated in the respective figures. BrdU solution (10 μM final concentration, BrdU Flow Kit, BD Biosciences) was added two hours before harvesting of cells.

Non-adherent cells were collected, adherent cells were washed in HEPES-buffered saline solution (Promocell, Heidelberg, Germany), detached by incubating in Accutase (Sigma Aldrich) and, together with non-adherent cells, resuspended in FACS buffer before flow cytometry analysis.

Statistical Analysis

All statistical analysis was conducted using GraphPad Prism version 9. Normality distribution was tested by the D'Agostino-Pearson omnibus K2 normality test or the Shapiro-Wilk test for sample sizes n<8. Two-group comparisons were performed using two-sided Student´s *t*-test (normally distributed data; Welch's *t*-test was used if variances between both groups were significantly different, as tested by *F*-test) or two-sided Mann-Whitney *U*-test (non-normally distributed data), as shown in the figure legends in combination with sample sizes. Comparisons of three or more groups were performed using repeated measures one-way ANOVA followed by Dunnett's multiple comparisons test (normally distributed data) and Friedman test followed by Dunn's multiple comparisons test (non-normally distributed data), as appropriate and indicated in the figure legends. A two-sided ROUT´s test was applied to determine statistical outliers. All graphs illustrate data as mean + s.e.m. Statistical significance was assumed if *P*-values were <0.05. Mouse experiments were performed at least twice or with n ≥ 10. Where appropriate, variation between experiments was adjusted by normalizing absolute values to a representative experiment.

RESULTS

Colchicine Treatment Reduced Inflammatory Leukocyte Accumulation in Atherosclerotic Aortas

To explore the mechanisms by which colchicine beneficially alters the course of atherosclerosis, we treated atherosclerosis-prone mice (*Apoe*$^{-/-}$ mice on a high cholesterol diet for eight weeks) with either vehicle or colchicine for four weeks. We found that colchicine reduced inflammatory leukocyte numbers over vehicle in atherosclerotic aortas (**Figures 1A, B**, **Supplementary Figure 1A, B**). We corroborated our flow cytometry findings using immunohistochemistry and observed fewer intimal myeloid cells (monocytes/macrophages and neutrophils) and neutrophils in aortic root sections from colchicine treated mice stained for the myeloid marker CD11b and the neutrophil marker Ly6G, respectively (**Figures 1C, D**). Next, we tested whether reduced plaque inflammation changed the overall plaque character. Phenotyping of plaques using quantitative polymerase chain reaction (qPCR) revealed that colchicine treatment reduced expression of mRNAs that encode the pro-inflammatory cytokine TNF (tumor necrosis factor), while it had no effect on transcriptional levels of IL-1β (interleukin-1 beta)

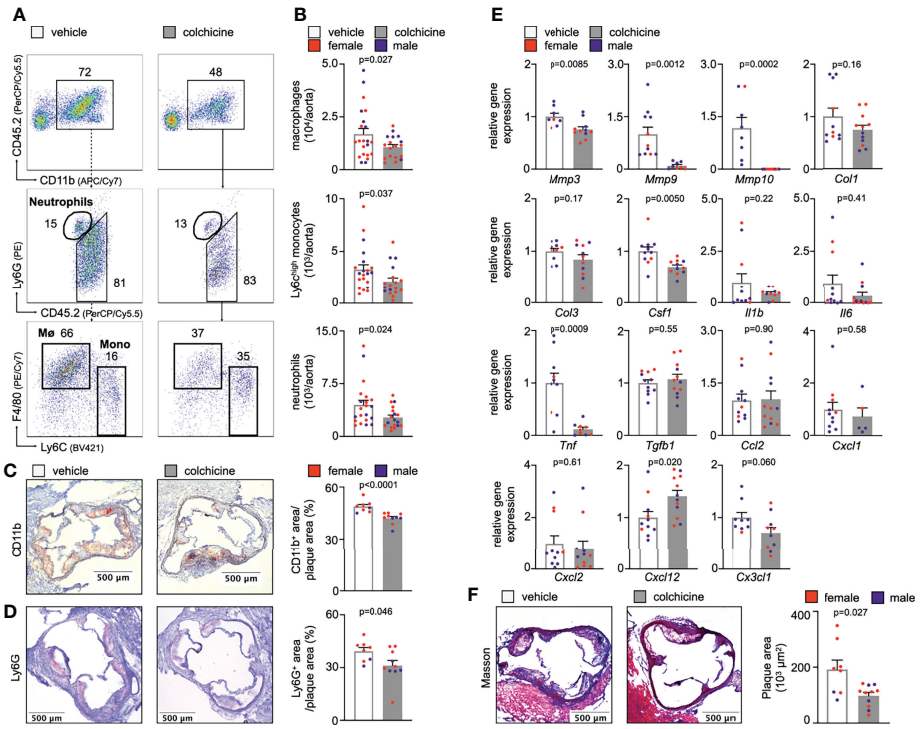

FIGURE 1 | Colchicine treatment reduces plaque inflammation. **(A)** Flow cytometric gating and **(B)** quantification of myeloid cells in atherosclerotic aortas in vehicle- vs. colchicine-treated *Apoe*$^{-/-}$ mice (*n*=18-21 per group, 62-67% female, Welch's *t*-test for macrophages (Mø), Mann-Whitney *U*-test for monocytes (Mono) and neutrophils as appropriate). Numbers next to gates indicate population frequencies (%). Representative immunohistochemical staining for **(C)** myeloid cells (CD11b) and **(D)** neutrophils (Ly6G) of sectioned aortic roots from vehicle- vs. colchicine-treated *Apoe*$^{-/-}$ mice (*n*=8-10 per group, 60-75% female, Mann-Whitney *U*-test for CD11b, Student's *t*-test for Ly6G). Bar graphs show quantification of positive CD11b- and Ly6G-area, respectively. Scale bars represent 500 µm. **(E)** Quantitative real-time PCR for gene expression quantification of fibrotic, inflammatory and cytokine genes in aortas of vehicle- vs. colchicine-treated *Apoe*$^{-/-}$ mice (*n*=5-12 per group, 55-88% female, Student's/Welch's *t*-test or Mann-Whitney *U*-test as appropriate). *Mmp3/Mmp9/Mmp10* (matrix metalloproteinase-3/9/10), *Col1/Col3* (collagen-1/3), *Csf1* (colony stimulating factor 1), *Il1β* (interleukin 1 beta), *Il6* (interleukin 6), *Tnf* (tumor necrosis factor), *Tgfb1* (transforming growth factor beta 1), *Ccl2* (C-C Motif Chemokine Ligand 2), *Cxcl1* (C-X-C Motif Chemokine Ligand 1), *Cxcl2* (C-X-C Motif Chemokine Ligand 2), *Cxcl12* (C-X-C Motif Chemokine Ligand 12), *Cx3cl1* (C-X3-C Motif Chemokine Ligand 1). Data are presented as mean+s.e.m. **(F)** Representative Masson Trichrome staining and quantification of total plaque area (*n*=8-11 per group, 64-75% female, Welch's *t*-test). Scale bars represent 500 µm. Dots within bar plots show the gender of the mice with a color code: purple (male) and red (female).

and IL-6 (interleukin-6) (**Figure 1E**). Levels of MMP (matrix metalloproteinase)-3, MMP-9, and MMP-10 decreased in colchicine treated mice (**Figure 1E**). MMPs support extracellular matrix degradation, a process that may lead to atherosclerotic plaque destabilization (12). Histology revealed a smaller total plaque size in the colchicine group (**Figure 1F**). Of note, colchicine treatment did not alter body weight or LDL cholesterol levels in mice. Colchicine treated mice did not show any type of discomfort or impairment compared to mice receiving vehicle (**Supplementary Figure 2A**). Taken together, these data indicate that colchicine treatment limited plaque inflammation and hence progression of atherosclerosis.

Colchicine Treatment Dampened Plaque Leukocyte Recruitment

We next addressed how colchicine treatment reduced inflammatory leukocyte accumulation in atherosclerotic aortas. To explore whether colchicine dampened blood inflammatory leukocyte recruitment into atherosclerotic aortas, we performed adoptive transfer experiments. Here, we isolated GFP^{high} myeloid cells (monocytes admixed with neutrophils) from naïve transgenic *Ubc-GFP* mice (all leukocytes express green fluorescent protein, GFP) and injected these cells intravenously into *Apoe*$^{-/-}$ mice (all cells are GFP^{negative}) which were treated with either vehicle or colchicine for 4 weeks (**Supplementary Figure 1C**). 24h after the transfer, we quantitated GFP^{high} myeloid cells inside atherosclerotic aortas using flow cytometry and found that colchicine treatment lowered GFP^{high} myeloid cell numbers, while GFP^{high} myeloid cell numbers in the blood did not show any differences between the two groups (**Figure 2A**, **Supplementary Figure 1D**). These data show that colchicine mitigates myeloid cell uptake from blood into atherosclerotic aortas.

Colchicine Treatment Altered the Recruitment Profile of Monocytes and Neutrophils

Leukocyte recruitment refers to a process in which endothelial cells and circulating leukocytes need to interact closely to

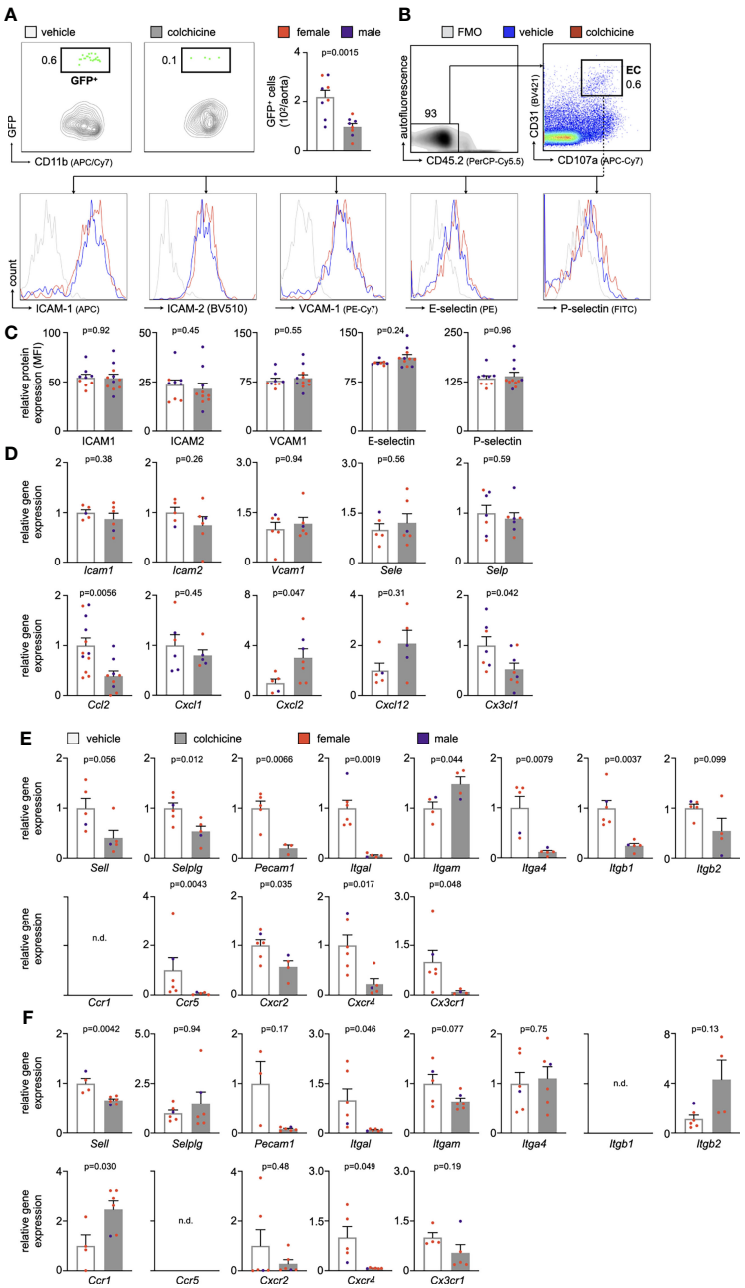

FIGURE 2 | Colchicine treatment dampens leukocyte recruitment to atherosclerotic aortas by silencing neutrophil and monocyte activation. **(A)** Flow cytometric gating and quantification of GFP^{high} (GFP^{+}) myeloid cells in atherosclerotic aortas 24h after adoptive transfer of GFP^{high} monocytes and neutrophils into vehicle- vs. colchicine-treated *Apoe*$^{-/-}$ mice (n=8 per group, 38-50% female, Student's t-test). **(B)** Gating strategy and histograms of leukocyte adhesion molecules on aortic endothelial cells (EC) from vehicle- vs. colchicine-treated *Apoe*$^{-/-}$ mice. **(C)** Quantification of mean fluorescent intensities (MFI, representing relative protein levels) of adhesion molecules expressed by aortic endothelial cells from vehicle- vs. colchicine-treated *Apoe*$^{-/-}$ mice (n=9-11 per group, 44-55% female, Student's t-test or Mann-Whitney U-test as appropriate). Bar graphs indicate relative change of MFI standardized to controls. FMO (fluorescence minus one (respective antibody omitted)) control. Quantitative real-time PCR for gene expression quantification in fluorescence-activated cell sorting (FACS)-purified **(D)** aortic endothelial cells, **(E)** blood neutrophils and **(F)** blood Ly6C^{high} monocytes of vehicle- vs. colchicine-treated *Apoe*$^{-/-}$ mice (n=3-12 per group, 33-100% female, Student's/Welch's t-test or Mann-Whitney U-test as appropriate). ICAM-1/*Icam1* (intercellular adhesion molecule 1), ICAM-2/*Icam2* (intercellular adhesion molecule 2), VCAM-1/*Vcam1* (vascular cell adhesion protein 1), E-selectin/*Sele*, P-selectin/*Selp*, L-selectin/*Sell*, selectin P ligand/*Selplg*, platelet endothelial cell adhesion molecule-1/*Pecam1*, integrin subunit alpha L/*Itgal*, integrin subunit alpha M/*Itgam*, integrin subunit alpha 4/*Itga4*, integrin subunit beta 1/*Itgb1*, integrin subunit beta 2/*Itgb2*, C-C motif chemokine ligand 2/*Ccl2*, C-X-C motif chemokine ligands 1 + 2+12/*Cxcl1/Cxcl2/Cxcl12*, C-X3-C motif ligand 1/*Cx3cl1*, C-C chemokine receptor types 1 + 5/*Ccr1/Ccr5*, C-X-C Motif chemokine receptor types 2 + 4/*Cxcr2/Cxcr4* and C-X3-C Motif Chemokine Receptor 1/*Cx3cr1*. Data are presented as mean+s.e.m. Numbers next to gates indicate population frequencies (%). Dots within bar plots show the gender of the mice with a color code: purple (male) and red (female).

mediate leukocytes rolling, adhesion and transmigration/extravasation (13, 14). To investigate how colchicine treatment limited myeloid cell recruitment from blood to atherosclerotic aortas, we used flow cytometry to assess levels of leukocyte adhesion molecules on endothelial cells from atherosclerotic aortas. Our data revealed that colchicine had no effect on protein levels of leukocyte adhesion molecules ICAM-1 (intercellular adhesion molecule-1), ICAM-2 (intercellular adhesion molecule 2), VCAM-1 (vascular cell adhesion protein 1), E-selectin and P-selectin (**Figures 2B, C**). Moreover, we found that colchicine treatment lowered transcriptional levels of only Ccl2 (chemokine (C-C motif) ligand 2) and Cx3cl1 (C-X3-C Motif Chemokine Ligand 1) – both known chemoattractants for monocytes – while expression of other leukocyte-attracting chemokines and leukocyte adhesion molecules remained unchanged in fluorescence-activated cell sorting (FACS)-purified endothelial cells from atherosclerotic aortas (**Figure 2D**). Next, we FACS-purified blood Ly6C^{high} monocytes and neutrophils from *Apoe*$^{-/-}$ mice treated with either vehicle or colchicine. In contrast to endothelial cells, we found that both blood Ly6C^{high} monocytes and neutrophils underwent profound phenotypic alteration in colchicine treated mice (**Figure 2E, F**). Blood neutrophils responded to colchicine treatment and downregulated leukocyte adhesion molecules [such as *Selplg* (selectin P ligand), *Pecam1* (platelet endothelial cell adhesion molecule), integrin subunits *Itgal* (Integrin Subunit Alpha L), *Itga4* (Integrin Subunit Alpha 4), *Itgb1* (Integrin Subunit Beta 1)], and chemokine receptors (such as *Ccr5* [C-C chemokine receptor type 5), *Cxcr2+4* (C-X-C Motif chemokine receptor types 2 + 4), and *Cx3cr1* (C-X3-C Motif Chemokine Receptor 1)], as revealed by gene expression profiling (**Figure 2E**). Similarly, blood Ly6C^{high} monocytes also underwent phenotypic changes in response to colchicine and downregulated leukocyte adhesion molecules (such as *Sell* (Selectin L, CD62L) and integrin subunit *Itgal*) and chemokine receptors (such as *Cxcr4*) (**Figure 2F**). We next tested *in vivo* how these colchicine-induced phenotypic changes impact leukocyte recruitment. We treated transgenic *Ubc-GFP* mice (all leukocytes are GFP^{high}) with colchicine for seven days and then retrieved both monocytes and neutrophils from these mice (experimental setup outlined in **Figure 3A**). These GFP^{high} leukocytes were then adoptively transferred into atherosclerotic *Apoe*$^{-/-}$ recipient mice, which were not treated with colchicine. In this setting, only transferred blood monocytes and neutrophils, but not endothelial cells, were exposed to colchicine. 24h after the transfer we enumerated GFP^{high} leukocytes inside atherosclerotic plaques using flow cytometry and found that colchicine-exposed neutrophils and monocytes were recruited less in comparison to vehicle-exposed neutrophils and monocytes (**Figures 3B, C**, **Supplementary Figure 3**). These data indicate that colchicine dampened recruitment of neutrophils and monocytes into plaques primarily by altering the recruitment profile of these immune cells. Leukocyte subset numbers were unchanged in the blood and bone marrow (**Figure 4**).

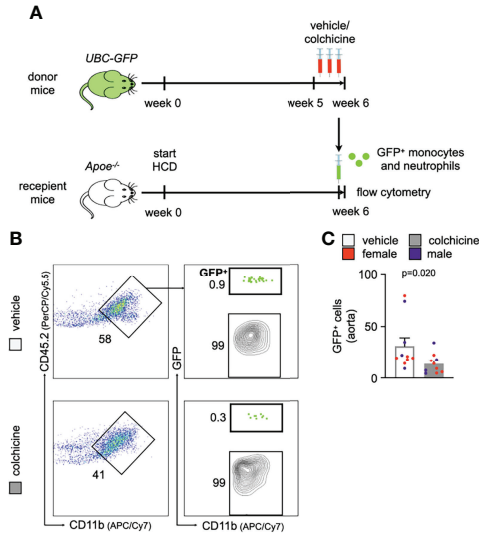

FIGURE 3 | Colchicine exposed neutrophils and monocytes show reduced recruitment capacities. **(A)** Experimental scheme. **(B)** Flow cytometric gating and **(C)** quantification of GFP^{high} myeloid cells (GFP^{+}) in atherosclerotic aortas 24h after adoptive transfer of either vehicle- or colchicine-exposed GFP^{high} monocytes and neutrophils into *Apoe*$^{-/-}$ mice (*n*=10 per group, 60% female, Mann-Whitney *U*-test). Data are presented as mean+s.e.m. Numbers next to gates indicate population frequencies (%). Dots within bar plots show the gender of the mice with a color code: purple (male) and red (female).

Colchicine Treatment Impacted Neither Transition of Monocytes to Macrophages nor Macrophage Proliferation

Apart from reducing uptake, we tested whether colchicine – a known anti-mitotic agent with anti-proliferative effects – also prevents accumulation of plaque macrophages by 1) inhibiting differentiation/maturation of recruited monocytes into macrophages or 2) reducing *in-situ* proliferation of plaque macrophages. To this end, we seeded murine bone marrow cells (retrieved from flushed femurs of wild-type mice) and incubated them with M-CSF (macrophage colony-stimulating factor) to generate bone marrow-derived macrophages (BMDM). In kinetic experiments, we found the strongest surge in macrophage numbers around days 3 to 5 (**Supplementary Figures 4A–C**). To interfere with macrophage generation, we added either vehicle or colchicine early on starting immediately after seeding (doses: 1 and 10 ng colchicine/ml; a 100 ng colchicine/ml dose was found to be cytotoxic) for six days (**Figure 5A**). We found macrophage numbers to be unchanged between vehicle and different doses of colchicine (**Figures 5B, C**). Experiments in which we added colchicine at a later time point and/or for shorter periods revealed the same results and again did not show differences in macrophage numbers (**Supplementary Figures 5A–H**). These data suggest that colchicine may not impact maturation/differentiation of monocyte progenitors/monocytes into macrophages. To assess a potential effect of colchicine on macrophage proliferation, we

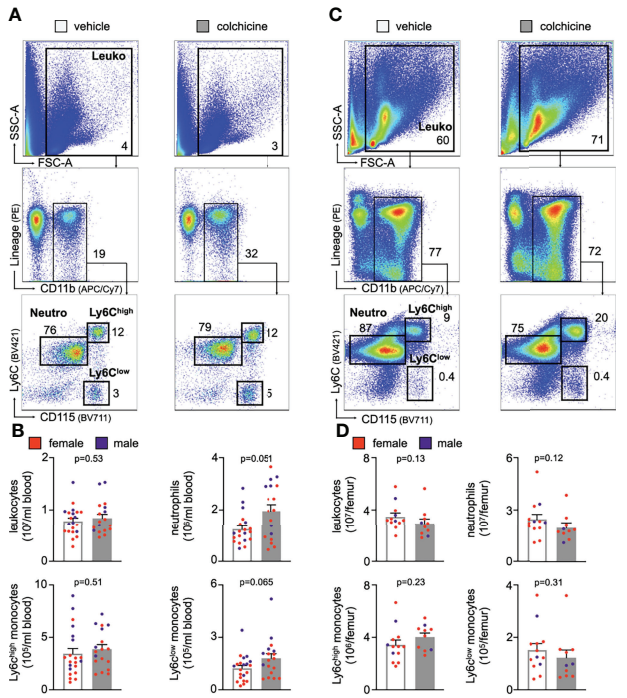

FIGURE 4 | Colchicine treatment did not alter numbers of blood leukocyte subsets. Flow cytometric gating and quantification of myeloid cells in the blood **(A, B)** (*n*=18-21 per group, 62-67% female, Student's *t*-test for total leukocytes (Leuko) and Ly6C^{high} monocytes (Ly6C^{high}), Mann-Whitney *U*-test for neutrophils (Neutro) and Ly6C^{low} monocytes (Ly6C^{low}) and bone marrow **(C, D)** in vehicle- vs. colchicine-treated *Apoe*$^{-/-}$ mice (*n*=10-13 per group, 77-80% female, Mann-Whitney *U*-test). Data are presented as mean+s.e.m. Numbers inside/next to gates indicate population frequencies (%). Dots within bar plots show the gender of the mice with a color code: purple (male) and red (female).

first generated BMDM and subsequently added colchicine on day 4 for 48h (**Figure 5D**). Using cell cycle analyses, we found that the macrophage proliferation rate (BrdU (bromodeoxyuridine) incorporation) did not differ between groups (**Figures 5E, F**). Consequently, colchicine did not change macrophage numbers over vehicle (**Figure 5F**) on day 6. Similar results regarding proliferation were obtained when we added colchicine earlier and/or used shorter incubation periods (**Supplementary Figures 6A–F**). Taken together, these data suggest that colchicine – used in dosages that resemble the colchicine plasma concentration range in treated patients (15) – may not reduce plaque macrophage accumulation by i) preventing the transition of monocytes into macrophages or by ii) impacting macrophage proliferation.

Colchicine Treatment Curtailed Leukocyte Accumulation in Atherosclerotic Aortas Also in Post-MI Accelerated Atherosclerosis

The above performed experiments explored how colchicine treatment impacts early atherosclerosis (atherogenesis), i.e. primary prevention. We next probed whether these beneficial effects also occur in secondary prevention, i.e. in the setting of prior MI as investigated in the COLCOT trial. We surgically induced MI (permanent left anterior descending coronary artery ligation) in atherosclerotic mice (**Figure 6A**) and administered either vehicle or colchicine for 4 weeks starting one week after MI. We then excised atherosclerotic aortas, enumerated leukocytes, and found that colchicine treatment reduced numbers of macrophages, Ly6C^{high} monocytes, and neutrophils (**Figures 6B, C**, **Supplementary Figure 7**). Using adoptive transfer, we tested whether colchicine also reduced uptake of monocytes and neutrophils and found fewer GFP^{high} myeloid cells inside atherosclerotic aortas in the treatment group in post-MI accelerated atherosclerosis (**Figure 6D**). Exploring the blood compartment, we found higher numbers of blood neutrophils (**Figure 6E**). These data suggest that colchicine treatment reduced inflammatory leukocyte recruitment in post-MI accelerated (**Figure 6**) as well as primary atherosclerosis (**Figures 1–4**).

Colchicine Treatment Limited Expansion of Myeloid Cells Also in Acute and Chronic Cardiac Inflammation

Finally, we tested colchicine also in the setting of cardiac inflammation (16). To this end, wild-type mice were subjected to experimental MI (permanent left anterior descending coronary artery ligation) and treated with either high dose colchicine or vehicle starting two hours after induction of cardiac ischemia (**Supplementary Figure 8A**). Three days after MI, we enumerated leukocyte numbers inside the ischemic cardiac area using flow cytometry (**Supplementary Figure 8B**). We found fewer neutrophils in colchicine treated mice with MI while numbers for other myeloid cells remained unchanged (**Supplementary Figure 8C**). Next, we extended our investigations from acute MI to chronic MI/chronic ischemic cardiomyopathy with chronic heart failure. Here, we infarcted *Apoe*$^{-/-}$ mice and started administering vehicle or colchicine 7 days after MI for 4 weeks (**Figure 6A**). Adoptive transfer experiments revealed reduced uptake of adoptively transferred GFP^{+} cells into infarcted hearts in the colchicine group (**Supplementary Figure 8D**). Consequently, numbers of cardiac inflammatory monocytes and macrophages decreased in colchicine treated mice (**Supplementary Figure 8E**). To conclude, colchicine reduced numbers of cardiac inflammatory leukocytes within infarcted hearts, especially affecting neutrophils in the acute setting, and monocytes/macrophages in the chronic phase after MI.

DISCUSSION

Colchicine, derived from the plant extract of *Colchicum autumnale*, is a broadly available, inexpensive, orally administered drug with multiple mechanisms of action, some of which are still under investigation (9, 15, 17, 18). The primary intracellular targets of colchicine are microtubules which are essential components of the cellular cytoskeleton. Microtubules

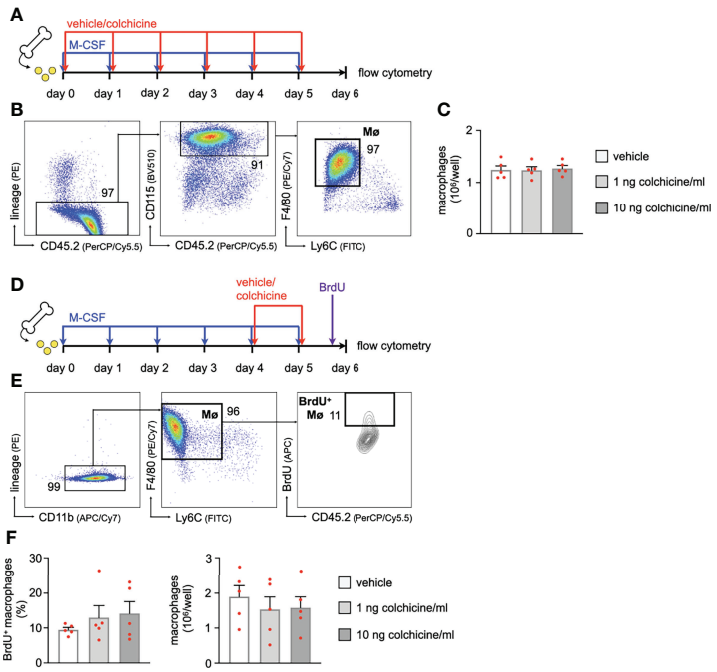

FIGURE 5 | Colchicine treatment impacts neither macrophage precursor differentiation nor macrophage proliferation. **(A)** Experimental scheme for precursor differentiation into macrophages (Fig. 6B+C). In brief, bone marrow cells were retrieved from one femur and cultured with M-CSF (macrophage colony-stimulating factor) for 6 days to generate bone marrow-derived macrophages (BMDM). Either vehicle or colchicine was added once every 24h starting immediately after seeding. **(B)** Flow cytometric gating and **(C)** quantification of macrophage (Mø) numbers 6 days after either vehicle or colchicine exposure (n=5 per group, each n represents one donor animal; repeated measures one-way ANOVA with Dunnett's multiple comparisons test). **(D)** Experimental scheme for macrophage proliferation (Fig. 6E+F). In brief, bone marrow cells were retrieved from one femur and cultured with M-CSF (macrophage colony-stimulating factor) for 6 days to generate bone marrow-derived macrophages (BMDM). Either vehicle or colchicine was added once every 24h starting 4d after seeding. BrdU (bromodeoxyuridine) was administered 2h before the harvest (day 6 after seeding). **(E)** Flow cytometric gating and **(F)** quantification of BrdU$^+$ macrophage (BrdU$^+$ Mø) frequencies (Friedman test followed by Dunn's multiple comparisons test) and total macrophage numbers 48h after either vehicle or colchicine exposure (repeated measures one-way ANOVA with Dunnett's multiple comparisons test). n=5 per group (each n represents one donor animal). Data are presented as mean+s.e.m. Numbers next to gates indicate population frequencies (%).

play a pivotal role in maintaining cell shape, intracellular trafficking, cytokine secretion, cell migration, and cell division (9). At low doses, colchicine prevents growth of microtubules, while it supports microtubule depolymerization at high doses. Colchicine's effect on tubulin disruption prevents the formation of the inflammasome which results in less secretion of pro-inflammatory cytokines and impaired neutrophil function (9, 19). Given this background, colchicine was explored as a novel anti-inflammatory treatment strategy in patients with coronary artery disease (CAD). In the LoDoCo trial, low-dose colchicine treatment reduced cardiovascular events in patients with stable CAD (20). These results were confirmed in the LoDoCo2 trial which reported a 31% relative risk reduction of cardiovascular events in stable CAD patients treated with colchicine compared to placebo (8). Regarding acute coronary syndromes, the COLCOT trial reported that among patients with recent MI, colchicine at a dose of 0.5 mg daily reduced cardiovascular outcomes over placebo, an effect that was mainly driven by a lower incidence of strokes and urgent hospitalizations for angina leading to coronary revascularization (7).

Although these results are encouraging, we do not fully understand the underlying mechanisms for the cardiovascular benefits of colchicine. In this study we provide evidence that colchicine reduces vascular inflammation and dampens progression of atherosclerosis. Causally, we found that colchicine decreased accumulation of inflammatory leukocytes inside atherosclerotic plaques which in turn altered the overall plaque character. In line with our study, a recent report showed that colchicine decreased plaque vulnerability with reductions in plaque inflammation, medial fibrosis and vascular remodeling in atherosclerotic rabbits (21). According to our data, colchicine reduced expansion of inflammatory leukocytes by preventing influx of inflammatory monocytes and neutrophils from the blood into aortic plaques. Previously, it was described that colchicine can act on both endothelial cells and neutrophils: in endothelial cells colchicine reduced expression of E-selectin, in neutrophils colchicine decreased expression of L-selectin and neutrophil extracellular trap formation (22, 23). In line, we also found that blood monocytes/neutrophils and plaque endothelial cells underwent phenotypic changes in response to colchicine. However, colchicine seems to affect blood leukocytes stronger than endothelial cells. While transcriptomic profiling of FACS-purified plaque endothelial cells revealed only mild colchicine-induced alterations, we found substantial changes in blood

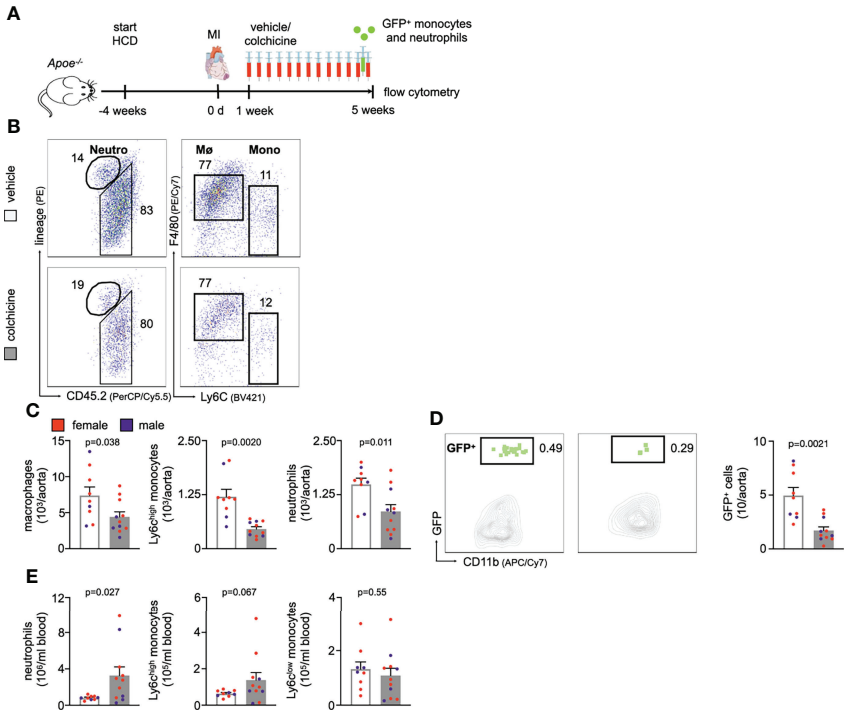

FIGURE 6 | Colchicine treatment reduces vascular inflammation in post-myocardial infarction accelerated atherosclerosis. **(A)** Experimental scheme for **Figures 6B-E**. In brief, *Apoe*$^{-/-}$ mice on a high cholesterol diet (HCD) were subjected to myocardial infarction (MI) and treated with either vehicle or colchicine for four weeks starting one week after induction of MI. **(B)** Flow cytometric gating and **(C)** quantification of leukocyte subsets in atherosclerotic aortas in vehicle- vs. colchicine-treated *Apoe*$^{-/-}$ mice which were infarcted five weeks prior (*n*=9-11 per group, 64-67% female, Student's *t*-test for macrophages and neutrophils, Welch's *t*-test for monocytes). Neutro: neutrophils, Mø: macrophages and Mono: monocytes **(D)** Flow cytometric gating and quantification of GFP^{high} myeloid cells (GFP^{+}) in atherosclerotic aortas 24h after adoptive transfer of GFP^{high} monocytes and neutrophils into vehicle- vs. colchicine-treated *Apoe*$^{-/-}$ mice which were infarcted five weeks prior (*n*=9-11 per group, 64-67% female, Welch's *t*-test). **(E)** Quantification of blood leukocyte subsets in vehicle- vs. colchicine-treated *Apoe*$^{-/-}$ mice which were infarcted five weeks prior (*n*=9-11 per group, 64-67% female, Welch's *t*-test for neutrophils, Mann-Whitney *U*-test for Ly6C^{high} monocytes, Student's *t*-test for Ly6C^{low} monocytes). Data are presented as mean+s.e.m. Numbers next to gates indicate population frequencies (%). Dots within bar plots show the gender of the mice with a color code: purple (male) and red (female).

neutrophils and Ly6C^{high} monocytes. We determined the consequences of reduced myeloid cell accumulation in colchicine treated mice using qPCR. Whether the observed reduction in expression levels led to reduced protein levels remains to be investigated. In sum, these data demonstrate that colchicine mitigates blood leukocyte recruitment into atherosclerotic aortas predominantly by silencing blood neutrophil and monocyte activation, suggesting a largely endothelial cell-independent effect of colchicine on inflammatory leukocyte recruitment. However, we cannot exclude that colchicine also impacts the recruitment profile of endothelial cells beyond adhesion molecule and chemokine expression (24).

Further research is needed to decipher whether colchicine exerts its action 1) exclusively on circulating blood monocytes and neutrophils or 2) on monocytes and neutrophils in other compartments prior to egress into the blood. The fact that we did not observe a retention of neutrophils and monocytes in the bone marrow (their numbers were unchanged), however, argues for an effect that is mediated in the circulation. Moreover, further investigations that explore how exactly colchicine leads to downregulation of adhesion molecules and chemokine receptors on monocytes and neutrophils are needed. One may speculate that colchicine-induced microtubules'/cytoskeleton alterations affect cell adhesion molecules since both are known to bidirectionally interact (25).

Apart from increased monocyte recruitment, macrophages may also expand inside plaques through accelerated conversion/differentiation of recruited monocytes and/or *in-situ* proliferation (26). We cultured mouse whole bone marrow cells with M-CSF – a cytokine that causes bone marrow cells to differentiate into macrophages – and added either vehicle or colchicine early on. Our kinetics experiments revealed that macrophage numbers were not at any time point affected by colchicine treatment. These findings are in line with a prior report where colchicine also failed to influence monocyte differentiation (27). We next tested the possibility that colchicine dampened accumulation of plaque macrophages by reducing *in-situ* macrophage proliferation. Although described for vascular smooth muscle cells (28), colchicine did not influence macrophage proliferation. Taken together, colchicine does not seem to impact i) monocyte trans-differentiation into

macrophages or ii) macrophage proliferation in *in-vitro* experiments using colchicine concentrations comparable to clinical settings.

Colchicine was also tested to treat acute coronary syndromes in humans. In this context, high-dose colchicine was administered over a short period starting early after onset of chest pain/MI. While one study revealed smaller infarct sizes in MI patients treated with colchicine, two other recent trials failed to document a clear benefit of colchicine in the acute stetting (29–31). This motivated us to investigate colchicine also in acute and chronic MI. Our experiments reveal that colchicine – as in the setting of atherosclerosis – reduced accumulation of cardiac inflammatory myeloid cells, indicating the operation of convergent mechanisms (reduced uptake of inflammatory leukocytes).

CONCLUSION

Taken together, our data suggest that colchicine – an inhibitor of microtubule assembly with anti-inflammatory properties – reduces vascular inflammation and plaque progression by silencing monocyte and neutrophil activation and thereby preventing uptake of these cells into atherosclerotic plaques. Our data shed new light on the mechanism by which colchicine reduces the risk of cardiovascular complications.

DATA AVAILABILITY STATEMENT

The original contributions presented in the study are included in the article/**Supplementary Material**. Further inquiries can be directed to the corresponding author.

ETHICS STATEMENT

The animal study was reviewed and approved by the local animal care committee (Regierung von Oberbayern).

AUTHOR CONTRIBUTIONS

HSa and TK generated the hypothesis and conceived the project. HSa, TK, UM-L, CM, A-CS, and AM designed experiments. HSa, UM-L, CM, A-CS, AM, JHi, JHe, DK, CG, and AD performed experiments. HSa, UM-L, CM, A-CS, and AM analyzed and interpreted data. XL performed MI surgeries. TK and HSc provided intellectual input and edited the manuscript. HSa, UM-L, CM, A-CS, and AM made the figures. HSa, CM, and UM-L wrote the manuscript, which was approved by all authors.

FUNDING

HSa has received funding from the European Research Council under the European Union's Horizon 2020 Research and Innovation Programme (STRATO, grant agreement No. 759272), the "Else-Kröner-Fresenius-Stiftung" (2020_EKSE.07) and the "Deutsche Herzstiftung" (F/28/17). This study was further supported by the "Deutsche Forschungsgemeinschaft (DFG)" (SA 1668/5-1 and 470462396). TK is supported by the Corona Foundation [Junior Research Group *Translational Cardiovascular Genomics*) and the "Deutsche Forschungsgemeinschaft (DFG)" (CRC 1123 (B02)]. Additionally, we gratefully acknowledge the support of the German Federal Ministry of Education and Research (BMBF), to HSc, within the framework of ERA-NET on Cardiovascular Disease (Druggable-MI-genes: 01KL1802) and the scheme of target validation (BlockCAD: 16GW0198K), as well as the German Centre of Cardiovascular Research (DZHK) Munich Heart Alliance, within the framework of the e:Med research and funding concept (AbCD-Net: 01ZX1706C). The British Heart Foundation (BHF)/German Centre of Cardiovascular Research (DZHK) Collaboration, for which we are co-applicants, has also provided support and funding. HSc has received further support from the German Research Foundation (DFG) as part of the "Sonderforschungsbereich" 1123 (B02) and the "Sonderforschungsbereich" TRR 267 (B05). Bavarian State Ministry of Health and Care also funded this work as part of "DigiMed Bayern" (grant No: DMB-1805-0001).

SUPPLEMENTARY MATERIAL

The Supplementary Material for this article can be found online at: https://www.frontiersin.org/articles/10.3389/fimmu.2022.898690/full#supplementary-material

REFERENCES

1. Libby P. Inflammation During the Life Cycle of the Atherosclerotic Plaque. *Cardiovasc Res* (2021) 117:cvab303.
2. Schloss MJ, Swirski FK, Nahrendorf M. Modifiable Cardiovascular Risk, Hematopoiesis, and Innate Immunity. *Circ Res* (2020) 126:1242–59.
3. Hinterdobler J, Schunkert H, Kessler T, Sager HB. Impact of Acute and Chronic Psychosocial Stress on Vascular Inflammation. *Antioxid Redox Sign* (2021) 35:1531–50.
4. Soehnlein O, Libby P. Targeting Inflammation in Atherosclerosis — From Experimental Insights to the Clinic. *Nat Rev Drug Discovery* (2021) 20:589–610.
5. Ridker PM, Everett BM, Thuren T, MacFadyen JG, Chang WH, Ballantyne C, et al. Antiinflammatory Therapy With Canakinumab for Atherosclerotic Disease. *New Engl J Med* (2017) 377:1119–31.
6. Hettwer J, Hinterdobler J, Miritsch B, Deutsch M-A, Li X, Mauersberger C, et al. Interleukin-1β Suppression Dampens Inflammatory Leukocyte Production and Uptake in Atherosclerosis. *Cardiovasc Res* (2021).
7. Tardif J-C, Kouz S, Waters DD, Bertrand OF, Diaz R, Maggioni AP, et al. Efficacy and Safety of Low-Dose Colchicine After Myocardial Infarction. *New Engl J Med* (2019) 381:2497–505.
8. Nidorf SM, Fiolet ATL, Mosterd A, Eikelboom JW, Schut A, Opstal TSJ, et al. Colchicine in Patients With Chronic Coronary Disease. *New Engl J Med* (2020) 383:1838–47.

9. Imazio M, Nidorf M. Colchicine and the Heart. *Eur Heart J* (2021) 42:2745–60.
10. Akodad M, Fauconnier J, Sicard P, Huet F, Blandel F, Bourret A, et al. Interest of Colchicine in the Treatment of Acute Myocardial Infarct Responsible for Heart Failure in a Mouse Model. *Int J Cardiol* (2017) 240:347–53.
11. Fujisue K, Sugamura K, Kurokawa H, Matsubara J, Ishii M, Izumiya Y, et al. Colchicine Improves Survival, Left Ventricular Remodeling, and Chronic Cardiac Function After Acute Myocardial Infarction. *Circ J* (2017) 81:CJ–16-0949.
12. Galis ZS, Khatri JJ. Matrix Metalloproteinases in Vascular Remodeling and Atherogenesis: The Good, the Bad, and the Ugly. *Circ Res* (2002) 90:251–62.
13. Mauersberger C, Hinterdobler J, Schunkert H, Kessler T, Sager HB. Where the Action Is—Leukocyte Recruitment in Atherosclerosis. *Front Cardiovasc Med* (2022) 8:813984.
14. Sager HB, Nahrendorf M. Inflammation: A Trigger for Acute Coronary Syndrome. *Q J Nucl Med Mol Imaging* (2016) 60:185–93.
15. Deftereos S, Giannopoulos G, Papoutsidakis N, Panagopoulou V, Kossyvakis C, Raisakis K, et al. Colchicine and the Heart. *J Am Coll Cardiol* (2013) 62:1817–25.
16. Sager HB, Kessler T, Schunkert H. Monocytes and Macrophages in Cardiac Injury and Repair. *J Thorac Dis* (2016) 9:S30–5.
17. Angelini F, Bocchino PP, Imazio M. Colchicine and Coronary Artery Disease: A Virtuous Adoption. *Eur Heart J* (2021) 42:2796–7.
18. Deftereos SG, Beerkens FJ, Shah B, Giannopoulos G, Vrachatis DA, Giotaki SG, et al. Colchicine in Cardiovascular Disease: In-Depth Review. *Circulation* (2021) 145:61–78.
19. Zhang F-S, He Q-Z, Qin CH, Little PJ, Weng J-P, Xu S-W. Therapeutic Potential of Colchicine in Cardiovascular Medicine: A Pharmacological Review. *Acta Pharmacol Sin* (2022) 1–18.
20. Nidorf SM, Eikelboom JW, Budgeon CA, Thompson PL. Low-Dose Colchicine for Secondary Prevention of Cardiovascular Disease. *J Am Coll Cardiol* (2013) 61:404–10.
21. Roubille F, Merlet N, Busseuil D, Ferron M, Shi Y, Mihalache-Avram T, et al. Colchicine Reduces Atherosclerotic Plaque Vulnerability in Rabbits. *Atheroscler Plus* (2021) 45:1–9.
22. Vaidya K, Tucker B, Kurup R, Khandkar C, Pandzic E, Barraclough J, et al. Colchicine Inhibits Neutrophil Extracellular Trap Formation in Patients With Acute Coronary Syndrome After Percutaneous Coronary Intervention. *J Am Heart Assoc* (2021) 10:e018993.
23. Cronstein BN, Molad Y, Reibman J, Balakhane E, Levin RI, Weissmann G. Colchicine Alters the Quantitative and Qualitative Display of Selectins on Endothelial Cells and Neutrophils. *J Clin Invest* (1995) 96:994–1002.
24. Weber A, Iturri J, Benitez R, Zemljic-Jokhadar S, Toca-Herrera JL. Microtubule Disruption Changes Endothelial Cell Mechanics and Adhesion. *Sci Rep-uk* (2019) 9:14903.
25. Parsons JT, Horwitz AR, Schwartz MA. Cell Adhesion: Integrating Cytoskeletal Dynamics and Cellular Tension. *Nat Rev Mol Cell Biol* (2010) 11:633–43.
26. Frodermann V, Nahrendorf M. Macrophages and Cardiovascular Health. *Physiol Rev* (2018) 98:2523–69.
27. RBW II, Meng X, Godin D, Galis ZS. Extracellular Matrix Modulates Macrophage Functions Characteristic to Atheroma. *Arterioscler Thromb Vasc Biol* (1998) 18:432–40.
28. Bauriedel G, Heimerl J, Beinert T, Welsch U, Höfling B. Colchicine Antagonizes the Activity of Human Smooth Muscle Cells Cultivated From Arteriosclerotic Lesions After Atherectomy. *Coronary Artery Dis* (1994) 5:531–9.
29. Mewton N, Roubille F, Bresson D, Prieur C, Bouleti C, Bochaton T, et al. Effect of Colchicine on Myocardial Injury in Acute Myocardial Infarction. *Circulation* (2021) 144:859–69.
30. Deftereos S, Giannopoulos G, Angelidis C, Alexopoulos N, Filippatos G, Papoutsidakis N, et al. Anti-Inflammatory Treatment With Colchicine in Acute Myocardial Infarction. *Circulation* (2015) 132:1395–403.
31. Tong DC, Quinn S, Nasis A, Hiew C, Roberts-Thomson P, Adams H, et al. Colchicine in Patients With Acute Coronary Syndrome: The Australian COPS Randomized Clinical Trial. *Circulation* (2020) 142:1890–900.

Conflict of Interest: HSa reports grants from the European Research Council, the "Else-Kröner-Fresenius-Stiftung", the "Deutsche Herzstiftung" and the "Deutsche Forschungsgemeinschaft" during the conduct of the study. HSa received lecture fees from Novo Nordisk. HSc reports personal fees from MSD Sharp & Dohme, personal fees from AMGEN, personal fees from Bayer Vital GmbH, personal fees from Boehringer Ingelheim, personal fees from Daiichi-Sankyo, personal fees from Novartis, personal fees from Servier, personal fees from Brahms, personal fees from Bristol-Myers Squibb, personal fees from Medtronic, personal fees from Sanofi Aventis, personal fees from Synlab, personal fees from Pfizer, grants and personal fees from Astra-Zeneca and personal fees from Vifor, outside the submitted work. HSc and TK are named inventors on a patent application for prevention of restenosis after angioplasty and stent implantation outside the submitted work. TK received lecture fees from Bayer AG, Pharmaceuticals.

The remaining authors declare that the research was conducted in the absence of any commercial or financial relationships that could be construed as a potential conflict of interest.

Publisher's Note: All claims expressed in this article are solely those of the authors and do not necessarily represent those of their affiliated organizations, or those of the publisher, the editors and the reviewers. Any product that may be evaluated in this article, or claim that may be made by its manufacturer, is not guaranteed or endorsed by the publisher.

frontiers | Frontiers in Immunology

ORIGINAL RESEARCH
published: 04 July 2022
doi: 10.3389/fimmu.2022.935787

Autoimmunity to Sphingosine-1-Phosphate-Receptors in Systemic Sclerosis and Pulmonary Arterial Hypertension

Hans Gluschke[1], Elise Siegert[2,3], Waldemar B. Minich[1], Julian Hackler[1], Gabriela Riemekasten[4], Wolfgang M. Kuebler[5,6], Szandor Simmons[5,6] and Lutz Schomburg[1]**

[1] Institute for Experimental Endocrinology, Charité – Universitätsmedizin Berlin, Berlin, Germany, [2] Department of Rheumatology and Clinical Immunology, Charité – Universitätsmedizin Berlin, Berlin, Germany, [3] Berlin Institute of Health at Charité – Universitätsmedizin Berlin, Berlin, Germany, [4] Department of Rheumatology, University Medical Center Schleswig Holstein, Lübeck, Germany, [5] Institute of Physiology, Charité – Universitätsmedizin Berlin, Berlin, Germany, [6] Deutschs Zentrum für Herz-Kreislauf-Forschung e.V. (DZHK) (German Centre for Cardiovascular Research), Partner Site Berlin, Berlin, Germany

OPEN ACCESS

Edited by:
Juan Bautista De Sanctis, Palacký University Olomouc, Czechia

Reviewed by:
Michael Rodney Mijaes Tussaint, Central University of Venezuela, Venezuela
Luis E. Munoz, Friedrich-Alexander-University Erlangen-Nürnberg (FAU), Germany

***Correspondence:**
Szandor Simmons
szandor.simmons@charite.de
Lutz Schomburg
lutz.schomburg@charite.de

Specialty section:
This article was submitted to Inflammation, a section of the journal Frontiers in Immunology

Received: *04 May 2022*
Accepted: *07 June 2022*
Published: *04 July 2022*

Citation:
Gluschke H, Siegert E, Minich WB, Hackler J, Riemekasten G, Kuebler WM, Simmons S and Schomburg L (2022) Autoimmunity to Sphingosine-1-Phosphate-Receptors in Systemic Sclerosis and Pulmonary Arterial Hypertension. Front. Immunol. 13:935787. doi: 10.3389/fimmu.2022.935787

Context: Pulmonary arterial hypertension (PAH) is a frequent extracutaneous manifestation of systemic sclerosis (SSc). PAH is characterized by increased vasomotor tone, progressive remodeling of pulmonary arteries and arterioles, consequentially increased pulmonary vascular resistance, right heart hypertrophy, and eventually right ventricular failure. Autoimmunity against G-protein coupled receptors (GPCRs) has been implicated in the development of SSc-associated PAH. Sphingosine-1-phosphate (S1P) receptors (S1PR) present a potential, yet so far untested antigen for PAH autoimmunity, given the documented role of S1P/S1PR signaling in PAH pathogenesis.

Objective: We hypothesized that S1P receptors (S1PR) may constitute autoantigens in human patients, and that the prevalence of autoantibodies (aAb) to S1PR1, S1PR2 and S1PR3 is elevated in SSc patients and associated with PAH.

Methods: For this exploratory study, serum samples from 158 SSc patients, 58 of whom with PAH, along with 333 healthy control subjects were screened for S1PR-aAb. S1PR1-3 were expressed as fusion proteins with luciferase in human embryonic kidney cells and used to establish novel *in-vitro* assays for detecting and quantifying S1PR-aAb. The fusion proteins were incubated with serum samples, the aAb-S1PR complexes formed were precipitated by protein-A, washed and tested for luciferase activity. Commercial anti-S1PR-antibodies were used to verify specificity of the assays.

Results: All three assays showed dose-dependent signal intensities when tested with S1PR-subtype specific commercial antibodies. Natural aAb to each S1PR were detected in healthy controls with a prevalence of <10% each, i.e., 2.7% for S1PR1-aAb, 3.6% for S1PR2-aAb, and 8.3% for S1PR3. The respective prevalence was higher in the cohort of SSc patients without PAH, with 17.1% for S1PR1-aAb, 19.0% for S1PR2-aAb, and

21.5% for S1PR3. In the subgroup of SSc patients with PAH, prevalence of aAb to S1PR2 and S1PR3 was further elevated to 25.9% for S1PR2-aAb, and 27.6% for S1PR3. Notably, the majority of patients with positive S1PR2-aAb (60.7%) or S1PR3-aAb (71.9%) displayed interstitial lung disease.

Conclusion: S1PR1–3 can constitute autoantigens in humans, particularly in SSC patients with PAH. The potential pathophysiological significance for the etiology of the disease is currently unknown, but the elevated prevalence of S1PR2-aAb and S1PR3-aAb in SSC patients with PAH merits further mechanistic investigations.

Keywords: autoantibodies, G-protein coupled receptor, autoimmune disease, immunoglobulin, rheumatology, immunology, sphingolipid, sphingosine-1-phosphate

INTRODUCTION

Pulmonary hypertension (PH) is characterized by a mean pulmonary arterial pressure (mPAP) of ≥ 20 mmHg at rest. Its clinical features may gradually progress from an initial asymptomatic course to dyspnea and orthopnea, and eventually to right heart hypertrophy, failure and death. The pathophysiology of PH is characterized by vascular remodeling, endothelial dysfunction and increased vascular tone, predominantly in small to medium-sized pulmonary arterioles (1). Precapillary pulmonary arterial hypertension (PAH) constitutes the first group in the 2018 consensus on the clinical classification of PH into five groups (2). 'PAH' is diagnosed when mPAP at rest is measured ≥ 20 mmHg, yet pulmonary artery wedge pressure is ≤ 15 mmHg and other causes of pre-capillary PH (e.g. lung disease or chronic thromboembolic pulmonary hypertension) are excluded (3). The subcategory PAH can be specified further by etiology into idiopathic, hereditary, drug- and toxin-induced forms of PAH, or PAH associated with connective tissue disease, HIV or congenital heart disease (4). While essential pathophysiological elements have been elucidated over the past decades, the etiology of PAH remains incompletely understood (5). Besides an epigenetic dysregulation, alterations in bone morphogenetic protein signaling, abnormalities in mitochondrial metabolism, and dynamic inflammatory, autoimmune processes contribute to the pathogenesis of PAH (6). Specifically, cell-based and autoantibody (aAb) related immune dysregulation have been implicated in the development of PAH, predominantly with respect to idiopathic and connective tissue disease-associated PAH (7). Antinuclear Ab (ANA) serve as diagnostic hallmark of connective tissue disease, and specific ANA are associated with an increased risk for PAH. In addition, aAb to certain G-protein coupled receptors (GPCR) such as angiotensin 1-receptor or endothelin receptor-1 have recently been associated with PAH, and may promote pathological vasoconstriction and vascular remodeling by acting as agonists of the respective GPCR (8). Another line of research has recently identified signaling *via* the small bioactive lipid mediator sphingosine-1-phosphate (S1P) and its receptors (S1PR), which regulate vasoconstriction, fibrosis, and lymphocyte trafficking (9–11) as potential pathomechanism in PAH.

S1P can be generated at the inner layer of the cell membrane from its sphingolipid precursor sphingosine by sphingosine-kinase (SPHK)-1 or -2 *via* the specific S1P-transporters major facilitator superfamily domain-containing protein 2B (MFSD2B, in erythrocytes and platelets) (12), or spinster-homologue-2 (SPNS2, in blood and lymphatic endothelial cells) S1P can then be released into the extracellular space and the circulation (13, 14). Extracellular S1P can bind and activate five different human S1P-receptors (S1PR), namely S1PR1 to S1PR5, all of which belong to the superfamily of GPCR (15, 16). Besides the crucial role of S1PR1, S1PR2 and S1PR3 in the maturation, activation and chemotaxis of immune cells (11, 17), these ubiquitously expressed S1PR are also the major receptor subtypes in the cardiovascular system with high expression in pulmonary artery smooth muscle cells (PASMC) (18). Of note, S1PR1- and S1PR3-signaling plays an important role in preserving vascular functions and blood pressure homeostasis by controlling endothelial nitric oxide synthase (eNOS)-derived nitric oxide (NO) production, which underlies the anti-hypertensive effect of S1P (19). However, elevated levels of SPHK1 in PASMC result in an autocrine "inside-out" S1PR-signaling that can stimulate PASMC proliferation *via* S1PR2, which has been proposed appears upregulated in PASMC of idiopathic PAH patients (9, 15). In parallel, activation of S1PR2 (and potentially also S1PR4) in PASMC causes pulmonary vasoconstriction (20–22). In combination, the effects of S1P on pulmonary arterial endothelial and smooth muscle cells emphasize the importance of a tightly controlled S1P/S1PR-signaling in vascular homeostasis that when impaired can drive vasoconstriction, vascular remodeling, and endothelial dysfunction, which increase pulmonary vascular resistance and mPAP ultimately resulting in the development of PAH. Experimental proof-of-principle for this concept was demonstrated by the fact that genetic deficiency or pharmacological inhibition of either SPHK1 or S1PR2 effectively attenuated the development of PH in rodent models of chronic hypoxic PH (9). Further, a specific role of S1PR2 and S1PR3 has been described in fibrosis, in particular in relation to inflammation and tissue injury, leading to cell death, matrix deposition and finally end organ dysfunction (23). Due to the crucial role of S1P-signaling in homeostasis of the immune system and the endothelium, specific S1PR-modulators are

already used in autoimmune disease such as multiple sclerosis and inflammatory bowel disease and constitute a promising therapeutic option for rheumatoid arthritis, systemic lupus erythematosus or systemic sclerosis (SSc) (24–26).

Systemic sclerosis, as one of the rheumatic diseases with the highest mortality, is also characterized by autoimmune dysregulation, endothelial dysfunction and chronic inflammation (27, 28). In more than 90% of patients, ANA are detected, constituting an important cornerstone of the diagnosis and supporting the classification of SSc as an autoimmune disease (29). Additional aAb to other members of the GPCR superfamily have recently been described in SSc by us and others (28, 30). The complication of PAH on a background of SSc (SSc-PAH) affects up to 12% of patients with SSc, constituting the major cause of death in SSc. Still, diagnostic and prognostic markers for PAH are few, therapeutic measures remain poorly effective and treatment options are limited, causing physicians to pursue symptomatic approaches rather than curative strategies (31, 32). Besides established immunosuppressive therapies, S1P modulators such as cenerimod already showed promising results in a mouse model of bleomycin-induced fibroses (33).

In view of the ubiquitous function of S1P/S1PR1/eNOS signaling in the vasculature, the established role of S1P/S1PR2 signaling in PASMC proliferation, contraction, and the development of PH, and the specific contribution of S1PR2 and S1PR3 to disease-related extracellular matrix deposition and tissue fibrosis, we speculated that any alterations to the function of one of these three S1PR may be associated with SSc, in particular with respect to PAH development. To this end, we established as a first step novel *in vitro* assays for detection and quantification of aAb binding to S1PR1, S1PR2 or S1PR3, and compared the prevalence of these GPCR-specific aAb in serum samples from healthy controls and SSc patients with or without PAH. Our results indicate an elevated prevalence of S1PR-specific aAb in SSc, in particular for S1PR2-aAb and S1PR3-aAb in patients with SSc-PAH.

MATERIALS AND METHODS

Human Samples From Healthy Controls and SSc Patients

An explorative study was conducted on the prevalence of S1PR-aAb. To this end, a set of commercially available serum samples (n=303) from subjects with a self-assessed status as 'healthy' (HC; healthy controls) served as reference (in.vent Diagnostica GmbH, Hennigsdorf, Germany). An additional set of 30 serum samples from healthy subjects were collected at the Rheumatology Department in Lübeck, Germany. Patients suffering from SSc with or without PAH were identified and enrolled into the study at the Rheumatology Department at the Charité – University Medicine Berlin, Berlin, Germany, or at the University Hospital Lübeck, Schleswig Holstein, Germany, in the time period from Nov. 2004 to Dec. 2019. The final cohort consisted of n=158 serum samples from SSc patients, n=58 of which had an additional diagnosis of PAH. Samples were stored at -80°C until transfer to the analytical laboratory in Berlin, and provided to the scientists conducting the laboratory analyses in a blinded fashion. All patients provided their written informed consent for enrollment into the study after detailed explanation of purpose, procedures (blood sampling and analysis) and right to withdraw from participation at any time point. The study was conducted in accordance with the Declaration of Helsinki. Ethical counselling was provided by the Charité Medical School Berlin (10/30/2017, EA1/178/17) and the Board of Ethics of the University of Cologne (#04-037). Baseline characteristics of patients and healthy controls are displayed in **Table 1**.

Construction of the Receptor–Luciferase Fusion Proteins for Autoantibody Detection

The construction of these novel assays followed an established path, whereby the full open reading frames of the human coding sequences of the three S1PR were individually fused in frame to a luciferase (Luc) reading frame. The resulting receptor-luciferase fusion proteins served as autoantigen baits for autoantibody detection. Briefly, the open reading frames of the human S1PR1, S1PR2 and S1PR3 were synthesized by a commercial supplier (BioTeZ, Berlin-Buch GmbH, Berlin, Germany), each containing suitable restriction sites for directed insertion into a eukaryotic expression plasmid. The strategy is similar to the recently generated assays for the insulin-like growth factor receptor 1, the thyroid hormone transporters MCT8 and MCT10, the GPCR for gonadotropin-releasing hormone, luteinizing hormone or follicle-stimulating hormone or the iodide transporters sodium-iodide symporter and pendrin (34–38). The stop codons were each replaced by a sense codon in order to enable read-through. The expression

TABLE 1 | Baseline characteristics of the study cohorts.

	Rheumatology Departments Univ. of Lübeck & Charité Berlin		In.vent Diagnostica
Diagnosis	**Systemic sclerosis n=158**	**Healthy controls n=30**	**Healthy controls n=303**
Sex			
Female, n (%)	116 (73.9%)	19 (63.3%)	171 (56.4%)
Male, n (%)	41 (26.1%)	11 (36.7%)	132 (43.6%)
Age, median (range) [y]	63 (26–84)	52 (22–59)	32 (19–63)
BMI, median (range) [kg/m2]	24 (16–48)	–	–
Disease duration, median (range) [months]	84 (0–588)	–	–

Missing values were excluded from the calculation.

plasmid backbone pSP-Luc+NF was obtained from Promega (Promega GmbH, Walldorf, Germany). DNA-sequencing for verification of the correct expression cassettes was conducted by LGC Genomics (LGC Genomics GmbH, Berlin, Germany).

Stable Expression of Fusion Proteins in Human Embryonic Kidney Cells

In order to achieve stable and reproducible expression of the fusion proteins, human embryonic kidney cells (HEK 293) were transfected with the expression vectors and cultured in DMEM/F12 supplemented with 10% fetal bovine serum (FBS) and 1% penicillin/streptomycin. Two days after transfection, 0.8 mg/mL G418 (geneticin, Sigma-Aldrich GmbH, Steinheim, Germany) was added to the medium, and stable clones were selected by the criteria of robust cell growth characteristics and high luciferase activity. Selected clones were expanded and seeded on 165 cm^2 cell culture dishes for recombinant protein production in medium supplemented with 0.2 mg/dL G418.

Preparation of Cell–Extracts for Autoantibody Tests

After reaching confluency of 80% or more, stable HEK293 cells expressing the fusion protein of choice were harvested with a cell scraper and collected by centrifugation (10 min, 1000 g, 4°C). Cell pellets were washed twice with pre-cooled PBS and collected again by centrifugation. The resulting pellet was resolved in collection buffer (50 mM Tris-HCl, 100 mM NaCl, 10% glycerol, 0.01% NaN_3 in dH_20) and subsequently lysed by adding 1% Triton X-100 (Sigma-Aldrich). After gentle shaking and final centrifugation (15 min, 4000 g, 4°C), the supernatants were tested for luciferase activity. The resulting cell extracts were diluted in collection buffer to achieve signal intensities of > $1*10^6$ relative light units (RLU) per measurement and stored in aliquots at -80°C until use.

Quantitative Analysis of Antibodies Binding to Human S1P Receptors

For the quantitative analysis of antibodies reactive with S1P receptors, the cell extracts containing S1PR-Luc fusion proteins were diluted in reaction buffer (50 mM Tris-HCl, 100 mM NaCl, 10% glycerol, 5% milk powder, 5% glucose, 1% Triton X-100, 0.005% NaN_3 in dH_2O) to a concentration equivalent to providing $2\text{-}4*10^5$ RLU per reaction (Automat Plus LB953, Berthold Technologies, Bad Wildbad, Germany). Each measurement was conducted by incubating 40 µL of diluted cell extract overnight at 4°C with 10 µL of serum sample diluted 1:1 (v/v) with serum buffer (50% glycerol, 100 mM NaCl, 50 mM Tris-HCL, 0.01% NaN_3 in dH_2O). After 24 h, an aliquot of 40 µL of protein-A sepharose (ASKA Biosciences GmbH, Berlin, Germany) diluted in reaction buffer (20% v/v) was added to capture the fusion-protein-aAb-complexes that had formed overnight. The samples were centrifuged (1000 g, 2 min, 4°C) and pellets were washed five times using 200 µL Tris-based buffer (50 mM Tris-HCl, pH 7.4, 100 mM NaCl, 10% glycerol, 0.5% Triton X-100 in dH_2O). After resuspension, luciferase activity was determined by injection of luciferase substrate, signal intensities were measured as RLU with a luminometer (Automat Plus LB953 or Mithras LB943), and used to calculate specific binding indices (BI) as factor above background noise.

Statistical Analysis

Under the assumption of less than 50% of positive samples in the analysis, average background noise of negative samples was determined for each experimental run in 96-well plates by calculating the mean RLU from the lower half of the obtained signals. This signal was defined as binding index one (BI = 1.0). For analytical comparison, all signals [RLU] were divided by this background signal [RLU] and expressed as BI, denoting the signal strength as times background signal. In order to determine the cut-off for S1PR-aAb-positve samples, a mathematical outlier criterion was used. To this end, a threshold was calculated representing the BI of the 75^{th} percentile of all signals plus 1.5-times the inter quartile range (P75 + 1.5 x IQR). In this manner, a separation of aAb-positive from aAb-negative samples was achieved. All statistical analyses were performed using GraphPad Prism v8.4.0 (GraphPad Software Inc., San Diego, CA, USA). Intra-assay coefficients of variation were determined from repeated measurements of the same positive samples. Tests for normal distribution (D'Agostino-Pearson test, Shapiro-Wilk test, Kolmogorov-Smirnov test) showed a non-parametric distribution of S1PR-aAb-positivity and of the clinical parameters. Group comparisons of continuous clinical characteristics were analyzed for significant differences with two-sided Mann-Whitney test. Binary variables were compared with one-sided (expected direction of difference) or two-sided (explorative hypothesis) Chi Square test for statistical significance, as indicated. Significance was assumed when the p-value was below 0.05; however, the p-values may not be interpreted as confirmative as all analyses were considered exploratory and not adjusted for multiple testing.

RESULTS

Establishment of Quantitative Tests for Measuring Autoantibodies to the S1P Receptors

Stable HEK293 cell clones were established expressing human S1PR1-, S1PR2- and S1PR3-luciferase (S1PR1-Luc, S1PR2-Luc, S1PR3-Luc) fusion proteins, respectively. Recombinant expression of the fusion proteins to be used as bait in the aAb analyses yielded comparable luciferase activities per preparation. To verify specificity, commercial antibodies recognizing human S1PR1, S1PR2 or S1PR3 were obtained and used as positive standards. Each of the commercial antibodies produced strong signals in the respective assay. Intra-assay coefficients of variation were 14.3% for the S1PR1-, 6.6% for the S1PR2- and 5.3% for the S1PR3-assay. Stepwise dilution experiments using commercial antibodies revealed concentration-dependent signals for all three aAb assays (**Figure 1**).

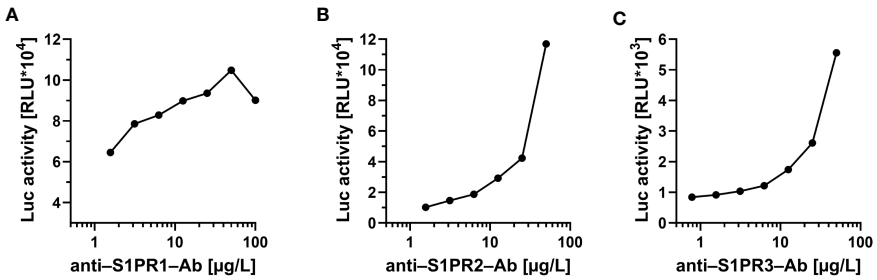

FIGURE 1 | Proof of concept for the novel tests to quantify commercial antibodies to the S1P-receptors. Signal development was tested with commercial antibodies to **(A)** S1PR1, **(B)** S1PR2 and **(C)** S1PR3, respectively. In all three newly developed detection assays, a concentration-dependent decline of signal intensity (expressed as relative light units; RLU) was observed in dilution experiments of commercial receptor-specific antibodies. No cross-reactivity to other receptors was observed. Control measurements were conducted using either monoclonal (to S1PR1 and S1PR2) or polyclonal (to S1PR3) antibody preparations.

Stability of S1PR–aAb in Serum Samples Upon Freezing and Thawing

To ensure that freezing and thawing does not interfere with the analysis of S1PR-aAb in human serum, selected samples that had been screened positive for S1PR–aAb were tested after one to four consecutive freeze and thaw cycles. Freezing was achieved on dry ice at –80°C and thawing by standing without agitation at room temperature until completely thawed. The signal intensities remained relatively unaffected by the repeated freezing and thawing, and final signal strength after four rounds of freezing and thawing was within 20% of the initial values determined after the first thawing in all three analytical assays (**Figure 2**). The results support the suitability of frozen human serum samples for assessing aAb to the S1PR by the newly generated analytical tests.

Prevalence of S1PR–aAb in SSc Patients Versus Healthy Controls

A cohort of serum samples from patients with SSc (n=158) and a collection of serum samples from healthy controls (n=333) was analyzed for natural aAb to S1PR by the three receptor-specific tests. The signals (RLU) were converted into relative binding indices (BI), with BI=1.0 representing background noise. Thresholds for positive aAb signals were determined by applying the mathematical outlier criterion of P75+1.5-times IQR as indicated by a dotted line (**Figure 3**). According to these criteria, several samples with positive aAb were identified in all three tests in both control and patient group. Prevalence of natural S1PR1–aAb was 17.1% in SSc versus 2.7% in controls (**Figure 3A**). Similarly, prevalence of S1PR2–aAb was elevated with 19.0% in SSc patients versus 3.6% in controls (**Figure 3B**). In comparison of all three assays, S1PR3-aAb displayed the highest prevalence, with 8.3% in controls and 21.5% in patients, with one sample showing exceptionally high signal intensity with a BI of 13 (**Figure 3C**). A direct comparison of the prevalence for each of the three S1PR-aAb is provided in (**Figure 3D**) and highlights the statistically significant differences in S1PR-aAb prevalence in SSc versus controls.

Prevalence of S1PR–aAb in Patients as a Function of Pulmonary Arterial Hypertension

Pursuing the hypothesis that S1PR-aAb may be involved in the pathogenesis of PAH and therefore more prevalent in PAH, we subsequently divided the group of SSc patients into patients without PAH (SSc w/o PAH, n=100) and a smaller group of

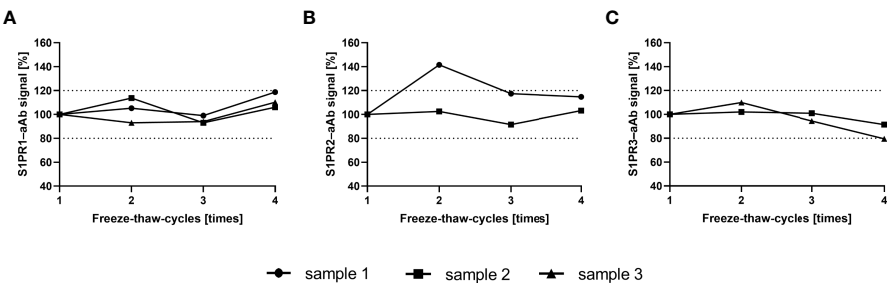

FIGURE 2 | Signal stability upon multiple freeze-thaw-cycles. S1PR–aAb signal stability of aAb-positive serum was assessed with selected samples in the newly generated assays for **(A)** S1PR1–aAb, **(B)** S1PR2–aAb, and **(C)** S1PR3–aAb assay. Samples were subjected consecutively to four freeze and thaw cycles, and all measurements with one exception displayed signal intensities within a 20% range from the initial signal strength determined upon first thawing.

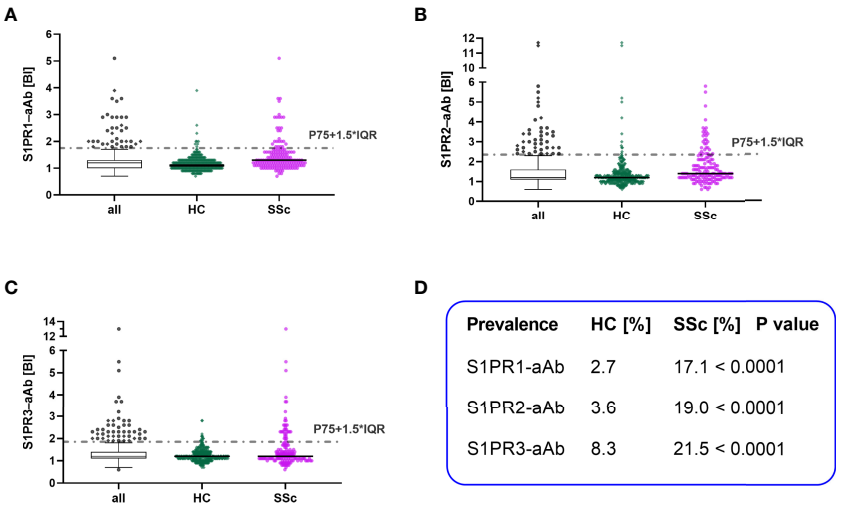

FIGURE 3 | Comparison of S1PR–aAb in healthy controls versus patients with systemic sclerosis. The presence of aAb to the three human S1PR (1–3) was determined in the group of healthy controls (HC) and patients with systemic sclerosis (SSc), and the relative prevalence was compared between both groups. Thresholds are indicated by dotted lines, and values are displayed as scattered dot plots. Black lines represent the median. Whiskers of the box plots denote P25 and P75. Results from HC are denoted in green and of SSc in pink. The prevalence for **(A)** S1PR1–aAb, **(B)** S1PR2–aAb, and **(C)** S1PR3–aAb was elevated in the patient cohort as compared to healthy controls. **(D)** A statistical comparison of SSc and HC for S1PR-aAb was conducted by two-sided Chi square test and revealed significant group differences.

PAH-positive SSc patients (SSc-PAH, n=58). S1PR1-aAb appeared unrelated to PAH, and prevalence in the SSc w/o PAH group (18/100, 18.0%) was similar to the prevalence in the SSc-PAH group (9/58, 15.5%) (**Figure 4A**). In contrast, a quarter of samples in the SSc-PAH group displayed positivity for S1PR2-aAb (15/58, 25.9%), whereas a smaller percentage of SSc patients without PAH was positive for S1PR2-aAb (15/100, 15.0%), with the difference reaching statistical significance (P=0.0467) (**Figure 4B**). With regards to the prevalence of S1PR3-aAb, a higher fraction of samples from the SSc-PAH was identified as positive (16/58, 27.6%) in comparison to the SSc w/o PAH group (18/100, 18.0%), albeit without reaching statistical significance (P=0.1133) (**Figure 4C**). An overview of these three sets of measurements highlights the differential picture, with a particularly elevated prevalence of S1PR2-aAb in patients with SSc-PAH.

Serum Samples With Positive Autoantibodies to More Than One S1PR

The samples showing positive autoimmunity were further analyzed with respect to recognizing more than one receptor, i.e., being positive in two or even in all three S1PR-aAb assays. In total, six positive samples were identified with aAb exceeding the threshold in all three S1PR-aAb assays, suggesting either a cross-reactivity of a single aAb to the different receptors or a polyclonal nature of the aAb within a given serum, with aAb co-existing and recognizing either S1PR1, or S1PR2 or S1PR3. All of the respective patients were female, five derived from the SSc

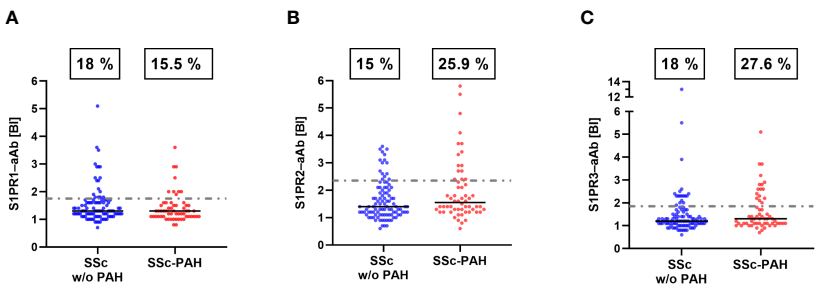

FIGURE 4 | Prevalence of S1PR–aAb in SSc patients as a function of a diagnosis of PAH. SSc patients were subdivided into those with or without a diagnosis of PAH. **(A)** Prevalence of S1PR1-aAb was similar in both groups of patients, whereas **(B)** the prevalence of S1PR2-aAb was higher in SSc patients with PAH than in patients without PAH (P<0.05). **(C)** The difference in prevalence of S1PR3-aAb between both groups did not reach statistical significance (P>0.05). The binding indices (BI) along with the percentages of positive samples are provided. Prevalence was compared by one-sided Chi square test.

cohort whereas only one healthy control was triple positive. Three of the triple positive subjects were suffering from SSc-PAH. Four samples were tested positive for both S1PR1-aAb and S1PR3-aAb. In addition, two SSc patient samples were simultaneously positive in the tests for S1PR1-aAb and S1PR2-aAb. A total number of 19 other samples were positive for S1PR2-aAb and S1PR3-aAb. The commercial antibodies yielded high signals only when tested for one receptor subtype, and not in the related assays.

Comparison of Clinical Characteristics With Respect to S1PR–aAb

The full cohort of SSc patients was analyzed for clinical characteristics in relation to the results from the S1PR-aAb tests. In general, patients with S1PR3-aAb were younger than average (median age; 51 vs. 63). With respect to cutaneous manifestation of SSc, 85.2% of patients positive for S1PR1-aAb had a limited cutaneous form, whereas the diffuse manifestations were dominating in patients that were positive for S1PR2-aAb or S1PR3-aAb. Besides the elevated prevalence of S1PR2-aAb and S1PR3-aAb in the group of SSc patients with PAH, there was also a higher share of patients suffering from lung fibrosis in these groups (S1PR2-aAb; 60.7% vs. 45.3%, S1PR3–aAb; 71.9% vs. 41.9%). None of the groups showed remarkable differences in the prevalence of specific anti-nuclear Ab (**Table 2**).

DISCUSSION

In this manuscript, we describe the establishment of novel analytical *in vitro* assays for assessing the prevalence of natural autoantibodies recognizing human S1PR1, S1PR2 or S1PR3. A first analysis on the specificity of the assays was positively passed by using commercial receptor-specific antibodies, recognizing only the respective receptor type and not cross-reacting to a related S1PR. Dependence of signals to antibody levels was observed in dilution experiments with commercial antibodies. As another important prerequisite for the present analysis, signal stability was shown by repeated freezing and thawing of aAb-positive human samples. In agreement with our hypothesis, prevalence of natural S1PR-aAb was significantly elevated in SSc patients as compared to healthy controls, with some further increase in the subgroup of patients who developed PAH. S1PR2-aAb and S1PR3-aAb showed a particular association with both PAH and lung fibrosis, in line with their established local biochemical function (39).

The balance between vasoconstriction and vasodilation in the (pulmonary) arterial system is fine-tuned by the expression of S1PR1, S1PR2 and S1PR3 on vascular endothelial cells and smooth muscle cells. While S1PR1 agonism in endothelial cells stimulates NO formation and causes vasodilation, S1PR2 and S1PR3 signaling in smooth muscle cells mediate vasoconstriction. Analyses in primary pulmonary artery smooth muscle cells, isolated perfused lungs and *in vivo* models of PH specifically identified signaling *via* S1PR2 to trigger pulmonary vasoconstriction and vascular remodeling (21, 22), while pharmacological inhibition of S1PR2 effectively prevented the development of chronic hypoxic PH in mice (9). Agonism of S1PR3, on the other hand, has been implicated in the development of radiation- and bleomycin-induced pulmonary fibrosis in mice (40, 41).

TABLE 2 | Characterization of the cohort of patients with systemic sclerosis regarding S1PR–aAb.

		S1PR1–aAb		S1PR2–aAb		S1PR3–aAb	
	SSc n=158	**positive* n=27 (17.1%)**	**negative n=131 (82.9%)**	**positive* n=30 (19%)**	**negative n=128 (81%)**	**positive* n=34 (21.5%)**	**negative n=124 (78.5%)**
Cutanous manifestation							
Limited, n (%)	91 (58%)	23 (85.2%)	68 (52.3%)	14 (48.3%)	77 (60.2%)	13 (39.4%)	78 (62.9%)
Diffuse, n (%)	59 (38%)	4 (14.8%)	55 (42.3%)	14 (48.3%)	45 (35.2%)	19 (57.6%)	40 (32.3%)
Sine scleroderma, n (%)	7 (4%)	0 (0%)	7 (5.4%)	1 (3.4%)	6 (4.7%)	1 (3.0%)	6 (4.8%)
mRSS, median (range)	6 (0–39)	4 (0–24)	6 (0–39)	5 (0–27)	6 (0–39)	5 (0–27)	6 (0–39)
Pulmonary & cardiac involvement							
NTproBNP [ng/L], median (range)	206 (5–19066)	296 (46–4884)	196 (5–19066)	135 (5–19066)	235 (29–14414)	135 (5–4884)	242 (29–19066)
PAH, n (%)	58 (37%)	9 (33.3%)	49 (37.4%)	15 (50%)	43 (33.6%)	16 (47.1%)	42 (33.9%)
ILD, n (%)	75 (48%)	11 (40.7%)	64 (49.6%)	17 (60.7%)	58 (45.3%)	23 (71.9%)	52 (41.9%)
Autoantibodies**							
anti-topoisomerase-1 (Scl70) Ab, n (%)	50 (33%)	4 (15.4%)	46 (36.2%)	11 (39.3%)	39 (31.2%)	16 (48.5%)	34 (28.3%)
anti-RNA-Pol-III Ab (ARA), n (%)	13 (8%)	2 (7.4%)	11 (8.7%)	2 (7.4%)	11 (8.7%)	4 (12.5%)	9 (7.4%)
anti-centromere-CENP-B Ab, n (%)	63 (41.4%)	21 (75%)	42 (33.6%)	11 (40.7%)	52 (41.6%)	9 (29.0%)	54 (44.6%)
anti-citrullinated-peptide Ab, n (%)***	30 (54.5%)	6 (66.7%)	24 (52.2%)	10 (71.4%)	20 (48.8%)	8 (53.3%)	22 (55%)

*Missing values were excluded from the calculation; mRSS, modified Rodnan-Skin-Score; ILD, interstitial lung disease; *P75+1.5xIQR, **all were antinuclear Ab (ANA) positive, ***positive: ≥7 U/ml.*

The increased prevalence of S1PR2- and S1PR3- but not S1PR1-specific aAb in SSc-PAH patients may thus point towards an autoimmune-supported pathomechanism that could contribute to elevated pulmonary vascular resistance and the development of lung fibrosis in SSc-associated PAH. In line with this notion, PAH patients show elevated expression of S1PR2 on PASMC (9). Given that pharmacologic S1PR2 inhibition could prevent the development of hypoxic PH in rodents, an agonistic aAb against S1PR2/3 may conceivably promote PASMC proliferation and medial thickening (9). Yet, the biochemical nature of the S1PR-aAb and their functional effects on receptor signaling are presently unclear, as our newly developed assays only detect binding characteristics, while data probing whether the identified aAb act as antagonists to inhibit the receptors, as agonists to stimulate receptor signaling, or rather elicit allosteric effects are lacking and remain to be elucidated in future studies (40).

Our findings support earlier reports describing a set of GPCR-specific aAb in patients with autoimmune disease such as systemic sclerosis (28, 41). While aAb against a variety of GPCR including the endothelin type A receptor and angiotensin II receptor type 2 have been identified in a wide range of cardiovascular diseases where they have been proposed to contribute critically to disease initiation and/or progression, aAb against S1PR have so far only been reported in a single case report. In this lymphopenic patient with recurrent infections, aAb to human S1PR1 were identified (42). Adoptive transfer of the purified human aAb into mice caused immunosuppression, decreased T-cell chemotaxis and reduced lymph node egress *via* direct interaction with a subset of T-cells (42), thus highlighting the functional relevance of these aAb. The epitope recognized by the S1PR1-aAb was within the amino-terminal domain of S1PR1. Yet as therapeutic antibodies against certain S1PR demonstrated, binding is often not restricted to just one receptor (43). As such, it will be important to characterize the major antigenic epitopes for the specific receptor subtypes identified in the present study. Here, we describe for the first time the prevalence of S1PR-aAb including the first identification of S1PR2- and S1PR3-aAb in a large cohort of patients and healthy individuals, and report their potential use as both biomarkers and potential therapeutic targets in SSc, PAH, and/or lung fibrosis.

Among the particular strengths of our study are the rigorous assay designs, using full-length human receptor molecules as bait and human cells as system for the recombinant expression, thereby enabling regular posttranslational modifications, full coverage of potential epitopes and correct trafficking (44, 45). Moreover, the identification of commercial receptor-specific antibodies to each of the three receptor subtypes verified specificity of the assays, and enables other research groups to conduct similar analyses using the same type of positive controls, thereby increasing transparency and comparability between analytical techniques. The cohort size of the controls and of the patients provided considerable numbers of samples, allowing for a solid case-control comparison and a focused analysis of patients with versus without PAH. Finally, assay sensitivity was high and only small amounts of serum were required to obtain the aAb result, enabling fast, cost-effective and high throughput analyses in future studies on larger cohorts of samples with related cardiovascular phenotypes.

No study is without limitation, and the lack of biological characterization of the identified aAb as potential agonists, antagonists or modulators of receptor function constitutes an important knowledge gap. Unfortunately, sample volumes were limited and not sufficient to isolate immunoglobulins for further biochemical analyses. The nature of the study design as case-control study precludes any causal interpretations, and detailed structural and functional analyses of the identified aAb along with analyses with longitudinal patient samples and clinical data are required to elucidate a potential etiologic role of the aAb in SSc, and in particular in PAH. In addition, information on anthropometric and clinical characteristics of the participants contributing to the cohort of healthy subjects is sparse, as the samples were obtained from a commercial supplier, and subject-specific information was not provided for reasons of data safety. Finally, genetic background and place of residency of the patients was relatively uniform, precluding extrapolations to patients from other populations or different genetic background. That notwithstanding, this is the first systematic analysis of aAb to human S1PR in healthy and diseased subjects, providing some positive results in relation to PAH which warrant further analysis in larger clinical studies.

DATA AVAILABILITY STATEMENT

The original contributions presented in the study are included in the article/supplementary material. Further inquiries can be directed to the corresponding authors.

ETHICS STATEMENT

The studies involving human participants were reviewed and approved by Charité Medical School Berlin (10/30/2017, EA1/178/17) and the Board of Ethics of the University of Cologne (#04-037). The patients/participants provided their written informed consent to participate in this study.

AUTHOR CONTRIBUTIONS

Conceptualization, ES, SS, and LS; Methodology: HG, WM, and JH; Software: HG and JH; Validation, SS, GR, and WK; Formal Analysis: HG, JH, SS, and LS; Investigation: HG, ES, WM, SS, and LS; Resources: ES, WM, GR, and LS; Data Curation: HG, JH, SS, and LS; Writing—Original Draft Preparation, HG, ES, SS, and LS; Writing, Review and Editing; WM, JH, GR, and WK; Supervision, SS and LS; Project Administration, LS; Funding Acquisition, LS. All authors have read and agreed to the published version of the manuscript.

FUNDING

The research was supported by the Deutsche Forschungsgemeinschaft (DFG), research unit FOR-2558 "TraceAge" (Scho 849/6-2), and CRC/TR 296 "Local control of TH action" (LocoTact), to LS, and SFB-TR84 and KU1218/12-1 to WK. Additional support was received from the German Centre for Cardiovascular Research (DZHK) and German Foundation for Heart Research (F-09-19) to SS. ES was supported by the Berlin Institute of Health Biomedical Innovation Academy with a Fellowship of the BIH Charité Clinician Scientist Program.

ACKNOWLEDGMENTS

The authors thank their clinical colleagues for patient care, enrolling the patients into the study and obtaining the blood samples. We thank all patients and healthy subjects for their kind participation. A special thanks goes to our colleague Dr. Eddy Rijntjes and Julian Hackler for statistical support and conceptual expertise. Gabriela Boehm, Vartiter Seher and Anja Fischbach contributed with their excellent technical assistance.

REFERENCES

1. Kurakula K, Smolders V, Tura-Ceide O, Jukema JW, Quax PHA, Goumans MJ. Endothelial Dysfunction in Pulmonary Hypertension: Cause or Consequence? *Biomedicines* (2021) 9(1). doi: 10.3390/biomedicines9010057
2. Sarah B, Ashrith G, Sandeep S. Evaluation, Diagnosis, and Classification of Pulmonary Hypertension. *Methodist Debakey Cardiovasc J* (2021) 17(2):86–91. doi: 10.14797/OCDF4453
3. Galiè N, Humbert M, Vachiery J-L, Gibbs S, Lang I, Torbicki A, et al. 2015 ESC/ERS Guidelines for the Diagnosis and Treatment of Pulmonary Hypertension. The Joint Task Force for the Diagnosis and Treatment of Pulmonary Hypertension of the European Society of Cardiology (ESC) and the European Respiratory Society (ERS) Endorsed by: Association for European Paediatric and Congenital Cardiology (AEPC), International Society for Heart and Lung Transplantation (ISHLT). *Eur Respir J* (2015) 46(4):903–75. doi: 10.1183/13993003.01032-2015
4. Hoeper MM, Bogaard HJ, Condliffe R, Frantz R, Khanna D, Kurzyna M, et al. Definitions and Diagnosis of Pulmonary Hypertension. *J Am Coll Cardiol* (2013) 62(25 Suppl):D42–50. doi: 10.1016/j.jacc.2013.10.032
5. Hudson J, Farkas L. Epigenetic Regulation of Endothelial Dysfunction and Inflammation in Pulmonary Arterial Hypertension. *Int J Mol Sci* (2021) 22 (22). doi: 10.3390/ijms222212098
6. Li MX, Jiang DQ, Wang Y, Chen QZ, Ma YJ, Yu SS, et al. Signal Mechanisms of Vascular Remodeling in the Development of Pulmonary Arterial Hypertension. *J Cardiovasc Pharmacol* (2016) 67(2):182–90. doi: 10.1097/FJC.0000000000000328
7. Li C, Liu P, Song R, Zhang Y, Lei S, Wu S. Immune Cells and Autoantibodies in Pulmonary Arterial Hypertension. *Acta Biochim Biophys Sin* (2017) 49 (12):1047–57. doi: 10.1093/abbs/gmx095
8. Günther J, Kill A, Becker MO, Heidecke H, Rademacher J, Siegert E, et al. Angiotensin Receptor Type 1 and Endothelin Receptor Type A on Immune Cells Mediate Migration and the Expression of IL-8 and CCL18 When Stimulated by Autoantibodies From Systemic Sclerosis Patients. *Arthritis Res Ther* (2014) 16(2):R65. doi: 10.1186/ar4503
9. Chen J, Tang H, Sysol JR, Moreno-Vinasco L, Shioura KM, Chen T, et al. The Sphingosine Kinase 1/Sphingosine-1-Phosphate Pathway in Pulmonary Arterial Hypertension. *Am J Respir Crit Care Med* (2014) 190(9):1032–43. doi: 10.1164/rccm.201401-0121OC
10. Gairhe S, Joshi SR, Bastola MM, McLendon JM, Oka M, Fagan KA, et al. Sphingosine-1-Phosphate is Involved in the Occlusive Arteriopathy of Pulmonary Arterial Hypertension. *Pulmonary Circulation* (2016) 6(3):369–80. doi: 10.1086/687766
11. Cartier A, Hla T. Sphingosine 1-Phosphate: Lipid Signaling in Pathology and Therapy. *Science* (2019) 366(6463). doi: 10.1126/science.aar5551
12. Vu TM, Ishizu AN, Foo JC, Toh XR, Zhang F, Whee DM, et al. Mfsd2b is Essential for the Sphingosine-1-Phosphate Export in Erythrocytes and Platelets. *Nature* (2017) 550(7677):524–8. doi: 10.1038/nature24053
13. Fukuhara S, Simmons S, Kawamura S, Inoue A, Orba Y, Tokudome T, et al. The Sphingosine-1-Phosphate Transporter Spns2 Expressed on Endothelial Cells Regulates Lymphocyte Trafficking in Mice. *J Clin Invest* (2012) 122 (4):1416–26. doi: 10.1172/JCI60746
14. Simmons S, Sasaki N, Umemoto E, Uchida Y, Fukuhara S, Kitazawa Y, et al. High-Endothelial Cell-Derived S1P Regulates Dendritic Cell Localization and Vascular Integrity in the Lymph Node. *Elife* (2019) 8. doi: 10.7554/eLife.41239
15. Takabe K, Paugh SW, Milstien S, Spiegel S. "Inside-Out" Signaling of Sphingosine-1-Phosphate: Therapeutic Targets. *Pharmacol Rev* (2008) 60 (2):181–95. doi: 10.1124/pr.107.07113
16. Blaho VA, Chun J. 'Crystal' Clear? Lysophospholipid Receptor Structure Insights and Controversies. *Trends Pharmacol Sci* (2018) 39(11):953–66. doi: 10.1016/j.tips.2018.08.006
17. Matloubian M, Lo CG, Cinamon G, Lesneski MJ, Xu Y, Brinkmann V, et al. Lymphocyte Egress From Thymus and Peripheral Lymphoid Organs is Dependent on S1P Receptor 1. *Nature* (2004) 427(6972):355–60. doi: 10.1038/nature02284
18. Birker-Robaczewska M, Studer R, Haenig B, Menyhart K, Hofmann S, Nayler O. bFGF Induces S1P1 Receptor Expression and Functionality in Human Pulmonary Artery Smooth Muscle Cells. *J Cell Biochem* (2008) 105(4):1139–45. doi: 10.1002/jcb.21918
19. Cantalupo A, Gargiulo A, Dautaj E, Liu C, Zhang Y, Hla T, et al. S1PR1 (Sphingosine-1-Phosphate Receptor 1) Signaling Regulates Blood Flow and Pressure. *Hypertens (Dallas Tex 1979)* (2017) 70(2):426–34. doi: 10.1161/HYPERTENSIONAHA.117.09088
20. Ota H, Beutz MA, Ito M, Abe K, Oka M, McMurtry IF. S1P(4) Receptor Mediates S1P-Induced Vasoconstriction in Normotensive and Hypertensive Rat Lungs. *Pulmonary Circulation* (2011) 1(3):399–404. doi: 10.4103/2045-8932.87309
21. Tabeling C, Yu H, Wang L, Ranke H, Goldenberg NM, Zabini D, et al. CFTR and Sphingolipids Mediate Hypoxic Pulmonary Vasoconstriction. *Proc Natl Acad Sci U S A* (2015) 112(13):E1614–23. doi: 10.1073/pnas.1421190112
22. Grimmer B, Kuebler WM. The Endothelium in Hypoxic Pulmonary Vasoconstriction. *J Appl Physiol (1985)* (2017) 123(6):1635–46. doi: 10.1152/japplphysiol.00120.2017
23. Yang L, Han Z, Tian L, Mai P, Zhang Y, Wang L, et al. Sphingosine 1-Phosphate Receptor 2 and 3 Mediate Bone Marrow-Derived Monocyte/Macrophage Motility in Cholestatic Liver Injury in Mice. *Sci Rep* (2015) 5:13423. doi: 10.1038/srep13423
24. Burg N, Salmon JE, Hla T. Sphingosine 1-Phosphate Receptor-Targeted Therapeutics in Rheumatic Diseases. *Nat Rev Rheumatol* (2022) 18(6):335–51. doi: 10.1038/s41584-022-00784-6
25. Tian J, Huang T, Chang S, Wang Y, Fan W, Ji H, et al. Role of Sphingosine-1-Phosphate Mediated Signalling in Systemic Lupus Erythematosus. *Prostaglandins Other Lipid Mediat* (2021) 156:106584. doi: 10.1016/j.prostaglandins.2021.106584
26. Pérez-Jeldres T, Alvarez-Lobos M, Rivera-Nieves J. Targeting Sphingosine-1-Phosphate Signaling in Immune-Mediated Diseases: Beyond Multiple Sclerosis. *Drugs* (2021) 81(9):985–1002. doi: 10.1007/s40265-021-01528-8
27. Chaisson NF, Hassoun PM. Systemic Sclerosis-Associated Pulmonary Arterial Hypertension. *Chest* (2013) 144(4):1346–56. doi: 10.1378/chest.12-2396
28. Cabral-Marques O, Marques A, Giil LM, De Vito R, Rademacher J, Gunther J, et al. GPCR-Specific Autoantibody Signatures are Associated With Physiological and Pathological Immune Homeostasis. *Nat Commun* (2018) 9(1):5224. doi: 10.1038/s41467-018-07598-9
29. Hamaguchi Y. [Autoantibodies and Their Clinical Characteristics in Systemic Sclerosis]. *Nihon Rinsho Meneki Gakkai Kaishi* (2013) 36(3):139–47. doi: 10.2177/jsci.36.139
30. Becker MO, Kill A, Kutsche M, Guenther J, Rose A, Tabeling C, et al. Vascular Receptor Autoantibodies in Pulmonary Arterial Hypertension Associated

With Systemic Sclerosis. *Am J Respir Crit Care Med* (2014) 190(7):808–17. doi: 10.1164/rccm.201403-0442OC
31. Fisher MR, Mathai SC, Champion HC, Girgis RE, Housten-Harris T, Hummers L, et al. Clinical Differences Between Idiopathic and Scleroderma-Related Pulmonary Hypertension. *Arthritis Rheumatol* (2006) 54(9):3043–50. doi: 10.1002/art.22069
32. Hoeper MM, Ghofrani HA, Grunig E, Klose H, Olschewski H, Rosenkranz S. Pulmonary Hypertension. *Dtsch Arztebl Int* (2017) 114(5):73–84. doi: 10.3238/arztebl.2016.0073
33. Kano M, Kobayashi T, Date M, Tennichi M, Hamaguchi Y, Strasser DS, et al. Attenuation of Murine Sclerodermatous Models by the Selective S1P(1) Receptor Modulator Cenerimod. *Sci Rep* (2019) 9(1):658. doi: 10.1038/s41598-018-37074-9
34. Eleftheriadou AM, Mehl S, Renko K, Kasim RH, Schaefer JA, Minich WB, et al. Re-Visiting Autoimmunity to Sodium-Iodide Symporter and Pendrin in Thyroid Disease. *Eur J Endocrinol* (2020) 183(6):571–80. doi: 10.1530/EJE-20-0566
35. Schwiebert C, Kuhnen P, Becker NP, Welsink T, Keller T, Minich WB, et al. Antagonistic Autoantibodies to Insulin-Like Growth Factor-1 Receptor Associate With Poor Physical Strength. *Int J Mol Sci* (2020) 21(2). doi: 10.3390/ijms21020463
36. Porst T, Johannes J, Gluschke H, Kohler R, Mehl S, Kuhnen P, et al. Natural Autoimmunity to the Thyroid Hormone Monocarboxylate Transporters MCT8 and MCT10. *Biomedicines* (2021) 9(5). doi: 10.3390/biomedicines9050496
37. Sattler LM, Schniewind HA, Minich WB, Haudum CW, Niklowitz P, Munzker J, et al. Natural Autoantibodies to the Gonadotropin-Releasing Hormone Receptor in Polycystic Ovarian Syndrome. *PloS One* (2021) 16(4): e0249639. doi: 10.1371/journal.pone.0249639
38. Schniewind HA, Sattler LM, Haudum CW, Munzker J, Minich WB, Obermayer-Pietsch B, et al. Autoimmunity to the Follicle-Stimulating Hormone Receptor (FSHR) and Luteinizing Hormone Receptor (LHR) in Polycystic Ovarian Syndrome. *Int J Mol Sci* (2021) 22(24). doi: 10.3390/ijms222413667
39. Waeber C, Blondeau N, Salomone S. Vascular Sphingosine-1-Phosphate S1P1 and S1P3 Receptors. *Drug News Perspect* (2004) 17(6):365–82. doi: 10.1358/dnp.2004.17.6.829028
40. Ludwig RJ, Vanhoorelbeke K, Leypoldt F, Kaya Z, Bieber K, McLachlan SM, et al. Mechanisms of Autoantibody-Induced Pathology. *Front Immunol* (2017) 8. doi: 10.3389/fimmu.2017.00603
41. Cabral-Marques O, Riemekasten G. Functional Autoantibodies Targeting G Protein-Coupled Receptors in Rheumatic Diseases. *Nat Rev Rheumatol* (2017) 13(11):648–56. doi: 10.1038/nrrheum.2017.134
42. Liao JJ, Huang MC, Fast K, Gundling K, Yadav M, Van Brocklyn JR, et al. Immunosuppressive Human Anti-Lymphocyte Autoantibodies Specific for the Type 1 Sphingosine 1-Phosphate Receptor. *FASEB J* (2009) 23(6):1786–96. doi: 10.1096/fj.08-124891
43. Wang J, Goren I, Yang B, Lin S, Li J, Elias M, et al. Review Article: The Sphingosine 1 Phosphate/Sphingosine 1 Phosphate Receptor Axis - a Unique Therapeutic Target in Inflammatory Bowel Disease. *Aliment Pharmacol Ther* (2022) 55(3):277–91. doi: 10.1111/apt.16741
44. Ju MS, Jung ST. Antigen Design for Successful Isolation of Highly Challenging Therapeutic Anti-GPCR Antibodies. *Int J Mol Sci* (2020) 21(21). doi: 10.3390/ijms21218240
45. Corin K, Baaske P, Ravel DB, Song J, Brown E, Wang X, et al. A Robust and Rapid Method of Producing Soluble, Stable, and Functional G-Protein Coupled Receptors. *PloS One* (2011) 6(10):e23036. doi: 10.1371/journal.pone.0023036

Conflict of Interest: The authors declare that the research was conducted in the absence of any commercial or financial relationships that could be construed as a potential conflict of interest.

Publisher's Note: All claims expressed in this article are solely those of the authors and do not necessarily represent those of their affiliated organizations, or those of the publisher, the editors and the reviewers. Any product that may be evaluated in this article, or claim that may be made by its manufacturer, is not guaranteed or endorsed by the publisher.

frontiers | Frontiers in Immunology

ORIGINAL RESEARCH
published: 08 July 2022
doi: 10.3389/fimmu.2022.845526

Restricted T-Cell Repertoire in the Epicardial Adipose Tissue of Non-ST Segment Elevation Myocardial Infarction Patients

Daniela Pedicino[1†], Anna Severino[1,2†], Gabriele Di Sante[3,4†], Maria Cristina De Rosa[5], Davide Pirolli[5], Ramona Vinci[1,2], Vincenzo Pazzano[6], Ada F. Giglio[7], Francesco Trotta[8], Giulio Russo[2], Aureliano Ruggio[1], Eugenia Pisano[2], Alessia d'Aiello[1], Francesco Canonico[1,2], Pellegrino Ciampi[2], Domenico Cianflone[9], Lorenzo Cianfanelli[9], Maria Chiara Grimaldi[2], Simone Filomia[2], Nicola Luciani[1,2], Franco Glieca[1,9], Piergiorgio Bruno[1,2], Massimo Massetti[1,2], Francesco Ria[3,10‡], Filippo Crea[1,2‡] and Giovanna Liuzzo[1,2‡]*

[1] Dipartimento di Scienze Cardiovascolari, Fondazione Policlinico Universitario A. Gemelli Istituto di Ricovero e Cura a Carattere Scientifico (IRCCS), Rome, Italy, [2] Dipartimento di Scienze Cardiovascolari e Pneumologiche, Università Cattolica del Sacro Cuore, Rome, Italy, [3] Dipartimento di Medicina e Chirurgia traslazionale, Università Cattolica del Sacro Cuore, Rome, Italy, [4] Dipartimento di Medicina e Chirurgia, Sezione di Anatomia Umana, Clinica e Forense, Università di Perugia, Perugia, Italy, [5] Istituto di Scienze e Tecnologie Chimiche "Giulio Natta" (SCITEC) - Consiglio Nazionale delle Ricerche (CNR), Rome, Italy, [6] Paediatric Cardiology and Cardiac Arrhythmia/Syncope Unit, Bambino Gesù Children's Hospital Istituto di Ricovero e Cura a Carattere Scientifico (IRCCS), Rome, Italy, [7] Dipartimento di Cardiologia, Aziende Socio Sanitarie Territoriali (ASST) Fatebenefratelli Sacco, Milano, Italy, [8] Cardiology Unit "F. Perinei" Hospital, Bari, Italy, [9] Cardiac Rehabilitation Unit, Istituto di Ricovero e Cura a Carattere Scientifico (IRCCS) Ospedale San Raffaele, Università Vita-Salute San Raffaele, Milan, Italy, [10] Dipartimento di Scienze di Laboratorio ed Infettivologiche, Fondazione Policlinico Universitario A. Gemelli Istituto di Ricovero e Cura a Carattere Scientifico (IRCCS), Rome, Italy

Aims: Human epicardial adipose tissue, a dynamic source of multiple bioactive factors, holds a close functional and anatomic relationship with the epicardial coronary arteries and communicates with the coronary artery wall through paracrine and vasocrine secretions. We explored the hypothesis that T-cell recruitment into epicardial adipose tissue (EAT) in patients with non-ST segment elevation myocardial infarction (NSTEMI) could be part of a specific antigen-driven response implicated in acute coronary syndrome onset and progression.

Methods and Results: We enrolled 32 NSTEMI patients and 34 chronic coronary syndrome (CCS) patients undergoing coronary artery bypass grafting (CABG) and 12 mitral valve disease (MVD) patients undergoing surgery. We performed EAT proteome profiling on pooled specimens from three NSTEMI and three CCS patients. We performed T-cell receptor (TCR) spectratyping and CDR3 sequencing in EAT and peripheral blood mononuclear cells of 29 NSTEMI, 31 CCS, and 12 MVD patients. We then used computational modeling studies to predict interactions of the TCR beta chain variable region (TRBV) and explore sequence alignments. The EAT proteome profiling displayed a

OPEN ACCESS

Edited by:
Kathleen Pappritz,
Charité Medical University of Berlin, Germany

Reviewed by:
Vyacheslav Ryabov,
Tomsk National Research Medical Center (RAS), Russia
Marinos Kallikourdis,
Humanitas University, Italy

***Correspondence:**
Daniela Pedicino
danialla@gmail.com;
daniela.pedicino@policlinogemelli.it
orcid.org/0000-0002-4218-3066

†These authors share first authorship

‡These authors share last authorship

Specialty section:
This article was submitted to Inflammation, a section of the journal Frontiers in Immunology

Received: 29 December 2021
Accepted: 31 May 2022
Published: 08 July 2022

Citation:
Pedicino D, Severino A, Di Sante G, De Rosa MC, Pirolli D, Vinci R, Pazzano V, Giglio AF, Trotta F, Russo G, Ruggio A, Pisano E, d'Aiello A, Canonico F, Ciampi P, Cianflone D, Cianfanelli L, Grimaldi MC, Filomia S, Luciani N, Glieca F, Bruno P, Massetti M, Ria F, Crea F and Liuzzo G (2022) Restricted T-Cell Repertoire in the Epicardial Adipose Tissue of Non-ST Segment Elevation Myocardial Infarction Patients. Front. Immunol. 13:845526. doi: 10.3389/fimmu.2022.845526

higher content of pro-inflammatory molecules (CD31, CHI3L1, CRP, EMPRINN, ENG, IL-17, IL-33, MMP-9, MPO, NGAL, RBP-4, RETN, VDB) in NSTEMI as compared to CCS ($P < 0.0001$). CDR3-beta spectratyping showed a TRBV21 enrichment in EAT of NSTEMI (12/29 patients; 41%) as compared with CCS (1/31 patients; 3%) and MVD (none) (ANOVA for trend $P < 0.001$). Of note, 11/12 (92%) NSTEMI patients with TRBV21 perturbation were at their first manifestation of ACS. Four patients with the first event shared a distinctive TRBV21-CDR3 sequence of 178 bp length and 2/4 were carriers of the human leukocyte antigen (HLA)-A*03:01 allele. A 3D analysis predicted the most likely epitope able to bind HLA-A3*01 and interact with the TRBV21-CDR3 sequence of 178 bp length, while the alignment results were consistent with microbial DNA sequences.

Conclusions: Our study revealed a unique immune signature of the epicardial adipose tissue, which led to a 3D modeling of the TCRBV/peptide/HLA-A3 complex, in acute coronary syndrome patients at their first event, paving the way for epitope-driven therapeutic strategies.

Keywords: epicardial adipose tissue (EAT), NSTE ACS, T-cell receptor (TCR), immune response, precision medicine, first acute myocardial infarction, antigen-driven immunity, computational modeling

INTRODUCTION

Human epicardial adipose tissue (EAT), a dynamic source of multiple bioactive factors, owns a close functional and anatomic relationship with the epicardial coronary arteries and communicates with the coronary artery wall through paracrine and vasocrine secretions (1). Several studies suggesting the role of EAT in the pathogenesis of atherosclerosis consistently reported that EAT thickness is an independent indicator of cardiovascular risk (2, 3).

Cytokine release and pro-inflammatory cell infiltration of macrophages, lymphocytes, and basophils have been associated with the EAT of patients with established coronary artery disease who underwent elective coronary artery bypass graft (CABG) (4, 5); in these patients, macrophage polarization in EAT is shifted toward the pro-inflammatory M1 phenotype (6, 7).

Although less abundant than macrophages, T cells orchestrate the antigen-specific immune response in the coronary plaque (8–10). This occurs after the T-cell receptor (TCR) has mediated the recognition of short peptides on the human leukocyte antigen (HLA) on presenting cells. The enormous TCR diversity allows for the recognition of a wide range of potential pathogenic molecules and accounts for the difficulties in determining the antigen specificity of each receptor (11, 12).

In the present study, we sought to investigate if T-cell recruitment within EAT in acute coronary syndrome (ACS) patients with non-ST segment elevation myocardial infarction (NSTEMI) might be part of a specific antigen-driven response potentially implicated in ACS onset and progression. To this aim, we performed the EAT proteome profiling and an extended analysis of the TCR beta chain variable region (TRBV) in EAT using the T-cell repertoire of peripheral blood mononuclear cells (PBMCs) as a reference for selective EAT enrichment which led to the design of a 3D model of the cognate/specific peptide-major histocompatibility complex (MHC) target, associated with the first acute coronary event.

METHODS

For a detailed description of the methods, see the **Online Supplementary Material**.

Study Population Design

We enrolled 1) 32 patients admitted to our Coronary Care Unit with a diagnosis of NSTEMI, who underwent CABG within 14 days of symptom onset, either at their first manifestation ($n = 19$) or with previous acute coronary events ($n = 13$); 2) 34 patients with a history of chronic stable effort angina (CCS) lasting more than 12 months, severe coronary artery disease (CAD) requiring CABG, and no clinically evident effort or rest ischemic episodes during the previous 2 weeks; and 3) 12 patients presenting with mitral valve disease (MVD) undergoing cardiac surgery for mitral valve regurgitation due to degenerative disease, with angiographically normal coronary arteries. **Figure 1** displays a schematic allocation of the study population in each experimental setting. For a detailed description of the inclusion and exclusion criteria, see the **Online Supplementary Material**. The Clinical and Research Ethics Committee of Fondazione Policlinico A. Gemelli-IRCCS and the Catholic University of the Sacred Heart of Rome approved the study protocol (protocol no. 2047) that has been conducted in accordance with the principles of the Declaration of Helsinki. All participants provided their written informed consent.

Peripheral Blood Sampling

Venous blood samples were taken a day before the surgery. PBMCs were obtained from whole blood by density gradient

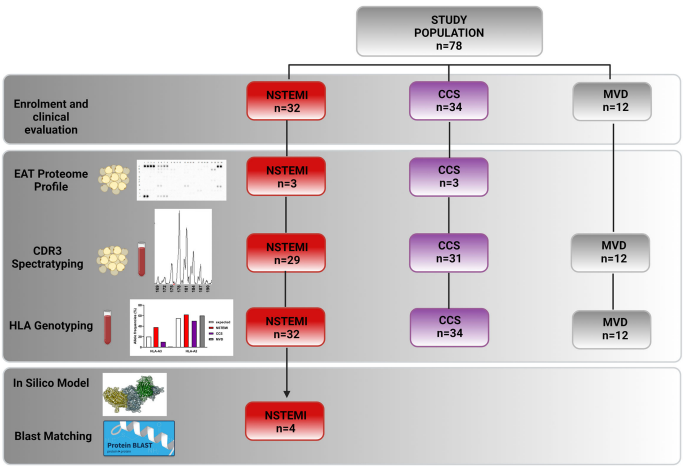

FIGURE 1 | Flowchart showing enrolled patients and their experimental and study result allocations. We obtained EAT biopsies and peripheral blood from 32 NSTEMI patients, 34 CCS patients, and 12 MVD patients undergoing surgery. Three EAT specimens from NSTEMI and CCS patients were used for proteome profiling. We therefore performed TCR spectratyping and CDR3 sequencing in EAT and PBMCs of 29 NSTEMI, 31 CCS, and 12 MVD patients. We performed HLA-A molecular typing from DNA extracted from the PBMCs of the same patients. Twelve NSTEMI patients showed a TRBV21 perturbation, four of which shared a distinctive TRBV21-CDR3 sequence of 178 bp length and 2/4 were carriers of the human leukocyte antigen (HLA)-A*03:01 allele. We then used computational 3D modeling studies to predict interactions between HLA-A3*01 and the TRBV21-CDR3 sequence of 178 bp length, employing BLAST to compare the predicted peptide sequence to specific microbial databases. BLAST, Basic Local Alignment Search Tool; EAT, epicardial adipose tissue; HLA, human leukocyte antigen; MVD, mitral valve disease; NSTEMI, non-ST elevation myocardial infarction; PBMC, peripheral blood mononuclear cells; CCS, chronic coronary syndrome; TCR, T-cell receptor.

centrifugation over Ficoll-Hypaque (GE Healthcare Bio-Sciences, Piscataway, NJ, USA) and stored at −80°C for RNA extraction. Coded serum samples were stored at −80°C and analyzed for high-sensitivity C-reactive protein (hs-CRP) in a single batch at the end of the study. In NSTEMI patients, serum cardiac troponin I (cTnI) was determined at the time of hospital admission as a routine measurement. All categorization and management of patients were independent from these results.

EAT Sampling and Profiling

EAT biopsy (average 0.9 g) was collected before surgery in all cases. In CCS and MVD patients, EAT was collected near the proximal right coronary artery, while in NSTEMI patients, it was collected near the culprit coronary artery, i.e., left coronary artery (LCA) in 20 cases and right coronary artery (RCA) in 12 cases. Liquid nitrogen EAT specimens were stored at −80°C and subsequently used for RNA isolation. Isolated and stimulated EAT T cells were stained with fluorochrome-conjugated mAbs anti-CD4-FITC and anti-CD8-PE-Cy5 (all from Beckman Coulter, Brea, CA, USA). A total of 100,000 events have been acquired. Non-specific staining with isotype-matched control mAb was <1%; the intra- and interassay variability was <10%. Flow cytometry analysis was conducted with FC 500 (Beckman Coulter, Brea, CA, USA) and the data were analyzed with Kaluza software (Beckman Coulter, Brea, CA, USA). EAT biopsies (average weight = 0.2 g) from CCS (n = 3) and NSTEMI (n = 3), collected as described above, were pooled to evaluate the inflammatory proteome profile (Proteome Profiler Array, R&D, USA). Details of EAT T-cell isolation and stimulation and profiling are described in the **Online Supplementary Material**.

TCR Repertoire Analysis and CDR3 Sequencing

TCR repertoire analysis and CDR3 sequencing were performed as previously published (13–15). The method for quantifying TCR repertoire perturbation in EAT as compared with PBMCs was adapted from Gorochov et al. (16) (see the **Online Supplementary Material** and **Figure S1**).

DNA Extraction and HLA-A Genotyping

Genomic DNA from peripheral whole blood was extracted by QIAamp DNA Mini kits (Qiagen GmbH, Hilden, Germany) and 0.1 µg of purified genomic DNA was used for HLA-DRB1 exon PCR amplification. After PCR amplification, HLA-A molecular typing was performed by a reverse hybridization method using the INNO-LiPA HLA-A kit (Fujirebio, Tokyo, Japan), following the manufacturer's instructions. Interpretation of hybridization of HLA-A probes was made using the LiRAS software (Fujirebio, Tokyo, Japan) to predict one-digit HLA.

In-Silico 3D Modeling of the TRBV/Peptide/HLA-A3 Complex

We employed a computational modeling study to predict TRBV/peptide/MHC interactions (17, 18). The homology modeling algorithm MODELLER v9.10 as implemented in Discovery Studio 4.0 (Dassault Systèmes, San Diego, CA, USA) was used to generate the computational model structure of TRBV21* (19). The 3D structure of the human anti-pre-pro insulin (PPI) protein T-cell receptor (1E6) bound to an HLA-A*0201-restricted glucose-sensitive PPI peptide (PDB code: 3UTT REF 10.1038/ni.2206), showing 70.0% sequence identity, was used as template (**Online**

Supplementary Material Figure S2). The best-ranked model based on the probability density function (PDF) was selected, and the quality of the structure was assessed by PROCHECK and VERIFY3D (**Online Supplementary Material Figures S3**, **S4**). The structure of the human MHC class I molecule HLA-A*0301 (HLA-A3), in complex with a peptide (KLIETYFSK) from proteolipid protein (PDB code: 2XPG REF 10.1107/S0907444911007888), was used as the interaction partner for the modeled TRBV21*. The quaternary complex 1BD2 was used as a reference for the relative orientation of the interacting structures (20). Following the replacement of each residue by glycine (glycine), the peptide backbone was used to build putative epitope peptides by side chain construction and CHARMM's energy minimization. This process was automatically performed by the Grow Scaffold module in Discovery Studio 4.0 by identifying the top-ranking residue in each position. After calculating and scoring, the best peptide to act as a ligand was selected for further analyses (see the **Online Supplementary Material** for references).

Sequence Alignment and Similarity Analysis

The Basic Local Alignment Search Tool (BLAST) (21) was used to compare the predicted peptide sequence to specific microbial databases and to calculate the statistical significance of matches (see the **Online Supplementary Material**).

Statistical Analysis

Categorical variables were described as numbers and percentages (%), and they were analyzed using the chi-square (χ^2) test or Fisher's test, depending on sample size restrictions. The continuous variables that were normally distributed, as assessed by the Shapiro–Wilk test, were described as mean ± SD and analyzed with parametric tests. For comparisons among the three groups, we used one-way (or two-way) analysis of variance (ANOVA) with Bonferroni or Sidak correction. For between-group comparisons, we used unpaired or paired Student's *t*-test. Data that did not follow a normal distribution were described as median and interquartile range and analyzed by using a non-parametric test. We used the Kruskal–Wallis non-parametric ANOVA and the Dunn's test for comparisons among groups. For between-group comparisons, we used the Mann–Whitney *U*-test. To compare two related samples within groups, we used the Wilcoxon test. A two-tailed *P*-value <0.05 was considered statistically significant. Statistical analysis was performed by using SPSS Statistics 20.0 (IBM Corp., Armonk, NY, USA) and Prism software 8.02 (GraphPad, San Diego, CA 92121, USA).

RESULTS

The baseline characteristics of the patients are presented in **Table S1**. The study design is described in **Figure 1**.

EAT T-Cell Infiltration and Proteome Profiling

In order to characterize the presence of immune infiltrates in EAT, we analyzed the cell suspensions obtained from EAT specimens of NSTEMI (n = 10) and CCS (n = 10) patients by flow cytometry. We observed that 50% of EAT-infiltrating T cells were $CD4^+$, while the 30% were $CD8^+$ without differences between groups (**Figure 2A**).

To determine the relative amount of inflammatory mediators at the local level, proteome profiling of pooled EAT specimens from NSTEMI (n = 3) and CCS (n = 3) patients was performed. The results displayed highly significant differences between the two groups for multiple molecules involved in the pro-inflammatory response, cell recruitment and adhesion to the arterial wall, and vascular remodeling (**Figures 2B, C; Table S2**), thus highlighting the unique composition of the EAT in patients with NSTEMI.

T Cells in EAT Display a Broad TCR Repertoire

To deepen the characterization of T lymphocyte infiltrates, a TRBV-TRBJ spectratyping was performed. We examined the size distribution of the TCR CDR3 region for 25 BV families by immunoscope spectratyping (**Table S3**). A total of 3,600 spectra were analyzed in PBMC and EAT samples from 72 patients (NSTEMI, n = 29; CCS, n = 31; MVD, n = 12). PBMCs and EAT T cells displayed no difference in TCR BV usage pattern. EAT obtained from MVD patients showed a comparable width of T-cell repertoire. The repertoire used by each individual is highly variable, although among the 25 BV families (**Table S3**) analyzed, 14 were used more consistently among SA and NSTEMI patients, while only 6 BV among MVD patients (**Figure 3** and **Figure S5**). Despite the high variability of the TCR repertoire used by each individual, it was possible to detect several TCR signatures characterizing specifically NSTEMI, CCS, or MVD patients.

Perturbation of the TCR Repertoire (TRBV21) in EAT Is Associated With the First Manifestation of NSTEMI

Focusing on the most shared TCRs, we calculated using algorithms the threshold values and determined the cutoffs to identify specific disease-related TCRs as biomarkers. The perturbation (D) degree (%) of the TCR repertoire was calculated for each patient in PBMC and EAT specimens as a function of the difference between the P distribution of the EAT sample and the P distribution of the PBMC sample (reference sample). This approach provides a quantitative determination of repertoire perturbations with a D value carrying from 0% to 100% (**Online Supplementary Material, Figure S1**). As illustrated in **Figure 3** and **Figure S5**, the perturbations of the TCR repertoire in EAT are distributed differently in NSTEMI and CCS patients: in NSTEMI patients, alterations of TRBV21 were strongly prevalent, while perturbations of TRBV28 were observed in CCS and MVD patients, although not statistically significant. Indeed, TRBV21 perturbation was significantly higher in NSTEMI (median, range: 7.4, 0.3–56) as compared to CCS (1.4, 0.02–11.6) and MVD (1.2, 0.2–1.7; ANOVA by Kruskal–Wallis $P < 0.001$; Dunn's multiple comparisons test: both $P = 0.002$) (**Figure 4A**). A TRBV21* perturbation ($D >$

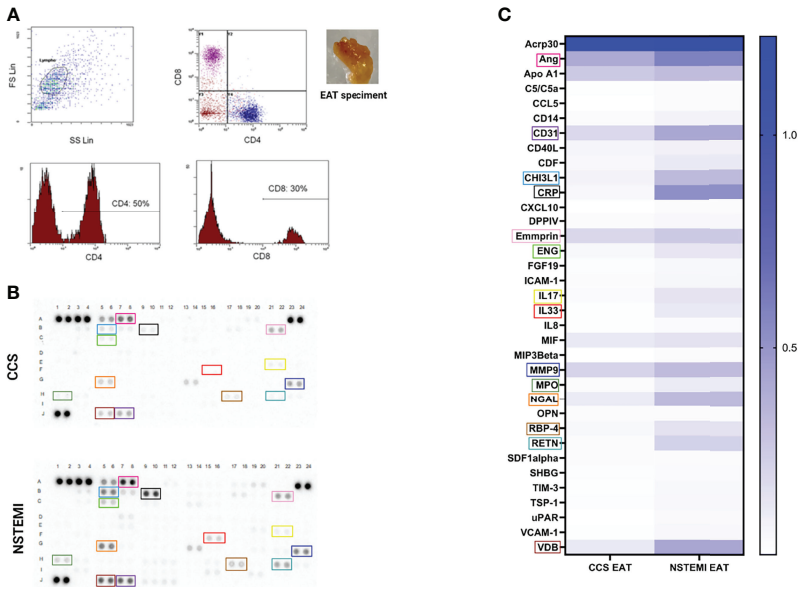

FIGURE 2 | Flow cytometry characterization of EAT-resident T cells and proteome profiling of EAT specimens. **(A)** A phenotypic characterization of EAT-resident T cells was performed by flow cytometry in NSTEMI (n = 10) and CCS (n = 10) patients. A representative flow cytometry analysis is displayed and the EAT specimen of one patient is shown. About 50% of EAT-infiltrating T cells were $CD4^+$, while 30% were $CD8^+$ without differences among groups. **(B)** An inflammatory proteome profiling was performed in NSTEMI (n = 3) and CCS (n = 3) patients; X-ray films **(B)** and heatmap analyses **(C)** are shown [squares of the same color indicate the same molecule in **(B**, **C)**]. NSTEMI and CCS patients significantly differed for multiple immune-related molecules.

10%) was observed in 12/29 (41%) of NSTEMI patients (compared with an expected 1%, in a random use of TCR gene segments) (22). TRBV21 was not enriched in EAT of CCS and MVD patients (3% and 0%, respectively; ANOVA for trend $P < 0.001$). Of note, 11/12 (92%) NSTEMI patients with TRBV21* perturbation ($D > 10\%$) were at their first manifestation and only one patient (8%) had previous acute coronary events ($P = 0.008$) (**Figure 4B**). **Figure S6** shows the receiver-operating characteristic (ROC) curves for TRBV21* perturbation. Furthermore, most perturbations of the TRBV21 distribution in NSTEMI patients focused on one single CDR3 of 178 bp length (**Figure 4C** and **Figure S7**). The same analysis was performed for TRBV28 (**Online Supplementary Material Figure S8**), demonstrating the clonal peculiarity of EAT T cells.

The NSTEMI-Associated TRBV21 Family Shares a Common CDR3 Sequence

To understand whether the enriched NSTEMI-associated TCR shared the same hypervariable region, several sequencing analyses were performed. Each CDR3 BV peak contains thousands of different sequences, each coding for a unique TCR with a particular antigen specificity. To determine whether the perturbation observed for EAT CDR3 profiles reflected a clonal expansion of T cells, CDR3 sequences of EAT samples were analyzed. Two hundred and eighty-eight sequences were obtained from nine NSTEMI patients, after a screening of about 50 plasmids per sample. Surprisingly, the same sequence (TRBV21 CASSKA ETDE ETQYFGPGTRL) was obtained in four out of the nine NSTEMI patients, all at their first manifestation. This observation supported the idea that T cells carrying this TCR were selectively enriched or expanded in EAT, at the onset of NSTEMI.

A similar CDR3 sequence analysis was carried out with the BV28 family for which several perturbations were also observed in CDR3 spectratyping profiles of CCS patients. In this case, however, we could not find sequences frequently recurring among samples. The resulting sequences and the expected length for TRBV21 and TRBV28 are reported in the **Online Supplementary Material Tables S4–S6**.

HLA-A Genotyping

In Caucasians, the most frequent HLA alleles belong to the HLA-A2 family, which collectively has an allelic frequency of approximately 30%, leading to an ≅50% of individuals being HLA-A2 positive in the population (23).

However, two of four NSTEMI patients at their first manifestation of disease with EAT samples displaying the usage of sequence TRBV21 CASSKA ETDE ETQYFGPGTRL were HLA-A*03$^+$ (**Figure 4D**). These observations led us to propose HLA-A*03 as the candidate restricting element for the public TCR (TRBV21 CASSKA ETDE ETQYFGPGTRL) in our NSTEMI patients, for further studies.

In-Silico 3D Modeling

We decided to design a 3D molecular modeling strategy aimed at identifying putative antigen peptide sequence and conformation in the TCRBV/HLA-class I/epitope complex. A scoring algorithm was used to rank sequence candidates, and the top-

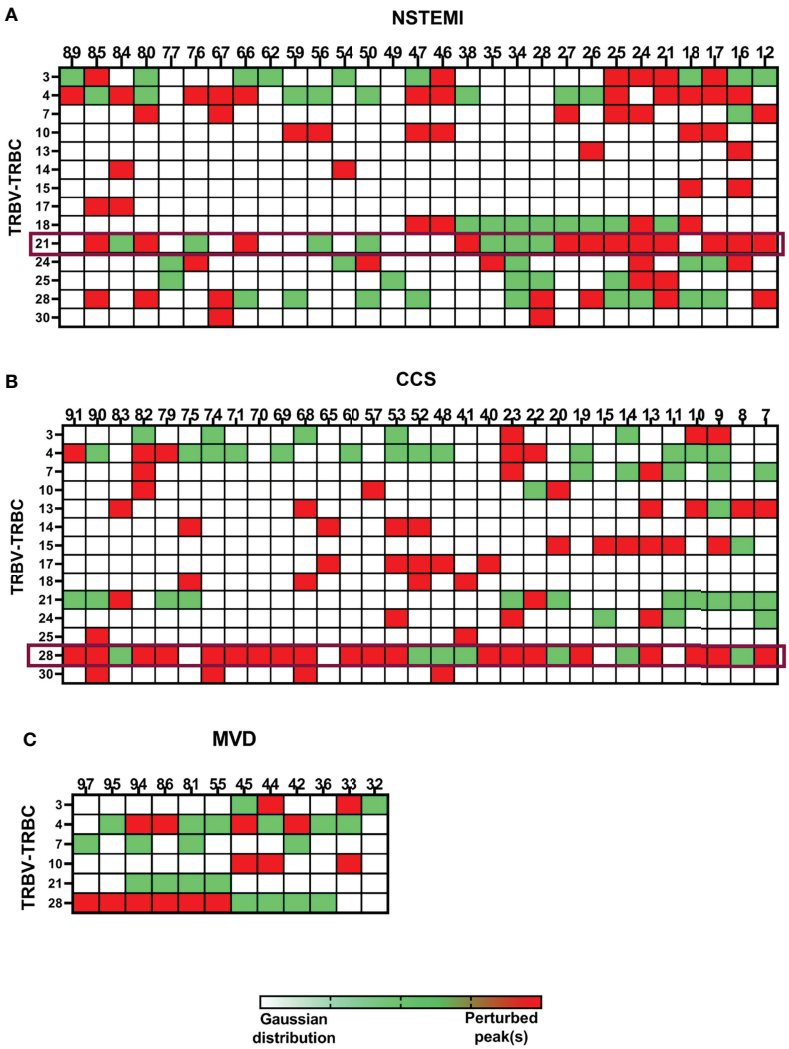

FIGURE 3 | Quantitative analysis of TCR repertoire perturbations. The TRBV-TRBC spectratyping technique was applied to analyze the TCR repertoires of the enrolled patients. EAT samples were compared with the respective PBMCs. Three matrixes are displayed, one for each group of patients [**(A)** for NSTEMI, **(B)** for CCS, and **(C)** for MVD]. Single patients are displayed in columns, while the rows represent the same TRBV-TRBC TCR recombination for all patients in each group. Each square of the matrixes represents a TRBV-TRBC rearrangement for every single patient. TRBV-TRBC spectratypes from an ideal naive TCR repertoire follow an approximate Gaussian distribution containing eight or more peaks. Skewed TRBV-TRBC profiles can be detected as perturbation of this distribution. White squares represent non-perturbed Gaussian. Green squares display minimally perturbed Gaussian. Red squares indicate a high enrichment of the same peak(s) in the EAT sample compared with the homologous PBMC sample. Despite the high variability of the TCR repertoire used by each individual, it was possible to detect specific TCR signatures characterizing NSTEMI, CCS, or MVD patients.

ranking sequence KVFLHFRVK was selected as the most likely epitope able to bind HLA-A3*01 and interact with the TRBV21* CASSKA ETDE ETQYFGPGTRL. The 3D model structures of the TCRBV/HLA-class I/epitope complex and the interacting residues are shown in **Figure 5** and **Table 1**.

Proteins of EAT Microbiota Contain Sequences Homologous to the Putative Epitope Sequence

Our group has recently demonstrated the existence of a local microbiome signature in EAT (24). Based on this scenario, a sequence similarity analysis between the putative antigen sequence ($K^1V^2F^3L^4H^5F^6R^7V^8K^9$) and the EAT microbiota genome was performed by BLASTp (21). We find that several sequences from these bacteria display homology higher than 80% with our candidate epitope sequence (**Table 2**).

Among the *Firmicutes*-derived sequences, two display the RV residues in the appropriate position, with one having an R for the H^5 in the query. Since R (arginine) and H (histidine) have distinct chemical properties, we are not certain that this peptide would be able to interact properly with the HLA-A*0301 molecule. In the sequences obtained from *Cyanobacteria* (VFLH**Y**RVK), Y substitutes for F^6. Although this is not a conservative substitution, in our model, F^6

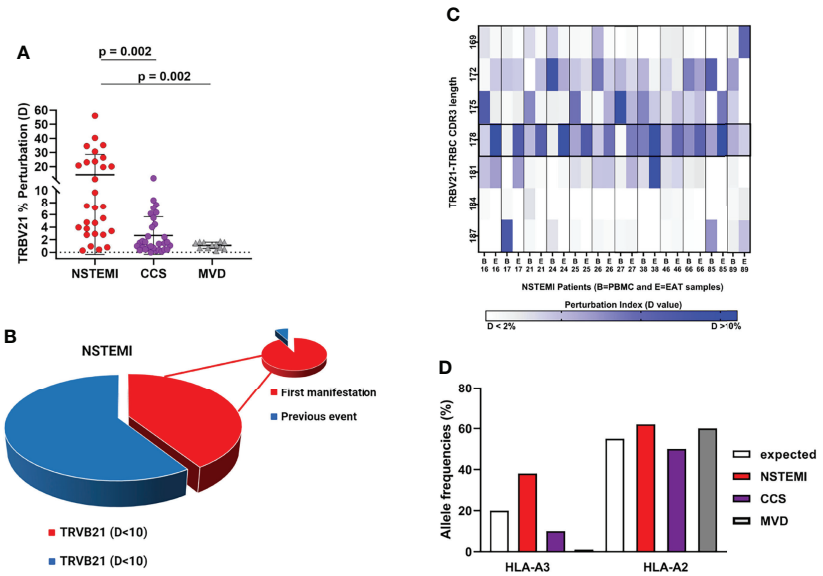

FIGURE 4 | Quantitative analysis of TRBV21 perturbation. **(A)** Comparison of the TRBV21 perturbations in the three groups of patients. The TRBV21 average perturbation between EAT and PBMC samples is different in the three groups of patients (ANOVA for trends $P < 0.001$). It is significantly higher in NSTEMI patients as compared with CCS and MVD patients ($P < 0.01$ for both comparisons), but similar between CCS and MVD patients. This analysis revealed a perturbation threshold of 10% for TRBV21. **(B)** Pie chart showing the percentage of NSTEMI with TRVB21 D >10% (41%) and the proportion of patients at their first event (pie of pie chart) (92%). **(C)** Quantitative analysis of TRBV21 perturbation in NSTEMI patients. NSTEMI patients with high perturbation of TRBV21 (D > 10%) are displayed in the matrix with dark blue rectangles, highlighting that the most frequently perturbed peak is the 178-bp length. **(D)** Frequency (%) of HLA-A*02+ and HLA-A*03+ in the three groups of patients tested. HLA-A*03^{+} frequency is higher in the NSTEMI group (38%) than in the CCS group (10%). In MVD patients, A3 was not present in the analyzed cohort. The graph shows the expected frequency of HLA-A in a reference Caucasian population deduced from http://allelefrequencies.net (>110,000 individuals). As a referral, we also reported the frequency of the commonly used HLA in the Caucasian population.

interacts only with an A (alanine^{69}) of HLA-A*0301, an interaction that may occur also for a Y (tyrosine) residue in the same position.

Overall, we propose that sequences from *Firmicutes/Ruminococcus* (LHFRVK) and *Cyanobacteria* (VFLHYRVK) display most of the characteristics required for the interaction with HLA-A*0301 and TRBV21* and can be considered good candidates as epitopes triggering the activation of T cells at the first episode of NSTEMI.

DISCUSSION

The close anatomical relationship between EAT and coronary arteries has always suggested a likely involvement of the adipose tissue in CAD (1). However, the functional role of the adipose tissue surrounding the heart is still barely elucidated. Several clues indicate that EAT is one of the key characteristics of CAD pathophysiology (25–27). Therefore, in addition to its storage and protective functions, EAT must be considered by all accounts a lymphatic organ, characterized by leukocyte trafficking and cytokine and adipokine release. Our NSTEMI EAT specimens effectively hold a peculiar proteome profile displaying an increased content of a bunch of pro-inflammatory molecules (CRP, IL-17, IL-33, CDF, RETN, RBP-4, CHI3L1) as well as proteins involved in cell recruitment and adhesion to the arterial wall and vascular remodeling (CD14, NGAL, CD31, MMP-9, VCAM1, MPO, ENG, ANG), thereby strengthening the EAT multifaced nature.

Indeed, the EAT of patients with CAD undergoing CABG shows high levels of pro-inflammatory cytokines and cell infiltration with lymphocytes, basophils, and macrophages (4, 5), mostly displaying the pro-inflammatory M1 phenotype (6, 7). The total amount of T lymphocytes is increased in EAT of CAD patients as compared with subcutaneous adipose tissue and EAT of non-CAD patients (28).

A sizeable proportion of patients presenting with ACS shows a unique adaptive immune system profile, characterized by higher levels of effector T cells and reduced levels and/or function of circulating T regulatory cells, together with a disproportionate TCR activation (29–31). T-cell clonal restriction has been demonstrated both in peripheral blood and in coronary thrombi of ACS patients (9, 10), suggesting a specific antigen-driven response. Given the role of adaptive immune dysregulation in the pathogenesis of ACS, EAT might likely contribute, as immunologically active tissue, to the immune unbalance leading to the unstable plaque (4).

Microbial DNA has been found in the EAT environment of ACS patients in association with the NOD-like receptor P3/inflammasome activation (24), suggesting, along with other evidence (32), that the gut-resident microbiome might directly or indirectly influence the progression toward plaque instability through an antigen-driven response. These data have brought

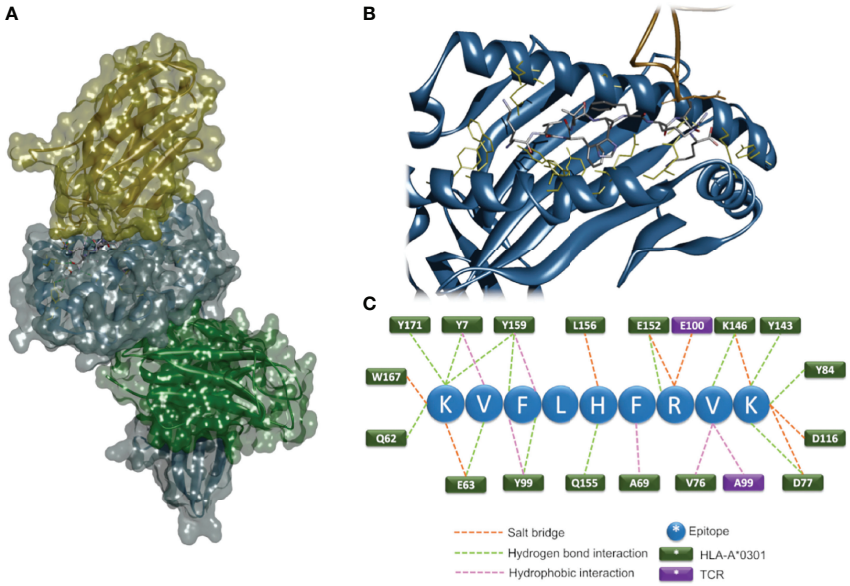

FIGURE 5 | *In-silico* 3D modeling. Molecular modeling of the TCRBV/HLA-class I/epitope complex. Overall 3D structure of the quaternary complex **(A)**. The backbone structures of TCRBV21 (yellow), HLA-A3*01 α-chain (blue), and β2-microglobulin (green) are displayed in ribbon and solvent-accessible surface representations. The epitope residues are in stick representation color-coded by atom types. A zoom view of the contact interface showing the residues important for the stabilization of the complex **(B)**. Sketch of the predicted interactions at the interface **(C)**; epitope residues are shown as blue circles, and HLA and TCR residues as green and violet rectangles, respectively.

TABLE 1 | Intermolecular non-bond interactions established by the predicted epitope with HLA-A*0301 and TCR.

Epitope	HLA-A*0301	TCR	Non-bond interactions
LYS1 (N)	TYR7 (OH)		H-bond
LYS1 (N)	TYR171 (OH)		H-bond
LYS1 (NZ)	GLN62 (OE1)		H-bond
LYS1 (NZ)	TYR159 (OH)		H-bond
LYS1 (NZ)	GLU63 (OE2)		Salt bridge
LYS1 (NZ)	TRP167 (AR)		Pi-cation
VAL2 (CG1)	TYR7		Hydrophobic
VAL2 (N)	GLU63 (OE1)		H-bond
PHE3 (AR)	TYR159 (AR)		Hydrophobic
PHE3 (AR)	TYR99 (AR)		Hydrophobic
PHE3 (N)	TYR99 (OH)		H-bond
PHE3 (OH)	TYR159 (OH)		H-bond
HIS5 (AR)	LEU156 (AR)		Hydrophobic
HIS5 (ND1)	GLN155 (OE1)		H-bond
PHE6 (AR)	ALA69 (AR)		Hydrophobic
ARG7 (NH1)	GLU152 (OE2)		Salt bridge
ARG7 (NH2)	GLU152 (OE2)		H-bond
ARG7 (NH2)	GLU100 (OE2)		Salt bridge
VAL8 (CG1)	ALA99 (CB)		Hydrophobic
VAL8 (O)	LYS146 (NZ)		H-bond
VAL8 (CG2)	VAL76 (CG1)		Hydrophobic
LYS9 (OXT)	LYS146 (NZ)		Salt bridge
LYS9 (N)	ASP77 (OD2)		Salt bridge
LYS9 (NZ)	ASP116 (OD2)		Salt bridge
LYS9 (NZ)	ASP77 (OD1)		H-bond
LYS9 (O)	THR143 (OG1)		H-bond
LYS9 (O)	TYR84 (OH)		H-bond

*Intermolecular non-bond interactions established by the predicted epitope with HLA-A*0301 and TCR as identified by Discovery Studio 4.0 (Dassault Systèmes 2018). A three-letter amino acid code followed by position number is used. Atoms involved in the interaction are reported in standard PDB atom names.*

TABLE 2 | Sequence similarity analysis between the putative antigen sequence ($K^1V^2F^3L^4H^5F^6R^7V^8K^9$) and EAT microbiota genome as performed by BLASTp (25).

Phylum	Genus	Accession	Protein	Peptide sequence	Max score	Total score	Query cover (%)	E-value	Identity (%)
Actinobacteria	*Actinomyces*	WP_075414257.1	Hypothetical protein	VFLHFR	24	24	66	4.7	100
	Actinomyces	BAV83756.1	Hypothetical protein	VFLHFR	24	24	66	4.7	100
	Actinomyces	WP_073708799.1	Oligoribonuclease	FLHFR	21	21	55	55	100
	Propionibacterium	WP_055345539.1	ABC transporter ATP-binding protein	IFLHFRGK	22.7	22.7	88	1.2	75
	Propionibacterium	SCQ71317.1	Nod factor export ATP-binding protein I (nodulation ATP-binding protein I)	IFLHFRGK	22.7	22.7	88	1.2	75
	Propionibacterium	SCQ60498.1	ABC daunorubicin resistance transporter, ATP-binding component (precursor)	IFLHFRGK	22.7	22.7	88	1.2	75
Firmicutes	*Ruminococcus*	WP_028510096.1	Hypothetical protein	LHFRVK	23.1	23.1	66	13	100
	Ruminococcus	CDE11995.1	cRISPR-associated protein Csd1 family	VFLRFRV	22.3	22.3	77	26	85.71
	Ruminococcus	WP_118609816.1	Sensor histidine kinase*	KVFLEFSVK	22.3	22.3	100	26	77.78
Proteobacteria	*Rickettsiales*	RPF74257.1	Glucose-1-phosphate thymidylyltransferase*	KVFLHRVK	24.8	24.8	100	1.9	88.89
	Rickettsiales	MAR56391.1	Hypothetical protein CMM93_04335	IFLHFR	21.8	21.8	66	22	83.33
	Rickettsiales	MBJ94827.1	Hypothetical protein CMP23_10205	VFMHFR	21.4	21.4	66	31	83.33
Cyanobacteria	*Cyanobacteria*	WP_068817593.1	RibD family protein [*Phormidesmis priestleyi*]*	VFLHYRVK	26.9	26.9	88	3.0	87.50
	Cyanobacteria	WP_015194555.1	RibD family protein [*Stanieria cyanosphaera*]*	VFLHYRVK	26.9	26.9	88	3.0	87.50
	Cyanobacteria	WP_095722341.1	RibD family protein [*Calothrix elsteri*]	VFLHYRVK	26.9	26.9	88	3.0	87.50

**Best candidate sequences as epitopes triggering the activation of T cells at thefirst episode of NSTEMI.*

back the "infection hypothesis," according to which an infectious event, or even just an altered composition of gut microbiome without clinical signs of infection, could act as a trigger for ACS (33). Given this, our missing piece in the history was to understand whether and how the EAT *milieu* might contribute to the immune alterations leading to coronary plaque instability. The goal of this work was to prove that an immune response to specific antigens might occur in the EAT as one of the steps toward ACS.

T-cell accumulation in non-lymphoid tissues (EAT in our study) is shaped by several mechanisms including migration and retention of circulating T cells as well as expansion of clones specific for tissue-specific antigens. The local chemokine and cytokine milieu and the expression of specific antigens in the tissue promote chemotaxis and clonal expansion of T cells (10, 12). Here, we report for the first time that EAT of NSTEMI patients at their first clinical manifestation showed the enrichment of an exclusive TRBV21* public T-cell receptor, demonstrating a consistent pattern of clonal restriction in EAT T cells. We could also observe that the presence of TRBV21* was co-occurring with an HLA-A*03$^+$ haplotype that in turn was more frequent in our NSTEMI patients when compared with CCS patients and the expected frequency in the general population. These observations reinforced the hypothesis of a specific, antigen-driven, T-cell expansion in EAT along with the first presentation of ACS.

We previously reported in human (14) and experimental (34) autoimmune diseases that the first wave of T cells specific for a given antigen during the immune response is often characterized by the use of public TCRs, leading to a skewed TCR repertoire. At later times, during chronic disease, the early T-cell repertoire can be modified by exhaustion of some of the activated antigen-specific T cells expanded by the first event (34), in tandem with epitope spreading and TCR repertoire enlargement. Thus, the memory repertoire generated following primary immunization and expanded upon secondary encounter(s) with the antigen changes its clonal composition over time, at least in part to address a presumably larger epitope repertoire. This might account for the differences observed in the TCR repertoire composition between NSTEMI patients with and without previous events.

TCRs recognize short peptides presented on the HLA. To date, several strategies have been used to determine the antigen specificities of T cells knowing the TCR sequence and the restricting element (35). In this study, we used *in-silico* molecular modeling to describe the TCRBV/HLA-class I/epitope quaternary complex and predict a putative sequence of the target epitope, starting with an unbiased interrogation of TCR specificity. Finally, this computational modeling allowed us to highlight a similarity between the putative epitope sequence and the sequences found in bacterial phyla associated with ACS and found in the gut microbiota (24). Overall, this scenario is in line with recent demonstrations of cross-reactive CD4$^+$ T cells, primed by epitopes derived from microbes colonizing different mucosal tissues, able to infiltrate target organs, causing or exacerbating both autoimmune (36) and autoinflammatory diseases (37). Moreover, in agreement with our findings, another study has recently described the involvement and the activation of heart-specific Th cells by bacterial peptide mimics derived from the intestinal microbiota, able to enter the myocardium, enhancing the damage caused by infection during lethal inflammatory cardiomyopathy (38).

Thanks to its privileged position of close proximity to the coronary arteries, EAT represents the ideal environment for a specific T-cell clonal expansion in response to antigen exposure. Whether the enriched T cells and the antigens detected in the EAT result from direct microbial colonization or represent the consequence of previous peripheral immune responses needs to be proven in further studies. However, the evidence for an antigen-driven immune response as a molecular and cellular marker of the first coronary event represents the first step toward a personalized approach in cardiovascular medicine for the ideation of epitope-based vaccines in the treatment of ACS. In the future, more

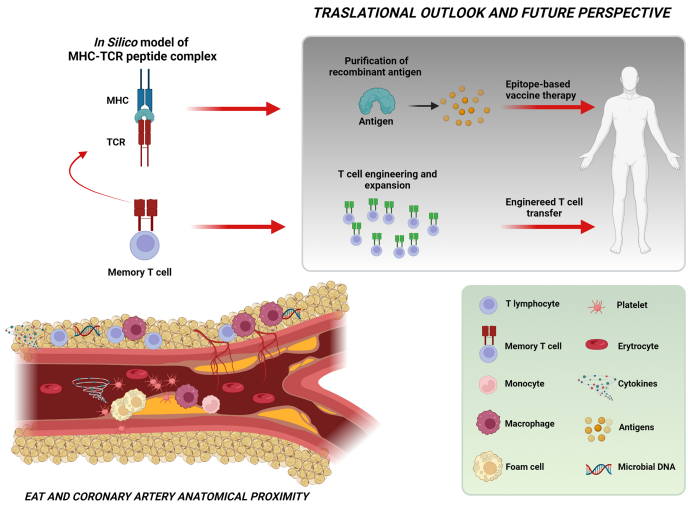

FIGURE 6 | Take-home figure. The figure shows the close relationship between EAT and coronary arteries and the intricate cellular and molecular network possibly implicated in the pathogenesis of ACS. The identification of a specific T-cell clonal expansion in the EAT of NSTEMI patients at their first clinical manifestation and the prediction of the putative sequence of the MHC–TCR–peptide complex (through *in-silico* modeling) indicate the existence in the EAT of an antigen-driven immune response likely involving microbiome-derived antigens as triggers for instability. These observations represent a significant step toward the perspective of engineered T-cell or epitope-based vaccine therapies. Created with BioRender.com.

advanced methods that integrate computational biology and structural modeling might be used to design highly specific and powerful TCRs for use in T-cell therapies (**Figure 6**).

CONCLUSIONS

The identification of a specific T-cell enrichment in the EAT of patients presenting at their first coronary event represents the clue of a specific antigen-driven immune response in the pathogenesis of ACS. Together with the available evidence on the role of dysbiosis in plaque instability, our data pave the way for the fascinating hypothesis of microbiome-derived antigens as triggers for plaque instability. These observations represent a significant step toward the intriguing perspective of engineered T-cell or epitope-based vaccine therapies that begins from a genome-based computational model and terminates with advanced, personalized healthcare (**Figure 6**).

LIMITATIONS AND PERSPECTIVES

Our study is more hypothesis-generating than hypothesis-proving by its nature. Some limitations should be recognized. First, T cells may have encountered bacteria somewhere else, and we cannot exclude that the restricted TCR diversity observed in the EAT surrounding diseased coronary arteries may reflect differential entrapment of antigen primed T cells from the circulating T-cell pool. One possibility is the cross-reactivity of T cells exposed to peptide motifs shared by the human proteome and gastrointestinal microbiota (39) or, as it happens for other autoimmune/autoinflammatory mechanisms, a TCR-independent pathway or a bystander effect (40). Second, in a previous study, we have documented the presence of bacterial DNA of gut microbiota phyla in the EAT of NSTEMI patients (24). However, we did not demonstrate a direct bacterial colonization in EAT, since bacterial DNA in EAT might represent both the clue of direct bacterial colonization and the result of antigen-presenting cell translocation following phagocytosis that occurred elsewhere. In the current study, we did not have the opportunity to directly search bacterial DNA in the EAT samples showing the related TRBV21 sequences because of the scarcity of tissue. Third, we could not directly prove that induction of pro-inflammatory signaling by the related T cells in EAT plays a role in the generation of unstable plaques. However, taking together the present work and our previous data, the demonstration of T-cell enrichment in EAT of NSTEMI patients agrees with the already demonstrated upregulation of NLRP3 inflammasome (24) and with the available evidence of an altered immune response as a trigger for plaque instability. Whether or not microbial colonization of EAT antecedes this immune response, the demonstration of enriched T cells in the EAT of NSTEMI patients at their first manifestation represents sufficient proof of an antigen-driven immune response taking place in the adipose tissue surrounding the coronary artery.

DATA AVAILABILITY STATEMENT

The datasets presented in this study can be found in online repositories. The name of the repository and link to the data can be found below: Figshare; 10.6084/m9.figshare.19932182.

ETHICS STATEMENT

The studies involving human participants were reviewed and approved by the Clinical and Research Ethics Committee of Fondazione Policlinico A. Gemelli-IRCCS and the Catholic University of the Sacred Heart of Rome. The patients/participants provided their written informed consent to participate in this study.

AUTHOR CONTRIBUTIONS

GL, DPe, AS, FR and GDS designed the research. GL provided funding support. FT, AFG, Ad'A, PC, AR, and PB collected the biological materials. AS, VP, GDS, RV, FCa, and EP processed the biological materials and performed the statistical analyses. DC, LC, DPe, GR, NL, FG, PB, MCG, and SF performed the screening and selection of patients MCDR and DPi performed computational modelling. AS, DPe, FR, and GDS investigated and analyzed the data and wrote the original manuscript. DPe, AS, RV, GL, GDS, and FR reviewed and edited the final manuscript. GL, FCr, MM, and FR provided suggestions and performed critical reading of the manuscript. All authors read and approved the submitted version.

FUNDING

The present study was partially supported by the Catholic University of the Sacred Heart Linea D1 2016 Grant and by the Italian National Project Grant PRIN 2017, Protocol 2017WJBKKW_001.

ACKNOWLEDGMENTS

The authors thank the Minister of Health Ricerca Corrente 2021 for the support. The authors thank all their colleagues, technicians, and nurses for their technical and scientific support. The authors strongly believe in translational research involving clinicians, interventional cardiologists, surgeons, and molecular biologists to promote personalized medicine.

SUPPLEMENTARY MATERIAL

The Supplementary Material for this article can be found online at: https://www.frontiersin.org/articles/10.3389/fimmu.2022.;845526/full#supplementary-material

REFERENCES

1. Chaowalit N, Lopez-Jimenez F. Epicardial Adipose Tissue: Friendly Companion or Hazardous Neighbour for Adjacent Coronary Arteries? *Eur Heart J* (2008) 29:695–7. doi: 10.1093/eurheartj/ehm643
2. Maimaituxun G, Shimabukuro M, Fukuda D, Yagi S, Hirata Y, Iwase T, et al. Local Thickness of Epicardial Adipose Tissue Surrounding the Left Anterior Descending Artery Is a Simple Predictor of Coronary Artery Disease - New Prediction Model in Combination With Framingham Risk Score. *Circ J* (2018) 82:1369–78. doi: 10.1253/circj.CJ-17-1289
3. Hassan M, Said K, Rizk H, ElMogy F, Donya M, Houseni M, et al. Segmental Peri-Coronary Epicardial Adipose Tissue Volume and Coronary Plaque Characteristics. *Eur Heart J Cardiovasc Imaging* (2016) 17:1169–77. doi: 10.1093/ehjci/jev298
4. Mazurek T, Zhang L, Zalewski A, Mannion JD, Diehl JT, Arafat H, et al. Human Epicardial Adipose Tissue Is a Source of Inflammatory Mediators. *Circulation* (2003) 108:2460–6. doi: 10.1161/01.CIR.0000099542.57313.C5
5. Karastergiou K, Evans I, Ogston N, Miheisi N, Nair D, Kaski JC, et al. Epicardial Adipokines in Obesity and Coronary Artery Disease Induce Atherogenic Changes in Monocytes and Endothelial Cells. *Arterioscler Thromb Vasc Biol* (2010) 30:1340–6. doi: 10.1161/ATVBAHA.110.204719
6. Hirata Y, Tabata M, Kurobe H, Motoki T, Akaike M, Nishio C, et al. Coronary Atherosclerosis is Associated With Macrophage Polarization in Epicardial Adipose Tissue. *J Am Coll Cardiol* (2011) 58:248–55. doi: 10.1016/j.jacc.2011.01.048
7. Hirata Y, Kurobe H, Akaike M, Chikugo F, Hori T, Bando Y, et al. Enhanced Inflammation in Epicardial Fat in Patients With Coronary Artery Disease. *Int Heart J* (2011) 52:139–42. doi: 10.1536/ihj.52.139
8. Liuzzo G, Goronzy JJ, Yang H, Kopecky SL, Holmes DR, Frye RL, et al. Monoclonal T-Cell Proliferation and Plaque Instability in Acute Coronary Syndromes. *Circulation* (2000) 101(25):2883–8. doi: 10.1161/01.CIR.101.25.2883
9. De Palma R, Del Galdo F, Abbate G, Chiariello M, Calabró R, Forte L, et al. Patients With Acute Coronary Syndrome Show Oligoclonal T-Cell Recruitment Within Unstable Plaque: Evidence for a Local, Intracoronary Immunologic Mechanism. *Circulation* (2006) 113:640–6. doi: 10.1161/CIRCULATIONAHA.105.537712
10. Klingenberg R, Brokopp CE, Grivès A, Courtier A, Jaguszewski M, Pasqual N, et al. Clonal Restriction and Predominance of Regulatory T Cells in Coronary Thrombi of Patients With Acute Coronary Syndromes. *Eur Heart J* (2015) 36:1041–8. doi: 10.1093/eurheartj/eht543
11. Swanson SJ, Rosenzweig A, Seidman JG, Libby P. Diversity of T-Cell Antigen Receptor V Beta Gene Utilization in Advanced Human Atheroma. *Arterioscler Thromb* (1994) 14:1210–4. doi: 10.1161/01.ATV.14.7.1210
12. Glanville J, Huang H, Nau A, Hatton O, Wagar LE, Rubelt F, et al. Identifying Specificity Groups in the T Cell Receptor Repertoire. *Nature* (2017) 547:94–8. doi: 10.1038/nature22976
13. Ria F, Gallard A, Gabaglia CR, Guéry J-C, Sercarz EE, Adorini L. Selection of Similar Naive T Cell Repertoires But Induction of Distinct T Cell Responses by Native and Modified Antigen. *J Immunol* (2004) 172:3447–53. doi: 10.4049/jimmunol.172.6.3447
14. Ria F, Penitente R, De Santis M, Nicolò C, Di Sante G, Orsini M, et al. Collagen-Specific T-Cell Repertoire in Blood and Synovial Fluid Varies With Disease Activity in Early Rheumatoid Arthritis. *Arthritis Res Ther* (2008) 10: R135. doi: 10.1186/ar2553
15. Di Sante G, Tolusso B, Fedele AL, Gremese E, Alivernini S, Nicolò C, et al. Collagen Specific T-Cell Repertoire and HLA-DR Alleles: Biomarkers of Active Refractory Rheumatoid Arthritis. *EBioMedicine* (2015) 2:2037–45. doi: 10.1016/j.ebiom.2015.11.019
16. Gorochov G, Neumann AU, Kereveur A, Parizot C, Li T, Katlama C, et al. Perturbation of CD4+ and CD8+ T-Cell Repertoires During Progression to AIDS and Regulation of the CD4+ Repertoire During Antiviral Therapy. *Nat Med* (1998) 4:215–21. doi: 10.1038/nm0298-215
17. De Rosa MC, Giardina B, Bianchi C, Carelli Alinovi C, Pirolli D, Ferraccioli G, et al. Modeling the Ternary Complex TCR-Vbeta/CollagenII(261-273)/HLA-DR4 Associated With Rheumatoid Arthritis. *PLoS One* (2010) 5:e11550. doi: 10.1371/journal.pone.0011550
18. Ria F, Pirolli D, Di Sante G, Righino B, Gremese E, Gervasoni J, et al. Selective Inhibitors of T Cell Receptor Recognition of Antigen-MHC Complexes for Rheumatoid Arthritis. *ACS Med Chem Lett* (2019) 10:644–9. doi: 10.1021/acsmedchemlett.8b00601
19. Eswar N, Webb B, Marti-Renom MA, Madhusudhan MS, Eramian D, Shen MY, et al. Comparative Protein Structure Modeling Using Modeller. *Curr Protoc Bioinformatics* (2006) 5:5.6. doi: 10.1002/0471250953.bi0506s15
20. Ding YH, Smith KJ, Garboczi DN, Utz U, Biddison WE, Wiley DC. Two Human T Cell Receptors Bind in a Similar Diagonal Mode to the HLA-A2/Tax Peptide Complex Using Different TCR Amino Acids. *Immunity* (1998) 8:403–11. doi: 10.1016/S1074-7613(00)80546-4

21. Camacho C, Coulouris G, Avagyan V, Ma N, Papadopoulos J, Bealer K, et al. BLAST+: Architecture and Applications. *BMC Bioinformatics* (2009) 10:421. doi: 10.1186/1471-2105-10-421
22. Freeman JD, Warren RL, Webb JR, Nelson BH, Holt RA. Profiling the T-Cell Receptor Beta-Chain Repertoire by Massively Parallel Sequencing. *Genome Res* (2009) 19:1817–24. doi: 10.1101/gr.092924.109
23. González-Galarza FF, Takeshita LY, Santos EJ, Kempson F, Maia MH, da Silva AL, et al. Allele Frequency Net 2015 Update: New Features for HLA Epitopes, KIR and Disease and HLA Adverse Drug Reaction Associations. *Nucleic Acids Res* (2015) 43(Database issue):D784–8. doi: 10.1093/nar/gku1166
24. Pedicino D, Severino A, Ucci S, Bugli F, Flego D, Giglio AF, et al. Epicardial Adipose Tissue Microbial Colonization and Inflammasome Activation in Acute Coronary Syndrome. *Int J Cardiol* (2017) 236:95–9. doi: 10.1016/j.ijcard.2017.02.040
25. Baker AR, Silva NF, Quinn DW, Harte AL, Pagano D, Bonser RS, et al. Human Epicardial Adipose Tissue Expresses a Pathogenic Profile of Adipocytokines in Patients With Cardiovascular Disease. *Cardiovasc Diabetol* (2006) 5:1. doi: 10.1186/1475-2840-5-1
26. Oikonomou EK, Marwan M, Desai MY, Mancio J, Alashi A, Hutt Centeno E, et al. Non-Invasive Detection of Coronary Inflammation Using Computed Tomography and Prediction of Residual Cardiovascular Risk (the CRISP CT Study): A Post-Hoc Analysis of Prospective Outcome Data. *Lancet* (2018) 392:929–39. doi: 10.1016/S0140-6736(18)31114-0
27. Bermúdez V, Durán P, Rojas E, Díaz MP, Rivas J, Nava M, et al. The Sick Adipose Tissue: New Insights Into Defective Signaling and Crosstalk With the Myocardium. *Front Endocrinol (Lausanne)* (2021) 12. doi: 10.3389/fendo.2021.735070
28. Mráz M, Cinkajzlová A, Kloučková J, Lacinová Z, Kratochvílová H, Lipš M, et al. Coronary Artery Disease Is Associated With an Increased Amount of T Lymphocytes in Human Epicardial Adipose Tissue. *Mediators Inflamm* (2019) 2019:4075086. doi: 10.1155/2019/4075086
29. Flego D, Severino A, Trotta F, Previtero M, Ucci S, Zara C, et al. Increased PTPN22 Expression and Defective CREB Activation Impair Regulatory T-Cell Differentiation in non-ST-Segment Elevation Acute Coronary Syndromes. *J Am Coll Cardiol* (2015) 65:1175–86. doi: 10.1016/j.jacc.2015.01.027
30. Flego D, Liuzzo G, Weyand CM, Crea F. Adaptive Immunity Dysregulation in Acute Coronary Syndromes: From Cellular and Molecular Basis to Clinical Implications. *J Am Coll Cardiol* (2016) 68:2107–17. doi: 10.1016/j.jacc.2016.08.036
31. Angelini G, Flego D, Vinci R, Pedicino D, Trotta F, Ruggio A, et al. Matrix Metalloproteinase-9 Might Affect Adaptive Immunity in non-ST Segment Elevation Acute Coronary Syndromes by Increasing CD31 Cleavage on CD4+ T-Cells. *Eur Heart J* (2018) 39:1089–97. doi: 10.1093/eurheartj/ehx684
32. Li XS, Obeid S, Klingenberg R, Gencer B, Mach F, Räber L, et al. Gut Microbiota-Dependent Trimethylamine N-Oxide in Acute Coronary Syndromes: A Prognostic Marker for Incident Cardiovascular Events Beyond Traditional Risk Factors. *Eur Heart J* (2017) 38:814–24. doi: 10.1093/eurheartj/ehw582
33. Pedicino D, Giglio AF, Galiffa VA, Cialdella P, Trotta F, Graziani F, et al. Infections, Immunity and Atherosclerosis: Pathogenic Mechanisms and Unsolved Questions. *Int J Cardiol* (2013) 166:572–83. doi: 10.1016/j.ijcard.2012.05.098
34. Penitente R, Nicolò C, Van den Elzen P, Di Sante G, Agrati C, Aloisi F, et al. Administration of PLP139-151 Primes T Cells Distinct From Those Spontaneously Responsive *In Vitro* to This Antigen. *J Immunol* (2008) 180:6611–22. doi: 10.4049/jimmunol.180.10.6611
35. Birnbaum ME, Dong S, Garcia KC. Diversity-Oriented Approaches for Interrogating T-Cell Receptor Repertoire, Ligand Recognition, and Function. *Immunol Rev* (2012) 250:82–101. doi: 10.1111/imr.12006
36. Di Sante G, Gremese E, Tolusso B, Cattani P, Di Mario C, Marchetti S, et al. Haemophilus Parasuis (Glaesserella Parasuis) as a Potential Driver of Molecular Mimicry and Inflammation in Rheumatoid Arthritis. *Front Med (Lausanne)* (2021) 17:8:671018. doi: 10.3389/fmed.2021.671018
37. Greaves SA, Ravindran A, Santos RG, Chen L, Falta MT, Wang Y , et al. CD4+ T Cells in the Lungs of Acute Sarcoidosis Patients Recognize an Aspergillus Nidulans Epitope. *J Exp Med* (2021) 218(10):e20210785. doi: 10.1084/jem.20210785
38. Gil-Cruz C, Perez-Shibayama C, De Martin A, Ronchi F, van derBorght K, Niederer R, et al. Microbiota-Derived Peptide Mimics Drive Lethal Inflammatory Cardiomyopathy. *Science* (2019) 366(6467):881–6. doi: 10.1126/science.aav3487
39. Nanjundappa RH, Ronchi F, Wang J, Clemente-Casares X, Yamanouchi J, Sokke Umeshappa C, et al. A Gut Microbial Mimic That Hijacks Diabetogenic Autoreactivity to Suppress Colitis. *Cell* (2017) 171:655–67. doi: 10.1016/j.cell.2017.09.022
40. Tredicine M, Camponeschi C, Pirolli D, Lucchini M, Valentini M, Geloso MC, et al. A TLR/CD44 Axis Regulates T Cell Trafficking in Experimental and Human Multiple Sclerosis. *iScience* (2022) 25(2):103763. doi: 10.1016/j.isci.2022.103763

Conflict of Interest: The authors declare that the research was conducted in the absence of any commercial or financial relationships that could be construed as a potential conflict of interest.

frontiers | Frontiers in Immunology

TYPE Original Research
PUBLISHED 28 July 2022
DOI 10.3389/fimmu.2022.947267

OPEN ACCESS

EDITED BY
Manuela Mengozzi,
Brighton and Sussex Medical School,
United Kingdom

REVIEWED BY
Laura Coelho,
Oswaldo Cruz Foundation (Fiocruz),
Brazil
Jarle Vaage,
University of Oslo, Norway

*CORRESPONDENCE
Sophie Van Linthout
sophie.van-linthout@bih-charite.de

SPECIALTY SECTION
This article was submitted to Inflammation,
a section of the journal
Frontiers in Immunology

RECEIVED 19 May 2022
ACCEPTED 04 July 2022
PUBLISHED 28 July 2022

CITATION
Matz I, Pappritz K, Springer J and Van Linthout S (2022) Left ventricle- and skeletal muscle-derived fibroblasts exhibit a differential inflammatory and metabolic responsiveness to interleukin-6.
Front. Immunol. 13:947267.
doi: 10.3389/fimmu.2022.947267

Left ventricle- and skeletal muscle-derived fibroblasts exhibit a differential inflammatory and metabolic responsiveness to interleukin-6

Isabell Matz[1,2], Kathleen Pappritz[1,2], Jochen Springer[1,2] and Sophie Van Linthout[1,2]*

[1]Berlin Institute of Health at Charité - Universitätmedizin Berlin,Berlin Institute of Health (BIH) Center for Regenerative Therapies (BCRT), Berlin, Germany, [2]German Center for Cardiovascular Research (DZHK), Partner Site Berlin, Berlin, Germany

Interleukin-6 (IL-6) is an important player in chronic inflammation associated with heart failure and tumor-induced cachexia. Fibroblasts are salient mediators of both inflammation and fibrosis. Whereas the general outcome of IL-6 on the heart's function and muscle wasting has been intensively studied, the influence of IL-6 on fibroblasts of the heart and skeletal muscle (SM) has not been analyzed so far. We illustrate that SM-derived fibroblasts exhibit higher basal mRNA expression of α-SMA, extracellular matrix molecules (collagen1a1/3a1/5a1), and chemokines (CCL2, CCL7, and CX3CL1) as compared to the left ventricle (LV)-derived fibroblasts. IL-6 drives the transdifferentiation of fibroblasts into myofibroblasts as indicated by an increase in α-SMA expression and upregulates NLRP3 inflammasome activity in both LV- and SM-derived fibroblasts. IL-6 increases the release of CCL7 to CX3CL1 in the supernatant of SM-derived fibroblasts associated with the attraction of more pro(Ly6C^{hi}) versus anti(Ly6C^{lo}) inflammatory monocytes as compared to unstimulated fibroblasts. IL-6-stimulated LV-derived fibroblasts attract less Ly6C^{hi} to Ly6C^{lo} monocytes compared to IL-6-stimulated SM-derived fibroblasts. In addition, SM-derived fibroblasts have a higher mitochondrial energy turnover and lower glycolytic activity versus LV-derived fibroblasts under basal and IL-6 conditions. In conclusion, IL-6 modulates the inflammatory and metabolic phenotype of LV- and SM-originated fibroblasts.

KEYWORDS

fibroblasts, left ventricle, skeletal muscle, IL-6, NLRP3 inflammasome

Introduction

Heart failure (HF) and cancer are both main causes of morbidity and mortality worldwide (1). Increasing evidence suggests a multifaceted relationship between both disease entities. The relevance of inflammation as a trigger and valuable therapeutic target in HF and cancer was shown in the CANTOS (Canakinumab Anti-Inflammatory Thrombosis Outcome Study) trial. Beyond the primary observation that rates of cardiovascular events were lower in canakinumab-treated patients with previous myocardial infarction as compared to the placebo group (2), the largest cytokine inhibition trial ever performed illustrated that interleukin (IL)-1β antagonism reduced the incidence of lung cancer and cancer-related mortality (3). Beyond being a common contributor to the pathogenesis of cancer and HF, inflammation associated with cancer can provoke HF (4). In addition, there is further recognition that systemic inflammation associated with HF (5) stimulates tumorigenesis (6). Furthermore, in both disease entities, chronic inflammation can lead to cachexia, a metabolic syndrome that is characterized by high morbidity and mortality due to involuntary weight loss caused by the depletion of fat mass and a prominent loss of muscle tissue (7) leading to a severely impaired muscle function. Less known is the evidence from experimental (8–10) and patient (11) studies illustrating that HF-elevated serum cytokine levels are associated with increased local inflammation in the skeletal muscle (SM).

One of the inflammatory factors secreted from various cancers known to heavily impact cachexia, and which is stimulated, *inter alia*, by IL-1, is IL-6 (12–14). Blocking IL-6 signaling leads to decreased wasting of muscles and prevents cancer cachexia in melanoma and prostate tumor cachectic mouse models (15). Permanent excess of IL-6 during chronic inflammation exerts malignant effects on cardiac function (16), whereas IL-6 spillover in the peripheral circulation increases with the severity of HF, and enhanced IL-6 levels are associated with reduced clinical outcomes (17, 18). IL-6 gene expression is elevated in the heart of tumor-bearing mice, which are characterized by impaired cardiac function and increased fibrosis (19), hinting to the possible involvement of cardiac fibroblasts in tumor-induced cardiac dysfunction in rodents and humans (20, 21).

In addition to their function of extracellular matrix (ECM) regulation, fibroblasts gain more and more recognition for their role as inflammatory supporter cells in the heart (22–26). Fibroblasts present a heterogeneous cell population, located at different sites of the body, and are of mesenchymal origin (27). Recent single-cell analysis of fibroblasts from the heart and SM illustrated fibroblast heterogeneity and an organ-specific fibroblast-mediated ECM profile (28), although how fibroblasts from the left ventricle (LV) versus SM may exhibit an organ-specific response to IL-6 has not been analyzed before.

Although the overall effect of IL-6 on cardiac function (16–19) and SM function/wasting (15) has been deeply investigated, little is known so far about the effect of IL-6 on cardiac and SM fibroblasts. As fibroblasts are one of the main drivers of inflammation (22–26), including the main source of NLRP3 inflammasome activity (29) in the heart, and their role as inflammatory supporter cells is underexplored in the SM, this work aimed to elucidate the impact of IL-6 on both LV- and SM-derived fibroblasts. These investigations provide further insights into how fibroblasts from different organs may respond differently toward a common systemic inflammatory response (here IL-6) and can support local and potentially chronic systemic inflammation.

Methods

Animal material

LV and SM tissues were isolated from 12-week-old healthy male C57BL6/j mice (n = 6; Charles River, Sulzfeld, Germany). All animals were housed under standard housing conditions (12-h light/dark cycle, 50%–70% humidity, 19°C–21°C) with free access to food and water. The experiments were performed in accordance with the European Directive 2010/63/EU and were approved by the local ethical committee (Landesamt für Gesundheit und Soziales, Berlin, T0025/15).

Outgrowth culture of murine left ventricle- and skeletal muscle-derived fibroblasts

In order to isolate and expand fibroblasts from the LV and SM, an outgrowth culture (22) was performed. Therefore, LV and SM tissues were cut into 1-mm-sized pieces and were subsequently fixed in 12-well plates by scratching the pieces in the plastic of the bottom of the plates. During outgrowth, the fibroblasts were cultured in Dulbecco's modified Eagle medium (DMEM; Gibco, Thermo Fisher Scientific Inc., Waltham, MA, USA) containing 20% fetal bovine serum (FBS) (Bio&Sell GmbH, Feucht, Germany) and 1% penicillin and streptomycin (P/S) (Gibco) at 37°C and 5% CO_2. Stimulation experiments were performed between passages 4 and 9.

Immunofluorescence staining of left ventricle- and skeletal muscle-derived fibroblasts

To characterize the outgrowth cells of LV and SM tissues, outgrowth cells in passage 1 were stained with markers of mesenchymal cells, cardiomyocytes, and endothelial cells, as

previously described (30), using murine C4 fibroblasts (Sigma Aldrich, Munich, Germany), HL-1 cells (cardiomyocytes), and brain-derived endothelial cells (bEnd.3 cells) (ATCC, Tell City, IN, USA) as reference cells (Supplementary Figure 1). In detail, each cell type was seeded at a density of 10,000 cells/well in a 48-well format. Upon reaching 80% confluence, the cells were washed once with DPBS (Gibco) and subsequently fixed in 4% paraformaldehyde (PFA) (Sigma Aldrich) for 10 min and stored at 4°C until staining. For this, the cells were first permeabilized with Triton X-100 for 5 min, followed by 30 min incubation with avidin blocking solution (Vector Laboratories, California, USA). Subsequently, the cells were incubated with the primary antibody, all diluted at 1:50, for 1 h at room temperature (RT). The following primary antibodies were used: anti-vimentin (GTX 100619, GeneTex, distributed *via* Biozol, Echingen, Germany), anti-desmin (SC-7559, Santa Cruz, Heidelberg, Germany), and anti-CD31 antibody (BD550274, BD Biosciences, Heidelberg, Germany). After washing two times with DPBS (Gibco), staining with a 1:250 diluted biotinylated secondary antibody (Dianova, Hamburg, Germany) was performed. According to our established protocol, cells were finally incubated with Cy3-conjugated streptavidin diluted at 1:250 (Jackson ImmunoResearch Laboratories Inc., West Grove, PA, USA). For nuclear staining, the cells were incubated with 1:100 diluted diamidinophenylindol (Invitrogen, Darmstadt, Germany). Pictures were acquired using an Axio Observer.Z1 (Carl Zeiss Microscopy GmbH, Oberkochen, Germany) at a magnification of ×200. The microscopic images were taken and processed with the Axio Vision SE64 software (version 4.9.1, Carl Zeiss Microscopy GmbH).

Stimulation experiments of left ventricle- and skeletal muscle-derived fibroblasts

For stimulation experiments, murine fibroblasts were seeded in 6-well plates (50,000 cells/well) for collection of supernatant and flow cytometry, in 48-well plates (20,000 cells/well) for RNA isolation, in 96-well plates (7,500 cells/well) for Crystal Violet and Sirius Red assay, or in Seahorse 96-well Utility plates (Agilent Technologies, Santa Clara, CA, USA) (20,000 cells/well) for analysis of mitochondrial function and glycolysis. The number of biological and technical replicates for each experiment is indicated in the legends of the figures. When the cells reached at least 80% confluency, the medium was replaced, after washing with DPBS (Gibco), by a DMEM containing 5% FBS and 1% P/S (basal medium). The cells were next cultured under basal conditions for 3 h. In the following step, the basal medium was removed, and the cells were incubated with either fresh basal medium (no stimulation) or DMEM including 5% FBS, 1% P/S, and 10 ng/ml of IL-6 (31) (PeproTech, Rocky Hill, NJ, USA) for up to 72 h.

RNA isolation

For RNA isolation, the fibroblasts were harvested after 24-h stimulation with 0 or 10 ng/ml of IL-6, and the TRIzol® (Life Technologies, Carlsbad, CA, USA) method was used. Following the addition of chloroform and subsequent centrifugation, the upper aqueous phase, containing the RNA, was removed and precipitated with isopropanol (Carl Roth GmbH, Karlsruhe, Germany). The RNA was washed in 70% ethanol, and the pellet was next dissolved in 10 µl of RNase-free water (Invitrogen).

cDNA synthesis and real-time PCR

After DNase treatment (DNAse Kit, Peqlab, VWR International, Radnor, PA, USA) and the addition of an RNase Inhibitor (Promega, Fitchburg, WI, USA), 1,000 ng of RNA was transcribed into complementary DNA (cDNA) using the High-Capacity Reverse Transcriptase Kit (Applied Biosystems, Darmstadt, Germany). To assess the mRNA expression of the target genes, real-time PCR was performed using the Quant Studio 6 Flex TaqMan system (Applied Biosystems).The following commercially available gene expression assays (all Applied Biosystems) were used: alpha-smooth muscle actin (α-SMA; Mm00725412_s1), collagen 1a1 (Col1a1; Mm01302043_g1), collagen 3a1 (Col3a1; Mm00802331_m1), collagen 5a1 (Col5a1; Mm00489299_m1), glyceraldehyde 3-phosphate dehydrogenase (GAPDH; Mm99999915_g1), lysyl oxidase 1 (LOX1; Mm00495386_m1), lysyl oxidase-like 2 (LOXL2; Mm00804740_m1), C-C Motif Chemokine Ligand 2 (CCL2; Mm00441242_m1), C-C Motif Chemokine Ligand 7 (CCL7; Mm00443113_m1), C-X3-C Motif Chemokine Ligand 1 (CX3CL1; Mm00436454_m1), and interleukin-6 receptor (IL6R; Mm01211445_m1). For quantification of gene expression, quantitative real-time PCR data were acquired using the QuantStudio software (version 1.2, Thermo Fisher Scientific). For the expression analysis under basal conditions, the target genes were normalized to the GAPDH housekeeping gene and expressed as $2^{-\Delta CT}$. For the stimulation experiments, data were expressed as $2^{-\Delta\Delta CT}$, reflecting normalization of the target genes toward GAPDH and subsequent normalization toward the mean of the basal conditions of each tissue.

Crystal Violet and Sirius Red assay

To assess the total collagen content per well of (un) stimulated LV- and SM-derived fibroblasts, a Sirius Red assay was performed 24 h after stimulation with or without (basal condition) 10 ng/ml of IL-6 as previously described (32, 33). The cells were fixed in 100 µl of methanol (Thermo Fisher Scientific) per well and stored at −20°C overnight. After washing with

DPBS (Gibco), 100 µl 25% Direct Red 80 solution was added per well and incubated for 60 min at RT. The cells were three times washed with 0.1% acetic acid solution (Thermo Fisher Scientific). To elude the staining solution, 100 µl of 0.1 N of natriumhydroxide was added, and the cells were incubated for 1 h at RT while shaking. The absorbance was measured at 540 nm using a spectrophotometer (SpectraMax 340 PC, Molecular Devices, San Jose, CA, USA), and the spectroscopic data were acquired using the SoftMax®7Pro software (Molecular Devices).

In order to be able to normalize the total collagen content to the amount of cells/well, a Crystal Violet assay was performed according to the same cell culture conditions as the Sirius Red assay. The cells were fixed in 100 µl of 4% PFA per well, and the cells were stored at 4°C overnight. Upon washing with bi-distilled water, 50 µl of Crystal Violet solution (Sigma Aldrich) was added per well. After 30 min of incubation at RT, the cells were washed three times with bi-distilled water. Next, 100 µl of a 1% sodium dodecyl sulfate (Sigma Aldrich) solution was added, and the cells were incubated for 1 h at RT while shaking to dissolve the Crystal Violet. The absorbance was measured at 595 nm as written above.

CCL2, CCL7, Cx3CL1, and gp130 ELISA

To determine the amounts of secreted CCL2, CCL7, and Cx3CL1 chemokines (14) from (un)stimulated LV- and SM-derived fibroblasts, 72 h post-stimulation with 0 or 10 ng/ml of IL-6, the murine MCP-1 (CCL2) standard ABTS ELISA Development Kit and murine MCP-3 (CCL7) Standard ABTS ELISA Development Kit (both PeproTech), and the murine Cx3CL1 ELISA kit (Abcam, Cambridge, UK) were used according to the manufacturer's protocol, respectively. For analysis of glycoprotein (gp)130 secretion in the supernatant of (un)stimulated LV- and SM-derived fibroblasts, the mouse gp130 ELISA kit (Abcam) was used as indicated by the manufacturer. To enable normalization of CCL2, CCL7, Cx3CL1, and gp130 to the protein concentration of the supernatant, a bicinchoninic acid (BCA) assay (Pierce™ BCA™ Protein-Assay, Thermo Fisher Scientific) was performed according to the manufacturer's protocol.

CytoSelect™ cell migration assay

To assess the chemotactic potential of fibroblast's secreted factors, a cell migration assay (Cell Biolabs, San Diego, CA, USA) was performed as described by Pappritz et al. (2018) (14). In detail, 10^5 splenocytes isolated from 9–12-week-old healthy male C57BL6/j mice (Charles River, Sulzfeld, Germany) were plated per well in 100 µl of RPMI 1640 medium containing 0.01% FBS and placed into the migration chamber. In the next step, 150 µl of pooled supernatant of (un)stimulated LV- or SM-derived fibroblasts from three mice was added to the feeder tray (n = 7 per condition). After incubation for 24 h at 37°C and 5% CO_2, the migrated cells were harvested, pooled (7 wells per condition), and analyzed *via* flow cytometry staining for CD11b, CD115, and Ly6C (see below).

Flow cytometry

Flow cytometry experiments were conducted in order to assess protein expression of α-SMA and NLRP3 inflammasome components including NLRP3, caspase-1, and IL-1β in fibroblasts. LV- and SM-derived fibroblasts were harvested after 24-h stimulation with 10 ng/ml of IL-6, resuspended in Fixation/Permeabilization solution (BD Cytofix/Cytoperm™, BD Biosciences) followed by incubation for 20 min at 4°C, and washed in BD Perm/Wash™ buffer (BD Biosciences). After an additional centrifuge step was performed and the supernatant was removed, the fibroblasts were resuspended in 100 µl of BD Perm/Wash™ buffer (BD Biosciences) containing the respective antibody conjugate diluted at a ratio of 1:100. The following antibody conjugates were used for flow cytometry: anti-α-SMA Phycoerythrin and anti-NLRP3 AlexaFluor647 (both R&D Systems, Minneapolis, MN, USA), anti-IL-1β Pacific Blue (BioLegend, San Diego, CA, USA), and anti-caspase-1 FITC (Bioss, Woburn, MA, USA). After incubation for 30 min at 18°C to 24°C in the dark, cells were washed with BD Perm/Wash™ buffer (BD Biosciences) and next resuspended in 100 µl of DPBS (Gibco) for subsequent analysis using the MACSQuant Erato (Miltenyi Biotech GmbH, Bergisch Gladbach, Germany) flow cytometer.

Migrated splenocytes were analyzed by staining of CD11b (anti-CD11b Alexa488, diluted 1:100), CD115 (anti-CD115 PerCP/Cy5.5, diluted 1:100), and Ly6C (anti-Ly6C Brilliant Violet 421, diluted 1:50) (all BioLegend). The flow cytometry data were collected using the MACSQuantify software (version 2.6, Miltenyi Biotech). Appropriate gating (Supplementary Figures 2–4) and analysis of flow cytometry data were performed using the FlowJo software (version 8.7, BD Life Sciences, Franklin Lakes, NJ, USA).

Mitochondrial and glycolytic stress test

To analyze the metabolic activity of LV- and SM-derived fibroblasts after 4-h stimulation with 10 ng of IL-6, mitochondrial and glycolytic stress tests using the Seahorse XF Cell Mito Stress test kit and Seahorse XF Glycolysis Stress test kit (both Agilent Technologies) were applied, respectively. The kits were used according to the manufacturer's protocol. In brief, the sensor cartridge was hydrated with 200 µl of Seahorse XF Calibrant (Agilent Technologies) pipetted into each well of the utility plate and incubated overnight at 37°C and 5% CO_2. The

next day, the assay medium for the mitochondrial stress test (pre-warmed at 37°C) was prepared, comprising DMEM XF Base medium (Agilent Technologies), 25 mM of D-(+)-glucose (Sigma Aldrich), 1 mM of sodium pyruvate (Gibco), and 2 mM of L-glutamine (Biochrom GmbH, Berlin, Germany). The assay medium for the glycolytic stress test consisted of 2 mM of L-glutamine (Biochrom GmbH). As assay reagents for the mitochondrial stress test, 2 µM of oligomycin (Sigma Aldrich), 1 µm of FCCP (Sigma Aldrich), 0.5 µM of rotenone (Sigma Aldrich), or 0.5 µM of antimycin (Sigma Aldrich) was added to the assay media. For the glycolytic stress test, 10 mM of D-(+)-glucose (Sigma Aldrich), 2 µM of oligomycin (Sigma Aldrich), and 50 mM of 2-deoxy-glucose (Roth) were used. Next, 25 µl of each media was pipetted into the respective port of the sensor cartridge. The cell culture medium in the utility plate was replaced by the respective assay medium. The plate was incubated under non-CO_2 conditions at 37°C for 10 min. After the initial calibration of the sensor plate, the utility plate was placed on the tray to start the Seahorse run using the XFe96 Extracellular Flux Analyzer (Agilent Technologies). The data for Seahorse experiments were recorded and evaluated by applying Seahorse Wave Desktop Software (version 2.6.1, Agilent Technologies). After the assay was finished, the supernatant was removed from each well, and the plate was frozen at −20°C for subsequent measurement of the protein content using the Micro BCA™ Protein-Assay Kit (Thermo Scientific), which was applied according to the manufacturer's protocol.

Statistical analysis

Data analysis and graphical presentation were performed using the software Prism 8 (version 8.4.3, GraphPad Software, La Jolla, CA, USA). The data were presented as mean ± 95% confidence interval (CI). All the data were tested for normal distribution by using the Shapiro–Wilk test. To assess statistical differences between multiple groups, a one-way ANOVA test or the Kruskal–Wallis test with *post-hoc* Benjamini–Hochberg correction was used. Statistical difference between the two groups was assessed using the Mann–Whitney U test or Welch test. Differences between groups are presented to be statistically different with an (adjusted) p-value smaller than 0.05.

Results

Outgrowth culture from left ventricle and skeletal muscle tissues generates primary fibroblasts

The outgrowth cells from LV and SM tissues were characterized according to their expression of the mesenchymal marker vimentin, and the markers desmin and CD31 were able to discriminate the generated primary cells from cardiomyocytes and endothelial cells, respectively, as described previously (30). LV- and SM-derived cells were positive for vimentin but negative for desmin and the endothelial cell marker CD31. In parallel, C4 fibroblasts, serving as a positive control, showed the same signal pattern as compared to LV- and SM-derived fibroblasts. The cardiomyocyte and endothelial cell lines, which served as negative controls, were positive for their cell-specific markers desmin and CD31, respectively (Supplementary Figure 1).

Skeletal muscle-derived fibroblasts exhibit a higher gene expression of α-SMA, components of the extracellular matrix, and chemokines compared to left ventricle-derived fibroblasts

In view of evaluating potential differences between fibroblasts from the LV and SM, basal mRNA expression of α-SMA, ECM components, and modulators as well as chemokines was analyzed from fibroblasts that originated from the two different tissues. Under basal conditions, fibroblasts from the SM showed 3.9-fold ($p < 0.0001$), 2.0-fold, ($p < 0.0001$), 2.7-fold ($p < 0.0001$), 2.3-fold ($p < 0.0001$), and 3.1-fold ($p < 0.0001$) higher mRNA expression of α-SMA, collagen1a1, collagen3a1, collagen5a1, and LOX1 compared to LV-derived fibroblasts (Figure 1A), respectively. Relative to fibroblasts from the LV, SM-derived fibroblasts revealed higher mRNA expression of the chemokines CCL2 (2.4-fold, $p < 0.0001$), CCL7 (7.6-fold, $p < 0.0001$), and Cx3CL1 (2.2-fold, $p = 0.0132$) (Figure 1B). These results hint at a higher basal activity with regard to ECM modulation as well as monocyte attraction in unstimulated SM- versus LV-derived fibroblasts.

IL-6 stimulation leads to transdifferentiation of left ventricle- and skeletal muscle-derived fibroblasts to myofibroblasts

To assess the effect of IL-6 stimulation in LV- and SM-derived fibroblasts on their transdifferentiation into (myo) fibroblasts, α-SMA gene and protein expression were analyzed (34). In addition, the impact of IL-6 on ECM components and modulators of LV- and SM-derived fibroblasts was determined. IL-6 did not affect α-SMA mRNA expression in LV-derived fibroblasts (Figure 2A). In SM-derived fibroblasts, IL-6 stimulation for 24 h led to the reduction of α-SMA on mRNA level compared to basal conditions (0.7-fold, $p = 0.0007$) (Figure 2B). We observed no changes in mRNA expression of components of the ECM upon IL-6 stimulation, in neither LV- nor SM-derived fibroblasts (Figures 2A, B). At the protein level, 24-h IL-6 stimulation induced an increase of α-SMA-positive

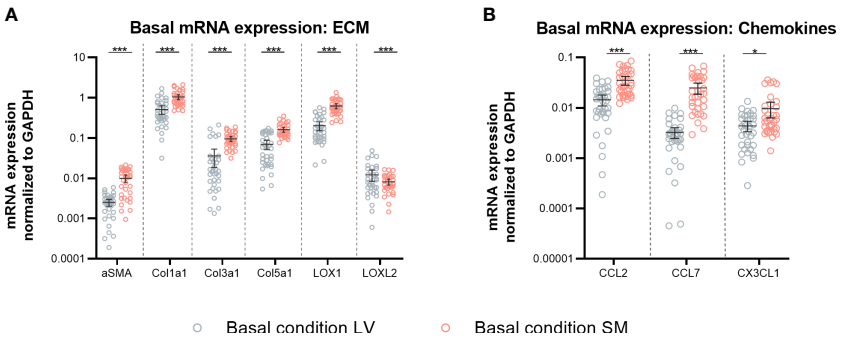

FIGURE 1
Skeletal muscle (SM)-derived fibroblasts show a higher gene expression of α-SMA, components of the extracellular matrix (ECM), and chemokines compared to left ventricle (LV)-derived fibroblasts. mRNA expression of **(A)** α-SMA, ECM components, and modulators (Col1a1, Col3a1, Col5a1, LOX, and LOXL2) and **(B)** chemokines (CCL2, CCL7, Cx3CL1) normalized to GAPDH of LV-derived (black) and SM-derived (red) fibroblasts after 24-h culture with basal medium without IL-6 (basal condition; bright hollow circle). Mean ± 95% CI; n = 36, N = 6; Mann–Whitney/Welch's test with *post-hoc* Benjamini–Hochberg correction; adjusted p-value: *p < 0.05,***p < 0.001.

cells in both LV- and SM-derived fibroblasts (2.4-fold and 2.6-fold, $p < 0.0001$) versus respective unstimulated fibroblasts (Figure 2C). However, a difference in α-SMA$^+$ cells upon IL-6 stimulation between fibroblasts from both tissues was not observed. IL-6 increased the number of SM-derived fibroblasts ($p < 0.0001$), depicted as Crystal Violet-stained cells, whereas no difference in cell count was seen following IL-6 stimulation of LV-derived fibroblasts ($p < 0.0001$) (Figure 2D). IL-6 did not affect collagen deposition, in neither LV- nor SM-derived fibroblasts (Figures 2E, F).

IL-6 stimulation leads to the attraction of different monocyte subsets to left ventricle- versus skeletal muscle-derived fibroblasts

To determine the capacity of IL-6 to stimulate LV- and SM-derived fibroblasts to attract monocytes, the expression of different chemokines in LV- and SM-derived fibroblasts following IL-6 stimulation was analyzed. An impact of IL-6 on CCL2, CCL7, and Cx3CL1 gene expression could not be found in neither LV- nor SM-derived fibroblasts (Figures 3A, B). However, in response to IL-6 stimulation, the secreted CCL7 in the supernatant of cultured LV- and SM-derived fibroblasts was increased (1.3-fold, $p = 0.0183$) and tended to be higher in LV-derived fibroblasts versus basal conditions (1.2-fold; not significant). In parallel, IL-6 stimulation raised Cx3CL1 by 1.1-fold ($p = 0.0306$) in the supernatant of LV-derived fibroblasts, whereas no changes were detected in the supernatant of SM-derived fibroblasts (Figures 3C–E). CCL2 and CCL7 have been identified as chemokines attracting pro-inflammatory monocytes, whereas Cx3CL1 attracts anti-inflammatory monocytes (35, 36) CCL2/Cx3CL1 and CCL7/Cx3CL1 ratios were calculated. Whereas the CCL2/Cx3CL1 ratio did not differ among the LV and SM groups, the CCL7 to Cx3CL1 ratio was 3.0-fold ($p = 0.0196$) increased in stimulated SM-derived fibroblasts compared to the respective LV group (Figures 3F, G), indicating that—upon IL-6 stimulation—fibroblasts from the SM attract a higher proportion of pro-inflammatory monocytes compared to fibroblasts from the LV.

Following the observed differences in chemokine expression profile, we further analyzed the potential to attract different monocyte subsets by performing a migration assay. We found a 1.4-fold ($p = 0.0197$) higher attraction of Ly6C^{hi} cells toward supernatant of unstimulated SM- versus LV-derived fibroblasts. The higher ratio of CCL7/Cx3CL1 in the supernatant of IL-6-stimulated SM-derived versus LV-derived fibroblasts went along with a 2.1-fold ($p < 0.0001$) higher attraction of Ly6C^{hi} monocytes. Furthermore, IL-6 stimulation led to a 1.3-fold ($p = 0.0330$) lower attraction of Ly6C^{lo} monocytes by the supernatant of SM-derived fibroblasts compared to basal conditions. Compared to IL-6-stimulated LV-derived fibroblasts, the supernatant of IL-6-stimulated SM-derived fibroblasts resulted in a 2.0-fold ($p = 0.0009$) reduction in Ly6C^{lo} monocytes. In accordance with this, IL-6-stimulated SM- versus LV-derived fibroblasts IL-6 stimulation led to a 4.3-fold ($p = 0.0003$) increase in attracted Ly6C^{hi} versus Ly6C^{lo} monocytes by the supernatant of fibroblasts from the SM compared to the LV (Figures 4A–C).

IL-6 stimulation induces NLRP3 inflammasome activity in left ventricle- and skeletal muscle-derived fibroblasts

Next, we investigated the potential of LV- and SM-derived fibroblasts to regulate inflammatory processes in the respective

10.3389/fimmu.2022.947267

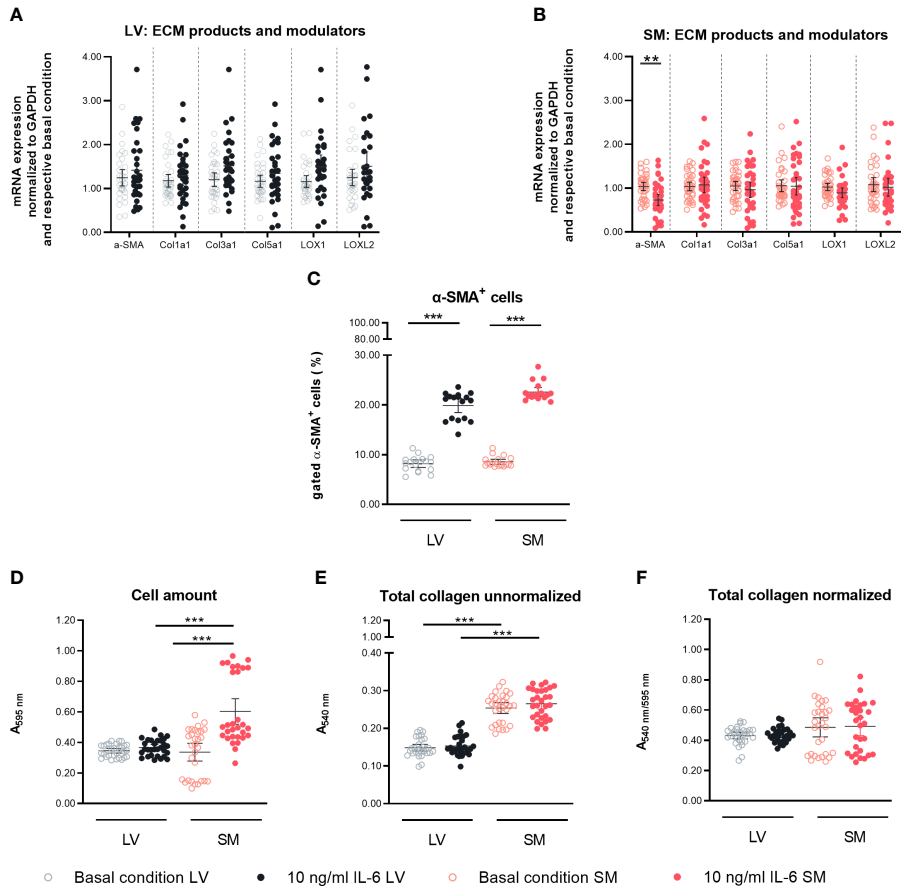

FIGURE 2
IL-6 stimulation leads to differential regulation of α-SMA in left ventricle (LV)- and skeletal muscle (SM)-derived fibroblasts. mRNA expression of α-SMA, ECM components, and modulators (Col1a1, Col3a1, Col5a1, LOX, and LOXL2) normalized to GAPDH and the respective basal condition of **(A)** LV-derived (black) and **(B)** SM-derived (red) fibroblasts after 24-h culture with basal medium without IL-6 (basal condition; bright hollow circle) or with 10 ng/ml of IL-6 (dark filled circle); n = 36, N = 6, Mann–Whitney/Welch's test. **(C)** Percentage of gated α-SMA$^+$ cells (flow cytometry data) of LV-derived (black) and SM-derived (red) fibroblasts after 24-h culture with basal medium without IL-6 (basal condition; bright hollow circle) or with 10 ng/ml of IL-6 (dark filled circle); n = 18, N = 3, Kruskal–Wallis/one-way ANOVA. **(D)** Cell number assessed *via* Crystal Violet assay and absorption at 595 nm from LV-derived (black) and SM-derived (red) fibroblasts after 24-h culture with basal medium without IL-6 (basal condition; bright hollow circle) or with 10 ng/ml of IL-6 (dark filled circle). Total collagen content of LV-derived (black) and SM-derived (red) fibroblasts after 24-h culture with basal medium without IL-6 (basal condition; bright hollow circle) or with 10 ng/ml of IL-6 (dark filled circle) measured *via* Sirius Red assay and absorption at 540 nm **(E)** unnormalized and **(F)** normalized to cell number (Crystal Violet assay data); n = 30, N = 3, Kruskal–Wallis/one-way ANOVA; all data are presented as mean ± 95% CI and tested with *post-hoc* Benjamini–Hochberg correction; adjusted p-values: **p < 0.01, ***p < 0.001.

tissues in response to IL-6 in more depth. Fibroblasts are the main source of cardiac NLRP3 inflammasome activity (29), whereas the inflammatory potential of SM-derived fibroblasts is still underexplored. Thus, the expression of NLRP3 inflammasome components in LV- and SM-derived fibroblasts was evaluated. Protein expression of NLRP3 was 1.6-fold ($p < 0.0001$) and 2.0-fold ($p < 0.0001$) increased as compared to basal conditions in LV- and SM-originated IL-6-stimulated fibroblasts, respectively. Caspase-1 expression was similarly upregulated in stimulated fibroblasts of both tissues (2.1-fold versus 2.5-fold, $p = 0.0003$ versus $p < 0.0001$) in LV- versus SM-derived fibroblasts compared to unstimulated cells. In accordance with the previous results, the expression of the end product of the inflammasome formation, IL-1β, was enhanced in stimulated LV- (3.5-fold, $p < 0.0001$) and SM-derived fibroblasts (4.0-fold, $p < 0.0001$) compared to respective unstimulated controls. No difference in NLRP3 inflammasome activity was observed between LV- and SM-derived fibroblasts, under neither basal conditions nor IL-6 stimulation (Figure 5A). Following this observation, we further analyzed whether there was a difference in the expression of inflammasome components depending on the α-SMA$^+$ versus α-SMA$^-$ fibroblast population. Independent of the expression of α-SMA, the NLRP3 inflammasome activity was increased in LV- and SM-derived fibroblasts upon

10.3389/fimmu.2022.947267

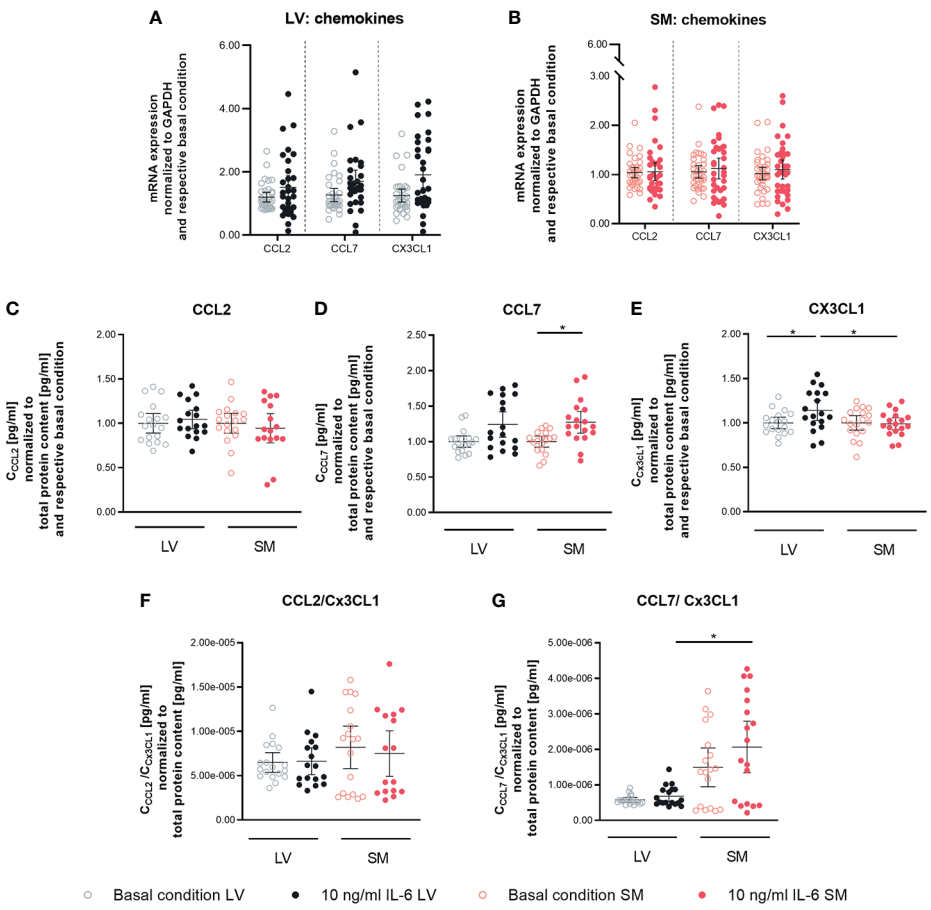

FIGURE 3
IL-6 stimulation leads to secretion of anti- and pro-inflammatory chemokines in left ventricle- and skeletal muscle-derived fibroblasts. mRNA expression of CCL2, CCL7 and CX3CL1 normalized to GAPDH and the respective basal condition of **(A)** LV-(black) and **(B)** SM- (red) derived fibroblasts after 24 h culture with basal medium without IL-6 (basal condition; hollow circle) or with10 ng/ml IL-6 (filled circle); n=36, N=6, Mann-Whitney/Welch's test; Protein expression of **(C)** CCL2, **(D)** CCL7 and (E) CX3CL1 in the supernatant and ratio of **(F)** CCL2 and CX3CL1 and **(G)** CCL7 and CX3CL1 normalized to total protein content measured via bicinchoninic acid assay and respective basal condition of LV (black)- and SM (red)-derived fibroblasts after 72 h culture with basal medium without IL-6 (basal condition; bright hollow circle) or with 10 ng/ml IL-6 (dark filled circle); n=24, N=4, Kruskal-Wallis/One-Way ANOVA; All data are presented as mean ± 95 % CI and tested with post hoc Benjamini-Hochberg correction; adjusted p-values: *p < 0.05.

stimulation with IL-6, and no differences among the fibroblasts of the different tissues were observed (Figures 5B, C).

Left ventricle- and skeletal muscle-derived fibroblasts have a differentially regulated mitochondrial and glycolytic metabolism

Since increased IL-6 is strongly associated with disturbances in metabolism in both the heart and SM (37–40) and since inflammation and cellular metabolism are linked *via* NLRP3 inflammasome activity (41, 42), we next investigated the impact of IL-6 on the fibroblast's mitochondrial function and glycolytic function using a Seahorse assay. Under basal conditions, fibroblasts from the SM showed a higher mitochondrial energy consumption characterized by increased basal respiration (1.6-fold, $p < 0.0001$), ATP production (1.6-fold, $p < 0.0001$), proton leakage (1.4-fold, $p = 0.0498$), maximal respiration (1.8-fold, $p < 0.0001$), and spare respiratory capacity (2.1-fold, $p = 0.0301$) as compared to LV-derived fibroblasts. In response to IL-6, LV- and SM-derived fibroblasts showed a decreased mitochondrial metabolic activity indicated by reduced basal respiration (1.5-fold versus 1.3-fold, both $p = 0.0014$), ATP production (1.3-fold versus 1.2-fold, $p = 0.0206$ versus $p = 0.0024$) compared to basal conditions. Both proton leakage and spare respiratory capacity were not regulated upon cytokine stimulation with IL-6, in neither LV- nor SM-derived fibroblasts (Figure 6A). We next showed that LV-derived fibroblasts have an increased glycolytic metabolism as compared to fibroblasts from the SM. The

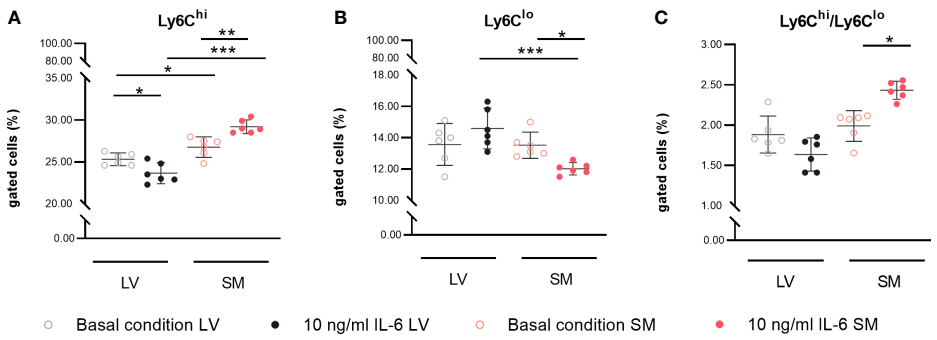

FIGURE 4
IL-6 stimulation leads to attraction of different monocyte subsets to left ventricle (LV)- versus skeletal muscle (SM)-derived fibroblasts. Percentage of gated **(A)** $CD11b^+CD115^+Ly6C^{hi}$ and **(B)** $CD11b^+CD115^+Ly6C^{lo}$ monocytes and **(C)** ratio of $Ly6C^{hi}$ versus $Ly6C^{lo}$ monocytes attracted by the medium of LV-derived (black) and SM-derived (red) fibroblasts after 72-h culture with basal medium without IL-6 (basal condition; bright hollow circle) or with 10 ng/ml of IL-6 (dark filled circle), n = 18, N = 3; Kruskal–Wallis/one-way ANOVA. All data are presented as mean ± 95% CI and tested with *post-hoc* Benjamini–Hochberg correction; adjusted p-values: *p < 0.05, **p < 0.01, ***p < 0.001.

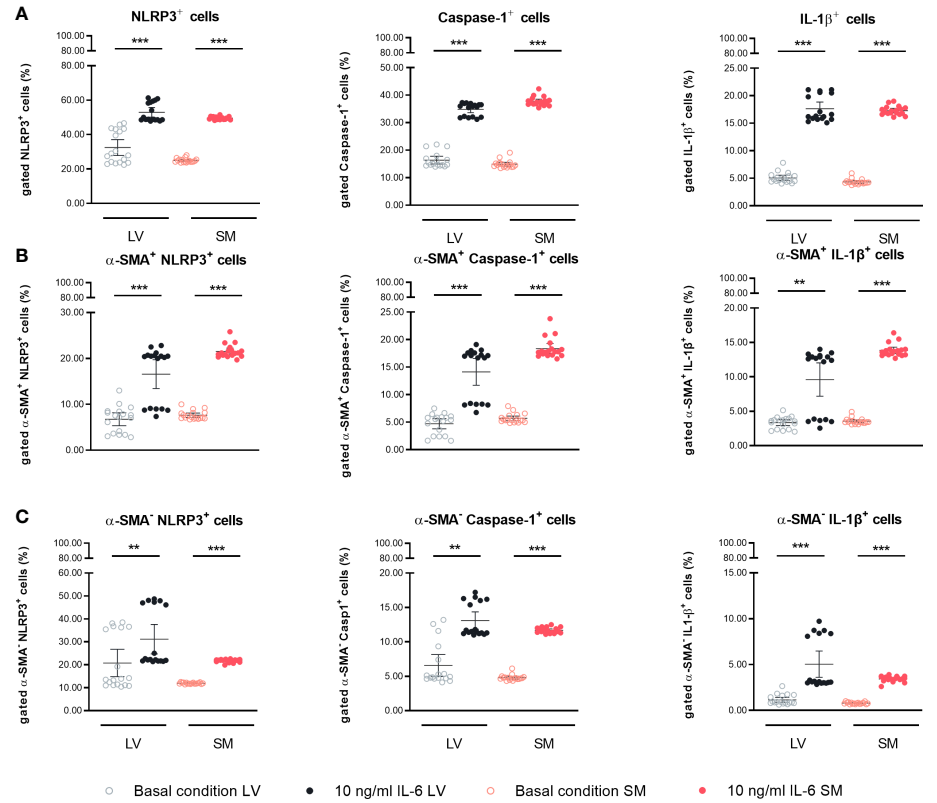

FIGURE 5
IL-6 stimulation leads to upregulation of NLRP3 inflammasome activity in left ventricle (LV)- and skeletal muscle (SM)-derived fibroblasts. Percentage of gated **(A)** $NLRP3^+$, Caspase-1^+, and IL-$1\beta^+$ cells in the global population; **(B)** $NLRP3^+$, Caspase-1^+, and IL-$1\beta^+$ cells in the α-SMA^+ subpopulation; and **(C)** $NLRP3^+$, Caspase-1^+, and IL-$1\beta^+$ cells in the α-SMA^- subpopulation of LV-derived (black) and SM-derived (red) fibroblasts after 24-h culture with basal medium without IL-6 (basal condition; bright hollow circle) or with 10 ng/ml of IL-6 (dark filled circle), n = 18, N = 3. All data are presented as mean ± 95% CI and tested with *post-hoc* Benjamini–Hochberg correction; adjusted p-values: **p < 0.01,***p < 0.001.

glucose-induced overall glycolysis tended to be higher (1.6-fold; not significant), and oligomycin-induced glycolysis (glycolytic capacity) was increased in LV- versus SM-derived fibroblasts (2.1-fold, p = 0.0246). The competence of the LV-derived fibroblasts to adapt to the energy demand (glycolytic reserve; 2-DG-induced glycolysis) was 2.7-fold (p = 0.0087) higher under basal conditions compared to fibroblasts of the SM, further indicating that LV fibroblasts rather rely on glycolytic energy production than SM-derived fibroblasts. IL-6 stimulation did not affect glycolytic function in neither LV- nor SM-derived fibroblasts. Likewise, IL-6 stimulation did not alter other sources of extracellular acidification (non-glycolytic acidification) (Figure 6B). Thus, IL-6 induces a metabolic shift toward reduced mitochondrial energy production rather than altered glycolysis in LV- and SM-derived fibroblasts.

Secretion of gp130 receptor in left ventricle- versus skeletal muscle-derived fibroblasts

To obtain insights into the different biological responses in fibroblasts from the LV and SM upon IL-6 stimulation, we analyzed the expression of the IL-6R and gp130. According to our data, IL-6 stimulation did not affect IL-6R expression on mRNA level. However, secretion of the IL-6 co-receptor gp130 tended to be higher in unstimulated (4.3-fold, not significant) and stimulated LV-derived fibroblasts (3.7-fold, not significant) compared to fibroblasts from the SM (Figure 7), suggesting a different potential in the regulation of IL-6 *trans*-signaling between LV- and SM-derived fibroblasts.

Discussion

In this study, we showed that LV- and SM-derived fibroblasts differ in basal expression of ECM components and chemokines. IL-6 stimulation led to the induction of an α-SMA-expressing phenotype, increased NLRP3 inflammasome activity, and de-regulated mitochondrial metabolism in both tissue fibroblasts, by which LV-derived fibroblasts are characterized with a chemokines profile attracting anti-inflammatory monocytes, whereas SM-derived fibroblasts attract pro-inflammatory monocytes.

Single-cell analysis of fibroblasts from the heart and SM indicates different fibroblast phenotypes and an organ-specific fibroblast-mediated ECM profile (28). Biologically, intra-organ heterogeneity of fibroblasts on a basal level may be related to the diverse microenvironment of the fibroblasts in different tissues, including different surrounding cells, different mechanosensation, and metabolism. Indeed, the LV and quadriceps consist of two different types of muscles (cardiomyocytes versus SM cells) exhibiting a location-dependent physiological environment and cellular demand. In agreement, we show that LV- and SM-derived fibroblasts differ in their basal expression of ECM components and chemokines by which fibroblasts from the SM have a higher expression, except for basal LOXL2 expression, which is reduced compared to fibroblasts from the LV. In addition, while LV-derived fibroblasts seem to be more dependent on glucose metabolism compared to SM-derived fibroblasts, the mitochondrial activity is higher in unstimulated SM- compared to LV-derived fibroblasts.

We next investigated whether LV- and SM-specific fibroblasts differ in their responsiveness to IL-6, analyzing potential distinct biological functions of fibroblasts at different local sites. Stimulation of LV- and SM-originated fibroblasts with IL-6 led to transdifferentiation of fibroblasts from both tissues into an α-SMA-expressing phenotype. In addition to producing and modulating ECM, activated (myo)fibroblasts are well known to strongly influence cardiac inflammation (29, 34). A central function of cardiac fibroblasts is the attraction of immune cells *via* chemokine expression (34). The comparison of chemokine expression from fibroblasts of both tissues did not show any difference in CCL2 expression between LV- and SM-derived fibroblasts supplemented with IL-6. In contrast, CCL7 expression was increased in IL-6-stimulated LV- and SM-derived fibroblasts, whereas CX3CL1 was only upregulated following IL-6 stimulation in LV fibroblasts. CCL7 is a pro-inflammatory regulator of cardiac remodeling and critical for the recruitment of monocyte subsets in the myocardium (43, 44). CX3CL1 functions in a later phase of the myocardial healing process by mediating the attraction of anti-inflammatory monocytes and subsequent support of tissue repair by modulating the aggregation of activated cardiac (myo) fibroblasts (35). Little is known about the impact of fibroblasts in the SM on inflammation and notably about the influence on the induction of tissue-specific immune responses. Here, we show that IL-6 stimulation increased the release of CCL7 to CX3CL1 in the supernatant of SM-originated fibroblasts, hinting to a possible role of SM-derived fibroblasts driving a pro-inflammatory immune response. This is supported by our migration assay data, illustrating the attraction of more pro-inflammatory $Ly6C^{hi}$ than anti-inflammatory $Ly6C^{lo}$ monocytes versus supernatant of IL-6-stimulated SM fibroblasts. In addition, IL-6 increased NLRP3 inflammasome activity in SM fibroblasts. These findings corroborate the contribution of SM fibroblasts in the less recognized presence of muscle inflammation (8, 9) and pro-inflammatory monocyte presence (10, 45) in muscles of patients with HF and circulating cytokines. Instead, fibroblasts from the LV potentially play an ambivalent role in driving inflammation following IL-6 by, on the one hand, supporting anti-inflammatory immune responses attracting $Ly6C^{lo}$ monocytes and, on the other hand, exhibiting high NLRP3 inflammasome activity, thus supporting pro-inflammatory reactions upon IL-6 stimulation. It further accentuates how LV fibroblasts may act differently on the

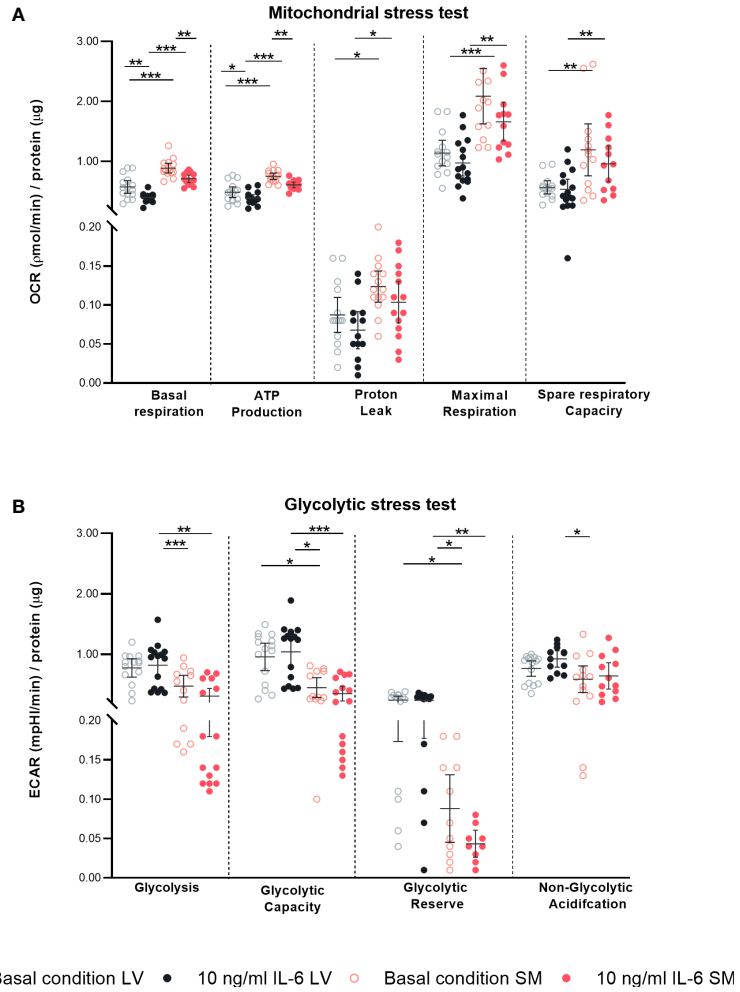

FIGURE 6
IL-6 stimulation leads to differential regulated mitochondrial and glycolytic disturbances in left ventricle (LV)- versus skeletal muscle (SM)-derived fibroblasts. Mitochondrial stress test measuring **(A)** oxygen consumption rate (OCR) describing basal respiration, ATP production, proton leak, maximal respiration, and spare respiratory and glycolytic stress test assessing **(B)** extracellular acidification rate (ECAR) describing glycolysis, glycolytic capacity, glycolytic reserve, and non-glycolytic acidification normalized to protein amount in µg of LV-derived (black) and SM-derived (red) fibroblasts after 4-h culture with basal medium without IL-6 (basal condition; bright hollow circle) or with 10 ng/ml of IL-6 (dark filled circle); n = 15, N = 3. All data are presented as mean ± 95% CI and tested with *post-hoc* Benjamini–Hochberg correction; adjusted p-values: * $p < 0.05$, ** $p < 0.01$, *** $p < 0.001$.

inflammatory response as previously already shown for TGF-β and IFN-γ (22).

Differences in the responsiveness of LV- and SM-derived fibroblasts to stimulation with IL-6 might be explained by variations in the fibroblast's IL-6R expression (46, 47), involving signaling over membrane-bound IL-6R (via *cis* signaling). Following our findings, IL-6R expression did not differ among LV- and SM-derived fibroblasts, although we observed a higher secretion of the natural antagonist of the soluble IL-6R, soluble gp130 receptor (48, 49) by LV- compared to SM-derived fibroblasts. Fibroblasts also respond to *trans* IL-6 signaling (47), involving the binding of a IL-6/IL-6R complex to the ubiquitously expressed gp130 receptor (50). Thus, differences in *trans* IL-6 signaling in LV- and SM-derived fibroblasts might be a reason for the diverse response to IL-6. The higher secretion of the natural antagonist of the soluble IL-6R, soluble gp130 receptor (48, 49), by LV- compared to SM-fibroblasts hints at a function of LV-derived fibroblasts in protecting the heart from detrimental systemic effects of IL-6, which is also supported by the chemokine profile in stimulated cells. IL-6 is known to be the first protective during acute cardiac inflammation, but excessive IL-6 during chronic inflammation leads to malignant effects on cardiac function (16, 51). Here, LV-derived fibroblasts might play an important role in mediating the

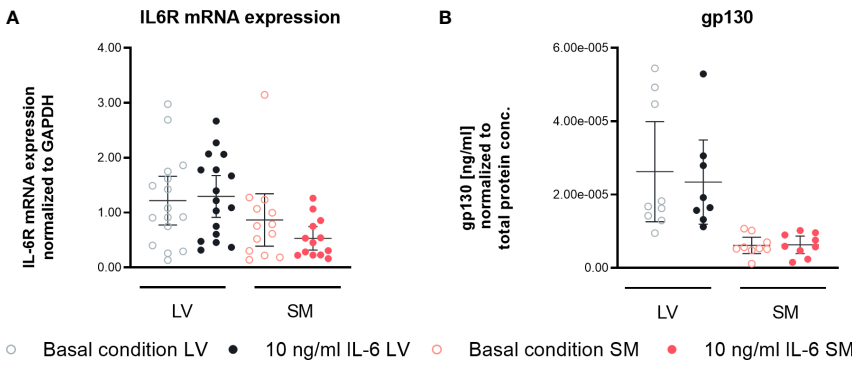

FIGURE 7
IL-6 *trans*-signaling is differently regulated in left ventricle (LV)- versus skeletal muscle (SM)-derived fibroblasts. **(A)** IL6R mRNA expression normalized to GAPDH and respective control of LV-derived (black) and SM-derived (red) fibroblasts after 24-h culture with basal medium without IL-6 (basal condition; bright hollow circle) or with 10 ng/ml of IL-6 (dark filled circle), n = 18, N = 3, Kruskal–Wallis/one-way ANOVA. **(B)** Protein expression of gp130 in the supernatant normalized to total protein content measured *via* bicinchoninic acid assay of LV-derived (black) and SM-derived (red) fibroblasts after 72-h culture with basal medium without IL-6 (basal condition; bright hollow circle) or with 10 ng/ml of IL-6 (dark filled circle). All data are presented as mean ± 95% CI and tested with *post-hoc* Benjamini–Hochberg correction.

balance between cardio-protection and chronic inflammatory response in the heart. IL-6 induces NLRP3 inflammasome activity and IL-1β production in macrophages (52). IL-1β further drives the production of IL-6, creating a positive feedback loop in fibroblasts (53), which might, due to an excess of local IL-6, lead to a shift in the fibroblast's phenotype in the heart in the course of systemic inflammation.

In the SM instead, the effect of IL-6 on the fibroblasts rather implicates direct regulation of the immune reaction to pro-inflammatory responses, further demonstrating the location-dependent biological function of fibroblasts from different organs in the context of inflammation. In the SM, it has been shown that IL-6 induced aberrant mitochondrial metabolism (37). This further draws attention to the role of the NLRP3 inflammasome activity in linking metabolism and inflammation not only in the heart (42) but in the muscle as well. The NLRP3 inflammasome is known to become activated upon metabolic disturbances and boosts pro-inflammatory immune reactions *via* IL-1β, which not only drives myocardial remodeling (42) but also is the hallmark of cachexia, metabolic de-regulation (54, 55). According to the data presented here, IL-6 could be here an important mediator between de-regulated metabolism in cachexia and inflammatory response in fibroblasts from the LV and SM regarding NLRP3 inflammasome activity. Furthermore, on a cellular level, analysis of mitochondrial function revealed that treatment with IL-6 leads to a significant reduction of basal and ATP-linked respiration in fibroblasts from both tissues, indicating either deregulation of ATP use or synthesis of substrates being used for oxidization. In a physiological state, the heart highly depends on the generation of ATP *via* oxidative phosphorylation in the mitochondria (>95%) and only to a less extent *via* glycolysis (56). In the SM, fast switches from glycolytic to mitochondrial metabolism allow to metabolically adapt to short-term and sustained activities (57). Disturbances in mitochondrial energy production have been reported in both SM cells and the cardiomyocytes of cachectic mice (19, 58, 59). As a response to disturbed mitochondrial metabolism in HF, a switch to a higher contribution of glycolysis to overall energy production is observed (60). Therefore, we performed a glycolytic stress test to further understand the shifted metabolic processes in IL-6-stimulated fibroblasts. Here, we showed that IL-6 did not affect glycolysis in LV-derived fibroblasts, whereas glycolysis, glycolytic capacity, and reserve tended to be lower in SM fibroblasts following IL-6 stimulation, suggesting a higher sensitivity to change in glycolysis in SM fibroblasts, although with respect to both tissues, IL-6 mainly regulates mitochondrial metabolism, which can further drive the fibroblast's inflammatory phenotype. This highlights that the NLRP3 inflammasome might be directly regulated either by IL-6 or *via* disturbances in mitochondrial rather than in glycolytic metabolism in fibroblasts from the LV and SM.

IL-6 is a mediator of systemic inflammatory responses not only in cancer and HF but also in other inflammatory and infectious diseases. For instance, a link between cardiovascular diseases and SARS-CoV-2 infection is represented by high IL-6 levels in patients with severe disease progression. IL-6 is here discussed not only to be a biomarker describing the severity and outcome of the disease but also to play a role as a potential therapeutic target against COVID-19 (61).

Based on our findings illustrating that IL-6 induces NLRP3 inflammasome activity and hence the inflammatory potential of fibroblasts in the SM and LV, fibroblasts might be able to serve as positive feedback amplifiers of local and subsequent systemic IL-

1β and IL-6 production, which would lead to severe functional effects in the heart (5). Beneficial effects are shown following NLRP3-, IL-1β-, and IL-6-inhibiting drugs on HF (62, 63), which might therefore be partly explained by the inhibition of the pro-inflammatory potential of LV and SM fibroblasts.

We conclude that SM- and LV-derived fibroblasts differ under basal conditions and following IL-6 supplementation. Their differential responsiveness to IL-6 in terms of attraction of different monocyte subclasses suggests a different contribution of SM and LV fibroblasts to local and (potential) systemic inflammation in cancer, HF, and hereto related cachexia. However, the similar responsiveness of SM and LV fibroblasts related to NLRP3 activation following IL-6 suggests that SM-derived fibroblasts could be potentially used as a tool to mirror the cardiac inflammatory NLRP3 response during cancer progression prior to cardiac damage.

Data availability statement

The original contributions presented in the study are included in the article/supplementary material. Further inquiries can be directed to the corresponding author.

Ethics statement

The animal study was reviewed and approved by Landesamt für Gesundheit und Soziales, Berlin (LAGeSo), Turmstraße 21, Haus A, 10559 Berlin.

Author contributions

IM wrote the manuscript and substantially contributed to the study design, data acquisition, data analysis, and data interpretation. KP substantially contributed to the cell culture of the cardiac and SM fibroblasts and subsequent molecular investigations. JS contributed to the study design and revised the manuscript. SVL conceived the study, provided funding, contributed to the data analysis and data interpretation, and revised the manuscript. All authors revised the manuscript for intellectual content and gave their final approval for publication.

Funding

The project was supported by the DFG, SFB 1470 to SL.

Acknowledgments

We thank Annika Koschel, Kerstin Puhl, and Marzena Sosnowski (in alphabetical order) for excellent technical support. Furthermore, we thank Alba del Rio Serrato (AG Infante-Duarte, Experimental and Clinical Research Centre, Max-Delbrück Centre (MDC) and Charité Universitätmedizin Berlin, Berlin) for kindly providing the bEnd.3 cells.

Conflict of interest

The authors declare that the research was conducted in the absence of any commercial or financial relationships that could be construed as a potential conflict of interest.

Publisher's note

Supplementary material

The Supplementary Material for this article can be found online at: https://www.frontiersin.org/articles/10.3389/fimmu.2022.947267/full#supplementary-material

References

1. Evaluation, I.f.H.M.a.. *Findings from the global burden of disease study 2017*. Seattle, WA: Institute for Health Metrics and Evaluation (IHME) (2018).

2. Ridker PM, Everett BM, Thuren T, MacFadyen JG, Chang WH, Ballantyne C, et al. Antiinflammatory therapy with canakinumab for atherosclerotic disease. *N Engl J Med* (2017) 377(12):1119–31. doi: 10.1056/NEJMoa1707914

3. Ridker PM, MacFadyen JG, Thuren T, Everett BM, Libby P, Glynn RJ, et al. Effect of interleukin-1β inhibition with canakinumab on incident lung cancer in patients with atherosclerosis: exploratory results from a randomised, double-blind, placebo-controlled trial. *Lancet* (2017) 390(10105):1833–42. doi: 10.1016/S0140-6736(17)32247-X

4. Finke D, Heckmann MB, Frey N, Lehmann LH., et al. Cancer–a major cardiac comorbidity with implications on cardiovascular metabolism. *Front Physiol* (2021) 12. doi: 10.3389/fphys.2021.729713

5. Van Linthout S, Tschöpe C. Inflammation – cause or consequence of heart failure or both? *Curr Heart Failure Rep* (2017) 14(4):251–65. doi: 10.1007/s11897-017-0337-9

6. Al-u'datt DA, Allen BG, Nattel S. Role of the lysyl oxidase enzyme family in cardiac function and disease. *Cardiovasc Res* (2019) 115(13):1820–37. doi: 10.1093/cvr/cvz176

7. McGovern J, Dolan RD, Skipworth RJ, Laird BJ, McMillan DC., et al. Cancer cachexia: a nutritional or a systemic inflammatory syndrome? *Br J Cancer* (2022), 1–4. doi: 10.1038/s41416-022-01826-2

8. Batista MLJr., Rosa JC, Lopes RD, Lira FS, Martins E, Yamashita AS, et al. Exercise training changes IL-10/TNF-alpha ratio in the skeletal muscle of post-MI rats. *Cytokine* (2010) 49(1):102–8. doi: 10.1016/j.cyto.2009.10.007

9. Rossato DD, Dal Lago P, Hentschke VS, Rucatti AL, Signori LU, Silveira MN, et al. Ultrasound modulates skeletal muscle cytokine levels in rats with heart failure. *Ultrasound Med Biol* (2015) 41(3):797–805. doi: 10.1016/j.ultrasmedbio.2014.11.017

10. Song T, Manoharan P, Millay DP, Koch SE, Rubinstein J, Heiny JA, et al. Dilated cardiomyopathy-mediated heart failure induces a unique skeletal muscle myopathy with inflammation. *Skeletal Muscle* (2019) 9(1):4. doi: 10.1186/s13395-019-0189-y

11. Gielen S, Adams V, Möbius-Winkler S, Linke A, Erbs S, Yu J, et al. Anti-inflammatory effects of exercise training in the skeletal muscle of patients with chronic heart failure. *J Am Coll Cardiol* (2003) 42(5):861–8. doi: 10.1016/S0735-1097(03)00848-9

12. Ausoni S, Azzarello G. Development of cancer in patients with heart failure: How systemic inflammation can lay the groundwork. *Front Cardiovasc Med* (2020) 7. doi: 10.3389/fcvm.2020.598384

13. Nilsson MB, Langley RR, Fidler IJ. Interleukin-6, secreted by human ovarian carcinoma cells, is a potent proangiogenic cytokine. *Cancer Res* (2005) 65 (23):10794–800. doi: 10.1158/0008-5472.CAN-05-0623

14. Seelaender M, Batista M, Lira F, Silverio R, Rossi-Fanelli F., et al. Inflammation in cancer cachexia: To resolve or not to resolve (is that the question?). *Clin Nutr* (2012) 31(4):562–6. doi: 10.1016/j.clnu.2012.01.011

15. Zaki MH, Nemeth JA, Trikha M. CNTO 328, a monoclonal antibody to IL-6, inhibits human tumor-induced cachexia in nude mice. *Int J Cancer* (2004) 111 (4):592–5. doi: 10.1002/ijc.20270

16. Fontes JA, Rose NR, Čiháková D. The varying faces of IL-6: From cardiac protection to cardiac failure. *Cytokine* (2015) 74(1):62–8. doi: 10.1016/j.cyto.2014.12.024

17. Markousis-Mavrogenis G, Tromp J, Ouwerkerk W, Devalaraja M, Anker SD, Cleland JG, et al. The clinical significance of interleukin-6 in heart failure: results from the BIOSTAT-CHF study. *Eur J Heart Fail* (2019) 21(8):965–73. doi: 10.1002/ejhf.1482

18. Tsutamoto T, Hisanaga T, Wada A, Maeda K, Ohnishi M, Fukai D, et al. Interleukin-6 spillover in the peripheral circulation increases with the severity of heart failure, and the high plasma level of interleukin-6 is an important prognostic predictor in patients with congestive heart failure. *J Am Coll Cardiol* (1998) 31 (2):391–8. doi: 10.1016/S0735-1097(97)00494-4

19. Tian M, Nishijima Y, Asp ML, Stout MB, Reiser PJ, Belury MA., et al. Cardiac alterations in cancer-induced cachexia in mice. *Int J Oncol* (2010) 37 (2):347–53. doi: 10.3892/ijo_00000683

20. Springer J, Tschirner A, Haghikia A, Haehling von Lal S H, Grzesiak A, et al. Prevention of liver cancer cachexia-induced cardiac wasting and heart failure. *Eur Heart J* (2014) 35(14):932–41. doi: 10.1093/eurheartj/eht302

21. Barkhudaryan A, Scherbakov N, Springer J, Doehner W., et al. Cardiac muscle wasting in individuals with cancer cachexia. *ESC Heart Fail* (2017) 4 (4):458–67. doi: 10.1002/ehf2.12184

22. Pappritz K, Savvatis K, Koschel A, Miteva K, Tschöpe C, van Linthout S.. Cardiac (myo)fibroblasts modulate the migration of monocyte subsets. *Sci Rep* (2018) 8(1):5575. doi: 10.1038/s41598-018-23881-7

23. Van Linthout S, Miteva K, Tschöpe C. Crosstalk between fibroblasts and inflammatory cells. *Cardiovasc Res* (2014) 102(2):258–69. doi: 10.1093/cvr/cvu062

24. Lindner D, Zietsch C, Tank J, Sossalla S, Fluschnik N, Hinrichs S, et al. Cardiac fibroblasts support cardiac inflammation in heart failure. *Basic Res Cardiol* (2014) 109(5):428. doi: 10.1007/s00395-014-0428-7

25. Shinde AV, Frangogiannis NG. Fibroblasts in myocardial infarction: A role in inflammation and repair. *J Mol Cell Cardiol* (2014) 70:74–82. doi: 10.1016/j.yjmcc.2013.11.015

26. Steffens S, van Linthout S, Sluijter JP, Tocchetti CG, Thum T, Madonna R., et al. Stimulating pro-reparative immune responses to prevent adverse cardiac remodelling: consensus document from the joint 2019 meeting of the ESC working groups of cellular biology of the heart and myocardial function. *Cardiovasc Res* (2020) 116(11):1850–62. doi: 10.1093/cvr/cvaa137

27. Phan SH. Biology of fibroblasts and myofibroblasts. *Proc Am Thorac Soc* (2008) 5(3):334–7. doi: 10.1513/pats.200708-146DR

28. Muhl L, Genové G, Leptidis S, Liu J, He L, Mocci G, et al. Single-cell analysis uncovers fibroblast heterogeneity and criteria for fibroblast and mural cell identification and discrimination. *Nat Commun* (2020) 11(1):3953. doi: 10.1038/s41467-020-17740-1

29. Sandanger Ø, Ranheim T, Vinge LE, Bliksøen M, Alfsnes K, Finsen AV, et al. The NLRP3 inflammasome is up-regulated in cardiac fibroblasts and mediates myocardial ischaemia-reperfusion injury. *Cardiovasc Res* (2013) 99(1):164–74. doi: 10.1093/cvr/cvt091

30. Lindner D, Zietsch C, Becher PM, Schulze K, Schultheiss H-P, Tschöpe C, et al. Differential expression of matrix metalloproteases in human fibroblasts with different origins. *Biochem Res Int 2012* (2012), 875742. doi: 10.1155/2012/875742

31. Savvatis K, Müller I, Fröhlich M, Pappritz K, Zietsch C, Hamdani N, et al. Interleukin-6 receptor inhibition modulates the immune reaction and restores titin phosphorylation in experimental myocarditis. *Basic Res Cardiol* (2014) 109(6):449. doi: 10.1007/s00395-014-0449-2

32. Spillmann F, Miteva K, Pieske B, Tschöpe C, van Linthout S.. High-density lipoproteins reduce endothelial-to-Mesenchymal transition. *Arteriosclerosis Thrombosis Vasc Biol* (2015) 35(8):1774–7. doi: 10.1161/ATVBAHA.115.305887

33. Van Linthout S, Hamdani N, Miteva K, Koschel A, Müller I, Pinzur L, et al. Placenta-derived adherent stromal cells improve diabetes mellitus-associated left ventricular diastolic performance. *Stem Cells Trans Med* (2017) 6(12):2135–45. doi: 10.1002/sctm.17-0130

34. Baum J, Duffy HS. Fibroblasts and myofibroblasts: what are we talking about? *J Cardiovasc Pharmacol* (2011) 57(4):376–9. doi: 10.1097/FJC.0b013e3182116e39

35. Nahrendorf M, Swirski FK, Aikawa E, Stangenberg L, Wurdinger T, Figueiredo J-L, et al. The healing myocardium sequentially mobilizes two monocyte subsets with divergent and complementary functions. *J Exp Med* (2007) 204(12):3037–47. doi: 10.1084/jem.20070885

36. Cavalera M, Frangogiannis NG. Targeting the chemokines in cardiac repair. *Curr Pharm Design* (2014) 20(12):1971–9. doi: 10.2174/13816128113199990449

37. Abid H, Ryan ZC, Delmotte P, Sieck GC, Lanza IR.. Extramyocellular interleukin-6 influences skeletal muscle mitochondrial physiology through canonical JAK/STAT signaling pathways. *FASEB J* (2020) 34(11):14458–72. doi: 10.1096/fj.202000965RR

38. Al-Khalili L, Bouzakri K, Glund S, Lönnqvist F, Koistinen HA, Krook A.. Signaling specificity of interleukin-6 action on glucose and lipid metabolism in skeletal muscle. *Mol Endocrinol* (2006) 20(12):3364–75. doi: 10.1210/me.2005-0490

39. Zhang Y, Wang J-H, Zhang Y-Y, Wang Y-Z, Wang J, Zhao Y, et al. Deletion of interleukin-6 alleviated interstitial fibrosis in streptozotocin-induced diabetic cardiomyopathy of mice through affecting TGFβ1 and miR-29 pathways. *Sci Rep* (2016) 6(1):23010. doi: 10.1038/srep23010

40. Jiang T, Peng D, Shi W, Guo J, Huo S, Men L, et al. IL-6/STAT3 signaling promotes cardiac dysfunction by upregulating FUNDC1-dependent mitochondria-associated endoplasmic reticulum membranes formation in sepsis mice. *Front Cardiovasc Med* (2022) 8. doi: 10.3389/fcvm.2021.790612

41. Ye Q, Chen S, Wang D. Metabolic regulation of the NLRP3 inflammasome. *Infect Microbes Dis* (2021) 3:183–6. doi: 10.1097/IM9.0000000000000057

42. Sokolova M, Ranheim T, Louwe MC, Halvorsen B, Yndestad A, Aukrust P., et al. NLRP3 inflammasome: A novel player in metabolically induced inflammation–potential influence on the myocardium. *J Cardiovasc Pharmacol* (2019) 74(4):276–84. doi: 10.1097/FJC.0000000000000704

43. Tsou C-L, Peters W, Si Y, Slaymaker S, Aslanian AM, Weisberg SP, et al. Critical roles for CCR2 and MCP-3 in monocyte mobilization from bone marrow and recruitment to inflammatory sites. *J Clin Invest* (2007) 117(4):902–9. doi: 10.1172/JCI29919

44. Westermann D, Savvatis K, Lindner D, Zietsch C, Becher PM, Hammer E, et al. Reduced degradation of the chemokine MCP-3 by matrix metalloproteinase-2 exacerbates myocardial inflammation in experimental viral cardiomyopathy. *Circulation* (2011) 124(19):2082–93. doi: 10.1161/CIRCULATIONAHA.111.035964

45. Lavine KJ, Sierra OL. Skeletal muscle inflammation and atrophy in heart failure. *Heart Failure Rev* (2017) 22(2):179–89. doi: 10.1007/s10741-016-9593-0

46. Gallucci RM, Lee EG, Tomasek JJ. IL-6 modulates alpha-smooth muscle actin expression in dermal fibroblasts from IL-6-Deficient mice. *J Invest Dermatol* (2006) 126(3):561–8. doi: 10.1038/sj.jid.5700109

47. Irwin CR, Myrillas TT, Traynor P, Leadbetter N, Cawston TE, et al. The role of soluble interleukin (IL)-6 receptor in mediating the effects of IL-6 on matrix metalloproteinase-1 and tissue inhibitor of metalloproteinase-1 expression by gingival fibroblasts. *J Periodontol* (2002) 73(7):741–7. doi: 10.1902/jop.2002.73.7.741

48. Rose-John S. Interleukin-6 biology is coordinated by membrane bound and soluble receptors. *Acta Biochim Polonica* (2003) 50(3):603–11. doi: 10.18388/abp.2003_3654

49. Jostock T, Müllberg J, Ozbek S, Atreya R, Blinn G, Voltz N, et al. Soluble gp130 is the natural inhibitor of soluble interleukin-6 receptor transsignaling

responses. *Eur J Biochem* (2001) 268(1):160–7. doi: 10.1046/j.1432-1327.2001.01867.x

50. Heinrich PC, Behrmann I, Müller-Newen G, Schaper F, Graeve L, et al. Interleukin-6-type cytokine signalling through the gp130/Jak/STAT pathway. *Biochem J* (1998) 334(Pt 2):297–314. doi: 10.1042/bj3340297

51. Fisher DT, Appenheimer MM, Evans SS. The two faces of IL-6 in the tumor microenvironment. *Semin Immunol* (2014) 26(1):38–47. doi: 10.1016/j.smim.2014.01.008

52. Wang H, Wang Z, Wang L, Sun L, Liu W, Li Q, et al. IL-6 promotes collagen-induced arthritis by activating the NLRP3 inflammasome through the cathepsin B/S100A9-mediated pathway. *Int Immunopharmacol* (2020) 88:106985. doi: 10.1016/j.intimp.2020.106985

53. Chen B, Tsui S, Smith TJ. IL-1β induces IL-6 expression in human orbital fibroblasts: Identification of an anatomic-site specific phenotypic attribute relevant to thyroid-associated ophthalmopathy. *J Immunol* (2005) 175(2):1310. doi: 10.4049/jimmunol.175.2.1310

54. Evans WJ, Morley JE, Argilés J, Bales C, Baracos V, Guttridge D, et al. Cachexia: A new definition. *Clin Nutr* (2008) 27(6):793–9. doi: 10.1016/j.clnu.2008.06.013

55. Manole E, Ceafalan LC, Popescu BO, Dumitru C, Bastian AE, et al. Myokines as possible therapeutic targets in cancer cachexia. *J Immunol Res* (2018) 2018:8260742. doi: 10.1155/2018/8260742

56. Stanley WC, Recchia FA, Lopaschuk GD. Myocardial substrate metabolism in the normal and failing heart. *Physiol Rev* (2005) 85(3):1093–129. doi: 10.1152/physrev.00006.2004

57. Chen C-n. Chapter 28 - Late-onset caloric restriction alters skeletal muscle metabolism. In: RR Watson, editor. *Mechanisms from animal and human studies, in nutrition and functional foods for healthy aging*. Cambridge:Academic Press (2017). p. 337–44.

58. Penna F, Ballarò R, Beltrá M, Lucia de Costelli S P., et al. Modulating metabolism to improve cancer-induced muscle wasting. *Oxid Med Cell Longevity* (2018) 2018:7153610–7153610. doi: 10.1155/2018/7153610

59. Miyagawa Y, Nukaga S, Mori T, Fujiwara-Tani R, Fujii K, Mori S, et al. Evaluation of cancer-derived myocardial impairments using a mouse model. *Oncotarget* (2020) 11(41):3712–22. doi: 10.18632/oncotarget.27759

60. Allard MF, Schönekess BO, Henning SL, English DR, Lopaschuk GD., et al. Contribution of oxidative metabolism and glycolysis to ATP production in hypertrophied hearts. *Am J Physiol-Heart Circulatory Physiol* (1994) 267(2):H742–50. doi: 10.1152/ajpheart.1994.267.2.H742

61. Pesce M, Agostoni P, Bøtker H-E, Brundel B, Davidson SM, Caterina de R, et al. COVID-19-related cardiac complications from clinical evidences to basic mechanisms: opinion paper of the ESC working group on cellular biology of the heart. *Cardiovasc Res* (2021) 117(10):2148–60. doi: 10.1093/cvr/cvab201

62. Deftereos SG, Beerkens FJ, Shah B, Giannopoulos G, Vrachatis DA, Giotaki SG, et al. Colchicine in cardiovascular disease: In-depth review. *Circulation* (2022) 145(1):61–78. doi: 110.1161/CIRCULATIONAHA.121.056171

63. Ridker PM, Rane M. Interleukin-6 signaling and anti-Interleukin-6 therapeutics in cardiovascular disease. *Circ Res* (2021) 128(11):1728–46. doi: 10.1161/CIRCRESAHA.121.319077

frontiers | Frontiers in Immunology

TYPE Original Research
PUBLISHED 01 August 2022
DOI 10.3389/fimmu.2022.884362

OPEN ACCESS

EDITED BY
Szandor Simmons,
Charité,
Universitätsmedizin Berlin,
Germany

REVIEWED BY
Juliana Falivene,
Consejo Nacional de Investigaciones Científicas y Técnicas (CONICET),
Argentina
Guangliang Hong,
First Affiliated Hospital of Wenzhou Medical University, China

*CORRESPONDENCE
Xuemin Song
xueminsong@whu.edu.cn
Xinyi Li
lxy08272021@126.com

†These authors have contributed equally to this work

SPECIALTY SECTION
This article was submitted to Inflammation,
a section of the journal
Frontiers in Immunology

RECEIVED 26 February 2022
ACCEPTED 04 July 2022
PUBLISHED 01 August 2022

CITATION
Zhang J, Zheng Y, Wang Y, Wang J, Sang A, Song X and Li X (2022) YAP1 alleviates sepsis-induced acute lung injury *via* inhibiting ferritinophagy-mediated ferroptosis.
Front. Immunol. 13:884362.
doi: 10.3389/fimmu.2022.884362

YAP1 alleviates sepsis-induced acute lung injury *via* inhibiting ferritinophagy-mediated ferroptosis

Jing Zhang[1†], Yongping Zheng[1†], Yun Wang[1†], Jin Wang[1], Aming Sang[1], Xuemin Song[2*] and Xinyi Li[1*]

[1]Department of Anesthesiology, Zhongnan Hospital of Wuhan University, Wuhan, China, [2]Research Centre of Anesthesiology and Critical Care Medicine, Department of Anesthesiology, Zhongnan Hospital of Wuhan University, Wuhan, China

Ferroptosis is a phospholipid peroxidation-mediated and iron-dependent cell death form, involved in sepsis-induced organ injury and other lung diseases. Yes-associated protein 1 (YAP1), a key regulator of the Hippo signaling pathway, could target multiple ferroptosis regulators. Herein, this study aimed to explore the involvement of ferroptosis in the etiopathogenesis of sepsis-induced acute lung injury (ALI) and demonstrate that YAP1 could disrupt ferritinophagy and moderate sepsis-induced ALI. Cecal ligation and puncture (CLP) models were constructed in wild-type (WT) and pulmonary epithelium-conditional knockout ($YAP1^{f/f}$) mice to induce ALI, while MLE-12 cells with or without YAP1 overexpression were stimulated by lipopolysaccharide (LPS) *in vitro*. *In-vivo* modes showed that YAP1 knockout aggravated CLP-induced ALI and also accelerated pulmonary ferroptosis, as presented by the downregulated expression of GPX4, FTH1, and SLC7A11, along with the upregulated expression of SFXN1 and NCOA4. Transcriptome research identified these key genes and ferroptosis pathways involved in sepsis-induced ALI. *In-vitro* modes consistently verified that YAP1 deficiency boosted the ferrous iron accumulation and mitochondrial dysfunction in response to LPS. Furthermore, the co-IP assay revealed that YAP1 overexpression could prevent the degradation of ferritin to a mass of Fe^{2+} (ferritinophagy) *via* disrupting the NCOA4–FTH1 interaction, which blocked the transport of cytoplasmic Fe^{2+} into the mitochondria *via* the mitochondrial membrane protein (SFXN1), further reducing the generation of mitochondrial ROS. Therefore, these findings revealed that YAP1 could inhibit ferroptosis in a

10.3389/fimmu.2022.884362

ferritinophagy-mediated manner, thus alleviating sepsis-induced ALI, which may provide a new approach to the therapeutic orientation for sepsis-induced ALI.

KEYWORDS

sepsis-induced acute lung injury, YAP1, NCOA4, ferritinophagy, ferroptosis

Introduction

Sepsis is acute multiple organ dysfunctions induced by the complicated response of the host to intruding pathogenic microorganisms (1, 2), results in expensive hospitalization, and is primarily responsible for hospital mortality (3, 4). The acute systemic inflammatory response arising from sepsis contributes to a cascade of pathological and physiological changes that first spreads to the respiratory system. The lung is especially susceptible to sepsis, which is mediated by inflammation and oxidative stress, leading to acute respiratory distress syndrome or acute lung injury (ARDS/ALI). Sepsis is the dominant cause of ARDS/ALI (6%–42%) (5). ARDS/ALI chiefly manifests as acute inflammation, disruption of endothelial barrier integrity, and injury of the alveolar epithelium, which lead to protein-rich pulmonary interstitial edema and leakage of immune cells into the alveolar cavities (6, 7). Facilitating lung repair and promoting the resolution of lung inflammation are potential therapeutic strategies for ARDS/ALI (7).

Yes-associated protein 1 (YAP1; also regarded as YAP) and transcriptional coactivator TAZ are the essential downstream effectors of the Hippo pathway, which modulates organ development and cell proliferation. The Hippo/YAP1 pathway is a kinase cascade, and YAP1 can be directly phosphorylated and inactivated by the large tumor suppressor 1/2 (LATS1/2), leading to the reservation of YAP1 in the cytoplasm (8). YAP1 could affect the production of autophagosomes and regulate autophagy (9), which are crucial elements of ferritinophagy (10). Previous studies have shown diffuse expression of YAP1/TAZ in multiple tissues, airway and bronchial smooth muscle cells, fibroblasts, and epithelial cells of lung tissue (11–13). YAP1/TAZ expression dysregulation diminished surfactant protein C (SPC) generation, which is a representative element of ARDS (14), and the interaction of TAZ with TTF-1 regulated the activation of SPC in pulmonary epithelial cells (15). Collectively, YAP1/TAZ could bring about lung organogenesis by precisely controlling cell differentiation and proliferation. However, how YAP1 regulates lung epithelial cell proliferation is still indistinct.

As an innovative form of regulated cell death, ferroptosis is described as an iron-dependent phospholipid peroxidation in consequence of reactive oxygen species (ROS) production due to the iron-mediated Fenton reaction (16). Recombinant solute carrier family 7 member 11 (SLC7A11), glutathione (GSH), and glutathione peroxidase 4 (GPX4) are pivotal regulators of the ferroptosis pathway (17). Reductions in GPX4 and GSH levels can be observed during ferroptosis, leading to lipid peroxidation (17, 18). Ferroptosis is mainly regulated by iron homeostasis and oxidative stress, and iron homeostasis is partly controlled by ferritin. Ferritin consists of ferritin light chain (FTL) and ferritin heavy chain 1 (FTH1), the latter being the primary iron-storage protein. Ferritin could be degraded by autophagy (19), which was mediated by nuclear receptor coactivator 4 (NCOA4)—a selective cargo receptor of ferritin. NCOA4-dependent autophagy was defined as ferritinophagy and resulted in increased intracellular iron levels and Fenton reaction (10). One recent research elucidated that the degradation of ferritin was required for ferroptosis cell death of vascular endothelial cells exposed to zinc oxide nanoparticles (20). Bronchial epithelial cell ferroptosis induced by cigarette smoke was closely linked to NCOA4-mediated ferritinophagy (21). Nevertheless, the connection between NCOA4-mediated ferritinophagy and sepsis-induced ALI remains unclear.

Furthermore, the positive effect of YAP1 on pulmonary epithelial cells has already been reported. Research on the intervention of YAP1 in ferroptosis springs up gradually, and the newest study found that YAP depletion could abolish the myocardial protective effect of melatonin by upregulating acyl-CoA synthetase long-chain family member 4 (ACSL4) expression (22). Based on these reports, our study aimed to investigate whether YAP1 was involved in pulmonary epithelial cell ferroptosis in response to LPS stimulation and to explore the underlying mechanism of ferroptosis in sepsis-induced ALI.

Materials and methods

Mice

Male mice (8–12 weeks) were used in this experiment. All mice were on the C57BL/6 background, which were obtained

from Cyagen (Suzhou, China). YAP1$^{flox/flox}$ mice were crossbred with Sftpc-CreERT2 mice to generate epithelial-specific YAP1-conditional knockout mice (termed as YAP1$^{f/f}$). To obtain epithelial-specific YAP1-conditional knockout mice, 6- to 8-week-old mice received tamoxifen (75 mg/kg dissolved in corn oil, once a day) by intraperitoneal injection for 5 days and had a rest for 4 weeks. Then, we successfully obtained the epithelial-specific YAP1-conditional knockout mice. We used only YAP1$^{flox/flox}$ mice as wild-type mice (termed as WT), and they were used as controls. WT mice and YAP1-knockout mice were randomly allotted into the WT+Sham, WT+CLP, YAP1$^{f/f}$ +Sham, and YAP1$^{f/f}$+CLP groups. All experiments were executed following the criteria of the NIH and authorized by the Animal Ethics Committee of Wuhan University (No. 2021187).

Cecal ligation puncture in mice

The sepsis-associated lung injury model mice were created by cecal ligation and puncture (CLP) according to previous studies (23). After using 50 mg/kg of pentobarbital sodium (1%, Sigma, USA) to anesthetize the experimental mice, about a 1-cm midline incision was operated in the mice's lower abdomen. The procedure was made to dissociate and ligate the cecum, which was punctured with a 20-gauge needle twice. After gently squeezing the cecum to push the feces into the abdominal cavity, the cecum was anastomosed and the abdomen was sutured layer by layer. Volumetric resuscitation was performed immediately after surgery with 25 ml/kg of Ringer saline in mice. For the mice in the sham group, the cecum was just turned over when the abdomen was opened, and no treatment was given as mentioned above except closing the abdomen. After the treatment, the mice were administered 1 ml of warming sterile saline for fluid resuscitation immediately. The mice enjoyed free access to food and water and were monitored until sacrificed 24 h after the operation.

Cell models

MLE-12 cells (1×10^5 cells, provided by the ATCCATCC, USA) were cultured with 100 U/ml of streptomycin/penicillin and fetal bovine serum (10%) in DMEM (Gibco, USA) and arranged in an incubator containing 5% CO_2 with a suitable temperature (37°C). Cells were seeded in 24-well plates. To overexpress a certain gene—*YAP1*, the YAP1 overexpression clone lentiviral particle (YAP1 OE) of MLE-12 cells was supplied by GeneChem Co. Ltd. (P40122, Shanghai, China). For the stable overexpression of the *YAP1* gene, the cells were cultured in 24-well plates. Transfection of *YAP1* was accomplished referring to the working instructions, and cells transfected with scramble were used as controls. Both scramble and YAP1 OE were transfected into the MLE-12 cells for 48 h before LPS stimulation. Following expansion and maintenance, stable MLE-12 cells expressing YAP1 overexpression were used for the subsequent experiments. The transfection efficiency was detected by Western blot, and the nuclear translocation of YAP1 was captured by fluorescence microscopy. To generate pulmonary injury models *in vitro*, LPS (1 μg/ml, Sigma, USA) was given to the scramble or YAP1 overexpression cells for 24 h (Figures S1A–D). MLE-12 cells were randomly allotted into the control group (Con+Scramble), LPS group (LPS+Scramble), control+YAP1 overexpression-treated group (Con +YAP1 OE), and LPS+YAP1 overexpression-treated group (LPS +YAP1 OE).

Determination of protein content in bronchoalveolar lavage fluid

Bronchoalveolar lavage fluid (BALF) was obtained from the left lung post-experiment. Abiding with the manufacturer's protocols, after euthanizing the mice, they were fixed, the skin was incised in the middle of the neck, the trachea was isolated, and the right bronchus was ligated. The left bronchus was punctured by a fine needle and fixed with silk thread. Then, 0.5 ml of PBS solution was injected into the bronchus, and the BALF was recovered slowly after 1 min. The above operation was repeated five times. The collected BALF was centrifuged 1,500 rpm at 4°C for 10 min, and the supernatant was recovered and stored at −20°C for protein concentration determination. The content of protein was checked by the commercial bicinchoninic acid protein assay kit (Beyotime, China).

Histological analysis

The lung samples were isolated and fixed with 4% paraformaldehyde for 48 h and then dehydrated by ethanol solution with different concentrations (70%–100%) for 40 min. Following paraffin embedding, the samples were preserved for the subsequent experiments. The sections were sliced into 4 μm sections and placed in xylene, anhydrous ethanol, and alcohol to dewax in sequence. Hematoxylin–eosin (HE) was utilized to stain the lung samples. The slides were dyed with hematoxylin for 5 min and rinsed with water, and then after returning to blue, the slides were stained with eosin for 1–3 min. The degree of lung damage was assessed by two independent technicians who were blinded to the experimental group protocols in line with the recently published criterion (24). The scores were recorded according to the degree of neutrophil infiltration, alveolar and interstitial edema, and hemorrhage in lung tissues. The range of scores was from 0 to 4: 0, normal lung; 1, mild lung injury (less

than 25% injury); 2, moderate lung injury (25%–50% injury); 3, broad lung injury (50%–75% injury); and 4, extreme lung injury (more than 75% injury). The individual scores of each criterion were added and calculated as the final lung injury score. The histological photographs were observed by optical microscopy (Nikon, Japan).

Immunohistochemical staining

Lung tissues were paraffin-fixed and incubated overnight at 37°C. Then, these lung sections were deparaffinized and hatched with 3% hydrogen peroxide for 15 min. The slices were heated at microwave treatment and then naturally cooled for 40 min. After performing antigen retrieval, the samples were blocked with 1% BSA for 0.5 h and incubated with primary rabbit anti-NCOA4 (1:100, DF4255, Affinity Biosciences, Jiangsu, China) and anti-SLC7A11 (1:100, DF12509, Affinity Biosciences, Jiangsu, China), respectively, overnight at 4°C. Lastly, homologous fluorescent or biotin-labeled secondary antibodies were incubated with the lung tissues for 2 h at 37°C. The images were captured using a microscope (Nikon, Japan).

Cell viability assay

Following the previous illustration, cell viability was examined by the CCK-8 assay kit (Beyotime, China) (25). The CCK-8 solution (10 µl) was diluted into the working concentration and given into each well of MLE-12 cells and cultured with cells. After 3 h, the microplate reader (PerkinElmer, USA) was used to analyze the absorbance (450 nm).

Transmission electron microscopy

The fresh lung lobe was removed and placed in a fixed solution quickly. Briefly, about 1-mm^3 piece of lung sections was fixed in 2.5% glutaraldehyde, and then the samples were fixed with 1% osmium tetroxide for 90 min. Next, the samples were stained with 2% uranyl acetate and in turn dehydrated with a cascade of ethanol series. The slices were embedded in acetone (100%, 4°C) all night and cut into ultrathin slices (100 nm). Lastly, these slices were double-dyed with lead citrate and uranyl acetate. The graphs were observed using an HT-7500 transmission electron microscope (Hitachi Co., Japan).

Determination of reactive oxygen species

MLE-12 cells were suspended by 0.25% trypsin and subsequently centrifuged at 1,500 rpm (4°C, 5 min). The cells were cultured in 24-well plates and received the corresponding treatment at the given time according to the indicated groups. The cells were incubated with the 2′,7′-dichlorodihydrofluorescein diacetate (DCFH-DA) fluorescent probe (D6883, Sigma-Aldrich, MO, USA) in a serum-free medium following the manufacturer's protocols. Shortly, the probe incubation solution should be firstly prepared under dark conditions, and the probe was diluted (1:1,000) to 10 µM of the working concentration. Secondly, the cells were washed with PBS and incubated with a 500-µl probe solution of each well for 15 min at 37°C. Finally, discarding the probe solution and washing it three times, the cells were added with a 400-µl medium. The level of ROS in MLE-12 cells was acquired by a TE-2000 fluorescent microscope (Nikon, Japan) at an excitation (Ex) wavelength of 485 nm and an emission (Em) wavelength of 530 nm.

Lipid ROS was detected by the BODIPY 581/591 C11 reagent (D3861, Invitrogen, California, USA). Briefly, after the indicated treatment, the cells were dyed with a 5-µM reagent and incubated for 30 min. Flow cytometry (BD Accuri C6 Plus, BD Biosciences, USA) and FlowJo software were adopted to detect the lipid ROS level. Quantification of ROS and lipid ROS in individual cells was analyzed and calculated by the software Image-Pro Plus 6.0, (Rockville, USA) and the Con+Scramble group was used for the normalization of the data (regarded as fold change 1).

Determination of reactive oxygen species in lung tissue

The ROS level of lung tissue was evaluated with the dihydroethidium (DHE) fluorescent probe (D7008, Sigma-Aldrich, USA). The lung tissues were fixed in 4% paraformaldehyde for 48 h and dehydrated in gradient sucrose. Then, the samples were embedded in optimal cutting temperature compound (OCT gel) and serially sectioned to 8 µm. The already frozen sections were incubated with 50 µM DHE away from light at 37°C for 30 min and 1 mg/ml DAPI for 10 min. To obtain the images, we used a Nikon TE-2000 fluorescent microscope (Tokyo, Japan) at (Ex/Em) 525 nm/610 nm. Quantification of ROS in lung tissue was analyzed and calculated by the software Image-Pro Plus 6.0 targeted to the hole images, and the WT+Sham group was used for the normalization of the data (regarded as fold change 1).

Determination of mitochondria ROS

MLE-12 cells were seeded in 24-well lucifugal plates, then incubated with 5 µM MitoSOX™ reagent solution (Beyotime, China) for 10 min. The cells were washed two times with PBS, and the level of mitochondria ROS was assessed by a fluorescence microscope (TE-2000, Nikon Co., Japan). Quantification of the mitochondrial ROS in individual cells was analyzed and calculated by the software Image-Pro Plus

6.0, and the Con+Scramble group was used for the normalization of the data (regarded as fold change 1).

Detection of related indicators

The levels of ferrous iron (Fe^{2+}), malondialdehyde (MDA), and glutathione (GSH) in MLE-12 cells and lung tissue lysate were detected by the iron assay kit (MAK025, Sigma-Aldrich, USA), MDA assay kit (S0131, Beyotime, China), and GSH assay kit (S0053, Beyotime, China) according to relevant manufacturers' protocols.

Western blot

We extracted the lysate from lung tissues or cells in a RIPA buffer, and protein contents were quantified by the BCA protein assay kit (P0011, Beyotime, China). Protein samples (50 μg) from each group underwent the 10% SDS-PAGE gel electrophoresis and then transferred to a PVDF membrane. After being blocked with non-fat dry milk (5%), these blots were hatched with the primary antibodies all night at 4°C. The proteins used in the study were as follows: GPX4 (DF6701, Affinity Biosciences, Jiangsu, China), ACSL4 (1:1,000, A14439, ABclonal Technology, Wuhan, China), SFXN1 (1:1,000, DF12509, Proteintech Group, Wuhan, China), LC3 (1:1,000, AF5402, Affinity Biosciences, Jiangsu, China), NCOA4 (1:10,000, DF4255, Affinity Biosciences, Jiangsu, China), FTH1 (1:1,000, DF6278, Affinity Biosciences, Jiangsu, China), SLC7A11 (1:1,000, DF12509, Affinity Biosciences, Jiangsu, China), YAP1 (1:1,000, DF3182, Affinity Biosciences, Jiangsu, China), or β-actin (BM0627, Boster Biological Technology, Wuhan, China). Finally, the proteins were incubated with HRP-conjugated secondary antibody (1:5,000, Proteintech) at room temperature for 1 h. An ECL kit (Beyotime) was applied to detect the bands, which were assayed by the ImageJ software.

Distribution of ferrous iron in lysosomes

MLE-12 cells were plated in a 96-well culture dish and hatched overnight. After simulating the four groups of cells indicatively, the 50-nM LysoTracker Green (Beyotime, C1047s, China) and 1-μM FerroOrange (Dojindo, F374, Japan) were added to the cells for 30 min to co-stain the cells and incubated at room temperature for 30 min, and then the previous solution was replaced with fresh PBS. After washing with PBS, the samples were incubated with secondary antibodies including rabbit anti-mouse IgG Ab (A11059, Invitrogen), goat anti-rabbit IgG Ab (A-11012, Invitrogen), or DAPI. The cell photographs were captured by a confocal microscope (TCS-SP2, Leica, Germany) to acquire the mitochondrial ferrous iron and green fluorescent lysosomes at Ex and Em wavelengths of 488 and 510–550 nm, respectively. Quantification of the FerroOrange and colocalization in each hole cell were analyzed and calculated by the software Image-Pro Plus 6.0, and the Con+Scramble group was used for the normalization of the data (regarded as fold change 1).

Ferritin and LAMP2

MLE-12 cells were fixed as pre-described and immunostained by anti-ferritin (Abcam, ab75973, UK) and anti-LAMP2 (Proteintech, 66301-1-Ig, USA). Then, the samples were incubated with secondary antibodies or DAPI. MLE-12 cells were photographed using confocal laser scanning microscopy and fluorescence microscopy (TE-2000, Nikon Co., Tokyo, Japan). Quantification of the ferritin and lysosomes in each hole cell was analyzed and calculated by the software Image-Pro Plus 6.0, and the Con+Scramble group was used for the normalization of the data (regarded as fold change 1).

Colocalization of LC3 and ferritin

Firstly, MLE-12 cells with stable YAP1 overexpression were transfected with LC3-GFP (Beyotime, D2815, China) and cultured in eight-well plates for 24 h. Secondly, the cells in each group were treated with LPS and bafilomycin A1 (BafA1) (Abcam, ab120497, UK) for 24 h. Thirdly, the cells were permeated by 0.03% Triton X-100 (Beyotime, China) for 60 min and then fixed and blocked with 0.1% BSA (Beyotime, China) for 1 h. Finally, the primary anti-ferritin (Abcam, ab75973, UK) and secondary antibodies were applied to the medium in turn. MLE-12 cells were analyzed *via* confocal laser scanning microscopy and evaluated by fluorescence microscopy (Nikon TE-2000, Tokyo, Japan).

For immunofluorescence staining in lung tissues, the samples were fixed in 4% paraformaldehyde for 1 h, washed completely with PBST (1× PBS added with 0.1% Triton X-100) for three times, and permeabilized with 0.1% Triton X-100 for 1 h. Then, the samples were incubated with primary antibodies including anti-LC3 (1:100, AF5402, Affinity Biosciences) and anti-ferritin (1:100, Abcam, ab75973) for 10 h at 4°C. After three times of washing with PBST, the samples were incubated with secondary antibodies, and nuclei were stained with DAPI. After washing again, the samples were imaged with a confocal microscope (Nikon TE-2000).

Co-immunoprecipitation assay

Following the corresponding pretreatment in the indicated groups, the concentration of protein in MLE-12 cells was assessed by the BCA protein (Beyotime, Shanghai, China) assay kit. MLE-12 cells were lysed in mixed buffer (50 mmol/L

Tris–HCl, 150 mmol/L NaCl, 1% NP-40, 1 mmol/L NaF, 1 mmol/L EDTA, 1 mmol/L PMSF, 1 mmol/L Na_3VO_4, and protease inhibitor cocktail). The protein supernatant was hatched with 1–2 μg rabbit polyclonal IgG control antibody and 25 μl resuspended volume of protein A/G plus agarose (Beyotime, P2055) for 1 h. Then, the protein supernatant was incubated with 1 μl anti-NCOA4 (Affinity Biosciences, DF4255, 1:1,000) for 24 h at 4°C. The cells were cultured again lasting 2 h. The immunoprecipitation buffer was washed several times, and 50 μl of SDS-PAGE loading buffer was added and then denatured. Finally, the co-IP assay was performed.

RNA sequence analysis

First, RNA was extracted from CLP or normal lung tissue. Bioanalyzer 2100 system was used to detect RNA purity. Ribo-off rRNA Depletion Kit (N406-02, Vazyme, China) and MGIEasy RNA Library Prep Kit (1000006385, MGI, China) were used to generate sequencing libraries according to the manufacturer's instructions. Then, after purifying the PCR products with the AMPure XP system, the library quality was analyzed (Agilent Bioanalyzer 2100 system). Finally, the index codes were clustered by Cluster Kit of HiSeq 4000 PE (Illumina, USA), and the sequenced library preparations were performed for 150 cycles on the former platform. Total library constructions and sequencing were implemented at BGI Wuhan. Hierarchical clustered heatmap and genome enrichment analysis were adopted to detect the differential expression of both groups. Differentially expressed genes (DEGs) were displayed for log2 fold change >1 and adjusted *p*-value <0.05.

Statistical analysis

All data are presented as the means ± standard deviation and analyzed by SPSS software 23.0. Graphs were drawn by GraphPad Prism 8.0. Discrepancies among the four groups were checked by one-way ANOVA analysis. p <0.05 was defined as statistically significant.

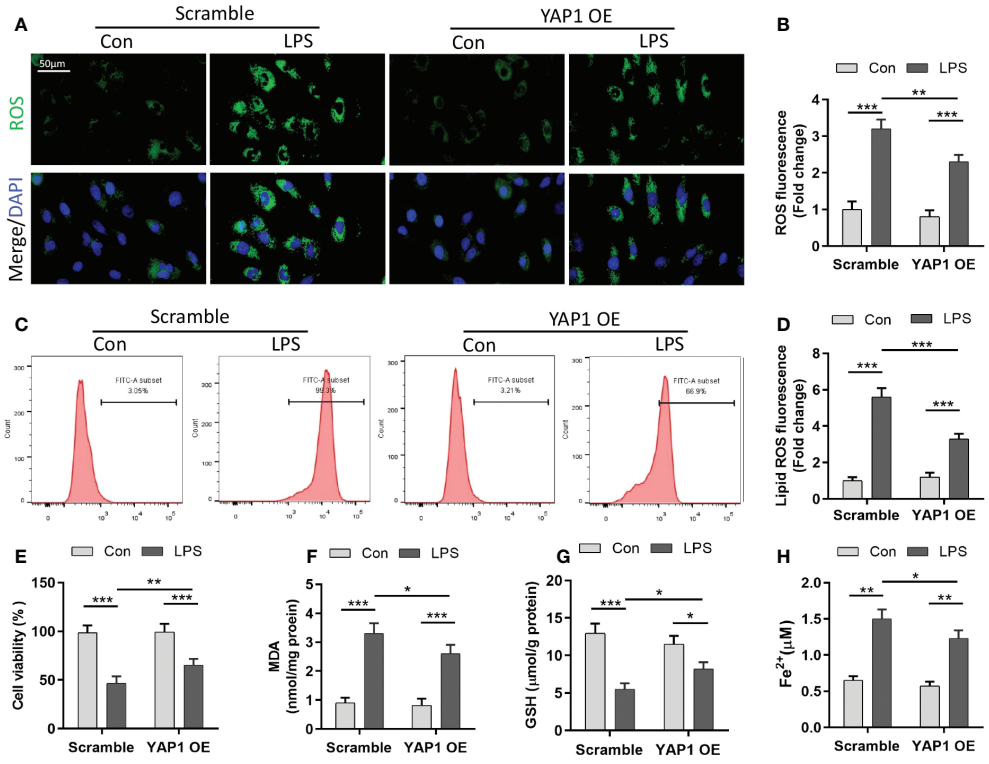

FIGURE 1
Yes-associated protein 1 (YAP1) alleviated reactive oxygen species (ROS) accumulation and lipid peroxidation in LPS-induced MLE-12 cells. **(A)** Representative images of fluorescence probes (DCFH-DA) for intracellular ROS production and **(B)** quantification of ROS fluorescence intensity. **(C)** Lipid ROS generation was analyzed by using BODIPY 581/591 and determined by flow cytometry in MLE-12 cells treated with the contextual stimuli and **(D)** quantification of lipid ROS. **(E)** Cell viability was evaluated by the cell counting kit-8. The contents of MDA **(F)**, GSH **(G)**, and Fe^{2+} **(H)** were determined using the indicated commercial kits. Data are expressed as mean ± SD. n = 3; *p < 0.05, **p < 0.01, ***p < 0.001. LPS, lipopolysaccharide; Con, control group; Scramble, negative control; YAP1 OE, YAP1 overexpression.

Results

YAP1 overexpression prevented ferroptosis in LPS-stimulated MLE-12 cells

We explored that LPS could induce ferroptosis in LPS-treated pulmonary epithelial cells (Figures S2A–D). To delineate the presence of ferroptosis in LPS-induced ALI, MLE-12 cells were transfected with YAP1 overexpressing lentivirus (YAP1 OE). First, we detected the verification of YAP1 overexpression (Figures S3A, B) and nuclear translocation of YAP1 in MLE-12 cells (Figures S3C). Elevated cellular ROS accumulation and lipid peroxidation were not merely the vital origins of ferroptosis but also the hallmarks of ferroptosis. We found that LPS treatment induced remarkable ROS accumulation in MLE-12 cells, which was captured by the enhancement of green fluorescence, while YAP1 overexpression significantly diminished the fluorescence intensity of ROS (Figures 1A, B). In line with ROS tendency, abundant accumulation of lipid ROS was observed in LPS-treated cells; however, YAP1 overexpression partially reversed the lipid ROS accumulation induced by LPS from flow cytometry (Figures 1C, D). Moreover, LPS distinctly gave rise to the mortality of MLE-12 cells; meanwhile, YAP1 overexpression could increase the number of viable cells upon LPS treatment (Figure 1E). The lipid peroxide production (MDA) levels and the content of iron (Fe^{2+}) increased (Figures 1F, H), whereas the levels of GSH declined (Figure 1G) following LPS treatment, both of which are the representative

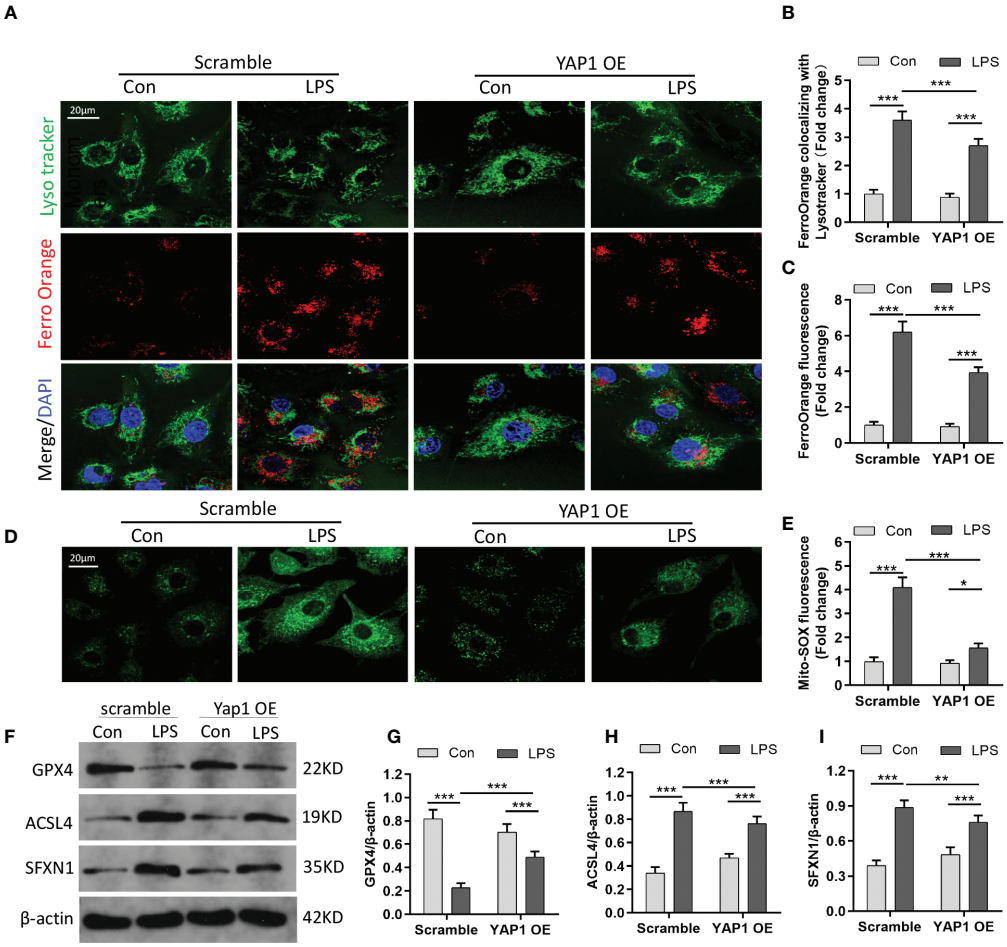

FIGURE 2
YAP1 activation inhibited ferroptosis by decreasing the amount of intracellular free ferrous iron. **(A)** LysoTracker (green) and FerroOrange (red) were shown by confocal imaging in MLE-12 cells stimulated with LPS. The images exhibited the localization of ferrous iron in survival cells. The lysosomes were stained by LysoTracker Green fluorescence. Nuclei were stained with DAPI (blue). **(B)** Quantification of the fluorescence intensity of FerroOrange colocalized with LysoTracker (green). **(C)** Quantification of the FerroOrange fluorescence intensity. **(D)** Representative images of mitochondrial ROS stained with MitoSOX (green). **(E)** Quantitative results of mitochondrial ROS. **(F–I)** The expression levels of GPX4 **(G)**, ACSL4 **(H)**, and SFXN1 **(I)** were shown by WB. Data are expressed as mean ± SD. $n = 3$; $^{*}p < 0.05$, $^{**}p < 0.01$, $^{***}p < 0.001$.

hallmarks of ferroptosis. These aforesaid related markers were converted to beneficial tendency *via* overexpressing YAP1 in MLE-12 cells (Figures 1F–H). Altogether, these outcomes suggested that LPS induced ferroptosis, which could be partially counteracted by YAP1 overexpression in MLE-12 cells.

YAP1 overexpression decreased the amount of intracellular free-divalent iron to inhibit ferroptosis

Divalent metal ion transporter 1 (SLC11A2) mediates the release of Fe^{2+} into a labile iron pool of cytoplasm. Excessive iron would contribute to the Fenton reaction to produce massive ROS and activate iron-containing enzymes to facilitate lipid peroxidation and ferroptosis. We chose the Fe^{2+}-specific probe FerroOrange to explore whether YAP1 could affect the contents of bioavailable Fe^{2+}. The level of Fe^{2+} (FerroOrange) remarkably decreased in YAP1 overexpression cells on the basis of the LPS stimuli (Figures 2A, C). We also observed that colocalization of LysoTracker (green) and FerroOrange (red) was strengthened after LPS stimulation, indicating that large amounts of iron were present in lysosomes. However, the location of free Fe^{2+} in lysosomes was weakened in YAP1 overexpression cells upon LPS stimulation (Figures 2A, B). The number of lysosomes remained the same in each group (Figures S4A), illustrating that the decrease in the amount of lysosomal Fe^{2+} was independent of the number of lysosomes.

SFXN1 (as a mitochondrial amino acid transporter) can facilitate the component of iron utilization traversing the mitochondria (26). In the pathological states, the expression of SFXN1 protein was elevated, combined with the enhancement of iron absorption (27). We explored that mitochondrial ROS sharply increased in LPS-induced cells *via* the MitoSOX green fluorescence probe. However, YAP1 overexpression could significantly reduce the mitochondrial ROS accumulation in LPS-treated cells (Figures 2D, E). GPX4, which acts as one of the redundant defense mechanisms in the mitochondria, was inhibited after LPS stimulation and turned high level when in alliance with YAP1 overexpression (Figures 2F, G). As shown, apart from diminishing the expression level of ACSL4, YAP1 overexpression could inhibit the expression of SFXN1 when cells accepted LPS inducement (Figures 2F, H, I). To some extent, YAP1 inhibited ferroptosis by reducing free iron and ROS located in lysosomes.

YAP1 overexpression blocked the degradation of ferritin in lysosomes (ferritinophagy) and *was* localized in autophagosomes

Ferritin is the primary iron-storage protein in mammals and a crucial element in maintaining iron homeostasis and preventing Fenton reaction. Ferritin can alter sequestered iron *via* the process of autophagy (ferritinophagy). Since YAP1 overexpression decreased the amount of intracellular free-divalent iron (as shown in Figure 2A), we speculated that this process might be linked to ferritinophagy (degradation of ferritin in lysosomes); we thus hypothesized that YAP1 overexpression could interrupt ferritinophagy. To validate the assumption, we carried out immunofluorescence assays to observe the lysosomal location of ferritin. The MLE-12 cells were fixed and immunostained using antibodies of ferritin (red fluorescence) and LAMP2 (green fluorescence). In baseline conditions, the control group with no LPS treatment presented high ferritin fluorescence, indicating a small quantity of degraded ferritin. Surprisingly, upon LPS treatment of the control cells, ferritin fluorescence was substantially decreased due to the degradation of ferritin located in lysosomes. Furthermore, in LPS-stimulated cells, the levels of ferritin were partially restored (YAP1 OE+LPS vs. Scramble+LPS) upon YAP1 overexpression compared to the scramble group (Figures 3A, C). The number of lysosomes was unchanged (Figure 3B). The results suggested that YAP1 inhibited the lysosomal ferritin degradation upon LPS treatment and led to impaired ferritinophagy after LPS-stimulated injury.

It had been reported that NCOA4 can combine with FTH1 and targeted ferritin to lysosome for autophagy degradation to release free iron. Blocking autophagy or knocking out NCOA4 inhibits the labile accumulation of iron and ROS associated with ferroptosis and prevents eventual iron-related cell death (28). To further investigate ferritinophagy, we determined the levels of LC3, NCOA4, and FTH1 by Western blotting. We found that the expression of the autophagic marker (LC3) and NCOA4 was elevated in MLE-12 cells exposed to LPS, while YAP1 overexpression declined the expression levels on the basis of LPS stimulation (Figures 3D–F). Along with the fluorescence images, YAP1 overexpression partially recovered the decreasing levels of FTH1 caused by LPS treatment (Figures 3D, G). Overall, YAP1 could inhibit ferritinophagy in LPS-challenged MLE-12 cells.

YAP1 overexpression inhibited ferritinophagy by disrupting the NCOA4–FTH1 interaction

Ferritinophagy (autophagic degradation of ferritin) can promote ferroptosis and is mediated by the cargo receptor NCOA4. The immunofluorescence analysis showed that LPS treatment decreased ferritin fluorescence and enhanced the expression of LC3-GFP in MLE-12 cells. The colocalization fluorescence of ferritin with LC3-GFP was strengthened by LPS exposure, whereas YAP1 overexpression reduced the numbers of LC3-GFP puncta (green puncta) and colocalization puncta of ferritin with LC3-GFP (yellow puncta)

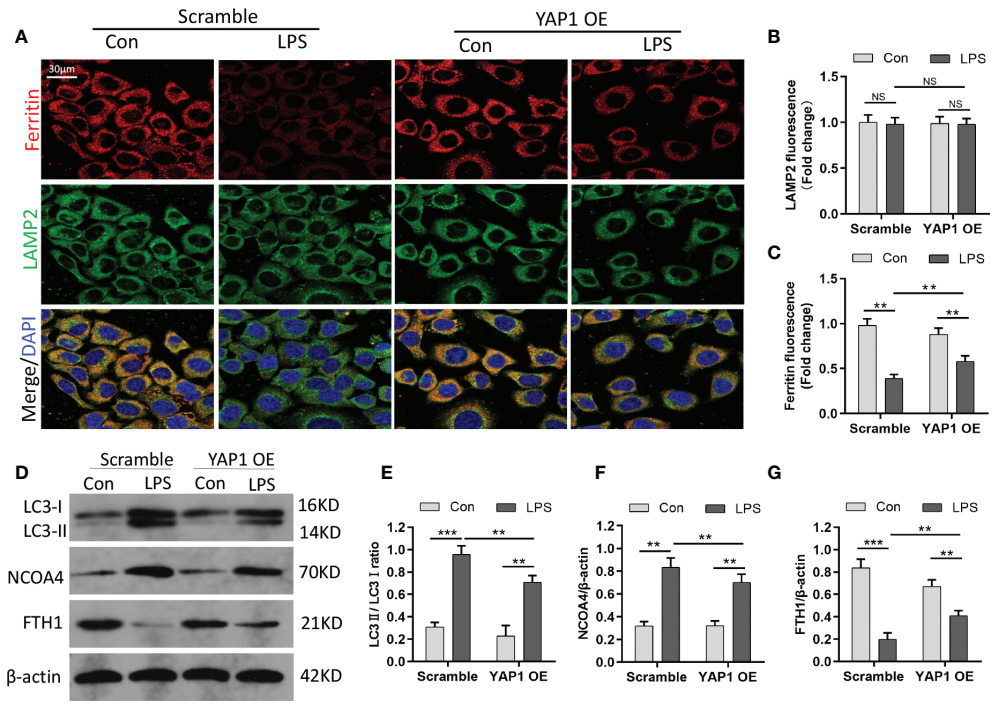

FIGURE 3
YAP1 restrained the degradation of ferritin in lysosomes to suppress ferritinophagy. **(A)** Confocal images of ferritin (red) and LAMP2 (green) were shown in LPS-treated MLE-12 cells, while lysosomes were stained with LAMP2 (green). **(B)** Quantification measurement of lysosome fluorescence intensity. **(C)** Quantification measurement of ferritin fluorescence intensity. **(D–G)** Data showed the expression contents of LC3II/LC3I **(E)**, NCOA4 **(F)**, and FTH1 **(G)**. Data are expressed as mean ± SD. $n = 3$; $^{*}p < 0.05$, $^{**}p < 0.01$, $^{***}p < 0.001$. NS: no significance, P>0.05

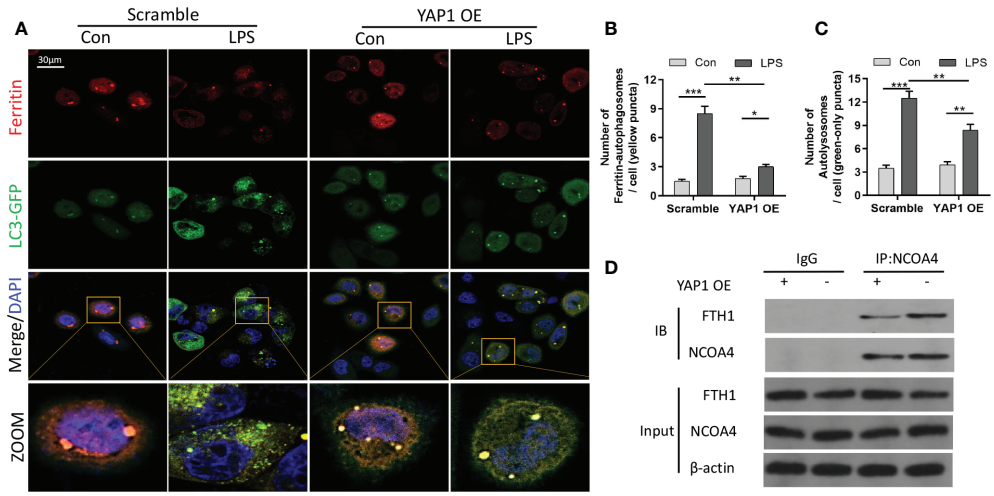

FIGURE 4
YAP1 inhibited ferritinophagy by disrupting the NCOA4–FTH1 interaction. **(A)** Cells in the indicated groups were transfected with the LC3-GFP plasmid, and the autophagosome in cells presented green fluorescence puncta. Representative confocal images of cells exhibited fluorescent colocalization (yellow puncta) of ferritin (red fluorescence) with LC3-GFP (green puncta). Cells were treated with LPS for 24 (h) **(B)** Fluorescence quantification of ferritin colocalizing with autophagosomes (LC3-GFP). The colocalization puncta per cell were calculated. **(C)** Fluorescence quantification of autophagosomes (LC3-GFP). The autophagosome puncta per cell were calculated. **(D)** Immunoprecipitation analysis of NCOA4 and FTH1 interaction in MLE-12 cells. IgG was used for control. Data are expressed as mean ± SD. $n = 3$; $^{*}p < 0.05$, $^{**}p < 0.01$, $^{***}p < 0.001$.

in the LPS-treated cells (Figures 4A–C). To further investigate the interaction of NCOA4-mediated ferritinophagy and FTH1, we performed co-IP assays to detect the inner interaction between NCOA4 and FTH1 in the MLE-12 cells. YAP1 overexpression significantly decreased the association of FTH1 with NCOA4 (Figure 4D), suggesting that YAP1 might disrupt the interaction of NCOA4 and FTH1.

Taken together, these outcomes hinted that YAP1 inhibited ferritinophagy by suspending the NCOA4–FTH1 interaction in LPS-treated MLE-12 cells.

YAP1 inactivation accelerated ferroptosis activation during CLP-induced acute lung injury

To verify the role of YAP1 with ferroptosis in sepsis-induced ALI *in vivo*, we used the YAP1 conditional knockout mice for further research. As shown, CLP treatment created significant pathological changes, including alveolar hemorrhage and massive inflammatory cell infiltration, while YAP1 conditional knockout mice suffered larger trauma (Figures 5A, B). Furthermore, YAP1 deletion exacerbated CLP-stimulated pulmonary edema significantly as evidenced by protein leakage in BALF (Figure 5C). These results confirmed that YAP1 was a crucial element in CLP-induced ALI.

Similar to MLE-12 cells, to prove the anti-ferroptotic role of YAP1 in CLP-treated mice, we measured the ROS production and lipid peroxidation-related markers (MDA and GSH) with or without YAP1 deficiency in the murine lung tissue. Western blot data exhibited that the YAP1 protein level was significantly decreased in YAP1$^{f/f}$ mice (Figure 5E). CLP treatment markedly increased the generation of ROS and MDA levels and diminished GSH contents, while YAP1 deficiency deteriorated the oxidative damage caused by CLP treatment (Figures 5D–G). Collectively, we considered that YAP1 conditional knockout in mice aggravated pulmonary ferroptosis in response to CLP stimulation.

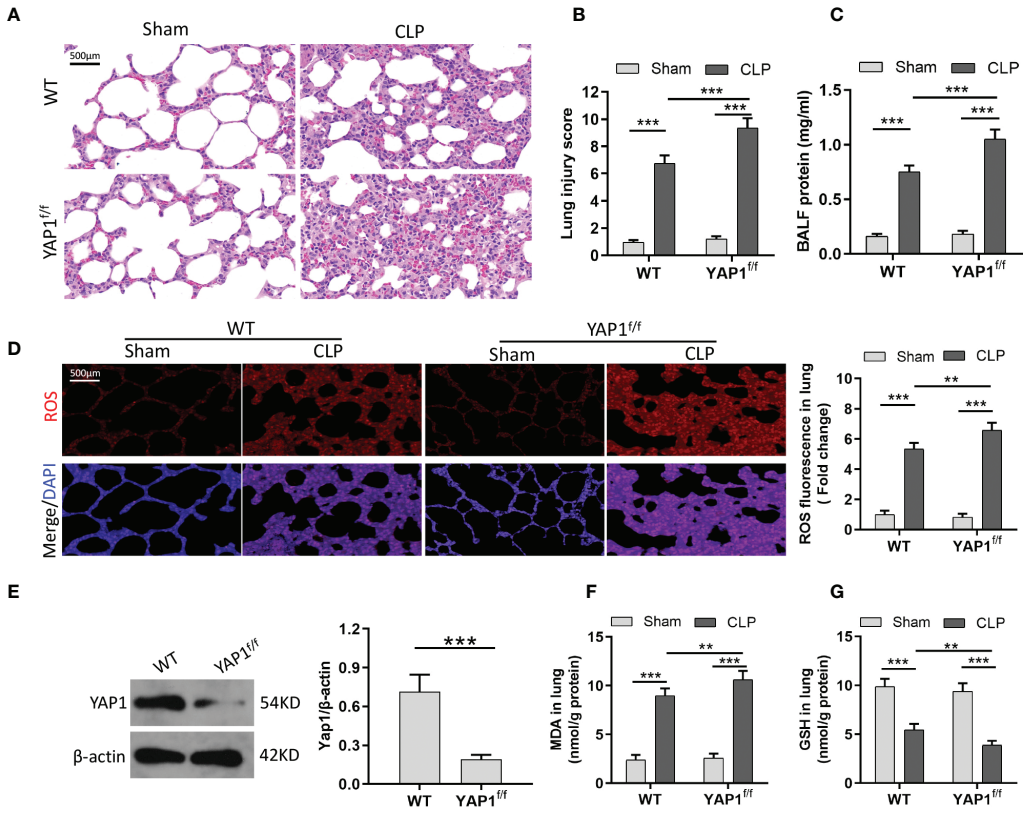

FIGURE 5
YAP1 deficiency aggravated oxidative stress-mediated lung injury in CLP mice. **(A)** Histological images of lung samples exhibited by HE staining in mice following CLP, YAP1$^{f/f}$, and CLP+YAP1$^{f/f}$ treatment. **(B)** The pathological lesion scores. **(C)** The content of BALF protein. **(D)** Representative fluorescent images of ROS staining and the quantification of ROS fluorescence intensity in lung tissue. **(E)** The certification of YAP1 conditional knockout in mice pulmonary epithelial cells. **(F–G)** Pulmonary content of MDA **(F)** and GSH **(G)** was assessed by the corresponding commercial kit. Data are expressed as mean ± SD. $n = 6$; *$p < 0.05$, **$p < 0.01$, ***$p < 0.001$.

10.3389/fimmu.2022.884362

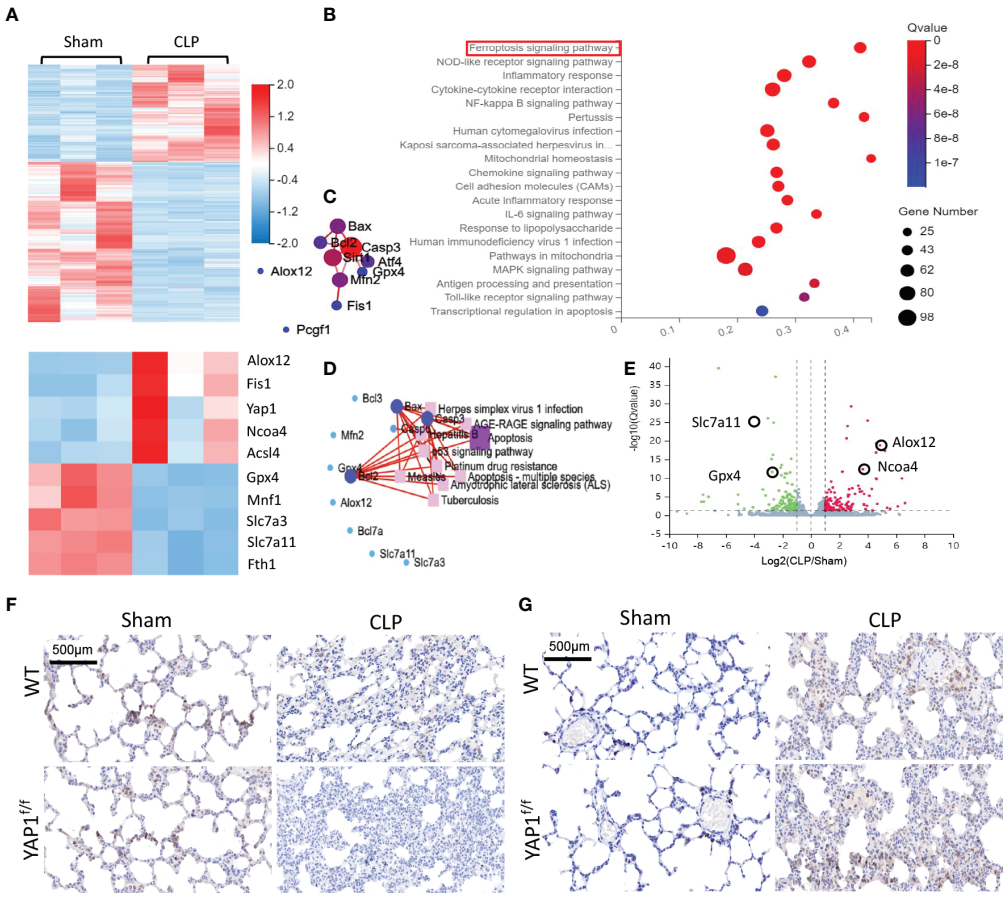

FIGURE 6
Gene expression analysis of lung tissue in WT+CLP mice and WT+Sham mice. **(A)** Hierarchical clustered heatmap of differentially expressed genes (DEGs) in lung tissues between WT+CLP mice and WT+Sham mice, *n* = 3. **(B)** The Kyoto Encyclopedia of Genes and Genomes enrichment analysis (KEGG pathway) was adopted to identify the most significantly altered signaling pathways in lung tissues of CLP mice. The differentially expressed genes enriched in the ferroptosis-related pathway, indicating that the ferroptosis signaling pathway was obviously activated, *n* = 3. **(C)** Construction of protein–protein interaction (PPI) regulatory network based on DEGs. **(D)** Network of KEGG pathway based on similarity of their gene expression profiles. These enrichment genes were related to several signaling pathways. **(E)** The volcano plot shows DEGs between CLP mice and WT mice. Genes colored in red represented dramatically upregulated genes, genes colored in green displayed remarkably downregulated genes, while insignificantly altered genes are colored in gray, log2 FC > 1, *Q* value < 0.05. **(F)** SLC7A11 of mouse lung parenchyma was stained by immunohistochemical (IHC) staining. **(G)** NCOA4 of mouse lung parenchyma was stained by IHC staining.

RNA-seq identified the enriched ferroptosis pathway and upregulated YAP1 in sepsis-induced ALI

To quantify the gene expression profiles of CLP treatment, RNA sequencing (RNA-seq) was performed in lung tissues of CLP mice or sham group. Firstly, we created an overall heatmap of all differentially expressed genes (log2 fold change > 1, *Q* value < 0.05). Then, we picked out genes that had the most significant differences (top 50) and focused on several target genes. Hierarchical clustered heatmap identified a series of upregulated genes (*ALOX12*, *NCOA4*, *Fis1*, *YAP1*) linked to ferroptosis and mitochondria fission and mitigation of genes (*GPX4*, *SLC7A11*, *FTH1*) associated with antioxidative stress and anti-ferroptosis (Figure 6A). The Kyoto Encyclopedia of Genes and Genomes (KEGG) enrichment analysis was utilized to determine the most significantly altered signaling pathways involved in CLP-treated lung tissues, including the NF-κB signaling pathway and ferroptosis signaling pathway (Figure 6B). The protein–protein interaction (PPI) regulatory network analysis predicted a high clustering coefficient and potential interaction among several related genes, such as apoptosis, ferroptosis, and mitochondrial fission (Figure 6C). These enrichment genes regulated relevant signaling pathways.

10.3389/fimmu.2022.884362

The network of KEGG pathways elucidated the potential crosstalk of these different signaling pathways (Figure 6D). The volcano plot also showed DEGs of CLP mice and the sham group (Figure 6E). Taken together, RNA-seq results indicated that YAP1 promoted ferroptosis in CLP mice lung tissue IHC staining showed that CLP stimulation reduced the accumulation of SLC7A11 (brown dye) in the lung tissue, while YAP1 knockout further diminished the content of SLC7A11 (Figure 6F). Moreover, we also observed that CLP stimulation gave rise to the accumulation of NCOA4 (brown dye), and YAP1 knockout exhibited more accumulation of NCOA4 (Figure 6G).

YAP1 deficiency aggravated CLP-induced ferroptosis and ferritinophagy in lung tissue

The morphological characteristics of ferroptosis were captured with TEM. The photographs revealed that the mitochondrial morphological structures were normal in WT mice and YAP$^{f/f}$ mice without CLP injury. Following the CLP challenge, we observed significant aberrant mitochondria (red arrows in the WT+CLP group and the YAP$^{f/f}$+CLP group), including reduction and even disappearance of

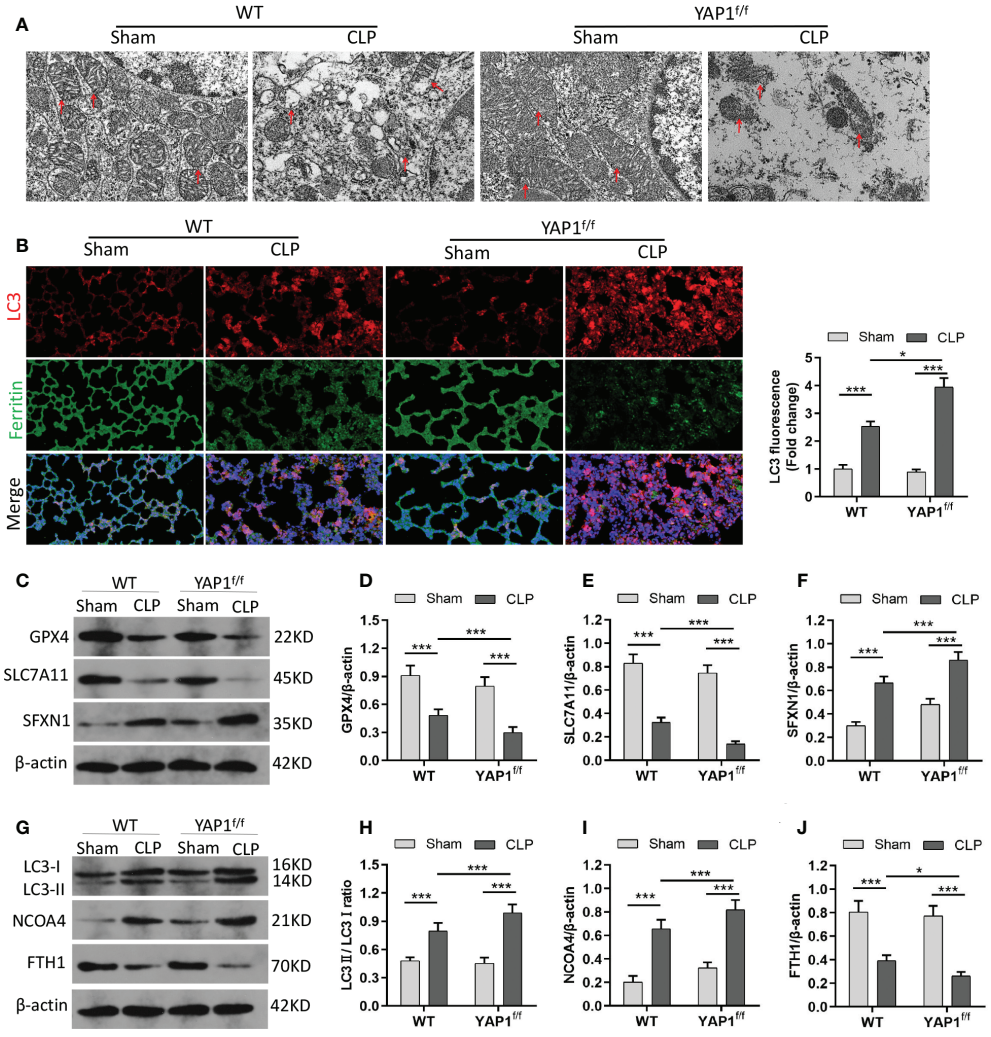

FIGURE 7
YAP1 deficiency aggravated CLP-induced ferroptosis and ferritinophagy in lung tissues. **(A)** Representative images shown by TEM. The red arrow indicates representative mitochondria in WT and YAP1$^{f/f}$ mice lungs treated by CLP or not (n = 3 mice/group). **(B)** Fluorescence analysis showed representative images of ferritin colocalization (green) with tissue expression of LC3 (red) and quantification fluorescence intensity of LC3. Nuclei were counterstained by DAPI (blue). Light pink fluorescence represented the colocalization of ferritin and LC3. **(C–F)** Immunoblotting detection of the expression contents of GPX4 **(D)**, SLC7A11 **(E)**, and SFXN1 **(F)** in mice with indicated treatment. **(G–J)** Immunoblotting determination of the expression levels of LC3II/LC3I **(H)**, NCOA4 **(I)**, and FTH1 **(J)** in mice with equivalent treatment. Data are expressed as mean ± SD. n = 6; *p < 0.05, **p < 0.01, ***p < 0.001.

mitochondria cristae and rupture of the mitochondrial outer membrane. Moreover, YAP1 deficiency further worsened CLP-induced mitochondrial damage (Figure 7A). In addition, the protein expression of GPX4 and SLC7A11 linked to ferroptosis and SFXN1 was determined. The data showed the significant upregulation of SFXN1 and downregulation of GPX4 and SLC7A11 during CLP treatment. However, these changes were further aggravated by YAP1 deficiency (Figures 7C–F).

Similar to the colocalization of LC3-GFP with ferritin in MLE-12 cells, we observed the fluorescent localization in CLP-treated mice with the presence or absence of YAP1 deficiency. As expected, YAP1 conditional knockout triggered the autophagy and promoted the degradation of ferritin in CLP-induced ALI (Figure 7B) (Figures S4B, C), indicating that YAP1 might affect ferroptosis by mediating ferritinophagy in sepsis-induced ALI. Western blotting showed that CLP treatment caused increases in LC3II/I ratio and NCOA4 levels and a decline in FTH1 levels. When mice experienced YAP1 conditional deletion, the LC3II/I ratio and NCOA4 climbed to higher levels, and FTH1 presented massive degradation (Figures 7G–J). In summary, our results suggested that the absence of YAP1 was able to aggravate ferroptosis and ferritinophagy in CLP-operated mice.

Discussion

In this study, we unveiled that ferroptosis in pulmonary epithelial cells was generated in sepsis-induced ALI, and YAP1 may be a feasible protective agent that prevents ALI by inhibiting ferroptosis.

To explore the potential regulated mechanism of sepsis-induced ALI, we first performed the RNA sequence analysis. We discovered that the ferroptosis-related pathway was closely linked to the differentially expressed genes, and YAP1 was upregulated in sepsis-induced ALI models. Based on these observations, we picked out the ferroptosis-related genes and YAP1 for further experiments.

Since the term ferroptosis was formally put forward in 2012, related research has experienced exponential growth in the past several years. Ferroptosis is featured by the surplus iron-dependent accumulation of lipid peroxidation, causing membrane damage and non-reversible cell death (29, 30). Multiple cellular metabolic events could regulate ferroptosis, for instance, redox homeostasis, iron load, mitochondrial function, and lipid metabolism, as well as disease-relevant signaling pathways. Abundant evidence indicated that ROS partook in the pathogenesis of septic cardiac or liver injury (28, 31). Intracellular overburden of ferrous iron can lead to the accumulation of lipid ROS, which makes an imbalance of redox in cells and cell death. This study determined the levels of oxidative stress marker and discovered increasing intracellular Fe^{2+} and lipid ROS in both the MLE-12 cells and lung tissues after stimulation with LPS or CLP.

YAP1, which is an important transcription factor in the Hippo pathway, has been studied extensively and regarded as a potential approach for the onset mechanism of various diseases, such as cancer, atherosclerosis, fibrosis, and inflammation. Currently, YAP1 has been proven to promote alveolar epithelial regeneration and repair in a growing number of studies. The nuclear localization of YAP1 is pervasively distributed in pulmonary structural cells like lung epithelial cells. Homozygous deletion of YAP1 resulted in no new lung bud production, while selective loss of YAP1 disrupted lung branching morphogenesis and reduced cell proliferation (32). YAP could abolish inflammation and regulate pulmonary endothelial cell activation through preventing TRAF6-mediated NF-κB activation (33). In mice with bacterial pneumonia, YAP/TAZ deficiency in epithelial type II cells exhibited long-term inflammatory responses and tardive alveolar epithelial regeneration after lung injury (34). Furthermore, YAP1/TAZ mutant expression decreased the production of surfactant protein C (SPC), which is a representative feature of ALI/ARDS (14). Apart from the role of YAP1 in lung tissue, YAP activation reduced congenital inflammatory response to oxidative stress and necrosis/apoptosis to prevent the liver from ischemia–reperfusion (IR) stress (35). Nuclear YAP1 drove intestinal epithelial cell proliferation, which could cause post-inflammatory epithelial regeneration in ulcerative colitis (36). Hence, considering the protective role of YAP1 in promoting cell proliferation, we explored whether sepsis was a vital process in facilitating the ferroptosis of epithelial cells, which could be concerned with YAP1 activity. Our *in-vivo* study found that YAP1 deficiency aggravated sepsis-induced lung pathological damage and produced Fe^{2+} overload and higher MDA levels as well as more ROS accumulation in $YAP1^{f/f}$ mice after CLP. Concurrently, YAP1 overexpression exhibited an anti-ferroptotic ability, as presented by the reduction in ROS accumulation and suppression of lipid peroxidation *in vitro*. These outcomes reminded us that ferroptosis participates in the genesis and development of sepsis-induced ALI, and YAP1 modulates the process by controlling Fe^{2+} and lipid peroxidation, which might provide a targeted strategy for mitigating sepsis-induced ALI.

Then, we detected other ferroptosis-related regulators. SLC7A11 and GPX4 were downregulated, while MDA and iron accumulation were upregulated in the LPS-treated human bronchial epithelial cell line (37), indicating that ferroptosis was

on the front burner in LPS-induced ALI. ACSL4 is also necessary for facilitating ferroptosis and can insert unsaturated arachidonic acid into the cellular membrane, which produces a mass of lipid ROS. Pharmacological inhibition of ACSL4 can prevent ferroptosis-related diseases (38). In doxorubicin-induced myocardial damage models, YAP could decrease the expression level of ACSL4 (22). In lung adenocarcinoma, YAP diminished intracellular iron levels by promoting FTL transcription through transcription factor CP2 (TRCP2) (39). To clarify the mechanism of ferroptosis in sepsis-induced ALI, a transcriptome study of RNA sequencing was carried out, suggesting that the ferroptosis signaling pathway was involved in the pathogenesis of sepsis-induced ALI. Subsequently, our findings revealed that YAP1 knockdown attenuated the expression of GPX4 and SLC7A11 in CLP-treated mice, and YAP1 overexpression enhanced the expression of GPX4 *in vitro* and *in vivo*. YAP1 overexpression limited the expression of ACSL4 in LPS-treated cells. Briefly, YAP1 played a pivotal role in ferroptosis suppression *via* regulating the ferroptosis mediator in sepsis-induced ALI.

The mitochondria are the main sites of energy metabolism and the apoptotic targets of excessive ROS. Mitochondrial double membrane is the ideal site for ferroptosis. Increased mitochondrial ROS could trigger ferritinophagy and elevate the content of intracellular iron, eventually leading to ferroptosis (20). SFXN1 contributes to iron transportation into the mitochondria and promotes the utilization of erythroid mitochondrial iron. Furthermore, previous research discovered that SFXN1 is closely related to pathologic mitochondrial iron accumulation, which led to sideroblastic anemia (26). In YAP1$^{f/f}$ septic mice, we detected more serious mitochondria damage and a higher expression level of SFXN1. Inversely, YAP1 overexpression blocked the expression of SFXN1 *in vitro* and allayed the generation of mitochondrial ROS.

Previous findings indicated that suppression of autophagy alleviated ferroptosis (19, 40). The catabolic process of autophagy involves the continuous degradation of substrates in lysosomes for maintaining cell homeostasis in response to hypoxia and stress as well as sepsis attack. Along with the occurrence of ferroptosis, autophagy is motivated, causing the

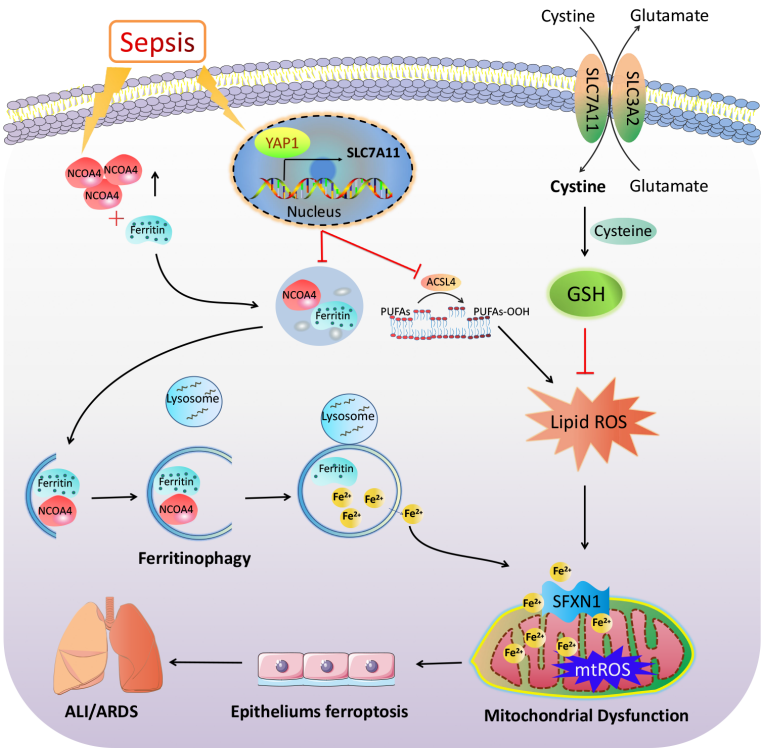

FIGURE 8
The mechanism illustration on the involvement of YAP1 in ferritinophagy and ferroptosis in sepsis-induced acute lung injury. Sepsis induces increased intracellular NCOA4 expression, which then has an interaction with ferritin and brings about the autophagic degradation of ferritin. YAP1 can suppress the degradation of ferritin into autophagosomes *via* inhibiting NCOA4-mediated ferritinophagy, then prevent ferrous iron from transporting into the mitochondria. YAP1 attenuates the accumulation of mitochondrial reactive oxygen species and lipid peroxidation and contributes to protecting mitochondrial function and repressing ferroptosis. Therefore, we conclude that YAP1 is involved in sepsis-induced acute lung injury by regulating the process of ferritinophagy-mediated ferroptosis.

consequent degradation of ferritin *via* NCOA4–FTH1 binding (41). NCOA4 mediated the autophagic degradation of ferritin in lysosomes; thus, cellular free iron is released to initiate the Fenton reaction. These cascades of reactions could be blocked by NCOA4 inhibition or autophagy disrupting, hence abrogating the accumulation of ferrous iron and ROS due to ferroptosis (42). Fang et al. (43) observed that compound 9a diminished the colocalization of Fe^{2+} in lysosomes and inhibited the NCOA4–FTH1 reaction. Qi et al. (44) clarified that curcumol could inhibit NCOA4 regulation of ferritinophagy to prevent hepatocyte senescence through the promotion of YAP. Zhang et al. (45) noted that YAP suppression might sensitize ferroptosis by inhibiting FTH1 in lung adenocarcinoma. In our experiments, the colocalization of ferritin and autophagosomes was observed by confocal microscopic evaluation, reflecting that YAP1 overexpression decreased the release of ferrous iron from lysosomes and lysosomal ferritin degradation. Moreover, we also found that YAP1 could inhibit the NCOA4–FTH1 interaction by co-IP assays, which was consistent with a previous report (45). An amount of Fe^{2+} from ferritin degradation stimulates SFXN1 production in the mitochondrial membrane, which subsequently transports Fe^{2+} into the mitochondria, triggering the cascade of mitochondrial ROS and eventually contributing to ferroptosis (28). SFXN1-induced mitochondria iron accumulation might be caused by NCOA4-mediated ferritinophagy in apelin-13 myocardiopathy (27). Our current observation supports the theory that YAP1 is linked to the NCOA4–FTH1 interaction. This interaction may affect SFXN1-regulated mitochondrial iron overload and mitochondrial ROS production, ultimately generating epithelial cell ferroptosis. Taken together, these experimental data suggested that YAP1 could suppress FTH1 autophagic degradation mediated by NCOA4, which was crucial for protecting pulmonary epithelial cells from sepsis-induced ferroptosis. Sepsis-induced ALI in mice was probably connected to ferritinophagy-mediated ferroptosis activation.

In conclusion, our results demonstrate the important participation of ferroptosis and YAP1 in the pathophysiology of sepsis-induced ALI. YAP1 disrupted the NCOA4–FTH1 reaction and inhibited NCOA4-mediated ferritinophagy to prevent ferroptosis and subsequent mitochondrial ROS-related dysfunction in septic lung injury (Figure 8). These previous publications raise the possibility that YAP1 may be a protective ingredient of ALI/ARDS, and sustaining the expression of YAP1 could become an emerging therapeutic approach. Notably, elevated YAP levels have been formally confirmed to be related to cancer development. Consequently, one of the future challenges toward the application of YAP1 in lung diseases is activating YAP1 precisely without inducing cancer. Further investigation should be expected to explore the accurate regulation of YAP1 in sepsis-induced pulmonary diseases targeting ferroptosis.

Data availability statement

The data presented in the study are deposited in the SRA (Sequence Read Archive) repository, accession number PRJNA836168.

Ethics statement

The animal study was reviewed and approved by the Animal Ethics Committee of Wuhan University (No. 2021187).

Author contributions

XL and XS conceptualized and designed the study. JZ, YZ, and YW performed the study and acquired the data. JW and AS analyzed the data. JZ drafted the manuscript. XL and XS revised the paper. All authors read and approved the final manuscript. All authors contributed to the article and approved the submitted version.

Conflict of interest

The authors declare that the research was conducted in the absence of any commercial or financial relationships that could be construed as a potential conflict of interest.

Publisher's note

Supplementary material

The Supplementary Material for this article can be found online at: https://www.frontiersin.org/articles/10.3389/fimmu.2022.884362/full#supplementary-material

References

1. Singer M, Deutschman CS, Seymour CW, Shankar-Hari M, Annane D, Bauer M, et al. The third international consensus definitions for sepsis and septic shock (sepsis-3). *JAMA* (2016) 315(8):801–10. doi: 10.1001/jama.2016.0287

2. Angus DC, van der Poll T. Severe sepsis and septic shock. *N Engl J Med* (2013) 369(9):840–51. doi: 10.1056/NEJMra1208623

3. Torio CM, Moore BJ. National inpatient hospital costs: The most expensive conditions by payer, 2013 Stat Brief. In: *Healthcare Cost and Utilization Project (HCUP) Statistical Briefs* (2006) 204 Agency for Healthcare Research and Quality (US):Rockville (MD).

4. Hall MJ, Levant S, DeFrances CJ. Trends in inpatient hospital deaths: National hospital discharge survey, 2000-2010 NCHS Data Brief. *US Department of Health and Human Services, Centers for Disease Control and Prevention* (2013) 118):1–8. National Center for Health Statistics.

5. Sessler CN, Bloomfield GL, Fowler AA3rd. Current concepts of sepsis and acute lung injury. *Clin Chest Med* (1996) 17(2):213–35. doi: 10.1016/S0272-5231(05)70310-5

6. Ware LB, Matthay MA. The acute respiratory distress syndrome. *N Engl J Med* (2000) 342(18):1334–49. doi: 10.1056/NEJM200005043421806

7. Matthay MA, Zimmerman GA. Acute lung injury and the acute respiratory distress syndrome: four decades of inquiry into pathogenesis and rational management. *Am J Respir Cell Mol Biol* (2005) 33(4):319–27. doi: 10.1165/rcmb.F305

8. Panciera T, Azzolin L, Cordenonsi M, Piccolo S. Mechanobiology of YAP and TAZ in physiology and disease. *Nat Rev Mol Cell Biol* (2017) 18(12):758–70. doi: 10.1038/nrm.2017.87

9. Pavel M, Renna M, Park SJ, Menzies FM, Ricketts T, Füllgrabe J, et al. Contact inhibition controls cell survival and proliferation *via* YAP/TAZ-autophagy axis. *Nat Commun* (2018) 9(1):2961. doi: 10.1038/s41467-018-05388-x

10. Mancias JD, Wang X, Gygi SP, Harper JW, Kimmelman AC. Quantitative proteomics identifies NCOA4 as the cargo receptor mediating ferritinophagy. *Nature* (2014) 509(7498):105–9. doi: 10.1038/nature13148

11. Szymaniak AD, Mahoney JE, Cardoso WV, Varelas X. Crumbs3-mediated polarity directs airway epithelial cell fate through the hippo pathway effector yap. *Dev Cell* (2015) 34(3):283–96. doi: 10.1016/j.devcel.2015.06.020

12. Zhao R, Fallon TR, Saladi SV, Pardo-Saganta A, Villoria J, Mou H, et al. Yap tunes airway epithelial size and architecture by regulating the identity, maintenance, and self-renewal of stem cells. *Dev Cell* (2014) 30(2):151–65. doi: 10.1016/j.devcel.2014.06.004

13. iu F, Lagares D, Choi KM, Stopfer L, Marinković A, Vrbanac V, et al. Mechanosignaling through YAP and TAZ drives fibroblast activation and fibrosis. *Am J Physiol Lung Cell Mol Physiol* (2015) 308(4):L344–57. doi: 10.1152/ajplung.00300.2014

14. Otsubo K, Goto H, Nishio M, Kawamura K, Yanagi S, Nishie W, et al. MOB1-YAP1/TAZ-NKX2.1 axis controls bronchioalveolar cell differentiation, adhesion and tumour formation. *Oncogene* (2017) 36(29):4201–11. doi: 10.1038/onc.2017.58

15. Park KS, Whitsett JA, Di Palma T, Hong JH, Yaffe MB, Zannini M. TAZ interacts with TTF-1 and regulates expression of surfactant protein-c. *J Biol Chem* (2004) 279(17):17384–90. doi: 10.1074/jbc.M312569200

16. Dixon SJ, Lemberg KM, Lamprecht MR, Skouta R, Zaitsev EM, Gleason CE, et al. Ferroptosis: an iron-dependent form of nonapoptotic cell death. *Cell* (2012) 149(5):1060–72. doi: 10.1016/j.cell.2012.03.042

17. Yang WS, SriRamaratnam R, Welsch ME, Shimada K, Skouta R, Viswanathan VS, et al. Regulation of ferroptotic cancer cell death by GPX4. *Cell* (2014) 156(1-2):317–31. doi: 10.1016/j.cell.2013.12.010

18. Cao JY, Dixon SJ. Mechanisms of ferroptosis. *Cell Mol Life Sci* (2016) 73(11-12):2195–209. doi: 10.1007/s00018-016-2194-1

19. Hou W, Xie Y, Song X, Sun X, Lotze MT, Zeh HJ 3rd, et al. Autophagy promotes ferroptosis by degradation of ferritin. *Autophagy* (2016) 12(8):1425–8. doi: 10.1080/15548627.2016.1187366

20. Qin X, Zhang J, Wang B, Xu G, Yang X, Zou Z, et al. Ferritinophagy is involved in the zinc oxide nanoparticles-induced ferroptosis of vascular endothelial cells. *Autophagy* (2021) 17(12):4266–85. doi: 10.1080/15548627.2021.1911016

21. Yoshida M, Minagawa S, Araya J, Sakamoto T, Hara H, Tsubouchi K, et al. Involvement of cigarette smoke-induced epithelial cell ferroptosis in COPD pathogenesis. *Nat Commun* (2019) 10(1):3145. doi: 10.1038/s41467-019-10991-7

22. Sun X, Sun P, Zhen D, Xu X, Yang L, Fu D, et al. Melatonin alleviates doxorubicin-induced mitochondrial oxidative damage and ferroptosis in cardiomyocytes by regulating YAP expression. *Toxicol Appl Pharmacol* (2022) 437:115902. doi: 10.1016/j.taap.2022.115902

23. Qian M, Lou Y, Wang Y, Zhang M, Jiang Q, Mo Y, et al. PICK1 deficiency exacerbates sepsis-associated acute lung injury and impairs glutathione synthesis *via* reduction of xCT. *Free Radic Biol Med* (2018) 118:23–34. doi: 10.1016/j.freeradbiomed.2018.02.028

24. Qiang Z, Dong H, Xia Y, Chai D, Hu R, Jiang H. Nrf2 and STAT3 alleviates ferroptosis-mediated IIR-ALI by regulating SLC7A11. *Oxid Med Cell Longev* (2020) 2020:5146982. doi: 10.1155/2020/5146982

25. Qiu YB, Wan BB, Liu G, Wu YX, Chen D, Lu MD, et al. Nrf2 protects against seawater drowning-induced acute lung injury *via* inhibiting ferroptosis. *Respir Res* (2020) 21(1):232. doi: 10.1186/s12931-020-01500-2

26. Fleming MD, Campagna DR, Haslett JN, Trenor CC3rd, Andrews NC. A mutation in a mitochondrial transmembrane protein is responsible for the pleiotropic hematological and skeletal phenotype of flexed-tail (f/f) mice. *Genes Dev* (2001) 15(6):652–7. doi: 10.1101/gad.873001

27. Tang M, Huang Z, Luo X, Liu M, Wang L, Qi Z, et al. Ferritinophagy activation and sideroflexin1-dependent mitochondria iron overload is involved in apelin-13-induced cardiomyocytes hypertrophy. *Free Radic Biol Med* (2019) 134:445–57. doi: 10.1016/j.freeradbiomed.2019.01.052

28. Li N, Wang W, Zhou H, Wu Q, Duan M, Liu C, et al. Ferritinophagy-mediated ferroptosis is involved in sepsis-induced cardiac injury. *Free Radic Biol Med* (2020) 160:303–18. doi: 10.1016/j.freeradbiomed.2020.08.009

29. Gan B. Mitochondrial regulation of ferroptosis. *J Cell Biol* (2021) 220(9):e202105043. doi: 10.1083/jcb.202105043

30. Chen X, Li J, Kang R, Klionsky DJ, Tang D. Ferroptosis: machinery and regulation. *Autophagy* (2021) 17:2054–81. doi: 10.1080/15548627.2020.1810918

31. Wei S, Bi J, Yang L, Zhang J, Wan Y, Chen X, et al. Serum irisin levels are decreased in patients with sepsis, and exogenous irisin suppresses ferroptosis in the liver of septic mice. *Clin Transl Med* (2020) 10(5):e173. doi: 10.1002/ctm2.173

32. Lin C, Yao E, Zhang K, Jiang X, Croll S, Thompson-Peer K, et al. YAP is essential for mechanical force production and epithelial cell proliferation during lung branching morphogenesis. *Elife* (2017) 6:e21130. doi: 10.7554/eLife.21130

33. Lv Y, Kim K, Sheng Y, Cho J, Qian Z, Zhao YY, et al. YAP controls endothelial activation and vascular inflammation through TRAF6. *Circ Res* (2018) 123(1):43–56. doi: 10.1161/CIRCRESAHA.118.313143

34. LaCanna R, Liccardo D, Zhang P, Tragesser L, Wang Y, Cao T, et al. Yap/Taz regulate alveolar regeneration and resolution of lung inflammation. *J Clin Invest* (2019) 129(5):2107–22. doi: 10.1172/JCI125014

35. Liu Y, Lu T, Zhang C, Xu J, Xue Z, Busuttil RW, et al. Activation of YAP attenuates hepatic damage and fibrosis in liver ischemia-reperfusion injury. *J Hepatol* (2019) 71(4):719–30. doi: 10.1016/j.jhep.2019.05.029

36. Deng F, Peng L, Li Z, Tan G, Liang E, Chen S, et al. YAP triggers the wnt/β-catenin signalling pathway and promotes enterocyte self-renewal, regeneration and tumorigenesis after DSS-induced injury. *Cell Death Dis* (2018) 9(2):153. doi: 10.1038/s41419-017-0244-8

37. Liu P, Feng Y, Li H, Chen X, Wang G, Xu S, et al. Ferrostatin-1 alleviates lipopolysaccharide-induced acute lung injury *via* inhibiting ferroptosis. *Cell Mol Biol Lett* (2020) 25:10. doi: 10.1186/s11658-020-00205-0

38. Doll S, Proneth B, Tyurina YY, Panzilius E, Kobayashi S, Ingold I, et al. ACSL4 dictates ferroptosis sensitivity by shaping cellular lipid composition. *Nat Chem Biol* (2017) 13(1):91–8. doi: 10.1038/nchembio.2239

39. Wang Y, Qiu S, Wang H, Cui J, Tian X, Miao Y, et al. Transcriptional repression of ferritin light chain increases ferroptosis sensitivity in lung adenocarcinoma. *Front Cell Dev Biol* (2021) 9:719187. doi: 10.3389/fcell.2021.719187

40. Gao M, Monian P, Pan Q, Zhang W, Xiang J, Jiang X. Ferroptosis is an autophagic cell death process. *Cell Res* (2016) 26(9):1021–32. doi: 10.1038/cr.2016.95

41. Dowdle WE, Nyfeler B, Nagel J, Elling RA, Liu S, Triantafellow E, et al. Selective VPS34 inhibitor blocks autophagy and uncovers a role for NCOA4 in ferritin degradation and iron homeostasis in vivo. *Nat Cell Biol* (2014) 16(11):1069–79. doi: 10.1038/ncb3053

42. Latunde-Dada GO. Ferroptosis: Role of lipid peroxidation, iron and ferritinophagy. *Biochim Biophys Acta Gen Subj* (2017) 1861(8):1893–900. doi: 10.1016/j.bbagen.2017.05.019

43. Fang Y, Chen X, Tan Q, Zhou H, Xu J, Gu Q. Inhibiting ferroptosis through disrupting the NCOA4-FTH1 interaction: A new mechanism of action. *ACS Cent Sci* (2021) 7(6):980–9. doi: 10.1021/acscentsci.0c01592

44. Qi X, Song A, Ma M, Wang P, Zhang X, Lu C, et al. Curcumol inhibits ferritinophagy to restrain hepatocyte senescence through YAP/NCOA4 in non-alcoholic fatty liver disease. *Cell Prolif* (2021) 54(9):e13107. doi: 10.1111/cpr.13107

45. Zhang X, Yu K, Ma L, Qian Z, Tian X, Miao Y, et al. Endogenous glutamate determines ferroptosis sensitivity *via* ADCY10-dependent YAP suppression in lung adenocarcinoma. *Theranostics* (2021) 11(12):5650–74. doi: 10.7150/thno.55482

frontiers | Frontiers in Immunology

TYPE Original Research
PUBLISHED 03 October 2022
DOI 10.3389/fimmu.2022.928979

OPEN ACCESS

EDITED BY
Szandor Simmons,
Junior Research Group
"Immunodynamics", Germany

REVIEWED BY
Marcos Lessa,
Oswaldo Cruz Foundation
(Fiocruz), Brazil
Uirassu Borges,
German Sport University
Cologne, Germany

*CORRESPONDENCE
Marc N. Jarczok
Marc.jarczok@uni-ulm.de

SPECIALTY SECTION
This article was submitted to
Inflammation,
a section of the journal
Frontiers in Immunology

RECEIVED 26 April 2022
ACCEPTED 26 August 2022
PUBLISHED 03 October 2022

CITATION
Balint EM, Grüner B, Haase S, Kaw-Geppert M, Thayer JF, Gündel H and Jarczok MN (2022) A randomized clinical trial to stimulate the cholinergic anti-inflammatory pathway in patients with moderate COVID-19-pneumonia using a slow-paced breathing technique.
Front. Immunol. 13:928979.
doi: 10.3389/fimmu.2022.928979

A randomized clinical trial to stimulate the cholinergic anti-inflammatory pathway in patients with moderate COVID-19-pneumonia using a slow-paced breathing technique

Elisabeth Maria Balint [1,2], Beate Grüner [3], Sophia Haase [1], Mandakini Kaw-Geppert [1], Julian F. Thayer [4], Harald Gündel [1] and Marc N. Jarczok [1*]

[1]Clinic for Psychosomatic Medicine and Psychotherapy, University Hospital Ulm, Ulm, Germany, [2]Center for mental health, Privatklinik Meiringen, Meiringen, Switzerland, [3]Clinic for Internal Medicine III, Division of Infectious Diseases, University Hospital Ulm, Ulm, Germany, [4]Department of Psychological Science, University of California, Irvine, Irvine, CA, United States

Purpose: A characteristic problem occurring in COVID-19 is excessive elevations of pro-inflammatory cytokines (e.g. IL-6 and CRP) which are associated with worse clinical outcomes. Stimulation of the vagally-mediated cholinergic anti-inflammatory reflex by slow paced breathing with prolonged exhalation may present a clinically relevant way to reduce circulating IL-6.

Method: Single-center randomized controlled clinical trial with enrolment of 46 patients hospitalized with confirmed severe acute respiratory syndrome Coronavirus 2 (SARS-CoV-2) infection and moderate COVID-19 pneumonia (primary diagnosis). Differences between intervention (4sec inhalation, 6sec exhalation for 20 minutes 3x daily) and control group in IL-6 calculated using multilevel mixed-effect linear regression models with random slope including the covariates relevant comorbidities, COVID-19 medication, and age. Both groups received standard care.

Results: Mean age was 57 years ± 13 years, N= 28 (60%) male, N=30 (65%) with relevant comorbidities. The model including group-by-time interaction revealed a significantly lower trajectory of IL-6 in the intervention group (effect size Cohens f^2 = 0.11, LR-test p=.040) in the intention-to-treat sample, confirmed by per-protocol analysis (f^2 = 0.15, LR-test p=.022). Exploratory analysis using the median split of practice time to predict IL-6 of the next morning indicated a dose-response relationship with beneficial effects of practice time above 45 minutes per day. Oxygen saturation remained unchanged during slow-paced breathing (95.1% ± 2.1% to 95.4% ± 1.6%).

Conclusion: Patients practicing slow-paced breathing had significantly lower IL-6 values than controls with a small to medium effect size and without relevant side effects. Further trials should evaluate clinical outcomes and an earlier start of the intervention. Slow-paced breathing could be an easy to implement, low-cost, safe and feasible adjuvant therapeutic approach to reduce circulating IL-6 in moderate COVID-19 pneumonia.

Clinical Trial Registration: https://www.drks.de, identifier DRKS00023971, Universal Trial Number (UTN) U1111-1263-8658.

KEYWORDS

Cholinergic anti-inflammatory reflex, slow-paced breathing, IL-6, acute viral infection, moderate COVID-19 pneumonia, dose-response relationship, CRP, TNF-alpha

Introduction

The pandemic of severe acute respiratory syndrome coronavirus 2 (SARS-CoV-2) still occupies politics and health care. Though immunization is available now and knowledge about therapy options has widely progressed, there is still an urgent need especially for cheap, broadly accessible interventions that could be spread globally.

A characteristic problem occurring in coronavirus disease 2019 (COVID-19) are excessive elevations of pro-inflammatory cytokines such as interleukin-6 (IL-6) and C-reactive protein (CRP) which are associated with worse clinical courses (1, 2). Several trials have tested anti-inflammatory agents, including dexamethasone or IL-6 antagonists with beneficial outcomes (3–5). Beside drugs, there exists a clinically relevant, non-pharmaceutical way to reduce inflammation through vagus nerve stimulation (VNS). The latter is involved in the regulation of the immune response *via* the cholinergic anti-inflammatory reflex (6). Specifically, the efferent vagally mediated reflex arc regulates systemic inflammation and the release of pro-inflammatory cytokines such as IL-6 from acetylcholine-synthesizing T-cells (7). In detail, the nucleus of the solitary tract (NTS) neurons activates the dorsal motor nucleus of the vagus nerve (DMNV) whose efferent fibers trigger the cholinergic anti-inflammatory reflex (8), stimulating the cholinergic motoneurons that project to the splenic nerve in the celiac ganglion. Acetylcholine (ACh), released from the preganglionic terminals, excites celiac neurons and provoke the release of norepinephrine (NE) in the spleen. Then, splenic response inhibits the release of macrophage cytokines, decreasing inflammation (9).

Accordingly, plasma levels of pro-inflammatory cytokines increase with cervical or subdiaphragmatic vagotomy, whereas electrical VNS or acetylcholine administration decrease IL-6 cytokine levels in human and mouse models (7). Therefore, measures of vagal activity and inflammatory parameters such as IL-6, CRP, and tumor necrosis factor α (TNF-α) are strongly correlated (10). In the specific case of infection with SARS-CoV-2, as the cholinergic anti-inflammatory mechanism controls NF-κB action through Acetylcholine coupled to the α7n-Acetylcholin-receptor (11), insufficient vagal activity appears to be the cause of both unhindered viral replication and uncontrolled cytokine release along the virus-driven NF-κB pathway (12). Therefore, increasing vagal activity seems to be a promising therapeutic approach.

The vagus nerve can be stimulated with electric devices (13, 14), whic has been suggested early on in the treatment of Acute Respiratory Distress Syndrome in COVID-19 patients (15).The authors of a randomized controlled study proved feasibility for auricular electrical VNS in 31 patients hospitalized due to COVID-19 and did not report side effects, but were not able to show clinical improvement (16). Two case reports describe decreasing IL-6 and CRP after onset of electrical VNS in four COVID-19 patients suffering from moderate or severe COVID-19-pneumonia (17, 18). However, electrical VNS has the limitation that no device has yet been certified for this anti-inflammatory use, this intervention must be performed by medical professionals, and is therefore limited with respect to personal and financial resources. To our knowledge, no study investigated the effect of non-electrical VNS in patients with COVID-19. A simple way to increase the activity of the vagus nerve is a specific breathing technique with reduced frequency and a prolonged exhalation phase (slow-paced breathing) (19, 20). A recent meta-analysis clearly showed increased vagal and mixed measures of HRV during and after slow-paced breathing interventions (21). The mechanism how slow-paced breathing stimulates vagal activity is described in great detail (22). Though some studies show effects of slow-paced breathing on IL-6, CRP

or TNF-α after several days or weeks in patients with hypertension (23) and irritable bowel syndrome (24), the effect of vagal stimulation through slow-paced breathing in infectious diseases was not yet investigated.

Therefore, we performed a randomized controlled trial in patients with moderate COVID-19 pneumonia to investigate the hypothesis whether a breathing technique that increases vagal activity reduces inflammatory levels (primary outcome: IL-6; secondary outcome: CRP, leukocytes) in patients with COVID -19 pneumonia compared to a control group of patients with treatment as usual.

Materials and methods

The present study design is a prospective, two-arm, open-label, single-center randomized controlled trial. The protocol was approved by the Institutional Review Board of Ulm University (No. 3/21, 01/02/2021) and registered prior to screening start at the German Clinical Trials Register (ID: DRKS00023971), Universal Trial Number (UTN) U1111-1263-8658. The study was conducted in compliance with the Declaration of Helsinki, the Guideline for Good Clinical Practice, and local regulatory requirements. All patients provided written informed consent prior to inclusion.

Patients

Inclusion criteria were hospitalization with SARS-CoV-2-pneumonia (primary diagnosis) in non-ICU-wards with a moderate degree of disease according to the definition of the German Robert Koch Institute (RKI) adapted from WHO (www.rki.de/covid-19-therapie-stakob), age of 18 years or older and being able to give written informed consent at study enrollment. The SARS-CoV-2-infection was confirmed by positive polymerase chain reaction (PCR) assay. The following exclusion criteria were applied: 1) Severe and critical COVID-19 pneumonia with respiratory rate>30/min or SpO2<90% on room air (www.rki.de/covid-19-therapie-stakob), or 2) condition after surgery/trauma/acute event (stroke, myocardial infarction, acute COVID-independent infection) in the last four weeks, i.e., other primary diagnoses than COVID-19, or 3) current pregnancy, or 4) patients with pre-existing pulmonary disease who were on oxygen prior to infection (e.g., due to pulmonary fibrosis, COPD), or 5) limited ability to give consent (e.g., due to dementia), or 6) limited ability to perform breathing maneuvers independently (e.g., high frailty), or 7) limited ability to provide self-care (German care level two or three), or 8) insufficient language skills, or 9) seizures in the medical history.

Study design

Screening was performed starting from 23/02/2021 until 17/06/2021 on either the ward for infectious diseases or the temporary ward for patients suffering from COVID-19 at the Clinic for Internal Medicine III (Infectious Diseases, hematology, oncology) of the University Medical Center Ulm (Germany). Consenting patients were randomized in a 1:1 ratio to receive the breathing intervention additional to standard care (intervention group, IG) or standard care only (control group, CG). The randomization list was created prior to screening start by MNJ with blocks of 20, 16, 14, and 16 numbers to account for the adaptive design (see below Statistical methods section) using the software STATA (Stata Corp, College Station Texas, USA) (25) and was not accessible to recruiting study personnel (EMB, SH, MKG).

Standard care consisted of O2 supplementation (non-invasive), dexamethasone, antiviral and antibiotic drugs as well as additional anti-inflammatory medication and other medication on requirement according to the RKI-criteria valid at that time (www.rki.de/covid-19-therapie-stakob). All patients received anticoagulant therapy. Relevant medication is listed in Table 1.

Patients randomized to intervention group were asked to perform the 20-minute breathing exercise three times a day with 6 breaths per minute and an inhalation to exhalation ratio of 4:6 seconds (see Supplement material for the instruction) in the hospital bed with the backrest in an upright position. To support the correct technique, the free application BreathBall (https://breathball.com/de/home-de/) was shown on a smartphone. For hygienic reasons, it was preferred that patients used their own smartphone and installed the add-free app. A study smartphone was available for the very few patients without a smartphone (N=2). The application facilitates paced breathing by displaying a decreasing (exhale) and increasing (inhale) ball, combined with sound if preferred. The study personnel monitored the first exercise to guide the correct implementation of the breathing exercise and to assist and register side effects. If the patients were unable to follow the breathing scheme, it was adapted slightly up to a breathing frequency of maximal 10 per minute. Further exercises were to be done independently and the time spent in the exercise was self-recorded. The control group received standard care. Both groups were visited every second day by the study personnel to assure the correct implementation of the breathing exercise, assess symptoms, check for side effects, record the practice times and to collect oxygen saturation, oxygen flow, breathing frequency and one-channel ECG for calculation of heart rate variability measurements (HRV). Blood samples were taken in routine at approximately 8am in the morning and analyzed by

10.3389/fimmu.2022.928979

TABLE 1 Characteristics of the patients at baseline according to treatment assignment.

	Intervention group (N = 23)		Control group (N = 23)	
	Mean (or N)	Standard Deviation (or %)	Mean (or N)	Standard Deviation (or %)
Age [years]	58.8	13.2	54.3	13.4
Sex [male]	14	61%	14	61%
Ethnicity:				
German [N, %]	10	43%	9	39%
Turkish [N, %]	5	22%	2	9%
Russian [N, %]	3	13%	5	22%
Other [N, %]	5	22%	7	30%
BMI [kg/m^2]	30.6	5.1	30.2	6.1
Living in partnership [N, %]	18	78%	16	70%
Active Smoking [N, %]	1	4%	1	4%
Regular physical activity [N, %]	9	39%	9	39%
Working status: working [N, %]	13	57%	13	57%
Practicing a relaxation method at least once a week [N, %]	0	0%	2	9%
Self-rated health (last 6 months)	6.9	2.6	7.5	2.6
Screened positive for depressive symptoms [N, %]	2	9%	5	22%
Screened positive for anxious symptoms [N, %]	3	13%	5	22%
CT Thorax/X-ray Bipulmonale infiltrates [N, %]	23	100%	22	96%
No. of patients with relevant comorbidities* [N, %]	18	78%	12	52%
Diabetes [N, %]	5	22%	4	17%
Hypertension [N, %]	12	52%	9	39%
Asthma [N, %]	4	17%	1	4%
Obesity (BMI>30) [N, %]	13	57%	13	57%
Medication at admission: total number	3.4	4.1	2.0	2.3
Asthma spray [N, %]	3	13%	2	9%
Beta-blocking agent [N, %]	7	30%	5	22%
IL-6 (pg/ml) at inclusion	29.7	12.4	33.9	11.8
CRP (mg/l) at inclusion	82.6	19.9	60.4	11.4
TNF-a (pg/ml) at inclusion	8.4	0.7	9.4	1.0
IL-1b (pg/ml) at inclusion	6.7	1.6	3.6	1.0
Number of COVID-19- and pneumonia-associated medication	2.8	1.0	2.3	1.3
In detail:				
Dexamethason [N, %]	21	91%	19	83%
Casirivimab/Imdevimab (monoclonal antibodies) [N, %]	5	22%	1	4%
Ruxcoflam [N, %]	5	22%	5	22%
Antiviral agent (Remdesivir) [N, %]	13	57%	11	48%
Antibiotics [N, %]	20	87%	17	74%
Virus variant				
Wildtype [N, %]	1	4%	1	4%
B 1.1.7 alpha [N, %]	11	48%	11	48%
Unknown [N, %]	11	48%	11	48%
Temporary COVID-19-only ward [N, %]	8	35%	8	35%
Ward for infectious diseases [N, %]	15	62%	15	65%
Hospital stay [days]	10.1	2.9	9.3	3.2

*cardiovascular, renal, respiratory, autoimmune disease, diabetes.

the clinical chemistry within four hours by accredited procedures to assess IL-6, CRP, and leucocytes and tumor-necrosis-factor alpha (TNF-α).

Four weeks after discharge, patients were contacted *via* telephone to assess symptoms and adverse events (follow-up). Follow-up was completed on July 22nd, 2021.

Measures

Oxygen saturation was measured with the pulse oximeter available at the ward for measurement on the finger. Only one blood sample measurement was included per day. If several blood samples were available, we included the measurement closest to 8am. Values below the detection limit (IL6<1.5 pg/ml, CRP < 0.6 mg/l, TNF-α < 8.1 pg/ml) were set to the value of the detection limit.

Breathing protocol adherence was defined as follows: if the breathing intervention was performed at least once autonomously and if the percentage of minutes in paced breathing were at least 50% of the required minutes, i.e., min. 30 minutes per day averaged over the whole stay. Treatment per protocol sample (TPP) included only those patients meeting the adherence criteria.

Adverse events were defined as transfer to ICU or death.

Screening for depressive and anxious symptoms was performed using the PHQ-4 (positive screening if sum score ≥ 3) (26).

Statistical analysis

The Institutional Review Board requested an adaptive design (power of 80% and an alpha of.05). After N=30, N=46 and N=60 of patients, the effect size can be calculated. The intervention can be stopped at N=46 if an effect size of greater than f^2=0.16 exists. After N=46, data were reviewed resulting in a significant effect size of f^2=0.11 (ITT) and f^2=0.14 (TPP). Considering the given seasonal circumstances (infection rate lowering, no further patient admissions) the study was discontinued mid of June 2021 to avoid delay (new patient admissions expected only five months later) and to limit the sample to one wave.

Statistics: For comparisons between the intervention and control group, chi square tests and the Mann-Whitney U test were used if appropriate. For repeated measurements (oxygen saturation, oxygen flow, breathing frequency), multilevel-mixed effect linear regression models were calculated.

Due to a skewed distribution, IL-6, TNF-α, leucocytes, and CRP were natural log-transformed prior to parametric statistical testing to better approximate Gaussian distribution. The level of significance was set *a priori* to p<.05 (two-sided). Data management and analysis were performed using STATA 15.1 SE (STATA Corp., College Station, Texas, USA).

Trial outcome analysis method

Per outcome, four multilevel mixed-effect linear regression models were calculated and compared, as recommended by a recently published best practice guidance for linear mixed-effects models (27). The covariance was set to unstructured. The first model included random effect only (on the individual level), the second additionally included the main fixed effects for group (IG vs. CG) and time (days since study inclusion). Since clinically meaningful differences existed between the study groups (see Table 1) additional covariates were also included. These were: relevant comorbidities (no vs. yes), COVID-19 pneumonia medication (count), and age (years). The third model additionally included the variable time to the random effect equation. The fourth model additionally included the interaction between group and time in the fixed effect part. The model fit was compared between these four models and parsimonious model improvement was tested using likelihood ratio tests (see Table 2). Additionally, information criteria (Akaike IC and Bayesian IC) were assessed.

These models were calculated for each outcome and each analysis sample (ITT and TPP). The analyses were restricted to a maximum of thirteen days after study inclusion, because afterwards no observations were available in the IG. This led to a deletion of three observations from three patients of the CG.

Post hoc analyses

Potential dose-response effects from categorized breathing minutes on daily IL-6 values were analyzed in all patients from the intervention group. Daily total breathing minutes were dichotomized at median value (45 minutes). Categorized minutes of breathing were related to blood samples from the following morning to retain temporal relationship. Two multilevel mixed-effect linear regression models were calculated for the primary outcome IL-6. The first model included the categorized practice time in the fixed effect part. The random effect part included the individual slopes as well as the binary practice time as cross-level interaction. Findings for analyses of end points other than the primary end point should be interpreted as exploratory due to the potential for type I error using multiple comparisons.

10.3389/fimmu.2022.928979

TABLE 2 Model comparison of intention-to-treat analysis by outcome (N = 46).

DV	Obs	Model Number	Model specification	Fixed Effects added	Random effects		Model fit				LR Test against nested		
					Subjects (ID)	Item (Day)	AIC	BIC	LL	dfmodel	df LR-test	X^2	Prob > X
IL-6 ln[pg/ml]	208 (min. 2, avg 4.5, max 10)	1	RE only	–	intercepts	–	684.1391	694.1518	-339.06957	3	–	–	–
		2	M1 + FE main effects	Group + Day	intercepts	–	682.5409	749.2917	-321.2705	20	17	35.60	0.0052
		3	M2 + RE	–	intercepts	intercepts	674.3049	747.7307	-315.1524	22	2	12.24	0.0022
		4	**M3 + Interaction**	**Group X Time**	**intercepts**	**intercepts**	**677.1227**	**793.9366**	**-303.5614**	**35**	**13**	**23.18**	**0.0395**
Leucocytes (ln[giga/l])	214 (min. 2, avg 4.7, max 10)	1	RE only	–	intercepts	–	195.8852	205.9832	-94.94262	3	–	–	–
		2	M1 + FE main effects	Group + Day	intercepts	–	127.7382	195.0577	-43.86911	20	17	102.15	<0.0001
		3	**M2 + RE**	**-**	**intercepts**	**intercepts**	**111.1439**	**185.1954**	**-33.57196**	**22**	**2**	**20.59**	**<0.0001**
		4	M3 + Interaction	Group X Time	intercepts	intercepts	124.6047	239.0478	-28.30233	34	12	10.54	0.5688
CRP (ln [mg/l])	222 (min. 2, avg 4.8, max 10)	1	RE only	–	intercepts	–	718.8937	729.1018	-356.4469	3	–	–	–
		2	M1 + FE main effects	Group + Day	intercepts	–	589.4273	657.4808	-274.7136	20	17	163.47	<0.0001
		3	**M2 + RE**	**-**	**intercepts**	**intercepts**	**504.5118**	**579.3707**	**-230.2559**	**22**	**2**	**88.92**	**<0.0001**
		4	M3 + Interaction	Group X Time	intercepts	intercepts	516.4878	635.5815	-223.2439	35	13	14.02	0.3722
TNF-α (ln [pg/ml])	151 (min. 1, avg 3.4, max 8)	1	RE only	–	intercepts	–	189.4543	198.5061	-91.72714	3	–	–	–
		2	M1 + FE main effects	Group + Day	intercepts	–	182.9308	243.2764	-71.46538	20	17	40.52	0.0011
		3	**M2 + RE**	**-**	**intercepts**	**intercepts**	**170.7575**	**237.1376**	**-63.37873**	**22**	**2**	**16.17**	**0.0003**
		4	M3 + Interaction	Group X Time	intercepts	intercepts	175.1232	274.6934	-54.5616	33	11	17.63	0.0905

df, degrees of freedom; DV, Dependent Variable; Obs, Observations in model (not Participants); LL, log-likelihood; LR-Test, Likelihood ratio test; AIC, Akaike's information criterion; BIC, Schwarz's Bayesian information criterion; X^2, CHI^2-value.
BOLD lines indicate favored model.

Results

Study population

Of 131 patients screened, 81 met exclusion criteria (see Figure 1). Main exclusion reasons were invasive procedures, trauma or acute myocardial infarction/stroke during the last four weeks (N=35, 43%), followed by high frailty and dementia (N=23, 28%) and insufficient knowledge of German language (N=16, 20%). Out of the remaining 50 patients, two patients (4%) were not willing to participate. A total of 48 patients (37% out of 131 patients screened) were randomized. Monitoring during the study revealed an exclusion criterion in two patients (severe COVID-19 pneumonia before study entry). Therefore, 46 patients (N=23 patients per group) were available for intention to treat (ITT) analysis. Seven patients in the intervention group practiced less than 50%. Two stopped because they had difficulties with the implementation of the breathing exercise in terms of concentration and technique. Two were transferred to ICU within two days of study entry due to deterioration of COVID-19 pneumonia. Three practiced continuously, but with shorter duration or less frequently, in total less than 50% of the required time. Thus, 16 patients of the IG and 23 of the CG entered the treatment per protocol (TPP) analysis.

Characteristics of the study samples are shown in Table 1. The study sample was between 23 and 83 years old (57 years ± 13 years), 60% were male. N=30 (65%) had relevant comorbidities. Only one patient was vaccinated against SARS-CoV, as vaccination capacity was very limited at that time in Germany. All patients showed pulmonary infiltrates in thoracic computer tomography. Mean hospitalization length was 9.8 ± 3.1 days (range 5-19 days).

Although no statistically significant differences were found between intervention and control group for baseline variables, clinically relevant differences were apparent. Patients in the intervention group were older (M=58.8 ± 13.2 vs. M=54.3 ± 13.4), had more relevant comorbidities (N= 18, 78% vs. N=12, 52%) and a higher amount of COVID-19- and pneumonia-associated medication during hospital stay (M=2.8 ± 1.0 vs. M=2.3 ± 1.3) (see Table 1).

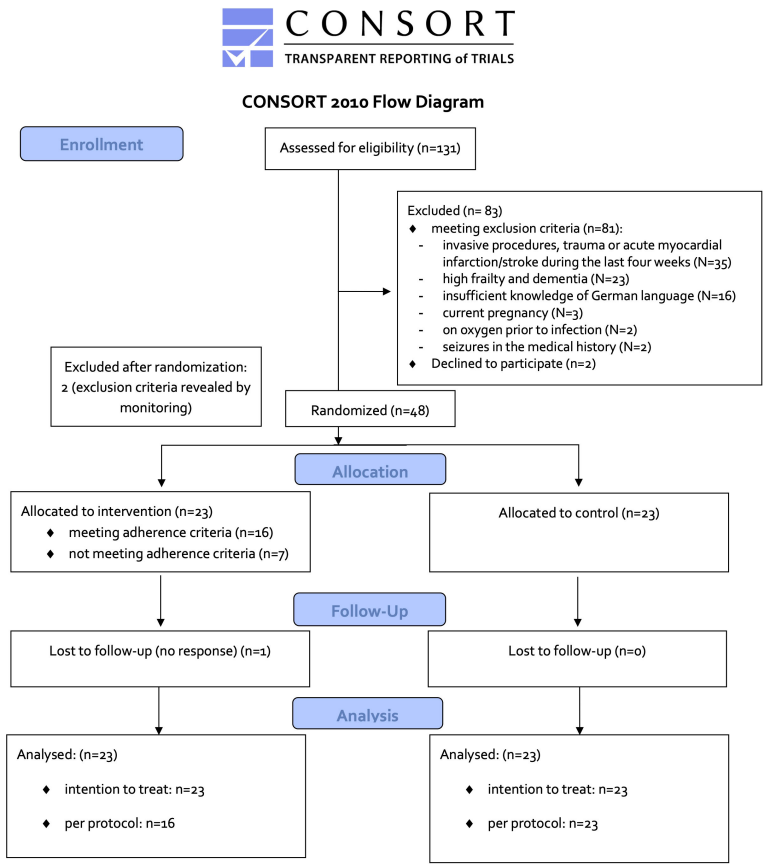

FIGURE 1
Flowchart Recruitment.

Primary outcome

Estimated marginal mean course of log-transformed IL-6 for all patients of the ITT-sample (N=46) is shown in Figure 2A. The prediction models included the covariates set to mean (relevant comorbidities (no/yes), count of COVID-19 pneumonia medication, and age (years). Multilevel fixed-effect linear regression models were compared using likelihood-ratio tests (see Table 2). These LR tests identified a random slope model with a group by time interaction as the superior model for IL-6 (LR $chi^2(13)=23.18$; p=.040). The graphical results of the model (marginal means displayed in Figure 1) on average show lower values of IL-6 in the IG (effect size Cohens $f^2 = 0.11$, LR-test p=.040). Per-protocol analysis (N=39) confirmed these results ($f^2 = 0.14$, LR-test p=.022).

Supplemental Table 1 and Supplemental Figure 1 showcase the change in the High and Low frequency bands of HRV from 5 minute resting phase pre-intervention, during intervention (4x 5 minutes) and 5 minute resting phase post-intervention. An increase in both frequency bands is observed during breathing intervention.

Secondary outcomes

Estimated marginal mean course of log-transformed leucocytes, CRP and TNF-α for all patients of the ITT sample (N=46) are shown in Figures 2B–D. The model comparison for the secondary outcomes Leucocytes, CRP and TNF-α showed no relevant group by time interaction (see Table 2).

Post hoc analyses

To further explore the relationship between slow-paced breathing and IL-6, we modeled a dose-response analysis using the daily minutes of slow-paced breathing to predict IL-6 of the next

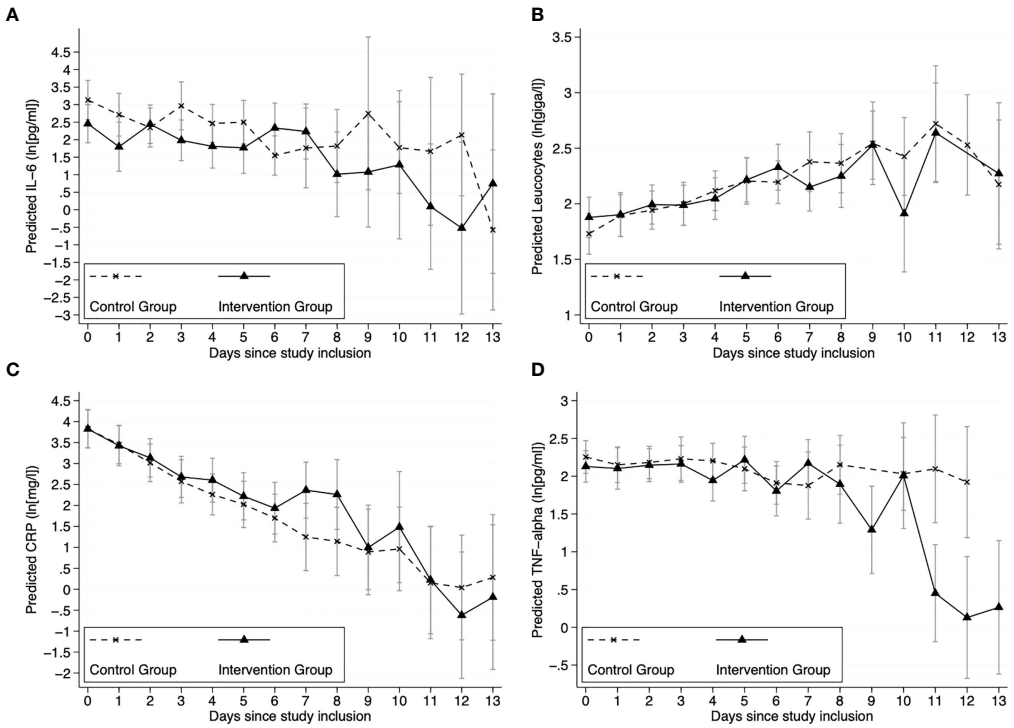

FIGURE 2
Trajectories of inflammatory outcomes. Marginal mean prediction of **(A)** ln(IL-6[pg/ml]), **(B)** ln(leucocytes[giga/l]), **(C)** ln(CRP[mg/l)] and **(D)** ln(TNF-α [pg/ml]) values for IG and CG from multilevel fixed-effect linear regression models with random slope (N = 46 individuals with N = 208 observations; average observations per individual=4.5). Note: Negative ln values translate to parameter values <1. Covariates: relevant comorbidities (no vs. yes), COVID-19 pneumonia medication (count), and age (years). Model predictions were calculated at covariate mean values.

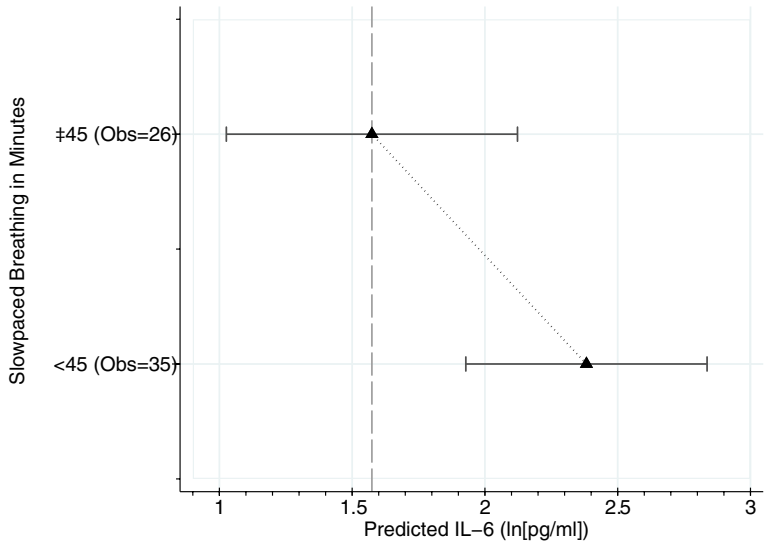

FIGURE 3
Dose response analysis using categorized breathing minutes from 22 patients and 61 days. Marginal mean values from multilevel mixed-effect linear regression models adjusted for relevant comorbidities (no vs. yes), COVID-19 pneumonia medication (count), and age (years). Prediction at covariate mean values. Obs. = Observations (Days of breathing practice).

day. Marginal mean values from adjusted multilevel mixed-effect linear regression models are shown in Figure 3. The model indicates a dose-response relationship with beneficial effects of practice time above 45 minutes a day (b=-.82, 95%CI lower -1.55; upper -.01).

Adverse events

Six patients (N=3, 13% in each study group) were admitted to the ICU, of whom one patient died (CG). All 23 patients practiced at least once. Most patients (N=18, 78%) managed the breathing exercise well. Nine patients (39%) reported the exercise at least from time to time as demanding. Two stopped due to difficulties with the implementation of the breathing exercise in terms of concentration and technique. There was one case of dizziness that resolved by reducing the depth of breathing slightly. Four out of the 23 patients (17%) who practiced at least once complained about coughing especially at the beginning of the exercise, and one had to stop the exercise once due to coughing. Weighted mean breathing frequency at rest was 18.5/min ± 4.5/min (range 10-30.5/min) for IG with no significant difference to the CG (M= 19.2/min ± 3.6/min, range 13.5-28.3/min; p=0.431. During the exercise, mean breathing frequency was 6.4/min ± 1.0/min (range 5.7-10/min) in IG. Six patients felt uncomfortable breathing at 6/min and had adjusted frequencies up to 10/min. 34 patients received nasal oxygen at least once during the hospital stay with a patient weighted mean flow of 1.9l ± 1.8l per min. Oxygen saturation was comparable between IG (95.1% ± 2.1%) and CG (94.7% ± 1.8%) at rest (p=0.444) but marginally increased during slow-paced breathing (95.4% ± 1.6%, p=0.003).

Discussion

This clinical trial of patients with moderate COVID-19 pneumonia showed that slow-paced breathing is effective to reduce IL-6 in COVID-19 pneumonia, though with uncertain clinical importance. Further, the data showed that reducing breathing frequency to 6/min is safe and feasible in moderate COVID-19 pneumonia and did not deteriorate oxygen saturation.

A non-invasive, non-pharmaceutical, not device dependent treatment option in COVID-19 disease has several advantages. The intervention may reduce plasma IL-6 levels without bearing potential side effects of administrated IL-6 receptor antagonists. Costs are low as no devices have to be bought or certified. The technique itself is easy to learn and the exercises can be supported *via* free apps on the patient's own smartphone. Therefore, the intervention can be scaled easily by training medical assistance staff that instructs the breathing techniques and supports first practice sessions. This would offer an access to a therapy option not only for industrial, but also for low-income countries.

Slow-paced breathing could be an additional treatment option for patients with moderate covid-19 pneumonia (www.rki.de/covid-19-therapie-stakob) who can still breathe independently. For severely and critically ill patients mostly receiving invasive ventilation, electrical VNS could be another treatment option that should be further evaluated.

Our data adds to the knowledge about the effect of VNS on inflammation marker. To our knowledge, this is the first study showing a statistically significant direct effect of non-invasive VNS *via* paced-breathing on IL-6 of the following day. The exploratory dose-response analysis proposes a linear relationship with more minutes in slow-paced breathing reducing IL-6 values more the next day. The dose necessary for this effect was 45 minutes of paced breathing a day at a breathing frequency of 6/min with an inhalation to exhalation ratio of 4:6. Though data about the effect of slow breathing in acute inflammation is scarce, the data available for the effect of interventions including slow breathing on IL-6 seems to depend highly on the frequency and duration, with an effect only in studies with at least half an hour of practice daily (28, 29). More detailed studies should further explore the necessary frequency, ratio and dose for a meaningful reduction in IL-6. In addition, the optimal time to start the intervention should be investigated. The patients in our study were already in an advanced stage of the disease. Intervention might be even more effective at the onset of symptoms. A randomized controlled trial in which patients were recruited immediately after PCR testing showed less dyspnea and higher aerobic capacity after 14 days in the breathing exercise group (30).

We cannot distinguish effects of VNS and placebo. Psychosocial interventions have been shown to affect the immune system (31). Though the amount of attention by study personnel was approximately the same in both groups, patients in the IG might have felt more self-efficient and this might have influenced their inflammatory marker. Though this effect would not be triggered by VNS, it would still originate in the central autonomic network and still, the anti-inflammatory pathway would be triggered drug- and device-free. From a patient's point of view, this is very important. We had a very high rate of patients willing to participate (97.6%) because most patients were very interested in a study that investigates a therapeutic approach without drugs and devices. Furthermore, most patients were very happy to perform the intervention because it was their only possibility to manage their disease. This alleviated their feeling of being helpless and without control, introducing the feeling of self-efficacy.

Limitations

The first limitation is the sample size that could not address clinical outcomes. Second, early discharge was not included in the model. Third, the intervention was not blinded. Another trial could include a sham intervention. Fourth, we did not control

objectively the amount of time spent in slow-paced breathing but relied on self-report.

Conclusion

This small, single-center randomized controlled clinical trial showed that reducing breathing frequency to 6/min is effective in reducing IL-6 levels in moderate COVID-19 pneumonia without relevant side effects. Larger RCTs need to confirm these results as well as evaluate clinical outcomes. This would offer access to a therapy option not only for industrial, but also for low-income countries.

Data availability statement

Data and analysis code underlying this study can be accessed through the OPen Access Repository of Ulm University and Ulm University of Applied Sciences (OPARU) at: http://dx.doi.org/10.18725/OPARU-44647. Data and analysis code are available under the terms of the Creative Commons Attribution 4.0 International (CC BY NC 4.0).

Ethics statement

The studies involving human participants were reviewed and approved by the Institutional Review Board of Ulm University (No. 3/21, 01/02/2021). The patients/participants provided their written informed consent to participate in this study.

Author contributions

Conceptualization: MJ and EB. Data curation: MJ and EMB. Formal analysis: MJ and EB. Investigation: EB, BG, SH, and MK-G. Methodology: MJ, EB, and JT. Project administration: EB, MJ, and BG. Resources: HG and BG. Software: EB, MJ, SH, and MK-G. Validation: EB, MJ, SH, and MK-G. Visualization: MJ and EB. Writing – original draft: EB and MJ. Writing – review & editing: EB, BG, SH, MK-G, JT, HG, and MJ.

Funding

No funding was received. The research cost and personnel costs were covered by internal funds of the Clinic for Psychosomatic Medicine and Psychotherapy, Clinic for Internal Medicine III, Division of Infectious Diseases, University Hospital Ulm, Germany

Acknowledgments

We thank the directors of the Clinic for Internal Medicine III, Prof. Hartmut Döhner, and Clinic for Internal Medicine I, Prof. Thomas Seufferlein, for their support in conducting this study. Special thanks to Andreas Binzberger, Jinny Scheffler, the ward physicians in charge, who supported us during study conduction. Thanks to Michael Holl, developer of the BreathBall App, for the inspiring interaction.

Conflict of interest

The authors declare that the research was conducted in the absence of any commercial or financial relationships that could be construed as a potential conflict of interest.

Publisher's note

All claims expressed in this article are solely those of the authors and do not necessarily represent those of their affiliated organizations, or those of the publisher, the editors and the reviewers. Any product that may be evaluated in this article, or claim that may be made by its manufacturer, is not guaranteed or endorsed by the publisher.

Supplementary material

The Supplementary Material for this article can be found online at: https://www.frontiersin.org/articles/10.3389/fimmu.2022.928979/full#supplementary-material

References

1. Madjid M, Safavi-Naeini P, Solomon SD, Vardeny O. Potential effects of coronaviruses on the cardiovascular system: A review. *JAMA Cardiol* (2020) 10:1–10. doi: 10.1001/jamacardio.2020.1286

2. Herold T, Jurinovic V, Arnreich C, Lipworth BJ, Hellmuth JC, von Bergwelt-Baildon M, et al. Elevated levels of IL-6 and CRP predict the need for mechanical ventilation in COVID-19. *J Allergy Clin Immunol* (2020) 146:128–36.e4. doi: 10.1016/j.jaci.2020.05.008

3. RECOVERY Collaborative Group, Horby P, Lim WS, Emberson JR, Mafham M, Bell L, et al. Dexamethasone in hospitalized patients with covid-19. *N Engl J Med* (2021) 384:693–704. doi: 10.1056/nejmoa2021436

4. Pinzon RT, Wijaya VO, Buana RB. Interleukin-6 (IL-6) inhibitors as therapeutic agents for coronavirus disease 2019 (COVID-19): A systematic review and meta-analysis. *J Infect Public Health* (2021) 14:1001–9. doi: 10.1016/j.jiph.2021.06.004

5. Shankar-Hari M, Vale CL, Godolphin PJ, Fisher D, Higgins JPT, Spiga F, et al. Association between administration of IL-6 antagonists and mortality among patients hospitalized for COVID-19: A meta-analysis. *JAMA - J Am Med Assoc* (2021) 326:499–518. doi: 10.1001/jama.2021.11330

6. Pavlov VA, Tracey KJ. Neural regulation of immunity: molecular mechanisms and clinical translation. *Nat Neurosci* (2017) 20:156–66. doi: 10.1038/nn.4477

7. Pavlov VA, Chavan SS, Tracey KJ. Molecular and functional neuroscience in immunity. *Annu Rev Immunol* (2018) 36:783–812. doi: 10.1146/annurev-immunol-042617-053158

8. Bonaz B, Sinniger V, Pellissier S. Vagus nerve stimulation: a new promising therapeutic tool in inflammatory bowel disease. *J Intern Med* (2017) 282:46–63. doi: 10.1111/joim.12611

9. Wang H, Yu M, Ochani M, Amella CA, Tanovic M, Susarla S. Nicotinic acetylcholine receptor α7 subunit is an essential regulator of inflammation. *Nature* (2003) 421:384–8. doi: 10.1038/nature01339

10. Williams DP, Koenig J, Carnevali L, Sgoifo A, Jarczok MN, Sternberg EM, et al. Heart rate variability and inflammation: A meta-analysis of human studies. *Brain Behav Immun* (2019) 80:219–26. doi: 10.1016/j.bbi.2019.03.009

11. Kevin J, Tracey KJ. Physiology and immunology of the cholinergic antiinflammatory pathway. *J Clin Invest* (2007) 117:230–44. doi: 10.1172/JCI30555

12. Poppe M, Wittig S, Jurida L, Bartkuhn M, Wilhelm J, Müller H, et al. The NF-κB-dependent and -independent transcriptome and chromatin landscapes of human coronavirus 229E-infected cells. *PloS Pathog* (2017) 13:1–29. doi: 10.1371/journal.ppat.1006286

13. Martin JLR, Martín-Sánchez E. Systematic review and meta-analysis of vagus nerve stimulation in the treatment of depression: Variable results based on study designs. *Eur Psychiatry* (2012) 27:147–55. doi: 10.1016/j.eurpsy.2011.07.006

14. Yuan H, Silberstein SD. Vagus nerve and vagus nerve stimulation, a comprehensive review: Part II. *Headache* (2016) 56:259–66. doi: 10.1111/head.12650

15. Kaniusas E, Szeles JC, Kampusch S, Alfageme-Lopez N, Yucuma-Conde D, Li X, et al. Non-invasive auricular vagus nerve stimulation as a potential treatment for Covid19-originated acute respiratory distress syndrome. *Front Physiol* (2020) 11:1–11. doi: 10.3389/fphys.2020.00890

16. Rangon C-M, Barruet R, Mazouni A, Cossec C, Thevenin S, Guillaume J, et al. Auricular neuromodulation for mass vagus nerve stimulation: Insights from SOS COVID-19 a multicentric, randomized, controlled, double-blind French pilot study. *Front Physiol* (2021) 12. doi: 10.3389/fphys.2021.704599

17. Boezaart AP, Botha DA. Treatment of stage 3 COVID-19 with transcutaneous auricular vagus nerve stimulation drastically reduces interleukin-6 blood levels: A report on two cases. *Neuromodulation* (2021) 24:166–7. doi: 10.1111/ner.13293

18. Nemechek P, Evlogiev I. Clinical immunology & research case Report : Successful treatment of COVID-19 ARDS with transcutaneous vagus nerve stimulation. *Clin Immunol Res* (2021) 5:1–6. Availablbe at: https://www.scivisionpub.com/pdfs/case-report-successful-treatment-of-covid19-ards-with-transcutaneous-vagus-nerve-stimulation-1953.pdf

19. Lehrer PM, Gevirtz R. Heart rate variability biofeedback: how and why does it work? *Front Psychol* (2014) 5:1–9. doi: 10.3389/fpsyg.2014.00756

20. Schwerdtfeger AR, Schwarz G, Pfurtscheller K, Thayer JF, Jarczok MN, Pfurtscheller G. Heart rate variability (HRV): From brain death to resonance breathing at 6 breaths per minute. *Clin Neurophysiol* (2020) 131:676–93. doi: 10.1016/j.clinph.2019.11.013

21. Laborde S, Allen MS, Borges U, Dosseville F, Hosang TJ, Iskra M, et al. Effects of voluntary slow breathing on heart rate and heart rate variability: A systematic review and a meta-analysis. *Neurosci Biobehav Rev* (2022) 138:104711. doi: 10.1016/j.neubiorev.2022.104711

22. Sevoz-Couche C, Laborde S. Heart rate variability and slow-paced breathing:when coherence meets resonance. *Neurosci Biobehav Rev* (2022) 135:104576. doi: 10.1016/j.neubiorev.2022.104576

23. Nolan RP, Floras JS, Ahmed L, Harvey PJ, Hiscock N, Hendrickx H, et al. Behavioural modification of the cholinergic anti-inflammatory response to c-reactive protein in patients with hypertension. *J Intern Med* (2012) 272:161–9. doi: 10.1111/j.1365-2796.2012.02523.x

24. Gerbarg PL, Jacob VE, Stevens L, Bosworth BP, Chabouni F, Defilippis EM, et al. The effect of breathing, movement, and meditation on psychological and physical symptoms and inflammatory biomarkers in inflammatory bowel disease: A randomized controlled trial. *Inflammation Bowel Dis* (2015) 21:2886–96. doi: 10.1097/MIB.0000000000000568

25. Morgan KL, Rubin DB. Rerandomization to improve covariate balance in experiments. *Ann Stat* (2012) 40:1263–82. doi: 10.1214/12-AOS1008

26. Löwe B, Wahl I, Rose M, Spitzer C, Glaesmer H, Wingenfeld K, et al. A 4-item measure of depression and anxiety: Validation and standardization of the patient health questionnaire-4 (PHQ-4) in the general population. *J Affect Disord* (2010) 122:86–95. doi: 10.1016/j.jad.2009.06.019

27. Meteyard L, Davies RAI. Best practice guidance for linear mixed-effects models in psychological science. *J Mem Lang* (2020) 112:104092. doi: 10.1016/j.jml.2020.104092

28. Djalilova DM, Schulz PS, Berger AM, Case AJ, Kupzyk KA, Ross AC. Impact of yoga on inflammatory biomarkers: A systematic review. *Biol Res Nurs* (2019) 21:198–209. doi: 10.1177/1099800418820162

29. Wang CH, Yang HW, Huang HL, Hsiao CY, Jiu BK, Lin C, et al. Long-term effect of device-guided slow breathing on blood pressure regulation and chronic inflammation in patients with essential hypertension using a wearable ECG device. *Acta Cardiol Sin* (2021) 37:195. doi: 10.6515/ACS.202103_37(2).20200907A

30. Rodríguez-Blanco C, Bernal-Utrera C, Anarte-Lazo E, Saavedra-Hernandez M, De-La-Barrera-Aranda E, et al. Breathing exercises versus strength exercises through telerehabilitation in coronavirus disease 2019 patients in the acute phase: A randomized controlled trial. *Clin Rehabil* (2022) 36:486–97. doi: 10.1177/02692155211061221

31. Shields GS, Spahr CM, Slavich GM. Psychosocial interventions and immune system function: A systematic review and meta-analysis of randomized clinical trials. *JAMA Psychiatry* (2020) 77:1031–43. doi: 10.1001/jamapsychiatry.2020.0431

frontiers | Frontiers in Immunology

TYPE Review
PUBLISHED 05 October 2022
DOI 10.3389/fimmu.2022.959209

OPEN ACCESS

EDITED BY
Rizgar A Mageed,
Queen Mary University of London, United Kingdom

REVIEWED BY
Robert Naeije,
Université libre de Bruxelles, Belgium
Morgan Salmon,
Michigan Medicine, University of Michigan, United States

*CORRESPONDENCE
Mariya M. Kucherenko
mariya.kucherenko@charite.de

†These authors have contributed equally to this work

SPECIALTY SECTION
This article was submitted to Inflammation, a section of the journal Frontiers in Immunology

RECEIVED 01 June 2022
ACCEPTED 14 September 2022
PUBLISHED 05 October 2022

CITATION
Liu S-F, Nambiar Veetil N, Li Q, Kucherenko MM, Knosalla C and Kuebler WM (2022) Pulmonary hypertension: Linking inflammation and pulmonary arterial stiffening. *Front. Immunol.* 13:959209. doi: 10.3389/fimmu.2022.959209

Pulmonary hypertension: Linking inflammation and pulmonary arterial stiffening

Shao-Fei Liu[1,2†], Netra Nambiar Veetil[1,2,3†], Qiuhua Li[1,2], Mariya M. Kucherenko[1,2,3*], Christoph Knosalla[2,3,4] and Wolfgang M. Kuebler[1,2,5,6,7]

[1]Institute of Physiology, Charité-Universitätsmedizin Berlin, Corporate Member of Freie Universität Berlin and Humboldt-Universität zu Berlin, Berlin, Germany, [2]German Centre for Cardiovascular Research (DZHK), Berlin, Germany, [3]Department of Cardiothoracic and Vascular Surgery, German Heart Center, Berlin, Germany, [4]Charité-Universitätsmedizin Berlin, Corporate Member of Freie Universität Berlin and Humboldt-Universität zu Berlin, Berlin, Germany, [5]German Center for Lung Research (DZL), Gießen, Germany, [6]The Keenan Research Centre for Biomedical Science, St. Michael's Hospital, Toronto, ON, Canada, [7]Department of Surgery and Physiology, University of Toronto, Toronto, ON, Canada

Pulmonary hypertension (PH) is a progressive disease that arises from multiple etiologies and ultimately leads to right heart failure as the predominant cause of morbidity and mortality. In patients, distinct inflammatory responses are a prominent feature in different types of PH, and various immunomodulatory interventions have been shown to modulate disease development and progression in animal models. Specifically, PH-associated inflammation comprises infiltration of both innate and adaptive immune cells into the vascular wall of the pulmonary vasculature—specifically in pulmonary vascular lesions—as well as increased levels of cytokines and chemokines in circulating blood and in the perivascular tissue of pulmonary arteries (PAs). Previous studies suggest that altered hemodynamic forces cause lung endothelial dysfunction and, in turn, adherence of immune cells and release of inflammatory mediators, while the resulting perivascular inflammation, in turn, promotes vascular remodeling and the progression of PH. As such, a vicious cycle of endothelial activation, inflammation, and vascular remodeling may develop and drive the disease process. PA stiffening constitutes an emerging research area in PH, with relevance in PH diagnostics, prognostics, and as a therapeutic target. With respect to its prognostic value, PA stiffness rivals the well-established measurement of pulmonary vascular resistance as a predictor of disease outcome. Vascular remodeling of the arterial extracellular matrix (ECM) as well as vascular calcification, smooth muscle cell stiffening, vascular wall thickening, and tissue fibrosis contribute to PA stiffening. While associations between inflammation and vascular stiffening are well-established in systemic vascular diseases such as atherosclerosis or the vascular manifestations of systemic sclerosis, a similar connection between inflammatory processes and PA stiffening has so far not been addressed in

the context of PH. In this review, we discuss potential links between inflammation and PA stiffening with a specific focus on vascular calcification and ECM remodeling in PH.

KEYWORDS

pulmonary hypertension, inflammation, vascular stiffness, vascular calcification, ECM remodeling

Introduction

Pulmonary hypertension (PH) comprises a group of diseases in which the mean pulmonary artery pressure (mPAP) exceeds 25 mmHg at rest according to current guidelines (1). Recently, the 6th World Symposium on PH has recommended to lower this cutoff further to 20 mmHg (2). The World Health Organization (WHO) classifies PH into five groups based on identifiable cause and risk factors (3). Although the treatment of pulmonary arterial hypertension (PAH) (WHO Group 1) has entered the stage of targeted therapy, the 5-year survival rate of patients with PAH is still only approximately 50% (4), presumably due to the multifactorial pathophysiological mechanisms of PAH, which evade targeting by a single pharmacological drug, in particular at the advanced disease stage (5). Therefore, identification and therapeutic targeting of common upstream mechanisms that trigger multiple downstream cellular and molecular processes governing pulmonary vascular remodeling in different PH groups remains the ultimate goal for an improved care of PH patients.

Lately, pulmonary perivascular inflammation has gradually gained increased attention as an early common hallmark across different PH groups. In the early stage of the disease, PAH patients and corresponding animal models not only display an accumulation of immune cells such as macrophages (6, 7) and mast cells (8) in their lungs (9), but also have elevated levels of inflammatory mediators in their pulmonary circulation (10, 11) (Figure 1). In most forms of PH, this inflammatory response is predominantly localized to the pulmonary adventitia (7). In fact, changes in the adventitia, which consists of a complex mix of heterogeneous cells, tend to precede those in other vascular compartments and are required for vascular remodeling (12). In PAH, this spatial predilection has been linked to the fact that fibroblasts in the pulmonary adventitia exhibit a pro-inflammatory phenotype with an increased expression of inflammatory mediators that drive the recruitment of innate immune cells (7, 13, 14). The resulting perivascular inflammation is now considered to constitute a critical pathomechanism orchestrating remodeling from the outside-in not only in PH associated with disorders of the immune system, such as connective tissue disease-associated pulmonary arterial hypertension (CTD-PAH) (15), but also in other forms of PAH (11, 16) as well as in PH due to left heart disease (PH-LHD) (17). In parallel, the adventitia releases a myriad of factors that regulate differentiation, proliferation, apoptosis, migration, and collagen synthesis by other cells in the vessel wall, while adventitial fibroblasts can transform to myofibroblasts and migrate into the intima through the medial layer (12). As such, it has been proposed that inflammatory processes alter vascular and immune cell metabolism, ultimately enhancing pulmonary artery (PA) remodeling and aggravating PH (Figure 1).

Concomitantly over the past decade, PA stiffening has emerged as an early hallmark, pathomechanism, and predictor of morbidity and mortality in PH (18–20). Vascular stiffening, defined as increased resistance of the arterial wall to deformation during blood influx, is a consequence of pathological vascular remodeling that can occur in both large proximal arteries and small distal arteries and arterioles. The mechanical consequences of these structural changes are decreased compliance in proximal PAs, and increased resistance to blood flow (pulmonary vascular resistance, PVR) in distal PAs (21). PA compliance (PAC) is essential to transform the pulsatile blood flow that enters the large conduit arteries *via* the Windkessel effect into the nearly laminar flow at the level of the distal pulmonary vascular tree. As such, PAC reduces right ventricular (RV) afterload and maintains near-constant lung perfusion over the cardiac cycle. In line with the impact of PAC for RV function, invasive or non-invasive assessment of PAC (or capacitance) has revealed PA stiffening in PAH patients as a sensitive predictor of pathological RV remodeling and mortality (21–24). It has further been proposed that stiffening of proximal PAs, through elevation of pulse-wave velocity and the shear stress exerted by the blood, promotes injury and remodeling in distal vessels, thus driving the pathology of PH in a positive feed-forward loop (25). Such interdependency between proximal and distal PA regions would predict that pathological remodeling should occur in parallel in large and small vessels. Indeed, work by Stuart R. Reuben first identified a hyperbolic relationship between PAC and PVR (26). The product of PAC × PVR yields the resistance–compliance (RC) time, which is considered to remain almost constant in PH patients of WHO class I (PAH), III (PH due to chronic lung

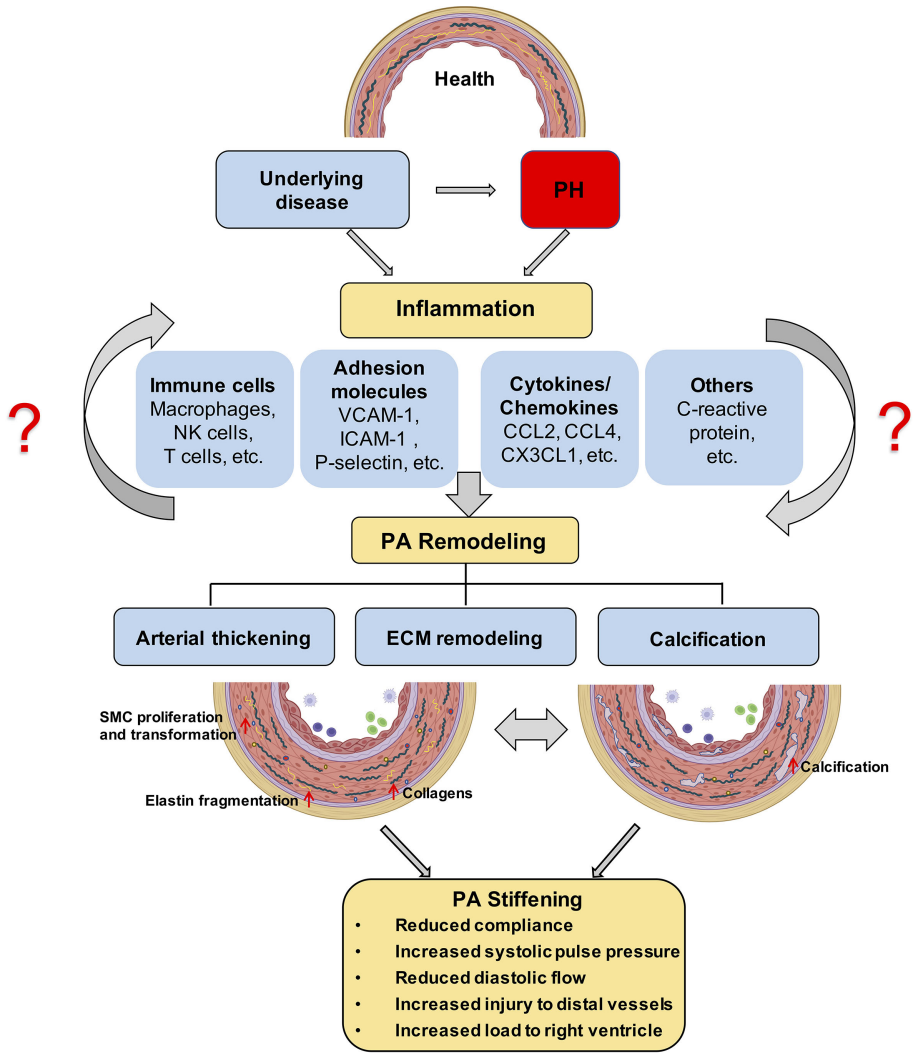

FIGURE 1
Proposed role of inflammation in PA stiffening; The development of PH is associated with an inflammatory response in the pulmonary vasculature, characterized by immune cell infiltration and the secretion of immune factors. ECM stiffening, especially proximal large pulmonary vascular sclerosis, occurs in the early stages of PH and has a prognostic value for patient outcome and later calcification, and is driven by inflammation. Prolonged angiosclerosis, in turn, further promotes an inflammatory response that exacerbates pulmonary vascular calcification and thickening. PH, pulmonary hypertension; ECM, extracellular matrix; PA, pulmonary artery.

disease), IV (chronic thrombo-embolic PH), or V (PH with unclear multifactorial mechanisms) and independent of medical therapy (27). Interestingly, however, for patients with WHO class II PH (PH due to left heart disease), RC time is reduced, i.e., for any given PVR, the corresponding PAC is lower as compared to PH patients from other causes. Notably, this reduction in RC time is also associated with an increase in RV afterload (27). This interesting finding may indicate distinct pathomechanisms and/or a higher degree of stiffening in proximal PAs in PH patients with underlying left heart disease as compared to other forms of PH; yet, this notion remains to be rigorously tested and mechanistically explored.

Conversely, mechanical communication between proximal PAs and the distal pulmonary vasculature may also promote restoration of pulmonary vascular homeostasis. Evidence of such a reverse remodeling process derives from a few clinical studies in patients with congenital heart disease and PH due to intracardiac left-to-right shunts causing lung overperfusion. In these patients, surgical banding of the PA—performed with the intent to protect the proximal PA from excessive pressure and flow—could successfully improve PH and, in some cases, reverse vascular remodeling in distal arteries (28, 29).

A growing number of studies reporting techniques to estimate stiffness of proximal PAs *in vivo* show promise for

the use of PA stiffness estimates as a prognostic tool in PH. Most commonly, PA stiffness is estimated by calculation of pulmonary arterial capacitance as ratio of stroke volume over pulmonary pulse pressure, assessed by either cardiac catheterization or non-invasively by echocardiography (20, 30–37), or by calculation of a stiffness index as change in PA pressure (again assessed by right heart catheterization) divided by the corresponding change in PA diameter (determined by real-time imaging modalities, such as cardiac magnetic resonance imaging) (18, 38).

Artery stiffening in cardiovascular disease is mainly attributed to remodeling of the extracellular matrix (ECM) and/or calcification within the arterial wall (39–42) (Figure 1). In particular, PAH is characterized by remodeling of the ECM and thickening of all three layers of the PA wall (43), which ultimately reduces arterial compliance. PAs of PAH patients exhibit an increased deposition of interstitial collagen, including collagen I, collagen XIV, and basement membrane-specific collagens, especially collagen IV (43–45). Additionally, increased expression of other ECM proteins such as elastin and fibronectin, or the matricellular ECM protein tenascin-C by dedifferentiated adventitial fibroblasts has been reported in PAH patients (46). Increased production and deposition of ECM constituents in PAs is considered to occur as an adaptive response to increased digestion of medial and basement membrane (BM) ECM by matrix metalloproteinases (MMPs), which have been found to be increased in PAH (47) and IPAH patients (45). The elevated expression of collagens by endothelial cells (ECs), smooth muscle cells (SMCs), and adventitial fibroblasts is associated with increased collagen-cross-linking by lysyl oxidases (LOXs) (48). In addition, proteolytic enzymes also induce degradation of elastic fibers, which are challenging to rebuild despite increased elastin gene expression due to the multicomponent complex 3D structure of these fibers (49–53). As such, PA stiffening emerges as a progressive imbalance of collagen over elastin fiber components in the PA wall.

Vascular stiffening has also been attributed to vascular calcification (40), a pathological deposition of solid minerals within the intima or media of arterial walls (54) (Figure 1). Importantly, pulmonary vascular calcification has been associated with transdifferentiation of SMCs into osteogenic-like lineages, driven by the activity of the pro-osteogenic transcription factor Runt-related transcription factor 2 (RUNX2) (55). As such, increased nuclear expression of RUNX2 in PA SMCs not only activates expression of calcification-related biomineralization genes (56), but also promotes cell proliferation and resistance to apoptosis by activating hypoxia-inducible factor-1α (HIF-1α) (55).

Stiffening of proximal PAs in PAH patients (18, 57) increases pulse pressure and shear stress in the pulmonary vasculature. Of relevance, these alterations in biomechanical forces acting upon the lung vascular wall can induce pro-inflammatory responses in ECs of distal PAs (58, 59) and promote the aggregation of immune cells (58). This includes inflammatory cell recruitment and release of immune-cell-derived cytokines, such as IL-6 (60, 61) and TNF (62) and bioactive enzymes, including MMPs (46), which may, in turn, promote vascular remodeling and stiffening processes, thus establishing a progressive vicious cycle. Such interplay between inflammation-triggered signaling events that, in turn, initiate wound healing processes and ECM remodeling, ultimately culminating in tissue fibrosis and scar formation, is well established in cardiac and systemic vascular diseases (63–65). In PH, however, the cause–effect relationship between inflammatory signaling and vascular stiffening has so far neither clinically nor experimentally been addressed. As such, the present review aims to link known inflammatory responses in PH to processes related to vascular stiffening, namely, ECM remodeling and vascular calcification, identified in either PH or other vascular diseases and *vice versa*. Proposed links and relevant literature are summarized in Table 1 and will be discussed in detail below. As such, we intend to highlight the potential relevance of a pathophysiological axis between inflammation and PA stiffening, and to incite mechanistic studies to address this conceptual gap in our present understanding of PH.

Inflammation-induced arterial wall thickening and ECM remodeling

PA stiffening and inflammatory responses are both paramount characteristics of PH. While inflammation is commonly associated with PH in both animal models and clinical scenarios, little is known about the role of inflammation in inducing vascular remodeling in PH. Only a limited number of studies have so far addressed the role of inflammation in promoting the production of ECM components (154), namely, collagens (155), fibronectin (156), and tenascin-C (156) in PH. Yet, in other cardiovascular diseases, the connection between inflammation and increased vascular stiffness has been better characterized: here, inflammatory processes have been shown to promote arterial stiffening through a variety of mechanisms, including the induction of endothelial dysfunction and BM stiffening, increased proliferation of SMCs (49)—resulting in arterial wall thickening and reduced compliance—and remodeling and stiffening of the ECM in different segments of the arterial wall.

In PH, elevated pressure and high pulsatile flow as a consequence of reduced vascular compliance can be sensed by ECs of the pulmonary vascular bed. Specifically in hypoxia-induced PH, ECs produce elevated levels of the inflammatory cytokines IL-1β (9) and IL-6 (9, 60), and express increased levels of immune cell adhesion molecules including vascular cell adhesion molecule-1 (VCAM-1), intercellular adhesion molecule-1 (ICAM-1), and P-selectin (9). Concomitantly, other vascular resident cells, such as SMCs and fibroblasts,

TABLE 1 Inflammatory mediators associated with vascular stiffening.

Cytokines, immune cells, and adhesion molecules in PH				Regulation of vascular stiffening-related pathways
Category/name		**Cell/tissue type of increased mediator abundance in PH patients/animal models**	**WHO-defined PH group**	
Cytokines	IL-1β	Lung (66–69), Plasma (70), Fibroblasts (71), CTEPH-EC (72)	I (68, 69, 71), III (66, 67, 70), IV (72)	**Atherosclerosis** IL-1β is associated with calcium content and calcification of the aortic wall (73). **Cardiovascular disease** IL-1β and TGF-β initiate the transdifferentiation of cardiac fibroblasts to myofibroblasts that produce elevated levels of collagens after cardiac injury (74). **Aortic calcification** IL-1β and TNF modulate EndoMT of aortic ECs and make ECs more sensitive to osteogenic transdifferentiation by BMP-9 *in vitro*, predominantly by reducing BMPR2 expression and increasing JNK signaling (75).
	IL-2	Plasma (76)	I (76)	**Aortic stiffening** In mice, IL-2 reduces angiotensin II-mediated inflammation and aortic stiffening *via* activation of $CD4^+CD25^+Foxp3^+$ regulatory T cells (77).
	IL-6	Plasma (70, 76, 78–80), Lung (61, 66–69, 81–83), Serum (16, 61, 84, 85), SMC (84), Pulmonary veins (61), PA (61), Exhaled breath condensate (85), Fibroblast (71)	I (16, 68, 69, 71, 76, 79, 80, 83, 84), II (61, 81), III (66, 67, 70, 78, 82, 85)	**IL-6 in PH-LHD** In a rat model of PH-LHD, macrophage accumulation and increased IL-6 production were observed in the lung (8, 81). IL-6 activates STAT3 signaling, inducing PA SMC overproliferation (81). **IL-6 and calcification in PAH** MicroRNA-204 regulates BRD4 expression, which upregulates IL-6 and drives vascular calcification in PAH (86, 87). **Coronary artery disease (CAD)** CAD patients have increased osteoprotegerin, osteopontin, and IL-6 levels in serum (88). **Hypertension-induced aortic stiffening** Positive correlation between IL-6 and aortic stiffness (89) **Arterial stiffening in chronic kidney disease (CKD)** IL-6 levels in patient plasma are positively correlated to arterial wall stiffness (90). **Vascular remodeling in PH** IL-6 promotes SMC proliferation and migration in PH, leading to medial wall thickening in distal PAs (60). IL-6 upregulates MMP-expression in PH, promoting ECM remodeling (60). IL-6 depletion attenuates lung vascular remodeling in a rat MCT model of PH (8).
	IL-10	Plasma (79, 80, 91), Lung (69)	I (69, 79, 80), IV (91)	**Aortic stiffness** IL-10 knockout mice develop aortic stiffening due to increased COX-2 activity and resulting thromboxane A2 receptor activation (92).
	IL-12	Plasma (79, 93), Serum (94, 95)	I (79, 93–95)	**Atherosclerotic cardiovascular disease** In CVD patients, IL-12 serum levels positively correlate with arterial stiffness (96).
	IL-17	Lung (83), Plasma (79), CD4+T cell (97)	I (79, 83), III (97)	**Psoriasis** IL-17 increases aortic stiffness by reducing lipoprotein trafficking (98).
	TNF	Plasma (70, 99–101), Lung (61), Serum (61, 102), Pulmonary veins (61), PA (61), EC (103)	I (100, 101), II (61), III (70), IV (99, 102)	**Aortic calcification** TNF induces osteoblast markers and enhanced osteoblast differentiation and calcification in bovine aortic SMCs by activation of the cAMP pathway (104). **Psoriasis** The anti-TNF monoclonal antibody adalimumab reduces carotid arterial stiffness (105). **Estrogen deficiency in postmenopausal women** The TNF inhibitor etanercept reduces carotid arterial stiffness (106). **Inflammatory artheropathies** In a controlled clinical study, patients with rheumatoid arthritis, ankolysing spondylitis, and psoriatic arthritis that received anti-TNF

(Continued)

TABLE 1 Continued

Cytokines, immune cells, and adhesion molecules in PH				Regulation of vascular stiffening-related pathways
Category/name		**Cell/tissue type of increased mediator abundance in PH patients/animal models**	**WHO-defined PH group**	
				therapies (either adalimumab, ethanarcept, or infliximab) exhibited less aortic stiffness, assessed by aortic pulse wave velocity and augmentation index (107)
	IL-4	Lung (108), Plasma (79, 109)	I (79, 108), III (109)	Not studied in the context of vascular stiffening
	IL-7	Plasma (79)	I (79)	
	IL-8	Exhaled breath condensate (85), Plasma (79, 80), EC (72, 103)	I (79), III (85), IV (72, 80)	
	IL-13	Lung (108), Plasma (109)	I (108), III (109)	
	IL-18	Lung (66, 110)	III (66, 110)	
	IL-21	Lung (82)	III (82)	
	IL-33	Lung (111, 112), Serum (113)	I (111, 112), III (113)	
	IFN-γ	Plasma (76, 109)	I (76), III (109)	
	CCL2 (MCP-1)/CCR2	Lung (114), SMC (115), Macrophage (115, 116), Fibroblast (71), CTEPH-EC (72), Plasma (91, 99)	I (71, 115, 116), III (114), IV (72, 91, 99)	**Hypertension-induced aortic stiffness** Positive correlation between MCP-1 levels in patient plasma and aortic stiffness estimated by echocardiography (89). **Arterial stiffening in chronic kidney disease (CKD)** Positive correlation between angiopoietin-2 in serum of CKD patients and aortic stiffness. Angiopoietin-2 induces CCL2 in ECs (117)
	CCL7/CCR7	Plasma (79), Serum (94), Fibroblast (71)	I (71, 79, 94)	**Abdominal aortic stiffness** HIF-1α deficiency in vascular smooth muscle cells suppresses CCL7, which increases macrophage infiltration (118).
	CX3CL1/CX3CR1	Lung (114), Serum (94)	I (94), III (114)	Not studied in the context of vascular stiffening
	CCL4	Plasma (79)	I (79)	
	CCL5 (RANTES)/CCR5	PAEC (119), Plasma (79), PASMC (115, 120), Macrophages (115), Fibroblasts (71), Lung (121), CTEPH-EC (72), PAH-EC (122)	I (71, 79, 115, 119–122), III (120), IV (72, 91, 99)	
	CCL11	Plasma (79)	I (79)	
	CCL12 (SDF-1)	Fibroblasts (71), Lung (121)	I (71, 121)	
	CXCR1	Lung (121)	I (121)	
	CXCR4/CXCL12	Fibroblasts (71), Lung (123, 124)	I (71, 123), III (123, 124)	
	CXCL9	Plasma (80)	I (80), IV (80)	
	CXCL13	Plasma (80), Serum (125)	I (80, 125), IV (125)	
	CD40	Fibroblasts (71), Serum (126), Lung (127)	I (71), III (126), I, III (127)	
Immune cells	Macrophages	Bone marrow (128), Lung (81, 129, 130), CTEPH-EC (131, 132), Alveoli (128), Blood (133)	I (115, 128, 129, 133, 134), II (81), III (130), IV (131, 132)	**PAH** Infiltrated macrophages express MMP-10, resulting in ECM remodeling and PA stiffening (47). **Thoracic aorta stiffening in CKD** ETA receptor blockade reduces macrophage infiltration, aortic stiffness and calcification in rats (135). **Aortic stiffness in obesity** Peroxisome proliferator-activated receptor γ (PPARγ) activation by pioglitazone attenuates MMP-12 in macrophages *in vitro*, and reduces aortic stiffness *in vivo* (136). **Aortic stiffness in abdominal aortic aneurysm** Angiotensin II promotes the recruitment of M2-like macrophages in the

(Continued)

TABLE 1 Continued

Cytokines, immune cells, and adhesion molecules in PH				Regulation of vascular stiffening-related pathways
Category/name		Cell/tissue type of increased mediator abundance in PH patients/animal models	WHO-defined PH group	
				aorta of IL12p40-deficient mice, which promote medial remodeling and aortic stiffening through increased TGF-β production (137).
	$CD4^+CD25^+Foxp3^+$ regulatory T cells	Plasma (76)	I (76, 138), III (139)	**Aortic stiffening** *In vivo* $CD4^+CD25^+Foxp3^+$ regulatory T-cell stimulation in mice reduces angiotensin-II mediated aortic remodeling and stiffening (77).
	NK cells	Plasma (76), CTEPH-EC (132), Blood (140)	I (76, 140), IV (132)	**PA calcification** Granzyme B from nature killer cells increases calcification in smooth muscle cells (SMCs) under hypoxia (141)
	T cells	Plasma (76) Lung (142)	I (76), III (142)	**HIV-related arterial stiffening** $CD4^+$ and $CD8^+$ T-cell exhaustion is associated with arterial stiffness (143).
	Neutrophil cells	Blood/bone marrow (144)	I (144), III (144)	**Vasculature stiffening** Oxidized low-density lipoprotein (OxLDL) and stiffer substrates promote neutrophil transmigration *in vitro* (145)
	Mast cells B cells Dendritic cells Eosinophils	Lung (8, 146–148), CTEPH-EC (132), Blood (149) Lung (8) Lung (69) Lung (150)	I (8, 147–149), II (8, 146), III (8), IV (132) I (8) I (69) I (150)	Not studied in the context of vascular stiffening
Other mediators	C-reactive protein (CRP)	Plasma (91, 99, 116)	I (116), IV (91, 99)	**Arterial stiffening** Higher CPR levels are associated with increased arterial stiffness (151).
	Intercellular adhesion molecule-1 (ICAM-1)	Plasma (93)	I (93)	**Arterial stiffening in CKD** Plasma angiopoietin-2, which induces ICAM-1 in ECs (117), correlates with arterial stiffness in CKD. **Matrix stiffness** Stiff matrices induce ICAM-1 clustering in ECs, which promotes immune cell recruitment (152).
	Vascular cell adhesion molecule-1 (VCAM-1)	Plasma (93), Fibroblasts (71), Lung (121), CTEPH-EC (72)	I (71, 93, 121), IV (72)	**Atherosclerosis** MicroRNA-1185 correlates with arterial stiffness and VCAM-1 expression (153).
	Macrophage inflammatory protein-1α	Plasma (91)	IV (91)	Not studied in the context of vascular stiffening

respond to biomechanical cues by altered secretion of immune factors including inflammatory cytokines such as monocyte chemoattractant protein-1 (MCP-1), stromal cell-derived factor 1, and CCR5 (71) (Table 1). These inflammatory mediators can, in turn, induce PA remodeling and stiffening (9, 71, 157). While the links between increased inflammation and PA remodeling are so far little understood in PH, we will delineate in the following existing connections between key inflammatory signals and vascular stiffening in systemic cardiovascular diseases, with the aim to translate this knowledge into an advanced understanding of the potential role of inflammation in PA stiffening in PH.

Several key inflammatory signals induce PA remodeling by dysregulating the behavior and function of both ECs and SMCs in PH, ultimately leading to arterial wall thickening and stiffening. Among these, IL-6 and TNF were found to be increased in plasma, lung, pulmonary arteries and veins, as well as in PA ECs in both patients and animal models of various PH groups (Table 1). In PAH patients (60) and in PH-LHD rat models (61, 81), IL-6 contributes to PA remodeling by inducing medial wall thickening *via* SMC proliferation and muscularization of the distal pulmonary arterial tree due to migration of SMCs into precapillary arterioles (60, 61, 81) (Table 2; Figure 2), potentially affecting arterial compliance by increased wall thickening. In the pulmonary adventitia, fibroblasts activate recruited macrophages through paracrine IL-6 signaling, initiating a pro-inflammatory and pro-fibrotic phenotype that is associated with an increased inflammatory response and vascular remodeling in PH (7). Notably, IL-6 is a sensitive marker for systemic inflammation in cardiovascular

TABLE 2 Potential links between factors associated with PA stiffening and immune responses in PH.

Factors associated with PA stiffening	Potential link to immune responses in PH
Caveolin-knockout mice show increased PA stiffness (158).	Caveolin-1 inhibits adventitial macrophage-induced inflammation in mouse aortic vessels (159).
5-HT inhibition prevents hypoxia-induced PH and vascular remodeling of PAs in mice (160).	5-HT is widely expressed on immune cells such as dendritic cells, and triggers the release of IL-1 and IL-6 (161).
SMC overproliferation causes arterial thickening and distal PA muscularization leading to arterial stiffening in PH mice (60).	IL-6 overexpression in inflammation triggers SMC hypertrophy in PAs (60).
MMP-overexpression and activation lead to degradation of elastin fibers in the PA wall and arterial stiffening in PAH patients (162).	Activated macrophages secrete MMP-2 (162), MMP-9 (162), MMP-10 (47), and MMP-19 (6, 154) in PAH. IL-6 upregulates MMP-9 expression in SMCs in PAH (60).
Myofibroblasts in PH overexpress ECM components (i.e., collagens, fibronectin, tenascin-C, etc.) (163).	TGF-β increases collagen, fibronectin, and tenascin-C production by SMCs and fibroblasts (43). IL-6 and TGF-β induce differentiation of fibroblasts to myofibroblasts (21, 46, 71).

disease (60, 88). In rheumatoid arthritis (164) and acute ischemic stroke (165), elevated levels of IL-6 in patient serum were associated with aortic stiffening as estimated by pulse-wave velocity, which could be significantly reduced by therapeutic infusions of the anti-IL-6 receptor antibody tocilizumab (164).

Similarly, elevated TNF in rodent models of PAH and PH-LHD has been shown to result in increased PA EC and SMC proliferation and medial wall thickening (61, 166), which have been attributed to suppressed BMPR-II signaling in PAH (166). Due to its effects on SMC hyperplasia, TNF may also promote PA stiffening in PH; however, direct correlations between TNF levels and PA stiffness in PH have yet to be established. In other cardiovascular and inflammatory diseases, e.g., arteriosclerosis, TNF is an established key mediator of vascular remodeling (61, 62). Patients with inflammatory artheropathies, namely, rheumatoid arthritis, ankylosing spondylitis, and psoriatic arthritis, who received anti-TNF treatment with either adalimumab, etanercept, or infliximab, showed a reduction in aortic stiffness as assessed by pulse-wave velocity and augmentation index as compared to untreated controls (107, 167). Hence, pharmacological inhibition of inflammatory mediators such as IL-6 and TNF in PH could potentially reduce pulmonary vascular cell proliferation and PA thickening and may therefore present a targeted therapy for PA stiffening.

Furthermore, pro-inflammatory mediators can induce vascular stiffening in cardiovascular diseases by increased production of ECM components, namely, fibrillar and non-fibrillar collagens and fibronectin by resident vascular cells (168). After myocardial infarction as well as in ischemic and non-ischemic heart failure, pro-inflammatory mediators such as TGF-β (74, 169) and IL-1β (170) induce the conversion of fibroblasts into myofibroblasts, which can produce abundant ECM proteins (168) (Tables 1, 2; Figure 2). In PH, adventitial myofibroblasts contribute to PA remodeling and stiffening (46) *via* the production of structural ECM components such as collagens, elastin, fibronectin, and dynamic ECM constituents, including tenascin-C and osteopontin (43, 46, 74) (Table 2; Figure 2). Tenascin-C and osteopontin, in turn, increase fibroblast and SMC proliferation, contributing to myofibroblast conversion and medial thickening, and therefore vascular stiffening (43, 46, 171) (Figure 2). Activated macrophages recruited to the pulmonary adventitia may express ECM proteins such as collagen type I, thereby contributing to ECM stiffening in PH (172). In animal models of MCT-induced PH, NADPH oxidase 4 (Nox4) has also been found to be upregulated in the pulmonary adventitia, where it promotes TGF-β-mediated expression of matrix collagens by adventitial fibroblasts and, as such, ECM stiffening (172). Similarly, collagen deposition by resident fibroblasts into the adventitia was also found to be increased in an animal model of chronic hypoxic PH and resulted in a thicker and stiffer arterial wall (172–174). In order to form insoluble rigid fibers, excessive fibrillar collagens are then further cross-linked by cross-linking enzymes (43, 175). Specifically, elevated expression of LOX in SMCs and lysyl oxidase-like enzyme (LOXL) expression in adventitial fibroblasts leads to increased collagen cross-linking and PA stiffening in PAH (176). Moreover, adventitial fibroblasts *per se* exhibit a pro-inflammatory phenotype in PH, including the recruitment and activation of adventitial macrophages (7) and production of pro-inflammatory markers, such as the chemokines MCP-1, SDF-1, RANTES/CCR5, CCR7, CXCR4, and the co-stimulatory molecules CD40 and CD40L (7, 71). This secretory activity can, in turn, create another feedback loop that triggers further inflammation and, hence, ECM remodeling.

Apart from elevated levels of circulating inflammatory mediators, increased mPAP in PH also induces activation of the pro-inflammatory NF-κB signaling pathway in PA ECs and SMCs (58, 133, 157) (Figure 2). Based on studies in systemic cardiovascular diseases, such activation of NF-κB emerges as a potentially important step in PA stiffening. As such, nuclear NF-κB was shown to increase the expression of aortic collagen type I in a murine model of type 2 diabetes, resulting in aortic stiffening

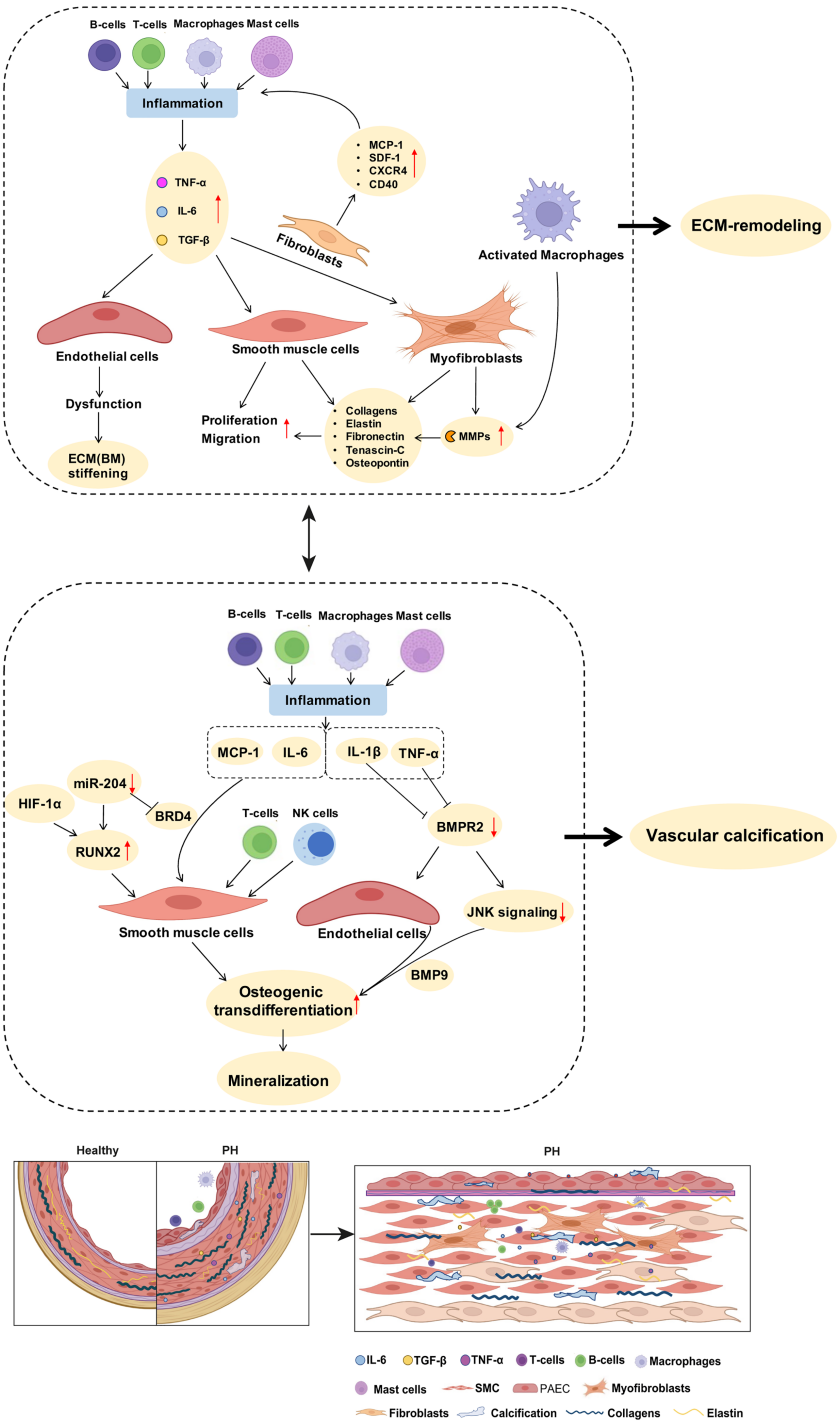

FIGURE 2
Potential links between inflammatory mediators and mechanisms of pulmonary arterial ECM remodeling and vascular calcification in PH. As described in detail in the manuscript text, perivascular accumulation of immune cells is a characteristic feature of PH. Inflammatory cells such as macrophages produce MMPs that promote ECM degradation and remodeling. Inflammatory cytokines such as IL-6 and TGF-β drive the proliferation of PA SMCs. Stimulation of fibroblasts by inflammatory mediators increases the expression of collagens, elastin, and fibronectin, further promoting PA stiffness. Activated immune cells and inflammatory mediators promote SMC transdifferentiation and enhance the expression of biomineralization genes, thus driving vascular calcification. BMPR2 downregulation, especially in response to the inflammatory factor TNF, promotes endothelial cell mesenchymalization and may as such contribute to the development of pulmonary vascular calcification. A detailed discussion of the proposed signaling pathways is provided in the manuscript text. ECM, extracellular matrix; MMPs, matrix metalloproteinases; SMC, smooth muscle cells; PH, pulmonary hypertension; PA, pulmonary artery; BM, basement membrane.

as measured *ex vivo* by pressure myography (177). Interestingly, these effects were mediated by an NF-κB-dependent overexpression of RUNX2, a key transcription factor relevant not only for ECM remodeling [through increased expression of ECM collagens by SMCs (177)], but also in the context of vascular calcification (55, 177) (as discussed below) (Figure 2). It may be speculated that activation of NF-κB could exhibit similar effects in PH, thus contributing to PA stiffening through ECM remodeling and vascular calcification.

Inflammation-induced overproduction of ECM components in cardiovascular diseases is rivaled by elevated proteolytic ECM degradation *via* a parallel increase in MMPs (46). In PH, activated macrophages and myofibroblasts in the adventitia secrete MMPs, specifically MMP-2 (154, 162), MMP-9 (6, 162), MMP-10 (47), and MMP-19 (6, 154), while tissue inhibitors of metalloproteinases (TIMPs) appear downregulated (46, 162) (Table 2; Figure 2). MMP-2 (50) and MMP-9 (49) degrade elastin, thereby decreasing vessel compliance, resulting in arterial stiffening (49–52). Furthermore, degradation of elastic fibers and other ECM components such as BM collagens, interstitial collagens, fibronectin, and several proteoglycans by MMPs, facilitates migration of adventitial fibroblasts and myofibroblasts into the media and intima, which, in turn, promotes PA stiffening and vascular stenosis (46, 154) (Table 2). Similarly, neointimal formation *via* increased proliferation and migration of SMC from the media into the intimal regions of the arterial wall is likewise facilitated by MMP-regulated ECM degradation (52, 178) and promotes vascular stenosis and stiffening (178). Products of ECM proteolysis—the matrikines [recently reviewed in detail by Mutgan et al. (179)]—can, in turn, serve as pro-inflammatory mediators, which accentuate inflammation and may, as such, create another positive feedback loop (43). Furthermore, ECM degradation allows for circulating serum factors to enter the media and stimulate serine elastase production by SMCs (178). These serine elastases aid elastin degradation and the release of activated growth factors, such as fibroblast growth factor (FGF) and TGF-β that, in turn, increase collagen, fibronectin, and tenascin-C production by SMCs and fibroblasts (43)—again furthering PA stiffening (Table 2). In other cardiovascular diseases such as ischemic heart failure, immune cells like macrophages, lymphocytes, and mast cells secrete MMPs that remodel the vascular and cardiac ECM in response to mechanical stress (168). In arteriosclerosis, elevated levels of both MMP-2 and MMP-9 were associated with increased arterial stiffness and cardiovascular disease risk, which has been attributed to their ability to degrade the elastic laminae in arteries (180, 181). Accordingly, MMP-2 knockdown reduces arterial stiffening of carotid arteries in mice by decreasing elastin degradation in the tissue (182).

As such, activation of immune cells and inflammatory pathways, and arterial wall thickening and ECM remodeling may reciprocally stimulate each other. Targeting inflammatory processes in cardiovascular diseases, for example, aortic aneurysms, has shown beneficial effects on key mechanisms of ECM remodeling such as elastin degradation, MMP expression, and macrophage infiltration (183). As such, a better understanding of the specific players and molecular pathways involved in this mutual interaction may reveal novel and potentially personalized targets for future PH therapy.

Pulmonary arterial calcification and inflammation

Biologically induced mineralization is an integral part of human physiology and tissue homeostasis that involves extracellular and intracellular mechanisms to direct the nucleation, growth, and location of the deposited minerals. In disease conditions, these processes may become dysbalanced due to changes in the local or global calcium milieu, DNA damage, endoplasmic reticulum stress, oxidative stress, or metabolic disorders—i.e., processes that are frequently associated with inflammatory responses—and ultimately result in pathological tissue or blood vessel calcification (184, 185). Mechanistically, these factors lead to (or are accompanied by) phenotypic conversion of various cell types into osteoprogenitor cells *via de novo* or increased expression, respectively, of the potent transcription activator RUNX2, which triggers the expression of downstream calcification-promoting proteins such as alkaline phosphatase (186–188). In comparison to systemic arteries, vascular calcification of the PA is scarcely addressed, yet it is actually a common feature in patients with severe prolonged PH (189), advanced PH, and PH with chronic renal failure (190) or end-stage renal disease (191). In fact, detection of peripheral PA calcification by computed tomography (CT) (192) predicts long-term outcome in PH (193) and in patients with atrial septal defect and Eisenmenger's syndrome (194).

In the context of PAH, a critical role in the regulation of PA calcification has been attributed to a microRNA-204-dependent upregulation of RUNX2 that, in turn, activates HIF-1α, leading to PA SMC hyperproliferation, resistance to apoptosis, and subsequent transdifferentiation into osteoblast-like cells (55). A second study reported that hypoxia-induced circular RNA CDR1 promotes osteogenic transdifferentiation of human PA SMCs by sponging microRNA-7-5p, and consequently upregulating its downstream targets calcium/calmodulin-dependent kinase II-delta (CAMK2D) and calponin 3 (CNN3) (195). Third, PA calcification has been linked to hypoxia, in that hypoxia decreases the expression of serine protease granzyme B stored in the granules of T lymphocytes and natural killer cells, which inhibits store-operated calcium channels (SOCCs) as the main source of calcium mineral by attenuating non-canonical Wnt signals in SMCs, thus increasing calcification of the PA (141). Independent of the underlying pathway, calcification

ultimately increases vascular stiffness and reduces the compliance of the pulmonary arterial wall, which is a manifestation of poor prognosis in PH (21).

In the systemic vasculature, inflammatory signals—as seen in PH—have been shown to regulate vascular calcification processes. Specifically, TNF promotes osteogenic differentiation and calcification of bovine aortic SMCs by inducing the expression of osteoblast markers, such as osteoblast-specific factor 2 (Osf2), activator protein 1 (AP1), and cAMP-responsive element-binding protein (CREB) *via* activation of cAMP signaling (104). Likewise, treatment of aortic SMCs with IL-1β or IL-6 caused a dose-dependent increase in alkaline phosphatase activity and increased cell mineralization *in vitro* (196). Interestingly, expression of the inflammatory cytokines IL-6, TNF, and MCP-1 is epigenetically regulated in various tissues by bromodomain protein 4 (BRD4) (86), which modulates the chromatin landscape and activates gene expression by scaffolding transcription factors at gene promoters and/or superenhancers. Notably, BRD4 is upregulated in PA SMCs of PAH patients and in lungs or distal PAs of rat PH models, and is posttranscriptionally regulated by microRNA-204 (87), which is concomitantly involved in PA calcification (55), providing for an additional epigenetic link between inflammation and vascular calcification. More importantly, the RUNX2 gene promoter has been shown to be under direct control of BRD4 during osteoblast differentiation (197) as well as in cancer (198), suggesting that BRD4 may serve as a "master-regulator" of both inflammation and vascular calcification in parallel. In line with this notion, BRD4 inhibition attenuated pulmonary and coronary artery remodeling in experimental PH, and this protective effect was associated with reduced levels of IL-6 and MCP-1 (199, 200).

Although studies linking calcification and inflammation in PH are scarce, cytokines have been implicated in the regulation of calcification in the extra-pulmonary vasculature. Importantly, vascular calcification also seems to be closely interconnected with ECM remodeling and stiffening (201), as SMC mineralization directly correlates with the production of collagen I and fibronectin and elastin degradation, while the latter forms scaffolds for calcium incorporation (201–203). These findings suggest that upstream inflammation may also promote vascular calcification through ECM remodeling.

Pulmonary arterial endothelial-to-mesenchymal transition and inflammation

While our interrogation of vascular calcification processes has at large focused on SMCs, it is important to keep in mind that ECs are also involved. In various cardiovascular diseases, ECs lose their characteristic morphology and undergo a shift toward a mesenchymal phenotype (204), a process that is termed endothelial-to-mesenchymal transition (EndoMT) and that is notably modulated by inflammation. Specifically, inflammatory cytokines such as IL-1β or TNF have been shown to induce EndoMT in PA ECs. In turn, these EndoMT cells start to secrete inflammatory cytokines including IL-4, IL-6, IL-8, IL-13, and TNF at much higher concentrations as compared to normal PA ECs (205), thus establishing a potentially vicious feed-forward loop. In line with the notion of inflammation-driven EndoMT in PH, activation of the pro-inflammatory NF-κB signaling pathway in a mouse model of monocrotaline (MCT)-induced PH was found to upregulate miR-130a, which induced loss of bone morphogenetic protein receptor type 2 (BMPR2), increased expression of High Mobility Group AT-hook 1 (HMGA1), and ultimately EndoMT in lung microvascular ECs (206). It is important to highlight that although EndoMT has been extensively documented in pulmonary and systemic ECs exposed to inflammatory mediators *in vitro*, the extent and relevance of EndoMT *in vivo* in recent studies using lineage tracing technologies remains controversial: By use of double transgenic mice stably expressing green fluorescent protein (GFP) in all ECs, Suzuki and colleagues detected GFP in 14.3 ± 1.8% of mesenchymal ($CD144^-CD45^-CD326^-$) cells, indicating substantial EndoMT (207). Similarly, endothelial lineage tracing using transgenic vascular endothelial-cadherin Cre recombinase or Tie-2 Cre mice intercrossed with mTomato/mGreen fluorescent protein double-fluorescent Cre reporter mice revealed abundant endothelial lineage-marked cells in the neointima where they expressed smooth muscle α-actin and smooth muscle myosin heavy chain following induction of PH by monocrotaline pyrrole (208). Yet, a recent lineage tracing study in chronic hypoxia and allergen-induced models of lung vascular remodeling showed retention of endothelial lineage-specific marker expression profiles without any indication of cell-type conversion (209). Notably, the recognition of limited or partial EndoMT does not necessarily conflict with its potential functional relevance in PA stiffening, but simply suggests that this relevance may potentially relate more to the release of proliferative, hypertrophic, and profibrotic signals—i.e., mediators of processes that will ultimately promote PA stiffness—by partial EndoMT cells rather than to the actual generation of significant mesenchymal cell mass *via* this mechanism. Indeed, a similar role is increasingly recognized for epithelial–mesenchymal transition in tissue fibrosis (210).

Over and above that, EndoMT may link inflammation to vascular calcification and, thus, PA stiffening in PH. Specifically, studies in aortic ECs show that inflammatory cytokines such as TNF and IL-1β modulate EndoMT and downregulate the expression of BMPR2 and JNK signaling, thereby sensitizing ECs for BMP9-induced osteogenic differentiation that culminates in mineralization (141). Similar regulatory mechanisms may drive PA EC calcification in different types of PH, and PAH patients with BMPR2 mutations or BMP signaling

pathway impairments (104) would be expected to be specifically vulnerable in this scenario given the association of impaired BMPR2 signaling with EndoMT (211). Lineage tracing studies in the systemic circulation support a role for EndoMT in vascular calcification, showing, e.g., that a subset of endocardial cells can undergo endocardial-to-mesenchymal transition resulting in calcification of mouse and human cardiac valves (212) or that vascular ECs can transition into osteogenic cells (213), which can be prevented by inhibition of glycogen synthase kinase 3 (GSK3) (214). The role of EndoMT (or partial EndoMT) in vascular calcification in the pulmonary circulation and in the contact of PH has, however, so far not been addressed.

Potential clinical relevance

While current PH therapies (i.e., prostacyclins, phosphodiesterase inhibitors, calcium channel blockers, endothelin receptor antagonists, or soluble guanylate cyclase stimulators) focus primarily on alleviating vasoconstriction as a symptomatic approach (215), the long-term therapeutic goal is to shift towards targeting mechanisms of disease onset and progression, including vascular remodeling and inflammation (215). In this regard, targeting the immune–PA stiffening axis may present a particularly promising strategy in light of the predictive and pathomechanistic role of PA stiffening in PH, and the armamentarium of immunomodulatory therapies already in clinical use or in development. In the systemic circulation, anti-inflammatory therapies have shown promise to reduce arterial stiffening in inflammatory artheropathies such as rheumatoid or psoriatic arthritis (167). Specifically, TNF antagonists, such as adalimumab, etanercept, or infliximab, represent established anti-inflammatory therapies in (auto-)immune conditions (216) that have explicitly lowered aortic stiffness in patients with inflammatory artheropathies (107, 167).

As such, immunomodulatory treatments are increasingly considered as potential therapeutic strategies for the treatment of PH. Yet, despite promising findings in preclinical models (8, 146, 215, 217), results from clinical trials have so far shown only modest benefit (149, 218, 219), thus stressing the need for more personalized approaches. Given the discussed link between immune responses, ECM remodeling, and vascular calcification, PA stiffness may present a promising biomarker to identify and monitor patients who may profit from immunomodulatory therapies; yet, assessment of PA stiffness in clinical trials is presently rare. Preclinical models, however, highlight the potential promise of anti-inflammatory therapies to target PA stiffness: For example, inhibition of carbonic anhydrases by acetazolamide or ammonium chloride (NH_4Cl) as a potential treatment for inflammation in PH was able to prevent SMC dedifferentiation and proliferation in a Sugen5416/hypoxia rat model (220). Other anti-inflammatory therapies, such as treatment with resveratrol, were similarly able to prevent PA remodeling and stiffening in chronic hypoxic rats (215), while inhibitors of the renin–angiotensin system such as captopril or losartan reduced the production of ECM components including interstitial collagen and the expression of MMP-2 and MMP-9 in PAH, thereby attenuating PA stiffening (215). Hence, targeting inflammation with a specific focus on PA stiffness may provide for a pathomechanism-based and individualized therapy to treat PH —a notion that should be considered and, ideally, may be tested in appropriate preclinical and clinical trials.

Author contributions

S-FL, NNV, and MK conceived and wrote the original draft manuscript. QL drew the figures. MK, CK, and WK conceived and revised the manuscript. All authors contributed to the article and approved the submitted version.

Funding

WK was supported by grants from the German Research Foundation (CRC 1470, A04; KU1218/12-1) and the German Center for Cardiovascular Research partner site Berlin, CK was supported by the German Centre for Cardiovascular Research partner site Berlin and by the German Ministry of Education and Research (BMBF), NNV was supported by the Doctoral Scholarship from the German Centre for Cardiovascular Research and the German Cardiology Association (DGK), MK was supported by the German Foundation for Heart Research (F23/20), and S-FL and QL were supported by the China Scholarship Council (No. 202008350142 and No.202108080221).

Acknowledgments

Parts of the figures were generated with the help of BioRender.

Conflict of interest

The authors declare that the research was conducted in the absence of any commercial or financial relationships that could be construed as a potential conflict of interest.

Publisher's note

References

1. Simonneau G, Montani D, Celermajer DS, Denton CP, Gatzoulis MA, Krowka M, et al. Haemodynamic definitions and updated clinical classification of pulmonary hypertension. *Eur Respir J* (2019) 53(1):1801913. doi: 10.1183/13993003.01913-2018

2. Condon DF, Nickel NP, Anderson R, Mirza S, de Jesus Perez VA. The 6th world symposium on pulmonary hypertension: What's old is new. *F1000Res* (2019) 8:F1000 Faculty Rev–888. doi: 10.12688/f1000research.18811.1

3. Simonneau G, Robbins IM, Beghetti M, Channick RN, Delcroix M, Denton CP, et al. Updated clinical classification of pulmonary hypertension. *J Am Coll Cardiol* (2009) 54:S43–54. doi: 10.1016/j.jacc.2009.04.012

4. Galie N, Humbert M, Vachiery JL, Gibbs S, Lang I, Torbicki A, et al. ESC/ERS guidelines for the diagnosis and treatment of pulmonary hypertension: The joint task force for the diagnosis and treatment of pulmonary hypertension of the European society of cardiology (ESC) and the European respiratory society (ERS): Endorsed by: Association for European paediatric and congenital cardiology (AEPC), international society for heart and lung transplantation (ISHLT). *Eur Respir J* (2015) 46:903–75. doi: 10.1183/13993003.01032-2015

5. Lan NSH, Massam BD, Kulkarni SS, Lang CC. Pulmonary arterial hypertension: Pathophysiology and treatment. *Diseases* (2018) 6 (2):38. doi: 10.3390/diseases6020038

6. Savai R, Pullamsetti SS, Kolbe J, Bieniek E, Voswinckel R, Fink L, et al. Immune and inflammatory cell involvement in the pathology of idiopathic pulmonary arterial hypertension. *Am J Respir Crit Care Med* (2012) 186:897–908. doi: 10.1164/rccm.201202-0335OC

7. El Kasmi KC, Pugliese SC, Riddle SR, Poth JM, Anderson AL, Frid MG, et al. Adventitial fibroblasts induce a distinct proinflammatory/profibrotic macrophage phenotype in pulmonary hypertension. *J Immunol* (2014) 193:597–609. doi: 10.4049/jimmunol.1303048

8. Breitling S, Hui Z, Zabini D, Hu Y, Hoffmann J, Goldenberg NM, et al. The mast cell-b cell axis in lung vascular remodeling and pulmonary hypertension. *Am J Physiol Lung Cell Mol Physiol* (2017) 312:L710–21. doi: 10.1152/ajplung.00311.2016

9. Pugliese SC, Poth JM, Fini MA, Olschewski A, El Kasmi KC, Stenmark KR. The role of inflammation in hypoxic pulmonary hypertension: From cellular mechanisms to clinical phenotypes. *Am J Physiol Lung Cell Mol Physiol* (2015) 308:L229–252. doi: 10.1152/ajplung.00238.2014

10. Soon E, Holmes AM, Treacy CM, Doughty NJ, Southgate L, Machado RD, et al. Elevated levels of inflammatory cytokines predict survival in idiopathic and familial pulmonary arterial hypertension. *Circulation* (2010) 122:920–7. doi: 10.1161/CIRCULATIONAHA.109.933762

11. Rabinovitch M, Guignabert C, Humbert M, Nicolls MR. Inflammation and immunity in the pathogenesis of pulmonary arterial hypertension. *Circ Res* (2014) 115:165–75. doi: 10.1161/CIRCRESAHA.113.301141

12. Spiekerkoetter E, Goncharova EA, Guignabert C, Stenmark K, Kwapiszewska G, Rabinovitch M, et al. Hot topics in the mechanisms of pulmonary arterial hypertension disease: Cancer-like pathobiology, the role of the adventitia, systemic involvement, and right ventricular failure. *Pulm Circ* (2019) 9:2045894019889775. doi: 10.1177/2045894019889775

13. Kuebler WM, Bonnet S, Tabuchi A. Inflammation and autoimmunity in pulmonary hypertension: Is there a role for endothelial adhesion molecules? (2017 grover conference series). *Pulm Circ* (2018) 8:2045893218757596. doi: 10.1177/2045893218757596

14. Hu Y, Chi L, Kuebler WM, Goldenberg NM. Perivascular inflammation in pulmonary arterial hypertension. *Cells* (2020) 9 (11):2338. doi: 10.3390/cells9112338

15. Sasaki N, Kamataki A, Sawai T. A histopathological study of pulmonary hypertension in connective tissue disease. *Allergol Int* (2011) 60:411–7. doi: 10.2332/allergolint.11-RAI-0337

16. Humbert M, Monti G, Brenot F, Sitbon O, Portier A, Grangeot-Keros L, et al. Increased interleukin-1 and interleukin-6 serum concentrations in severe primary pulmonary hypertension. *Am J Respir Crit Care Med* (1995) 151:1628–31. doi: 10.1164/ajrccm.151.5.7735624

17. Breitling S, Ravindran K, Goldenberg NM, Kuebler WM. The pathophysiology of pulmonary hypertension in left heart disease. *Am J Physiol Lung Cell Mol Physiol* (2015) 309:L924–941. doi: 10.1152/ajplung.00146.2015

18. Gan CT, Lankhaar JW, Westerhof N, Marcus JT, Becker A, Twisk JW, et al. Noninvasively assessed pulmonary artery stiffness predicts mortality in pulmonary arterial hypertension. *Chest* (2007) 132:1906–12. doi: 10.1378/chest.07-1246

19. Agoston-Coldea L, Lupu S, Mocan T. Pulmonary artery stiffness by cardiac magnetic resonance imaging predicts major adverse cardiovascular events in patients with chronic obstructive pulmonary disease. *Sci Rep* (2018) 8:14447. doi: 10.1038/s41598-018-32784-6

20. Al-Naamani N, Preston IR, Paulus JK, Hill NS, Roberts KE. Pulmonary arterial capacitance is an important predictor of mortality in heart failure with a preserved ejection fraction. *JACC Heart Fail* (2015) 3:467–74. doi: 10.1016/j.jchf.2015.01.013

21. Wang Z, Chesler NC. Pulmonary vascular wall stiffness: An important contributor to the increased right ventricular afterload with pulmonary hypertension. *Pulm Circ* (2011) 1:212–23. doi: 10.4103/2045-8932.83453

22. Papolos A, Tison GH, Mayfield J, Vasti E, DeMarco T. Echocardiographic assessment of pulmonary arterial capacitance predicts mortality in pulmonary hypertension. *J Cardiol* (2021) 77:279–84. doi: 10.1016/j.jjcc.2020.10.006

23. Sugimoto K, Yoshihisa A, Nakazato K, Jin Y, Suzuki S, Yokokawa T, et al. Pulmonary arterial capacitance predicts cardiac events in pulmonary hypertension due to left heart disease. *PloS One* (2016) 11:e0165603. doi: 10.1371/journal.pone.0165603

24. Friedberg MK, Feinstein JA, Rosenthal DN. Noninvasive assessment of pulmonary arterial capacitance by echocardiography. *J Am Soc Echocardiogr* (2007) 20:186–90. doi: 10.1016/j.echo.2006.08.009

25. Dieffenbach PB, Maracle M, Tschumperlin DJ, Fredenburgh LE. Mechanobiological feedback in pulmonary vascular disease. *Front Physiol* (2018) 9:951. doi: 10.3389/fphys.2018.00951

26. Reuben SR. Compliance of the human pulmonary arterial system in disease. *Circ Res* (1971) 29:40–50. doi: 10.1161/01.RES.29.1.40

27. Tedford RJ, Hassoun PM, Mathai SC, Girgis RE, Russell SD, Thiemann DR, et al. Pulmonary capillary wedge pressure augments right ventricular pulsatile loading. *Circulation* (2012) 125:289–97. doi: 10.1161/CIRCULATIONAHA.111.051540

28. Lin MT, Chen YS, Huang SC, Chiu HH, Chiu SN, Chen CA, et al. Alternative approach for selected severe pulmonary hypertension of congenital heart defect without initial correction–palliative surgical treatment. *Int J Cardiol* (2011) 151:313–7. doi: 10.1016/j.ijcard.2010.05.067

29. Wagenvoort CA, Wagenvoort N, Draulans-Noe Y. Reversibility of plexogenic pulmonary arteriopathy following banding of the pulmonary artery. *J Thorac Cardiovasc Surg* (1984) 87:876–86. doi: 10.1016/S0022-5223(19)38415-6

30. Cho JY, Kim KH. Evaluation of arterial stiffness by echocardiography: Methodological aspects. *Chonnam Med J* (2016) 52:101–6. doi: 10.4068/cmj.2016.52.2.101

31. Cheng XL, He JG, Liu ZH, Gu Q, Ni XH, Zhao ZH, et al. Pulmonary vascular capacitance is associated with vasoreactivity and long-term response to calcium channel blockers in idiopathic pulmonary arterial hypertension. *Lung* (2016) 194:613–8. doi: 10.1007/s00408-016-9905-0

32. Shafie D, Dohaei A, Amin A, Taghavi S, Naderi N. Pulmonary vascular capacitance as a predictor of vasoreactivity in idiopathic pulmonary arterial hypertension tested by adenosine. *Res Cardiovasc Med* (2015) 4(4):e28945. doi: 10.5812/cardiovascmed.28945

33. Sajan I, Manlhiot C, Reyes J, McCrindle BW, Humpl T, Friedberg MK. Pulmonary arterial capacitance in children with idiopathic pulmonary arterial hypertension and pulmonary arterial hypertension associated with congenital heart disease: relation to pulmonary vascular resistance, exercise capacity, and survival. *Am Heart J* (2011) 162:562–8. doi: 10.1016/j.ahj.2011.06.014

34. Pellegrini P, Rossi A, Pasotti M, Raineri C, Cicoira M, Bonapace S, et al. Prognostic relevance of pulmonary arterial compliance in patients with chronic heart failure. *Chest* (2014) 145:1064–70. doi: 10.1378/chest.13-1510

35. Dupont M, Mullens W, Skouri HN, Abrahams Z, Wu Y, Taylor DO, et al. Prognostic role of pulmonary arterial capacitance in advanced heart failure. *Circ Heart Fail* (2012) 5:778–85. doi: 10.1161/CIRCHEARTFAILURE.112.968511

36. Dragu R, Rispler S, Habib M, Sholy H, Hammerman H, Galie N, et al. Pulmonary arterial capacitance in patients with heart failure and reactive pulmonary hypertension. *Eur J Heart Fail* (2015) 17:74–80. doi: 10.1002/ejhf.192

37. Saito Y, Ohtani T, Kioka H, Onishi T, Tsukamoto Y, Nakamoto K, et al. Clinical significance of pulmonary arterial capacitance calculated by echocardiography in patients with advanced heart failure. *Circ J* (2017) 81:1871–8. doi: 10.1253/circj.CJ-16-1318

38. Sanz J, Kariisa M, Dellegrottaglie S, Prat-Gonzalez S, Garcia MJ, Fuster V, et al. Evaluation of pulmonary artery stiffness in pulmonary hypertension with cardiac magnetic resonance. *JACC Cardiovasc Imaging* (2009) 2:286–95. doi: 10.1016/j.jcmg.2008.08.007

39. Botney MD, Kaiser LR, Cooper JD, Mecham RP, Parghi D, Roby J, et al. Extracellular matrix protein gene expression in atherosclerotic hypertensive pulmonary arteries. *Am J Pathol* (1992) 140:357–64.

40. Kohn JC, Lampi MC, Reinhart-King CA. Age-related vascular stiffening: Causes and consequences. *Front Genet* (2015) 6:112. doi: 10.3389/fgene.2015.00112

41. Wagenseil JE, Mecham RP. Vascular extracellular matrix and arterial mechanics. *Physiol Rev* (2009) 89:957–89. doi: 10.1152/physrev.00041.2008

42. Wagenseil JE, Mecham RP. Elastin in large artery stiffness and hypertension. *J Cardiovasc Transl Res* (2012) 5:264–73. doi: 10.1007/s12265-012-9349-8

43. Thenappan T, Chan SY, Weir EK. Role of extracellular matrix in the pathogenesis of pulmonary arterial hypertension. *Am J Physiol Heart Circ Physiol* (2018) 315:H1322–31. doi: 10.1152/ajpheart.00136.2018

44. Botney MD, Liptay MJ, Kaiser LR, Cooper JD, Parks WC, Mecham RP. Active collagen synthesis by pulmonary arteries in human primary pulmonary hypertension. *Am J Pathol* (1993) 143:121–9.

45. Hoffmann J, Marsh LM, Pieper M, Stacher E, Ghanim B, Kovacs G, et al. Compartment-specific expression of collagens and their processing enzymes in intrapulmonary arteries of IPAH patients. *Am J Physiol Lung Cell Mol Physiol* (2015) 308:L1002–1013. doi: 10.1152/ajplung.00383.2014

46. Stenmark KR, Yeager ME, El Kasmi KC, Nozik-Grayck E, Gerasimovskaya EV, Li M, et al. The adventitia: Essential regulator of vascular wall structure and function. *Annu Rev Physiol* (2013) 75:23–47. doi: 10.1146/annurev-physiol-030212-183802

47. Chi PL, Cheng CC, Hung CC, Wang MT, Liu HY, Ke MW, et al. MMP-10 from M1 macrophages promotes pulmonary vascular remodeling and pulmonary arterial hypertension. *Int J Biol Sci* (2022) 18:331–48. doi: 10.7150/ijbs.66472

48. Bertero T, Oldham WM, Cottrill KA, Pisano S, Vanderpool RR, Yu Q, et al. Vascular stiffness mechanoactivates YAP/TAZ-dependent glutaminolysis to drive pulmonary hypertension. *J Clin Invest* (2016) 126:3313–35. doi: 10.1172/JCI86387

49. McEniery CM, Wilkinson IB. Large Artery stiffness and inflammation. *J Hum Hypertens* (2005) 19:507–9. doi: 10.1038/sj.jhh.1001814

50. Hardy E, Hardy-Sosa A, Fernandez-Patron C. MMP-2: Is too low as bad as too high in the cardiovascular system? *Am J Physiol Heart Circ Physiol* (2018) 315: H1332–40. doi: 10.1152/ajpheart.00198.2018

51. Loffek S, Schilling O, Franzke CW. Series "matrix metalloproteinases in lung health and disease": Biological role of matrix metalloproteinases: A critical balance. *Eur Respir J* (2011) 38:191–208. doi: 10.1183/09031936.00146510

52. Lepetit H, Eddahibi S, Fadel E, Frisdal E, Munaut C, Noel A, et al. Smooth muscle cell matrix metalloproteinases in idiopathic pulmonary arterial hypertension. *Eur Respir J* (2005) 25:834–42. doi: 10.1183/09031936.05.00072504

53. Golob MJ, Tabima DM, Wolf GD, Johnston JL, Forouzan O, Mulchrone AM, et al. Pulmonary arterial strain- and remodeling-induced stiffening are differentiated in a chronic model of pulmonary hypertension. *J Biomech* (2017) 55:92–8. doi: 10.1016/j.jbiomech.2017.02.003

54. Demer LL, Tintut Y. Vascular calcification: Pathobiology of a multifaceted disease. *Circulation* (2008) 117:2938–48. doi: 10.1161/CIRCULATIONAHA.107.743161

55. Ruffenach G, Chabot S, Tanguay VF, Courboulin A, Boucherat O, Potus F, et al. Role for runt-related transcription factor 2 in proliferative and calcified vascular lesions in pulmonary arterial hypertension. *Am J Respir Crit Care Med* (2016) 194:1273–85. doi: 10.1164/rccm.201512-2380OC

56. Sun Y, Byon CH, Yuan K, Chen J, Mao X, Heath JM, et al. Smooth muscle cell-specific runx2 deficiency inhibits vascular calcification. *Circ Res* (2012) 111:543–52. doi: 10.1161/CIRCRESAHA.112.267237

57. Friesen RM, Schafer M, Ivy DD, Abman SH, Stenmark K, Browne LP, et al. Proximal pulmonary vascular stiffness as a prognostic factor in children with pulmonary arterial hypertension. *Eur Heart J Cardiovasc Imaging* (2019) 20:209–17. doi: 10.1093/ehjci/jey069

58. Li M, Tan Y, Stenmark KR, Tan W. High pulsatility flow induces acute endothelial inflammation through overpolarizing cells to activate NF-kappaB. *Cardiovasc Eng Technol* (2013) 4:26–38. doi: 10.1007/s13239-012-0115-5

59. Steppan J, Barodka V, Berkowitz DE, Nyhan D. Vascular stiffness and increased pulse pressure in the aging cardiovascular system. *Cardiol Res Pract* (2011) 2011:263585. doi: 10.4061/2011/263585

60. Steiner MK, Syrkina OL, Kolliputi N, Mark EJ, Hales CA, Waxman AB. Interleukin-6 overexpression induces pulmonary hypertension. *Circ Res* (2009) 104:236–44. doi: 10.1161/CIRCRESAHA.108.182014

61. Huang W, Liu H, Pan Y, Yang H, Lin J, Zhang H. Mechanical stretching of the pulmonary vein mediates pulmonary hypertension due to left heart disease by regulating SAC/MAPK pathway and the expression of IL-6 and TNF-alpha. *J Cardiothorac Surg* (2021) 16:127. doi: 10.1186/s13019-021-01471-5

62. Hurlimann D, Forster A, Noll G, Enseleit F, Chenevard R, Distler O, et al. Anti-tumor necrosis factor-alpha treatment improves endothelial function in patients with rheumatoid arthritis. *Circulation* (2002) 106:2184–7. doi: 10.1161/01.CIR.0000037521.71373.44

63. Zhu Y, Huang Y, Ji Q, Fu S, Gu J, Tai N, et al. Interplay between extracellular matrix and neutrophils in diseases. *J Immunol Res* (2021) 2021:8243378. doi: 10.1155/2021/8243378

64. Tenkorang MAA, Chalise U, Daseke Ii MJ, Konfrst SR, Lindsey ML. Understanding the mechanisms that determine extracellular matrix remodeling in the infarcted myocardium. *Biochem Soc Trans* (2019) 47:1679–87. doi: 10.1042/BST20190113

65. Ma Z, Mao C, Jia Y, Fu Y, Kong W. Extracellular matrix dynamics in vascular remodeling. *Am J Physiol Cell Physiol* (2020) 319:C481–99. doi: 10.1152/ajpcell.00147.2020

66. Udjus C, Cero FT, Halvorsen B, Behmen D, Carlson CR, Bendiksen BA, et al. Caspase-1 induces smooth muscle cell growth in hypoxia-induced pulmonary hypertension. *Am J Physiol Lung Cell Mol Physiol* (2019) 316:L999–L1012. doi: 10.1152/ajplung.00322.2018

67. Parpaleix A, Amsellem V, Houssaini A, Abid S, Breau M, Marcos E, et al. Role of interleukin-1 receptor 1/MyD88 signalling in the development and progression of pulmonary hypertension. *Eur Respir J* (2016) 48:470–83. doi: 10.1183/13993003.01448-2015

68. Tang C, Luo Y, Li S, Huang B, Xu S, Li L. Characteristics of inflammation process in monocrotaline-induced pulmonary arterial hypertension in rats. *BioMed Pharmacother* (2021) 133:111081. doi: 10.1016/j.biopha.2020.111081

69. Koudstaal T, van Hulst JAC, Das T, Neys SFH, Merkus D, Bergen IM, et al. DNGR1-cre-mediated deletion of Tnfaip3/A20 in conventional dendritic cells induces pulmonary hypertension in mice. *Am J Respir Cell Mol Biol* (2020) 63:665–80. doi: 10.1165/rcmb.2019-0443OC

70. Wang J, Tian XT, Peng Z, Li WQ, Cao YY, Li Y, et al. HMGB1/TLR4 promotes hypoxic pulmonary hypertension *via* suppressing BMPR2 signaling. *Vascul Pharmacol* (2019) 117:35–44. doi: 10.1016/j.vph.2018.12.006

71. Li M, Riddle SR, Frid MG, El Kasmi KC, McKinsey TA, Sokol RJ, et al. Emergence of fibroblasts with a proinflammatory epigenetically altered phenotype in severe hypoxic pulmonary hypertension. *J Immunol* (2011) 187:2711–22. doi: 10.4049/jimmunol.1100479

72. Smolders V, Lodder K, Rodriguez C, Tura-Ceide O, Barbera JA, Jukema JW, et al. The inflammatory profile of CTEPH-derived endothelial cells is a possible driver of disease progression. *Cells* (2021) 10(4):737. doi: 10.3390/cells10040737

73. Gaillard V, Casellas D, Seguin-Devaux C, Schohn H, Dauca M, Atkinson J, et al. Pioglitazone improves aortic wall elasticity in a rat model of elastocalcinotic arteriosclerosis. *Hypertension* (2005) 46:372–9. doi: 10.1161/01.HYP.0000171472.24422.33

74. Santiago JJ, Dangerfield AL, Rattan SG, Bathe KL, Cunnington RH, Raizman JE, et al. Cardiac fibroblast to myofibroblast differentiation *in vivo* and *in vitro*: expression of focal adhesion components in neonatal and adult rat ventricular myofibroblasts. *Dev Dyn* (2010) 239:1573–84. doi: 10.1002/dvdy.22280

75. Sanchez-Duffhues G, Garcia de Vinuesa A, van de Pol V, Geerts ME, de Vries MR, Janson SG, et al. Inflammation induces endothelial-to-mesenchymal transition and promotes vascular calcification through downregulation of BMPR2. *J Pathol* (2019) 247:333–46. doi: 10.1002/path.5193

76. Tomaszewski M, Grywalska E, Tomaszewski A, Blaszczak P, Kurzyna M, Rolinski J, et al. Overexpression of PD-1 on peripheral blood lymphocytes in patients with idiopathic pulmonary arterial hypertension and its association with high viral loads of Epstein-Barr virus and poor clinical parameters. *J Clin Med* (2020) 9(6):1966. doi: 10.3390/jcm9061966

77. Majeed B, Tawinwung S, Eberson LS, Secomb TW, Larmonier N, Larson DF. Interleukin-2/Anti-Interleukin-2 immune complex expands regulatory T cells and reduces angiotensin II-induced aortic stiffening. *Int J Hypertens* (2014) 2014:126365. doi: 10.1155/2014/126365

78. Chaouat A, Savale L, Chouaid C, Tu L, Sztrymf B, Canuet M, et al. Role for interleukin-6 in COPD-related pulmonary hypertension. *Chest* (2009) 136:678–87. doi: 10.1378/chest.08-2420

79. Sweatt AJ, Hedlin HK, Balasubramanian V, Hsi A, Blum LK, Robinson WH, et al. Discovery of distinct immune phenotypes using machine learning in pulmonary arterial hypertension. *Circ Res* (2019) 124:904–19. doi: 10.1161/CIRCRESAHA.118.313911

80. Koudstaal T, van Uden D, van Hulst JAC, Heukels P, Bergen IM, Geenen LW, et al. Plasma markers in pulmonary hypertension subgroups correlate with patient survival. *Respir Res* (2021) 22:137. doi: 10.1186/s12931-021-01716-w

81. Ranchoux B, Nadeau V, Bourgeois A, Provencher S, Tremblay E, Omura J, et al. Metabolic syndrome exacerbates pulmonary hypertension due to left heart disease. *Circ Res* (2019) 125:449–66. doi: 10.1161/CIRCRESAHA.118.314555

82. Hashimoto-Kataoka T, Hosen N, Sonobe T, Arita Y, Yasui T, Masaki T, et al. Interleukin-6/interleukin-21 signaling axis is critical in the pathogenesis of pulmonary arterial hypertension. *Proc Natl Acad Sci U.S.A.* (2015) 112:E2677–2686. doi: 10.1073/pnas.1424774112

83. Batah SS, Alda MA, Rodrigues Lopes Roslindo Figueira R, Cruvinel HR, Perdona Rodrigues da Silva L, Machado-Rugolo J, et al. *In situ* evidence of collagen V and interleukin-6/Interleukin-17 activation in vascular remodeling of experimental pulmonary hypertension. *Pathobiol* (2020) 87:356–66. doi: 10.1159/000510048

84. Simpson CE, Chen JY, Damico RL, Hassoun PM, Martin LJ, Yang J, et al. Cellular sources of interleukin-6 and associations with clinical phenotypes and outcomes in pulmonary arterial hypertension. *Eur Respir J* (2020) 55(4):1901761. doi: 10.1183/13993003.01761-2019

85. He H, Tao Y, Chen X, Qiu H, Zhu J, Zhang J, et al. High levels of interleukin-6 and 8-iso-prostaglandin in the exhaled breath condensate and serum of patients with chronic obstructive pulmonary disease related pulmonary hypertension. *Chin Med J (Engl)* (2014) 127:1608–12.

86. Khan YM, Kirkham P, Barnes PJ, Adcock IM. Brd4 is essential for IL-1beta-induced inflammation in human airway epithelial cells. *PloS One* (2014) 9(4): e95051. doi: 10.1371/journal.pone.0095051

87. Meloche J, Potus F, Vaillancourt M, Bourgeois A, Johnson I, Deschamps L, et al. Bromodomain-containing protein 4: The epigenetic origin of pulmonary arterial hypertension. *Circ Res* (2015) 117:525–35. doi: 10.1161/CIRCRESAHA.115.307004

88. Maniatis K, Siasos G, Oikonomou E, Vavuranakis M, Zaromytidou M, Mourouzis K, et al. Osteoprotegerin and osteopontin serum levels are associated with vascular function and inflammation in coronary artery disease patients. *Curr Vasc Pharmacol* (2020) 18:523–30. doi: 10.2174/1570161117666191022095246

89. Gokaslan S, Ozer Gokaslan C, Demirel E, Celik S. Role of aortic stiffness and inflammation in the etiology of young-onset hypertension. *Turk J Med Sci* (2019) 49(6):1748–53. doi: 10.3906/sag-1908-137

90. Peyster E, Chen J, Feldman HI, Go AS, Gupta J, Mitra N, et al. Inflammation and arterial stiffness in chronic kidney disease: Findings from the CRIC study. *Am J Hypertens* (2017) 30:400–8. doi: 10.1093/ajh/hpw164

91. Quarck R, Wynants M, Verbeken E, Meyns B, Delcroix M. Contribution of inflammation and impaired angiogenesis to the pathobiology of chronic thromboembolic pulmonary hypertension. *Eur Respir J* (2015) 46:431–43. doi: 10.1183/09031936.00009914

92. Sikka G, Miller KL, Steppan J, Pandey D, Jung SM, Fraser CD3rd, et al. Interleukin 10 knockout frail mice develop cardiac and vascular dysfunction with increased age. . *Exp Gerontol* (2013) 48:128–35. doi: 10.1016/j.exger.2012.11.001

93. Calvier L, Legchenko E, Grimm L, Sallmon H, Hatch A, Plouffe BD, et al. Galectin-3 and aldosterone as potential tandem biomarkers in pulmonary arterial hypertension. *Heart* (2016) 102:390–6. doi: 10.1136/heartjnl-2015-308365

94. Larsen KO, Yndestad A, Sjaastad I, Loberg EM, Goverud IL, Halvorsen B, et al. Lack of CCR7 induces pulmonary hypertension involving perivascular leukocyte infiltration and inflammation. *Am J Physiol Lung Cell Mol Physiol* (2011) 301:L50–59. doi: 10.1152/ajplung.00048.2010

95. Wang W, Yan H, Zhu W, Cui Y, Chen J, Wang X, et al. Impairment of monocyte-derived dendritic cells in idiopathic pulmonary arterial hypertension. *J Clin Immunol* (2009) 29:705–13. doi: 10.1007/s10875-009-9322-8

96. Yong K, Dogra G, Boudville N, Chan D, Adams L, Ching H, et al. Interleukin-12 is associated with arterial stiffness in healthy individuals. *Am J Hypertens* (2013) 26:159–62. doi: 10.1093/ajh/hps032

97. Zhu R, Xie X, Wang N, Chen L, Hong Y. The T helper type 17/regulatory T cell imbalance was associated with ras-GTPase overexpression in patients with pulmonary hypertension associated with chronic obstructive pulmonary disease. *Immunology* (2019) 157(4):304–11. doi: 10.1111/imm.13084

98. Huang LH, Zinselmeyer BH, Chang CH, Saunders BT, Elvington A, Baba O, et al. Interleukin-17 drives interstitial entrapment of tissue lipoproteins in experimental psoriasis. *Cell Metab* (2019) 29:475–487 e477. doi: 10.1016/j.cmet.2018.10.006

99. Yang M, Deng C, Wu D, Zhong Z, Lv X, Huang Z, et al. The role of mononuclear cell tissue factor and inflammatory cytokines in patients with chronic thromboembolic pulmonary hypertension. *J Thromb Thrombol* (2016) 42:38–45. doi: 10.1007/s11239-015-1323-2

100. Saleby J, Bouzina H, Lundgren J, Radegran G. Angiogenic and inflammatory biomarkers in the differentiation of pulmonary hypertension. *Scand Cardiovasc J* (2017) 51:261–70. doi: 10.1080/14017431.2017.1359419

101. Kylhammar D, Hesselstrand R, Nielsen S, Scheele C, Radegran G. Angiogenic and inflammatory biomarkers for screening and follow-up in patients with pulmonary arterial hypertension. *Scand J Rheumatol* (2018) 47:319–24. doi: 10.1080/03009742.2017.1378714

102. Naito A, Sakao S, Terada J, Iwasawa S, Jujo Sanada T, Suda R, et al. Nocturnal hypoxemia and high circulating TNF-alpha levels in chronic thromboembolic pulmonary hypertension. *Intern Med* (2020) 59:1819–26. doi: 10.2169/internalmedicine.4458-20

103. Bai P, Lyu L, Yu T, Zuo C, Fu J, He Y, et al. Macrophage-derived legumain promotes pulmonary hypertension by activating the MMP (Matrix metalloproteinase)-2/TGF (Transforming growth factor)-beta1 signaling. *Arterioscler Thromb Vasc Biol* (2019) 39(4):e130–45. doi: 10.1161/ATVBAHA.118.312254

104. Tintut Y, Patel J, Parhami F, Demer LL. Tumor necrosis factor-alpha promotes *in vitro* calcification of vascular cells *via* the cAMP pathway. *Circulation* (2000) 102:2636–42. doi: 10.1161/01.CIR.102.21.2636

105. Pina T, Corrales A, Lopez-Mejias R, Armesto S, Gonzalez-Lopez MA, Gomez-Acebo I, et al. Anti-tumor necrosis factor-alpha therapy improves endothelial function and arterial stiffness in patients with moderate to severe psoriasis: A 6-month prospective study. *J Dermatol* (2016) 43:1267–72. doi: 10.1111/1346-8138.13398

106. Moreau KL, Deane KD, Meditz AL, Kohrt WM. Tumor necrosis factor-alpha inhibition improves endothelial function and decreases arterial stiffness in estrogen-deficient postmenopausal women. *Atherosclerosis* (2013) 230:390–6. doi: 10.1016/j.atherosclerosis.2013.07.057

107. Angel K, Provan SA, Gulseth HL, Mowinckel P, Kvien TK, Atar D. Tumor necrosis factor-alpha antagonists improve aortic stiffness in patients with inflammatory arthropathies: a controlled study. *Hypertension* (2010) 55:333–8. doi: 10.1161/HYPERTENSIONAHA.109.143982

108. Kumar R, Mickael C, Chabon J, Gebreab L, Rutebemberwa A, Garcia AR, et al. The causal role of IL-4 and IL-13 in schistosoma mansoni pulmonary hypertension. *Am J Respir Crit Care Med* (2015) 192:998–1008. doi: 10.1164/rccm.201410-1820OC

109. Li S, Ma X, Xie J, Yan X, Sun W. MicroRNA-206, IL-4, IL-13, and INF-gamma levels in lung tissue and plasma are increased by the stimulation of particulate matter with a diameter of </=2.5mum, and are associated with the poor prognosis of asthma induced pulmonary arterial hypertension patients. *Clin Exp Hypertens* (2021) 43:181–8. doi: 10.1080/10641963.2020.1836192

110. Cero FT, Hillestad V, Sjaastad I, Yndestad A, Aukrust P, Ranheim T, et al. Absence of the inflammasome adaptor ASC reduces hypoxia-induced pulmonary hypertension in mice. *Am J Physiol Lung Cell Mol Physiol* (2015) 309:L378–387. doi: 10.1152/ajplung.00342.2014

111. Shao D, Perros F, Caramori G, Meng C, Dormuller P, Chou PC, et al. Nuclear IL-33 regulates soluble ST2 receptor and IL-6 expression in primary human arterial endothelial cells and is decreased in idiopathic pulmonary arterial hypertension. *Biochem Biophys Res Commun* (2014) 451:8–14. doi: 10.1016/j.bbrc.2014.06.111

112. Carlomagno G, Messalli G, Melillo RM, Stanziola AA, Visciano C, Mercurio V, et al. Serum soluble ST2 and interleukin-33 levels in patients with pulmonary arterial hypertension. *Int J Cardiol* (2013) 168:1545–7. doi: 10.1016/j.ijcard.2012.12.031

113. Liu J, Wang W, Wang L, Chen S, Tian B, Huang K, et al. IL-33 initiates vascular remodelling in hypoxic pulmonary hypertension by up-regulating HIF-1alpha and VEGF expression in vascular endothelial cells. *EBioMedicine* (2018) 33:196–210. doi: 10.1016/j.ebiom.2018.06.003

114. Amsellem V, Abid S, Poupel L, Parpaleix A, Rodero M, Gary-Bobo G, et al. Roles for the CX3CL1/CX3CR1 and CCL2/CCR2 chemokine systems in hypoxic pulmonary hypertension. *Am J Respir Cell Mol Biol* (2017) 56:597–608. doi: 10.1165/rcmb.2016-0201OC

115. Abid S, Marcos E, Parpaleix A, Amsellem V, Breau M, Houssaini A, et al. CCR2/CCR5-mediated macrophage-smooth muscle cell crosstalk in pulmonary hypertension. *Eur Respir J* (2019) 54(4):1802308. doi: 10.1183/13993003.02308-2018

116. Bakouboula B, Morel O, Faure A, Zobairi F, Jesel L, Trinh A, et al. Procoagulant membrane microparticles correlate with the severity of pulmonary arterial hypertension. *Am J Respir Crit Care Med* (2008) 177:536–43. doi: 10.1164/rccm.200706-840OC

117. Chang FC, Chiang WC, Tsai MH, Chou YH, Pan SY, Chang YT, et al. Angiopoietin-2-induced arterial stiffness in CKD. *J Am Soc Nephrol* (2014) 25:1198–209. doi: 10.1681/ASN.2013050542

118. Qi D, Wei M, Jiao S, Song Y, Wang X, Xie G, et al. Hypoxia inducible factor 1alpha in vascular smooth muscle cells promotes angiotensin II-induced vascular remodeling *via* activation of CCL7-mediated macrophage recruitment. *Cell Death Dis* (2019) 10:544. doi: 10.1038/s41419-019-1757-0

119. Nie X, Tan J, Dai Y, Liu Y, Zou J, Sun J, et al. CCL5 deficiency rescues pulmonary vascular dysfunction, and reverses pulmonary hypertension *via* caveolin-1-dependent BMPR2 activation. *J Mol Cell Cardiol* (2018) 116:41–56. doi: 10.1016/j.yjmcc.2018.01.016

120. Amsellem V, Lipskaia L, Abid S, Poupel L, Houssaini A, Quarck R, et al. CCR5 as a treatment target in pulmonary arterial hypertension. *Circulation* (2014) 130:880–91. doi: 10.1161/CIRCULATIONAHA.114.010757

121. Zeng Y, Li N, Zheng Z, Chen R, Peng M, Liu W, et al. Screening of hub genes associated with pulmonary arterial hypertension by integrated bioinformatic analysis. *BioMed Res Int* (2021) 2021:6626094. doi: 10.1155/2021/6626094

122. Dorfmuller P, Zarka V, Durand-Gasselin I, Monti G, Balabanian K, Garcia G, et al. Chemokine RANTES in severe pulmonary arterial hypertension. *Am J Respir Crit Care Med* (2002) 165:534–9. doi: 10.1164/ajrccm.165.4.2012112

123. Xu J, Li X, Zhou S, Wang R, Wu M, Tan C, et al. Inhibition of CXCR4 ameliorates hypoxia-induced pulmonary arterial hypertension in rats. *Am J Transl Res* (2021) 13:1458–70.

124. Bordenave J, Thuillet R, Tu L, Phan C, Cumont A, Marsol C, et al. Neutralization of CXCL12 attenuates established pulmonary hypertension in rats. *Cardiovasc Res* (2020) 116:686–97. doi: 10.1093/cvr/cvz153

125. Olsson KM, Olle S, Fuge J, Welte T, Hoeper MM, Lerch C, et al. CXCL13 in idiopathic pulmonary arterial hypertension and chronic thromboembolic pulmonary hypertension. *Respir Res* (2016) 17:21. doi: 10.1186/s12931-016-0336-5

126. Zhang Y, Lin P, Hong C, Jiang Q, Xing Y, Tang X, et al. Serum cytokine profiles in patients with chronic obstructive pulmonary disease associated pulmonary hypertension identified using protein array. *Cytokine* (2018) 111:342–9. doi: 10.1016/j.cyto.2018.09.005

127. Delaney C, Davizon-Castillo P, Allawzi A, Posey J, Gandjeva A, Neeves K, et al. Platelet activation contributes to hypoxia-induced inflammation. *Am J Physiol Lung Cell Mol Physiol* (2021) 320:L413–21. doi: 10.1152/ajplung.00519.2020

128. Zawia A, Arnold ND, West L, Pickworth JA, Turton H, Iremonger J, et al. Altered macrophage polarization induces experimental pulmonary hypertension and is observed in patients with pulmonary arterial hypertension. *Arterioscler Thromb Vasc Biol* (2021) 41(1):430–45. doi: 10.1161/ATVBAHA.120.314639

129. Wang L, Zhang X, Cao Y, Ma Q, Mao X, Xu J, et al. Mice with a specific deficiency of Pfkfb3 in myeloid cells are protected from hypoxia-induced pulmonary hypertension. *Br J Pharmacol* (2021) 178:1055–72. doi: 10.1111/bph.15339

130. Xi X, Zhang J, Wang J, Chen Y, Zhang W, Zhang X, et al. SGK1 mediates hypoxic pulmonary hypertension through promoting macrophage infiltration and activation. *Anal Cell Pathol (Amst)* (2019) 2019:3013765. doi: 10.1155/2019/3013765

131. Bochenek ML, Rosinus NS, Lankeit M, Hobohm L, Bremmer F, Schutz E, et al. From thrombosis to fibrosis in chronic thromboembolic pulmonary hypertension. *Thromb Haemost* (2017) 117:769–83. doi: 10.1160/TH16-10-0790

132. Miao R, Dong X, Gong J, Li Y, Guo X, Wang J, et al. Cell landscape atlas for patients with chronic thromboembolic pulmonary hypertension after pulmonary endarterectomy constructed using single-cell RNA sequencing. *Aging (Albany NY)* (2021) 13:16485–99. doi: 10.18632/aging.203168

133. Price LC, Caramori G, Perros F, Meng C, Gambaryan N, Dorfmuller P, et al. Nuclear factor kappa-b is activated in the pulmonary vessels of patients with end-stage idiopathic pulmonary arterial hypertension. *PloS One* (2013) 8(10): e75415. doi: 10.1371/journal.pone.0075415

134. Masaki T, Okazawa M, Asano R, Inagaki T, Ishibashi T, Yamagishi A, et al. Aryl hydrocarbon receptor is essential for the pathogenesis of pulmonary arterial hypertension. *Proc Natl Acad Sci U.S.A.* (2021) 118(11):e2023899118. doi: 10.1073/pnas.2023899118

135. Lariviere R, Gauthier-Bastien A, Ung RV, St-Hilaire J, Mac-Way F, Richard DE, et al. Endothelin type a receptor blockade reduces vascular calcification and inflammation in rats with chronic kidney disease. *J Hypertens* (2017) 35:376–84. doi: 10.1097/HJH.0000000000001161

136. Chen JY, Wu YP, Li CY, Jheng HF, Kao LZ, Yang CC, et al. PPARgamma activation improves the microenvironment of perivascular adipose tissue and attenuates aortic stiffening in obesity. *J BioMed Sci* (2021) 28:22. doi: 10.1186/s12929-021-00720-y

137. Sharma N, Dev R, Belenchia AM, Aroor AR, Whaley-Connell A, Pulakat L, et al. Deficiency of IL12p40 (Interleukin 12 p40) promotes ang II (Angiotensin II)-induced abdominal aortic aneurysm. *Arterioscler Thromb Vasc Biol* (2019) 39:212–23. doi: 10.1161/ATVBAHA.118.311969

138. Tamosiuniene R, Manouvakhova O, Mesange P, Saito T, Qian J, Sanyal M, et al. Dominant role for regulatory T cells in protecting females against pulmonary hypertension. *Circ Res* (2018) 122:1689–702. doi: 10.1161/CIRCRESAHA.117.312058

139. Chu Y, Xiangli X, Xiao W. Regulatory T cells protect against hypoxia-induced pulmonary arterial hypertension in mice. *Mol Med Rep* (2015) 11:3181–7. doi: 10.3892/mmr.2014.3106

140. Ormiston ML, Chang C, Long LL, Soon E, Jones D, Machado R, et al. Impaired natural killer cell phenotype and function in idiopathic and heritable pulmonary arterial hypertension. *Circulation* (2012) 126:1099–109. doi: 10.1161/CIRCULATIONAHA.112.110619

141. Mao M, Zhang M, Ge A, Ge X, Gu R, Zhang C, et al. Granzyme b deficiency promotes osteoblastic differentiation and calcification of vascular smooth muscle cells in hypoxic pulmonary hypertension. *Cell Death Dis* (2018) 9:221. doi: 10.1038/s41419-018-0315-5

142. Maston LD, Jones DT, Giermakowska W, Howard TA, Cannon JL, Wang W, et al. Central role of T helper 17 cells in chronic hypoxia-induced pulmonary hypertension. *Am J Physiol Lung Cell Mol Physiol* (2017) 312:L609–24. doi: 10.1152/ajplung.00531.2016

143. Kelly C, Mwandumba HC, Heyderman RS, Jambo K, Kamng'ona R, Chammudzi M, et al. HIV-Related arterial stiffness in Malawian adults is associated with the proportion of PD-1-Expressing CD8+ T cells and reverses with antiretroviral therapy. *J Infect Dis* (2019) 219:1948–58. doi: 10.1093/infdis/jiz015

144. Florentin J, Zhao J, Tai YY, Vasamsetti SB, O'Neil SP, Kumar R, et al. Interleukin-6 mediates neutrophil mobilization from bone marrow in pulmonary hypertension. *Cell Mol Immunol* (2021) 18:374–84. doi: 10.1038/s41423-020-00608-1

145. Stroka KM, Levitan I, Aranda-Espinoza H. OxLDL and substrate stiffness promote neutrophil transmigration by enhanced endothelial cell contractility and ICAM-1. *J Biomech* (2012) 45:1828–34. doi: 10.1016/j.jbiomech.2012.04.011

146. Hoffmann J, Yin J, Kukucka M, Yin N, Saarikko I, Sterner-Kock A, et al. Mast cells promote lung vascular remodelling in pulmonary hypertension. *Eur Respir J* (2011) 37:1400–10. doi: 10.1183/09031936.00043310

147. Bartelds B, van Loon RLE, Mohaupt S, Wijnberg H, Dickinson MG, Boersma B, et al. Mast cell inhibition improves pulmonary vascular remodeling in pulmonary hypertension. *Chest* (2012) 141:651–60. doi: 10.1378/chest.11-0663

148. Dahal BK, Kosanovic D, Kaulen C, Cornitescu T, Savai R, Hoffmann J, et al. Involvement of mast cells in monocrotaline-induced pulmonary hypertension in rats. *Respir Res* (2011) 12:60. doi: 10.1186/1465-9921-12-60

149. Farha S, Sharp J, Asosingh K, Park M, Comhair SA, Tang WH, et al. Mast cell number, phenotype, and function in human pulmonary arterial hypertension. *Pulm Circ* (2012) 2:220–8. doi: 10.4103/2045-8932.97609

150. Weng M, Baron DM, Bloch KD, Luster AD, Lee JJ, Medoff BD. Eosinophils are necessary for pulmonary arterial remodeling in a mouse model of eosinophilic inflammation-induced pulmonary hypertension. *Am J Physiol Lung Cell Mol Physiol* (2011) 301:L927–936. doi: 10.1152/ajplung.00049.2011

151. Sun L, Ning C, Liu J, Yao T, Zhang L, Zhao L, et al. The association between cumulative c-reactive protein and brachial-ankle pulse wave velocity. *Aging Clin Exp Res* (2020) 32:789–96. doi: 10.1007/s40520-019-01274-8

152. Scott HA, Quach B, Yang X, Ardekani S, Cabrera AP, Wilson R, et al. Matrix stiffness exerts biphasic control over monocyte-endothelial adhesion *via* rho-mediated ICAM-1 clustering. *Integr Biol (Camb)* (2016) 8:869–78. doi: 10.1039/C6IB00084C

153. Deng H, Song Z, Xu H, Deng X, Zhang Q, Chen H, et al. MicroRNA-1185 promotes arterial stiffness though modulating VCAM-1 and e-selectin expression. *Cell Physiol Biochem* (2017) 41:2183–93. doi: 10.1159/000475576

154. Sun W, Chan SY. Pulmonary arterial stiffness: An early and pervasive driver of pulmonary arterial hypertension. *Front Med (Lausanne)* (2018) 5:204. doi: 10.3389/fmed.2018.00204

155. Wang Z, Lakes RS, Eickhoff JC, Chesler NC. Effects of collagen deposition on passive and active mechanical properties of large pulmonary arteries in hypoxic pulmonary hypertension. *Biomech Model Mechanobiol* (2013) 12:1115–25. doi: 10.1007/s10237-012-0467-7

156. Franz M, Grun K, Betge S, Rohm I, Ndongson-Dongmo B, Bauer R, et al. Lung tissue remodelling in MCT-induced pulmonary hypertension: A proposal for a novel scoring system and changes in extracellular matrix and fibrosis associated gene expression. *Oncotarget* (2016) 7:81241–54. doi: 10.18632/oncotarget.13220

157. Thenappan T, Prins KW, Pritzker MR, Scandurra J, Volmers K, Weir EK. The critical role of pulmonary arterial compliance in pulmonary hypertension. *Ann Am Thorac Soc* (2016) 13:276–84. doi: 10.1513/AnnalsATS.201509-599FR

158. Moreno J, Escobedo D, Calhoun C, Le Saux CJ, Han HC. Arterial wall stiffening in caveolin-1 deficiency-induced pulmonary artery hypertension in mice. *Exp Mech* (2021) 6:217–28. doi: 10.1007/s11340-020-00666-6

159. Mierke J, Christoph M, Augstein A, Pfluecke C, Jellinghaus S, Woitek F, et al. Influence of caveolin-1 and endothelial nitric oxide synthase on adventitial inflammation in aortic transplants. *Kardiol Pol* (2020) 78:124–30. doi: 10.33963/KP.15079

160. Bloodworth NC, Clark CR, West JD, Snider JC, Gaskill C, Shay S, et al. Bone marrow-derived proangiogenic cells mediate pulmonary arteriole stiffening *via* serotonin 2B receptor dependent mechanism. *Circ Res* (2018) 123:e51–64. doi: 10.1161/CIRCRESAHA.118.313397

161. Quintero-Villegas A, Valdes-Ferrer SI. Role of 5-HT7 receptors in the immune system in health and disease. *Mol Med* (2019) 26:2. doi: 10.1186/s10020-019-0126-x

162. Schafer M, Ivy DD, Nguyen K, Boncella K, Frank BS, Morgan GJ, et al. Metalloproteinases and their inhibitors are associated with pulmonary arterial stiffness and ventricular function in pediatric pulmonary hypertension. *Am J Physiol Heart Circ Physiol* (2021) 321:H242–52. doi: 10.1152/ajpheart.00750.2020

163. Lammers S, Scott D, Hunter K, Tan W, Shandas R, Stenmark KR. Mechanics and function of the pulmonary vasculature: implications for pulmonary vascular disease and right ventricular function. *Compr Physiol* (2012) 2:295–319. doi: 10.1002/cphy.c100070

164. Protogerou AD, Zampeli E, Fragiadaki K, Stamatelopoulos K, Papamichael C, Sfikakis PP. A pilot study of endothelial dysfunction and aortic stiffness after interleukin-6 receptor inhibition in rheumatoid arthritis. *Atherosclerosis* (2011) 219:734–6. doi: 10.1016/j.atherosclerosis.2011.09.015

165. Tuttolomondo A, Pecoraro R, Di Raimondo D, Di Sciacca R, Canino B, Arnao V, et al. Immune-inflammatory markers and arterial stiffness indexes in subjects with acute ischemic stroke with and without metabolic syndrome. *Diabetol Metab Syndr* (2014) 6:28. doi: 10.1186/1758-5996-6-28

166. Hurst LA, Dunmore BJ, Long L, Crosby A, Al-Lamki R, Deighton J, et al. TNFalpha drives pulmonary arterial hypertension by suppressing the BMP type-II receptor and altering NOTCH signalling. *Nat Commun* (2017) 8:14079. doi: 10.1038/ncomms14079

167. Vlachopoulos C, Gravos A, Georgiopoulos G, Terentes-Printzios D, Ioakeimidis N, Vassilopoulos D, et al. The effect of TNF-a antagonists on aortic stiffness and wave reflections: a meta-analysis. *Clin Rheumatol* (2018) 37:515–26. doi: 10.1007/s10067-017-3657-y

168. Frangogiannis NG. The extracellular matrix in ischemic and nonischemic heart failure. *Circ Res* (2019) 125:117–46. doi: 10.1161/CIRCRESAHA.119.311148

169. Zhang J, Tang L, Dai F, Qi Y, Yang L, Liu Z, et al. ROCK inhibitors alleviate myofibroblast transdifferentiation and vascular remodeling *via* decreasing TGFbeta1-mediated RhoGDI expression. *Gen Physiol Biophys* (2019) 38:271–80. doi: 10.4149/gpb_2019017

170. Baum J, Duffy HS. Fibroblasts and myofibroblasts: what are we talking about? *J Cardiovasc Pharmacol* (2011) 57:376–9. doi: 10.1097/FJC.0b013e3182116e39

171. Anwar A, Li M, Frid MG, Kumar B, Gerasimovskaya EV, Riddle SR, et al. Osteopontin is an endogenous modulator of the constitutively activated phenotype of pulmonary adventitial fibroblasts in hypoxic pulmonary hypertension. *Am J Physiol Lung Cell Mol Physiol* (2012) 303:L1–L11. doi: 10.1152/ajplung.00050.2012

172. Barman SA, Chen F, Su Y, Dimitropoulou C, Wang Y, Catravas JD, et al. NADPH oxidase 4 is expressed in pulmonary artery adventitia and contributes to hypertensive vascular remodeling. *Arterioscler Thromb Vasc Biol* (2014) 34:1704–15. doi: 10.1161/ATVBAHA.114.303848

173. Chazova I, Loyd JE, Zhdanov VS, Newman JH, Belenkov Y, Meyrick B. Pulmonary artery adventitial changes and venous involvement in primary pulmonary hypertension. *Am J Pathol* (1995) 146:389–97.

174. Chan EC, Peshavariya HM, Liu GS, Jiang F, Lim SY, Dusting GJ. Nox4 modulates collagen production stimulated by transforming growth factor beta1 *in vivo* and *in vitro*. *Biochem Biophys Res Commun* (2013) 430:918–25. doi: 10.1016/j.bbrc.2012.11.138

175. Lin YC, Sung YK, Jiang X, Peters-Golden M, Nicolls MR. Simultaneously targeting myofibroblast contractility and extracellular matrix cross-linking as a therapeutic concept in airway fibrosis. *Am J Transplant* (2017) 17:1229–41. doi: 10.1111/ajt.14103

176. Nave AH, Mizikova I, Niess G, Steenbock H, Reichenberger F, Talavera ML, et al. Lysyl oxidases play a causal role in vascular remodeling in clinical and experimental pulmonary arterial hypertension. *Arterioscler Thromb Vasc Biol* (2014) 34:1446–58. doi: 10.1161/ATVBAHA.114.303534

177. Raaz U, Schellinger IN, Chernogubova E, Warnecke C, Kayama Y, Penov K, et al. Transcription factor Runx2 promotes aortic fibrosis and stiffness in type 2 diabetes mellitus. *Circ Res* (2015) 117:513–24. doi: 10.1161/CIRCRESAHA.115.306341

178. Bendeck MP, Irvin C, Reidy MA. Inhibition of matrix metalloproteinase activity inhibits smooth muscle cell migration but not neointimal thickening after arterial injury. *Circ Res* (1996) 78:38–43. doi: 10.1161/01.RES.78.1.38

179. Mutgan AC, Jandl K, Kwapiszewska G. Endothelial basement membrane components and their products, matrikines: Active drivers of pulmonary hypertension? *Cells* (2020) 9(9):2029. doi: 10.3390/cells9092029

180. Bizbiz L, Bonithon-Kopp C, Ducimetiere P, Berr C, Alperovitch A, Robert L. Relation of serum elastase activity to ultrasonographically assessed carotid artery wall lesions and cardiovascular risk factors. *EVA study Atheroscl* (1996) 120:47–55. doi: 10.1016/0021-9150(95)05676-9

181. Yasmin, McEniery CM, Wallace S, Dakham Z, Pulsalkar P, Maki-Petaja K, et al. Matrix metalloproteinase-9 (MMP-9), MMP-2, and serum elastase activity are associated with systolic hypertension and arterial stiffness. *Arterioscler Thromb Vasc Biol* (2005) 25:372. doi: 10.1161/01.ATV.0000151373.33830.41

182. Diaz-Canestro C, Puspitasari YM, Liberale L, Guzik TJ, Flammer AJ, Bonetti NR, et al. MMP-2 knockdown blunts age-dependent carotid stiffness by decreasing elastin degradation and augmenting eNOS activation. *Cardiovasc Res* (2021) 118 (10):2385–96. doi: 10.1093/eurheartj/ehab724.3378

183. Xiong W, MacTaggart J, Knispel R, Worth J, Persidsky Y, Baxter BT. Blocking TNF-alpha attenuates aneurysm formation in a murine model. *J Immunol* (2009) 183:2741–6. doi: 10.4049/jimmunol.0803164

184. Leopold JA. Vascular calcification: Mechanisms of vascular smooth muscle cell calcification. *Trends Cardiovasc Med* (2015) 25:267–74. doi: 10.1016/j.tcm.2014.10.021

185. Hayden MR, Tyagi SC, Kolb L, Sowers JR, Khanna R. Vascular ossification-calcification in metabolic syndrome, type 2 diabetes mellitus, chronic kidney disease, and calciphylaxis-calcific uremic arteriolopathy: The emerging role of sodium thiosulfate. *Cardiovasc Diabetol* (2005) 4:4. doi: 10.1186/1475-2840-4-4

186. Weng JJ, Su Y. Nuclear matrix-targeting of the osteogenic factor Runx2 is essential for its recognition and activation of the alkaline phosphatase gene. *Biochim Biophys Acta* (2013) 1830:2839–52. doi: 10.1016/j.bbagen.2012.12.021

187. Cui RR, Li SJ, Liu LJ, Yi L, Liang QH, Zhu X, et al. MicroRNA-204 regulates vascular smooth muscle cell calcification *in vitro* and *in vivo*. *Cardiovasc Res* (2012) 96:320–9. doi: 10.1093/cvr/cvs258

188. Zhang J, Zheng B, Zhou PP, Zhang RN, He M, Yang Z, et al. Vascular calcification is coupled with phenotypic conversion of vascular smooth muscle cells through Klf5-mediated transactivation of the Runx2 promoter. *Biosci Rep* (2014) 34:e00148. doi: 10.1042/BSR20140103

189. Gutierrez FR, Moran CJ, Ludbrook PA, McKnight RC, Weldon CS. Pulmonary arterial calcification with reversible pulmonary hypertension. *AJR Am J Roentgenol* (1980) 135:177–8. doi: 10.2214/ajr.135.1.177

190. Akmal M, Barndt RR, Ansari AN, Mohler JG, Massry SG. Excess PTH in CRF induces pulmonary calcification, pulmonary hypertension and right ventricular hypertrophy. *Kidney Int* (1995) 47:158–63. doi: 10.1038/ki.1995.18

191. Ohyama Y, Tsuchiya H, Kurosawa K, Nakano A, Arai M, Nobusawa S, et al. Pulmonary hypertension with extensive calcification in small pulmonary vessels and alveolar capillary wall in a chronic hemodialysis patient. *J Cardiol cases* (2013) 8:e13–6. doi: 10.1016/j.jccase.2013.02.015

192. Aluja Jaramillo F, Gutierrez FR, Diaz Telli FG, Yevenes Aravena S, Javidan-Nejad C, Bhalla S. Approach to pulmonary hypertension: From CT to clinical diagnosis. *Radiographics* (2018) 38:357–73. doi: 10.1148/rg.2018170046

193. Tanguay VF, Babin C, Giardetti G, Sohier-Poirier C, Menard-Cholette V, Ranchoux B, et al. Enhanced pulmonary artery radiodensity in pulmonary arterial hypertension: A sign of early calcification? *Am J Respir Crit Care Med* (2019) 199:799–802. doi: 10.1164/rccm.201806-1027LE

194. Philp T. Pulmonary artery calcification. *Scott Med J* (1972) 17:104–7. doi: 10.1177/003693307201700305

195. Ma C, Gu R, Wang X, He S, Bai J, Zhang L, et al. circRNA CDR1as promotes pulmonary artery smooth muscle cell calcification by upregulating CAMK2D and CNN3 *via* sponging miR-7-5p. *Mol Ther Nucleic Acids* (2020) 22:530–41. doi: 10.1016/j.omtn.2020.09.018

196. Parhami F, Basseri B, Hwang J, Tintut Y, Demer LL. High-density lipoprotein regulates calcification of vascular cells. *Circ Res* (2002) 91:570–6. doi: 10.1161/01.RES.0000036607.05037.DA

197. Paradise CR, Galvan ML, Kubrova E, Bowden S, Liu E, Carstens MF, et al. The epigenetic reader Brd4 is required for osteoblast differentiation. *J Cell Physiol* (2020) 235:5293–304. doi: 10.1002/jcp.29415

198. Sancisi V, Manzotti G, Gugnoni M, Rossi T, Gandolfi G, Gobbi G, et al. RUNX2 expression in thyroid and breast cancer requires the cooperation of three non-redundant enhancers under the control of BRD4 and c-JUN. *Nucleic Acids Res* (2017) 45:11249–67. doi: 10.1093/nar/gkx802

199. Meloche J, Lampron MC, Nadeau V, Maltais M, Potus F, Lambert C, et al. Implication of inflammation and epigenetic readers in coronary artery remodeling in patients with pulmonary arterial hypertension. *Arterioscler Thromb Vasc Biol* (2017) 37:1513–23. doi: 10.1161/ATVBAHA.117.309156

200. Van der Feen DE, Kurakula K, Tremblay E, Boucherat O, Bossers GPL, Szulcek R, et al. Multicenter preclinical validation of BET inhibition for the treatment of pulmonary arterial hypertension. *Am J Respir Crit Care Med* (2019) 200:910–20. doi: 10.1164/rccm.201812-2275OC

201. Watson KE, Parhami F, Shin V, Demer LL. Fibronectin and collagen I matrixes promote calcification of vascular cells *in vitro*, whereas collagen IV matrix is inhibitory. *Arterioscler Thromb Vasc Biol* (1998) 18:1964–71. doi: 10.1161/01.ATV.18.12.1964

202. Krohn JB, Hutcheson JD, Martinez-Martinez E, Irvin WS, Bouten CV, Bertazzo S, et al. Discoidin domain receptor-1 regulates calcific extracellular vesicle release in vascular smooth muscle cell fibrocalcific response *via* transforming growth factor-beta signaling. *Arterioscler Thromb Vasc Biol* (2016) 36:525–33. doi: 10.1161/ATVBAHA.115.307009

203. Hodroge A, Trecherel E, Cornu M, Darwiche W, Mansour A, Ait-Mohand K, et al. Oligogalacturonic acid inhibits vascular calcification by two mechanisms: Inhibition of vascular smooth muscle cell osteogenic conversion and interaction with collagen. *Arterioscler Thromb Vasc Biol* (2017) 37:1391–401. doi: 10.1161/ATVBAHA.117.309513

204. Piera-Velazquez S, Jimenez SA. Endothelial to mesenchymal transition: Role in physiology and in the pathogenesis of human diseases. *Physiol Rev* (2019) 99:1281–324. doi: 10.1152/physrev.00021.2018

205. Good RB, Gilbane AJ, Trinder SL, Denton CP, Coghlan G, Abraham DJ, et al. Endothelial to mesenchymal transition contributes to endothelial dysfunction in pulmonary arterial hypertension. *Am J Pathol* (2015) 185:1850–8. doi: 10.1016/j.ajpath.2015.03.019

206. Li L, Kim IK, Chiasson V, Chatterjee P, Gupta S. NF-kappaB mediated miR-130a modulation in lung microvascular cell remodeling: Implication in pulmonary hypertension. *Exp Cell Res* (2017) 359:235–42. doi: 10.1016/j.yexcr.2017.07.024

207. Suzuki T, Carrier EJ, Talati MH, Rathinasabapathy A, Chen X, Nishimura R, et al. Isolation and characterization of endothelial-to-mesenchymal transition cells in pulmonary arterial hypertension. *Am J Physiol Lung Cell Mol Physiol* (2018) 314:L118–26. doi: 10.1152/ajplung.00296.2017

208. Qiao L, Nishimura T, Shi L, Sessions D, Thrasher A, Trudell JR, et al. Endothelial fate mapping in mice with pulmonary hypertension. *Circulation* (2014) 129:692–703. doi: 10.1161/CIRCULATIONAHA.113.003734

209. Crnkovic S, Marsh LM, El Agha E, Voswinckel R, Ghanim B, Klepetko W, et al. Resident cell lineages are preserved in pulmonary vascular remodeling. *J Pathol* (2018) 244:485–98. doi: 10.1002/path.5044

210. Dan Q, Shi Y, Rabani R, Venugopal S, Xiao J, Anwer S, et al. Claudin-2 suppresses GEF-H1, RHOA, and MRTF, thereby impacting proliferation and profibrotic phenotype of tubular cells. *J Biol Chem* (2019) 294:15446–65. doi: 10.1074/jbc.RA118.006484

211. Ranchoux B, Antigny F, Rucker-Martin C, Hautefort A, Pechoux C, Bogaard HJ, et al. Endothelial-to-mesenchymal transition in pulmonary hypertension. *Circulation* (2015) 131:1006–18. doi: 10.1161/CIRCULATIONAHA.114.008750

212. Farrar EJ, Hiriart E, Mahmut A, Jagla B, Peal DS, Milan DJ, et al. OCT4-mediated inflammation induces cell reprogramming at the origin of cardiac valve development and calcification. *Sci Adv* (2021) 7:eabf7910. doi: 10.1126/sciadv.abf7910

213. Yao Y, Jumabay M, Ly A, Radparvar M, Cubberly MR, Bostrom KI. A role for the endothelium in vascular calcification. *Circ Res* (2013) 113:495–504. doi: 10.1161/CIRCRESAHA.113.301792

214. Yao J, Wu X, Qiao X, Zhang D, Zhang L, Ma JA, et al. Shifting osteogenesis in vascular calcification. *JCI Insight* (2021) 6 (10):e143023. doi: 10.1172/jci.insight.143023

215. Xu D, Li Y, Zhang B, Wang Y, Liu Y, Luo Y, et al. Resveratrol alleviate hypoxic pulmonary hypertension *via* anti-inflammation and anti-oxidant pathways in rats. *Int J Med Sci* (2016) 13:942–54. doi: 10.7150/ijms.16810

216. Andreakos E. Targeting cytokines in autoimmunity: New approaches, new promise. *Expert Opin Biol Ther* (2003) 3:435–47. doi: 10.1517/14712598.3.3.435

217. Hernandez-Sanchez J, Harlow L, Church C, Gaine S, Knightbridge E, Bunclark K, et al. Clinical trial protocol for TRANSFORM-UK: A therapeutic open-label study of tocilizumab in the treatment of pulmonary arterial hypertension. *Pulm Circ* (2018) 8:2045893217735820. doi: 10.1177/2045893217735820

218. Zamanian RT, Badesch D, Chung L, Domsic RT, Medsger T, Pinckney A, et al. Safety and efficacy of b-cell depletion with rituximab for the treatment of systemic sclerosis-associated pulmonary arterial hypertension: A multicenter, double-blind, randomized, placebo-controlled trial. *Am J Respir Crit Care Med* (2021) 204:209–21. doi: 10.1164/rccm.202009-3481OC

219. Toshner M, Church C, Harbaum L, Rhodes C, Villar Moreschi SS, Liley J, et al. Mendelian randomisation and experimental medicine approaches to interleukin-6 as a drug target in pulmonary arterial hypertension. *Eur Respir J* (2022) 59(3):2002463. doi: 10.1183/13993003.02463-2020

220. Hudalla H, Michael Z, Christodoulou N, Willis GR, Fernandez-Gonzalez A, Filatava EJ, et al. Carbonic anhydrase inhibition ameliorates inflammation and experimental pulmonary hypertension. *Am J Respir Cell Mol Biol* (2019) 61:512–24. doi: 10.1165/rcmb.2018-0232OC

frontiers | Frontiers in Immunology

TYPE Mini Review
PUBLISHED 17 November 2022
DOI 10.3389/fimmu.2022.1018772

OPEN ACCESS

EDITED BY
Szandor Simmons,
Charité, Universitätsmedizin
Berlin, Germany

REVIEWED BY
Henrike Janssen,
Heidelberg University Hospital, Germany
Noor Momin,
University of Pennsylvania, United States

*CORRESPONDENCE
Sophie Van Linthout
sophie.van-linthout@bih-charite.de

SPECIALTY SECTION
This article was submitted to
Inflammation,
a section of the journal
Frontiers in Immunology

RECEIVED 13 August 2022
ACCEPTED 26 October 2022
PUBLISHED 17 November 2022

CITATION
Van Linthout S and Volk H-D (2022)
Immuno-cardio-oncology: Killing
two birds with one stone?
Front. Immunol. 13:1018772.
doi: 10.3389/fimmu.2022.1018772

Immuno-cardio-oncology: Killing two birds with one stone?

Sophie Van Linthout[1,2]* and Hans-Dieter Volk[1,3]

[1]Berlin Institute of Health (BIH) at Charité-University Medicine Berlin, BIH Center for Regenerative Therapies (BCRT), Berlin, Germany, [2]German Center for Cardiovascular Research (DZHK), Partner Site Berlin, Berlin, Germany, [3]Institute of Medical Immunology, Charité-University Medicine Berlin, Berlin, Germany

Inflammation and a dysregulated immune system are common denominators of cancer and cardiovascular disease (CVD). Immuno-cardio-oncology addresses the interconnected immunological aspect in both cancer and CVD and the integration of immunotherapies and anti-inflammatory therapies in both distinct disease entities. Building on prominent examples of convergent inflammation (IL-1ß biology) and immune disbalance (CD20 cells) in cancer and CVD/heart failure, the review tackles both the roadblocks and opportunities of repurposed use of IL-1ß drugs and anti-CD20 antibodies in both fields, and discusses the use of advanced therapies e.g. chimeric antigen receptor (CAR) T cells, that can address the raising burden of both cancer and CVD. Finally, it is discussed how inspired by precision medicine in oncology, the use of biomarker-driven patient stratification is needed to better guide anti-inflammatory/immunomodulatory therapeutic interventions in cardiology.

KEYWORDS

immuno-cardio-oncology, inflammation, immune cell dysbalance, repurposed therapies, patient stratification, interdisciplinarity

Introduction

Initially focused on the detrimental effects of cancer therapies on the cardiovascular system, the field of cardio-oncology has expanded, and further investigates the commonalities between cancer and CVD. In this regard, there is accumulating evidence that inflammation and a dysbalanced immune system are common triggers in the pathogenesis of cancer and CVD. This concept is covered in immuno-cardio-oncology, which beyond the use of immunotherapies or anti-inflammatory therapies to counteract cancer or cancer therapy-related side effects also addresses the interconnected immunological aspect in both cancer and CVD, and the hereto-related potential of

integrating immunomodulatory strategies in both disease entities. Important in this context is the raising appreciation that cancer and CVD/heart failure interact in a bidirectional manner with low-grade inflammation as common trigger. Improved cancer prognosis and survival rate due to the success of recently implemented onco-therapies, allowed the awareness that among survivors, CVD is the leading cause of noncancer-related mortality (1). For lung cancer, it has been reported that 89% of the patients have an increased risk of developing atherosclerotic heart disease compared to those not afflicted with cancer (2, 3). In general, a low-grade chronic inflammation provoked by the release of pro-inflammatory cytokines (tumor necrosis factor-α, interleukin (IL)-1β, IL-6, and interferon-γ), chemokines, and soluble factors by the primary tumor cells and cells of the microenvironment into the bloodstream is suggested to stimulate CVD and heart failure (4). On the other hand, there is epidemiological evidence that CVD patients are more prone to develop cancer (5, 6), stating CVD as an oncogenic risk factor (7, 8). This is further supported by experimental findings illustrating that failing hearts stimulate tumor growth (9–12) (reverse cardio-oncology) independent of hemodynamic impairment (10), *via* epigenetically driving myeloid cells in hematopoietic reservoirs toward an immunosuppressive state and inducing monocytosis (9) and *via* the release of inflammation markers like the matricellular protein periostin (11). The relevance of secreted tumor-promoting factors is further corroborated by the observation that heart failure and inflammation markers are associated with new onset cancer incidence among participants with heart failure (10). This bidirectional interaction of cancer and CVD with inflammation and a dysregulated immune system as common denominators offer the opportunity to transfer knowledge, technologies and concepts from the haema-/oncology field to the cardiovascular field and *vice versa*. It further opens avenues to accelerate the repurposed use of approved anti-inflammatory and immunomodulatory therapies, including advanced therapies e.g. chimeric antigen receptor (CAR) T cells, that can treat both disease entities (13).

With the activation of IL-1ß signaling and dysregulation of CD20 B immune cells being prominent examples illustrating the common involvement of inflammation and a dysregulated immune balance in cancer and CVD, this minireview addresses how further inspired by the CANTOS trial, anti-IL-1ß drugs are beyond CVD and heart failure, evaluated in cancer, and how *vice versa* the anti-CD20 monoclonal antibody (rituximab), the first therapeutic antibody approved for oncology patients, is evaluated in the context of CVD and heart failure. Next, the repurposed use of advanced therapies is discussed, to finally comment the roadblocks and challenges for anti-IL-1ß and anti-CD20 repurposed strategies in cancer and CVD, and the lessons learned for improved therapies, including the relevance of biomarker-driven stratification and treatment of patients.

Convergence of inflammation and immune cell disbalance in CVD, heart failure and cancer and repurposed therapies

IL-1ß biology and anti-Il-1ß therapies

The landmark CANTOS (Canakinumab Anti-Inflammatory Thrombosis Outcome Study) trial (14), the largest cytokine inhibition trial ever completed, providing compelling proof for the inflammatory hypothesis in atherothrombosis, further evidenced that inflammation is an important trigger and valuable target in both CVD and cancer. Along with the primary observation that rates of cardiovascular events were lower in canakinumab-treated patients compared to the placebo group, further investigations revealed that IL-1ß antagonism reduced the incidence of lung cancer and cancer-related mortality (15), accentuating convergence in IL-1ß biology in CVD and cancer. Canakinumab treatment did not alter all-cause mortality, which was due to offsetting effects of reduced cancer mortality but increased fatal infections. Finally, the outcome of CANTOS was FDA rejection and European license withdrawal. The full reasons for the rejection have not been disclosed by Novartis, which do not further pursue canakinumab for cardiovascular indications, but test now its anti-cancer potential in patients with no-small-cell lung cancer (16). The high pricing of canakinumab (ca. 200,000 €/year in the United States), further favors its use for (no-small-cell lung) cancer rather than for a common indication as a secondary prevention following myocardial infarction (MI) (17).

IL-1ß is generated by the Nod-like receptor protein 3 (NLRP3) inflammasome, a multiprotein complex, part of the innate immunity, which gets activated following dangerous associated molecular patterns, like the alarmins S100A8 and S100A9 (18, 19), tobacco (20) and cholesterol crystals (21), as well as by pathogen associated molecular patterns (PAMPs), like coxsackievirus B3 (22, 23) and human papillomavirus (24), covering a broad spectrum of triggers present in or provoking both CVD/heart failure and cancer (25). Oxidized LDL and cholesterol crystals are DAMPs which activate the NLRP3 inflammasome and lead to IL-1ß secretion. IL-1ß subsequently drives atherogenesis at different stages. It increases the adhesion and homing of pro-inflammatory monocytes as well as the expression of matrix metalloproteinases, the latter boosting plaque rupture (21). IL-1ß release following MI leads to myelopoiesis and splenic monocytosis (26). Hereby, it triggers the homing and infiltration of monocytes to the atherosclerotic plaque, supporting the so called "cardiovascular continuum" and begetting subsequent MI (27). The CANTOS study was built on this concept and the hypothesis that anti-IL-1ß antagonism could blunt the recurrence of cardiovascular events. Beyond atherosclerosis and ischemic heart disease, the NLRP3

inflammasome and downstream cytokines IL-1ß, IL-18, to IL-6 play a key pathogenic role in non-ischemic, inflammatory heart disease [myocarditis (22, 28–30), pericarditis (31)] and the progression to heart failure (32, 33).

Evidence states that polymorphisms in the *NLRP3* inflammasome gene are linked with CVD and cancer development (25). Clonal hematopoiesis, the occurrence of recurrent somatic mutations in leukemia-associated genes, most commonly in *DNMT3A, TET2, and ASXL1*, promoting expansion of clonal populations of hematopoietic stem or progenitor cells, is associated with hematologic malignancies like acute leukemia and can also occur in the absence of overt hematologic transformation. In fact, the latter, so called clonal hematopoiesis with intermediate potential (CHIP), contributes causally to the development of CVD and doubles the risk for CVD, whereas clonal hematopoiesis only accounts for 0.5% of hematologic cancers (34, 35). Intriguingly, loss of the *TET2* gene in hematopoietic cells, encoding an epigenetic regulatory protein involved in DNA methylation, accelerates atherogenesis involving increased NLRP3-mediated IL-1ß signaling (36). In addition, an explorative study demonstrated that presence of CHIP variant *TET2* clones may predispose patients to improved outcomes with targeted anti-IL-1ß therapy (37). Clonal hematopoiesis is an age-dependent risk factor for leukemia and CVD and can occur without candidate driver mutations (38). It is further common in patients with non-hematologic cancers following radiation or chemotherapy where it is associated with an increased risk of hematologic cancers and adverse clinical outcome (39).

In cancer, NLRP3 and IL-1ß drive cancer progression by different means, involving promotion of tumorigenesis, angiogenesis, immunosuppression, and metastasis (40). NLRP3, IL-1ß and downstream IL-6 are further activated following cancer therapies including doxorubicin (41–44), tumor cell-targeting CAR T cells (45, 46) and immune checkpoint inhibitors (47, 48), contributing to the cytokine release syndrome and cardiac toxicity. The relevance of NLRP3 and IL-1ß in cancer progression and cancer therapy-related (cardiac) detrimental effects form the rationale of several clinical trials currently investigating the efficacy of anti-IL-1ß drugs, mainly the IL-1ß antagonist canakinumab and the natural anti-ILR antagonist, anakinra, as anti-cancer therapy alone, or in combination with CAR T cells or the checkpoint inhibitors anti-PD1 or anti-PDL1 (40). Clinical trials directed to investigate the anti-cancer effect of specific NLRP3 inflammasome inhibitors which either target components of its canonical signaling pathway or are specific to the NLRP3 protein, have not been performed so far (49). This might be explained by the complexicity of NLRP3 in cancer and stresses the need for further preclinical studies. Indeed, beyond tumorigenic effects, also anti-tumorigenic effects of the NLRP3 inflammasome have been reported depending on the type of cancer (49). This involves among others the NLRP3-mediated release of IL-18 and subsequent promotion of natural killer cell tumoricidal activity (50, 51). The tumor-suppressive function of the NLRP3 inflammasome has mostly been demonstrated for colon cancer where its preventive role is achieved by tumor immunosurveillance, maintaining epithelial integrity, producing mucus and suppressing the proliferation of intestinal epithelial cells (52). It is the result of cell type-specific responses, which altogether determine the propensity for tumorigenesis in colon cancer (53). Several single-nucleotide polymorphisms in the NLRP3 region associated with hypoproduction of IL-1β and decreased *NLRP3* expression are associated with susceptibility to Crohn's disease (54), which is a strong risk factor for colon cancer. In addition, individuals with polymorphisms in *NLRP3*, and *caspase 1* have a greater risk of gastric cancer when they are infected with *Helicobacter pylori*, displaying the interplay between genetic and environmental factors in tumorigenesis (55). Further evidence from cancers with virus-triggered etiology and inflammasome genetics in susceptibility to cancer development suggests that the NLRP3 inflammasome may have a protective role in virus-associated cancers (24, 56). Though, further investigations are needed to solidate this hypothesis. A dysregulated inflammasome signaling and dysbiosis both affect intestinal inflammation and cancer development, accentuating that in addition to genetic factors, environmental factors such as diet influence the ecology of the gut microbiota, inflammasome activation, and cancer (52).

Related to heart failure, a phase 1B trial with the specific NLRP3 inhibitor dapansutrile (OLT1177) has been completed in patients with stable systolic heart failure (https://clinicaltrials.gov/ct2/show/NCT03534297, accessed October 2021). The non-specific NLRP3 inhibitor, colchicine, a microtubule destabilizer traditionally used for the treatment and prevention of gouty arthritis, has been shown to exert anticancer effects *in vitro* and in animal models. In addition, colchicine decreased the risk of incident all-cause cancers in male patients with gout (57). A pilot trial of colchicine in urothelial cancer and other solid tumors is ongoing (NCT05279690). Colchicine is also first-line therapy for first and recurrent pericarditis. Its cardiobeneficial effect is and has been explored in different clinical trials ranging from acute MI (58) over stable coronary artery disease (59) to stable systolic heart failure (60). The benefit of colchicine in community-treated patients with PCR-proven COVID-19 advocates its use in those at risk of complications like myocarditis (61). Three clinically approved biologics for blocking IL-1, of which none of the 3 have an indication for CVD at the present time: canakinumab, anakinra, and the soluble chimeric Fc fusion protein of IL-1R1 and IL-1R3, rilonacept, have been and are currently under evaluation in trials over the wide range of CVD. The IL-6 (with IL-6 being downstream IL-1) antagonist, tocilizumab, which blocks soluble and membrane-bound IL-6R, exerts beneficial effects in a high-risk population (rheumatoid arthritis patients), even as it increases total cholesterol and low-density lipoprotein levels (62). Its

potential has also been demonstrated for refractory severe immune checkpoint inhibitor associated myocarditis (63). Reduction in biomarkers of inflammation and thrombosis relevant to atherosclerosis has been shown in individuals with chronic kidney disease and elevated levels of C-reactive protein, following treatment with the novel IL-6 ligand inhibitor, ziltivekimab (64). The NLRP3 inflammasome activator, S100A9 has been identified as a promising biomarker and therapeutic target for different cancers (19, 65, 66) as well as for MI (67) and myocarditis (18, 68), accentuating the relevance of evaluating the potential of anti-S100A9 compounds in clinical studies of cancer (19) and heart failure (69).

CD20 B cells and anti-CD20 therapies

The chimeric mouse/human CD20-targeting monoclonal antibody (mAb) rituximab (RTX), the first therapeutic antibody approved for oncology patients, has since its initial approval in 1997, improved the prognosis of various B cell malignancies (70). About one million patients worldwide are given anti-CD0 antibodies such as RTX for the treatment of B cell-associated diseases. In clinical practice, CD20 depleting agents are not only approved for B cell-related cancers, but also increasingly used on- and off-label for autoimmune diseases, such as rheumatoid arthritis, multiple sclerosis and systemic lupus erythematosus (71). Though, RTX in patients with hematological cancers and autoimmune disease has been associated with both atrial and ventricular arrhythmias (72) and acute myocardial ischaemia (73). Its use in CVD is untested and currently contraindicated.

The transmembrane phospholipid protein CD20, which appears on surface in the physiological maturation from pre-B to mature B lymphocytes, is also expressed on B cell-derived malignancies. Anti-CD20 mAb acts by depleting normal and malignant B cells. Anti-tumor activity of anti-CD20 has been attributed to 4 main mechanisms: antibody-dependent cellular toxicity, complement-dependent cytotoxicity, antibody-dependent phagocytosis, and FcR-dependent mechanisms. Though, despite two decades of clinical use, there is still incomplete understanding of the mechanisms behind RTX efficacy, and the biological function of CD20. Part of the complexity is the importance of the cellular microenvironment and circulatory dynamics of B cells in the efficiency of CD20 mAb-directed therapies (74). In non-B cell derived cancers, presence of CD20+ B cells in tertiary lymphoid structures around tumors is predictive of improved cancer outcome and response to checkpoint blockade (75, 76). It is suggested that the B cells might contribute to the anti-tumor response by producing antibodies against the tumors (76), or they express regulatory potency, but further studies are needed to understand the specific anti-tumor mechanism. Nevertheless, this finding addresses the dichotomous role of CD20+ B cells depending of the microenvironment and immune context, accentuating the complexity of translating CD20+ immunotherapies in cancer.

Beyond their role in cancer, there is accumulated evidence that B cells, both directly (by differentiating into plasma cells and secreting antibodies) and indirectly (by antigen presentation and cytokines/chemokines secretion), play an essential role in the progression of atherosclerosis and heart failure (77–79). Several subsets of B cells exist which differentially affect atherosclerosis (80). B1 (B1a and B1b) cells are considered atheroprotective *via* their release of primarily IgM natural antibodies against oxidation-specific epitopes that block the uptake of oxidized LDL by macrophages, preventing foam cell formation and facilitating the clearance of apoptotic cells (81, 82). In contrast, B2 cells (marginal zone and follicular B cells) are proatherogenic *via* the release of proatherogenic (auto)antibodies (79, 83). B regulatory cells have been reported to protect against atherosclerosis *via* inducing immunosuppressive T regulatory cells (84), but their importance remains controversial (85). Innate response activator B cells exert proatherogeneic effects by promoting myeloid activation (80, 86). In mice, CD20-mediated B cell depletion affects predominantly B2 cells, while B1 cells are relatively maintained (87), and is atheroprotective (79, 83). In patients, RTX-treatment has been associated with reduced endothelial dysfunction (88), decreased intima-media thickness (89) and lower arterial stiffness (90).

In the heart, anti-cardiac autoantibodies contribute directly to cardiac injury by functional or cytotoxic effects following target cell binding as well as indirectly by the formation of antigen-antibody complexes and related complement activation and inflammation [for review (77)]. Experimental evidence illustrates the involvement of mature B lymphocytes in the mobilization of inflammatory monocytes into the heart after acute MI in mice, leading to increased infarct size and deterioration of cardiac function (78). In frame with the shown protective effect of RTX in this experimental acute MI setting, an early phase experimental medicine trial, recently demonstrated safety and feasibility of a single infusion of RTX given acutely in patients with ST-elevation MI (STEMI) (91) i.e. targeting the initial inflammatory phase of damage seen in acute MI. In patients with dilated cardiomyopathy, the frequency of TNF-α-secreting B cells is increased and positively correlates with procollagen type III (92). In chronic states, RTX has been successfully applied in a case series of patients with inflammatory cardiomyopathy (93), and improved survival in cardiac allograft patients with antibody-mediated rejection (94). Though, accelerated allograft vasculopathy with RTX after cardiac transplantation has also been demonstrated (95). Safety of RTX is currently evaluated in a phase II, single-centered, single group, prospective clinical trial in stable patients with functional class III/IV according to the NYHA classification with HFrEF with an inadequate response to treatment (96).

(Repurposed) use of advanced therapies

CAR T cell therapy has achieved durable clinical responses in patients with CD19-expressing refractory and relapsed B cell malignancies and CD269 (B-cell maturation antigen (BCMA))-expressing multiple myeloma cells and is increasingly investigated as a therapeutic option of other malignancies (97). Despite their clinical success, the use of CAR T cells can result in significant toxicities that are directly associated with the induction of powerful immune effector responses. This includes the induction of a potentially life-threatening cytokine release syndrome, which can lead to cardiovascular manifestations as tachycardia, hypotension, reduced ejection fraction and cardiogenic shock. Pretreatment with anti-inflammatory drugs, like anti-IL-6R mAb, new gene-editing technologies of *ex vivo* CAR T cell generation decreases this risk. In addition, next-generation of designed bispecific CD3-engager antibodies, targeting endogenous T cells to a defined target cell with high efficiency but limited side effects (98) opens new opportunities to use in cancer and non-cancer diseases without enhanced risk of CVD or even to treat CVD/heart failure by immune targeting (99).

Intriguingly, cardiac fibroblasts are the main source of NLRP3 inflammasome activity in the heart (100), whereas the NLRP3 inflammasome in cancer-associated fibroblasts links tissue damage with inflammation in breast cancer progression and metastasis (101). The raising relevance of fibroblasts as inflammatory supporter cells, together with their well-recognized importance as extracellular matrix-producing cells in both heart failure and cancer (102), identify fibroblasts as potential novel target cell in advanced therapies counteracting heart failure and cancer. Therefore, selective targeting "inflamed" fibroblasts would be a major breakthrough. Very recently, Rurik et al. designed a highly innovative immunotherapy strategy to generate transient CAR T cells that can recognize the fibrotic cells in the heart by *in vivo* RNA-delivery technology. Analysis of a mouse model of heart failure revealed that the approach was very successful in reducing fibrosis and restoring cardiac function (103).

Lessons from and opportunities for repurposed use of anti-IL-1ß and anti-CD20 therapies

Lessons from NLRP3/IL-1ß and CD20 cells in cancer and CVD indicate their complexity in the pathogenesis of both separate disease entities. Their contribution to the pathogenesis is time- and context-dependent, depending on the microenvironment and immune contexture, and for NLRP3/IL-1ß may even be cell-dependent. The dichotomous response of IL-1ß and CD20 cells on cancer and CVD/heart failure addresses the difficulty of immunotherapies within each field and of translating immunotherapies from one field to the other. On the other hand, findings from the CANTOS study illustrating how IL-1ß antagonism may reduce cardiovascular events and the incidence of lung cancer underscore the possibility of killing two birds with one stone. Though, further studies are needed to clarify whether, based on the current knowledge related to the involvement of the NLRP3 inflammasome in cancer progression and cancer-therapy (doxorubicin, CAR T cells, checkpoint inhibitors,…)-related cardiac toxicity and side effects, this statement also accounts for anti-IL-1ß drugs as combination therapy with an anti-cancer treatment. The double anticancer and cardioprotective effect of anti-IL-1ß drugs let raise the hypothesis that combination of an anti-IL1ß drug with an anti-cancer therapy will allow to decrease the dose of the primary anti-cancer drug and herewith related deleterious effects. Therefore, further preclinical investigations are needed evaluating both the anti-cancer effect and the cardioprotective potential of the adjuvant anti-IL-1ß drug *via* the use of translational models, i.e. tumor-bearing mice treated with the anti-cancer drug. A large limitation of studies exploring the protective effect of anti-IL-1ß on doxorubicin-induced cardiotoxicity so far was that mainly non-tumor bearing mice were used, lacking the contribution of the tumor-associated inflammation on cardiac dysfunction. Furthermore, many studies were/are often directed at exploring only one of both aspects, be it the oncologist investigating the anti-cancer aspect and the cardiologist evaluating the cardioprotective effect of the drug, underscoring the necessity of interdisciplinary investigations.

Biomarker-driven stratification

Learning from precision medicine in oncology and the disappointing results from past clinical trials with anti-inflammatory therapies in CVD and heart failure reflecting the diversity of inflammation in those patients (69), has led to the recognition of the need for patient stratification to better guide anti-inflammatory/immunomodulatory therapeutic interventions in the cardiology field (104). In fact, the outcome of the CANTOS trial (14), is partly built on the specific inclusion of post-MI patients with a residual inflammatory risk mirrored by high sensitive C-reactive protein levels, reflecting high IL-1ß levels (105), and their hereto treatment with the IL-1ß antibody canakinumab. Another example illustrating the power of biomarker-driven therapies, here the treatment of patients with a specific immune profile with a hereto-connected immune cell-targeted strategy, follows from virus-negative inflammatory cardiomyopathy patients with endomyocardial biopsies positive for CD20-positive B cells. Evidence from a case series illustrated that the clinical course of those patients,

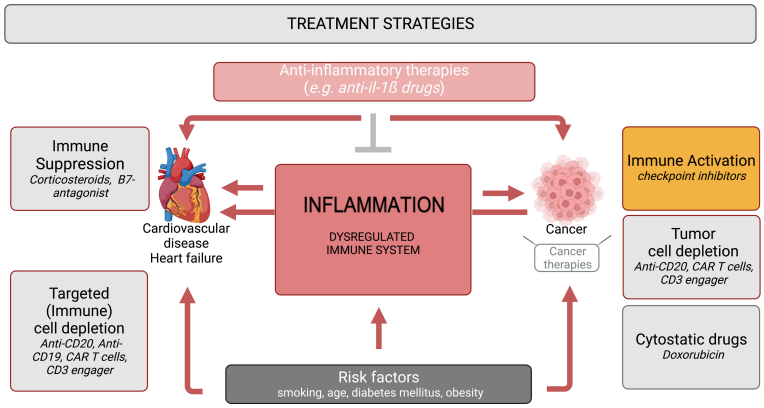

FIGURE 1
Immuno-cardio-oncology – anti-inflammatory and immunomodulatory strategies in CVD/heart failure and cancer. Inflammation and a dysbalanced immune system, provoked by risk factors such as smoking, age, diabetes mellitus and obesity, are common triggers in the pathogenesis of cancer and CVD/heart failure. Anti-cancer therapies comprise strategies directed to activate the immune response e.g. checkpoint inhibitors, to deplete tumor cells (anti-CD20, CAR T cells, CD3 engager), and cytostatic drugs e.g. doxorubicin, of which checkpoint inhibitors, CAR T cells and doxorubicin provoke cardiac inflammation. In contrast, immunosuppressive therapies like corticosteroids and B7-antagonists are used for the treatment of CVD and heart failure. Repurposed (immune) cell depletion strategies (anti-CD20, CD19 antibodies, CAR T cells, CD3 engager) have entered the cardiology field. Anti-inflammatory therapies (e.g. anti-IL-1ß drugs) are under investigation for the treatment of cancer, cancer therapy-related inflammation and CVD/heart failure.

refractory to a classical immunosuppressive therapy with prednisolone and azathioprine, improved following repurposed treatment with the anti-cancer drug RTX (93).

Despite the ability to identify and quantify specific immune cell subsets in endomyocardial biopsies of patients with suspected myocarditis/inflammatory cardiomyopathy, aetiology-specific therapies for myocarditis/inflammatory cardiomyopathy are still in their infancy (106, 107). This might be partly explained by the tools used to diagnose myocarditis/inflammatory cardiomyopathy, which is – following the ESC guidelines – based on the quantification of CD3 and CD68/Mac-1 infiltrating cells in endomyocardial biopsies *via* immunohistochemistry (≥ 14 leukocytes/mm^2 including up to 4 monocytes/mm^2 with the presence of CD3 positive T-lymphocytes ≥ 7 cells/mm^2) (108). This classical diagnostic work-up does not differentiate between T cell subsets (e.g. Treg/Teff), nor between pro- and inflammatory monocytes. This calls for a further defined and standardized evaluation of immune cells subtypes, gene expression profiles, or imaging to better mirror the cardiac immune homeostasis in those patients, allowing better patient stratification and differentiation of the stage in the pathogenesis. In this regard it is important to address that immune signatures (109) or ratios (Treg/Teff; pro-/anti-inflammatory monocytes) better reflect the immune status, not being restricted to only one specific marker or target, which due to redundancy of inflammation may be compensated *via* other inflammatory signaling pathways. Novel technologies initially used in the (immuno)-oncology field, including single cell (nucleus) sequencing, multiplex immunofluorescence, and mass cytometry may here be of value to close the current gaps related to the diagnosis of myocarditis based on immunohistochemistry. This does not imply their integration *per se* in daily diagnostic procedures. Though, screening of clinical samples *via* those state-of-the art techniques may identify novel diagnostic targets, which may then be integrated in routine diagnostic procedures.

Conclusion

Deeper understanding of the interaction between inflammation, cancer, CVD/heart failure – addressed in immuno-cardio-oncology – opens new options for preventing negative effects of cancer and cancer therapies on the heart on the one hand and for repurposing novel targeted therapeutic options and concepts from the cancer field for treating CVD (or *vice versa*) on the other hand (Figure 1). Hereto, further investigations are needed to disentangle context- and tissue-specific inflammation among the diversity of cancer types and CVD/heart failure.

Author contributions

SVL and H-DV wrote the manuscript. SVL concepted the manuscript. All authors revised the manuscript for intellectual content and gave their final approval for publication.

Conflict of interest

The authors declare that the research was conducted in the absence of any commercial or financial relationships that could be construed as a potential conflict of interest.

The handling editor SS declared a shared parent affiliation with the authors at the time of review.

Publisher's note

References

1. Mehta LS, Watson KE, Barac A, Beckie TM, Bittner V, Cruz-Flores S, et al. Cardiovascular disease and breast cancer: Where these entities intersect: A scientific statement from the American heart association. *Circulation* (2018) 137 (8):e30–66. doi: 10.1161/CIR.0000000000000556

2. Armenian SH, Xu L, Ky B, Sun C, Farol LT, Pal SK, et al. Cardiovascular disease among survivors of adult-onset cancer: A community-based retrospective cohort study. *J Clin Oncol* (2016) 34(10):1122–30. doi: 10.1200/JCO.2015.64.0409

3. Yuan M, Li QG. Lung cancer and risk of cardiovascular disease: A meta-analysis of cohort studies. *J Cardiothorac Vasc Anesth* (2018) 32(1):e25–e7. doi: 10.1053/j.jvca.2017.04.033

4. Finke D, Heckmann MB, Frey N, Lehmann LH. Cancer-a major cardiac comorbidity with implications on cardiovascular metabolism. *Front Physiol* (2021) 12:729713. doi: 10.3389/fphys.2021.729713

5. Banke A, Schou M, Videbaek L, Moller JE, Torp-Pedersen C, Gustafsson F, et al. Incidence of cancer in patients with chronic heart failure: a long-term follow-up study. *Eur J Heart Fail* (2016) 18(3):260–6. doi: 10.1002/ejhf.472

6. Hasin T, Gerber Y, McNallan SM, Weston SA, Kushwaha SS, Nelson TJ, et al. Patients with heart failure have an increased risk of incident cancer. *J Am Coll Cardiol* (2013) 62(10):881–6. doi: 10.1016/j.jacc.2013.04.088

7. Aboumsallem JP, Moslehi J, de Boer RA. Reverse cardio-oncology: Cancer development in patients with cardiovascular disease. *J Am Heart Assoc* (2020) 9(2): e013754. doi: 10.1161/JAHA.119.013754

8. Bertero E, Canepa M, Maack C, Ameri P. Linking heart failure to cancer. *Circulation* (2018) 138(7):735–42. doi: 10.1161/CIRCULATIONAHA.118.033603

9. Koelwyn GJ, Newman AAC, Afonso MS, van Solingen C, Corr EM, Brown EJ, et al. Myocardial infarction accelerates breast cancer *via* innate immune reprogramming. *Nat Med* (2020) 26(9):1452–8. doi: 10.1038/s41591-020-0964-7

10. Meijers WC, Maglione M, Bakker SJL, Oberhuber R, Kieneker LM, de Jong S, et al. Heart failure stimulates tumor growth by circulating factors. *Circulation* (2018) 138(7):678–91. doi: 10.1161/CIRCULATIONAHA.117.030816

11. Avraham S, Abu-Sharki S, Shofti R, Haas T, Korin B, Kalfon R, et al. Early cardiac remodeling promotes tumor growth and metastasis. *Circulation* (2020) 142 (7):670–83. doi: 10.1161/CIRCULATIONAHA.120.046471

12. Ausoni S, Azzarello G. Development of cancer in patients with heart failure: How systemic inflammation can lay the groundwork. *Front Cardiovasc Med* (2020) 7:598384. doi: 10.3389/fcvm.2020.598384

13. Libby P, Kobold S. Inflammation: A common contributor to cancer, aging, and cardiovascular diseases. *Cardiovasc Res* (2019) 115(5):824–9. doi: 10.1093/cvr/cvz058

14. Ridker PM, Everett BM, Thuren T, MacFadyen JG, Chang WH, Ballantyne C, et al. Antiinflammatory therapy with canakinumab for atherosclerotic disease. *N Engl J Med* (2017) 377(12):1119–31. doi: 10.1056/NEJMoa1707914

15. Ridker PM, MacFadyen JG, Thuren T, Everett BM, Libby P, Glynn RJ, et al. Effect of interleukin-1beta inhibition with canakinumab on incident lung cancer in patients with atherosclerosis: exploratory results from a randomised, double-blind, placebo-controlled trial. *Lancet* (2017) 390(10105):1833–42. doi: 10.1016/S0140-6736(17)32247-X

16. Mullard A. NLRP3 inhibitors stoke anti-inflammatory ambitions. *Nat Rev Drug Discovery* (2019) 18(6):405–7. doi: 10.1038/d41573-019-00086-9

17. Harrington RA. Targeting inflammation in coronary artery disease. *N Engl J Med* (2017) 377(12):1197–8. doi: 10.1056/NEJMe1709904

18. Muller I, Vogl T, Pappritz K, Miteva K, Savvatis K, Rohde D, et al. Pathogenic role of the damage-associated molecular patterns S100A8 and S100A9 in coxsackievirus B3-induced myocarditis. *Circ Heart Fail* (2017) 10(11): e004125. doi: 10.1161/CIRCHEARTFAILURE.117.004125

19. Raymond E, Dalgleish A, Damber JE, Smith M, Pili R. Mechanisms of action of tasquinimod on the tumour microenvironment. *Cancer Chemother Pharmacol* (2014) 73(1):1–8. doi: 10.1007/s00280-013-2321-8

20. Zhang MY, Jiang YX, Yang YC, Liu JY, Huo C, Ji XL, et al. Cigarette smoke extract induces pyroptosis in human bronchial epithelial cells through the ROS/NLRP3/caspase-1 pathway. *Life Sci* (2021) 269:119090. doi: 10.1016/j.lfs.2021.119090

21. Miteva K, Madonna R, De Caterina R, Van Linthout S. Innate and adaptive immunity in atherosclerosis. *Vascul Pharmacol* (2018) 107:67–77. doi: 10.1016/j.vph.2018.04.006

22. Tschope C, Muller I, Xia Y, Savvatis K, Pappritz K, Pinkert S, et al. NOD2 (Nucleotide-binding oligomerization domain 2) is a major pathogenic mediator of coxsackievirus B3-induced myocarditis. *Circ Heart Fail* (2017) 10(9):e003870. doi: 10.1161/CIRCHEARTFAILURE.117.003870

23. Pappritz K, Lin J, El-Shafeey M, Fechner H, Kuhl U, Alogna A, et al. Colchicine prevents disease progression in viral myocarditis *via* modulating the NLRP3 inflammasome in the cardiosplenic axis. *ESC Heart Fail* (2022) 9(2):925–41. doi: 10.1002/ehf2.13845

24. Pontillo A, Bricher P, Leal VN, Lima S, Souza PR, Crovella S. Role of inflammasome genetics in susceptibility to HPV infection and cervical cancer development. *J Med Virol* (2016) 88(9):1646–51. doi: 10.1002/jmv.24514

25. Fernandes FP, Leal VNC, Souza de Lima D, Reis EC, Pontillo A. Inflammasome genetics and complex diseases: a comprehensive review. *Eur J Hum Genet* (2020) 28(10):1307–21. doi: 10.1038/s41431-020-0631-y

26. Leuschner F, Rauch PJ, Ueno T, Gorbatov R, Marinelli B, Lee WW, et al. Rapid monocyte kinetics in acute myocardial infarction are sustained by extramedullary monocytopoiesis. *J Exp Med* (2012) 209(1):123–37. doi: 10.1084/jem.20111009

27. Libby P, Nahrendorf M, Swirski FK. Leukocytes link local and systemic inflammation in ischemic cardiovascular disease: An expanded "Cardiovascular continuum". *J Am Coll Cardiol* (2016) 67(9):1091–103. doi: 10.1016/j.jacc.2015.12.048

28. Toldo S, Kannan H, Bussani R, Anzini M, Sonnino C, Sinagra G, et al. Formation of the inflammasome in acute myocarditis. *Int J Cardiol* (2014) 171(3): e119–21. doi: 10.1016/j.ijcard.2013.12.137

29. Savvatis K, Muller I, Frohlich M, Pappritz K, Zietsch C, Hamdani N, et al. Interleukin-6 receptor inhibition modulates the immune reaction and restores titin phosphorylation in experimental myocarditis. *Basic Res Cardiol* (2014) 109(6):449. doi: 10.1007/s00395-014-0449-2

30. Kraft L, Erdenesukh T, Sauter M, Tschope C, Klingel K. Blocking the IL-1beta signalling pathway prevents chronic viral myocarditis and cardiac remodeling. *Basic Res Cardiol* (2019) 114(2):11. doi: 10.1007/s00395-019-0719-0

31. Mauro AG, Bonaventura A, Vecchie A, Mezzaroma E, Carbone S, Narayan P, et al. The role of NLRP3 inflammasome in pericarditis: Potential for therapeutic approaches. *JACC Basic Transl Sci* (2021) 6(2):137–50. doi: 10.1016/j.jacbts.2020.11.016

32. Everett BM, Cornel JH, Lainscak M, Anker SD, Abbate A, Thuren T, et al. Anti-inflammatory therapy with canakinumab for the prevention of hospitalization for heart failure. *Circulation* (2019) 139(10):1289–99. doi: 10.1161/CIRCULATIONAHA.118.038010

33. Deswal A, Petersen NJ, Feldman AM, Young JB, White BG, Mann DL. Cytokines and cytokine receptors in advanced heart failure: an analysis of the cytokine database from the vesnarinone trial (VEST). *Circulation* (2001) 103 (16):2055–9. doi: 10.1161/01.CIR.103.16.2055

34. Jaiswal S, Fontanillas P, Flannick J, Manning A, Grauman PV, Mar BG, et al. Age-related clonal hematopoiesis associated with adverse outcomes. *N Engl J Med* (2014) 371(26):2488–98. doi: 10.1056/NEJMoa1408617

35. Jaiswal S, Natarajan P, Silver AJ, Gibson CJ, Bick AG, Shvartz E, et al. Clonal hematopoiesis and risk of atherosclerotic cardiovascular disease. *N Engl J Med* (2017) 377(2):111–21. doi: 10.1056/NEJMoa1701719

36. Fuster JJ, MacLauchlan S, Zuriaga MA, Polackal MN, Ostriker AC, Chakraborty R, et al. Clonal hematopoiesis associated with TET2 deficiency accelerates atherosclerosis development in mice. *Science* (2017) 355(6327):842–7. doi: 10.1126/science.aag1381

37. Svensson EC, Madar A, Campbell CD, He Y, Sultan M, Healey ML, et al. TET2-driven clonal hematopoiesis and response to canakinumab: An exploratory analysis of the CANTOS randomized clinical trial. *JAMA Cardiol* (2022) 7(5):521–8. doi: 10.1001/jamacardio.2022.0386

38. Zink F, Stacey SN, Norddahl GL, Frigge ML, Magnusson OT, Jonsdottir I, et al. Clonal hematopoiesis, with and without candidate driver mutations, is common in the elderly. *Blood* (2017) 130(6):742–52. doi: 10.1182/blood-2017-02-769869

39. Coombs CC, Zehir A, Devlin SM, Kishtagari A, Syed A, Jonsson P, et al. Therapy-related clonal hematopoiesis in patients with non-hematologic cancers is common and associated with adverse clinical outcomes. *Cell Stem Cell* (2017) 21(3):374–82 e4. doi: 10.1016/j.stem.2017.07.010

40. Gelfo V, Romaniello D, Mazzeschi M, Sgarzi M, Grilli G, Morselli A, et al. Roles of IL-1 in cancer: From tumor progression to resistance to targeted therapies. *Int J Mol Sci* (2020) 21(17):6009. doi: 10.3390/ijms21176009

41. Wei S, Ma W, Li X, Jiang C, Sun T, Li Y, et al. Involvement of ROS/NLRP3 inflammasome signaling pathway in doxorubicin-induced cardiotoxicity. *Cardiovasc Toxicol* (2020) 20(5):507–19. doi: 10.1007/s12012-020-09576-4

42. Marchetti C, Toldo S, Chojnacki J, Mezzaroma E, Liu K, Salloum FN, et al. Pharmacologic inhibition of the NLRP3 inflammasome preserves cardiac function after ischemic and nonischemic injury in the mouse. *J Cardiovasc Pharmacol* (2015) 66(1):1–8. doi: 10.1097/FJC.0000000000000247

43. Zhu J, Zhang J, Xiang D, Zhang Z, Zhang L, Wu M, et al. Recombinant human interleukin-1 receptor antagonist protects mice against acute doxorubicin-induced cardiotoxicity. *Eur J Pharmacol* (2010) 643(2-3):247–53. doi: 10.1016/j.ejphar.2010.06.024

44. Bent EH, Millan-Barea LR, Zhuang I, Goulet DR, Frose J, Hemann MT. Microenvironmental IL-6 inhibits anti-cancer immune responses generated by cytotoxic chemotherapy. *Nat Commun* (2021) 12(1):6218. doi: 10.1038/s41467-021-26407-4

45. Morris EC, Neelapu SS, Giavridis T, Sadelain M. Cytokine release syndrome and associated neurotoxicity in cancer immunotherapy. *Nat Rev Immunol* (2022) 22(2):85–96. doi: 10.1038/s41577-021-00547-6

46. Giavridis T, van der Stegen SJC, Eyquem J, Hamieh M, Piersigilli A, Sadelain M. CAR T cell-induced cytokine release syndrome is mediated by macrophages and abated by IL-1 blockade. *Nat Med* (2018) 24(6):731–8. doi: 10.1038/s41591-018-0041-7

47. Tengesdal IW, Dinarello A, Powers NE, Burchill MA, Joosten LAB, Marchetti C, et al. Tumor NLRP3-derived IL-1beta drives the IL-6/STAT3 axis resulting in sustained MDSC-mediated immunosuppression. *Front Immunol* (2021) 12:661323. doi: 10.3389/fimmu.2021.661323

48. Kaplanov I, Carmi Y, Kornetsky R, Shemesh A, Shurin GV, Shurin MR, et al. Blocking IL-1beta reverses the immunosuppression in mouse breast cancer and synergizes with anti-PD-1 for tumor abrogation. *Proc Natl Acad Sci U S A* (2019) 116(4):1361–9. doi: 10.1073/pnas.1812266115

49. Hamarsheh S, Zeiser R. NLRP3 inflammasome activation in cancer: A double-edged sword. *Front Immunol* (2020) 11:1444. doi: 10.3389/fimmu.2020.01444

50. Fabbi M, Carbotti G, Ferrini S. Context-dependent role of IL-18 in cancer biology and counter-regulation by IL-18BP. *J Leukoc Biol* (2015) 97(4):665–75. doi: 10.1189/jlb.5RU0714-360RR

51. Dupaul-Chicoine J, Arabzadeh A, Dagenais M, Douglas T, Champagne C, Morizot A, et al. The Nlrp3 inflammasome suppresses colorectal cancer metastatic growth in the liver by promoting natural killer cell tumoricidal activity. *Immunity* (2015) 43(4):751–63. doi: 10.1016/j.immuni.2015.08.013

52. Karki R, Kanneganti TD. Diverging inflammasome signals in tumorigenesis and potential targeting. *Nat Rev Cancer* (2019) 19(4):197–214. doi: 10.1038/s41568-019-0123-y

53. Man SM. Inflammasomes in the gastrointestinal tract: infection, cancer and gut microbiota homeostasis. *Nat Rev Gastroenterol Hepatol* (2018) 15(12):721–37. doi: 10.1038/s41575-018-0054-1

54. Villani AC, Lemire M, Fortin G, Louis E, Silverberg MS, Collette C, et al. Common variants in the NLRP3 region contribute to crohn's disease susceptibility. *Nat Genet* (2009) 41(1):71–6. doi: 10.1038/ng.285

55. Castano-Rodriguez N, Kaakoush NO, Goh KL, Fock KM, Mitchell HM. The NOD-like receptor signalling pathway in helicobacter pylori infection and related gastric cancer: A case-control study and gene expression analyses. *PloS One* (2014) 9(6):e98899. doi: 10.1371/journal.pone.0098899

56. Chen LC, Wang LJ, Tsang NM, Ojcius DM, Chen CC, Ouyang CN, et al. Tumour inflammasome-derived IL-1beta recruits neutrophils and improves local recurrence-free survival in EBV-induced nasopharyngeal carcinoma. *EMBO Mol Med* (2012) 4(12):1276–93. doi: 10.1002/emmm.201201569

57. Kuo MC, Chang SJ, Hsieh MC. Colchicine significantly reduces incident cancer in gout Male patients: A 12-year cohort study. *Med (Baltimore)* (2015) 94(50):e1570. doi: 10.1097/MD.0000000000001570

58. Tardif JC, Kouz S, Waters DD, Bertrand OF, Diaz R, Maggioni AP, et al. Efficacy and safety of low-dose colchicine after myocardial infarction. *N Engl J Med* (2019) 381(26):2497–505. doi: 10.1056/NEJMoa1912388

59. Nidorf SM, Eikelboom JW, Budgeon CA, Thompson PL. Low-dose colchicine for secondary prevention of cardiovascular disease. *J Am Coll Cardiol* (2013) 61(4):404–10. doi: 10.1016/j.jacc.2012.10.027

60. Deftereos S, Giannopoulos G, Panagopoulou V, Bouras G, Raisakis K, Kossyvakis C, et al. Anti-inflammatory treatment with colchicine in stable chronic heart failure: a prospective, randomized study. *JACC Heart Fail* (2014) 2(2):131–7. doi: 10.1016/j.jchf.2013.11.006

61. Tardif JC, Bouabdallaoui N, L'Allier PL, Gaudet D, Shah B, Pillinger MH, et al. Colchicine for community-treated patients with COVID-19 (COLCORONA): A phase 3, randomised, double-blinded, adaptive, placebo-controlled, multicentre trial. *Lancet Respir Med* (2021) 9(8):924–32. doi: 10.1016/S2213-2600(21)00222-8

62. Bacchiega BC, Bacchiega AB, Usnayo MJ, Bedirian R, Singh G, Pinheiro GD. Interleukin 6 inhibition and coronary artery disease in a high-risk population: A prospective community-based clinical study. *J Am Heart Assoc* (2017) 6(3):e005038. doi: 10.1161/JAHA.116.005038

63. Doms J, Prior JO, Peters S, Obeid M. Tocilizumab for refractory severe immune checkpoint inhibitor-associated myocarditis. *Ann Oncol* (2020) 31(9):1273–5. doi: 10.1016/j.annonc.2020.05.005

64. Ridker PM, Devalaraja M, Baeres FMM, Engelmann MDM, Hovingh GK, Ivkovic M, et al. IL-6 inhibition with ziltivekimab in patients at high atherosclerotic risk (RESCUE): A double-blind, randomised, placebo-controlled, phase 2 trial. *Lancet* (2021) 397(10289):2060–9. doi: 10.1016/S0140-6736(21)00520-1

65. Wagner NB, Weide B, Gries M, Reith M, Tarnanidis K, Schuermans V, et al. Tumor microenvironment-derived S100A8/A9 is a novel prognostic biomarker for advanced melanoma patients and during immunotherapy with anti-PD-1 antibodies. *J Immunother Cancer* (2019) 7(1):343. doi: 10.1186/s40425-019-0828-1

66. Vogl T, Eisenblatter M, Voller T, Zenker S, Hermann S, van Lent P, et al. Alarmin S100A8/S100A9 as a biomarker for molecular imaging of local inflammatory activity. *Nat Commun* (2014) 5:4593. doi: 10.1038/ncomms5593

67. Marinkovic G, Koenis DS, de Camp L, Jablonowski R, Graber N, de Waard V, et al. S100A9 links inflammation and repair in myocardial infarction. *Circ Res* (2020) 127(5):664–76. doi: 10.1161/CIRCRESAHA.120.315865

68. Muller I, Vogl T, Kuhl U, Krannich A, Banks A, Trippel T, et al. Serum alarmin S100A8/S100A9 levels and its potential role as biomarker in myocarditis. *ESC Heart Fail* (2020) 7(4):1442–51. doi: 10.1002/ehf2.12760

69. Van Linthout S, Tschope C. The quest for antiinflammatory and immunomodulatory strategies in heart failure. *Clin Pharmacol Ther* (2019) 106(6):1198–208. doi: 10.1002/cpt.1637

70. Pierpont TM, Limper CB, Richards KL. Past, present, and future of rituximab-the world's first oncology monoclonal antibody therapy. *Front Oncol* (2018) 8:163. doi: 10.3389/fonc.2018.00163

71. Chan AC, Carter PJ. Therapeutic antibodies for autoimmunity and inflammation. *Nat Rev Immunol* (2010) 10(5):301–16. doi: 10.1038/nri2761

72. Poterucha JT, Westberg M, Nerheim P, Lovell JP. Rituximab-induced polymorphic ventricular tachycardia. *Tex Heart Inst J* (2010) 37(2):218–20.

73. Armitage JD, Montero C, Benner A, Armitage JO, Bociek G. Acute coronary syndromes complicating the first infusion of rituximab. *Clin Lymphoma Myeloma* (2008) 8(4):253–5. doi: 10.3816/CLM.2008.n.035

74. Gong Q, Ou Q, Ye S, Lee WP, Cornelius J, Diehl L, et al. Importance of cellular microenvironment and circulatory dynamics in b cell immunotherapy. *J Immunol* (2005) 174(2):817–26. doi: 10.4049/jimmunol.174.2.817

75. Helmink BA, Reddy SM, Gao J, Zhang S, Basar R, Thakur R, et al. B cells and tertiary lymphoid structures promote immunotherapy response. *Nature* (2020) 577(7791):549–55. doi: 10.1038/s41586-019-1922-8

76. Cabrita R, Lauss M, Sanna A, Donia M, Skaarup Larsen M, Mitra S, et al. Tertiary lymphoid structures improve immunotherapy and survival in melanoma. *Nature* (2020) 577(7791):561–5. doi: 10.1038/s41586-019-1914-8

77. Garcia-Rivas G, Castillo EC, Gonzalez-Gil AM, Maravillas-Montero JL, Brunck M, Torres-Quintanilla A, et al. The role of b cells in heart failure and implications for future immunomodulatory treatment strategies. *ESC Heart Fail* (2020) 7(4):1387–99. doi: 10.1002/ehf2.12744

78. Zouggari Y, Ait-Oufella H, Bonnin P, Simon T, Sage AP, Guérin C, et al. B lymphocytes trigger monocyte mobilization and impair heart function after acute myocardial infarction. *Nat Med* (2013) 19:1273–80. doi: 10.1038/nm.3284

79. Ait-Oufella H, Herbin O, Bouaziz JD, Binder CJ, Uyttenhove C, Laurans L, et al. B cell depletion reduces the development of atherosclerosis in mice. *J Exp Med* (2010) 207(8):1579–87. doi: 10.1084/jem.20100155

80. Porsch F, Binder CJ. Impact of b-Cell-Targeted therapies on cardiovascular disease. *Arterioscler Thromb Vasc Biol* (2019) 39(9):1705–14. doi: 10.1161/ATVBAHA.119.311996

81. Chou MY, Fogelstrand L, Hartvigsen K, Hansen LF, Woelkers D, Shaw PX, et al. Oxidation-specific epitopes are dominant targets of innate natural antibodies in mice and humans. *J Clin Invest* (2009) 119(5):1335–49. doi: 10.1172/JCI36800

82. Rosenfeld SM, Perry HM, Gonen A, Prohaska TA, Srikakulapu P, Grewal S, et al. B-1b cells secrete atheroprotective IgM and attenuate atherosclerosis. *Circ Res* (2015) 117(3):e28–39. doi: 10.1161/CIRCRESAHA.117.306044

83. Kyaw T, Tay C, Khan A, Dumouchel V, Cao A, To K, et al. Conventional B2 b cell depletion ameliorates whereas its adoptive transfer aggravates atherosclerosis. *J Immunol* (2010) 185(7):4410–9. doi: 10.4049/jimmunol.1000033

84. Douna H, Amersfoort J, Schaftenaar FH, Kroon S, van Puijvelde GHM, Kuiper J, et al. Bidirectional effects of IL-10(+) regulatory b cells in ldlr(-/-) mice. *Atherosclerosis* (2019) 280:118–25. doi: 10.1016/j.atherosclerosis.2018.11.019

85. Sage AP, Nus M, Baker LL, Finigan AJ, Masters LM, Mallat Z. Regulatory b cell-specific interleukin-10 is dispensable for atherosclerosis development in mice. *Arterioscler Thromb Vasc Biol* (2015) 35(8):1770–3. doi: 10.1161/ATVBAHA.115.305568

86. Hilgendorf I, Theurl I, Gerhardt LM, Robbins CS, Weber GF, Gonen A, et al. Innate response activator b cells aggravate atherosclerosis by stimulating T helper-1 adaptive immunity. *Circulation* (2014) 129(16):1677–87. doi: 10.1161/CIRCULATIONAHA.113.006381

87. Hamaguchi Y, Uchida J, Cain DW, Venturi GM, Poe JC, Haas KM, et al. The peritoneal cavity provides a protective niche for B1 and conventional b lymphocytes during anti-CD20 immunotherapy in mice. *J Immunol* (2005) 174 (7):4389–99. doi: 10.4049/jimmunol.174.7.4389

88. Kerekes G, Soltesz P, Der H, Veres K, Szabo Z, Vegvari A, et al. Effects of rituximab treatment on endothelial dysfunction, carotid atherosclerosis, and lipid profile in rheumatoid arthritis. *Clin Rheumatol* (2009) 28(6):705–10. doi: 10.1007/s10067-009-1095-1

89. Novikova DS, Popkova TV, Lukina GV, Luchikhina EL, Karateev DE, Volkov AV, et al. The effects of rituximab on lipids, arterial stiffness and carotid intima-media thickness in rheumatoid arthritis. *J Korean Med Sci* (2016) 31 (2):202–7. doi: 10.3346/jkms.2016.31.2.202

90. Provan SA, Berg IJ, Hammer HB, Mathiessen A, Kvien TK, Semb AG. The impact of newer biological disease modifying anti-rheumatic drugs on cardiovascular risk factors: A 12-month longitudinal study in rheumatoid arthritis patients treated with rituximab, abatacept and tociliziumab. *PloS One* (2015) 10(6):e0130709. doi: 10.1371/journal.pone.0130709

91. Zhao TX, Aetesam-Ur-Rahman M, Sage AP, Victor S, Kurian R, Fielding S, et al. Rituximab in patients with acute ST-elevation myocardial infarction: an experimental medicine safety study. *Cardiovasc Res* (2022) 118(3):872–82. doi: 10.1093/cvr/cvab113

92. Yu M, Wen S, Wang M, Liang W, Li HH, Long Q, et al. TNF-alpha-secreting b cells contribute to myocardial fibrosis in dilated cardiomyopathy. *J Clin Immunol* (2013) 33(5):1002–8. doi: 10.1007/s10875-013-9889-y

93. Tschope C, Van Linthout S, Spillmann F, Posch MG, Reinke P, Volk HD, et al. Targeting CD20+ b-lymphocytes in inflammatory dilated cardiomyopathy with rituximab improves clinical course: a case series. *Eur Heart J Case Rep* (2019) 3 (3):ytz131. doi: 10.1093/ehjcr/ytz131

94. Ravichandran AK, Schilling JD, Novak E, Pfeifer J, Ewald GA, Joseph SM. Rituximab is associated with improved survival in cardiac allograft patients with antibody-mediated rejection: A single center review. *Clin Transpl* (2013) 27 (6):961–7. doi: 10.1111/ctr.12277

95. Starling RC, Armstrong B, Bridges ND, Eisen H, Givertz MM, Kfoury AG, et al. Accelerated allograft vasculopathy with rituximab after cardiac transplantation. *J Am Coll Cardiol* (2019) 74(1):36–51. doi: 10.1016/j.jacc.2019.04.056

96. Sanchez-Trujillo L, Jerjes-Sanchez C, Rodriguez D, Panneflek J, Ortiz-Ledesma C, Garcia-Rivas G, et al. Phase II clinical trial testing the safety of a humanised monoclonal antibody anti-CD20 in patients with heart failure with reduced ejection fraction, ICFEr-RITU2: study protocol. *BMJ Open* (2019) 9(3): e022826. doi: 10.1136/bmjopen-2018-022826

97. Schroeder BA, Jess J, Sankaran H, Shah NN. Clinical trials for chimeric antigen receptor T-cell therapy: Lessons learned and future directions. *Curr Opin Hematol* (2022) 29(4):225–32. doi: 10.1097/MOH.0000000000000723

98. Leclercq G, Steinhoff N, Haegel H, De Marco D, Bacac M, Klein C. Novel strategies for the mitigation of cytokine release syndrome induced by T cell engaging therapies with a focus on the use of kinase inhibitors. *Oncoimmunology* (2022) 11(1):2083479. doi: 10.1080/2162402X.2022.2083479

99. Rurik JG, Aghajanian H, Epstein JA. Immune cells and immunotherapy for cardiac injury and repair. *Circulation Research* (2021) 128:1766–79.

100. Kawaguchi M, Takahashi M, Hata T, Kashima Y, Usui F, Morimoto H, et al. Inflammasome activation of cardiac fibroblasts is essential for myocardial ischemia/reperfusion injury. *Circulation* (2011) 123(6):594–604. doi: 10.1161/CIRCULATIONAHA.110.982777

101. Ershaid N, Sharon Y, Doron H, Raz Y, Shani O, Cohen N, et al. NLRP3 inflammasome in fibroblasts links tissue damage with inflammation in breast cancer progression and metastasis. *Nat Commun* (2019) 10(1):4375. doi: 10.1038/s41467-019-12370-8

102. Oatmen KE, Cull E, Spinale FG. Heart failure as interstitial cancer: emergence of a malignant fibroblast phenotype. *Nat Rev Cardiol* (2019) 17 (8):523–31. doi: 10.1038/s41569-019-0286-y

103. Rurik JG, Tombacz I, Yadegari A, Mendez Fernandez PO, Shewale SV, Li L, et al. CAR T cells produced *in vivo* to treat cardiac injury. *Science* (2022) 375 (6576):91–6. doi: 10.1126/science.abm0594

104. Antman EM, Loscalzo J. Precision medicine in cardiology. *Nat Rev Cardiol* (2016) 13(10):591–602. doi: 10.1038/nrcardio.2016.101

105. Ridker PM, Luscher TF. Anti-inflammatory therapies for cardiovascular disease. *Eur Heart J* (2014) 35(27):1782–91. doi: 10.1093/eurheartj/ehu203

106. Tschope C, Ammirati E, Bozkurt B, Caforio ALP, Cooper LT, Felix SB, et al. Myocarditis and inflammatory cardiomyopathy: Current evidence and future directions. *Nat Rev Cardiol* (2021) 18(3):169–93. doi: 10.1038/s41569-020-00435-x

107. Tschope C, Cooper LT, Torre-Amione G, Van Linthout S. Management of myocarditis-related cardiomyopathy in adults. *Circ Res* (2019) 124(11):1568–83. doi: 10.1161/CIRCRESAHA.118.313578

108. Caforio AL, Pankuweit S, Arbustini E, Basso C, Gimeno-Blanes J, Felix SB, et al. Current state of knowledge on aetiology, diagnosis, management, and therapy of myocarditis: A position statement of the European society of cardiology working group on myocardial and pericardial diseases. *Eur Heart J* (2013) 34(33):2636–48. doi: 10.1093/eurheartj/eht210

109. Pesenacker AM, Chen V, Gillies J, Speake C, Marwaha AK, Sun A, et al. Treg gene signatures predict and measure type 1 diabetes trajectory. *JCI Insight* (2019) 4(6):e123879. doi: 10.1172/jci.insight.123879

frontiers | Frontiers in Immunology

TYPE Original Research
PUBLISHED 25 November 2022
DOI 10.3389/fimmu.2022.947067

OPEN ACCESS

EDITED BY
Kathleen Pappritz,
Charité Medical University of Berlin, Germany

REVIEWED BY
Jie Liu,
Zunyi Medical University, China
Venkata Ramireddy Narala,
Yogi Vemana University, India

*CORRESPONDENCE
Xiaolu Shi
fsyy00721@njucm.edu.cn
Xia Zhao
Zhaoxiahy@njucm.edu.cn

†These authors have contributed equally to this work and share first authorship

SPECIALTY SECTION
This article was submitted to Inflammation, a section of the journal Frontiers in Immunology

RECEIVED 18 May 2022
ACCEPTED 08 November 2022
PUBLISHED 25 November 2022

CITATION
Tang L, Liu L, Sun X, Hu P, Zhang H, Wang B, Zhang X, Jiang J, Zhao X and Shi X (2022) BMAL1/FOXA2-induced rhythmic fluctuations in IL-6 contribute to nocturnal asthma attacks. *Front. Immunol.* 13:947067. doi: 10.3389/fimmu.2022.947067

BMAL1/FOXA2-induced rhythmic fluctuations in IL-6 contribute to nocturnal asthma attacks

Lingling Tang[1†], Li Liu[2†], Xianhong Sun[1†], Po Hu[3], Hui Zhang[4], Bohan Wang[1], Xiaona Zhang[1], Jinjin Jiang[5], Xia Zhao[5*] and Xiaolu Shi[1*]

[1]Jiangsu Province Hospital of Chinese Medicine, Affiliated Hospital of Nanjing University of Chinese Medicine, Nanjing, Jiangsu, China, [2]Department of Central lab, Affiliated Hospital of Nanjing University of Chinese Medicine, Nanjing, Jiangsu, China, [3]Department of Respiration, Changzhou Hospital of Traditional Chinese Medicine, Changzhou, Jiangsu, China, [4]Department of Respiration, Nanjing Hospital of Chinese Medicine Affiliated to Nanjing University of Chinese Medicine, Nanjing, Jiangsu, China, [5]Jiangsu Key Laboratory of Pediatric Respiratory Disease, Institute of Pediatrics, Affiliated Hospital of Nanjing University of Chinese Medicine, Nanjing, Jiangsu, China

The circadian clock is closely associated with inflammatory reactions. Increased inflammatory cytokine levels have been detected in the airways of nocturnal asthma. However, the mechanisms that contribute to the nocturnal increase in inflammatory responses and the relationship with circadian clock remain unknown.

Methods: Inflammatory cytokine levels were measured in asthma patients with and without nocturnal symptoms. Allergic airway disease was induced in mice by ovalbumin (OVA), and different periods of light/dark cycles were used to induce circadian rhythm disorders. Serum shock was used to stimulate the rhythmic expression in human bronchial epidermal cells (16HBE). The expression and oscillation of circadian clock genes and inflammatory cytokines in 16HBE cells subjected to brain and muscle ARNT-like protein-1 (BMAL1) and Forkhead Box A2 (FOXA2) knockdown and treatment with a FOXA2 overexpression plasmid were assessed.

Results: Serum IL-6 was found to be significantly higher in asthmatic patients with nocturnal symptoms than those without nocturnal symptoms. The OVA-induced asthma model with a circadian rhythm disorder and 16HBE cells treated with serum shock showed an increase in IL-6 levels and a negative correlation with BMAL1 and FOXA2. The knockdown of BMAL1 resulted in a lower correlation between IL-6 and other rhythm clock genes. Furthermore,

knockdown of the BMAL1 and FOXA2 in 16HBE cells reduced the expression and rhythmic fluctuations of IL-6.

Conclusions: Our findings suggest that there are increased IL-6 levels in nocturnal asthma resulting from inhibition of the BMAL1/FOXA2 signalling pathway in airway epithelial cells.

KEYWORDS

asthma, nocturnal symptom, circadian, inflammatory, airway epithelial cell

Introduction

Asthma is a heterogeneous disease of the airways involving a variety of cells and cellular components. Its clinical presentation includes recurrent wheezing, shortness of breath, chest tightness, coughs that vary over time and in intensity, and variable airflow limitations (1). One asthma symptom that worsens at night is nocturnal asthma, which affects nearly 30–70% of patients (2, 3). Nocturnal asthma also appears to be associated with an increased risk of mortality as 50–68% of asthma-related deaths and respiratory arrest occurred at night (4, 5). Previous studies have demonstrated a circadian variation in the fractional exhaled nitric oxide (FeNO) and lung function in nocturnal asthma (6–8), which may be triggered by inflammations in the airways at night. FeNO has emerged as an important biomarker of T helper 2 (Th2)-mediated airway inflammation in asthma (9). Nocturnal asthma is therefore associated with a significant increase in airway inflammation at night.

The circadian clock (approximately 24 h) is a collection of intrinsic, endogenous physiological oscillators that are found in almost all lung tissue cells (10). The circadian clock system plays a crucial role in the regulation of nearly all physiological activities. Disordered circadian rhythms therefore have severe consequences on human health. The disruption of circadian clock machinery leads to the dysregulation of the inflammatory response (11). Night shift workers with disrupted circadian rhythms eventually experience autoimmunity (a mistimed rise in IL-6), which compromises host defence mechanisms (12). The genes involved in circadian rhythms include period (PER1-2), cryptochrome (CRY1-2), nuclear receptor subfamily 1, group D, member 1 (NR1D1), CLOCK, and BMAL1. Mice lacking BMAL1 gene expression in myeloid cells have been found to exhibit markedly increased inflammation when challenged with OVA (13). An improved understanding of the correlation between circadian and inflammatory cytokines may therefore allow for strategies to be devised for the prevention, treatment, and recovery from asthma.

In this study, we detected inflammatory cytokines in asthma patients with and without nocturnal symptoms and found that inflammatory factors, such as IL-6, were increased in the peripheral blood of patients with nocturnal asthma. We further explored the relationship between circadian clock genes and inflammatory cytokines in a disordered circadian rhythm using OVA-challenged mice and cellular serum shock models. In addition, we discovered a negative regulatory effect of FOXA2 on IL-6 and determined that FOXA2 is involved in the circadian clock genes that co-regulate the rhythmic fluctuations of IL-6.

Materials and methods

Human samples

This study was approved by the Ethics Committee of the Affiliated Hospital of Nanjing University of Chinese Medicine (approval number 2019NL-024-02). All patients provided informed consent.

We retrospectively analysed the medical records of patients with asthma who were admitted to the Affiliated Hospital of Nanjing University of Chinese Medicine (Nanjing, Jiangsu, China) from November 2019 to December 2021. The inclusion criteria for patients with asthma included a clinical diagnosis of asthma according to the Global Initiative for Asthma Guidelines (2021) (14).

Patients with combined serious primary diseases or missing data were excluded from the analysis. The data that were assessed included baseline clinical data, pulmonary function tests, comorbidities, immunoglobulin E (IgE), routine blood tests, blood biochemistry, and cytokine measurements. Treatment decisions were made by the designated physician throughout the study period and were not influenced by the protocol for the study.

Nocturnal asthma, which is defined by symptoms that include coughing, wheezing, and dyspnoea, worsens at night and disturbs sleep (15). Blood samples from all patients were therefore collected in the morning between 4–5 A.M. Blood was collected from asthma patients with nocturnal symptoms on the days of attacks. Serum samples were frozen and stored at –80 °C.

Animals

All of the protocols involving animal use were approved by the Animal Ethics Committee of the Affiliated Hospital of Nanjing University of Traditional Chinese Medicine (NO:2021 DW-07-02). Thirty-six BALB/c mice (female, 18-22g, aged 6–8 weeks, Laboratory Animal Center of Jiangsu Academy of Traditional Chinese Medicine) were acclimatised in a specific pathogen-free room (temperature: 22°C ± 2°C, humidity: 55% ± 5%) with free access to food (irradiation feed) and water (sterilized). The animal experiments were performed in compliance with the ARRIVE guidelines.

OVA-induced mouse asthma model

The OVA-induced asthma model was established based on a previously described method (16). In brief, all mice were randomly assigned into two groups (control group n=6; asthma group, n=30). mice received intraperitoneal (i.p.) administrations of 100 μg of OVA complexed with 20 μg of alum (Sigma-Aldrich, St Louis, US) or saline on days 0 and 14. The mice were further challenged with 1 mg of OVA or saline intranasally (i.n.) on days 14, 25, 26, and 27 (Figure S1).

Circadian rhythm disorder mouse model

The circadian rhythm disorder mouse model used in this study was performed as previously described in other studies (17–19). On day 14 of asthma model construction, asthma group mice were randomly separated into five cohorts after sensitisation and challenge, with six mice per group. The control group (N) and normal asthma group (A) were housed with 12 h dark/12 h light (DL12) cycles. The mice from the other asthma group were individually housed with 3.5 h dark/3.5 h light (DL3.5) cycles, 24 h dark/24 h light (DL24) cycles, all-day darkness (DD), and all-daylight (LL) until day 28. Darkness began at 6:00 p.m. Lavage fluid, sera, and lung tissue were collected at 6:00 p.m. on day 28 (Figure S1).

Lung tissue analysis

Mice were anesthetised with pentobarbital (50 mg/kg). Blood plasma was collected by the abdominal aortic method. The cervical muscles and blood vessels were bluntly separated. The trachaeas were exposed by surgically opening the neck regions with minimum incisions. The lungs were lavaged using a trachaeal tube with 500 μL of chilled phosphate buffered saline (Servicebio, Wuhan, China) and a syringe while gently massaging the lung area to ensure adequate rinsing. This procedure was repeated three times. The collected bronchoalveolar lavage fluid (BALF) was immediately centrifuged at 500×g for 5 min at 4°C. The supernatant was stored at 4°C for further analysis. Flow cytometry was used to analyse the different cell types in the BALF (20). After collecting the BALF, the thoracic cavities of the mice were cut open. The inferior lobes of the left lungs in each group were removed and fixed in 4% paraformaldehyde aqueous solution (Servicebio) for the immunohistochemistry and haematoxylin-eosin (HE) staining procedures. The right lungs were immediately snap-frozen in liquid nitrogen and stored at –80°C until the total RNA and protein extractions for real-time quantitative polymerase chain reaction (RT-qPCR) and Western blot could occur.

Cell culture

Human bronchial epithelial cells (16HBE) and human embryonic kidney cells (293T) were obtained from the cell bank of the Chinese Academy of Sciences (Shanghai, China). 16HBE cells were cultured with RPMI 1640 media (Gibco, New York, USA) and 293T cells cultured with Dulbeccos's modified Eagle's medium (DMEM; Gibco), both containing 10% foetal bovine serum (FBS; Evergreen, Hangzhou, China), 100 mg/L penicillin, and 100 mg/L streptomycin (Gibco) in a 5% CO_2 incubator at 37°C. When cells grew to 70%-80% confluence, they were passaged using trypsin-ethylenediaminetetraacetic acid (Gibco).

Serum shock

Serum shock-induced synchronisation was performed based on a previously described method (21, 22). In brief, 16HBE cells were seeded in medium plates with 1×10^6 cells/plate and cultured in serum-free RPMI 1640 medium (Biological Industries, Haemek, Israel) for 24 h prior to the experiments. On the day of the experiments, the culture media were replaced with RPMI 1640 medium containing 50% horse serum (Yuanye, Shanghai, China) for 2 h. The media were then replaced with serum-free RPMI 1640. The cells were harvested and assayed at different time points (0, 4, 8, 12, 16, 20, 24, 28, 32, 36, 40, and 44 h) following serum shock and labelled as ZT0–ZT44, respectively.

Cell transfection

The 16HBE cells were seeded in 6-well plates. Follow-up experiments were performed when cell confluence reached 80%. Silent shRNAs (Hanbio, Shanghai, China) were transfected using the LipoFiter transfection reagent (Hanbio) in serum-free media. The cells were then transferred to 10% FBS-containing RPMI 1640 medium 6 h after transfection. After culturing for another 24 h, the positive populations were selected

using Blasticidin S (Beyotime, Shanghai, China). The target sequences of the shRNAs have been listed in Table S1. The FOXA2 overexpression plasmid was purchased from iGene Biotechnology Co., Ltd. The 16HBE cells were transfected with the plasmid using Lipofectamine 8000 (Beyotime) according to the manufacturer's instructions. Twenty-four hours after transfection, the medium was replaced with RPMI 1640 medium containing 10% FBS, and the cells were cultured for another 24 h. Gene silencing and overexpression were tested at the mRNA and protein levels.

ELISA

The human and mice blood samples were collected and centrifuged at 3000 rpm for 10 min at 4°C to obtain serum samples. The culture supernatant was harvested after serum shock at different time points. After centrifugation, the supernatant was taken and stored at −80°C. The serum levels of OVA-IgE were measured using an anti-OVA IgE ELISA kit (Cayman, Michigan, US). Interferon-α (INF-α), IL-2, IL-4, IL-5, IL-6, IL-8, IL-10, IL-12, IL-13, IL-17, IL-1β, and tumour necrosis factor (TNF)-α were quantified using ELISA kits (Multi Sciences, Hangzhou, China) following the manufacturer's instructions.

Immunohistochemistry

The mouse lung specimens were dehydrated, embedded in paraffin, and cut into 4-μm-thick sections. After deparaffinisation and rehydration, the sections were incubated with 3% hydrogen peroxide for 10 min to inactivate the endogenous peroxidase activity. After antigen retrieval, membrane permeabilisation was induced using 0.1% Triton X-100 in PBS for 20 min. The sections were blocked with 10% goat serum for 1 h. The slides were then incubated over night at 4°C with the primary antibodies (BMAL1, 1:200, Proteintech, 14268-1 and IL-6, 1:200, Affinity, DF6087). The secondary antibody consisting of HPR-labelled goat anti-rabbit IgG (1:200, Proteintech, S0001) was added and incubated for 1 h. Proteins were visualised with DAB (brown). Nuclei were counterstained with haematoxylin (blue).

Hematoxylin-eosin staining

The dewaxing and antigen retrieval steps were the same as those used for immunohistochemistry. First, the sections were stained with haematoxylin solution for 5 min and rinsed with tap water for 5 min. The sections were then differentiated in 1% acid alcohol for 30 s and washed again with tap water. In the bluing step, the sections were immersed in saturated lithium carbonate solution for 1 min and rinsed with tap water. Finally, the sections were counterstained with eosin Y solution for 3 min.

Western blot

The lung tissues were cut into small pieces. An appropriate amount of RIPA lysis buffer (Beyotime) containing a protease and phosphatase inhibitor mixture (Bimake, Houston, TX, US) and grinding steel balls were added and placed in a grinder to produce the homogenate. The homogenate was centrifuged at 12000× g for 20 min at 4°C. Supernatants were obtained after centrifugation. Protein concentrations were measured using the BCA protein detection kit (Beyotime). The whole cell lysates were added to a sodium dodecyl sulfate loading buffer, boiled for 10 min, and stored at −80°C. The proteins were isolated by sodium dodecyl sulfate-polyacrylamide gel electrophoresis and transferred to PVDF membranes using a membrane transfer apparatus. The membranes were blocked with 5% skimmed milk at room temperature. The corresponding primary antibodies (BMAL1, 1:1000, proteintech, 14268-1; IL-6, 1:1000, affinity, DF6087; FOXA2, 1:1000, abcam-ab108422) were then added. The membranes were incubated overnight at 4°C. After washing with Tris-buffered saline with 0.1% Tween® 20 Detergent (TBST) on the second day, the corresponding HRP-labelled goat anti-rabbit IgG antibody (1:5000, Proteintech, S0001) was added and incubated for 2 h. Finally, the protein bands were visualised following colouration with an enhanced chemiluminescence (ECL) reagent. Using GAPDH as the internal reference, the grey values of the target protein bands and the ratio of the grey values to the internal reference protein were analysed using ImageJ software.

Quantitative reverse transcription PCR

Partial lung lobes of mice and 16HBE cells were collected, and total RNA was extracted using an RNA Extraction Kit (Vazyme, Nanjing, China). cDNA was synthesised using a reverse transcription kit and stored at −20°C. The primer sequences for each gene have been listed in Table S2. The qPCR was performed using an ABI 7500 fast fluorescent quantitative PCR instrument. The thermocycling conditions were as follows: pre-denaturation at 95°C for 5 min, followed by 95°C for 10 s and 60°C for 30 s for 40 consecutive cycles. Using β-actin as an internal reference, the data were processed according to the calculation method of the relative expression amount = $2^{-\triangle\triangle Ct}$ to compare the changes in the mRNA expression levels of the samples in each group.

Luciferase reporter assays

The 293T and 16HBE cells were seeded into 96-well plates. They were transfected with IL-6 luciferase reporters, the pRL-TK vector, and the FOXA2 overexpression plasmid or blank pcDNA using LipoFiter3.0 (Hanbio). Twenty-four hours later, the

medium was removed, and the cells were collected for luciferase activity measurements using the Dual-Lumi™ II Luciferase Reporter Gene Assay Kit (Beyotime) according to the manufacturer's instructions. Firefly luciferase values were normalised to the Renilla luciferase values.

Statistical analysis

For the statistical analyses, we used SPSS21.0 (IBM Corp., Armonk, NY, USA). Sex, allergic history, corticosteroid therapy, and comorbidities comprised the qualitative data that were analysed using Fisher's exact test. Shapiro-Wilk and Levene's tests were used to confirm the normal distribution and homogeneity of variances of the quantitative data. Independent sample *t*-tests and a one-way analysis of variance (ANOVA) were used to compare the groups after the relevant conditions had been met. Tukey's multiple comparisons analysis method was used to compare the experimental and control groups. The Kruskal-Wallis test was performed on datasets with unequal variances. Pearson's correlation coefficient was used to determine the strength of the link between inflammatory cytokines and rhythm clock genes.

The Benjamini-Hochberg algorithm was used to adjust the *p*-values for the false discovery rate. All statistical tests were two-sided, and $p < 0.05$ was considered statistically significant

Role of Funders

The Funders did not have any role in study design, data collection, data analyses, interpretation, or writing of the report.

Results

Serum IL-6 expression is elevated in asthma patients with nocturnal symptoms

Between November 2019 and December 2021, 45 patients were diagnosed with asthma and admitted to our hospital. Patients without sufficient data (n = 7) and those with combined serious primary diseases (n = 1) were excluded. Eighteen asthma patients with nocturnal symptoms and 18 patients without nocturnal symptoms were included in the study. The baseline clinical, demographic, and biological characteristics of the patients (age, sex, BMI, heart rate, breathing rate, temperature, allergic history, corticosteroid therapy, pulmonary function tests, comorbidities, IgE, routine blood tests, and blood biochemistry) were similar between the groups, as shown in Table 1. The IL-6 levels for the asthma patients with nocturnal symptoms were markedly higher than those for patients without nocturnal symptoms (7.45 ± 6.57 vs. 2.81 ± 1.49 pg/mL, $p = 0.002$). In addition, the TNF-α levels were higher in the asthma patients with nocturnal symptoms (3.39 ± 1.90 vs. 2.09 ± 1.80 pg/ml, $p = 0.043$), but the between-group differences in the inflammatory cytokines, except IL-6 (adjusted $p = 0.022$), were not statistically significant after correction using the Benjamini–Hochberg method (Table 2).

Serum IL-6 expression is elevated in asthmatic mouse models with circadian rhythm disorders

The nocturnal asthma symptoms of coughing, wheezing, and dyspnoea are accompanied by circadian variations in airway inflammation, and the circadian clock may be responsible for this variability (23, 24). Therefore, we used different periods of light/dark cycles to induce circadian rhythm disorders in asthmatic mice and investigated the correlation between inflammatory cytokines and rhythm clock genes. The asthmatic mice lost weight (Figure 1A), had a significantly higher number of inflammatory cells in the BALF (Figure 1B), a marked increase in the infiltration of inflammatory cells and airway smooth muscle thickness (Figure 1C), and increased OVA-specific serum IgE levels (Figure 1D). However, these results did not differ from those of the asthmatic mice with circadian rhythm disorders. This indicates that different periods of light/dark cycles do not increase lung pathological changes in asthmatic mice. We further analysed the inflammatory cytokines in the sera of the mice and found that 24 h dark/24 h light cycles increased TNF-α levels (Figure 1I). Four different periods of light/dark cycles all increased IL-6 levels in the sera of asthmatic mice (Figure 1E), which was similar to the inflammatory cytokine results of the asthmatic patients. We did not observe significant differences in IL-4, IL-5, and IL-13 levels after the asthmatic mice had undergone different periods of light/dark cycles (Figures 1F–H).

Potential relationship between IL-6 and circadian clock genes

The altered expression of circadian clock genes has been observed in asthmatic patients with nocturnal symptoms (13). In our mouse model of asthma with circadian rhythm disorders, the circadian clock genes were also altered. Compared to the asthmatic mice in the 12 h dark/12 h light cycles, those who did not undergo these cycles exhibited an upregulation in the transcriptions of the circadian clock genes CLOCK, CRY1, CRY2, PER2, and NR1D1 (Figures 2A–F). We further investigated whether the upregulated circadian clock genes were associated with inflammatory cytokines. Interestingly,

TABLE 1 Demographic and clinical characteristics of the patients.

Variable	Asthma patients with nocturnal symptoms (n = 18)	Asthma patients without nocturnal symptoms (n = 18)	*p*-value
Age (y), mean(range)	59.61 ± 14.58 (24–87)	61.50 ± 11.46 (47–83)	0.464
Sex			
Male (%)	10 (55.56%)	4 (22.22%)	0.086
Female (%)	8 (44.44%)	14 (77.78%)	
BMI (kg/m^2), mean (range)	23.55 ± 3.20 (16.65-26.67)	24.63 ± 3.54 (19.77-33.3)	0.248
Heart rate (bpm), mean (range)	86.94 ± 16.01 (56–119)	82.94 ± 6.73 (76–100)	0.495
Breathing rate (br/min), mean (range)	19.17 ± 1.79 (16–22)	18.44 ± 1.42 (16–20)	0.188
Temperature (°C), mean (range)	36.35 ± 0.38 (35.8-37.4)	36.42 ± 0.29 (36.0-37.2)	0.406
Allergic history (%)	12 (66.67%)	9 (50.00%)	0.500
Corticosteroids therapy (%)	14 (77.78%)	9 (50.00%)	0.164
FEV1 (%predicted), mean (range)	79.88 ± 26.42 (24.5-107.4)	68.48 ± 17.83 (31.1-102.9)	0.138
FEV1/FVC, mean (range)	74.73 ± 15.71 (36.48-98.36)	68.49 ± 15.52 (39.0-98.82)	0.239
Comorbidities			
Hypertension (%)	5 (27.78%)	6 (33.33%)	>0.999
COPD (%)	6 (33.33%)	4 (22.22%)	0.711
Coronary heart disease (%)	3 (16.67%)	1 (5.56%)	0.603
IgE (IU/mL), mean (range)	242.28 ± 367.93 (10–1421)	304.44 ± 397.42 (8–1410)	0.656
Routine blood test			
WBC (10^9/L), mean (range)	8.24 ± 2.64 (5.01-11.81)	6.96 ± 2.18 (4.6-11.74)	0.121
RBC (10^{12}/L), mean (range)	4.39 ± 0.55 (3.53-5.43)	4.18 ± 0.50 (3.43-5.38)	0.244
HGB (g/L), mean (range)	132.17 ± 15.82 (98–162)	122.61 ± 14.68 (84–152)	0.069
PLT (10^9/L), mean (range)	201.11 ± 50.35 (72–300)	237.28 ± 108.31 (133–541)	0.944
EO%, mean (range)	2.79 ± 4.38 (0–17)	7.19 ± 12.63 (0-53.5)	0.171
LYM%, mean (range)	20.01 ± 9.56 (4.4-36.1)	25.79 ± 9.67 (3.4-46.8)	0.080
NEUT%, mean (range)	69.89 ± 13.02 (51.9-94.2)	61.86 ± 11.96 (38.8-92.8)	0.062
Blood biochemistry			
AST (U/L), mean (range)	16.89 ± 5.98 (9–28)	15.89 ± 4.43 (9–25)	0.572
ALT (U/L), mean (range)	17.39 ± 8.49 (10–46)	15.33 ± 5.54 (8–27)	0.610
TP (g/L), mean (range)	65.75 ± 6.48 (54.93-78.41)	64.45 ± 5.93 (55.46-82.02)	0.628
ALB (g/L), mean (range)	40.79 ± 4.58 (30.4-47.8)	40.76 ± 3.91 (32.3-49.8)	0.978
GLOB (g/L), mean (range)	24.36 ± 5.10 (15.7-37.1)	23.00 ± 6.28 (18.1-45)	0.145
ALP (U/L), mean (range)	74.86 ± 28.04 (14–126)	70.89 ± 16.62 (42–106)	0.609
CREA (μmol/L), mean (range)	65.72 ± 14.45 (47.9-99.9)	60.13 ± 16.67 (32.3-101.3)	0.290
UREA (mmol/L), mean (range)	5.68 ± 2.00 (3.06-11.32)	5.16 ± 1.40 (2.43-7.92)	0.370

Data are presented as the mean ± SEM or percentages and were compared using Fisher's exact test, Kruskal-Wallis test, or independent sample t-tests. No significant differences were observed between the groups.

ALB, albumin; ALP, alkaline phosphatase; ALT, alanine aminotransferase; AST, aspartate amino transferase; BMI, body mass index; COPD, chronic obstructive pulmonary disease; CREA, creatinine; EO, eosinophils; FEV1, forced expiratory volume in 1 second; FEV1/FVC, forced expiratory volume in one second/forced vital capacity; GOLB, globulin; HGB, hemoglobin count; IgE, immunoglobulin E; LYM, lymphocytes; NEUT, neutrophils; PLT, platelet; RBC, red blood cell count; TP, total protein; WBC, white blood cell count.

only IL-6 and TNF-α were most closely associated with the circadian clock genes, which suggests that an increase in IL-6 and TNF-α in asthmatic patients with nocturnal symptoms may be related to circadian clock genes (Figure 2G). The correlation coefficient and *p*-value have been listed in Table S3. Serum shock was used to stimulate the rhythmic expression of circadian clock genes in the 16HBE cells. Figures 3A–F shows that the transcription of CLOCK, CRY1, CRY2, PER2, and NR1D1 displayed oscillatory activity in a period of 24 ± 4 h. The transcription of IL-6 also displayed oscillatory activity that converged with the circadian clock genes (Figure 3G). However, serum shock did not seem to stimulate the rhythmic expression of IL-4, IL-5, IL-13, and TNF-α mRNA (Figure 3H–K). Correlational analyses revealed that only IL-6 and TNF-α were closely associated with the circadian clock genes following the serum shock in the 16HBE cells, which was also reflected in the asthmatic mice with circadian rhythm disorders (Figure 3L and Table S4).

TABLE 2 Inflammatory cytokines of asthma patients with or without nocturnal symptoms.

Variable	Asthma patients with nocturnal symptoms (n = 18)	Asthma patients without nocturnal symptoms (n = 18)	*p*-value	adjust *p*-value
IL-5 (pg/mL), mean (range)	4.25 ± 9.56 (0.19-39.85)	5.09 ± 8.62 (0.2-30.5)	0.079	0.290
IFN-α (pg/mL), mean (range)	2.20 ± 1.90 (0.4-7.12)	1.60 ± 0.77 (0.3-3.74)	0.420	0.770
IL-2 (pg/mL), mean (range)	1.51 ± 0.36 (0.99-2.20)	1.45 ± 0.57 (0.59-3.01)	0.749	0.915
IL-6 (pg/mL), mean (range)	7.45 ± 6.57 (1.35-28.65)	2.81 ± 1.49 (0.66-6.53)	0.002**	0.022*
IL-1β (pg/mL), mean (range)	9.31 ± 6.22 (0.94-17.08)	7.86 ± 10.87 (0.47-42.6)	0.126	0.347
IL-10 (pg/mL), mean (range)	1.52 ± 0.71 (0.79-3.81)	1.65 ± 0.92 (0.45-4.15)	0.622	0.887
IL-8 (pg/mL), mean (range)	3.43 ± 3.43 (0.09-11.77)	3.21 ± 4.74 (0.14-19.83)	0.645	0.887
IL-17 (pg/mL), mean (range)	1.72 ± 0.74 (0.49-2.82)	1.42 ± 0.48 (0.31-1.99)	0.156	0.343
IL-4 (pg/mL), mean (range)	1.28 ± 0.59 (0.27-2.33)	1.26 ± 0.43 (0.35-1.67)	0.761	0.941
IL-12 (pg/mL), mean (range)	1.21 ± 0.67 (0.26-2.66)	1.23 ± 0.71 (0.01-3.01)	0.941	0.941
TNF-α (pg/mL), mean (range)	3.39 ± 1.90 (0.78-7.05)	2.09 ± 1.80 (0.58-6.8)	0.043*	0.237

Data are presented as mean values ± SEM, the two groups were compared with Kruskal-Wallis test or independent samples t-tests. The Benjamini-Hochberg algorithm was used to adjust p-values. *p < 0.05, **p < 0.01 compared with asthma patients without nocturnal symptoms.

BMAL1 is the key core clock gene that drives circadian rhythms and suppresses IL-6 mRNA expression

BMAL1 is the principal driver of the molecular clock in mammals, and its deletion ablates rhythmic oscillatory activity (25). Therefore, we aimed to further clarify whether BMAL1 is involved in the regulation of IL-6 and whether it interferes with the correlation between other circadian clock genes and IL-6. The immunohistochemistry analysis revealed that BMAL1 and IL-6 were mainly expressed in the airway epithelial cells of mice. Compared to the normal group, BMAL1 was reduced in the lung tissue of the asthmatic mice, and it was further reduced in the non-12 h dark/12 h light cycles (Figure 4A). The levels of IL-6 showed an opposite trend in the lung tissue and sera of the mice (Figures 4A, C). BMAL1 expression was negatively correlated with IL-6 expression in mouse airway epithelial cells ($r = -0.464$, $p = 0.004$) (Figure 4B). Consistent with the IHC findings, Western blot analysis confirmed the protein levels of BMAL1 and IL-6 in the lungs of the mice (Figures 4D–F). To investigate the effects of BMAL1 knockdown on the expression of IL-6, we infected cultured 16HBE cells with a lentiviral vector encoding a shRNA targeting BMAL1 (BMAL1 shRNA) and lentiviral control (control shRNA). BMAL1 mRNA and protein levels decreased by approximately 80% and 60%, respectively, compared to cells infected with the control shRNA (Figures 4G–I). The knockdown of BMAL1 significantly increased the mRNA (2.8-fold increase) and protein (2.2-fold increase) levels of IL-6 in 16HBE cells (Figures 4H–J). After the serum shock, the protein level of BMAL1 displayed oscillatory activity with a period of 20 ± 4 h. IL-6, on the other hand, displayed opposite oscillatory activity and also showed a 20 ± 4 h cycle. The correlation analysis showed that BMAL1 was strongly negatively correlated with IL-6 and had a correlation coefficient of –0.716 ($p = 0.001$). Interestingly, the oscillatory activity of IL-6 was greatly diminished after the knockdown of BMAL1 ($r = -0.172$, $p = 0.233$) (Figures 4K–M).

We further explored the correlation between inflammatory factors and other rhythm clock genes after the knockdown of BMAL1. The RT-qPCR analysis showed that the knockdown of BMAL1 significantly decreased and disrupted the circadian rhythms of the negative clock genes (Figures 5A–F) and elevated the transcription of IL-6 and IL-5 at each time point (Figures 5G, J). However, there were no significant effects on the transcriptional expression of, or periodic changes in, IL-4, IL-13, and TNF-α (Figures 5H, I, K). Furthermore, the knockdown of BMAL1 resulted in a lower correlation between IL-6 and TNF-α with the rhythm clock genes (Figure 5L and Table S5).

FOXA2 participates in the BMAL1 co-intervention of the circadian rhythm of IL-6

FOXA2 is required for normal airway epithelial differentiation. Its deletion leads to Th2-mediated pulmonary inflammation during postnatal development (26). In our study, the expression of FOXA2 decreased in the lung tissue of OVA-sensitised mice. Compared to the OVA-sensitised mice in the 12 h dark/12 h light cycles, those who underwent the non-12 h dark/12 h light cycles further exhibited downregulated FOXA2 (Figures 6A, C, D). We also found a negative correlation between FOXA2 and IL-6 transcription in the lung tissue of mice ($r = -0.629$, $p = 0.001$) (Figure 6B). To further confirm the negative regulatory effect of FOXA2 on IL-6, we examined the expression of IL-6 when FOXA2 was overexpressed and knocked down using the FOXA2 plasmid and recombinant FOXA2 lentivirus vectors in 16HBE cells. Transfected 16HBE cells with a FOXA2 plasmid and FOXA2 mRNA and protein levels increased by approximately 14-fold and

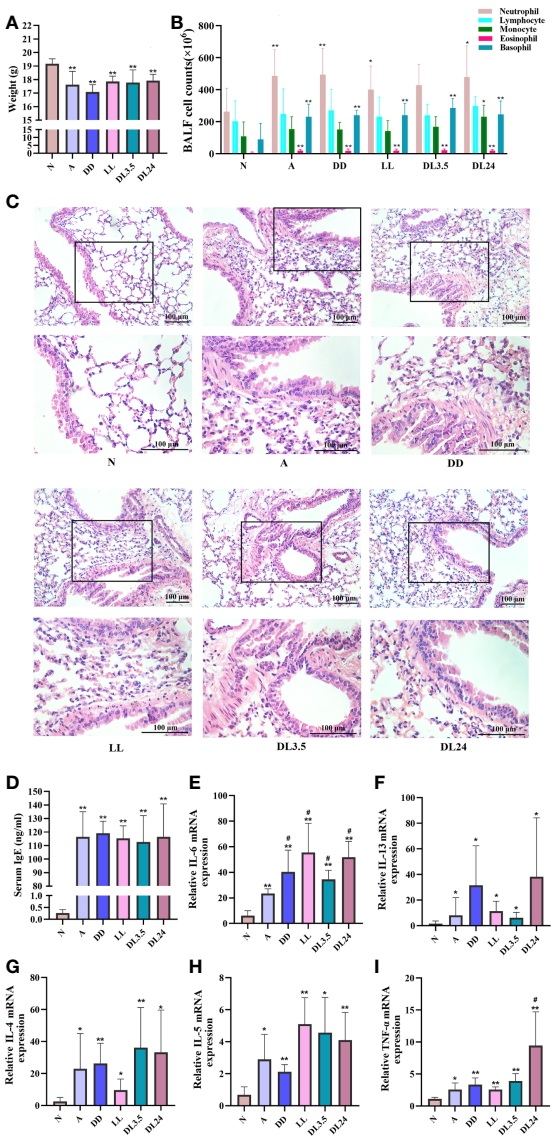

FIGURE 1
Effects of light-induced disturbances of rhythm on airway inflammation in the lung tissues of OVA-challenged mice. **(A)** Body weight variations at the end of the experiment in each group of mice. **(B)** Flow cytometric analysis of cell populations in the BALF of mice. **(C)** H&E staining of sections from OVA-challenged mouse lung tissue. Magnification: 100× (upper panel) and 200× (lower panel). Scale bar: 100 μm. **(D)** ELISA analysis of IgE levels in serum. **(E–I)** RT-qPCR analysis of the mRNA levels of inflammatory cytokines (IL-6, IL-13, IL-4, IL-5, and TNF-a) in the lung tissue. N=control group; A=OVA group; DD=OVA + all-day darkness group; LL= OVA + all-daylight; DL3.5= OVA + 3.5 h dark/3.5 h light group; DL24= OVA + 24 h dark/24 h light group. All data are presented as the mean ± standard error of the mean (SEM) of 6 mice per group, $^{*}p < 0.05$, $^{**}p < 0.01$, compared with the control group. $^{\#}p < 0.05$. One-way ANOVA with Tukey's multiple comparison analysis method.

2-fold, respectively, while IL-6 decreased by approximately 50% compared to cells infected with the control plasmid (Figures 6E–I). In contrast, Figures 6J–N shows that the knockdown of FOXA2 significantly improved the expression of IL-6. To demonstrate the function of FOXA2 in IL-6 regulation, co-transfection with the IL-6-luc and FOXA2 plasmids was performed. The transient transfection of FOXA2 significantly decreased luciferase expression compared with the empty vector in the 16HBE and 293T cells (Figure 6O). After serum shock, the protein level of FOXA2 displayed oscillatory activity, while IL-6 displayed an opposite oscillatory activity with a 24 ± 4 h cycle. The correlation analysis showed that the expression of FOXA2 was significantly negatively correlated with IL-6 expression ($r = -0.349$, $p = 0.037$). Nevertheless, the oscillatory activity of IL-6 was greatly diminished when FOXA2 was knocked down ($r = -0.036$, $p = 0.836$) (Figures 6P–R).

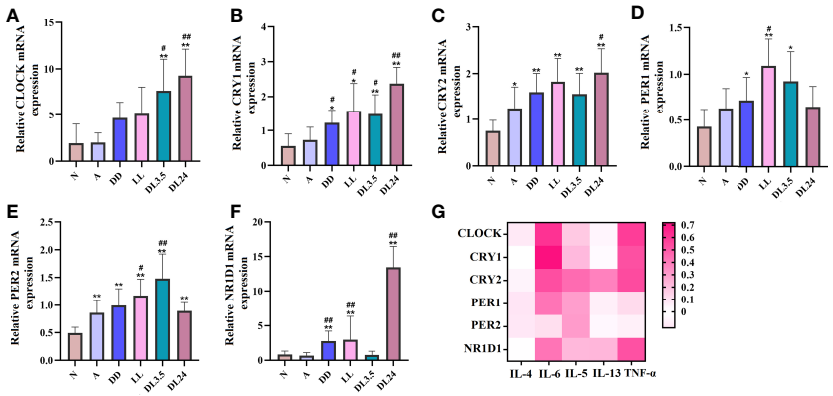

FIGURE 2
Association between circadian clock genes and inflammatory cytokines in mouse lung tissues. **(A–F)** RT-qPCR analysis of the mRNA levels of inflammatory cytokines (CLOCK, CRY1, CRY2, PER1, PER2, and NR1D1) in lung tissue. **(G)** Heat map of the matrix coefficient correlation of each circadian clock gene and inflammatory cytokines. The stronger Pearson's correlation coefficients (r) are represented in red. N=control group; A=OVA group; DD=OVA + all-day darkness group; LL= OVA + all-daylight; DL3.5= OVA + 3.5 h dark/3.5 h light group; DL24= OVA + 24 h dark/24 h light group; BLAF= bronchoalveolar lavage fluid. All data are presented as the mean ± SEM of 6 mice per group, $^{*}p < 0.05$, $^{**}p < 0.01$, compared with the control group. $^{\#}p < 0.05$, $^{\#\#}p < 0.01$ compared with the OVA group. One-way ANOVA with Tukey's multiple comparison analysis method, Pearson's correlation coefficient.

These results suggest that FOXA2 may function as a negative regulator in the regulation of IL-6 by rhythm clock genes. We further explored the expression of FOXA2 in BMAL1-knockdown 16HBE cells. The oscillatory activity of FOXA2 greatly disappeared after the serum shock in BMAL1-knockdown 16HBE cells (Figure 7A). A significant decrease in the expressions of FOXA2 mRNA and protein were observed after the knockdown of BMAL1 (Figures 7B–D). In addition, we found that IL-6 had a weakened increase by transfecting the FOXA2 overexpression plasmid in BMAL1-knockdown 16HBE cells (Figure S2). Subsequently, the 16HBE cells were subjected to the knockdown of FOXA2 and BMAL1. The double

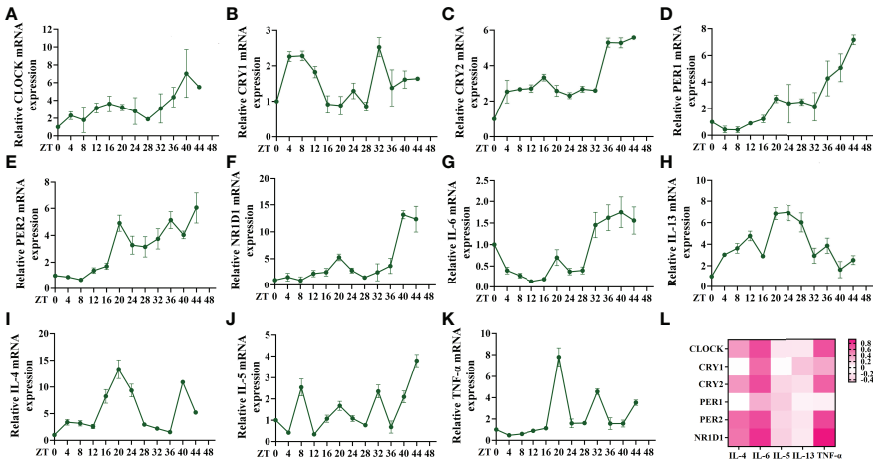

FIGURE 3
Serum shock induces circadian clock gene and inflammatory cytokine expression and association in 16HBE cells. **(A–F)** RT-qPCR analysis of the mRNA levels of circadian clock genes (CLOCK, CRY1, CRY2, PER1, PER2, and NR1D1) in 16HBE cells in response to serum shock synchronisation. **(G–K)** RT-qPCR analysis of the mRNA levels of inflammatory cytokines (IL-6, IL-13, IL-4, IL-5, and TNF-a) in 16HBE cells in response to serum shock synchronisation. **(L)** Heat map of the matrix coefficient correlation of each circadian clock gene and inflammatory cytokines. The stronger Pearson's correlation coefficients (r) are represented in red. ZT= zeitgeber time. All data shown are representative data of one out of at least 3 independent experiments, Pearson's correlation coefficient.

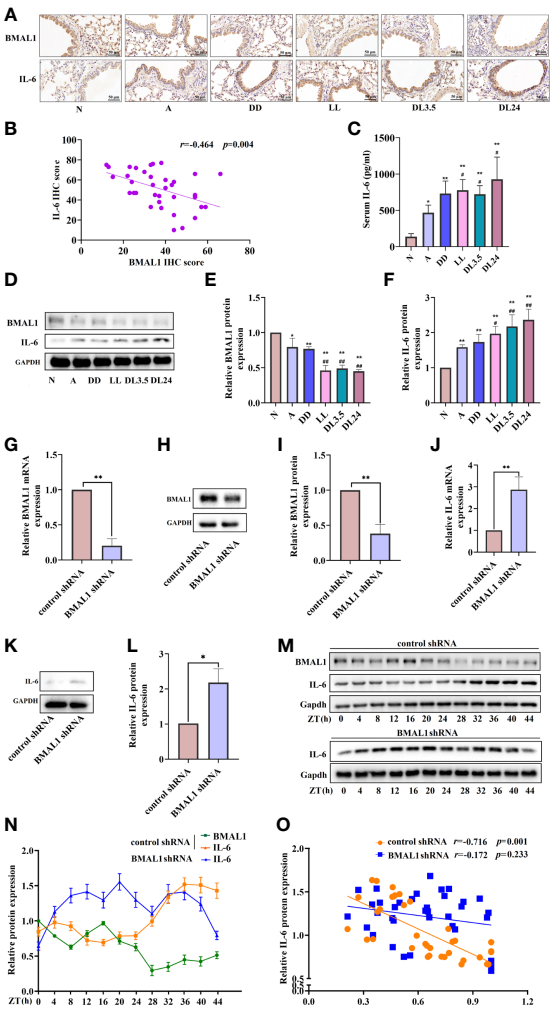

FIGURE 4
BMAL1 regulates the expression and rhythm fluctuations of IL-6. **(A)** Immunohistochemistry staining of BMAL1 and IL-6 in the mouse lung tissue of each group. Magnification: 200×. Scale bar: 50 μm. **(B)** Correlational analyses between BMAL1 and IL-6 protein expression levels in mouse lung tissue. **(C)** ELISA analysis of serum IL-6 in the mouse lung tissue of each group. **(D)** Western blot analysis of the protein levels of BMAL1 and IL-6 in the mouse lung tissue of each group. ImageJ software was used to quantify the BMAL1 **(E)** and IL-6 **(F)** bands. The mRNA **(G)** and protein **(H)** levels of BMAL1 expression in 16HBE cells with BMAL1 shRNA and control shRNA by RT-qPCR and Western blot, respectively. ImageJ software was used to quantify the BMAL1 bands **(I)**. RT-qPCR and Western blot analysis of IL-6 mRNA **(J)** and protein **(K)** levels of control shRNA and BMAL1 shRNA cells. IL-6 bands were quantitatively analysed by ImageJ software **(L)**. Western blot analysis of the protein levels of BMAL1 and IL-6 in control shRNA and BMAL1 shRNA cells in response to serum shock synchronisation **(M)**, IL-6 and BMAL1 bands were quantitatively analysed by ImageJ software **(N)**. **(O)** Correlational analyses between BMAL1 and IL-6 protein expression levels in control shRNA and BMAL1 shRNA cells. N=control group; A=OVA group; DD=OVA + all-day darkness group; LL= OVA + all-daylight; DL3.5= OVA + 3.5h dark/3.5h light group; DL24= OVA + 24h dark/24h light group; IHC, Immunohistochemistry. Data of animal experiment are presented as the mean ± SEM of 6 mice per group. Data of cell experiment shown are representative data of one out of at least 3 independent experiments. $^{*}p < 0.05$, $^{**}p < 0.01$, compared with the control group or control shRNA cells. $^{\#}p < 0.05$, $^{\#\#}p < 0.01$ compared with the OVA group. One-way ANOVA with Tukey's multiple comparison analysis method, and independent samples t-tests, Pearson's correlation coefficient.

knockdown of FOXA2 and BMAL1 caused a significant increase in IL-6 levels (Figures 8A–C). Furthermore, after the serum shock, the IL-6 transcription and secretion levels were significantly upregulated in BMAL1- and FOXA2-knockdown 16HBE cells compared to single FOXA2 or BMAL1 stable depletion cells (Figures 8D, E).

Discussion

The master pacemaker of the mammalian circadian clock is located in the hypothalamic suprachiasmatic nucleus (SCN). Intrinsically photosensitive retinal ganglion cells (ipRGCs) that respond to the lighting cycles and pass this information on to the

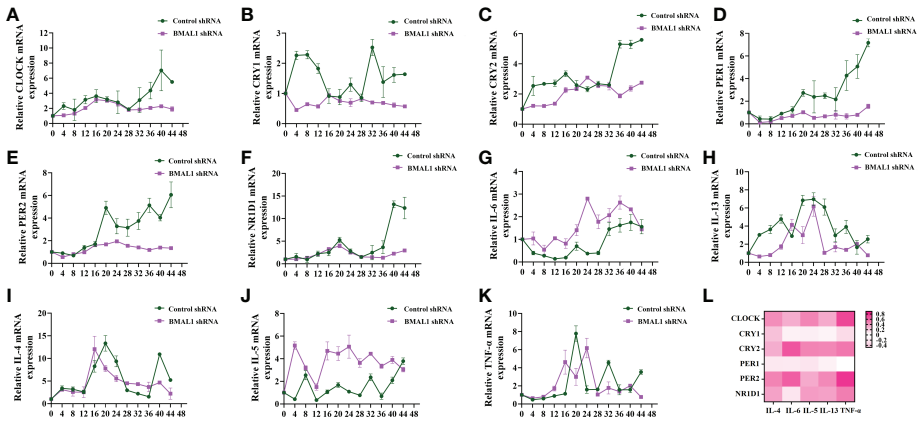

FIGURE 5
BMAL1 knockdown results in lower correlation between circadian clock genes with rhythm clock genes. **(A–F)** RT-qPCR analysis of the mRNA levels of circadian clock genes (CLOCK, CRY1, CRY2, PER1, PER2, and NR1D1) in control shRNA and BMAL1 shRNA cells in response to serum shock synchronisation. **(G–K)** RT-qPCR analysis of the mRNA levels of inflammatory cytokines (IL-6, IL-13, IL-4, IL-5, and TNF-a) in control shRNA and BMAL1 shRNA cells in response to serum shock synchronisation. **(L)** Heat map of the matrix coefficient correlation of each circadian clock gene and inflammatory cytokines in BMAL1 shRNA cells. Stronger Pearson's correlation coefficients (r) are represented in red. ZT, zeitgeber time. All data shown are representative data of one out of at least 3 independent experiments. Pearson's correlation coefficient.

SCN involve a complete network of clock genes (27). Complexes of the BMAL1-CLOCK transcription factor bind to cis-acting elements known as the E-box and activate the transcription of the PER1, PER2, CRY1, CRY2, NR1D1, and NR1D2 clock genes (28). The CRY and PER proteins form heterodimers and translocate back into the nucleus, inhibiting transcriptional activation by BMAL1-CLOCK to form the core negative feedback loop. Accompanied by the degradation of PER and CRY proteins, the repression of BMAL1 is gradually released, and a new PER/CRY transcription cycle is subsequently formed (29). BMAL1-CLOCK also forms a second core loop involving the NR1D1/2 nuclear receptor genes, which allows for the rhythmic expression of BMAL1 (30).

Light and darkness are the primary regulators of the circadian clock in mammals. With urbanisation and the rapid development of lighting systems, long-term exposure to artificial light leads to the breakdown of the circadian rhythm balance in the body and contributes to sleep disorders, gastrointestinal system disorders, accelerated aging, neurodegenerative disorders, obesity, cancer, and worsening asthmatic severity (31–33). Although the mechanisms by which circadian clocks contribute to these diseases are unclear, the diseases share common mechanisms, such as inflammation, which can further disrupt circadian rhythms (34). Mice carrying a clock gene mutation or deletion have exacerbated airway inflammation conditions. For example, mice lacking BMAL1 in myeloid cells have been found with increased lung inflammation, eosinophil infiltration, and inflammatory cytokines in their lungs and sera (35). The deletion of BMAL1 or disruption of the circadian clock environment exacerbates acute viral bronchiolitis caused by the Sendai and influenza A viruses in mice (36). Chronic jetlag has also been found to affect tumour-bearing mice and increases inflammation in the hypothalamus and liver, suggesting that the inflammatory signatures in the body can be further magnified by circadian disruption (33). Therefore, asthma with circadian rhythm disturbances may amplify the inflammatory signatures of the body, leading to inadequate asthma control and triggering of attacks at night.

Abnormal 12 h dark/12 h light cycles have been used to induce animal models with circadian rhythm disturbances. Adult male rats exposed to prolonged light for 12 consecutive weeks showed the upregulated relative mRNA expression of PER2, CRY2, and NR1D1 and downregulated mRNA expression of PER1, CRY1, BMAL1, and CLOCK (18). The expression of PER1 and PER2 in rat livers lost rhythmicity in a constant light environment, while the expression of NR1D1 maintained rhythmicity (37). Asthmatics showed increased rhythmic gene amplitudes (38). Furthermore, the circadian oscillation of BMAL1 content in the SCN of rats in constant darkness was stronger, and the peak/trough ratios were higher than those of rats undergoing 12 h dark/12 h light cycles (39). Although a consensus has been reached on the role of rhythmic disturbances in nocturnal asthma attacks, animal models of rhythmic disturbances are not the same (35). BMAL1-deficient mice have been used for rhythm research to show the disappearance of rhythmic oscillations, which is inconsistent with asthmatic rhythm gene expression patterns (40). In this study, we used four abnormal 12 h dark/12 h light cycles to induce rhythm disturbances in OVA-challenged mice, which showed varying degrees of downregulated BMAL1 expression and upregulated IL-6. This may explain the concomitant increase in IL-6 in patients with nocturnal asthma.

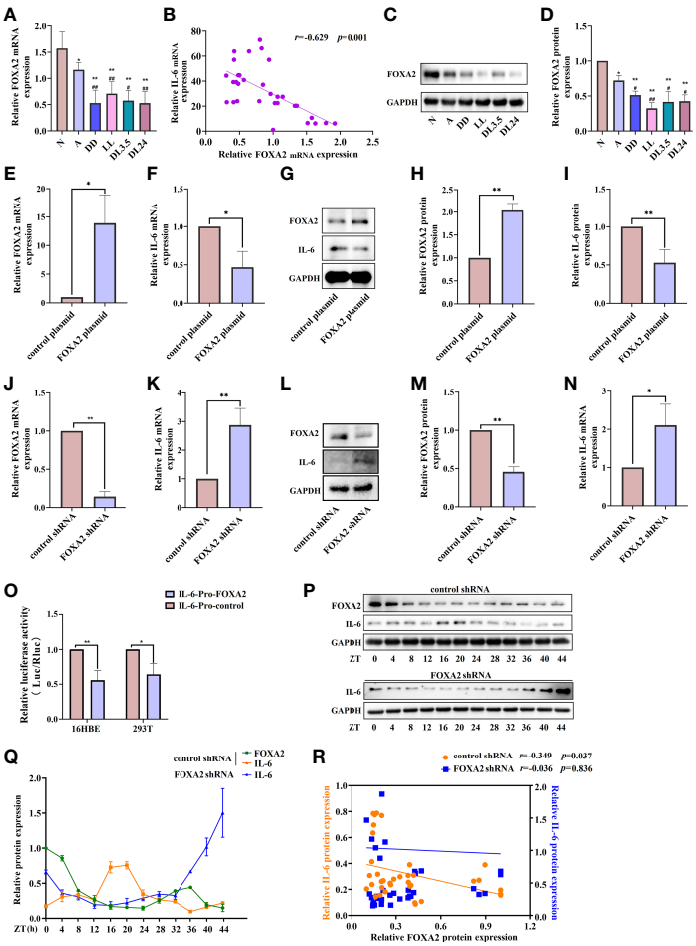

FIGURE 6
FOXA2 regulates the expression and rhythm fluctuations of IL-6. **(A)** RT-qPCR analysis of the mRNA levels of FOXA2 in lung tissue. **(B)** Correlational analyses between FOXA2 and IL-6 mRNA expression levels in lung tissue. **(C)** Western blot analysis of the protein levels of FOXA2 in mouse lung tissue of each group. ImageJ software was used to quantify FOXA2 **(D)**. RT-qPCR analysis of the mRNA levels of FOXA2 **(E)** and IL-6 **(F)** after the transfection of 16HBE cells with a FOXA2 over-expression (FOXA2 plasmid) and control plasmid. Western blot analysis of the protein levels of FOXA2 and IL-6 in 16HBE cells transfected with the FOXA2 and control plasmids **(G)**. ImageJ software was used to quantify FOXA2 **(H)** and IL-6 **(I)** bands. RT-qPCR analysis of the mRNA levels of FOXA2 **(J)** and IL-6 **(K)** expression in 16HBE cells with FOXA2 shRNA and control shRNA. Western blot analysis of the protein levels of FOXA2 and IL-6 in 16HBE cells transfected with FOXA2 shRNA and control shRNA **(L)**, ImageJ software was used to quantify FOXA2 **(M)** and IL-6 **(N)** bands. **(O)** Luciferase reporter assay analysis of the luciferase expression in the 16HBE and 293T cells transient transfection of FOXA2 and empty vector. Western blot analysis of the protein levels of FOXA2 and IL-6 in control shRNA and FOXA2 shRNA cells in response to serum shock synchronisation **(P)**, IL-6 and FOXA2 bands were quantitatively analysed by ImageJ software **(Q)**. **(R)** Correlational analyses between FOXA2 and IL-6 protein expression levels in control shRNA and FOXA2 shRNA cells. The left ordinate and the right ordinate represent the relative protein expression of IL-6 in control shRNA cells and FOXA2 shRNA cells, respectively. N=control group; A=OVA group; DD=OVA + all-day darkness group; LL= OVA + all-daylight; DL3.5= OVA + 3.5 h dark/3.5 h light group; DL24= OVA + 24 h dark/24 h light group. Data of animal experiment are presented as the mean ± SEM of 6 mice per group. Data of cell experiment shown are representative data of one out of at least 3 independent experiments. $^{*}p < 0.05$, $^{**}p < 0.01$, compared with the control group, control plasmid or control shRNA cells. $^{\#}p < 0.05$, $^{\#\#}p < 0.01$ compared with the OVA group. One-way ANOVA with Tukey's multiple comparison analysis method, and independent samples t-tests, Pearson's correlation coefficient.

Nocturnal asthma symptoms are associated with inflammation in the lung tissue. Previous studies have confirmed an increase in inflammatory cell populations and cytokines in the BALF of patients with nocturnal asthma (41–43). This inflammatory response, its induced airway epithelial damage, and small airway spasms may be important factors in the etiology of nocturnal asthma. By comparing the blood samples of asthmatic patients with and without nocturnal symptoms between 4–5 A.M., we found that the expression of IL-6 in patients with nocturnal asthma attacks was significantly higher than that in asthmatic patients without nocturnal symptoms. TNF-α also presented a significant difference in asthmatic patients with and without nocturnal symptoms, but it did not show a significant difference after adjustment by the

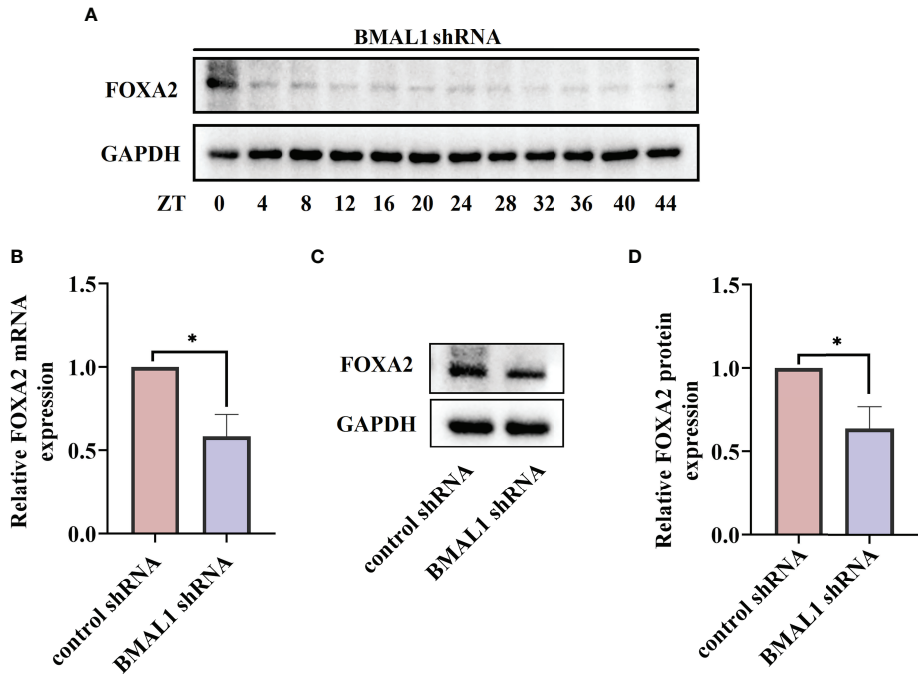

FIGURE 7
BMAL1 regulates the expression and rhythm fluctuations of FOXA2 in 16HBE cells. **(A)** Western blot analysis of the protein levels of FOXA2 in BMAL1 shRNA cells in response to serum shock synchronisation. The mRNA **(B)** and protein **(C)** levels of FOXA2 expression in 16HBE cells with BMAL1 shRNA constructs and control shRNA by RT-qPCR and Western blot, respectively. ImageJ software was used to quantify FOXA2 bands **(D)**. by RT-qPCR and Western blot, respectively. ImageJ software was used to quantify BMAL1 bands (g). ZT, zeitgeber time. All data shown are representative data of one out of at least 3 independent experiments, $*p < 0.05$ compared with control shRNA cells, independent samples t-tests.

Benjamini-Hochberg correction method for *p*-values. These results were the same as those obtained by Tom et al. (42), and may be related to insufficient sample size. The relationship between rhythmic genes and inflammation involves a complex traffic network. The dysregulation of the clock leads to dysregulated inflammation. Since inflammation can directly affect circadian rhythmicity, this constitutes a vicious cycle (44). We hope to use IL-6 as an example to provide research ideas for the study of circadian clock genes that regulate changes in airway inflammation.

The transcription factor BMAL1, an essential component of the molecular clock, regulates the upregulation of IL-6 in lipopolysaccharide-exposed microglia and plays a role in microglial inflammatory responses (45). The loss of BMAL1, or jetlag-sensitised mice, acts on the NF-κB/NLRP3 axis to promote inflammation, which exacerbates *Propionibacterium acnes*-induced skin inflammation (46). In addition, BMAL1 plays an important role in critical limb ischemia by activating IL-10, which transcriptionally suppresses inflammation and promotes angiogenesis *via* the transcriptional regulation of vascular endothelial growth factor expression (47). However, the role of BMAL1 in regulating lung inflammation remains unclear. Here, we found that the loss of the BMAL1 gene can lead to increased IL-6 expression and loss of rhythm in airway epithelial cells while reducing the correlation between IL-6 and other negatively regulated circadian clock genes. This suggests that the disorder of circadian clock genes and low expression of BMAL1 may lead to an increase in cytokines such as IL-6 and induce nocturnal asthma symptoms.

The transcription factor FOXA2, which belongs to the forkhead family, is involved in the development of lung tissues and is highly expressed in the airway epithelial cells of mature lungs. The deletion of FOXA2 has been found to cause goblet cell metaplasia and Th2-mediated lung inflammation in respiratory epithelia (48, 49). FOXA2 is expressed at low levels in asthmatic patients and is negatively correlated with the expression of mucins, such as MUC5AC and CLCA1 (48). FOXA2 is negatively correlated with IL-6 in patients with chronic rhinosinusitis. Increasing the expression of FOXA2 inhibits IL-6-induced MUC5AC production (50). The secretion of TNF-α, IL-1β, and IL-6 is inhibited in MLE-12 cells with low FOXA2 expression, and oxidative stress-induced apoptosis is also reduced (51). We also found a negative correlation between FOXA2 and IL-6 in OVA-challenged mice and the 16HBE cell serum shock model. Interestingly, FOXA2 also displayed oscillatory activity in serum shock, suggesting that FOXA2 may be involved in the transcriptional regulation of IL-6 by circadian clock genes.

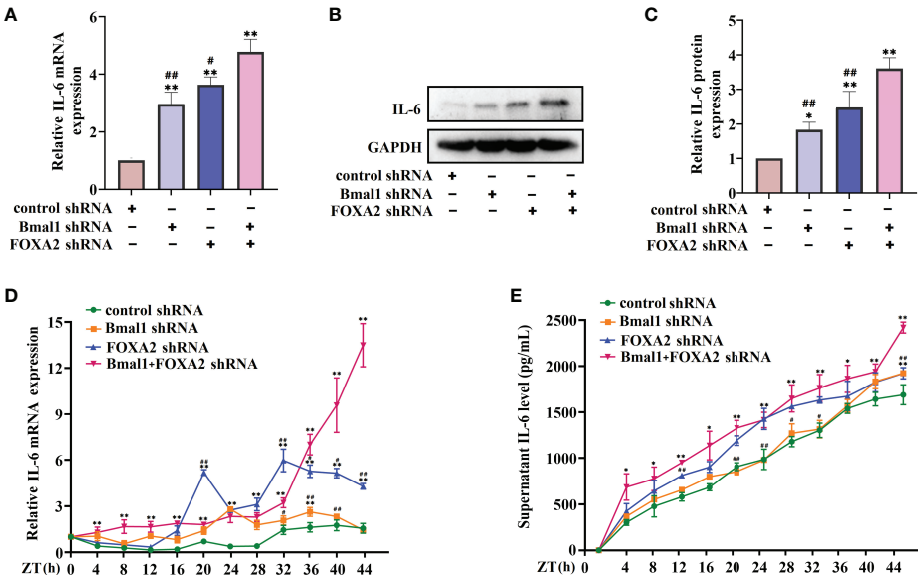

FIGURE 8
Double FOXA2 and BMAL1 stable depletion causes a significant increase of IL-6. The mRNA **(A)** and protein **(B)** levels of IL-6 in 16HBE cells transfected with control shRNA, FOXA2 shRNA, BMAL1 shRNA, and FOXA2+BMAL1 shRNA by RT-qPCR and Western blot, respectively. ImageJ software was used to quantify the IL-6 bands **(C)**. RT-qPCR **(D)** and ELISA **(E)** analysis of mRNA and secretion levels of IL-6 in 16HBE cells transfected with control shRNA, FOXA2 shRNA, BMAL1 shRNA, and FOXA2+BMAL1 shRNA cells in response to serum shock synchronisation. ZT, zeitgeber time. All data shown are representative data of one out of at least 3 independent experiments, $*p < 0.05$, $**p < 0.01$ compared with control shRNA cells. $^{\#}p < 0.05$, $^{\#\#}p < 0.01$ compared with FOXA2+BMAL1 shRNA cells. One-way ANOVA with Tukey's multiple comparison analysis method, and independent samples t-tests.

The molecular clock also plays an important regulatory role in mammalian embryonic development. The disruption of BMAL1 in mammals during embryonic development can lead to a reduced lifespan, locomotor activity level, body weight, and fertility (52). The activation of FOXA2 is severely hindered during the differentiation of BMAL1-knockdown mouse embryonic stem cells (53). Differentiated human colon adenocarcinoma cells have been found to correlate with

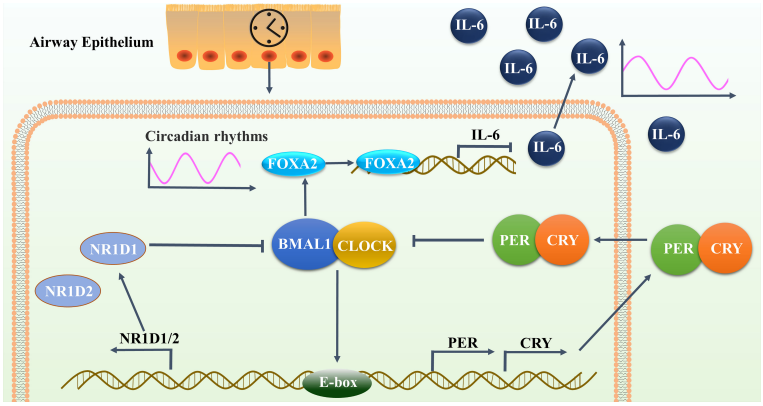

FIGURE 9
BMAL1 inhibited the expression and reduced the oscillation of IL-6 in airway epithelial cells by regulating the transcription factor FOXA2. This autoregulatory feedback loop cycles between the CLOCK/BMAL1 transcriptional activator complex and its repressors PER/CRY and NR1D1 to constitute the molecular clock oscillator in the airway epithelium, that drives the oscillatory activity of FOXA2. FOXA2 could bind to the promoter region of IL-6 and down-regulate its expression, resulting in periodic oscillations in the secretion level of IL-6.

decreased levels of FOXA2 upon treatment with shBMAL1. In turn, BMAL1 overexpression has no effect on FOXA2 expression (54). Here, we observed the lower expression and reduced rhythms of FOXA2 in 16HBE cells after BMAL1 suppression. We further noted the synergistic inhibitory effects of the double knockdown of FOXA2 and BMAL1 on the expression and oscillation of IL-6 in 16HBE cells. This study confirmed that BMAL1 inhibits the expression and oscillations of IL-6 in airway epithelial cells by regulating the transcription factor FOXA2 (Figure 9).

To the best of our knowledge, our findings are the first to demonstrate that there is a correlation between the increase in IL-6 inflammatory factors and rhythm clock genes in patients with nocturnal asthma. Mechanistic investigations supported the activation of BMAL1/FOXA2 pathway in reducing the secretion of IL-6 in airway epithelial cells. Targeting the BMAL1/FOXA2 pathway therefore represents a potential therapeutic option for inhibiting the increase of airway inflammation at night in asthmatic patients with nocturnal symptoms.

Data availability statement

The original contributions presented in the study are included in the article/Supplementary Material. Further inquiries can be directed to the corresponding authors.

Ethics statement

This study was approved by the Ethics Committee of the Affiliated Hospital of Nanjing University of Chinese Medicine (approval number 2019NL-024-02). All patients provided informed consent. The patients/participants provided their written informed consent to participate in this study. All of the protocols involving animal use were approved by the Animal Ethics Committee of the Affiliated Hospital of Nanjing University of Traditional Chinese Medicine (NO:2021 DW-07-02).

Author contributions

LT, XZ, XLS designed the experiments. PH, XZ participated in the collection and statistics of clinical cases. XHS, JJ, BW verified the underlying data. XHS, XNZ, and PH performed the animal model. LT and XHS completed the cell serum shock test. BW, XNZ and JJ processed the BALF and mouse lung tissue samples. LT and HZ carried out the RT-qPCR and IHC analysis. LT wrote the manuscript. All authors contributed to the article and approved the submitted version.

Funding

This work was financially supported by National Natural Science Foundation of China 82004265, 82004304, and General project of Jiangsu Natural Science Foundation BK20211391, and Graduate Research and Practice Innovation Plan of Graduate Education Innovation Project in Jiangsu Province SJCX21-0742. 2020 Nanjing Traditional Chinese Medicine Young Talents Training Project NJSZYYQNRC-2020-ZH.

Acknowledgments

The authors sincerely acknowledge the support of the Central Laboratory of Jiangsu Hospital of Traditional Chinese Medicine for providing the experimental platform and guidance.

Conflict of interest

The authors declare that the research was conducted in the absence of any commercial or financial relationships that could be construed as a potential conflict of interest.

Publisher's note

Supplementary material

The Supplementary Material for this article can be found online at: https://www.frontiersin.org/articles/10.3389/fimmu.2022.947067/full#supplementary-material

SUPPLEMENTARY FIGURE 1
Flowchart of creating light-induced disturbances of rhythm in OVA-challenged mice. i.p., intraperitoneal; i.n.= intranasal; N, control group; A=OVA group; DD=OVA + all-day darkness group; LL= OVA + all-daylight; DL3.5= OVA + 3.5 h dark/3.5 h light group; DL24= OVA + 24 h dark/24 h light group.

SUPPLEMENTARY FIGURE 2
IL-6 had a weakened increase by transfecting the FOXA2 overexpression plasmid in BMAL1-knockdown 16HBE cells. **(A)** Western blot analysis of the protein levels of IL-6 after the transfection of BMAL1-knockdown 16HBE cells with FOXA2 plasmid. **(B)** ImageJ software was used to quantify IL-6 bands. All data shown are representative data of one out of at least 3 independent experiments, $*p < 0.05$ compared with control

shRNA cells. #$p < 0.05$ compared with BMAL1 shRNA cells. One-way ANOVA with Tukey's multiple comparison analysis method.

SUPPLEMENTARY TABLE 1
The target sequences of shRNAs.

SUPPLEMENTARY TABLE 2
Sequences of primers used.

SUPPLEMENTARY TABLE 3
Pearson's correlation coefficient for the concentrations of circadian clock genes and inflammatory cytokines in the mice lung tissues. Pearson's correlation coefficient was used to measure the strength of the relationship between the two variables. *$p < 0.05$, **$p < 0.01$.

SUPPLEMENTARY TABLE 4
Pearson's correlation coefficient for the concentrations of circadian clock genes and inflammatory cytokines in 16HBE cells in response to serum shock synchronisation. Pearson's correlation coefficient was used to measure the strength of the relationship between the two variables. *$p < 0.05$, **$p < 0.01$.

SUPPLEMENTARY TABLE 5
Pearson's correlation coefficient for the concentrations of circadian clock genes and inflammatory cytokines in BMAL1 knockdown 16HBE cells in response to serum shock synchronisation. Pearson's correlation coefficient was used to measure the strength of the relationship between the two variables. *$p < 0.05$, **$p < 0.01$.

References

1. Reddel HK, Bacharier LB, Bateman ED, Brightling CE, Brusselle GG, Buhl R, et al. Global initiative for asthma strategy 2021: Executive summary and rationale for key changes. *Am J Respir Crit Care Med* (2022) 205(1):17–35. doi: 10.1164/rccm.202109-2205PP

2. Fagnano M, Bayer AL, Isensee CA, Hernandez T, Halterman JS. Nocturnal asthma symptoms and poor sleep quality among urban school children with asthma. *Acad Pediatr* (2011) 11(6):493–9. doi: 10.1016/j.acap.2011.05.006

3. Horner CC, Dula C, Bacharier LB, Garbutt JM, Gonzalez C, Deych E, et al. Daily global stress is associated with nocturnal asthma awakenings in school-age children. *J Allergy Clin Immunol* (2016) 138(4):1196–9.e3. doi: 10.1016/j.jaci.2016.01.054

4. Tough SC, Hessel PA, Ruff M, Green FH, Mitchell I, Butt JC. Features that distinguish those who die from asthma from community controls with asthma. *J Asthma* (1998) 35(8):657–65. doi: 10.3109/02770909809048968

5. Francisco CO, Yadollahi A. Thoracic fluid accumulation and asthma symptoms: A new contributor mechanism. *Porto BioMed J* (2019) 4(6):e40. doi: 10.1097/j.pbj.0000000000000040

6. Lehtimaki L, Kankaanranta H, Saarelainen S, Turjanmaa V, Moilanen E. Increased alveolar nitric oxide concentration in asthmatic patients with nocturnal symptoms. *Eur Respir J* (2002) 20(4):841–5. doi: 10.1183/09031936.02.00202002

7. Mattes J, Storm Van's Gravesande K, Moeller C, Moseler M, Brandis M, Kuehr J. Circadian variation of exhaled nitric oxide and urinary eosinophil protein X in asthmatic and healthy children. *Pediatr Res* (2002) 51(2):190–4. doi: 10.1203/00006450-200202000-00011

8. Abdo M, Trinkmann F, Kirsten AM, Biller H, Pedersen F, Waschki B, et al. The relevance of small airway dysfunction in asthma with nocturnal symptoms. *J Asthma Allergy* (2021) 14:897–905. doi: 10.2147/JAA.S313572

9. Marone G, Granata F, Pucino V, Pecoraro A, Heffler E, Loffredo S, et al. The intriguing role of interleukin 13 in the pathophysiology of asthma. *Front Pharmacol* (2019) 10:1387. doi: 10.3389/fphar.2019.01387

10. Zhang R, Lahens NF, Ballance HI, Hughes ME, Hogenesch JB. A circadian gene expression atlas in mammals: implications for biology and medicine. *Proc Natl Acad Sci U.S.A.* (2014) 111(45):16219–24. doi: 10.1073/pnas.1408886111

11. Studer P, Da Silva CG, Revuelta Cervantes JM, Mele A, Csizmadia E, Siracuse JJ, et al. Significant lethality following liver resection in A20 heterozygous knockout mice uncovers a key role for A20 in liver regeneration. *Cell Death Differ* (2015) 22(12):2068–77. doi: 10.1038/cdd.2015.52

12. Liu PY, Irwin MR, Krueger JM, Gaddameedhi S, Van Dongen HPA. Night shift schedule alters endogenous regulation of circulating cytokines. *Neurobiol Sleep Circadian Rhythms* (2021) 10:100063. doi: 10.1016/j.nbscr.2021.100063

13. Chen HC, Chen YC, Wang TN, Fang WF, Chang YC, Chen YM, et al. Disrupted expression of circadian clock genes in patients with bronchial asthma. *J Asthma Allergy* (2021) 14:371–80. doi: 10.2147/JAA.S302508

14. Global Initiative for Asthma. *Global strategy for asthma management and prevention* (2021). Available at: https://www.ginasthma.org/reports (Accessed April 1, 2022).

15. Mehra R. Understanding nocturnal asthma. the plot thickens. *Am J Respir Crit Care Med* (2014) 190(3):243–4. doi: 10.1164/rccm.201406-1130ED

16. Tang L, Zhu L, Zhang W, Yang X, Chen Q, Meng Z, et al. Qi-xian decoction upregulated e-cadherin expression in human lung epithelial cells and ovalbumin-challenged mice by inhibiting reactive oxygen species-mediated extracellular-Signal-Regulated kinase (ERK) activation. *Med Sci Monit* (2020) 26:e922003. doi: 10.12659/MSM.922003

17. Van Hoecke L, Job ER, Saelens X, Roose K. Bronchoalveolar lavage of murine lungs to analyze inflammatory cell infiltration. *J Vis Exp* (2017) 123):e55398. doi: 10.3791/55398

18. West AC, Iversen M, Jorgensen EH, Sandve SR, Hazlerigg DG, Wood SH. Diversified regulation of circadian clock gene expression following whole genome duplication. *PloS Genet* (2020) 16(10):e1009097. doi: 10.1371/journal.pgen.1009097

19. Engeland WC, Massman L, Mishra S, Yoder JM, Leng S, Pignatti E, et al. The adrenal clock prevents aberrant light-induced alterations in circadian glucocorticoid rhythms. *Endocrinology* (2018) 159(12):3950–64. doi: 10.1210/en.2018-00769

20. Balsalobre A, Damiola F, Schibler U. A serum shock induces circadian gene expression in mammalian tissue culture cells. *Cell* (1998) 93(6):929–37. doi: 10.1016/s0092-8674(00)81199-x

21. Lemos DR, Goodspeed L, Tonelli L, Antoch MP, Ojeda SR, Urbanski HF. Evidence for circadian regulation of activating transcription factor 5 but not tyrosine hydroxylase by the chromaffin cell clock. *Endocrinology* (2007) 148 (12):5811–21. doi: 10.1210/en.2007-0610

22. Durrington HJ, Farrow SN, Loudon AS, Ray DW. The circadian clock and asthma. *Thorax* (2014) 69(1):90–2. doi: 10.1136/thoraxjnl-2013-203482

23. Annamneedi VP, Park JW, Lee GS, Kang TJ. Cell autonomous circadian systems and their relation to inflammation. *Biomol Ther (Seoul)* (2021) 29(1):31–40. doi: 10.4062/biomolther.2020.215

24. Timmons GA, Carroll RG, O'siorain JR, Cervantes-Silva MP, Fagan LE, Cox SL, et al. The circadian clock protein BMAL1 acts as a metabolic sensor in macrophages to control the production of pro IL-1beta. *Front Immunol* (2021) 12:700431. doi: 10.3389/fimmu.2021.700431

25. Tang X, Liu XJ, Tian C, Su Q, Lei Y, Wu Q, et al. Foxa2 regulates leukotrienes to inhibit Th2-mediated pulmonary inflammation. *Am J Respir Cell Mol Biol* (2013) 49(6):960–70. doi: 10.1165/rcmb.2013-0122OC

26. Fonken LK, Nelson RJ. The effects of light at night on circadian clocks and metabolism. *Endocr Rev* (2014) 35(4):648–70. doi: 10.1210/er.2013-1051

27. Boden MJ, Varcoe TJ, Voultsios A, Kennaway DJ. Reproductive biology of female Bmal1 null mice. *Reproduction* (2010) 139(6):1077–90. doi: 10.1530/REP-09-0523

28. Ono D, Honma K, Honma S. Circadian and ultradian rhythms of clock gene expression in the suprachiasmatic nucleus of freely moving mice. *Sci Rep* (2015) 5:12310. doi: 10.1038/srep12310

29. Chiou YY, Yang Y, Rashid N, Ye R, Selby CP, Sancar A. Mammalian period represses and de-represses transcription by displacing CLOCK-BMAL1 from promoters in a cryptochrome-dependent manner. *Proc Natl Acad Sci U.S.A.* (2016) 113(41):E6072–E9. doi: 10.1073/pnas.1612917113

30. Froy O. Circadian aspects of energy metabolism and aging. *Ageing Res Rev* (2013) 12(4):931–40. doi: 10.1016/j.arr.2013.09.002

31. Valladares M, Obregon AM, Chaput JP. Association between genetic variants of the clock gene and obesity and sleep duration. *J Physiol Biochem* (2015) 71(4):855–60. doi: 10.1007/s13105-015-0447-3

32. Lawther AJ, Phillips AJK, Chung NC, Chang A, Ziegler AI, Debs S, et al. Disrupting circadian rhythms promotes cancer-induced inflammation in mice. *Brain Behav Immun Health* (2022) 21:100428. doi: 10.1016/j.bbih.2022.100428

33. Haspel JA, Chettimada S, Shaik RS, Chu JH, Raby BA, Cernadas M, et al. Circadian rhythm reprogramming during lung inflammation. *Nat Commun* (2014) 5:4753. doi: 10.1038/ncomms5753

34. Zaslona Z, Case S, Early JO, Lalor SJ, Mcloughlin RM, Curtis AM, et al. The circadian protein BMAL1 in myeloid cells is a negative regulator of allergic asthma. *Am J Physiol Lung Cell Mol Physiol* (2017) 312(6):L855–L60. doi: 10.1152/ajplung.00072.2017

35. Ehlers A, Xie W, Agapov E, Brown S, Steinberg D, Tidwell R, et al. BMAL1 links the circadian clock to viral airway pathology and asthma phenotypes. *Mucosal Immunol* (2018) 11(1):97–111. doi: 10.1038/mi.2017.24

36. Moustafa A. Effect of light-dark cycle misalignment on the hypothalamic-Pituitary-Gonadal axis, testicular oxidative stress, and expression of clock genes in adult Male rats. *Int J Endocrinol* (2020) 2020:1426846. doi: 10.1155/2020/1426846

37. Polidarova L, Sladek M, Sotak M, Pacha J, Sumova A. Hepatic, duodenal, and colonic circadian clocks differ in their persistence under conditions of constant light and in their entrainment by restricted feeding. *Chronobiol Int* (2011) 28 (3):204–15. doi: 10.3109/07420528.2010.548615

38. Sundar IK, Yao H, Sellix MT, Rahman I. Circadian molecular clock in lung pathophysiology. *Am J Physiol Lung Cell Mol Physiol* (2015) 309(10):L1056–75. doi: 10.1152/ajplung.00152.2015

39. Tamaru T, Isojima Y, Yamada T, Okada M, Nagai K, Takamatsu K. Light and glutamate-induced degradation of the circadian oscillating protein BMAL1 during the mammalian clock resetting. *J Neurosci* (2000) 20(20):7525–30. doi: 10.1523/JNEUROSCI.20-20-07525.2000

40. Yang G, Chen L, Zhang J, Ren B, Fitzgerald GA. Bmal1 deletion in mice facilitates adaptation to disrupted light/dark conditions. *JCI Insight* (2019) 5: e125133. doi: 10.1172/jci.insight.125133

41. Martin RJ, Cicutto LC, Smith HR, Ballard RD, Szefler SJ. Airways inflammation in nocturnal asthma. *Am Rev Respir Dis* (1991) 143(2):351–7. doi: 10.1164/ajrccm/143.2.351

42. Mackay TW, Wallace WA, Howie SE, Brown PH, Greening AP, Church MK, et al. Role of inflammation in nocturnal asthma. *Thorax* (1994) 49(3):257–62. doi: 10.1136/thx.49.3.257

43. Oosterhoff Y, Kauffman HF, Rutgers B, Zijlstra FJ, Koeter GH, Postma DS. Inflammatory cell number and mediators in bronchoalveolar lavage fluid and peripheral blood in subjects with asthma with increased nocturnal airways narrowing. *J Allergy Clin Immunol* (1995) 96(2):219–29. doi: 10.1016/s0091-6749(95)70011-0

44. Swanson GR, Kochman N, Amin J, Chouhan V, Yim W, Engen PA, et al. Disrupted circadian rest-activity cycles in inflammatory bowel disease are associated with aggressive disease phenotype, subclinical inflammation, and dysbiosis. *Front Med (Lausanne)* (2021) 8:770491. doi: 10.3389/fmed.2021.770491

45. Nakazato R, Hotta S, Yamada D, Kou M, Nakamura S, Takahata Y, et al. The intrinsic microglial clock system regulates interleukin-6 expression. *Glia* (2017) 65 (1):198–208. doi: 10.1002/glia.23087

46. Li F, Lin L, He Y, Sun G, Dong D, Wu B. BMAL1 regulates propionibacterium acnes-induced skin inflammation *via* REV-ERBalpha in mice. *Int J Biol Sci* (2022) 18(6):2597–608. doi: 10.7150/ijbs.71719

47. Xu L, Liu Y, Cheng Q, Shen Y, Yuan Y, Jiang X, et al. Bmal1 downregulation worsens critical limb ischemia by promoting inflammation and impairing angiogenesis. *Front Cardiovasc Med* (2021) 8:712903. doi: 10.3389/fcvm.2021.712903

48. Park SW, Verhaeghe C, Nguyenvu LT, Barbeau R, Eisley CJ, Nakagami Y, et al. Distinct roles of FOXA2 and FOXA3 in allergic airway disease and asthma. *Am J Respir Crit Care Med* (2009) 180(7):603–10. doi: 10.1164/rccm.200811-1768OC

49. Chen G, Wan H, Luo F, Zhang L, Xu Y, Lewkowich I, et al. Foxa2 programs Th2 cell-mediated innate immunity in the developing lung. *J Immunol* (2010) 184 (11):6133–41. doi: 10.4049/jimmunol.1000223

50. Luo Q, Zhang J, Wang H, Chen F, Luo X, Miao B, et al. Expression and regulation of transcription factor FoxA2 in chronic rhinosinusitis with and without nasal polyps. *Allergy Asthma Immunol Res* (2015) 7(5):458–66. doi: 10.4168/aair.2015.7.5.458

51. Mei M, Nie J, Sun H, Wang H, Rong L. LncRNA-NEF regulated the hyperoxia-induced injury of lung epithelial cells by FOXA2. *Am J Transl Res* (2020) 12(9):5563–74.

52. Mieda M, Hasegawa E, Kessaris N, Sakurai T. Fine-tuning circadian rhythms: The importance of Bmal1 expression in the ventral forebrain. *Front Neurosci* (2017) 11:55. doi: 10.3389/fnins.2017.00055

53. Gallardo A, Molina A, Asenjo HG, Martorell-Marugan J, Montes R, Ramos-Mejia V, et al. The molecular clock protein Bmal1 regulates cell differentiation in mouse embryonic stem cells. *Life Sci Alliance* (2020) 3(5):e201900535. doi: 10.26508/lsa.201900535

54. Sussman W, Stevenson M, Mowdawalla C, Mota S, Ragolia L, Pan X. BMAL1 controls glucose uptake through paired-homeodomain transcription factor 4 in differentiated caco-2 cells. *Am J Physiol Cell Physiol* (2019) 317(3): C492–501. doi: 10.1152/ajpcell.00058.2019

frontiers | Frontiers in Immunology

TYPE Original Research
PUBLISHED 22 December 2022
DOI 10.3389/fimmu.2022.958098

OPEN ACCESS

EDITED BY
Szandor Simmons,
Charité –Universitätsmedizin Berlin, Germany

REVIEWED BY
Hee Sam Na,
Pusan National University, Republic of Korea
Richard Kumaran Kandasamy,
Norwegian University of Science and Technology, Norway

*CORRESPONDENCE
Elena Lopez-Rodriguez
elena.lopez-rodriguez@charite.de

SPECIALTY SECTION
This article was submitted to Inflammation, a section of the journal Frontiers in Immunology

RECEIVED 31 May 2022
ACCEPTED 12 December 2022
PUBLISHED 22 December 2022

CITATION
Giambelluca S, Ochs M and Lopez-Rodriguez E (2022) Resting time after phorbol 12-myristate 13-acetate in THP-1 derived macrophages provides a non-biased model for the study of NLRP3 inflammasome.
Front. Immunol. 13:958098.
doi: 10.3389/fimmu.2022.958098

Resting time after phorbol 12-myristate 13-acetate in THP-1 derived macrophages provides a non-biased model for the study of NLRP3 inflammasome

Sonia Giambelluca[1], Matthias Ochs[1,2] and Elena Lopez-Rodriguez[1]*

[1]Institute of Functional Anatomy, Charité - Univeristätsmedizin Berlin, Berlin, Germany, [2]German Center for Lung Research (DZL), Berlin, Germany

Background: The activation of NLRP3 inflammasome in macrophages has been proven to play a crucial role in the development of cardiovascular diseases. THP-1 monocytes can be differentiated to macrophages by incubation with phorbol-12-myristate 13-acetate (PMA), providing a suitable model for *in vitro* studies. However, PMA has been shown to have effects on the levels of IL-1β, the main mediator of NLRP3 inflammasome, while the effects on the other mediators of the inflammasome have not been reported before.

Methods: THP-1 monocytes were incubated without (THP-1), with 5ng/ml PMA for 48h (PMA48h) or with 5ng/ml PMA for 48h plus 24h in fresh medium (PMArest). Morphological changes and the expression of macrophage surface markers (CD14, CD11b, CD36 and CD204) were evaluated by flow cytometry. Changes in intracellular levels of inflammasome components (NLRP3, ASC, pro-caspase-1, pro-IL1β) were analyzed by western blot and release of mature IL-1β in cell supernatant was analyzed by ELISA. ASC speck formation was determined by immunofluorescence.

Results: After 48h incubation with PMA or subsequent rest in fresh medium, cells became adherent, and the differential expression of CD36, CD11b, CD14 and CD204 compared to THP-1 cells confirmed that PMArest resemble macrophages from a molecular point of view. Changes in the levels were detected in PMA48h group for all the NLRP3-related proteins, with increase of NLRP3 and pro-IL-1β and secretion of mature IL-1β. In PMArest, no pro-IL-1β and lower amounts of mature IL-1β were detected. No ASC speck was found in PMA treated groups, but the addition of a second stimulus to PMArest resulted in ASC speck formation, together with IL-1β production, confirming the responsiveness of the model.

Conclusion: Differentiation of THP-1 with 5ng/ml PMA followed by 24h resting period provides a model that morphologically and molecularly resembles macrophages. However, even at low concentrations, PMA induces production of IL-1β. The 24h rest period provides for down-regulation of pro-IL-1β in PMArest group, without affecting its ability to respond to a second stimulus through activation of inflammasome.

KEYWORDS

phorbol 12-myristate 13-acetate (PMA), interleukin-1β (IL-1β), pro-caspase-1, cell differentiation, macrophage surface markers, monocyte - macrophage, *in vitro* model, ASC speck

1 Introduction

The Nod-like receptor family pyrin domain-containing 3 (NLRP3) inflammasome is a multiprotein complex that mediates caspase-1 activation, *via* apoptosis-associated speck like protein containing a caspase recruitment domain (ASC), in response to microbial infection and cellular damage. Upon assembly of the inflammasome, ASC is mobilized from his soluble cytoplasmic form to assemble into a large singular protein complex of about 1μm diameter, termed "speck", essential for caspase-1 activation, thus playing a critical role in innate immune response (1). Indeed, activated caspase-1 is involved in the maturation of proinflammatory cytokines, such as interleukin-1β (IL-1β) and IL-18, and in the promotion of pyroptotic cell death (pyroptosis), through cleavage and activation of gasdermin D.

Activation of the NLRP3 inflammasome has been shown to contribute to the development of a number of cardiovascular diseases (CVDs), representing a key pathogenetic mechanism in the formation and progression of atherosclerosis, and in the myocardial response to ischemic and nonischemic injury (2, 3). Moreover, in the last decade the effectiveness of NLRP3 inhibitors as therapeutic treatment for CVDs has been extensively investigated (4, 5).

The growing interest in the role of NLRP3 inflammasome in the onset of CVDs has given rise to a copious amount of *in vitro* studies investigating the mechanisms underlying its activation and regulation. Among the models employed, peripheral blood mononuclear cell (PBMC) and monocyte cell lines, such as THP-1 and U937, are the most frequent (6–10). PBMC are routinely used to derive monocytes and macrophages, while THP-1 can be differentiated into macrophage-like cells by using phorbol 12-myristate 13-acetate (PMA). After exposure to PMA, THP-1 cells start to adhere to culture plates and show morphological and functional changes, including flat and amoeboid shape and increased cell surface expression of macrophage markers, resulting in a phenotype that resembles PBMC-derived macrophages (11). The advantages of using THP-1 cell line over human PBMC-derived monocytes or macrophages have been recently reviewed by Chanput et al. (12), and include: a higher growing rate compared to that of PBMC-derived macrophages, stability in cell sensitivity and activity also when cultured for long term (up to passage 25), possibility to be stored for years in liquid nitrogen, and a homogeneous genetic background, thus facilitating the reproducibility of findings. Moreover, contamination with other blood components when isolating PBMC from buffy coat should be taken into account.

Although the convenience of using THP-1 cells as a model is widely accepted, when referring to the method used for the differentiation of THP-1 monocytes into macrophages, the lack of a standardized protocol may give rise to inconsistent and non-reproducible results among different studies. The multitude of applied protocols in the literature ranges from 5 to 400ng/mL PMA for 1–5 days of incubation (13–15), without concern for possible upregulation of some genes and changes in cytokine profile (16, 17). Indeed, PMA has been proven to have dose-dependent effects on the level of several molecules, included IL-1β (18–20). When aiming to investigate the activation of NLRP3 as a response to a specific treatment or to a particular experimental condition, it appears clear that the use of PMA as a differentiation agent deserves careful considerations. High concentrations or long exposure may represent potential sources of bias, making unclear if the triggering or release of the molecules of interest are a result of the biological question or of the bias itself. In this case, as IL-1β is one of the outcomes of PMA exposure, the use of IL-1β alone as primary read out of inflammasome activation may be biased.

In this paper, we investigated the effect of exposing THP-1 to PMA at 5ng/ml for 48h, with or without a rest period of 24h without stimulus, on the main components of NLRP3 pathway. This differentiation protocol has been previously reported to be the minimum amount of PMA sufficient to induce stable differentiation without undesirable gene upregulation upon

secondary stimuli (20). However, the effect on the main mediators of the NLRP3 pathway has never been reported. An optimized protocol may provide an *in vitro* macrophage model that is not only practical to use but can also better reflect the physiologic conditions with minimized risk of biased results.

2 Material and methods

2.1 Cell culture and treatment

THP-1 (ATCC® TIB202™, Virginia) monocytes were cultured in RPMI-1640 complete medium with L-glutamine, 25 mM HEPES (Corning, Virginia) containing 10% FBS (Sigma Aldrich, Germany) and 1% penicillin/streptomycin (10000 units penicillin + 10mg streptomycin/ml, Sigma Aldrich, Germany), plated at a density of 2 x 10^5 cells/ml in T25 flasks (Eppendorf, Germany), and incubated at 37°C in 5% CO_2. Cells from passage p8 to p20 were used for the study.

THP-1 monocytes were induced to differentiate to macrophages-like cells (MLCs) by incubation of 5 x 10^5 cells in a 6-well plate in 2ml complete medium without (THP-1) or with 5ng/ml of PMA (Stemcell technology, Switzerland) in dimethyl sulfoxide (final concentration 0.1%, DMSO, Sigma Aldrich, Germany) for 48h (PMA48h), or with 5ng/ml PMA for 48h plus 24h in fresh medium (PMArest). DMSO to a final concentration of 0.1% was added to THP-1 group to exclude differences in marker expressions due to the presence of DMSO. The chosen dose of 5ng/ml PMA has been previously reported as the minimal concentration of PMA for stable differentiation since cell adherence, a hallmark of differentiation, is unstable at lower concentration (19).

THP-1 cells differentiation to MLCs was evaluated at 48h (PMA48h) after incubation with PMA and 24h after stimulus removal (PMArest) by means of adherence test and fluorescence-activated cell sorting (FACS) analysis, as described below.

To obtain a positive control for the validation of the methods used to study the inflammasome activation, THP-1 cells were seeded in the presence of PMA 50ng/ml overnight followed by incubation with lipopolysaccharide (LPS) from Escherichia coli O26: B6 ≥10000EU/mg (Sigma Aldrich, Germany) (5µg/ml in phosphate-buffered saline, PBS) for 3h in complete media (CTLR+). The CTRL+ sample was only used for methods validation and not included in the statistical analysis.

2.2 Adherence test

The adherence test was performed after 48h incubation with 5ng/ml PMA in PMA48h group and after 24h rest in fresh medium for THP-1 and PMArest groups. The medium was collected in 15ml tubes and non-adherent cells were centrifuged at 200 xg for 4min at room temperature. The supernatant was collected and stored at -20°C until further ELISA analysis; non-adherent cells were resuspended in 200µl medium and counted to determine the adherence percentage. Adherent cells were detached by trypsinization with 1ml Trypsin EDTA 0.25% (Sigma Aldrich, Germany) for 10min at 37°C, collected by centrifugation, resuspended in 200µl medium, and counted. Results are expressed as percentage of total counted cells.

An automated Corning Cell Counter (CytoSMART Technologies, Netherland) was employed to calculate the number and viability of cells after trypan blue (Sigma Aldrich, Germany) staining.

Non-adherent cells, for THP-1 group, and adherent cells, for PMA48h and PMArest groups, were then pelleted again and stored at -20°C until western blot analysis.

Changes in morphology were detected by hematoxylin and eosin staining. Cells were seeded at a density of 150000 cells/ml in a 24-wells and treated as reported above. At collection time, cells were fixed in formalin 4%, washed twice in PBS, then stained as previously described (21). Images were acquired by Axio Imager.Z1 (Zeiss, Germany) and analyzed by ZEN software (v3.4, blue edition, Zeiss, Germany).

2.3 Fluorescence-activated cell sorting analysis

To confirm the differentiation into macrophages, morphological changes and macrophage marker expression were characterized on THP-1 (non-adherent) and PMA48h and PMArest (adherent) cells by FACS.

The combined positive staining for CD36, CD14, CD11b, and CD204 determined the differentiation into MLC (14, 20, 22, 23). Briefly, cells were collected as reported for adherence test, pelleted by centrifugation at 200 xg for 4min at room temperature, washed twice with wash buffer (5% FBS in PBS), and incubated for 30min at 4°C in wash buffer containing conjugated antibodies: anti-CD36 – PE (1:1000), anti-CD14 – APC (1:500), anti-CD11b - PE-Vio® 770 (1:500), and anti-CD204 - Vio® Bright FITC REAfinity (1:500) or isotype control antibody (IgG2a – PE, IgG2a – APC, IgG2b - PE-Vio® 770, IgG1- Vio Bright FITC REAfinity) (Miltenyi Biotec, Germany). Following incubation, samples were centrifuged at 200 xg for 4min at room temperature and pellets were resuspended in wash buffer.

A BD FACS Canto™ II Cell Analyzer (BD Biosciences, US) was employed. For every sample, 50000 events were recorded. Cells were gated by forward scatter – area (FSC-A) vs side scatter – area (SSC-A), then by SSC-A vs side scatter-width (SSC-W) and by FSC-A vs forward scatter – width (FSC-W).

Flow cytometric data were analyzed by FlowJo™ software (v10.7.2, BD, Ashland, OR, USA).

2.4 Inflammasome mediators analysis

To evaluate the effect of PMA treatment on the NLRP3 inflammasome, the levels of inflammasome mediators were assessed in THP-1, PMA48h and PMArest.

Commercially available ELISA kits were used to measure the levels of secreted human IL-1β (Human IL-1beta/IL-1F2), and caspase-1 (Human Caspase-1/ICE) (Quantikine ELISA Kit, R&D System, Minnesota, USA) in undiluted cell media, according to the manufacturer's instructions.

Western blot analysis was used to detect NLRP3, ASC, pro-caspase-1, pro-IL-1β, and caspase 8 in cell lysate. Cell pellet was lysed by addition of 200µl RIPA lysis buffer (Thermo Scientific, Germany) containing protease inhibitor cocktail (cOmplete, Sigma Aldrich, Germany). The cell debris and nuclei were removed by centrifugation at 12000 xg for 20min at 4°C.

The protein concentration in cell lysates was determined using the Micro BCA™ Protein Assay Kit (Thermo Fisher Scientific, Germany). Proteins were denatured in 1x Laemmli buffer (Tris-HCl 63 mM, Glycerol 10%, SDS 2%, Bromophenol blue 0.01%, 2-Mercaptoethanol 5%; pH 6.8) by heating for 10min at 95°C, were then resolved by SDS-PAGE, with 8-12% (wt/vol) separating gels, and transferred to PVDF membrane. Nonspecific sites on PVDF membrane were blocked with 5% non-fat milk powder (VWR, Belgium) in TBS + 0.1% Tween for 1h at room temperature. The membranes were then incubated overnight at 4°C with primary antibodies diluted 1:1000 in blocking solution or 5% BSA in TBS + 0.1% Tween: pro-IL-1β (ab216995), NLRP3 (ab263899), and pro-caspase-1 (ab179515) (Abcam, UK), ASC/TMS1 (#13833), and caspase-8 (#9746, Cell signalling technology, Massachusetts, USA). Proteins were detected by incubation with HRP-conjugated secondary antibodies at half of the primary antibody concentration, and protein bands were visualized by ECL western blotting detection reagents (Amersham Pharmacia Biotech, UK) and enhanced chemiluminescence (ECL Chemocam imager, Intas science imaging, Germany). β-actin (ab8229, Abcam, UK) served as loading control protein (24) to normalize western blot results and was analyzed following the same protocol at a dilution of 1:1000.

2.5 Responsiveness test

To test if, at the end of the 24h after PMA stimulus removal, PMArest cells were able to respond to secondary stimuli and activate the inflammasome, the PMArest group was further treated with LPS at 1 or 5µg/ml for 3h alone or followed by treatment with nigericin (NIG, #66419, Cell signalling technology, Massachusetts, USA) at 5 or 10µM for 45min (25, 26). The activation of canonical inflammasome was evaluated by analysis of pro-IL-1β and released IL-1β, as described above, in PMArest treated with LPS or with LPS+NIG, compared to untreated PMArest.

2.6 Detection of ASC specks

Due to the large size of ASC specks, their detection can be performed by imaging-based techniques. To determine if the treatment with PMA is associated with ASC specks oligomerization, immunofluorescence was used, as previously described (26). Briefly, THP-1 were seeded at a density of 150000 cells/ml in a 24-wells plate containing a glass coverslip per well, and treated as reported above to obtain the following experimental groups: PMA48h, PMArest, PMArest treated with LPS at 1 or 5µg/ml for 3h alone or followed by treatment with NIG at 5 or 10µM for 45min. At the collection time, cells that adhered to the coverslip, were washed in PBS and fixed in PBS-buffered formalin 4% for 30min at 37°C, then blocked in blocking/permeabilization (block/perm) buffer (10% goat serum, 1% FBS, and 0.5% Triton-x100 in PBS) for 30min at 37°C. The cells were then incubated with anti-ASC/TMS1 (#13833) primary antibody at 1:1000 dilution in block/perm buffer for 1h at room temperature. The staining for ASC was performed by incubation with conjugated secondary antibody, goat-anti-rabbit-PE (#79408, Cell signalling technology, Massachusetts, USA) at 1:2000 in block/perm buffer for 1h at room temperature. Nuclei were stained by incubation with Hoechst 34580 (Chemodex, Switzerland) at 1:1000 dilution in PBS for 30min at room temperature. Images were acquired by Axio Imager.Z2 (Zeiss, Germany) and analyzed by ZEN software (v3.4, blue edition, Zeiss, Germany). Unspecific signal due to secondary antibody has been excluded by immunofluorescence analysis of the CTRL+ incubated with the secondary antibody alone in absence of primary antibody (Neg CTRL).

2.7 Statistical analysis

For FACS, western blot and ELISA analyses, every treatment condition was replicated in 3 different wells in the same row of the plate (technical replicates). The row represented the experimental unit. To obtain three biological replicates the experiments were repeated three times in different plates with three different cell passages and freshly prepared stimuli (N=3). Data are shown as mean of the 3 biological replicates. Descriptive statistical analysis and graphs of the results were performed by GraphPad Prism 8 Software (San Diego, CA, USA).

For the analysis of ASC specks, the images are representative of three technical replicates.

10.3389/fimmu.2022.958098

3 Results

3.1 PMArest stably differentiated into MLCs

Differentiation from monocyte to macrophage is associated with morphological changes, such as an increase in size and granularity, as well as cell adhesion, a hallmark of macrophages (11). Representative micrographs showing morphological changes associated with differentiation are reported in Figure 1A. After induction by 5ng/ml PMA for 48h, 98.1% of counted PMA48h cells became adherent, with a viability of 94.4%. Following 24h rest after PMA stimulus removal, 87.1% of PMArest cells were adherent and showed a viability of 97.3%, compared to 99.4% of viability in THP-1 group. Alongside adherence, the treatment with PMA resulted in cells adopting a stellate or a spindle-like morphology after 48h and subsequent rest. Moreover, the hematoxylin and eosin staining resulted in a purple staining for the PMA treated cells, compared with THP-1 assuming a lighter pink staining, indicating changes in cytoplasmic and granular composition.

Morphological changes were confirmed by FACS analysis by comparing the FSC-A and SSC-A of the 3 groups. PMA48h and PMArest showed a gradual increase in size (FSC-A) and granularity (SSC-A) compared to the THP-1 cells (Figure 1B). Moreover, while for PMA48h group heterogeneity in size and granularity was detected, PMArest resulted in a homogenous cell population.

The differential expression of macrophage specific surface markers was assessed by FACS. Figure 1C shows the histogram plots for each marker expression in THP-1, PMA48h and PMArest, assessed by comparison with matched isotype

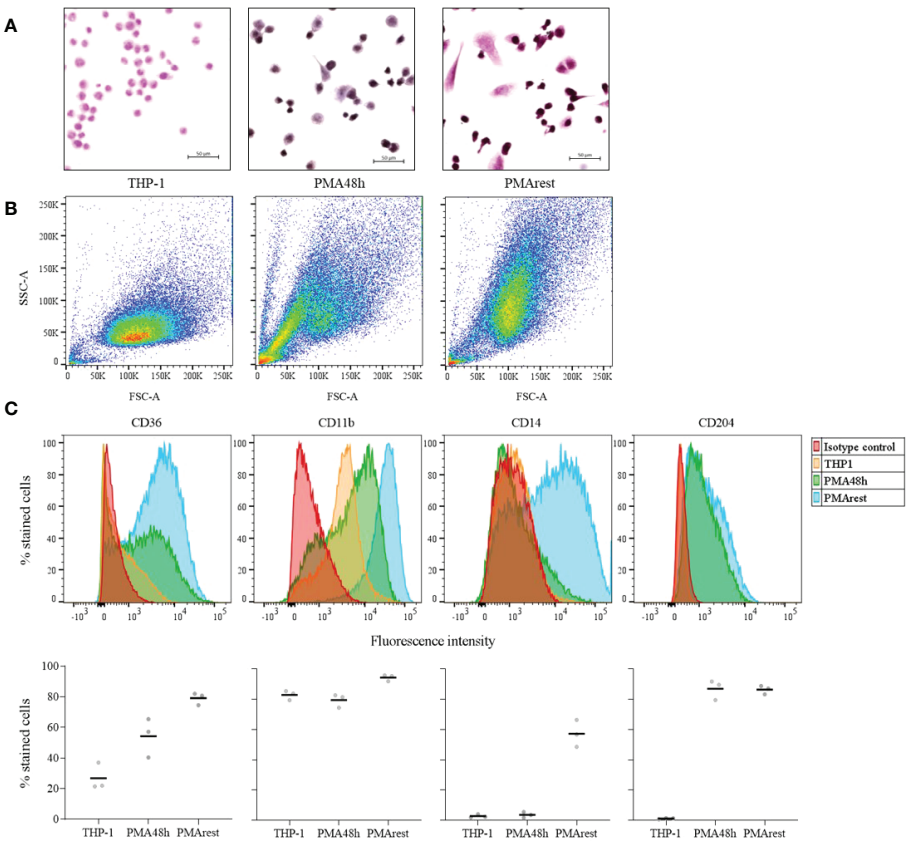

FIGURE 1
Assessment of the differentiation into macrophage-like cells. **(A)** Representative hematoxylin and eosin staining of THP-1 monocytes incubated without (THP-1), with 5ng/ml PMA for 48h (PMA48h) or with 5ng/ml PMA for 48h plus 24h in fresh medium (PMArest). All the micrographs were taken at the same magnification and reported with the same scale (scale bar = 50μm). **(B)** Representative forward (FSC-A) and side light scatter plot (SSC-A) of THP-1, PMA48h and PMArest. **(C)** Representative FACS analysis of THP-1 (yellow), PMA48h (green) and PMArest (blue) cells stained using anti- CD36, CD11b, CD14, or CD204 conjugated antibodies. For each marker, the expression was assessed by comparison with matched isotype control (red). Upper: histogram plots of marker expression (y: percentage of stained cells normalized by mode; x: fluorescence intensity); lower: mean value of the percentage of total events expressing the single markers. Data are shown as mean of three independent experiments in different plates with three different cell passages and freshly prepared stimuli (N=3).

control, and the mean value of the percentage of total events expressing the single markers. THP-1 monocytes showed no surface expression of CD14, and CD204 and low surface expression of CD36, the latter being higher expressed in both PMA48h and in PMArest. In contrast to THP-1, both PMA48h and PMArest exhibited surface expression of CD204, while surface expression of CD14 was only detected in PMArest. All the treatment groups showed expression of CD11b, with enhanced intensity in PMArest.

3.2 IL-1β level dropped down in PMArest

To determine if NLRP3 inflammasome activation occurred as a consequence of PMA treatment, we compared the detection of NLRP3, ASC, pro-caspase-1, and pro-IL-1β in cell lysate and release of mature IL-1β in the supernatant of THP-1, PMA48h and PMArest. Representative results for western blot analyses of cell lysate and the relative ratio of the detected proteins to the loading control are shown in Figures 2A, B, respectively. Western blot analysis confirmed that levels of pro-IL-1β (predicted band size 31kDa) and NLRP3 (predicted bands size 118kDa) were undetectable in THP-1 cells, while treatment with PMA stimulated the production of both pro-IL-1β and NLRP3 in PMA48h group. Along with the enhanced production of NLRP3, a different expression pattern was detected for ASC and for the zymogen forms of caspase-1 (predicted band size 45-42kDa) in PMA48h group compared to THP-1, with 3 times lower relative amount of ASC and 2.5 times lower amount of the 42 kDa band of pro-caspase-1 in PMA48h. On the other side, a higher relative expression of the 45kDa band of pro-caspase-1 was detected in PMA48h compared to THP-1 cells. However, no mature form of caspase-1 (predicted band size 10-12kDa) was detected by western blot in the cell lysate of any of the groups.

In PMArest group, after 24h resting period without PMA, the level of pro-IL-1β became undetectable again, and a decrease in NLRP3 level compared to PMA48h was detected. In contrast, the levels of ASC and pro-caspase-1 remained comparable to the PMA48h group.

In accordance with western blot analysis, secreted IL-1β was not detectable in the supernatant of THP-1, while released IL-1β was found in the supernatant of PMA48h. Levels of IL-1β dropped in PMArest group compared to PMA48h (Figure 2C). No released active caspase-1 was detected by ELISA in the supernatant of any of the groups (data not shown). The validity of the ELISA assays was confirmed by analysis of IL-

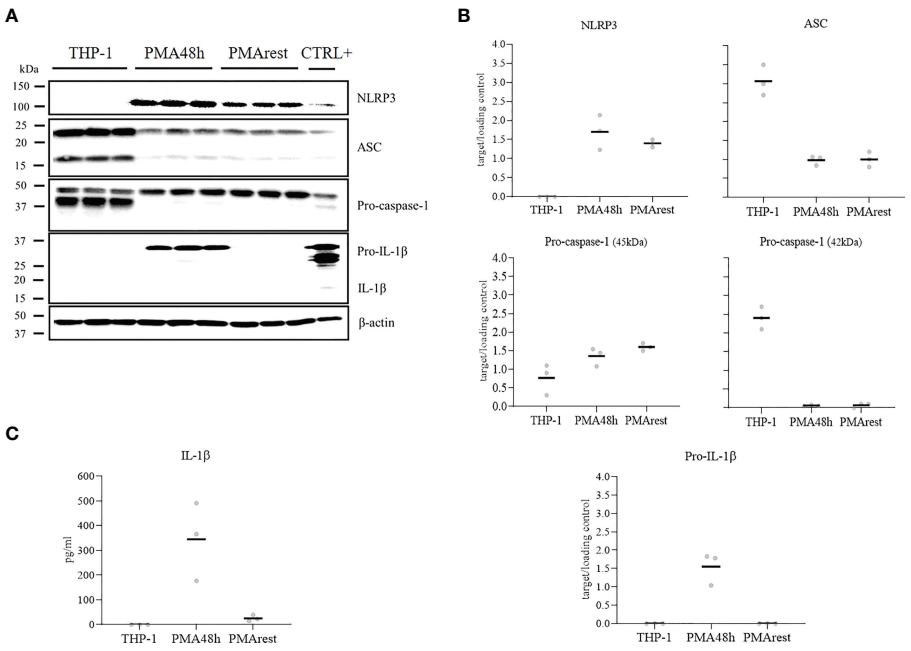

FIGURE 2
NLRP3 inflammasome mediators analysis. **(A)** Representative results of western blot analyses for NLRP3, ASC, pro-caspase-1, pro-IL-1β, and β-actin in cell lysate of THP-1 monocytes incubated without (THP-1), with 5ng/ml PMA for 48h (PMA48h) or with 5ng/ml PMA for 48h plus 24h in fresh medium (PMArest). The positive control (CTLR+) for the validation of western blot was obtained by incubation of THP-1 cells with PMA 50ng/ml overnight followed by incubation with 5μg/ml LPS for 3h in complete media. **(B)** Relative ratio of the expression of the target proteins to the loading control (β-actin), detected by western blot analysis in cell lysate of THP-1, PMA48h, and PMArest cells. **(C)** ELISA analysis of IL-1β in supernatant of THP-1, PMA48h, and PMArest cells. Data are shown as mean of three independent experiments in different plates with three different cell passages and freshly prepared stimuli (N=3).

1β and caspase-1 in the supernatant of the CTRL+, in which a concentration of 308 ± 27pg/mL and of 328pg/mL, respectively, was measured.

3.3 PMArest were responsive to canonical activation of inflammasome

To test the ability of the PMArest cells to respond to a canonical inflammasome activation stimulus, cells were treated with LPS at 1 or 5μg/ml alone or followed by NIG at 5 or 10μM. The results of the responsiveness test are reported in Figure 3. At any of the conditions tested, after treatment, PMArest were able to produce and release IL-1β, as confirmed by the presence of pro-IL-1β in the cell lysate (Figure 3A) and the higher levels of the cytokine in their supernatant (Figure 3B), compared to untreated PMArest. Although a little increasing trend was found in the groups treated with NIG compared to groups treated with LPS alone, not a clear dose dependent response was found.

3.4 ASC specks were not immunodetected in PMArest

Oligomerization of ASC into specks, as a readout for inflammasome activation (1), was investigated in PMA48h, PMArest, PMArest treated with LPS at 1 or 5μg/ml alone or followed by NIG at 5 or 10μM. Representative results are shown in Figure 4. Since no appreciable differences were found among different concentrations of LPS and NIG, only the results relative to LPS 5μg/ml alone (PMArest+LPS) or followed by NIG at 10μM (PMArest+LPS+NIG) are reported in Figure 4 and discussed. The remaining results are shown in Supplementary Figure 3. The staining for ASC is represented in white and nuclear staining (Hoechst) in blue. Activation of the inflammasome is characterized by a change in ASC status from diffuse cytoplasmic form to a speck, visualized as a singular perinuclear structure. The method was validated on our CTRL+ control in which a low amount of cytoplasmic ASC was detected along with several speck-like perinuclear bright dots. In PMA48h and PMArest groups, no speck structures were detected, and ASC showed a broad, weak cytosolic distribution. After treatment PMArest cells with LPS alone, showed an amount of diffuse ASC decreased compared to untreated PMArest and few specks were detected. In PMArest treated with LPS+NIG, cytoplasmic ASC was barely detectable, and instead they showed a high number of specks.

4 Discussion

The study aimed to assess the validity of THP-1 derived macrophages as a model to study the activation of the NLRP3 inflammasome. Several models are employed to study the inflammatory response of monocytes and macrophages, included primary PBMCs and monocyte cell lines. Due to donor variability and technical issues in long term handling of primary cells *in vitro*, THP-1 has been widely accepted as a macrophage model after differentiation by PMA treatment. However, the conditions used for differentiation, particularly the concentration of PMA and the duration of treatment, vary

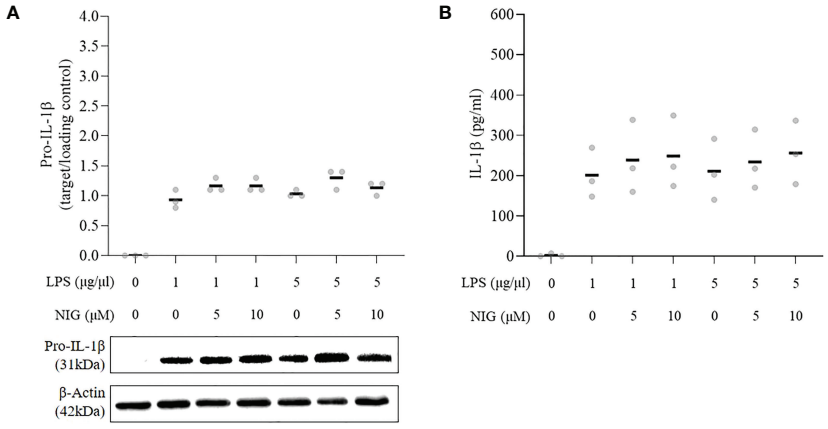

FIGURE 3
Responsiveness of THP-1 monocytes incubated with 5ng/ml PMA for 48h plus 24h in fresh medium (PMArest) to canonical inflammasome stimulus. **(A)** Relative ratio of the expression of pro-IL-1β to the loading control (β-actin), detected by western blot analysis in cell lysate and **(B)** ELISA analysis of IL-1β in supernatant of PMArest untreated or treated with LPS at 1 or 5μg/ml for 3h alone or followed by NIG at 5 or 10μM). Data are shown as mean of three independent experiments in different plates with three different cell passages and freshly prepared stimuli (N=3).

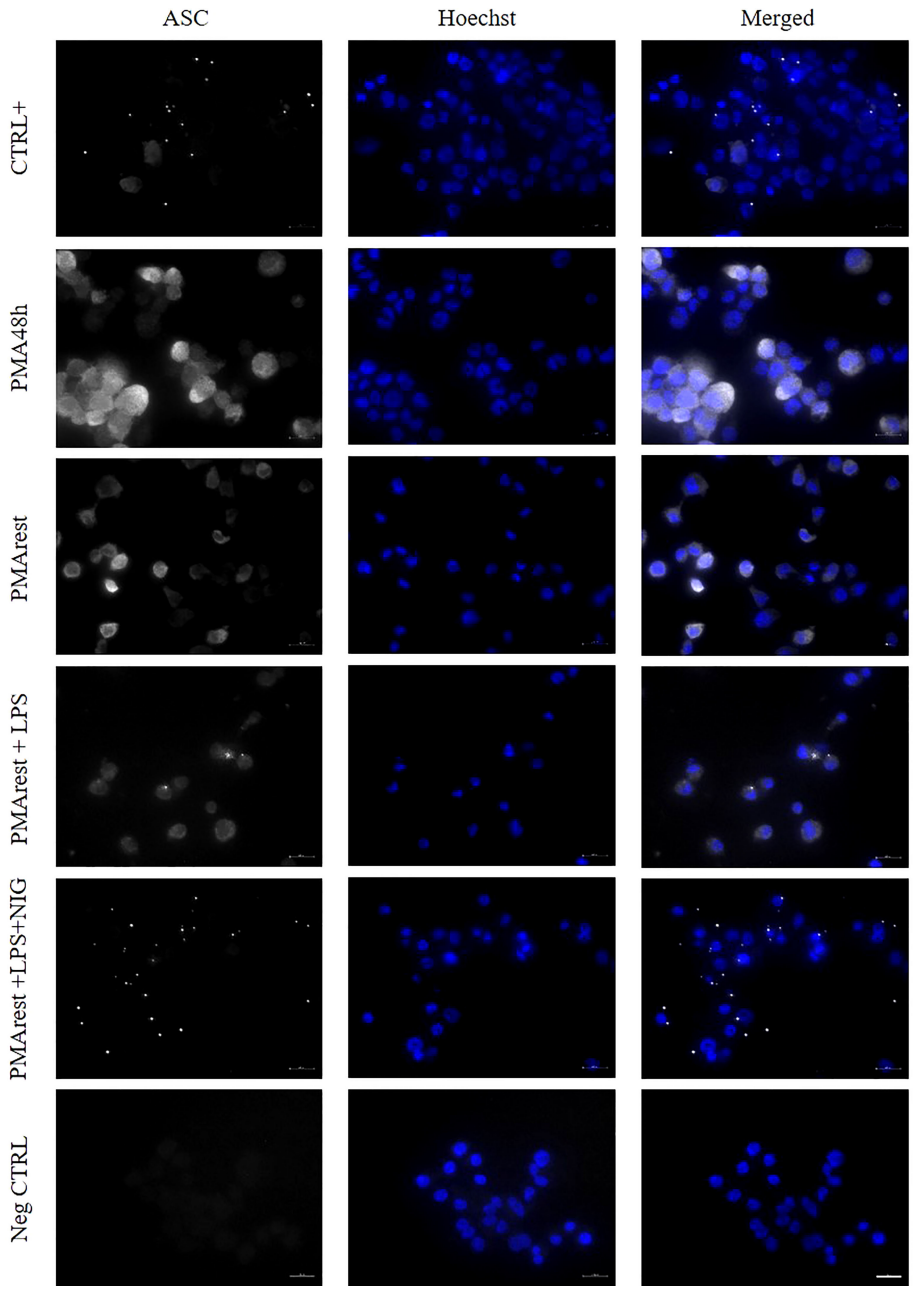

FIGURE 4
Immunofluorescence analysis of ASC specks. Representative results of ASC speck formation in (from top to bottom) THP-1 cells incubated with PMA 50ng/ml overnight followed by incubation with 5μg/ml LPS for 3h (CTRL+), 5ng/ml PMA for 48h (PMA48h), 5ng/ml PMA for 48h plus 24h in fresh medium (PMArest), PMArest treated with 5μg/ml LPS for 3h (PMArest+LPS), and PMArest treated with 5μg/ml LPS for 3h + 45min with 10μM nigericin (PMArest+LPS+NIG). Cells were fixed and stained with anti-ASC antibody, followed by staining with PE-coniugated secondary antibody (false colored in white). Nuclei were stained by incubation with Hoechst 34580 (colored in blue). As a negative control (Neg CTRL), cells were incubated with the secondary antibodies alone. All the micrographs were taken at the same magnification and reported with the same scale (scale bar = 20μm).

widely in the published literature, though a dose-dependent effect of PMA on the expression of inflammatory cytokines was already proved (20, 27). Indeed, PMA is a structural analogue of diacylglycerol, a potent activator of protein kinase-C (PKC) (28). PKC enzyme family comprise 10 cytosolic isoforms that upon activation are translocated to the plasma membrane, where they play a critical role in different signal transduction pathways and in the regulation of cell growth and

differentiation. In particular, the activation of certain isoforms of PKC by PMA results in the induction of pro-inflammatory cytokines synthesis, among which IL-6, TNF-α, and IL-1β (29).

In our model, the differentiation of THP-1 into MLCs was obtained by treatment with 5ng/ml PMA for 48h, followed by a rest period of 24h without PMA stimulus (PMArest). The chosen dose was reported to be the minimal concentration of PMA for stable differentiation (20). Moreover, since PMA has dose-dependent effects on monocytes, it is better to use lower dosages with longer incubation time (30), thus a 48h incubation time was chosen. The differentiation into MLCs was confirmed by adherence, morphological changes, and surface expression of macrophage markers (Figure 1). From a morphological point of view, 87% of PMArest cells were adherent and an increase in size and granularity was observed, in line with previous studies (27). The differential combined positive staining for CD36, CD11b, CD14 and CD204 compared to THP-1 cells indicated that PMArest cells resemble macrophages also from a molecular point of view. This result is consistent with previous studies, in which CD36 in particular is often used as a marker of THP-1 differentiation into macrophages (22–24), and also reported to be expressed in alveolar macrophages isolated from COPD patients (31). CD11b has been formerly described as a macrophage specific marker in both human macrophages (32) and THP-1 derived macrophages (14, 15, 22). Our data confirmed the expression of CD11b at higher intensity in our PMArest population. CD14 is a membrane glycoprotein expressed on cells of the myelomonocyte lineage, mainly by macrophages. Increased CD14 expression in PMA-treated compared to untreated THP-1 cells has been previously described and partly explains the better response of macrophages to LPS and $A\beta_{1\text{-}42}$ compared to monocytes (20). The lack of expression of CD14 in PMA48h group, along with heterogeneity in granularity and size detected by FACS analysis might indicate that the differentiation is still incomplete in this group. Noteworthy, the expression of CD14 was increased in PMArest, indicating a completed differentiation into MLC even at low concentration of PMA and validating the reported differentiation method. To check if the lack of CD14 in PMA48h group, compared to PMArest, may be due to the exposure length to PMA or to the time after the start of the PMA stimulus, we performed the FACS analysis for the expression of CD14 including a group of THP-1 cells treated with the same concentration of PMA for 72h. As reported in the Supplementary Figure 1, the percentage of cells expressing CD14 remains low (22%) also after 72h with PMA stimulus at 5ng/ml, while in the PMArest group about 70% of cells expressed the marker. This result suggests that not the timing after stimulus, but the resting period itself may play a role in the differentiation of THP-1 into MLCs.

NLRP3 inflammasome activation requires two signals, a priming signal that is typically provided by microbial components or endogenous cytokines and mediated by TLR4 activation and a second signal involving potassium ion efflux, lysosomal damage, particulate matter or reactive oxygen species generation. The priming signal may lead to the upregulation of NLRP3, which is thought to exist under resting conditions at too low concentrations to initiate inflammasome activation, and pro-IL-1β, which is not constitutively expressed in resting macrophages. The second signal causes the assembly of the inflammasome, a complex including NLRP3, ASC, and pro-caspase-1, with subsequent activation of caspase-1. Active caspase-1 cleaves pro-IL-1β and pro-IL-18 into their mature and biologically active forms (33). In THP-1 cells, PMA treatment has been shown to induce expression of IL-1β in a dose-dependent manner (20, 34). This aspect must be taken carefully into account when using the THP-1 derived macrophages as a model for the study of the inflammasome activation. In accordance with previous studies, our results confirm that even minimal amounts of PMA can induce the expression of pro-IL-1β in cell lysate and the secretion of IL-1β in the supernatant (Figure 2), thus PMA may provide not only for the priming but also for the second signal for the activation of the inflammasome.

Moreover, we report here for the first time the effect of PMA on the other mediators of the inflammasome, showing that the production of pro-IL-1β occurs alongside the overexpression of NLRP3 and decreased intracellular levels of pro-caspase-1 and ASC (Figure 2). Surprisingly, we were unable to detect any mature form of caspase-1, neither in the cell lysate, nor in the supernatant. Caspase-1 is normally present intracellularly in zymogen form, and after proteolytic cleavage, a tetrameric enzyme, (p20/p10)2, forms. The active subunits can be detected extracellularly, thus acting as a marker for inflammasome activation *in vitro* (35). Although the performed ELISA assay was validated by the analysis of caspase-1 in the CTRL+ sample, no appreciable level of the active enzyme was detected in any of the experimental groups, even in presence of released IL-1β in PMA48h group. One explanation may be that the activation of the NLRP3 inflammasome by PMA may be mediated by another caspase. Indeed, pro-IL-1β maturation and activation can be mediated by caspases other than caspase-1 or by other cell-type specific proteases, as recently reviewed by Pyrillou et al. (36). In particular, in dendritic cells and macrophages, cell stressors can promote caspase-8 dependent activation of NLRP3, and caspase-8 can provide proteolytic maturation of IL-1β in a caspase-1 independent manner (37). To address this hypothesis, we also analyzed the expression of caspase-8, however, no band for active caspase-8 in any experimental group was found (data not shown). Another explanation may be related to instability of the mature caspase-1. A previous study reported a very short half-life of the mature enzyme, with a full activity of about 9min. The authors related the rapid loss of activity to the instability of the quaternary structure of the active enzyme, resulting in loss of caspase-1 tetramers (38). On the other side, Shamaa and colleagues (39) distinguished between the activity of the enzyme in the cell extract, in which once activated, caspase-1 induced robust activity that was

totally lost within an hour, and the activity of the released caspase-1, which is sustained even after immunodepletion of the enzyme. In our study, the time of collection, may have limited our chance to detect the enzyme through immunoblotting assay. An analysis of caspase-1 activity could help to fill the gap of understanding in the release of IL-1β in absence of its proteolytic enzyme.

To better understand the activation status of the inflammasome in PMA48h and PMArest, the formation of ASC specks was analyzed. ASC speck formation has been used as a readout for the inflammasome activation, since it serves as a signal amplification mechanism for inflammasome-mediated cytokine production, required for processing of IL-1β (1, 40). The speck formation is a quick process, so that upon activation the cytosolic levels of ASC drop down and all cytosolic ASC can be incorporated into a speck in <3min (41). In our study, western blot analysis showed a decrease of ASC levels in cell lysate of both PMA48h and PMArest groups compared to THP-1 cells, however ASC specks were not present in none of the two groups (Figure 4). Again, the observation timing may have limited our possibility to detect them. We then performed an extra analysis on THP-1 cells treated with 5ng/ml of PMA for 4h, 12h and 24h, but in none of the groups the ASC specks were detected (Supplementary Figure 2). This data, together with the missed detection of active caspase-1, may suggest that the PMA treatment at 5ng/ml provides the first signal for inflammasome activation, and so the substrates and changes in the intracellular levels of its mediators, but we are not able to prove if it also provides for its assembly in the functionally activated form. In conclusion, the presence of mature IL-1β in the PMA48h is open for further research, out of the scope of this work.

Of note, after 24h rest, no pro-IL-1β and only low amounts of released IL-1β were detected, suggesting that the rest allows for the removal of the inflammasome substrate. Since the release of IL-1β is considered by many authors as the primary outcome of the NLRP3 inflammasome activation, the 24h rest is mandatory to reduce the levels of IL-1β to the basal conditions and exclude biases in the interpretation of the results after exposure to subsequent stimuli. However, NLRP3 is still present, although at lower relative amount, and levels of pro-caspase-1 and ASC remain comparable to those in PMA48h group. We further evaluated the validity of the PMArest as a model for the study of the inflammasome, not only morphologically and molecularly similar to macrophage, but also able to respond to stimuli, by analyzing the ASC formation and the release of pro-inflammatory cytokines after canonical stimulation (LPS+NIG). The decrease of cytosolic ASC together with presence of ASC specks, in particular in PMArest cells treated with LPS followed by NIG, confirmed the ability of these cells to respond to stimuli by activation of the inflammasome. Moreover, the analysis of IL-1β demonstrated that, although the cytokine is not detected in untreated PMArest, the treatment with LPS alone or in combination with nigericin activates an inflammatory response leading to the production (pro-IL-1β) and the release (IL-1β) of the investigated cytokine (Figure 3). Again, the expression of CD14 may make PMArest cells more responsive to LPS compared to undifferentiated THP-1 (20, 42), so that also in the absence of the nigericin stimulus, the cells respond by complete activation of the inflammasome. This confirms our protocol as a valuable non-biased model for the study of the NLRP3 inflammasome, which can be used in the future to analyze other canonical stimuli, such as ATP, oxidized LDL or monosodium urate (MSU) crystals, where IL-1β can be used, but not exclusively, as readout parameter.

We conclude that treatment of THP-1 with 5ng/ml PMA followed by 24h rest period without PMA provides the differentiation into MLCs, from both a morphological and molecular point of view. A 24h rest period without PMA stimulus allows for a complete differentiation into a homogeneous population of MLCs and for the removal of IL-1β, but does not affect the responsiveness of the cells to subsequent stimuli, thus providing a non-biased *in vitro* model for the study of NLRP3 inflammasome.

Data availability statement

The raw data supporting the conclusions of this article will be made available by the authors, without undue reservation.

Author contributions

SG, EL-R, and MO contributed to conception and design of the study. SG performed the laboratory analysis. SG and EL-R contributed to the analysis interpretation. SG wrote the first draft of the manuscript. All authors contributed to manuscript revision, read, and approved the submitted version.

Funding

Funded by the Deutsche Forschungsgemeinschaft (DFG, German Research Foundation) - project number: 462596862 (to SG) and the Else-Kröner-Fresenius Stiftung - project number 2020_EKEA.160 (to EL-R). We acknowledge financial support from the Open Access Publication Fund of Charité – Universitätsmedizin Berlin and the German Research Foundation (DFG).

Acknowledgments

We would like to acknowledge the assistance of the Flow Cytometry Core Facility at the Deutsches Rheuma-Forschungszentrum during the flow cytometry analysis. We would like to acknowledge Frauke Grams and Kerstin Riskowsky for their excellent technical support.

Conflict of interest

The authors declare that the research was conducted in the absence of any commercial or financial relationships that could be construed as a potential conflict of interest.

The handling editor SS declared a shared affiliation with the authors at the time of the review.

Publisher's note

All claims expressed in this article are solely those of the authors and do not necessarily represent those of their affiliated organizations, or those of the publisher, the editors and the reviewers. Any product that may be evaluated in this article, or claim that may be made by its manufacturer, is not guaranteed or endorsed by the publisher.

Supplementary material

The Supplementary Material for this article can be found online at: https://www.frontiersin.org/articles/10.3389/fimmu.2022.958098/full#supplementary-material

References

1. Stutz A, Horvath GL, Monks BG, Latz E. Asc speck formation as a readout for inflammasome activation. In: De Nardo C, Latz E, editors. *The inflammasome. methods in molecular biology*. Totowa, NJ: Humana Press (2013). p. 91–101.

2. Abbate A, Toldo S, Marchetti C, Kron J, Van Tassell BW, Dinarello CA. Interleukin-1 and the inflammasome as therapeutic targets in cardiovascular disease. *Circ Res* (2020) 126:1260–80. doi: 10.1161/CIRCRESAHA.120.315937

3. An N, Gao Y, Si Z, Zhang H, Wang L, Tian C, et al. Regulatory mechanisms of the NLRP3 inflammasome, a novel immune-inflammatory marker in cardiovascular diseases. *Front Immunol* (2019) 10:1592. doi: 10.3389/fimmu.2019.01592

4. Mezzaroma E, Abbate A, Toldo S. NLRP3 inflammasome inhibitors in cardiovascular diseases. *Molecules* (2021) 26:976. doi: 10.3390/molecules26040976

5. Wang Y, Liu X, Shi H, Yu Y, Yu Y, Li M, et al. NLRP3 inflammasome, an immune-inflammatory target in pathogenesis and treatment of cardiovascular diseases. *Clin Transl Med* (2020) 10(1):91–106. doi: 10.1002/CTM2.13

6. Duewell P, Kono H, Rayner KJ, Sirois CM, Vladimer G, Bauernfeind FG, et al. NLRP3 inflammasomes are required for atherogenesis and activated by cholesterol crystals. *Nature* (2010) 464(7293):1357–61. doi: 10.1038/nature08938

7. Samstad EO, Niyonzima N, Nymo S, Aune MH, Ryan L, Bakke SS, et al. Cholesterol crystals induce complement-dependent inflammasome activation and cytokine release. *J Immunol* (2014) 192(6):2837–45. doi: 10.4049/jimmunol.1302484

8. Qin Z. The use of THP-1 cells as a model for mimicking the function and regulation of monocytes and macrophages in the vasculature. *Atherosclerosis* (2012) 221:2–11. doi: 10.1016/j.atherosclerosis.2011.09.003

9. Mouasni S, Gonzalez V, Schmitt A, Bennana E, Guillonneau F, Mistou S, et al. The classical NLRP3 inflammasome controls fadd unconventional secretion through microvesicle shedding. *Cell Death Dis* (2019) 10(3):1–18. doi: 10.1038/s41419-019-1412-9

10. Chanput W, Peters V, Wichers H. THP-1 and U937 cells. In: Verhoeckx K, editor. *The impact of food bioactives on health*. Cham: Springer (2015). p. 147–59.

11. Daigneault M, Preston JA, Marriott HM, Whyte MKB, Dockrell DH. The identification of markers of macrophage differentiation in pma-stimulated THP-1 cells and monocyte-derived macrophages. *PloS One* (2010) 5(1):e8668–e. doi: 10.1371/journal.pone.0008668

12. Chanput W, Mes JJ, Wichers HJ. Thp-1 cell line: An *in vitro* cell model for immune modulation approach. *Int Immunopharmacol* (2014) 23(1):37–45. doi: 10.1016/J.INTIMP.2014.08.002

13. Rios FJO, Ferracini M, Pecenin M, Koga MM, Wang Y, Ketelhuth DFJ, et al. Uptake of oxldl and il-10 production by macrophages requires pafr and CD36 recruitment into the same lipid rafts. *PloS One* (2013) 8(10):e76893–e. doi: 10.1371/journal.pone.0076893

14. Starr T, Bauler TJ, Malik-Kale P, Steele-Mortimer O. The phorbol 12-Myristate-13-Acetate differentiation protocol is critical to the interaction of THP-1 macrophages with salmonella typhimurium. *PloS One* (2018) 13(3):e0193601–e. doi: 10.1371/journal.pone.0193601

15. Kletting S, Barthold S, Repnik U, Griffiths G, Loretz B, Schneider-Daum N, et al. Co-Culture of human alveolar epithelial (hAELVi) and macrophage (THP-1) cell lines. *ALTEX* (2018) 35(2):211–22. doi: 10.14573/altex.1607191

16. Kohro T, Tanaka T, Murakami T, Wada Y, Aburatani H, Hamakubo T, et al. A comparison of differences in the gene expression profiles of phorbol 12-myristate 13-acetate differentiated THP-1 cells and human monocyte-derived macrophage. *J Atheroscler Thromb* (2004) 11(2):88–97. doi: 10.5551/JAT.11.88

17. Aldo PB, Craveiro V, Guller S, Mor G. Effect of culture conditions on the phenotype of THP-1 monocyte cell line. *Am J Reprod Immunol* (2013) 70(1):80. doi: 10.1111/AJI.12129

18. Tedesco S, De Majo F, Kim J, Trenti A, Trevisi L, Fadini GP, et al. Convenience versus biological significance: Are pma-differentiated THP-1 cells a reliable substitute for blood-derived macrophages when studying. *Vitro Polarization? Front Pharmacol* (2018) 9:71. doi: 10.3389/fphar.2018.00071

19. Pinto SM, Kim H, Subbannayya Y, Giambelluca MS, Bösl K, Ryan L, et al. Comparative proteomic analysis reveals varying impact on immune responses in phorbol 12-Myristate-13-Acetate-Mediated THP-1 monocyte-to-Macrophage differentiation. *Front Immunol* (2021) 12:679458. doi: 10.3389/FIMMU.2021.679458

20. Park EK, Jung HS, Yang HI, Yoo MC, Kim C, Kim KS. Optimized THP-1 differentiation is required for the detection of responses to weak stimuli. *Inflammation Res* (2007) 56(1):45–50. doi: 10.1007/s00011-007-6115-5

21. Aescht E, Büchl-Zimmermann S, Burmester A, Dänhardt-Pfeiffer SD, Christine, Hamers C, et al. *Romeis, mikroskopische technik. 18 ed*. Heidelberg: Spektrum Akademischer Verlag (2010).

22. Sadofsky LR, Hayman YA, Vance J, Cervantes JL, Fraser SD, Wilkinson HN, et al. Characterisation of a new human alveolar macrophage-like cell line (Daisy). *Lung* (2019) 197(6):687–98. doi: 10.1007/s00408-019-00288-3

23. Forrester MA, Wassall HJ, Hall LS, Cao H, Wilson HM, Barker RN, et al. Similarities and differences in surface receptor expression by THP-1 monocytes and differentiated macrophages polarized using seven different conditioning regimens. *Cell Immunol* (2018) 332:55–76. doi: 10.1016/j.cellimm.2018.07.008

24. Maeß MB, Sendelbach S, Lorkowski S. Selection of reliable reference genes during THP-1 monocyte differentiation into macrophages. *BMC Mol Biol* (2010) 11(1):90. doi: 10.1186/1471-2199-11-90

25. Gritsenko A, Yu S, Martin-Sanchez F, Diaz-del-Olmo I, Nichols E-M, Davis DM, et al. Priming is dispensable for NLRP3 inflammasome activation in human monocytes in vitro. *Front Immunol* (2020) 11:565924. doi: 10.3389/fimmu.2020.565924

26. Beilharz M, De Nardo D, Latz E, Franklin BS. Measuring nlr oligomerization ii: Detection of ASC speck formation by confocal microscopy and immunofluorescence. In: Di Virgilio F, Pablo P, editors. *NLR proteins. methods in molecular biology*, vol. . p . New York: Humana Press (2016). p. 145–58. p. 1417.

27. Lund ME, To J, O'Brien BA, Donnelly S. The choice of phorbol 12-myristate 13-acetate differentiation protocol influences the response of THP-1 macrophages to a pro-inflammatory stimulus. *J Immunol Methods* (2016) 430:64–70. doi: 10.1016/j.jim.2016.01.012

28. Goel G, Makkar HP, Francis G, Becker K. Phorbol esters: Structure, biological activity, and toxicity in animals. *Int J Toxicol* (2007) 26(4):279–88. doi: 10.1080/10915810701464641

29. Kontny E, Ziółkowska M, Ryzewska A, W M. Protein kinase c-dependent pathway is critical for the production of pro-inflammatory cytokines (Tnf-α, il-1β, il-6). *Cytokine* (1999) 11(11):839–48. doi: 10.1006/cyto.1998.0496

30. Baxter EW, Graham AE, Re NA, Carr I, Robinson JI, Mackie SL, et al. Standardized protocols for differentiation of THP-1 cells to macrophages with distinct M(Ifnγ+Lps), M(Il-4) and M(Il-10) phenotypes. *J Immunol Methods* (2020) 478:112721. doi: 10.1016/j.jim.2019.112721

31. Dewhurst JA, Lea S, Hardaker E, Dungwa JV, Ravi AK, Singh D. Characterisation of lung macrophage subpopulations in copd patients and controls. *Sci Rep* (2017) 7(1):1–12. doi: 10.1038/s41598-017-07101-2

32. Bharat A, Bhorade SM, Morales-Nebreda L, McQuattie-Pimentel AC, Soberanes S, Ridge K, et al. Flow cytometry reveals similarities between lung macrophages in humans and mice. *Am J Respir Cell Mol Biol* (2016) 54(1):147–9. doi: 10.1165/rcmb.2015-0147LE

33. Kelley N, Jeltema D, Duan Y, He Y. The NLRP3 inflammasome: An overview of mechanisms of activation and regulation. *Int J Mol Sci* (2019) 20 (13):3328. doi: 10.3390/IJMS20133328

34. Fenton AMJ, Vermeulen MW, Clark BD, Webb AC. Human pro-Il-1 beta gene expression in monocytic cells is regulated by two distinct pathways. *J Immunol* (1988) 140(7):2267–73.

35. Laliberte RE, Eggler J, Gabel CA. Atp treatment of human monocytes promotes caspase-1 maturation and externalization. *J Biol Chem* (1999) 274 (52):36944–51. doi: 10.1074/JBC.274.52.36944

36. Pyrillou K, Burzynski LC, Clarke MCH. Alternative pathways of IL-1 activation, and its role in health and disease. *Front Immunol* (2020) 0:613170. doi: 10.3389/FIMMU.2020.613170

37. Antonopoulos C, Russo HM, El Sanadi C, Martin BN, Li X, Kaiser WJ, et al. Caspase-8 as an effector and regulator of NLRP3 inflammasome signaling. *J Biol Chem* (2015) 290(33):20167–84. doi: 10.1074/JBC.M115.652321

38. Walsh JG, Logue SE, Lu AU, Martin SJ. Caspase-1 promiscuity is counterbalanced by rapid inactivation of processed enzyme. *J Biol Chem* (2011) 286(37):32513–24. doi: 10.1074/jbc.M111.225862

39. Shamaa OR, Mitra S, Gavrilin MA, Wewers MD. Monocyte caspase-1 is released in a stable, active high molecular weight complex distinct from the unstable cell lysate-activated caspase-1. *PloS One* (2015) 10(11):e0142203. doi: 10.1371/journal.pone.0142203

40. Dick MS, Sborgi L, Ruhl S, Hiller S, Broz P. Asc filament formation serves as a signal amplification mechanism for inflammasomes. *Nat Commun* (2016) 7:11929. doi: 10.1038/ncomms11929

41. Fernandes-Alnemri T, Wu J, Yu JW, Datta P, Miller B, Jankowski W, et al. The pyroptosome: A supramolecular assembly of asc dimers mediating inflammatory cell death *Via* caspase-1 activation. *Cell Death Differ* (2007) 14 (9):1590–604. doi: 10.1038/sj.cdd.4402194

42. Bosshart H, Heinzelmann M. THP-1 cells as a model for human monocytes. *Ann Transl Med* (2016) 4(21):438. doi: 10.21037/atm.2016.08.53

Frontiers in Immunology

Explores novel approaches and diagnoses to treat immune disorders.

The official journal of the International Union of Immunological Societies (IUIS) and the most cited in its field, leading the way for research across basic, translational and clinical immunology.

Discover the latest Research Topics

See more →

Frontiers

Avenue du Tribunal-Fédéral 34
1005 Lausanne, Switzerland
frontiersin.org

Contact us

+41 (0)21 510 17 00
frontiersin.org/about/contact